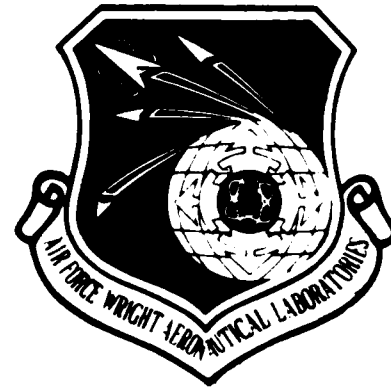AFWAL-TR-82-3014
VOLUME II

PROPOSED REVISIONS TO MIL-F-8785C
RELATED TO FLIGHT SAFETY OF AUGMENTED
AIRCRAFT
VOLUME II
APPENDICES A THROUGH F, REFERENCES

JOHN M. SCHULER
MARK A. DAHL
BOEING MILITARY AIRPLANE COMPANY
SEATTLE, WASHINGTON

APRIL 1982

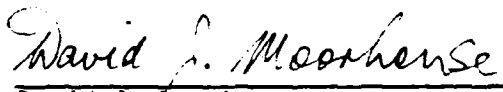Final Report for Period May 1978-August 1980

83 08 16 012

NOTICE

When Government drawings, specifications, or other data are used for any purpose other than in connection with a definitely related Government procurement operation, the United States Government thereby incurs no responsibility nor any obligation whatsoever; and the fact that the Government may have formulated, furnished, or in any way supplied the said drawings, specifications, or other data, is not to be regarded by implication or otherwise as in any manner licensing the holder or any other person or corporation, or conveying any rights or permission to manufacture, use, or sell any patented invention that may in any way be related thereto.
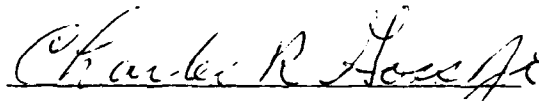
This report has been reviewed by the Public Affairs Office (ASD/PA) and is releasable to the National Technical Information Service (NTIS). At NTIS it will be available to the general public, including foreign nations.

This technical report has been reviewed and is approved for publication. The opinions expressed in this report are those of the authors and are not necessarily shared by the Air Force.

David J. Moorhouse
Project Engineer

Ronald O. Anderson, Chief
Control Dynamics Branch
Flight Control Division
Flight Dynamics Laboratory

FOR THE COMMANDER

CHARLES R. GOSS, JR, Lt Col, USAF
Chief, Flight Control Division
Flight Dynamics Laboratory

REPORT DOCUMENTATION PAGE	READ INSTRUCTIONS BEFORE COMPLETING FORM

1. REPORT NUMBER	2. GOVT ACCESSION NO.	3. RECIPIENT'S CATALOG NUMBER
AFWAL-TR-82-3014, Vol II		

4. TITLE (and Subtitle)	5. TYPE OF REPORT & PERIOD COVERED
PROPOSED REVISIONS TO MIL-F-8785C RELATED TO FLIGHT SAFETY OF AUGMENTED AIRCRAFT VOLUME II APPENDICES A THROUGH F, REFERENCES	Final Report May 1978 - August 1980
	6. PERFORMING ORG. REPORT NUMBER

7. AUTHOR(s)	8. CONTRACT OR GRANT NUMBER(s)
John M. Schuler Mark A. Dahl	F33615-78-C-3603

9. PERFORMING ORGANIZATION NAME AND ADDRESS	10. PROGRAM ELEMENT, PROJECT, TASK AREA & WORK UNIT NUMBERS
Boeing Military Airplane Company Advanced Airplane Branch P.O. Box 3707, Seattle, WA 98124	62201F 24030521

11. CONTROLLING OFFICE NAME AND ADDRESS	12. REPORT DATE
Flight Dynamics Laboratory (FIGC) Air Force Wright Aeronautical Laboratories Wright-Patterson AFB, Ohio 45433	April 1982
	13. NUMBER OF PAGES
	385

14. MONITORING AGENCY NAME & ADDRESS(if different from Controlling Office)	15. SECURITY CLASS. (of this report)
	Unclassified
	15a. DECLASSIFICATION/DOWNGRADING SCHEDULE

16. DISTRIBUTION STATEMENT (of this Report)

Approved for public release; distribution unlimited.

17. DISTRIBUTION STATEMENT (of the abstract entered in Block 20, if different from Report)

18. SUPPLEMENTARY NOTES

19. KEY WORDS (Continue on reverse side if necessary and identify by block number)

Longitudinal Flying Qualities   MIL Standard
Relaxed Static Stability   MIL Handbook
Approach and Landing
Military Specifications
Flight Control Systems

20. ABSTRACT (Continue on reverse side if necessary and identify by block number)

New tentative criteria have been developed for airplanes with relaxed static longitudinal stability based on approach and landing ground simulation, but augmented by the available flight test data. It is shown that a criterion based on just time-to-double amplitude is invalid, and other elements in the pitch attitude transfer function must be included. Criteria based on both closed-loop frequency response and airplane parameters (open-loop) are developed. This report covers the results obtained in one of a series of Air Force programs to update MIL-F-8785, Flying Qualities of Piloted Airplanes.

DD FORM 1 JAN 73 **1473**   EDITION OF 1 NOV 65 IS OBSOLETE

FOREWORD

This report was prepared for the United States Air Force by the Boeing Military Airplane Company, Seattle, Washington, in partial fulfillment of Contract Number F33615-78-C-3603, Project 2403, Flight Control, Task 05, Work Unit 21. The report describes proposed revisions to MIL-F-8785C related to flight safety of highly augmented aircraft, especially those with relaxed static stability. The proposed revisions are based on analysis and fixed base ground simulation.

The contract was under the direction first of Mr. R. Kevin Rowe, then Mr. G. Thomas Black, and finally Mr. David J. Moorhouse, all of the Control Criteria Branch, Air Force Flight Dynamics Laboratory, Wright-Patterson Air Force Base, Ohio. The support and encouragement provided by David Moorhouse are gratefully acknowledged.

The report represents the combined effort of many people of the Boeing Military Airplane Company, both in Seattle and Wichita. The technical work was under the direction of John M. Schuler, Principal Investigator, and Donald E. West, Program Manager. The accident/incident data analysis was performed by Pete Wylie, assisted by Gary Walker, Ove Moutka, and David Wilson of the Experience Analysis Center.

The proposed revisions to improve compatibility with MIL-F-9490D were developed by Garold Hodges and Olin Visor of the Flight Control Group and Donald Nordwall of the Aerodynamics Group, all of Boeing Wichita. The ground simulations were performed on the Boeing Visual Flight Simulator facility at Kent, Washington, under the trying circumstances imposed by significant off-hours operation, and the personnel of that facility are to be commended for their equanimity and outstanding effort, especially Gene Bird for overall operation and computer programming and Larry Hilliard and Bob Copeland for visual system operation and maintenance. The evaluation pilots, who performed their all important role with professional competence despite the trials of a compressed and irregular off-hours schedule, were Andrew Messer (Pilot A), Ray McPherson (Pilot R), and Terry Kriha (Pilot T).

Recognition is due Robert P. Harper, Rogers E. Smith, Charles R. Chalk, Robert C. Radford and James Lyons of the Flight Research Department of Calspan Corp. for their assistance in obtaining and

CONTENTS OF THE THREE VOLUMES [1]

VOLUME I

PAGE

VOLUME II

VOLUME III

[1] This is an abbreviated table of contents for all three volumes of this report.
Complete table of contents for Volume II follows.

TABLE OF CONTENTS

VOLUME II

LIST OF FIGURES

LIST OF FIGURES

LIST OF FIGURES

LIST OF FIGURES

LIST OF FIGURES

LIST OF TABLES

LIST OF TABLES

LIST OF TABLES

LIST OF SYMBOLS

$A_{S(fq)}$	flight safety allocation factor for flying qualities
A_θ	high frequency gain in θ/F_s transfer function
A_h	high frequency gain in h/F_s transfer function
c	wing chord, reference chord, ft
C_L	lift coefficient, L/qS
C_{L_α}	lift curve slope, $\partial C_L/\partial \alpha$
C_m	pitching moment coefficient, M/qSc
C_{m_α}	$\partial C_m/\partial \alpha$
$\bar{c}$	mean aerodynamic chord, ft
D	aerodynamic drag, parallel to flight path, lb
dB	decibels. $20 \log_{10}$ amplitude
F_s	pitch control force, applied by pilot, lb, pull = +
g	acceleration of gravity, ft/sec^2
h	altitude, ft
$\dot{h}$	rate of change of altitude, rate of climb, ft/sec^2
I_y	moment of inertia about y-axis, slug-ft^2
j	$\sqrt{-1}$
K_p	gain in pilot model
L	aerodynamic lift, normal to flight path, lb
M	Mach number
M	aerodynamic pitch moment about y-axis, ft-lb
m	mass of airplane, slugs
M_c	normalized pitching moment due to pitch control, $M_{control}/I_y$, rad/sec^2
$M_{c_{max}}$	maximum normalized pitching moment due to pitch control, rad/sec^2
M_i	$= \frac{1}{I_y} \frac{\partial M}{\partial i}$, $i = \alpha, u, q, \delta_e, \delta_h, \delta, \dot{\alpha}, w$
M_{F_s}	$= \frac{\delta_{ES}}{F_s} M_{\delta_{ES}}$, rad/sec^2/lb, deg/sec^2/lb

$M_{\delta_{ES}}$	$= \dfrac{\delta e}{\delta_{ES}} M_{\delta_e} = \dfrac{\delta_h}{\delta_{ES}} M_{\delta_h}$, rad/sec^2/in
n	normal acceleration or load factor, g's, up = +
n_z	normal acceleration along z-axis, g's, down = +
q	dynamic pressure, lb/ft^2
q	pitch rate about y-axis, rad/sec, deg/sec
$Q_{S(fq)}$	maximum allowable probability of worse than Level 3 flying qualities (aircraft loss rate), per flight
$\dot{q}$	time rate of change of pitch rate q, rad/sec^2
R_S	overall airplane flight safety requirement, per flight
s	Laplace operator
S	wing area, ft^2
t	time, sec
$T_{1/2}$	time to half amplitude, oscillation or convergence, sec
T_2	time to double amplitude, oscillation or divergence, sec
T_{θ_2}	time constant of larger zero in θ/F_s, sec
T_{θ_1}	time constant of smallest zero in θ/F_s, sec
T_{h_1}	time constant of smallest zero in h/F_s, sec
u	incremental velocity along x-axis, ft/sec
u_g	gust velocity along the x-axis, ft/sec
V	airspeed, ft/sec, knots
V_{min}	minimum service speed, knots
V_{max}	maximum service speed, knots
$V_{o_{min}}$	minimum operational speed, knots
$V_{o_{max}}$	maximum operational speed, knots
V_s	stall speed (equivalent airspeed), knots
W	airplane weight, lb
w	incremental velocity along z-axis, ft/sec

w_g	gust velocity along z-axis, ft/sec
x	body axis, longitudinal, origin at c.g.
y	body axis, right wing, origin at c.g.
$Y(s)_{cs}$	transfer function for airplane control system from control stick to control surface, rad/in
z	body axis, down, origin at c.g.
Z_{θ_1}	small zero in θ/F_s, $= -1/T_{\theta_1}$, rad/sec
Z_{θ_2}	large zero in θ/F_s, $= -1/T_{\theta_2}$, rad/sec
Z_{h_1}	smallest zero in h/F_s, $= -1/T_{h_1}$, rad/sec
Z_{h_2}	intermediate zero in h/F_s, rad/sec
Z_{h_3}	largest zero in h/F_s, rad/sec
Z_i	$= \frac{1}{M} \frac{\partial Z}{\partial i}$, $i = \alpha, u, q, \delta_e, \delta_h, \dot{\alpha}, w$
α	angle of attack, angle between x-axis and projection of air velocity vector in x-z plane, rad, deg
β	sideslip angle, angle between air velocity vector and its projection in x-z plane, rad, deg
γ	flight path angle, angle between velocity vector and horizontal, deg
$d\gamma/dV$	flight path stability parameter, steady state change in γ with V at constant throttle handle position, deg/knot
Δ	incremental
δ	control deflection
δ_e	elevator deflection, deg, rad, TE down = +
δ_{ES}	pitch control stick deflection (elevator stick), at stick grip, in, aft = +
δ_h	horizontal tail deflection, rad, deg, TE down = +
δ_e/δ_{ES}	gearing from control stick or column to pitch control surface, gain, rad/in, deg/in

δ_{ES}/F_S	gradient of stick deflection vs force, in/lb
ζ	damping ratio
ζ_{sp}	damping ratio of short period mode
ζ_p	damping ratio of phugoid mode
θ	pitch attitude, angle between x-axis and horizontal, deg
$\dot{\theta}$	time rate of change of θ, often used incorrectly for body pitch rate q, deg/sec
$\ddot{\theta}$	second derivative of θ, often uses incorrectly for body pitch angular acceleration, $\dot{q}$, deg/sec^2
λ	turbulence wave length, ft
λ	root of characteristic equation, usually real, rad/sec
λ_{sp_1}	most positive real root of short period mode
λ_{sp_2}	most negative real root of short period mode
λ_{csp_1}	most positive real root of short period mode with speed held constant
λ_{csp_2}	most negative real root of short period mode with speed held constant
$\lambda_{sp_{2_{CRIT}}}$	value of λ_{sp_2} (negative) for which pilot rating does not change for larger negative λ_{sp_2} (3.2.1.3)
ρ	air density, slug/ft^3
σ	real part of a complex root
σ	standard deviation, root-mean-square (rms) from the mean of a quantity
$\sigma_u, \sigma_v, \sigma_w$	rms of u_g, v_g, w_g, ft/sec
σ_V	rms of total gust velocity, ft/sec
τ	time constant, sec
$\tau_{p_1}, \tau_{p_2}, \tau_{p_3}$	time constants in pilot model
τ_d	time delay in pilot model, sec

τ_e time delay in equivalent system model, sec

ϕ bank angle, angle between y-axis and intersection of y-z plane with horizontal (about x-axis), deg, bank to right (right wing down) = +

ϕ_{PL} pilot lead (phase of pilot model excluding time delay), deg

ω frequency, imaginary part of complex root, rad/sec

$\omega_{n_{sp}}$ undamped natural frequency of short period mode with speed held constant, rad/sec

$\omega_{n_{csp}}$ undamped natural frequency of phugoid mode, rad/sec

$\mathfrak{z}$ angle of, phase angle of

ABBREVIATIONS

A	acceptable (pilot rating, Ref. 28)
AP	acceptable poor (pilot rating, Ref. 28)
BW	bandwidth frequency
c.g.	center of gravity
CAS	calibrated airspeed
CCV	control configured vehicle
FCS	flight control system
FTD	flare and touchdown
HZ	hertz, cycles per second
ILS	instrument landing system
LAHOS	landing approach higher order system, refers to investigation of Ref. 8
mac	mean aerodynamic chord
MAT	maximum augumented thrust
PCP	pitch control power
PIO	pilot induced oscillation
PR	pilot rating
PR_{CRIT}	pilot rating for $\lambda_{sp_{2_{CRIT}}}$ (3.2.1.3)
RA	resonant amplitude
RSSAS	relaxed static stability augmentation system
SAS	stability augumentation system
SST	supersonic transport
TE	trailing edge
U	unacceptable (pilot rating, Ref. 28)

APPENDIX A
ANALYSIS OF ACCIDENT AND INCIDENT DATA

Summaries of accidents and incidents related to flight control and flying qualities problems for highly augmented aircraft were obtained from the Air Force Safety Center, Norton AFB, and the Navy Safety Center, NAS Norfolk. The object was to see if statistics based on this data would show there was a need to revise MIL-F-8785C to improve its flight safety aspects, and if so, what areas most needed revision. To this intent, data were obtained which would show the frequency of occurrence of pilot error as well as other flight control related causes and failures. A high incidence of pilot error in a particular area should indicate a potential flying qualities deficiency.

A.1 Data Selection

The data requested was coded information and brief narrative descriptions of aircraft mishaps. This data is obtained by the Air Force and Navy Safety Centers from mishap reports on military aircraft, sanitized to eliminate specific mishap identification, and coded for computer sorting and printing. The categories of mishaps are indicated in Table A-1. Data were requested for selected aircraft and conditions for about

Table A-1. Outline of Data Request

CATEGORIES OF MISHAPS:		
MAJOR ACCIDENT - LOSS OF LIFE	HI	
MINOR ACCIDENT -	MED	COST TO REPAIR (M-HR,$)
INCIDENT -	LOW	
DATA REQUEST:		
AIRCRAFT	AIR FORCE	F-4, F-111, F-15
	NAVY	F-4; A-7, F-14
TIME PERIOD	JAN 1973 - MAR 1978	
UNSAFE ACTS AND CONDITIONS:		FLIGHT CONTROL RELATED
CONDITIONS AFFECTING MISHAP:		UNCONTROLLED AIRCRAFT IN FLIGHT

1

a five-year time period, indicated in Table A-1. The aircraft selected were those with higher levels of augmentation. The emphasis was on selecting mishaps which were caused by flight control system failures, primarily those of the augmentation system, and mishaps blamed on pilot error. The assumption was that repeated occurrences of a particular type of pilot error reflected in reality a flying qualities deficiency, rather than a human deficiency. Mishap data were requested for 23 unsafe acts and 7 unsafe conditions related to flight control, also all cases of "uncontrolled aircraft in flight", weather conditions, and three miscellaneous conditions. Subcategories of many of the above were also specified to narrow the data field. A description of the selected conditions is summarized by the broad categories listed in Table A-2.

Table A-2. Broad Categories Used In Data Request

UNSAFE ACTS OF PERSONNEL
MISCELLANEOUS
MISTREATED AIRPLANE
INCORRECT OPERATION OF FLIGHT CONTROLS AND SPEED BRAKES
INCORRECT OPERATION OF OTHER EQUIPMENT
DEMONSTRATED POOR TECHNIQUE IN GROUND AND TAKEOFF OPERATIONS
DEMONSTRATED POOR TECHNIQUE IN FLIGHT
DEMONSTRATED POOR TECHNIQUE IN APPROACH AND LANDING
UNSAFE CONDITIONS AND ENVIRONMENTAL FACTORS
FLIGHT CONTROL SYSTEM
ALLERON, ELEVATOR, RUDDER
AUTOPILOT
SPOILERS
CONTROL COLUMN
WEATHER
MISCELLANEOUS

An initial sifting of the data was made to select those cases pertinent to flying qualities and to obtain gross distributions with respect to airplane type and flight phase. This data is presented in Table A-3 along with statistics on all accidents for the selected aircraft types. The tabulated data shows that of 2216 cases received, 1300 were flying qualities related and were selected for detailed analysis. The criteria for selection addressed flight control system failures and pilot errors. Was there a flight control system failure or malfunction? Did the pilot misuse any controls, or lose control of the aircraft? Controls were defined to include any control affecting aircraft response - for example, the flaps, gear, drag chute and brakes, as well as stick, rudder pedals, and throttles. The distribution of mishaps by airplane type and mishap category-is tabulated in Table A-3 in terms of absolute number of occurrences. The bulk of the mishap data is for the F-4, either Air Force (C, D, E models) or Navy (J model). Most of the mishaps are incidents, but when an accident occurred, it tended to be major. Also tabulated is the distribution by flight phase in terms of fraction of mishaps in each phase per total mishaps for that aircraft type. Only those phases having more than 10% of the mishaps for a majority of the aircraft are shown. As well as those listed, the flight phases examined were pre-take-off, take-off, climb, descent, and "all others". Landing included approach through touchdown, but not landing roll. Combat maneuvering included aerobatics, air show maneuvers, low-level terrain following, and weapon delivery. Cruise included air refueling, but the number of mishaps during refueling was miniscule. The large fraction of mishaps that occurred in cruise for most of the aircraft is surprising. The overall accident statistics presented in Table A-3 are for the indicated five-year period. Only Air Force data on overall rates was made available. The ratio of the selected flight control related accidents to total accidents has been corrected for the additional five months covered by the case data of this study. As can be seen, we are generally dealing with more than 10% of the accidents.

3

A.2 Analysis Method

The description of each mishap was read, categorized according to the various factors involved, and coded for computer analysis. The major headings in the factor code were accident number, type aircraft, flight phase, damage class, injury class, ejection, day/night, cause factors, and conditions affecting the mishap. All factors had sub-headings. The major causes were environment, maintenance error, design deficiency, material failure or malfunction, and pilot error. The factors describing patterns in pilot error, the cause factor of primary importance, are shown in Table A-4 for landing and take-off; in Table A-5 for general up-and-away flight.

The factor code was not decided upon a priori, but rather, was developed as the data was analyzed. The data for the landing and air combat maneuvering flight phases was initially coded and analyzed by hand, that is without the aid of the digital computer, to develop the factor code and the method of analysis. Much of the data in the Appendix comes from this initial analysis. Then all mishaps were coded and the data entered onto cards for computer analysis. Computer programs were then written to sort out the data according to the various categories, causes, and factors which contributed to the mishap. The data with respect to flight phase comes from the computer analysis. The primary computer output is in the form of graphs of the distributions, but tabular data is available as well. A complete list of the factor codes used in the computer analysis of the data is presented in Table A-8 at the end of this Appendix.

A.3 Mishap Distribution by Flight Phase

The distribution of accidents and incidents by flight phase is shown in Figure A-1. The highest percentage of accidents occurs in landing (45%), followed closely by air combat and maneuvering (ACM, 35%). Surprisingly, take-off accidents are low (11%), and about the same as Category B flight phases combined (9%). The data for the cruise phase is not strictly Category B, since it includes a few (about 1%) air refueling cases. The highest percentage of incidents occurred in landing (25%),

4

Table A-3. Gross Distributions Of Mishap Data

MISHAPS PERTINENT TO FLIGHT CONTROL	AIR FORCE	NAVY						
CASES RECEIVED	1644	572						
SELECTED FOR ANALYSIS	985	315						

DISTRIBUTION BY ACCIDENT TYPE (NO)	A-7E	F-4J	F-14A	F-15A	F-4C TO E	F-111	FB-111
MAJOR ACCIDENTS	14	29	9	0	35	11	2
MINOR ACCIDENTS	3	11	1	1	6	0	0
INCIDENTS	135	59	54	29	706	130	65

DISTRIBUTION BY FLIGHT PHASE OF MISHAPS (FRACTION)	A-7E	F-4J	F-14A	F-15A	F-4C TO E	F-111	FB-111
LANDING	.24	.46	.34	.37	.24	.29	.19
COMBAT MAN.	.09	.26	.13	.33	.23	.38	.37
CRUISE	.20	.07	.07	.13	.28	.13	.22

DATA ON ALL ACCIDENTS 1973-1977	A-7E	F-4J	F-14A	F-15A	F-4C TO E	F-111	FB-111
NO. ACC (MAJ. & MIN.)	NA	NA	NA	24	230	56	15
NO. OF FLT. HRS. (1000's)	NA	NA	NA	67.6	2,158.3	387.5	88.7
ACC. RATE/10^5 FLT. HRS	NA	NA	NA	35.5	10.7	14.5	16.9
FC ACC/TOTAL ACC.	NA	NA	NA	.04	.16	.18	.12

Table A-4.   Pilot Error Factors, Landing And Take-Off

EXCESSIVE SINK RATE (ON GLIDESLOPE OR TOUCHDOWN)

IMPROPER (TOO HIGH) PITCH ATTITUDE (GO-AROUND, TOUCHDOWN, ROLLOUT)

UNFAVORABLE WINDS (CROSSWIND ,TAILWIND ,WIND SHEAR)

UNFAVORABLE WINDS FOLLOWED BY PILOT ERROR

OVER-ROTATE ON TAKEOFF

IMPROPER LANDING OR TAKEOFF CONFIGURATION (FLAPS, GEAR, WEIGHT
    DRAG CHUTE, WING SWEEP)

PITCHING DECK

IMPROPER TECHNIQUE LANDING ON WET RUNWAY

SCAN PATTERN PROBLEMS ON LANDING INDUCED BY REDUCED VISIBILITY

PILOT ERROR ON TAKEOFF

Table A-5.   Pilot Error Factors, Up-And-Away Flight

IMPROPER USE OF FLIGHT CONTROLS

IMPROPER USE OF FLIGHT CONTROLS RESULTED IN DEPARTURE

IMPROPER USE OF FLIGHT CONTROLS RESULTED IN SPIN

FAILURE TO RECOGNIZE APPROACH TO STALL

FAILURE TO USE CHECKLIST

MANEUVER TOO LOW TO RECOVER

DEPARTURES:
    EXCESSIVE ANGLE OF ATTACK
    AIRCRAFT INVERTED OR AT HIGH BANK ANGLE, V< 250 KIAS, "G" APPLIED
    AILERON ROLL AT TOO LOW V FOR HIGH GROSS WEIGHT OR EXTERNAL STORES
    OTHER

EXCESS "G":
    EXCESS PULL (AIRSPEED AND DIVE ANGLE NO FACTOR)
    TRANSONIC PITCH UP OR MACH TUCK
    DIVE RECOVERY
    OTHER

MAINTENANCE ERROR FOLLOWED BY PILOT ERROR

followed, surprisingly, by cruise (24%), with ACM (22%) a close third. If Category B flight phases are combined, this forms the flight phase with the highest rate of incidents (36%). Analysis of the incidents in cruise shows that, for all aircraft combined, the majority resulted from material failure or malfunction of augmentation system components. The major contributors were amplifiers or computers, followed by servos and then rate gyros. Most failures involved uncommanded transients as a factor in the incident.
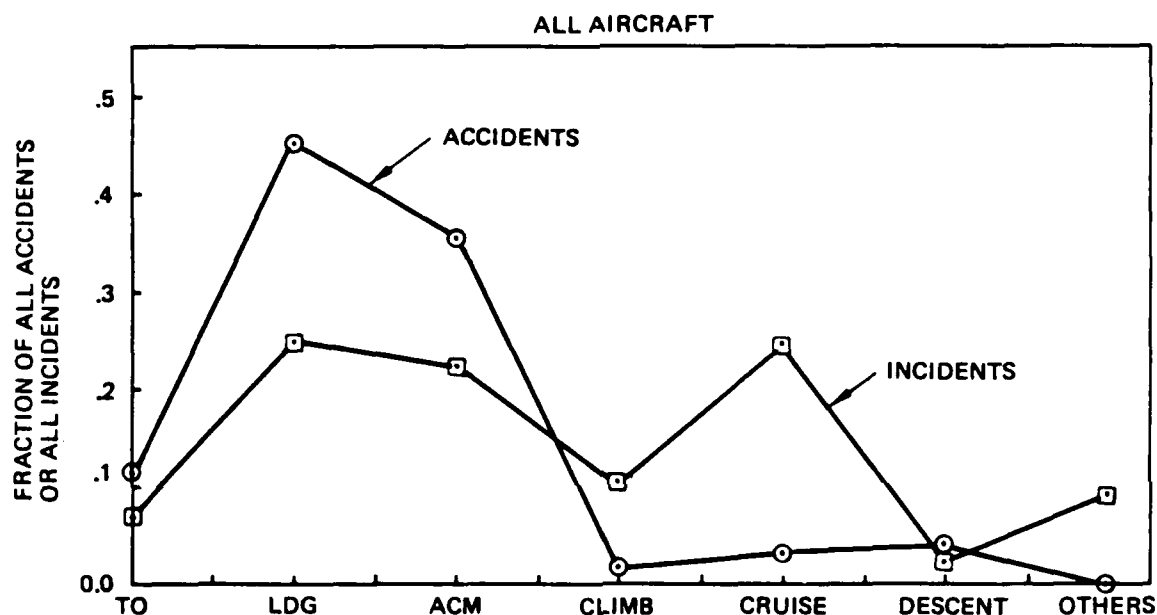
ALL AIRCRAFT

Figure A-1. Distribution of Accidents/Incidents By Flight Phase

The distribution of accidents and incidents with aircraft type for each flight phase is shown in Figure A-2. Climb, cruise, and descent have been combined into a single Category B flight phase. The distributions of accidents in landing (30-60%) and ACM (20-60%) are fairly flat, except the F-15. That anomaly is because there was only one F-15 accident, a case where the pilot pulled too much g, about 8 g, and the inlet failed. Take-off accidents are more prevalent for Navy (18%) than Air Force (3%) aircraft, but this is not due to carrier operations as might be supposed. The catapult and shore-based take-off accidents

7

were about equal in frequency of occurrence. Catapult take-off accidents were proportionately high for the F-4, but low for the A-7 and F-14. Accidents in Category B flight phases were almost exclusively a problem for the F-111 and FB-111. Analysis of the accidents shows that there were four in number and that all were characterized by uncommanded transients, pilot ejection, and loss of the aircraft. Three have known manual flight control system malfunctions, the cause for the fourth was unknown.

The distribution of incidents shown in Figure A-2 show some trends with flight phase that are different from accidents. Incidents in landing and ACM are high, but incidents in Category B flight phases are equally high. Several anomalous points appear in the data: the high values for "other" flight phases for the A-7 and F-14 aircraft, and the large value for Category B phases for the Air Force F-4 aircraft. For the A-7 and F-14, these incidents were almost exclusively augmentation system failures in pre-take-off. Most failures occurred in amplifier-computers, rate gyros, or accelerometers. More than half of the F-14 failures involved the spoiler fly-by-wire system. The Air Force F-4 incidents were primarily caused by material failures, primarily of augmentation system components, followed by manual flight controls and trim systems. Of the augmentation system components, amplifier-computers and rate gyros were the major culprits, with servo actuator a not-so-prevalent third.

The distribution of accidents and incidents is broken down in Figure A-3 for the three Category B flight phases, cruise, climb, and descent. The percent of accidents for the FB-111 in descent is high, but only two accidents were involved (Table A-3) so this is not statistically significant. The incidents occurred predominately in cruise, followed by climb and then descent. The sequence probably reflects the amount of time spent in each of the flight phases. Analysis of all incidents in cruise shows that the majority (58%) of incidents resulted from material failure of augmentation components: amplifier-computer, rate gyros, and servo actuators. About half of these failures involved uncommanded transients. The incidents represent potential accidents, and though not high in number, many of the Category B accidents did result from realization of this potential. So, Category B flying qualities criteria

8

FLIGHT PHASE

| ⊙ TO | ⊡ ACM | ★ OTHER |
| △ LDG | ◇ CAT B | |

ACCIDENTS

| ⊙ TO | ⊡ ACM | ★ OTHER |
| △ LDG | ◇ CAT B | |

INCIDENTS

USN ⟵ | ⟶ USAF
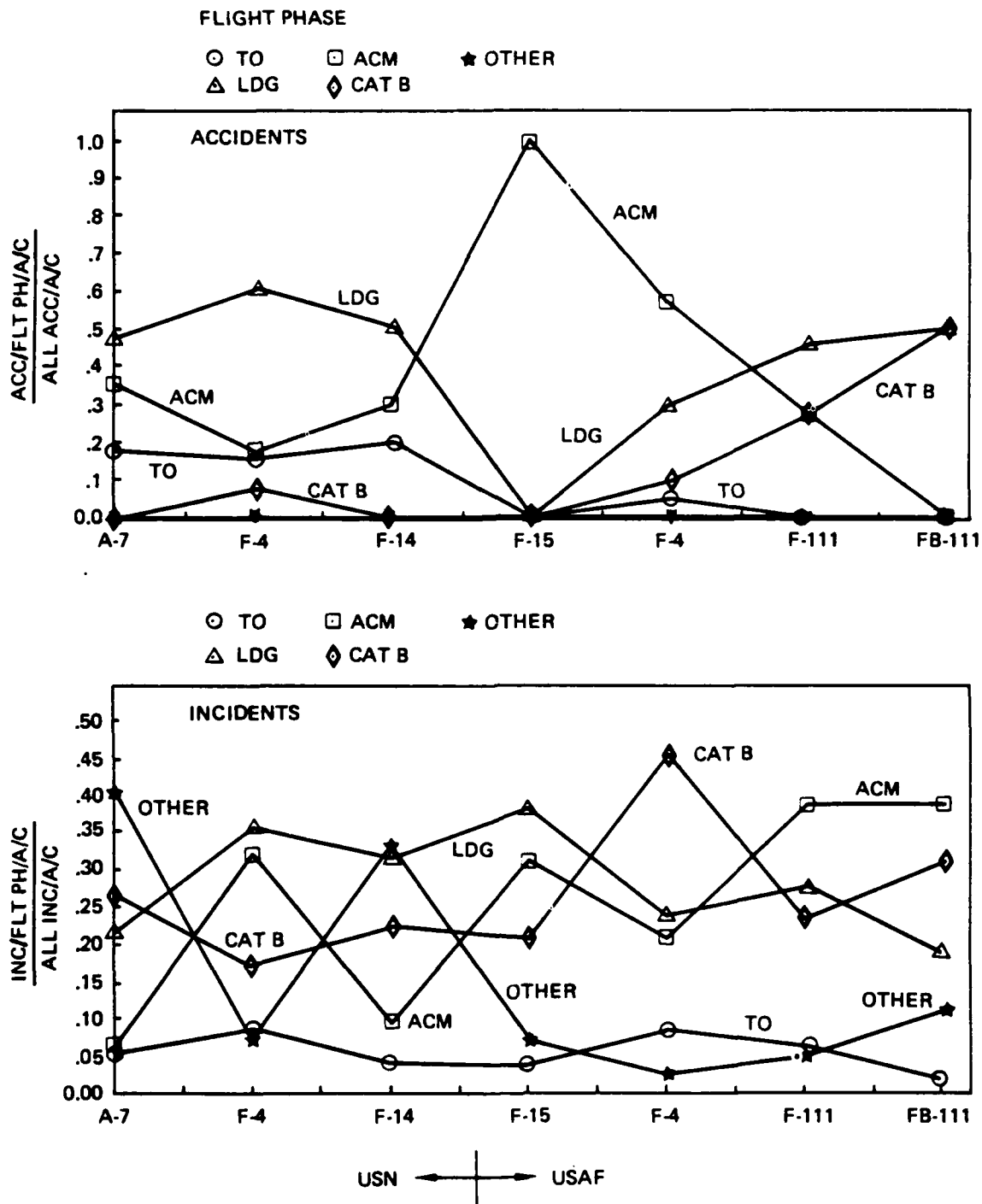
Figure A-2. *Distribution of Accidents/Incidents By Aircraft Type and Flight Phase*

9
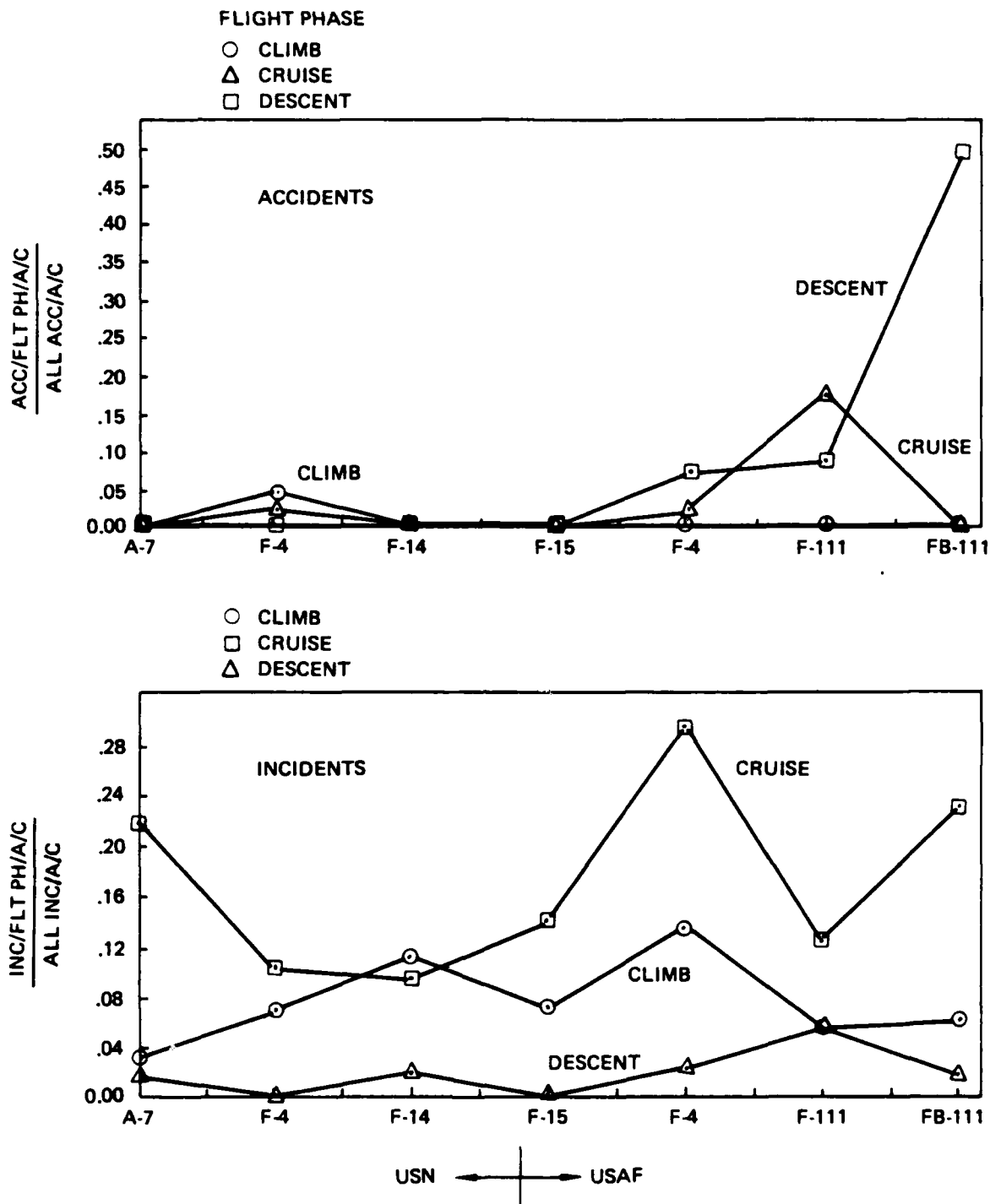
Figure A-3. Distribution of Accidents/Incidents By Aircraft Type for Category
B Flight Phases

do need to reflect protection against augmentation failures and the ability to maintain control and suppress transients resulting from the failures.

A.4 Mishap Cause in Landing and ACM

The majority of accidents occurred in the landing and air combat and maneuvering (ACM) flight phases. The distribution of the major causes of accidents and incidents in these two flight phases, by aircraft type, is shown in Figures A-4 and A-5. Note that the Air Force F-4 data (C, D, E models) is now found next to the Navy F-4 data (J model).

In landing (Figure A-4) pilot error was almost always involved in mishaps, either by itself, or following a material failure. Pilot error alone was the cause of most incidents, and a lesser number of accidents. Material failures alone did not cause a significant fraction of the incidents and only a significant fraction of the accidents for one aircraft, the F-111. But failures combined with pilot error were the major cause of accidents for most of the aircraft.

IN ACM (Figure A-5), again, pilot error was almost always involved in mishaps. Material failures alone or pilot error alone lead to most of the incidents. But pilot error alone, or following a material failure, was the cause for most of the accidents.

These results for landing and ACM suggest that flying qualities are deficient in both flight phases, especially flying qualities following a failure. To better define possible deficiencies, an analysis of the cause factors and types of pilot errors was made. The major patterns that evolved are shown in Figures A-6 and A-7. It should be noted that some mishaps involved multiple factors, so the sum of the fractions may exceed unity.

In landing (Fig. A-6), excessive sink rate was the standout contributor to accidents. But the data on incidents indicates that improper landing configuration and holding too high a pitch attitude were significant contributors. Unfavorable winds added problems and contributed to mishaps. These results suggest that pitch response and flight path control are inadequate, pilot workload is too high, and flying qualities deteriorate too much with crosswinds and turbulence.

11
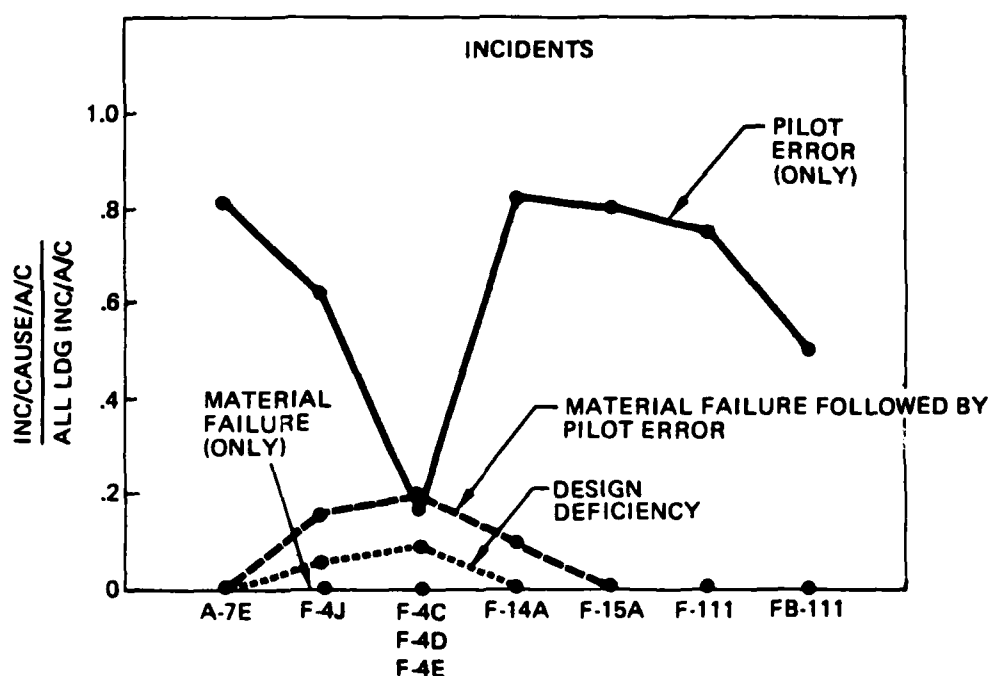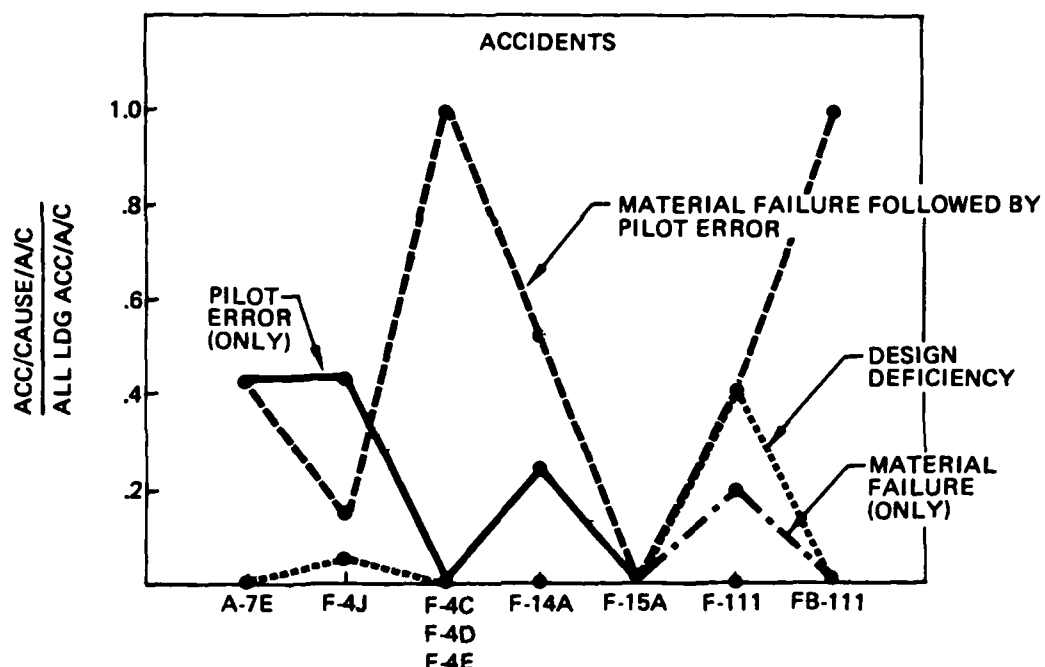
Figure A-4.   Major Causes of Mishaps in Approach and Landing
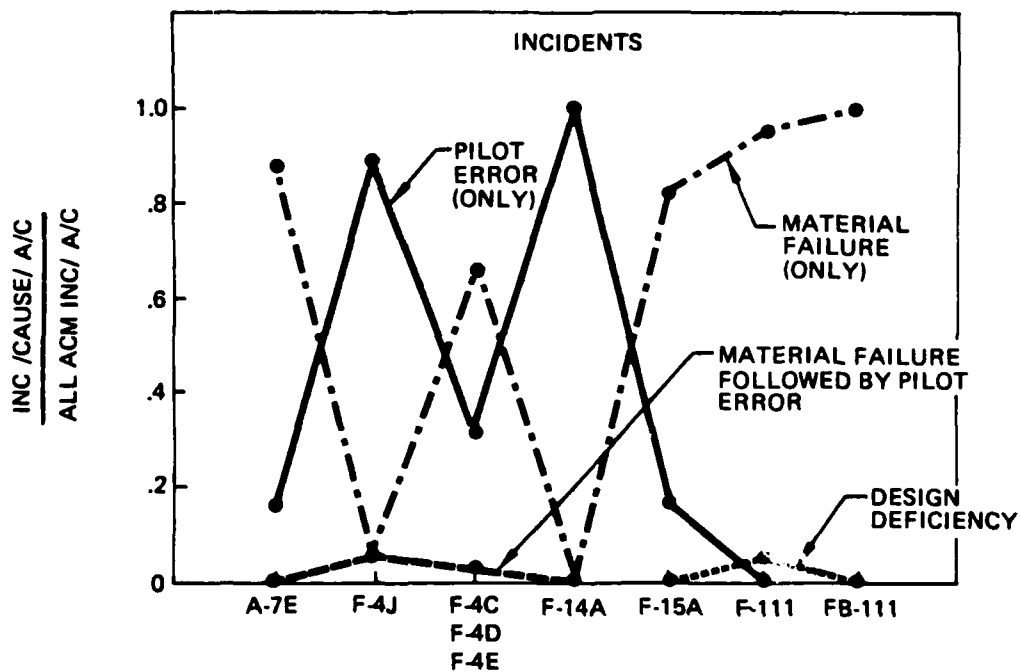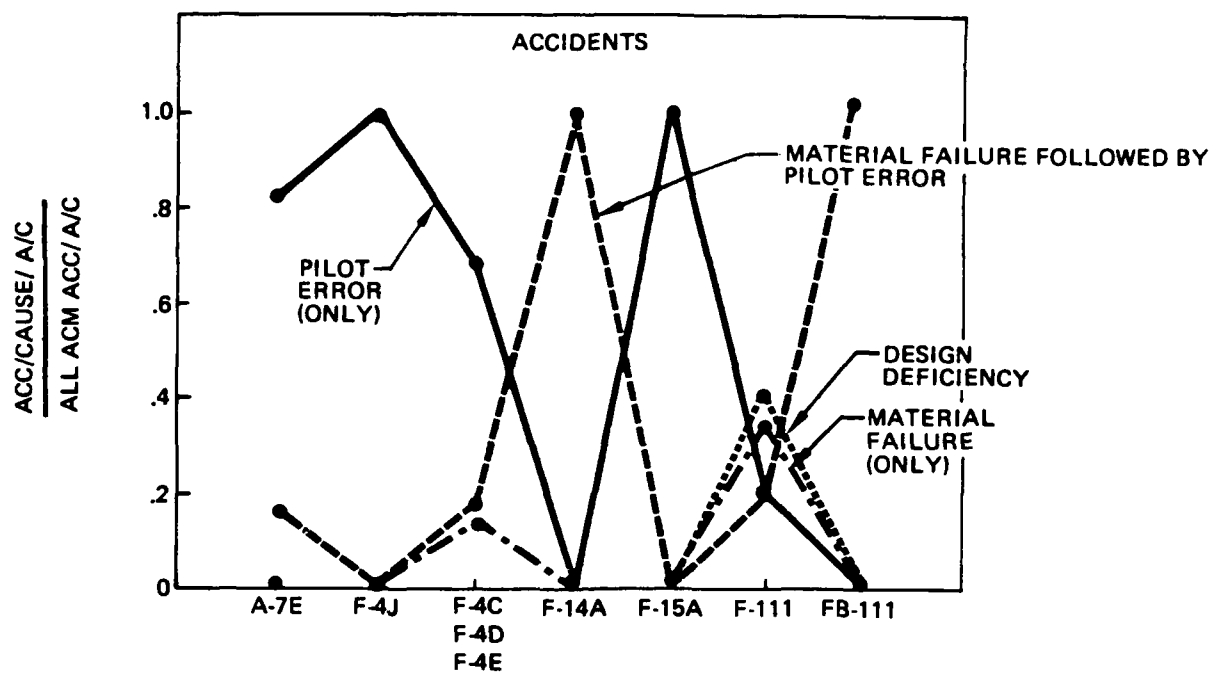
Figure A-5. Major Causes for Mishaps in Air Combat and Maneuvering Flight

13
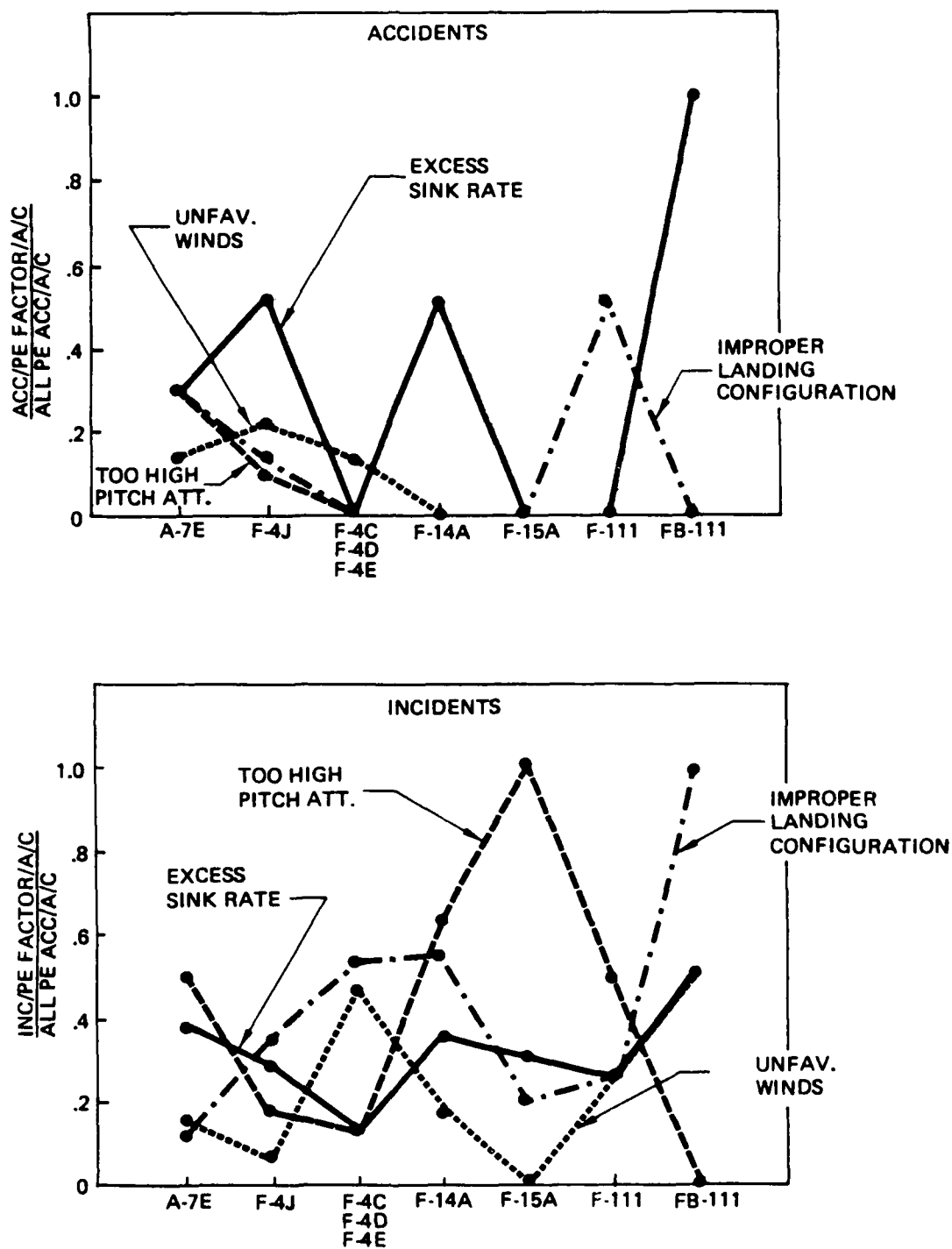
Figure A-6. Major Factors Involved in Pilot Errors for Mishaps in Approach and Landing

14
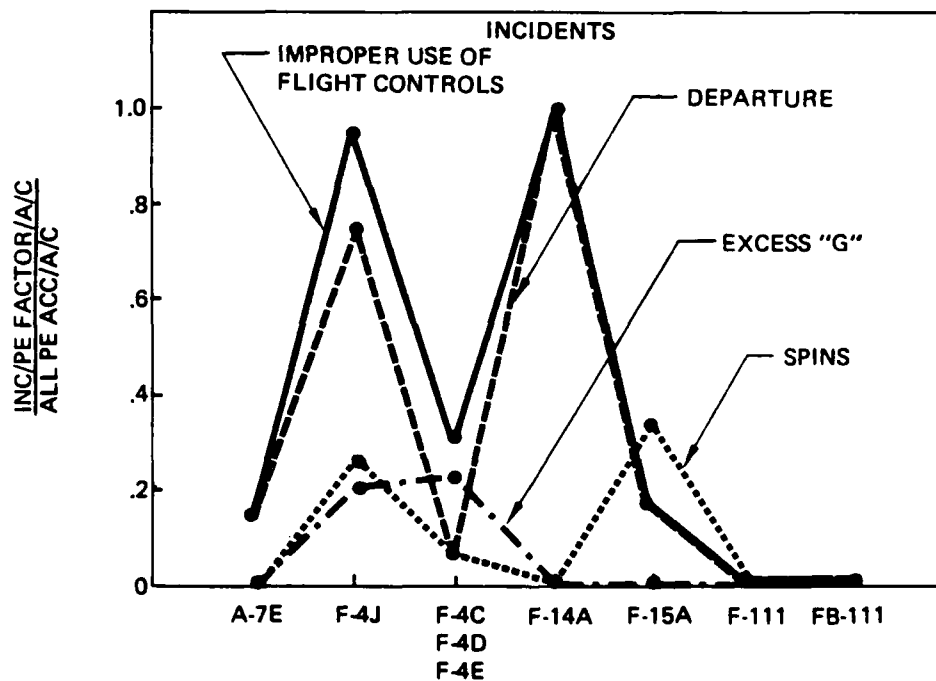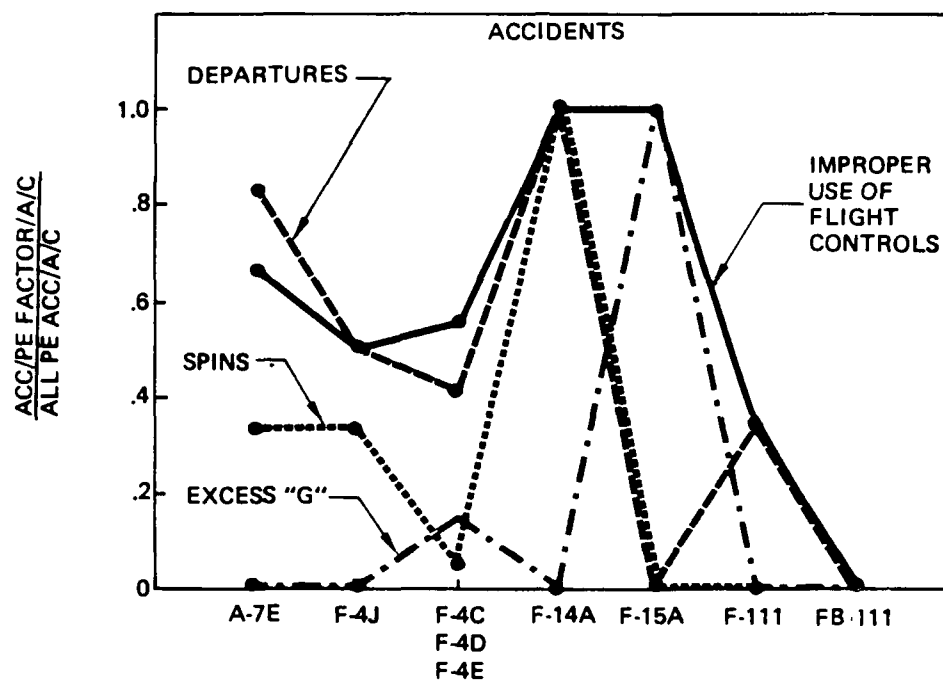
Figure A-7. Major Factors Involved in Pilot Errors for Mishaps in Air Combat
and Maneuvering Flight

The pilot cannot adequately handle configuration control (flaps, wing sweep, gear, drag chute, etc.) with the other demands imposed by the landing tasks.

In air combat and maneuvering (Figure A-7), most accidents and many incidents were attributed to improper use of flight controls by the pilot leading to departures, often subsequent spins, and some in loss of the aircraft. The other significant contributor to mishaps was when the pilot pulled "excess g", which as used here refers to excess normal acceleration in a pull-up or turn and not the result of rapid maneuver transients or departures. "Improper use of flight controls" generally refers to cases where the pilot failed to observe some restrictions, such as applying lateral control at high angles of attack or failing to turn off the roll SAS prior to high angle of attack maneuvers, both restrictions for the F-4 and F-14 aircraft. The stall/departure/spin problem is still obviously a major cause for concern. There is clearly a common demoninator to the major causes for mishaps in combat maneuvering, namely, they involve the pilot using the controls and maneuvering the airplane within possible limits but beyond permissible and safe limits. The results suggest that departure prevention and g-limiting devices are needed to relieve the pilot from having to observe control and structural limits while performing maneuvers close to aircraft and pilot limits in an intense and demanding environment such as air combat.

A.5 Augmentation Failures or Malfunctions

The aircraft types selected for examination in this study all had significant levels of augmentation, from the relatively simple three axis dampers and aileron-rudder interconnects of the F-4 and A-7 to the complex sophisticated adaptive system of the F-111. The types, frequency of occurrence, and consequences of failures in the augmentation system are of interest to flying qualities, and the results of such analysis for these are presented in Table A-6.

The accidents caused by augmentation system failures are relatively low, only 4% of the flight control related accidents. However, the number of incidents due to augmentation failures is high, 38%. In the few (five) accidents that involved augmentation system failures, three

Table A-6. Augmentation System Malfunction/Failure Occurrences

	A-7E	F-4J	F-14A	F-15A	F-4C-E	FB-111	F-111
1. Aug. accidents/total accidents	3/17	0/40	1/10	0/1	0/41	0/2	1/11
2. Aug. incidents/total incidents	88/135	16/60	32/54	10/29	257/715	25/65	46/130
3. Aug. components							
a. Control amplifier/amplifier computer							
(1) pitch	13	2	8	0	12	5	6
(2) roll	15	2	17	0	7	1	2
(3) yaw	17	4	4	0	10	6	2
b. Signal devices							
(1) rate gyros	21	3	3	0	66	2	0
(2) accelerometers	10	1	0	0	15	0	0
(3) stick force sensor/transducer	2	2	1	4	1	0	0
(4) air data computer	0	5	0	0	5	2	5
(5) other amplifiers	0	1(ARI)	0	0	53(SA)	4(TFR)	8(TF)
4. Aug. related equipment (actuators, power cylinders, servos, switches)	15	1	0	1	87	5	11
5. Uncommanded control transient, cause unknown	1	0	0	5	27	5	14

6. The 87 F-4C-E occurrences under Aug. related equipment are distributed between the following components:

    Pitch – Stabilizer power control cylinder 22
    Yaw – Rudder power control cylinder 50
    Roll – Lateral series servoactuator 15

7. Three Aug. accidents were caused by pilot error (1 A-7E, 1 F-14A, 1 F-111D) and two were caused by Aug. component malfunction/failure (1 rate gyro, 1 unknown) aggravated by pilot error (both A-7E). No Aug. incidents involved pilot error.

Abbreviation code:

    ARI – Aileron rudder interconnect amplifier   TF – Terrain following amplifier
    SA – Servo amplifier   TFR – Terrain following radar amplifier

were caused by pilot error and two were caused by augmentation system component failures, but aggravated by pilot error. Again the strong influence of pilot error is indicated. Of the many mishaps attributed to augmentation system failures, the only ones which became sufficiently serious as to become accidents were attributed either wholly or in part to pilot error.

The data in Table A-6 show the breakdown, by aircraft type, of component failures. The category, "augmentation related equipment", primarily relates to actuation equipment as indicated by the more detailed breakdown for the Air Force F-4 aircraft. The F-4 has an independent lateral-control series augmentation servo, but pitch and yaw augmentation are converted to mechanical inputs through integrated actuator packages, hence the listing of stabilizer and rudder power control cylinders as augmentation components. The cases of control transients of undetermined cause have been listed, but they have not been included in augmentation malfunction or failure totals.

Table A-7.   Summary of Augmentation Component Failures

Augmentation Component	All Types Aircraft (No.)	Air Force Aircraft (No.)	Failures/ 10^6 Flt. Hrs. (Air Force)
Amplifier — Computers	199	116	39
Actuators (power cylinders, servos, switches)	120	104	36
Rate gyros	95	68	23
Accelerometers	26	15	5
Others	25	15	5
All Augmentation Components	465	303	104

The data in Table A-6 has been reworked to provide component failures in somewhat more meaningful categories in Table A-7. Since no figures of flight hours were available for the Navy aircraft, the failure rates are based entirely on the Air Force aircraft. The category "Amplifier-Computers" in Table A-7 combines the pitch, roll and yaw amplifers and other amplifiers of Table A-6 to give a total control amplifier-computer figure. However, the air data computer has been included with stick force sensors in the "others" category.

A.6 Conclusion

The majority of flight control related accidents occur in the landing flight phase and the air combat and maneuvering (ACM) flight phase. The bulk of the incidents are, however, split between landing, ACM, and the Category B flight phases of climb, cruise, and descent.

LANDING MISHAPS:

High incidence of pilot error
93% of accidents
45% of mishaps

Most prevalent factor in pilot error
Pitch attitude too high
Excess sink rate
Improper landing configuration
Unfavorable winds

Flying qualities in landing are inadequate

Improve basic flying qualities
Response and control of pitch attitude, θ
Flight path response, V, γ
Auto throttle
Pitch and throttle system reliability

Reduce pilot workload in configuration control
Flaps, wing sweep, gear, weight effects, drag chute, speed brakes

Improve visibility

AIR COMBAT AND MANEUVERING MISHAPS:

High incidence of pilot error
83% of accidents
37% of mishaps

Most prevalent factors in pilot error
Improper use of flight controls
Departures
Spins
Excess "g"

Improve high angle of attack and maneuvering flying qualities
High resistance to departure
Positive simple spin recovery
Minimize need for pilot to limit control inputs to avoid departure or excess "g"

CATEGORY B FLIGHT PHASES:

High fraction of incidents - 36%

Causes
90% material failures
54% augumentation failures, most with uncommanded transients
Category B flying qualities must protect for failures and resulting transients

FLIGHT PATH CONTROL AFTER ENGINE FAILURE:

Experience

Three F-4J's lost on catapult take-off, engine out. Pilot failed to change configuration, drop stores.

Present requirement, MIL-F-8785B

Maintain "control" in straight flight without configuration change. "Control" means attitude.

Need

Requirement for control of flight path, without configuration change, in T.O. and landing.

AUGUMENTATION COMPONENTS:

Occurence

4% accidents - low

38% incidents -high

104 failures/10^6 flight hours (AF data)

Components

43% amplifier-computers

26% actuators

20% rate gyros

F-111 and BF-111

99% of ACM mishaps involved terrain following or related equipment.

MAJOR CONCLUSIONS:

- Landing Flight Phase - improve flying qualities and reduce pilot workload, especially with failures.

- Air Combat and Maneuvering Flight Phases - increase departure resistance, decrease need for pilot to limit control inputs in manuevers or at high angles of attack.

21

DATA ANALYSIS CATEGORIZATION CODES

0. ACCIDENT NO. - 9 DIGITS

1. TYPE ACFT. - OA007E__

2. ACCIDENT CLASS
0 MAJOR
2 MINOR
4 INCIDENT

3. FLIGHT PHASE
01 PRE-TAKEOFF
02 TAKEOFF
03 CATAPULT
04 CLIMB
05 CRUISE
C1 LOW LEVEL CRUISE
C2 WEAPON DELIVERY
C3 AIR COMBAT MANEUVERS
C4 AEROBATIC MANEUVERS
C5 AIRSHOW MANUEVERS
C6 REFUELING (REC)
06 TEST
07 UNKNOWN
08 DESCENT
L1 APPROACH
L2 WAVEOFF/GO-AROUND
L3 LANDING TOUCHDOWN
L4 LANDING ROLL
09 POST LANDING

4. TYPE OF LANDING
C SHIPBOARD - CARRIER
— SHOREBASED - AIRFIELD

5. DAMAGE CLASS
4 DESTROYED
3 SUBSTANTIAL
2 MINOR
1 LESS THAN MINOR

6. INJURY CLASS
5 MISSION
4 FATAL
3 MAJOR
2 MINOR
1 NO INJURY
0 UNKNOWN

7. EJECTION
Y YES
N NO

8. DAY/NIGHT
D DAY
N NIGHT
U UNKNOWN

9. CAUSE FACTORS
E__ENVIRONMENT
E CROSSWIND
J PITCHING DECK
L LIGHTNING
M WET RUNWAY
N NIGHT
S WIND SHEAR
T TURBULENCE
W WEATHER OBSCURATION/
   LOW CEILING
X JET WASH
Y TAIL WIND
Z BIRD STRIKE

KO MAINTENANCE ERROR
NO DESIGN DEFICIENCY
M — MATERIAL FAILURE/
   MALFUNCTION
A AUGMENTATION COMPONENT
B ENGINES
C ELECTRICAL
D HYDRAULIC
E MANUAL FLIGHT CONTROLS
S FLIGHT CONTROL SURFACE
T TRIM
F FUEL
G OIL
H BOUNDARY LAYER CONTROL
O OTHER
P — PILOT ERROR
A EXCESS SINK RATE
B ALLOWED AIRCRAFT.
   DEPARTURE
C HIGH PITCH ATTITUDE
D FAILED TO RECOGNIZE
   APPROACH TO STALL
H IMPROPER CONFIGURATION
L MANEUVER TOO LOW
T PILOT LAUNCHED AIRCRAFT
   WITH KNOWN MALFUNCTION
F FUEL MISMANAGEMENT
V OVER "G"
P INCORRECT PROCEDURES
   LANDING ROLL
O OTHER
SO OTHER PERSONNEL
TO FACILITIES
UO PUBLICATIONS
ZO CAUSE UNKNOWN

10. CONDITIONS AFFECTING
A__AUGMENTATION COMPONENTS
   1 PITCH AMPLIFIER-COMPUTER
   2 ROLL AMPLIFIER-COMPUTER
   3 YAW AMPLIFIER-COMPUTER
   4 RATE GYRO
   5 ACCELEROMETER
   6 STICK FORCE TRANSDUCER
   7 AIR DATA COMPUTER
   8 UNKNOWN
B__DEPARTURE CONDITIONS
   1 EXCESS ANGLE OF ATTACK
   2 INVERTED OR HIGH ANGLE
     OF BANK, "G" APPLIED
   3 ROLLED AT TOO SLOW AN AIR
     SPEED OR TOO HEAVY A
     GROSS WEIGHT
   4 OTHER
   5 RESULTED IN SPIN
V__EXCESS "G"
   1 EXCESS PULL (AIRSPEED
     AND DIVE ANGLE NO
     FACTOR)
   2 TRANSONIC PITCH OR
     MACH TUCK
   3 DIVE RECOVERY
   4 OTHER

H — CREW HUMAN FACTORS
   1 FATIGUE
   2 VERTIGO
   3 DISORIENTED
   4 PROFICIENCY
FLIGHT CONTROL/CONFIGURATION
M — MALFUNCTION OR
P — MISUSE
   A FLAPS (TRAILING EDGE)
   B SLATS/LEADING EDGE FLAP
   C SPOILERS
   D AILERONS
   E WING SWEEP
   F WING FOLD
   G ELEVATOR-STABILATOR
   H RUDDER
   I SPEEDBRAKE
   J FLIGHT ISOLATION SWITCH
   K AUGMENTATION
   L AFCS
   M APCS
   N EXTERNAL STORES
   O OTHER
   P LANDING GEAR
   Q DRAG CHUTE
   R NOSE WHEEL STEERING
   S BRAKES
   T GROSS WEIGHT
   U TRIM BELLOWS-FEEL
S__ FLIGHT CONTROL SURFACE
   SKIN/PANEL
   1 CRACKED
   2 DELAMINATED
   3 MISSING
I1 INFLIGHT ARRESTED LANDING
U__UNCOMMANDED TRANSIENTS
   1 PITCH
   2 ROLL
   3 YAW
C__IMPROPER CG
   1 PILOT ERROR
   2 AIRCRAFT FAILURE/
     MALFUNCTION
0—{ AUGMENTATION COMPONENTS
   { OTHER AMPLIFIERS-COMPUTERS
   1 AILERON RUDDER
     INTERCONNECT
   2 SERVO AMP
   3 TERRAIN FOLLOWING-
     COMPUTER
   4 OTHER
R—{ AUGMENTATION ACTUATORS -
   { SERVOS-DAMPERS
   1 ACTUATORS OTHER
   2 PITCH
   3 YAW
   4 ROLL
   5 SWITCHES
   6 OTHER
Z _ 0 NONE CODED

APPENDIX B

SIMULATION RESULTS AND ANALYSIS

B.1 Introduction

A fixed-base ground simulation program for the approach and landing
tasks was conducted to investigate the influence of various parameters
that might affect the flying qualities requirements for airplanes with
relaxed static stability, both for normal and failure states. The
simulation program had two distinct parts. The first, done as part of
the subject contract, investigated various pitch augmentation system
configurations including feedback gains (pitch rate, normal acceleration,
and angle of attack), control authority (position and rate limits), c.g.
position (stable, neutral, and unstable values), turbulence level
(negligible, moderate, and heavy), and landing task (side step maneuver
at 200 ft. break out), for normal (augmented) and failure (unaugmented)
states. The second part, done as a corollary study to the contract under
separate Boeing IR&D funds, was a fundamental investigation of the
various parameters, primarily in the θ/δ_e transfer function, that
affect the flying qualities of statically unstable airplanes. The
results of the simulation program will be treated as a whole in this
appendix, without regard to which part they came from.

B.1.1 Relaxed Static Stability (RSS)

Relaxed static stability refers to an airplane which has its center
of gravity located aft of the c.g. range normally chosen to obtain
performance benefits either in level or maneuvering flight. Normally the
c.g. range is chosen to assure good or acceptable longitudinal stability,
dynamic response, and maneuver characteristics. However, if the
requirement for static stability is relaxed so that a more aft c.g. range
can be chosen, then performance benefits can be realized from the
increased L/D produced by more efficient lift generation and the
reduction of trim and maneuvering drag. Lift efficiency and reduced drag
result from decreasing the down-load or having an up-load on the tail.
Desirable stability and response characteristics are provided by

23

augmentation in the flight control system (FCS). The horizontal tail may then be sized on the basis of control authority required and not stability, thus allowing a potential reduction in tail size and a further decrease in drag.

Recent studies directed at improving the energy efficiency of commercial transports (Ref. 47) have shown that a potential 10 to 15% improvement in block fuel efficiency can be realized from the use of relaxed static stability, about two thirds coming directly from the RSS, and one third from the reduced tail size. For best fuel efficiency the c.g. had to be well aft of the neutral point and the airplane very unstable, so the augmentation system had to be considered flight safety critical, requiring 10^{-9} reliability. By using a somewhat less aft c.g. location at some cost in fuel efficiency, and allowing transition to alternate flight conditions following FCS augmentation failure, the system could be treated as mission critical allowing relaxation of the reliability requirements. The airplane was considered to have pitch-up at high angles of attack, with a subseqent deep stall. To handle the stall, an angle of attack limiting device was included in the FCS which prevented entry into deep stall. At stall, a $-.08$ rad/sec^2 angular acceleration with full nose-down control was considered necessary for stall recovery.

Supersonic aircraft will benefit most from the use of RSS since trim drag is high for such aircraft, about 25% of the total drag for an airplane with conventional center of gravity range. The F-16 airplane is an example of where such benefits have been realized, though the degree of RSS is not extreme for this airplane. In supersonic flight the airplane aerodynamic center is generally well aft of that for subsonic flight. Thus an airplane with c.g. at the neutral point in supersonic flight, will have a c.g. well aft of the neutral point in subsonic flight and in the take off or landing configurations.

With landing being one of the most demanding tasks, the primary one pertinent to flight safety, and the one most likely to have to be accomplished with failed augmentation, the landing task appears to be the most critical one for failure-state or Level 2 and 3 flying qualities requirements. Also, landing under heavy turbulence conditions is one of the tasks critical for control authority, and hence important in the

24

development of augmented or normal-state requirements for control authority. For these reasons the approach and landing task must receive primary attention.

Other flight phases and conditions important to RSS flight-safety requirements are air combat maneuvering, any tasks requiring maximum performance maneuvers, also any conditions that will result in high angles of attack with possible subsequent stall or departure. Also, any flight condition that might have to be maintained for a long period of time with the augmentation system failed, such as cruise and descent to enable the airplane to reach a safe landing site, would be a critical condition. A pilot may well be able `. cope with a given level of instability for a short period of time, say five to ten minutes, but be unable to handle this level of instability for longer periods of time, perhaps one or more hours.

B.1.2 Dynamic Characteristics of Longitudinally Unstable Aircraft

Usually one considers an airplane to be statically unstable because M_α is positive, the primary result of moving the c.g. aft of the neutral point or airplane aerodynamics center. However, static instability can also be caused by negative M_u, which can result from power or thrust effects, from aeroelastic effects, or from variations in pitching moments in transonic flight as in "Mach tuck". The two root locus plots that follow illustrate the difference between the two causes of static instability.

For instability precipitated by a negative M_u as indicated in the locus to the left, it is the phugoid roots that become real, then separate with one root going unstable. The stable root converges on the indicated zero. The short period roots are relatively unaffected, and the instability is primarily one associated with speed. The constant-speed equations predict no change in maneuver response characteristics, stick force per g, or in any way indicate the presence of an instability. On the other hand, the presence of a significant M_u will result in rapid pitching motions due to turbulence.

25
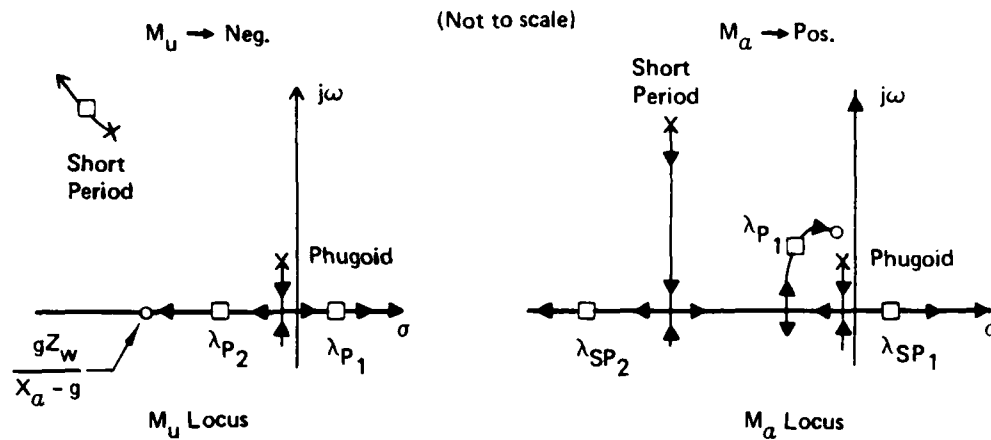
For instability produced by positive M_α as depicted in the locus to the right, the short period roots coalesce on the real axis, then split with one pole going unstable, the other going well into the left half plane. The pole going to the right will normally combine with the phugoid poles on the real axis, then these three will split again as indicated in the root locus to form the unstable root and an oscillatory mode which Etkin (Ref. 48) calls the "third mode". However, as demonstrated by the characteristics of the simulation configurations, the short-term attitude response is dominated by the two real poles while the oscillatory mode behaves much like a phugoid. For this reason the two real roots are labeled λ_{sp_1} (smaller, unstable root) and λ_{sp_2} (larger, stable root) while the remaining roots, normally oscillatory, are labeled λ_{p_1} and λ_{p_2}. Whereas conventional short period and phugoid separation with attendant constant-speed short-period approximation are maintained for an M_u type instability, these concepts generally do not apply for an M_α type instability.

The condition for one unstable root is that the constant term in the characteristic equation be negative,

$$E = g(Z_u M_w - M_u Z_w) < 0$$

or

$$Z_u M_w < M_u Z_w$$

26

or since Z_u is normally negative,

$$\frac{M_\alpha}{V} = M_w > M_u \frac{Z_w}{Z_u} \simeq M_u \left(\frac{C_{L\alpha}}{2C_L}\right)$$

Thus, if $M_u = 0$, then an unstable root is produced by static instability as defined by positive M_α or $C_{m\alpha}$ (c.g. aft of the neutral point or airplane a.c.). For $M_u < 0$, an unstable root can exist with negative or stable values of M_α.

B.2 Characteristics of RSS with F-111A Example

To study the dynamic characteristics implied by relaxed static stability, four widely separated flight conditions for the F-111A airplane are analyzed for the effect of aft c.g. location. Aerodynamic data came from Reference 49. The four flight conditions are

	M	Altitude ft	Wing Sweep deg	$\overline{x}_{cg}$
Landing Approach	.2	SL	16	.31
Terrain Following	.8	SL	50	.37
Subsonic Maneuvering	.8	35,000	50	.37
Supersonic, M=2	2.0	35,000	72.5	.39

The data necessary to estimate the coefficients in the linearized equations of motion for the unaugmented airplane are presented in Table B1 for longitudinal and Table B2 for lateral-directional characteristics. Transfer functions for landing approach at two c.g.'s are given in Table B3.

B.2.1 Stability Characteristics

Plots of the migration of the roots as the c.g. is moved aft for each of the four flight conditions are presented in Figures B1 to B4. Center of gravity limits for the F-111A are given in Figure B5 to provide some feel for the c.g. range covered.

Table B-1. F-111A Longitudinal Characteristics

Flight condition		Landing approach	Terrain following	Subsonic maneuvering	Supersonic M=2
Wing Sweep	Deg	16	50	50	72.5
Mach No.		.20	.80	.80	2.00
Altitude	Ft.	SL	SL	35,000	35,000
Trim Speed	KTAS	145	528	454	1152
Trim Alpha	Deg	4	2.75	8.20	3.18
Flap Setting	Deg	40/37.5	0	0	0
Wing Chord	Ft.	9.017	9.017	9.017	9.017
Wing Area	$Ft.^2$	525	525	525	525
Gross Weight	Lb	60,000	60,000	60,000	60,000
I_y	$Slug\text{-}Ft^2$	335,000	343,000	343,800	347,000
$\bar{x}_{ref}$		.45	.40	.40	.42
Neutral Point (N_o)		.434	.665	.700	1.123

Stability Derivatives (Stability Axis System)

C_{D_o}		+0.241	+.024	.0585	+0.0338
C_{D_u}		0	+0.0040	0.025	0
C_{D_α}	1/rad	+0.7774	0.112	.559	+0.114
$C_{D_{\delta_h}}$	1/rad	0	0	0	0
$\partial T/\partial V$	(Lb/fps)	−3.41	0	+3.45	+2.53
C_{L_o}		1.590	0.1207	0.5114	0.0818
C_{L_u}		0	0	0.160	0
C_{L_α}	1/rad	7.310	4.441	4.622	2.483
$C_{L_{\dot\alpha}}$	1/rad	2.550	3.650	4.870	1.00
C_{L_q}	1/rad	5.720	8.380	10.280	4.50
$C_{L_{\delta_h}}$	1/rad	0.860	0.788	0.573	0.430
C_{m_u}		0	+0.0260	+0.0174	−0.171
C_{m_α}	1/rad	+0.1150	−1.177	−1.387	−1.746
$C_{m_{\dot\alpha}}$	1/rad	−4.570	−7.200	−9.800	−1.850
C_{m_q}	1/rad	−15.0	−30.0	−47.8	−19.5
$C_{m_{\delta_h}}$	1/rad	−1.496	−1.715	−1.898	−0.958
Z_T	Ft	0	0	0	0

Note: (1) u derivatives do not include direct thrust effects

(2) $\delta_h = (\delta_{h_L} + \delta_{h_R})/2$

(3) $\bar{x}_{ref}$, location of reference moment center aft of LE of reference $(\bar{c})$ in chord lengths, $(x_{le}\text{-}x_{ref})/\bar{c}$

(4) N_o, c. g. location for $C_{m_\alpha} = 0$.

(5) u, $\dot\alpha$, q derivatives defined in Appendix F, Section F.2.2.

Flight condition		Landing approach	Terrain following	Subsonic maneuver	Supersonic M = 2
Wing Sweep	Deg	16	50	50	72.5
Mach No.		0.20	0.80	0.80	2.00
Altitude	Ft	SL	SL	35,000	35,000
Trim Speed	KTAS	145	528	454	1134
Trim Alpha	Deg	4	2.75	8.20	3.18
Flap Setting	Deg	40/37.5	0	0	0
Wing Span	Ft	63	63	63	63
Wing Area	ft^2	525	525	525	525
Gross Weight	Lb.	60,000	60,000	60,000	60,000
I_X	Slug-Ft^2	77,200	53,800	53,800	41,200
I_Z	Slug-Ft^2	399,000	383,700	383,700	374,000
I_{XZ}	Slug-Ft^2	3,640	4,920	4,920	5,260
$\bar{x}_{ref}$		.45	.40	.40	.42

Stability Derivatives (Stability Axis System)

C_{y_β}	1/rad	−1.198	−0.877	−0.877	−0.802
$C_{y_{\dot\beta}}$	1/rad	−0.122	−0.100	−0.1110	−0.098
C_{y_r}	1/rad	+0.280	+0.323	+0.304	+0.275
C_{y_p}	1/rad	0.100	+0.030	+0.070	−0.050
$C_{y_{\delta_a}}$	1/rad	0	−0.2464	−0.4584	+0.0361
$C_{y_{\delta sp}}$	1/rad	0	−	−	−
$C_{y_{\delta_r}}$	1/rad	+0.298	+0.1937	+0.2349	+0.0573
C_{n_β}	1/rad	+0.093	+0.0882	+0.0963	+0.0527
$C_{n_{\dot\beta}}$	1/rad	+0.038	+0.338	+0.0338	+0.0243
C_{n_r}	1/rad	−0.200	−0.188	−0.213	−0.1300
C_{n_p}	1/rad	+0.004	−0.0062	+0.002	−0.005
$C_{n_{\delta_a}}$	1/rad	+0.033	+0.0172	+0.0160	−0.0014
$C_{n_{\delta sp}}$	1/rad	−0.011	−	−	−
$C_{n_{\delta_r}}$	1/rad	−0.108	−0.0831	−0.0986	−0.0212
C_{ℓ_β}	1/rad	−0.080	−0.0705	−0.1163	−0.0607
$C_{\ell_{\dot\beta}}$	1/rad	−0.009	−0.0067	−0.0058	−0.0025
C_{ℓ_r}	1/rad	+0.065	+0.036	+0.054	+0.0200
C_{ℓ_p}	1/rad	−0.415	−0.155	−0.178	−0.0350
$C_{\ell_{\delta_a}}$	1/rad	+0.072	+0.0676	+0.0888	+0.0493
$C_{\ell_{\delta sp}}$	1/rad	−0.112	−	−	−
$C_{\ell_{\delta_r}}$	1/rad	+0.010	+0.0069	+0.0018	+0.0029

Note: $\delta_a = (\delta_{h_L} - \delta_{h_R})/2$; $\quad \delta_{sp} = \delta_{sp_L} - \delta_{sp_R}$

(1) $\dot\beta$, p,r derivatives defined with respect to $\dot\beta b/2v$, pb/2v, rb/2v.

Table B-3. *F-111A Longitudinal Aircraft Transfer Functions in Landing Approach for Stabilizer Inputs*

PARAMETER	$\bar{X}_{cg} = .35$	$\bar{X}_{cg} = .60$
Δ_{LONG}	$(S+.510\pm.743j)(S+.0089\pm.161j)$	$(S-0.68)(S+1.615)(S\cdot.0327\pm.192j)$
$\dfrac{u(S)}{\delta_h(S)}$	$\dfrac{-1.15(S-22.7)(S+1.16)}{\Delta_{LONG}}$	$\dfrac{-1.15(S-19.9)(S+1.32)}{\Delta_{LONG}}$
$\dfrac{w(S)}{\delta_h(S)}$	$\dfrac{-17.2(S+22.9)(S+.0199\pm.183j)}{\Delta_{LONG}}$	$\dfrac{-17.2(S+19.8)(S+.0198\pm.183j)}{\Delta_{LONG}}$
$\dfrac{\theta(S)}{\delta_h(S)}$	$\dfrac{-1.59(S+.560)(S+.0749)}{\Delta_{LONG}}$	$\dfrac{-1.37(S+.655)(S+.0696)}{\Delta_{LONG}}$
$\dfrac{n_z(S)}{\delta_h(S)}$	$\dfrac{-.535(S+3.83)(S-3.50)(S+.0129)S}{\Delta_{LONG}}$	$\dfrac{-.535(S+3.84)(S-3.47)(S+.0166)S}{\Delta_{LONG}}$
$\dfrac{\gamma(S)}{\delta_h(S)}$	$\dfrac{+.0703(S+3.83)(S-3.50)(S+.0129)}{\Delta_{LONG}}$	$\dfrac{+.0703(S+3.84)(S-3.47)(S+.0166)}{\Delta_{LONG}}$
$\dfrac{h(S)}{\delta_h(S)}$	$\dfrac{+17.2(S+3.38)(S-3.50)(S+.0129)}{\Delta_{LONG}}$	$\dfrac{+17.2(S+3.84)(S-3.47)(S+.0166)}{\Delta_{LONG}}$

Note: Numerator of u/δ_h is reduced one order since $X_{\delta_h} = 0$.

Figure B-1. Longitudinal Root Locus with C.G. Translation - Landing Approach

Some peculiarities in geometry are associated with the use of variable sweep. The reference mean aerodynamic chord ($\bar{c}$) is based on the geometry with the wings swept forward (16°). As the wings sweep back, the theoretical mean aerodynamic chord increases in length and moves aft. So, for large sweep angles, some quantities may appear to have rather extreme values (e.g.. neutral point at 1.123 $\bar{c}$ in Table B1). The c.g. translation aft with wing sweep from .31 to .39 as indicated in the foregoing table is typical, and is for the "no-payload" configuration of Reference 49.

Landing Approach

The landing approach root locus plot (Fig. B1) is very typical of the standard situation. C_{L_u} and C_{m_u} are zero and the major effect of c.g. is to change C_{m_α}. So we have a classical M_α root locus. The transfer functions for the landing approach are given in Table B3 for $\bar{x}_{cg}$ = .35 and .60. The changes in the numerators due to c.g. translation are small and essentially trivial. At neutral static

31

F-11?A
TERRAIN FOLLOWING

GW = 60,000 LBS

Λ = 50°

V = 528 KTAS

γ = 0°

h_p = S.L.

M = .80

Pitch Aug. OFF

$\overline{X}$ cg = .40

SHORT PERIOD →

.50

.60

.64

$j\omega$ rad/sec

4

3

2

1

.80 .70 .66 .66 .68 .74 .76 .80
-5   -4   -3   -2 -1   0   1
$\sigma \sim$ rad/sec

$j\omega$ rad/sec PHUGOID
.2 .70
.66 .68 .72
.60
.40
.76 .80 .80 .74 .73 .73
-.1 0   .1   .2
$\sigma \sim$ rad/sec

Figure B-2. Longitudinal Root Locus with C.G. Translation - Terrain Following

stability (root at the origin, $\overline{x}_{cg}$ = .44) or more aft c.g. locations, there is a low frequency oscillation with phugoid-like roots.

Terrain Following

The terrain-following root-locus plot (Fig. B2) shows different characteristics from the classical one since M_u is positive though invariant with c.g. as C_{L_u} = 0. The phugoid roots now increase in frequency and swing to the right, going dynamically unstable ($\zeta < 0$) for $\overline{x}_{cg}$ = .67. The neutral point (.665 from Table B1) corresponds closely to this value, but there is no obvious relationship indicating that this will be generally true. For $\overline{x}_{cg}$ = .68 through .72 there is a dynamically unstable ($\zeta < 0$) oscillation of phugoid frequency. For $\overline{x}_{cg}$ = .73 to .80 and larger,there are two unstable (positive) real roots.

32
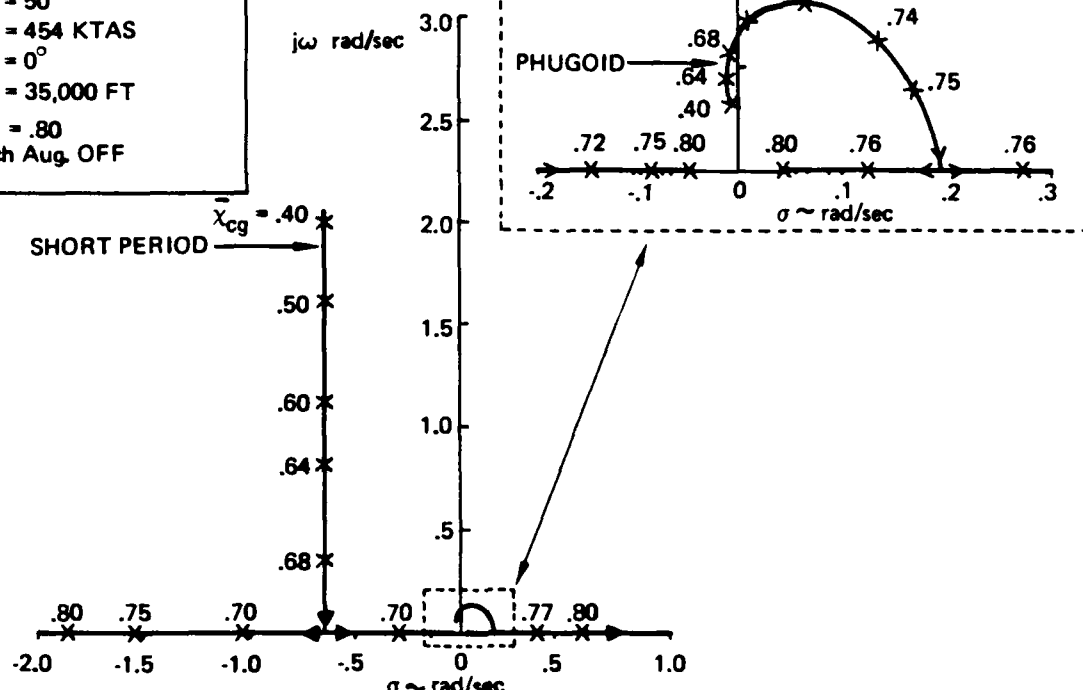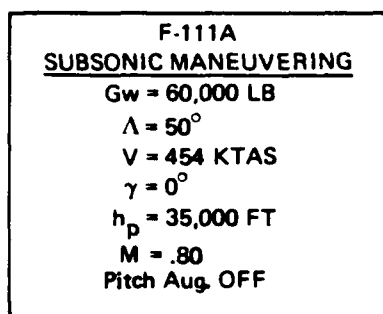
Figure B-3. Longitudinal Root Locus with C.G. Translation - Subsonic Maneuvering

Subsonic Maneuvering

The subsonic maneuvering root locus plot (Fig. B3) is qualitatively similar to the terrain-following root loci. Again M_u is positive, but it increases as the c.g. shifts aft due to the positive C_{L_u}. The phugoid goes dynamically unstable for $\overline{x}_{cg} = .69$, which again is close to the neutral point (.700). For $\overline{x}_{cg} = .76$ to .80 and larger, again there are two unstable real roots.

Supersonic, M=2

The root locus plot for the supersonic condition (Fig. B4) shows still a different characteristic. For the supersonic condition, C_{m_u} is quite large and negative, and the phugoid for $\overline{x}_{cg} = .42$ has two small real roots, one stable (-.037) and one unstable (+.029, with $T_2 = 24$ sec). The phugoid roots separate further. The stable root combines with
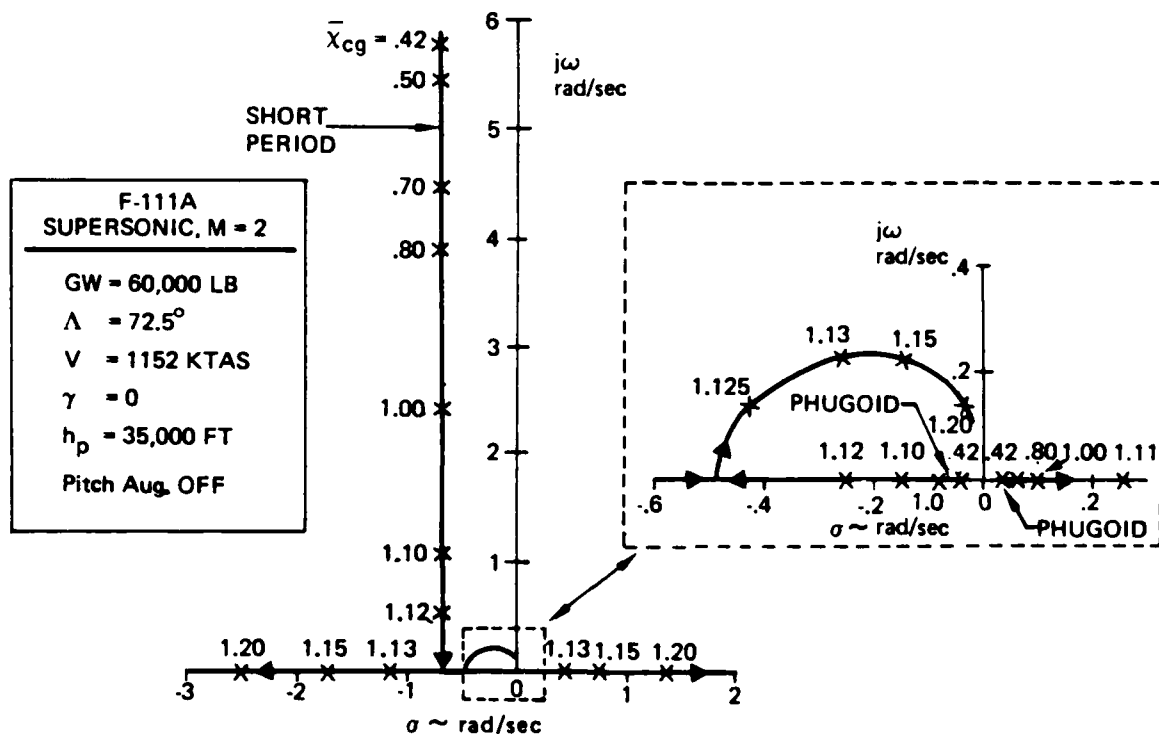
Figure B-4. Longitudinal Root Locus with C.G. Translation - Supersonic, M = 2

the short period root to form another phugoid while the unstable root, together with the large negative real root, become the dominant short period response. The phugoid roots, while they swing to the right, never become unstable for aft c.g. locations.

Overall Conditions

Taking an overview of the root loci in Figures B1 to B4, viewing just the larger scale plots which include the short period mode, it will be noted that they all have the same essential characteristic. As the c.g. moves aft the short period poles converge to the real axis, then split and one goes to the left, the other to the right. The pole going to the right, as it passes in the vicinity of the origin, gets intermixed with the phugoid for a narrow range of c.g. values. But beyond this range the pole continues into the right half plane independently of the phugoid.

34

Effectively, for aft c.g. locations, the phugoid roots remain near the origin while the short period mode has two real roots, a positive one and a larger magnitude negative one.

The F-111A was not designed to take advantage of relaxed static stability so relations between c.g. location, neutral point, and stability level over the flight envelope would not be those for an optimized RSS airplane. However, the trends should be similar and indicative. The following table displays some of the trends pertinent to use of RSS, especially if the airplane is to be considered flyable in some sense after augmentation failure.

CENTER OF GRAVITY ($\bar{X}_{cg}$)

	Neutral stability	$T_2 = 6$ sec	$T_2 = 2$ sec	N_o	F-111A typical
Landing approach	.44	.5	.51	.43	.31
Terrain following	.67[1]	.71[1]	.735[2]	.67	.37
Subsonic maneuvering	.69[1]	.74[1]	.77[3]	.70	.37
Supersonic, M=2	< .42	1.03	1.13	1.13	.39

(1) Phugoid oscillatory roots
(2) Two positive real roots, T_2 = 2 sec and 5 sec
(3) Two positive real roots, T_2 = 2 sec and 8 sec

The neutral point (N_o) is indicative of the desired value for the c.g., though to minimize trim or maneuvering drag the c.g. should be somewhat aft of N_o in order to have an upload on the tail. The c.g. locations for T_2 of 6 sec and 2 sec span the range of likely aft c.g. limits for a flyable airplane. For oscillatory instability, the c.g. for neutral stability ($\zeta = 0$, near the MIL-F-8785C limit of T_2 = 55 sec) might be considered the most aft usable c.g. instead of that for T_2 = 6 sec. (T.F. and subsonic maneuvering cases). The neutral point for all fight conditions lies within this range of limits (within .02 of it for landing approach). However, for a fixed c.g. the landing approach is critical (has the most forward limits) and even the wing sweep of the F-111A which moves the c.g. forward and aft 8% does not significantly ease the situation.
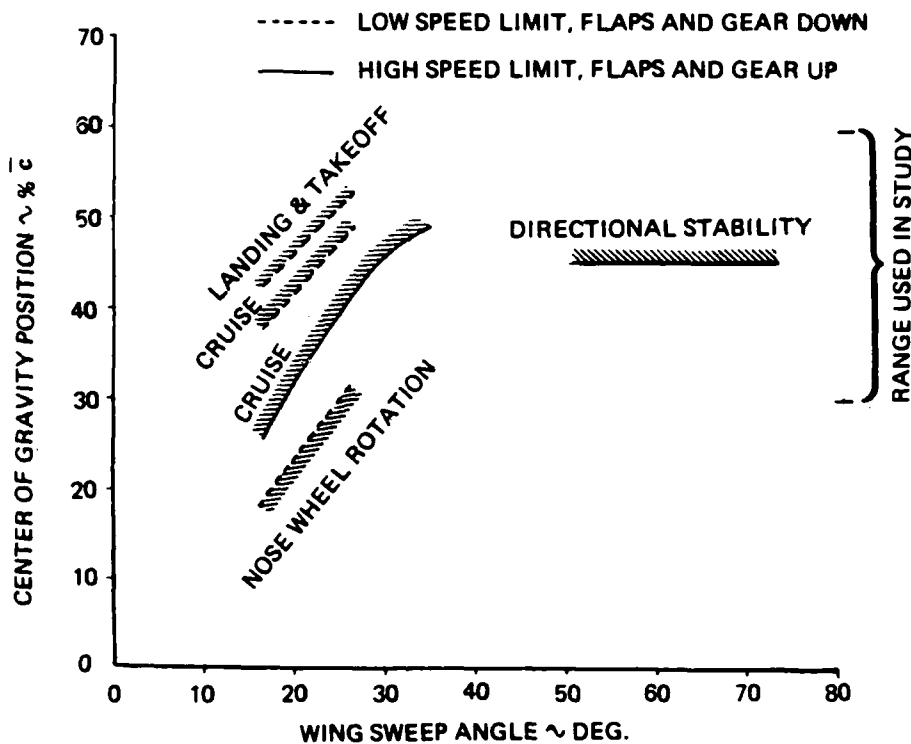
Figure B-5 Center of Gravity Limits for F111-A Airplane

If full use of RSS is employed for the supersonic condition, then clearly there is no possibility of having a flyable unaugmented airplane for lower speed conditions, and requirements for these conditions relate to reversion to a back-up or "Hard SAS" after normal augmentation failure. This situation is typical for supersonic airplanes (e.g., Ref. 15 and 16).

The c.g. limits vs wing sweep presented in Figure B5 give another overall picture of the situation. Low or forward sweep angles are clearly critical. This figure also points out the necessity for considering lateral-directional modes and directional stability for airplanes with large closely coupled (short tail length) vertical tails such as the F-111A.

The foregoing indicates clearly that the most critical area for the design of RSS airplanes is likely to be in the terminal area and especially the approach and landing problem. Accordingly, this investigation concentrates effort in that area.

B.2.2 Response Characteristics in Landing

The response characteristics are examined just for the critical landing approach case. However, the results can be extrapolated to other flight conditions. Since linearized equations provide us with the only generalized analysis methods, these are used first to examine the characteristics of RSS in three degrees of freedom, both in the time domain and in the frequency domain. Then linearized time responses are compared with those from the full nonlinear equations of motion. Finally a comparison is made with the responses computed from constant-speed equations in two degrees of freedom.

B.2.2.1 Linearized Equations - Three Degrees of Freedom

The pilot tends to fly near neutrally stable aircraft, stable or unstable, with pulse type inputs rather than the steps he tends to use for stable aircraft. So, time histories have been computed for the F-111A for a 0.4 second pitch pulse at the following selected c.g. positions. Linearized equations were used (Section F.2.1).

$\overline{x}_{cg}$	PR	Stability Level
.35	4	Stable short period
.434	5	Near neutral, but stable
.451	5.5	Unstable, T_2 = 6 sec
.506	7	Unstable, T_2 = 2 sec

The above pilot ratings (PR) are averages from the simulation program for smooth air. The roots for these four c.g. positions are presented in Table B4, along with the time to double or time to half amplitude for the short period mode.

Figure B6, parts (a) through (c), compares the time responses at the four c.g.'s for a duration of six seconds. The motion in this period of time characterizes the response the pilot sees as he tries to control the airplane closed-loop, particularly the primary attitude loop, and is characteristic of the short period motion. The things to note are as follows.

37

Table B-4. Longitudinal Roots for Selected C.G. Locations - F-111A Landing Approach

$\bar{X}_{cg}$	λ_{sp_1} (complex)	λ_{sp_2}	λ_{p_1} (complex)	λ_{p_2}	$T_2(T_{1/2})$ sec
.35	$(-,51 \pm .74j)$		$(-.009 \pm .16j)$		(1.4)
.434	$-.18$	$-.74$	$-.005$	$-.11$	(3.9)
.451	$+.11$	$-.92$	$(-.11 \pm .17j)$		6.1
.506	$+.35$	-1.26	$(-,05 \pm .20j)$		2.0

Notes: $T_2(T_{1/2})$ are for λ_{sp_1}.

- θ is the same for all cases for the first second after the pulse input.

- The forward c.g. response (.35), with its low $\omega_{n_{sp}}$ converges to $\Delta\alpha = 0$, $q = 0$ and a steady θ, but u diverges.

- The two intermediate c.g.'s (.434 and .451) have similar responses. Initially the large short period root (λ_{sp_2}) dominates the response, for about three seconds. Then the smaller short period root takes over (λ_{sp_1}), in one case causing weak convergence (.434), in the other, weak divergence (.451) which even at six seconds is not apparent in θ. Divergence of u, nearly the same for these two cases, is about twice as fast as for the stable (.35) case.

- The faster divergence of the aft c.g. (.506) case causes its response to be significantly different from the others. Most variables show divergence by three seconds, q earlier, and u diverges significantly more rapidly than for the other cases.

Figure B6, parts (d) through (f), compares the same responses but out to 60 seconds. These responses display the long-term stability charac-

teristics and the significance of the phugoid roots. The things to note are as follows.

- Each of the response variables, q, α, n_z, θ, and u, exhibits different characteristics for each of the four cases.

- For the stable (.35) case, the response shows conventional short period (see α) and phugoid modes (see θ and u).

- The near neutral but stable (.434) case has responses in q and n_z that are similar to the stable (.35) case. However, for this near neutral stability case, the α response resembles more the unstable cases out to 20 seconds; the θ response initially ramps like the unstable cases but then shows convergence as does u. The phugoid (two smallest) roots are real for this case (see Table B4) and do evidence their presence, especially in θ, by the convergence with $T_{1/2}$ = 6.5 sec to θ = 10° and then by the slower convergence with $T_{1/2}$ = 142 sec.

- For the two unstable cases, the short period (two real) roots dominate the response and the oscillatory phugoid roots are suppressed. The θ response to the pulse input is a ramp, with some indication of convergence for the least unstable case (T_2 = 6 sec) but with none for the more unstable case (T_2 = 2 sec). However, convergence associated with the negative real root (λ_{sp_2}) is initially indicated in the q, α, and n_z responses for both unstable cases, though much more strongly for the less unstable one.

A different view of the effects of relaxed static stabiity is presented by the θ/δ_h frequency responses in Figure B7. It should be noted that the transfer function is defined for negative stabilator deflection (- δ_h), equivalent to positive stick force or deflection. The following points are noted.

F-111A Landing Approach (Table B-1)
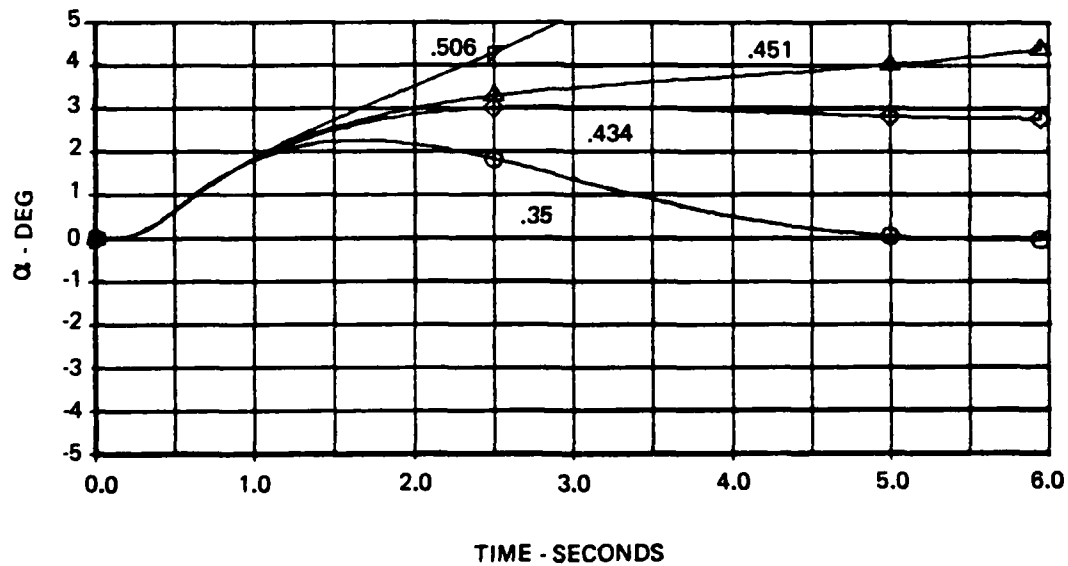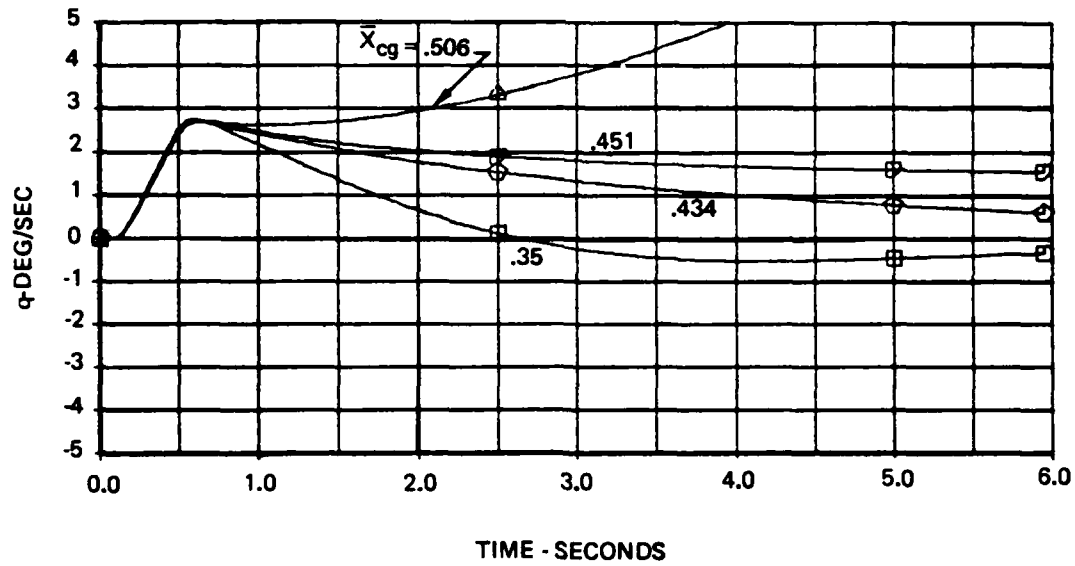
Figure B-6. Longitudinal Response for Selected c.g. Positions
(a) α and q for 6 sec.

(F-111A Landing Approach (Table B-1)
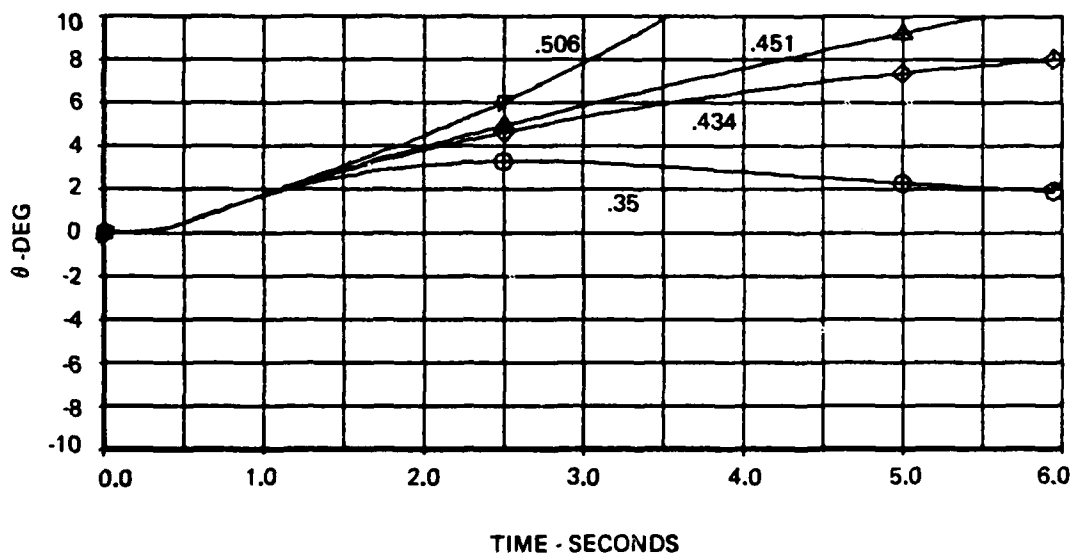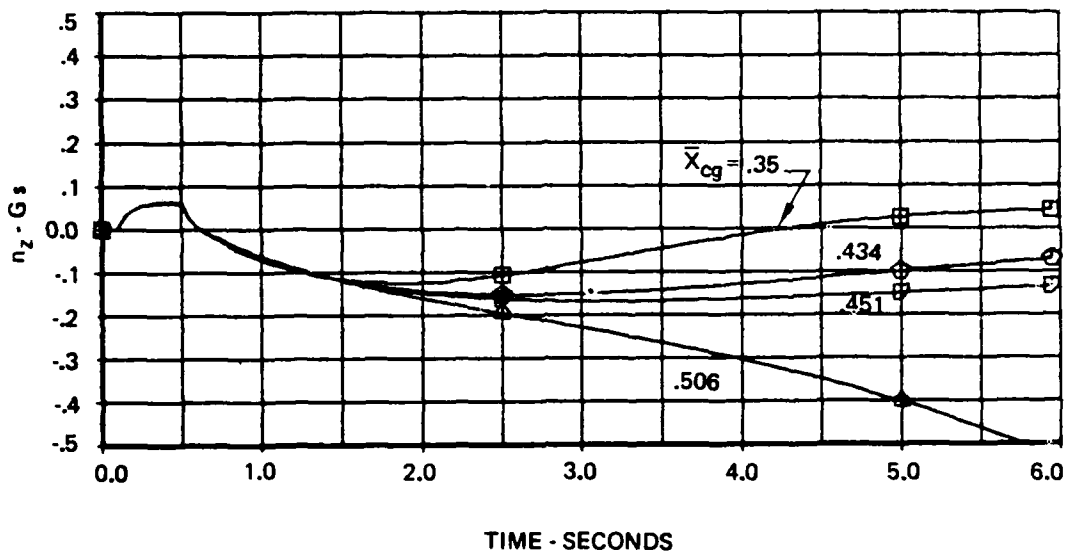
Figure B-6. Longitudinal Response for Selected c.g. Positions — Continued
(b) n_z and θ for 6 sec.

F-111A Landing Approach (Table B-1)
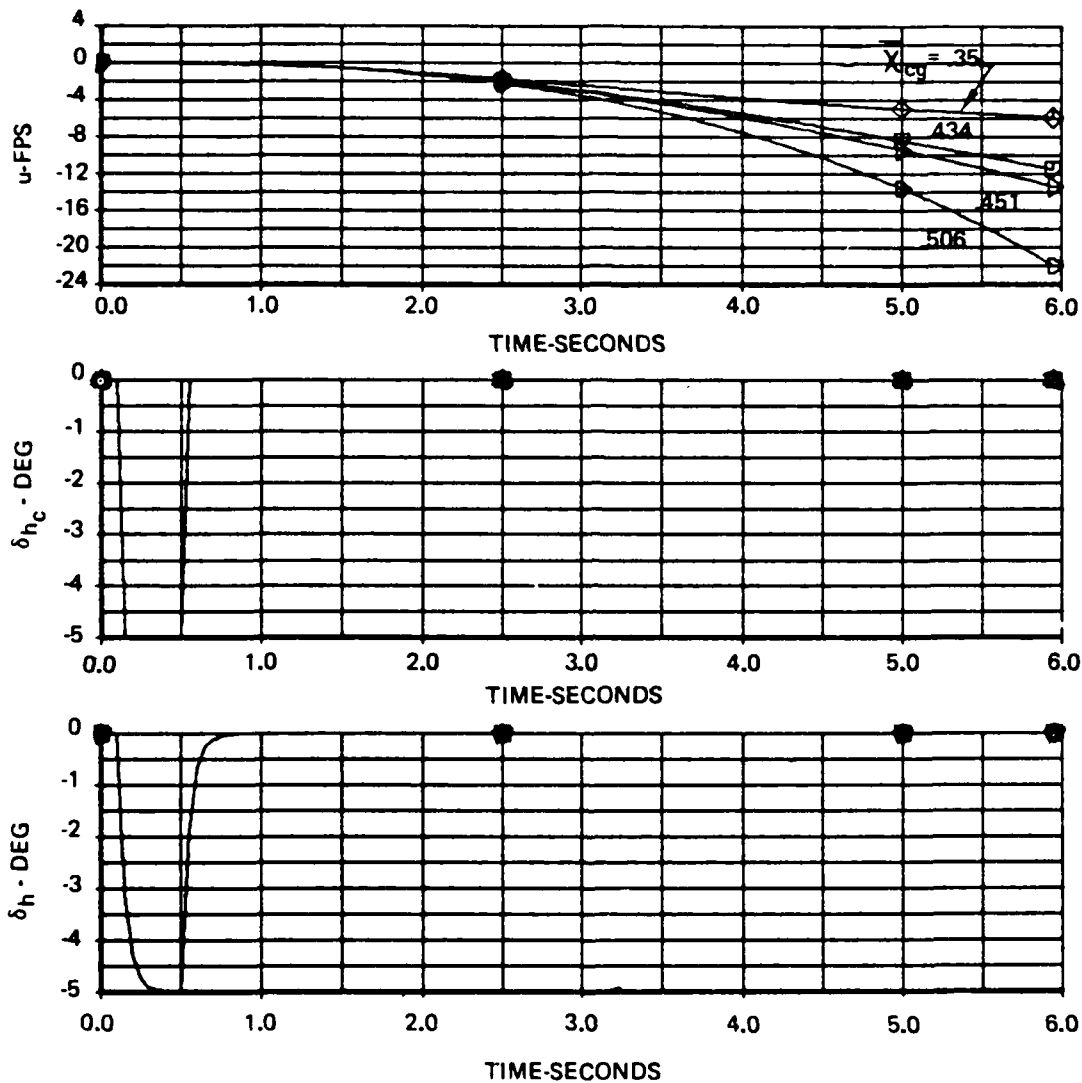
Figure B-6. Longitudinal Response for Selected c.g. Positions - Continued
(c) u, δ_h and δ_{h_c} for 6 sec.

42

F-111A Landing Approach (Table B-1)
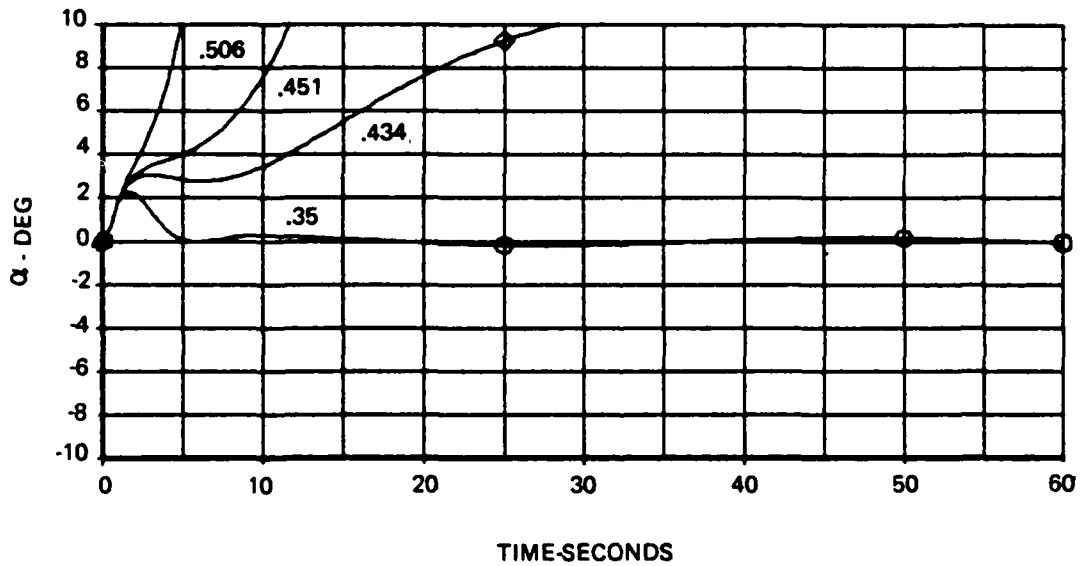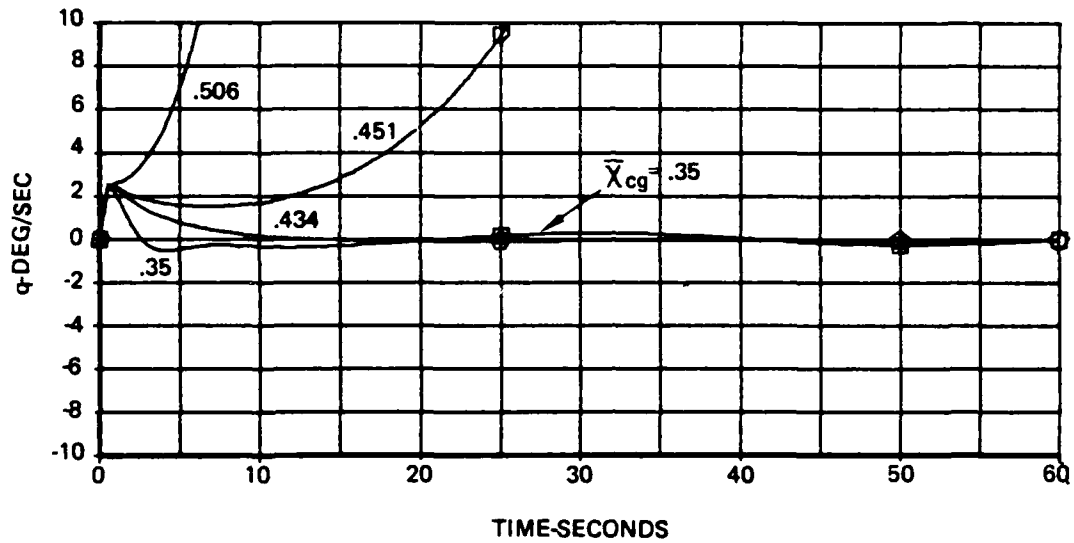
Figure B-6. Longitudinal Response for Selected c.g. Positions - Continued
(d) α and q for 60 sec.

43

F-111A Landing Approach (Table B-1)

TIME-SECONDS

TIME-SECONDS
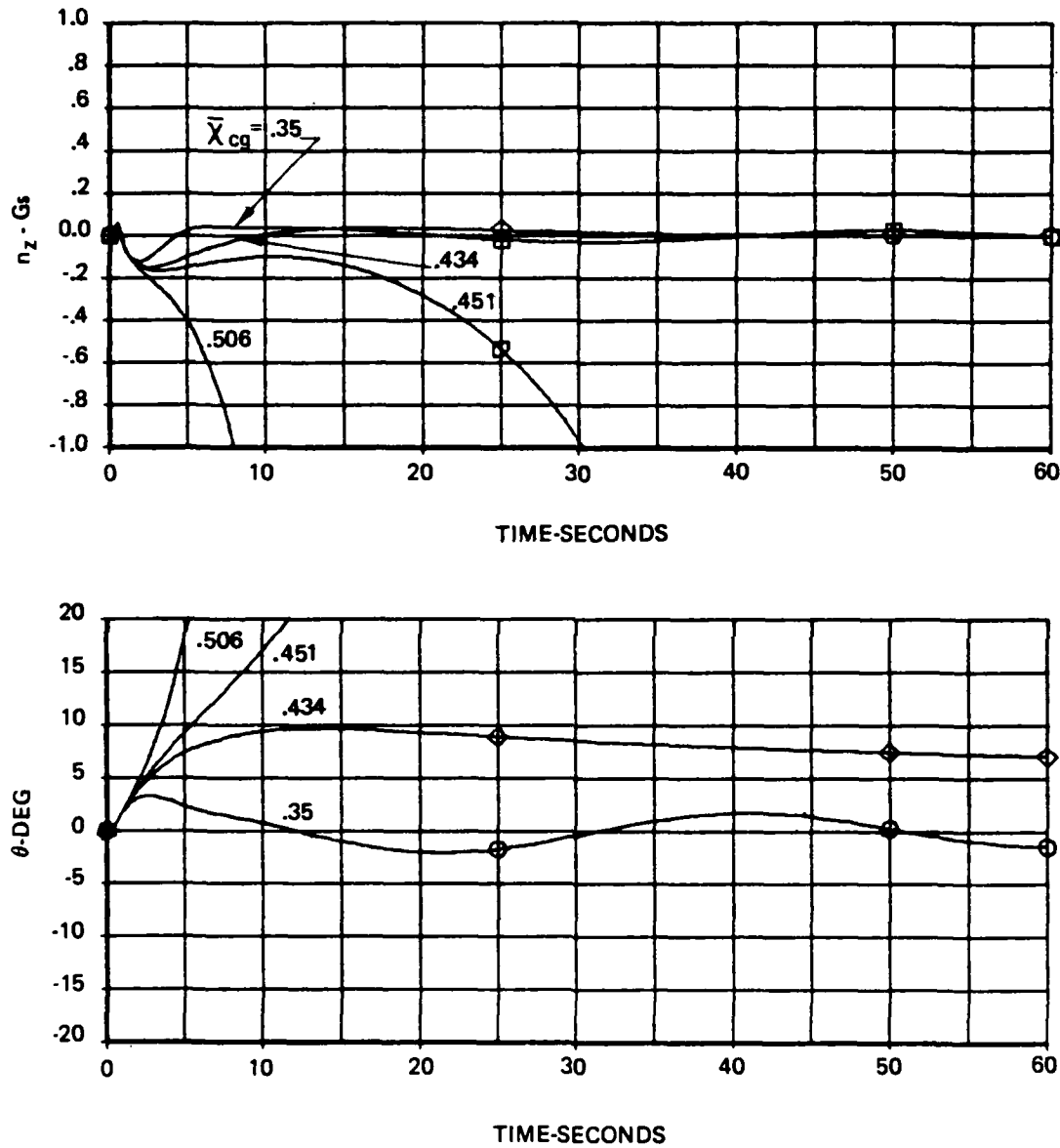
Figure B-6. Longitudinal   Response for Selected c. g. Positions - Continued
(e) n_z and θ for 60 sec.

44
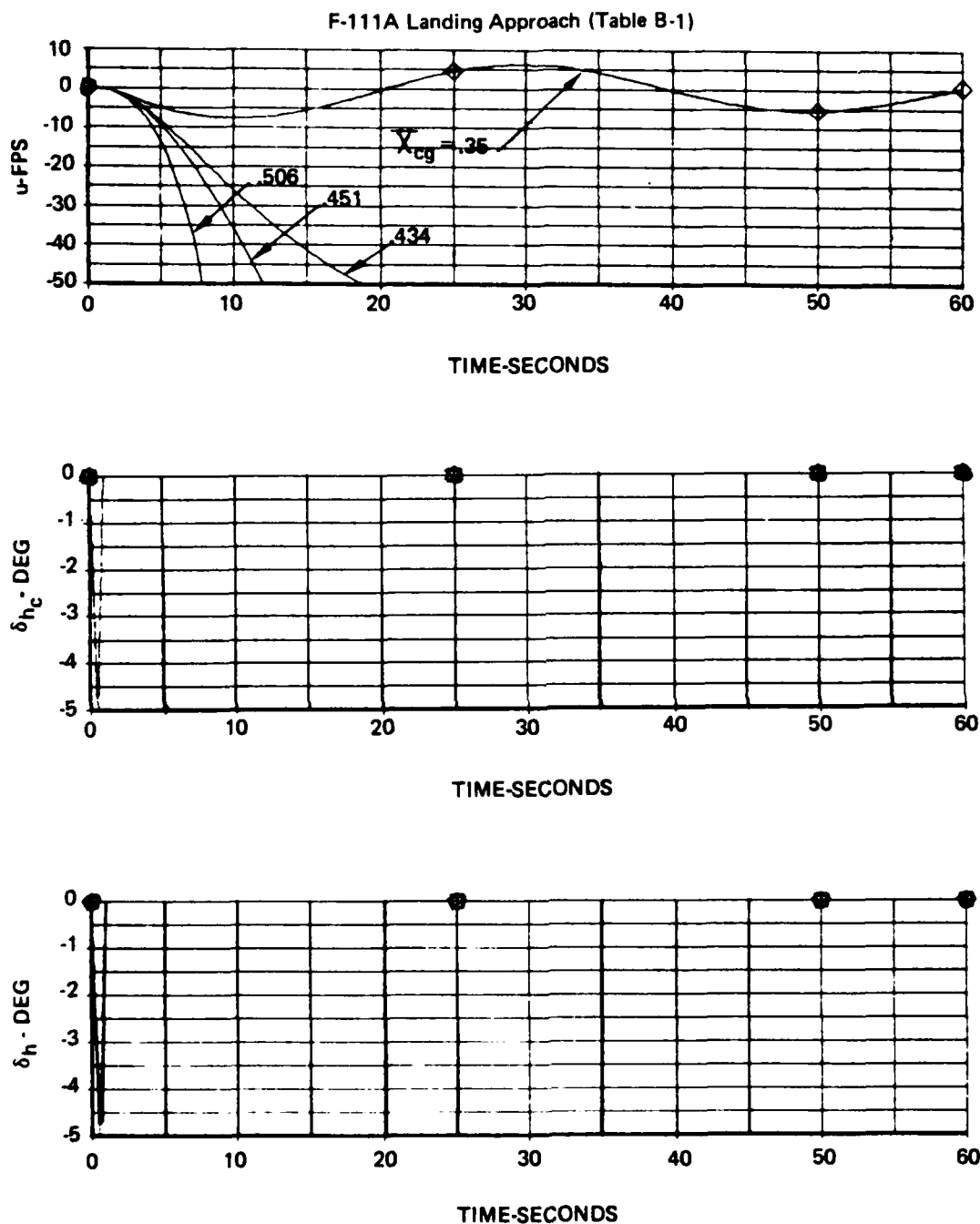
Figure B-6. Longitudinal Response for Selected c.g. Positions - Concluded
(f) u, δ_h and δ_{h_c} for 60 sec.
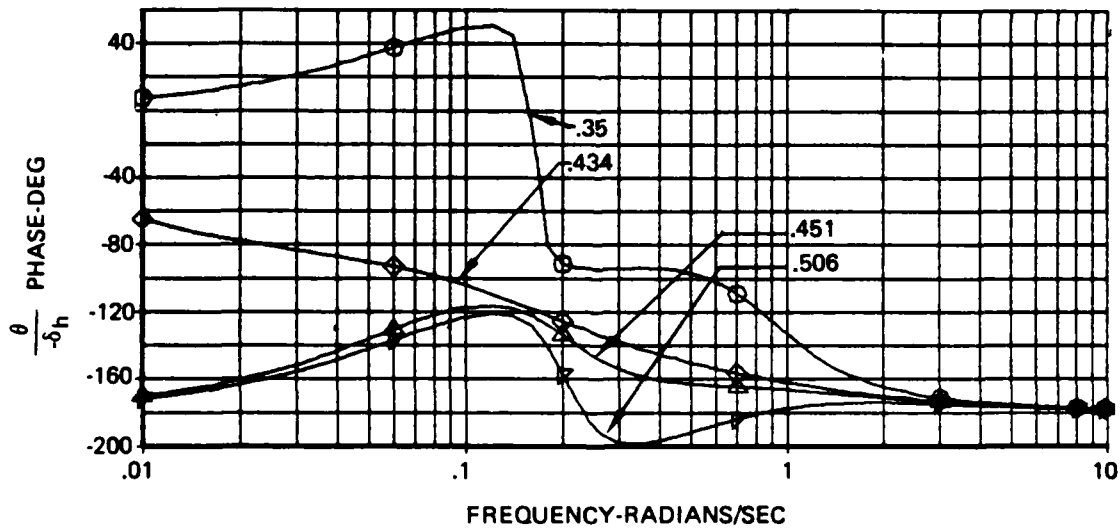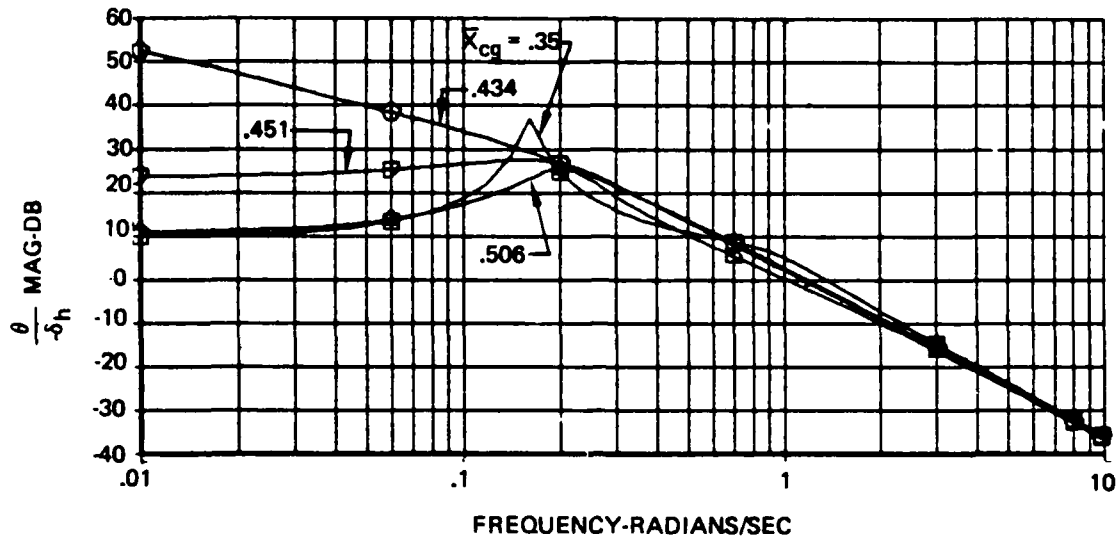
Figure B-7. Frequency Response, $\theta/-\delta_h$, for Selected C.G. Positions

o   Above ω = 0.2 rad/sec, the amplitude responses for all four c.g. locations are very nearly the same. But the phase angles for $0.2 < \omega < 2$ rad/sec are significantly different, with lag increasing with the degree of instability from -95° for the stable case to -200° for the most unstable case at $\omega \simeq 0.3$ rad/sec.

o   The two intermediate cases, one stable ($T_{1/2}$ = 4 sec) and the other unstable (T_2 = 6 sec), have nearly equal phase angles in the 0.2 to 2 rad/sec frequency range.

o   Below ω = 0.2 rad/sec, the frequency response is strongly affected by the phugoid or lower frequency roots as well as the short period or higher frequency roots. The phase angles for the two unstable cases are nearly equal, and converge to $\phi = 180^{\circ}$ as $\omega \to 0$. The stable case, with a typical phugoid, converges to $\phi = 0$. The phase angle for the near neutral but stable case goes from being near the unstable cases at ω = .15 rad/sec to approaching the stable case as $\omega \to 0$.

A recurring theme is apparent in the time histories and frequency responses, namely, the similarity between the two intermediate c.g. cases, one stable ($T_{1/2}$ = 4 sec) and the other unstable (T_2 = 6 sec). The similarity exists except for very low frequencies ($\omega < 0.1$ rad/sec) or for long times after the input (t > 6 sec). The expectation, borne out by the pilot ratings given at the beginning of this section, is that given real short-period roots with one near the origin, then the flying qualities will not be greatly affected by the location of the smaller root, whether stable or unstable. Two caveats should be heeded. The instability must not be too large (T_2 > 6 sec). The piloting task must be one requiring tight attitude control, such as approach and landing.

47

B.2.2.2 Full Nonlinear Equations - Three Degrees of Freedom

To assess the effect of linearizing the equations of motion, the linear stability derivatives in aerodynamic coefficient form (C_α, C_{m_α}, etc) were inserted in the full three-degree-of-freedom equations (Section C.2.1 and C.2.2.2) and these used to compute time responses for comparison with those from linearized equations. This comparison is shown in Figure B8 for a short, small, pulse input that excites mainly the unstable mode which is the characteristic of primary interest. The response from the linearized equations are compared with those from the full nonlinear equations for both nose-up and nose-down pulses for the three most aft c.g. locations (.434, .451, and .506). The primary difference between linear and nonlinear responses are due to changes in speed (exact computation of dynamic pressure, etc.) and attitude (exact computation of gravitational forces).

For the near neutral but stable case (.434), the response amplitudes are small and the linearized and nonlinear responses are essentially identical. For the unstable cases (.451, .506), the linearized response and the nose-down nonlinear response generally diverge faster than the nose-up response.

To quantify the differences and the characteristics of the responses, the times to double amplitude measured from the unstable responses in Figure B8 are presented in Table B5. Values of T_2 for each response were generally measured from half to full amplitude of the response, and from quarter to half amplitude of the response, using the value after the initial response to the pulse as the baseline. The values listed under "Roots" come from the unstable root, reflect the "true" value for the linearized responses, and are the same regardless of response variable. The values listed under "linear" were measured from the linear responses in Figure B8, and except for the noted case (.451, u) half and full amplitude values agreed within 0.1 seconds which shows that the measurement is reasonably accurate.

F-111A Landing Approach (Table B-1)
Full nonlinear: Eq. of Figure C5 and Section C.2.2.2.
Linear: Eq. F8
Stability - Body Axes. Pertubations added to reference values.
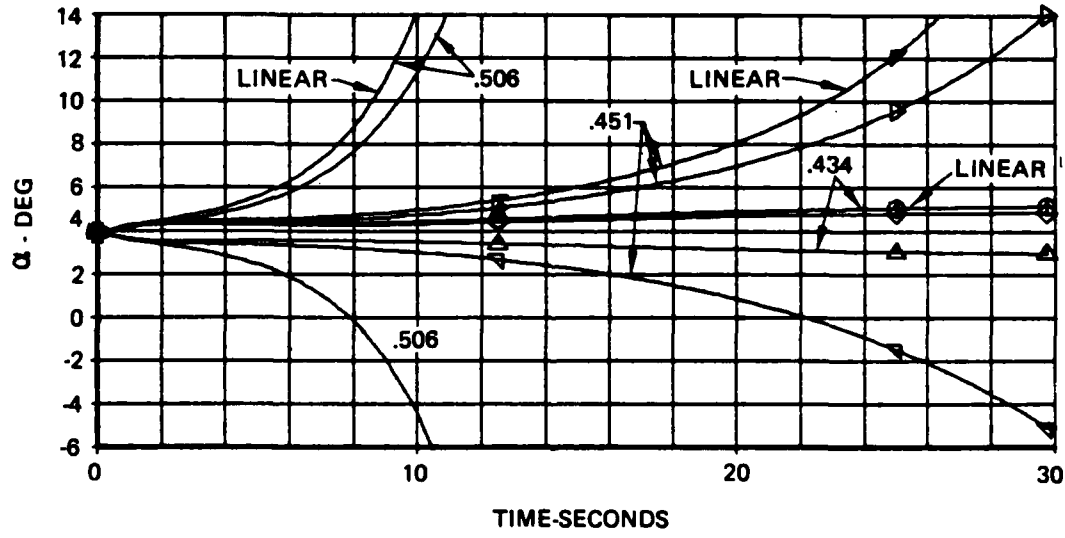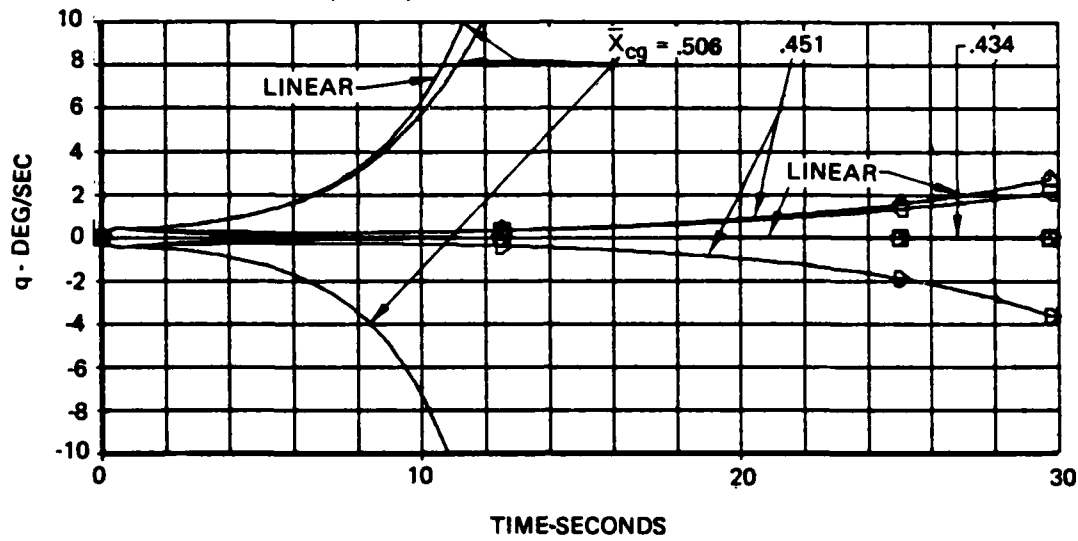
Figure B-8. Response From Full Nonlinear and Linearized Equations (Continued)
(a) q and α

49

Figure B-8. *Responses From Full Nonlinear and Linearized Equations - Continued*
(b) n_z and θ

50
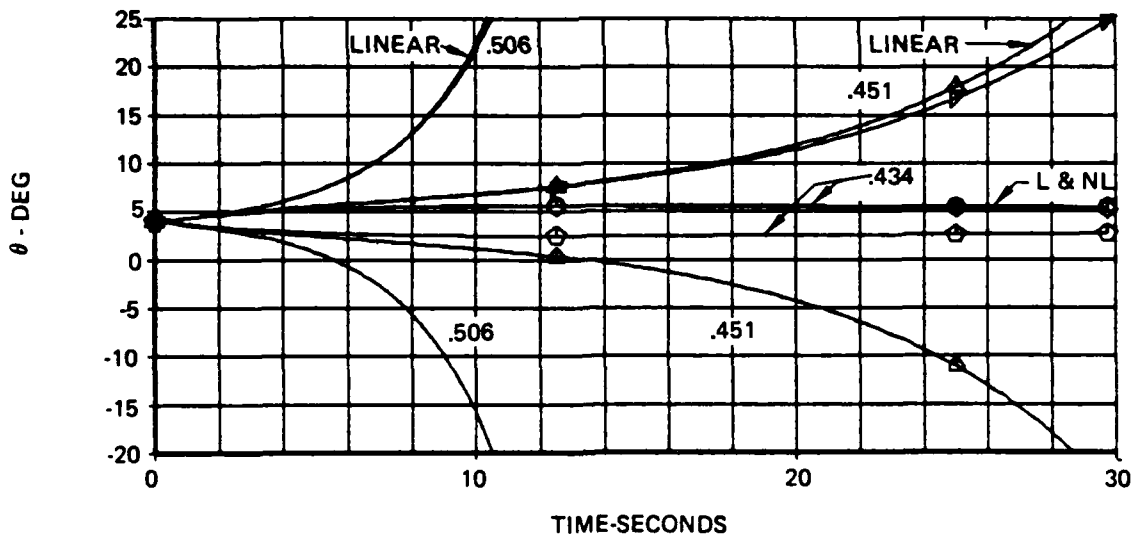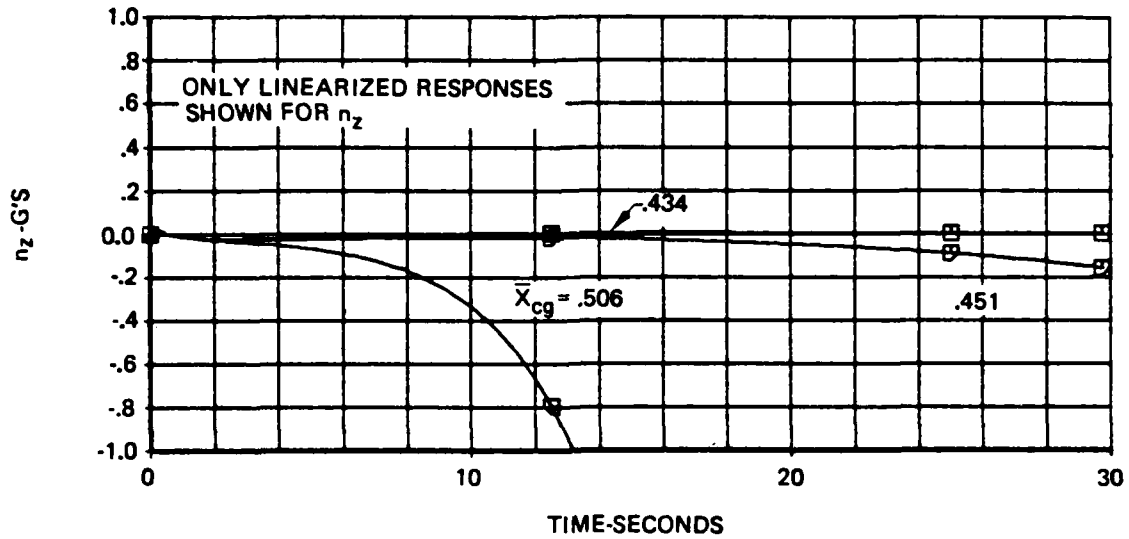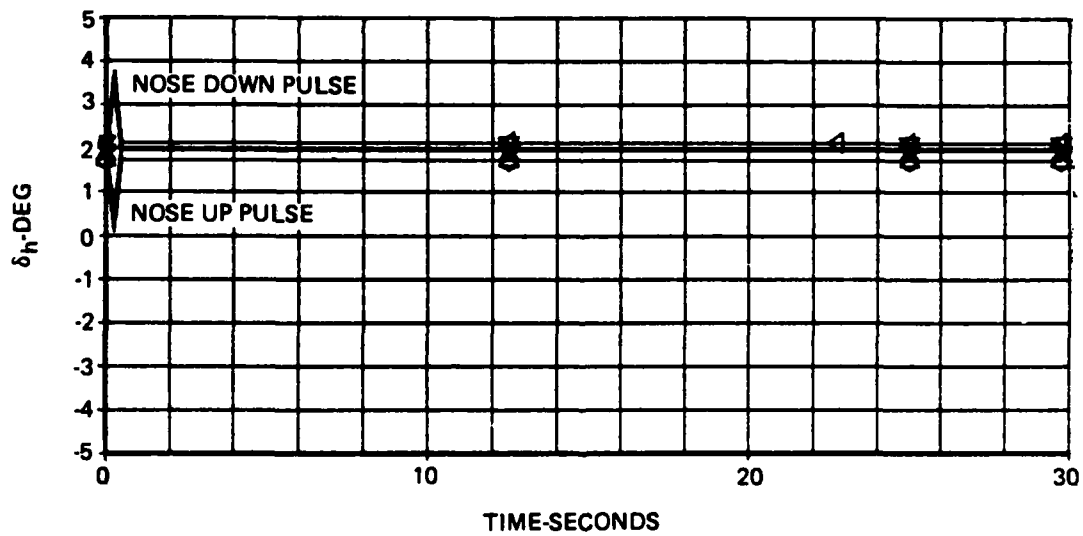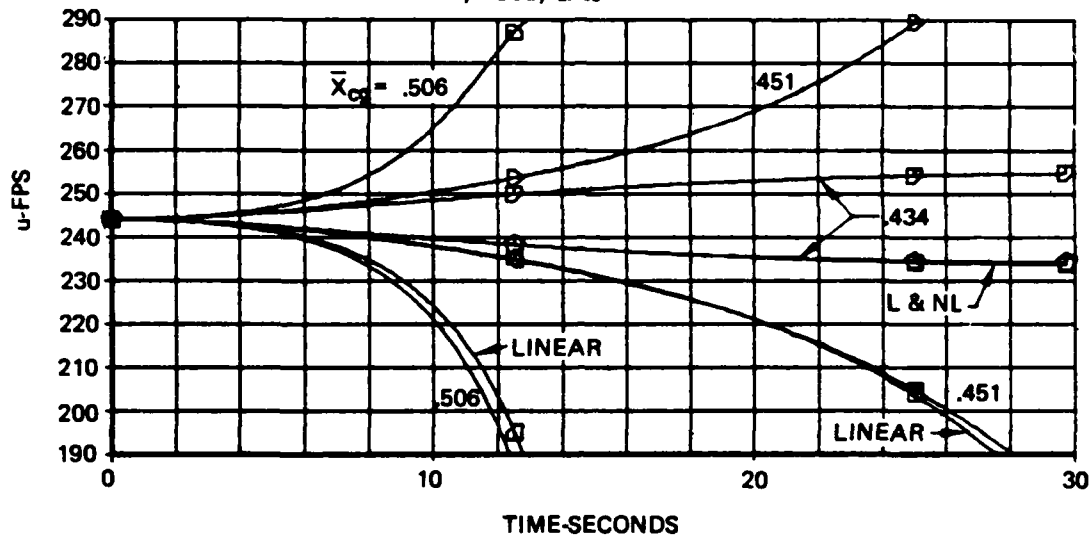
*Figure B-8. Responses From Full Nonlinear and Linearized Equations - Concluded
(c) u and δ_h*

Table B-5. Comparison of Time to Double Amplitude from Linear and Nonlinear Equations

$\overline{X}_{c.g.}$	Variable	TIME TO DOUBLE AMPLITUDE, T_2, IN SECONDS					
		Roots	Linear	Full amplitude		Half amplitude	
				NU	ND	NU	ND
.506	q	2.0	1.9	2.2	1.8	2.0	1.6
.506	α	2.0	1.6	1.9	1.8	1.7	1.7
.506	u	2.0	2.0	2.7	2.0	1.9	1.8
.451	q	6.1	4.9	5.5	4.8	–	–
.451	α	6.1	4.6	5.2	6.0	4.9	5.5
.451	u	6.1	6.1*	6.5	5.8	6.3	5.5

* Average of full (5.9) and half (6.3) amplitude values

Suprisingly, the divergence rate of the linear responses differs from variable to variable, with α having the shortest T_2 and u the longest. Also, the divergence rate of u agrees with that from the unstable root. This type of behavior was also found by Wasserman and Mitchell (Ref. 24) in their SST investigation when they attempted to extract $T_{1/2}$ and T_2 values for aft c.g. locations. They include plots of $T_{2\theta}$ (from q) and $T_{2\alpha}$ (from α) vs T_{2sp} (from λ_{sp_1}) as extracted from flight test data. They found that $T_{2\alpha}$ agreed with T_{2sp}, but $T_{2\theta}$ or $T_{1/2\theta}$ indicated considerably more stability. Their measurement technique involved the use of step inputs and semi-log plots of the response for extracting the values of $T_{1/2}$ or T_2. They also found that the values of $T_{2\theta}$ and $T_{1/2\theta}$ tended to agree with the roots of the constant-speed equations of motion (short-period approximation). They used $1/T_{2\theta}$ and $1/T_{1/2\theta}$ to correlate their pilot rating data.

Comparing T_2 for the linear and full-amplitude nonlinear responses as given in Table B5, the nose-up nonlinear responses diverge more slowly than the linear while the nose-down nonlinear responses diverge at about the same rate (α for .451 c.g. excepted). Examining the half-amplitude data, the difference between linear and nose-up nonlinear responses generally increases with amplitude as one would expect, but not so for nose down. The nose-down T_2 (α for .451 c.g. excepted) indicate more rapid divergence at half amplitude than the linear values, but return to the linear values at full amplitude. The primary

52

conclusion is that the linearized responses and equations reasonably represent the full nonlinear responses and equations through speed changes of as much as 50 fps or 30 knots, or about 20%. This applies to the effects of speed, dynamic pressure, and gravitational forces. It does not apply to significant aerodynamic nonlinearities such as a change in C_{m_α} with α.

In summary, for unstable configurations the use of a small pulse input excites primarily the unstable mode. The responses from the linearized equations have generally the same divergence rate as those from the full equations of motion. As measured from the time history, the divergence reflects the value of the unstable root, with q diverging slightly faster. Also the response in α diverges somewhat erratically, mostly faster, and is affected by more than just the unstable mode.

B.2.2.3 Constant-Speed Equations - Two Degrees of Freedom

The constant-speed equations have traditionally been used to characterize short-period and maneuvering characteristics. The equations are developed in Section F.3. The four selected c.g. cases for the F-111A in landing approach are analyzed for constant-speed characteristics which are compared with those for three degrees of freedom (3 DOF). Results are compared for transfer function poles and zeros, time histories, and frequency responses.

The transfer functions for horizontal tail inputs are given below, with parameters for the four selected cases listed in Table B6.

$$\frac{w(s)}{\delta_h(s)} = \frac{A_w (s - Z_w)}{s^2 + 2\zeta\omega_n s + \omega_n^2}$$

$$\frac{\theta(s)}{\delta_h(s)} = \frac{A_\theta (s - Z_\theta)}{s(s^2 + 2\zeta\omega_n s + \omega_n^2)}$$

Note that the above characteristics are for $\gamma_0 = 0$, so the third order constant-speed equations and transfer functions of Section F.3 reduce to second order. Also, the subscript "csp" is used to denote "constant-speed short period".

Table B-6. Constant-Speed Longitudinal Transfer Function Characteristics for F-111A in Landing Approach

$\bar{X}_{cg}$	λ_{csp_1}	λ_{csp_2}	A_w	Z_w	A_θ	Z_θ	$T_2(T_{1/2})$
.35	($-.49\pm.74j$)		-17.2	-22.9	-1.59	$-.59$	(1.4)
.434	$-.23$	$-.75$	-17.2	-21.8	-1.51	$-.62$	(3.0)
.451	$-.053$	$-.93$	-17.2	-21.6	-1.50	$-.63$	(13.2)
.506	$+.29$	-1.26	-17.2	-20.9	-1.45	$-.65$	2.4

Note: $T_2 (T_{1/2})$ values are for λ_{csp_1}

$$Z_w \cong Z_{w_1} = -1/T_{w_1}$$

$$Z_\theta \cong Z_{\theta_2} = -1/T_{\theta_2}$$

where Z_{w_1} and Z_{θ_2} are 3 DOF values.

Comparing the constant-speed roots (Table B6) with the 3 DOF roots (Table B4), we see that the phugoid roots (λ_{p_1}, λ_{p_2} in Table B4) have disappeared. The normal oscillatory short-period roots for $\bar{x}_{cg}$ = .35 are unchanged by holding speed constant, as is the the large negative real root for the other c.g. values. However, the small real root is more stable with speed constant, most noticeably for x_{cg} = .451, going from unstable (+.11) to stable (-.053).

Comparing the constant-speed gains and zeros (Table B6) with the 3 DOF ones in Table B3, we see that the complex zeros near the phugoid poles in w/δ_h have disappeared, the small real zero in θ/δ_h has disappeared, and there is an integrator (1/s) in θ/δ_h, so q/δ_h now has a steady state for a step input. The larger zeros in w/δ_h and θ/δ_h for the 3 DOF case are the same as the zeros in the constant-speed transfer functions.

Time histories for the two unstable cases comparing the 2 DOF and 3 DOF responses for pulse inputs are presented in Figure B9, where the 3 DOF responses are identical to those in Figure B6. As can be seen, for the six second duration there is negligible effect of holding speed constant in θ, and only α appears to have more than a trivial differ-

F-111A Landing Approach (Table B-1)
3 DOF equations: Eq. F8.
2 DOF, u = const. equations: Eq. F20.
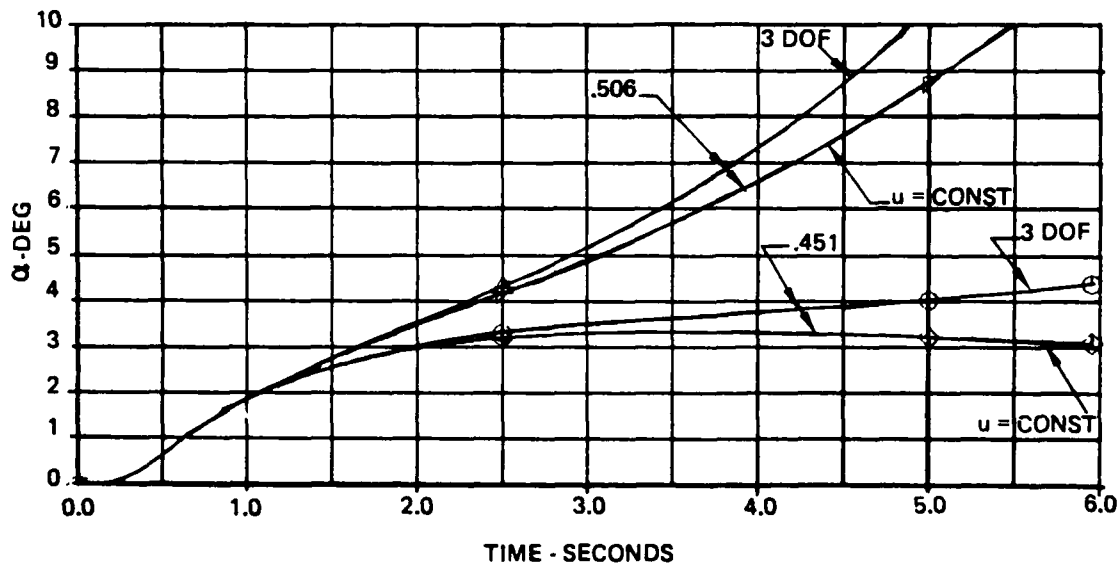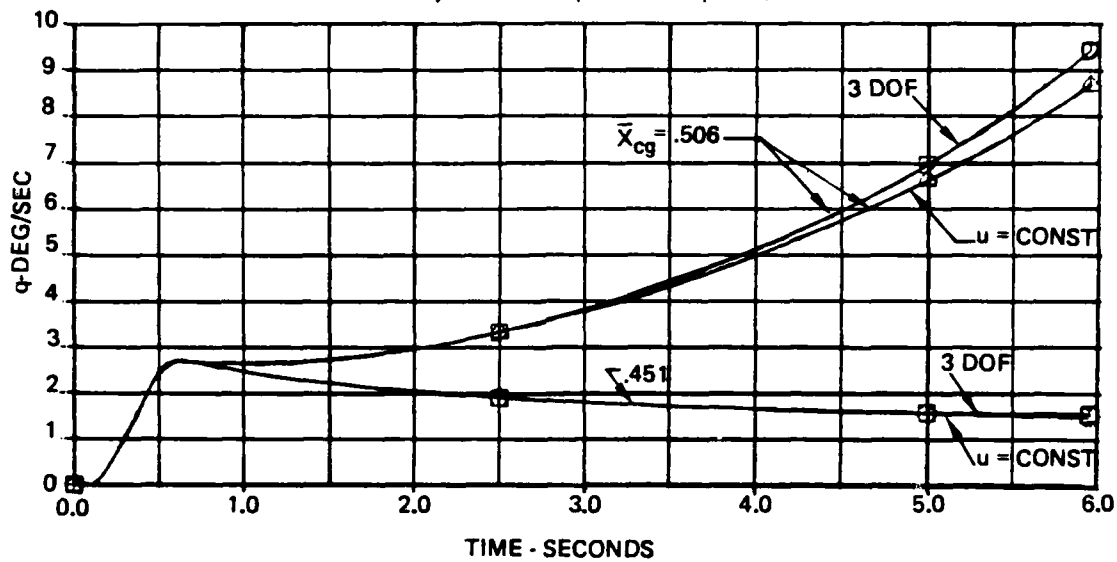
Figure B-9. Responses for Constant Speed and Three Degrees of Freedom
(a) q and α

Figure B-9. *Responses for Constant Speed and Three Degrees of Freedom - Continued*
(b) n_z and θ

F-111A Landing Approach (Table B-1)
See Part (a) for equation reference
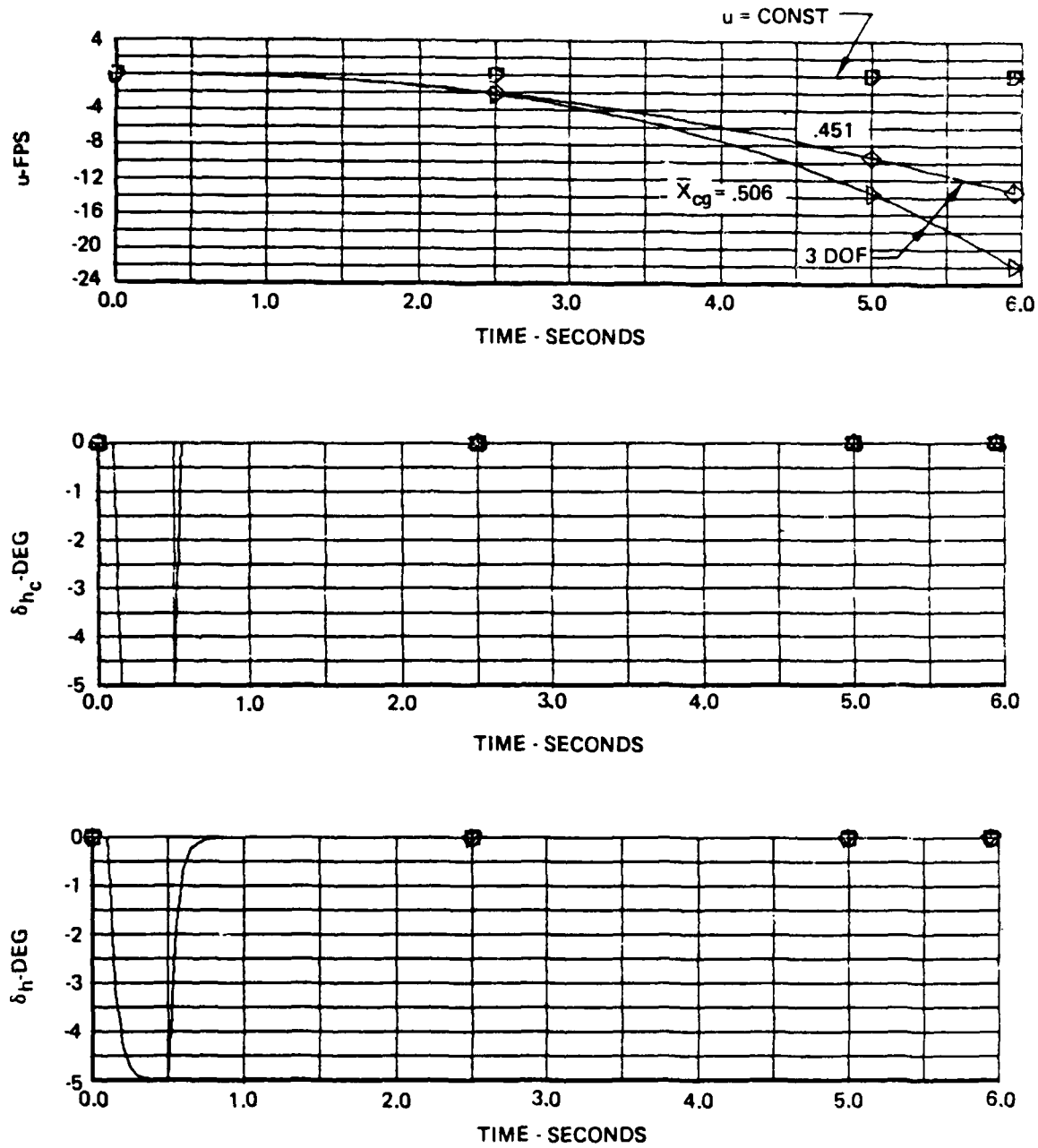
Figure B-9. Responses for Constant Speed and Three Degrees of Freedom - Concluded
(c) u, δ_{h_c} and δ_h

57

F-111A Landing Approach (Table B-1)
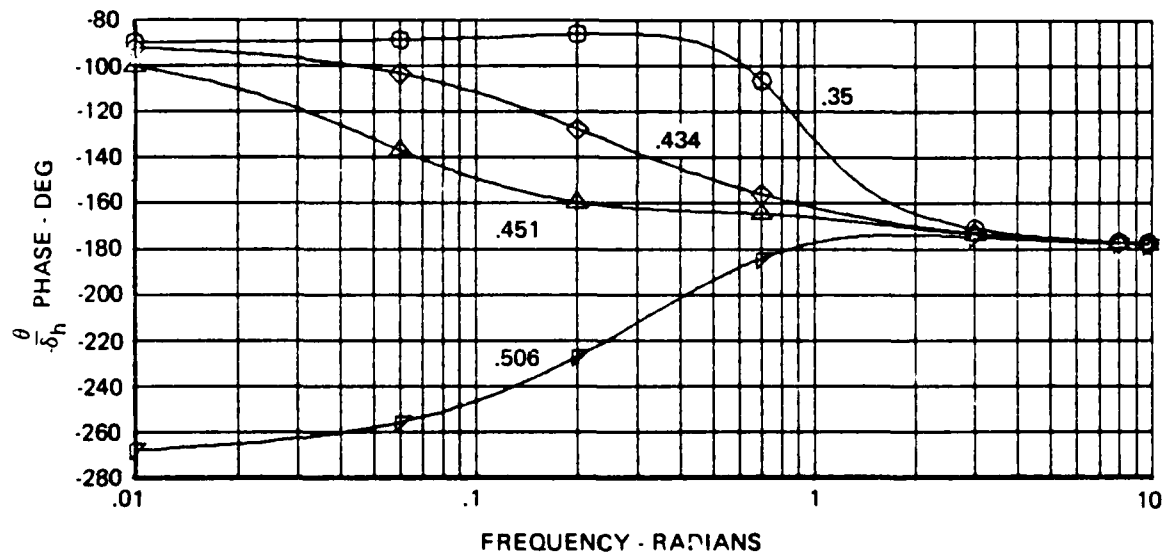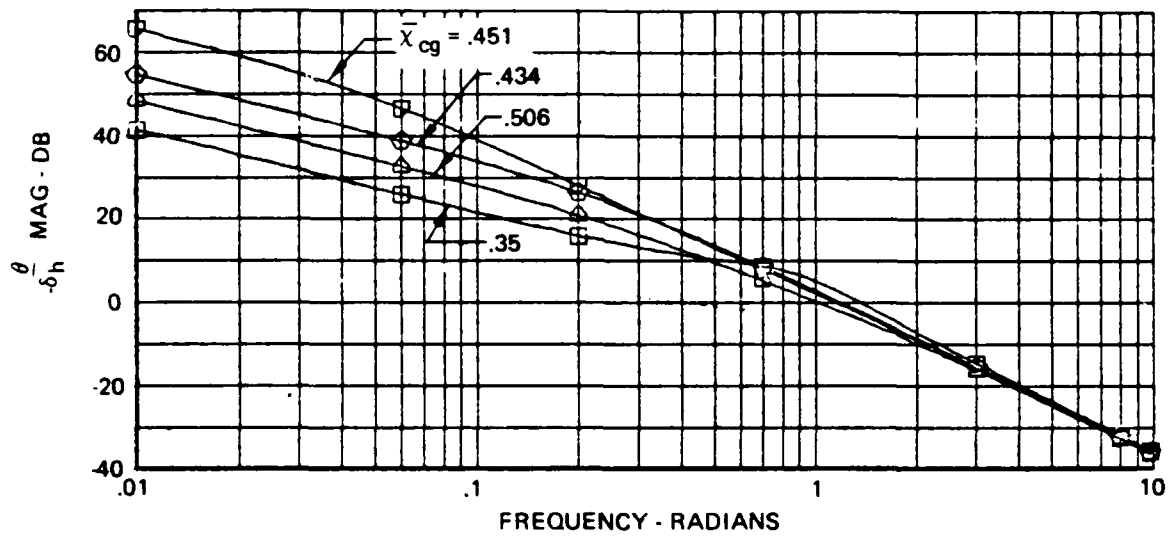
Figure B-10. Frequency Response, θ/δ_h, for Constant Speed (2 DOF)

58

ence (u excepted of course). For the more stable cases ($\bar{x}_{cg}$ = .35 and .434) there would be even less difference.

Frequency responses for $\theta/-\delta_h$ from the constant-speed two-degree-of-freedom equations for all four selected F-111A c.g. values are given in Figure B10. These, together with the 3 DOF responses in Figure B7, provide a good picture of the structure of the responses.

From the 2 DOF amplitude curves (Fig B10), we see that for $\omega > 1$ the responses are acceleration-like with a -40 db/decade slope, for $\omega < .04$ the responses are rate-like with a -20 db/decade slope, with transition varying from $\omega \simeq .06$ for c.g. at .451 to $\omega \simeq .7$ for c.g. at .35. The phase curves support this view, going from -90° to -180° with increasing ω for the stable (2 DOF) cases, and -270° to -180° for the unstable case. The responses appear to have the form

$$\frac{\theta}{-\delta_h} = \frac{K}{s(s + \lambda)}$$

with λ = -1.1, -.26, -.055, +.21 for c.g. at .35, .434, .451, .506 respectively, based on $\phi = -135^\circ$ at break frequency for the stable (2 DOF) cases and $\phi = -225^\circ$ for the unstable case. From the poles and zeros in Table B6, it appears that the Z_θ zero tends to cancel the λ_{csp_2} root, leaving the above net first order response in q (i.e. $\dot{\theta}$) with $\lambda \simeq \lambda_{csp_1}$ where λ_{csp_1} is the constant-speed value. This approach has in fact been suggested by Wasserman and Mitchell (Ref. 24) because it fit much of their data for which $Z_{\theta_2} \simeq \lambda_{sp_2}$. However, as the data in this report shows, this relationship is neither necessary nor desirable.

To delve briefly into the relationships, we make use of a special case which allows simple factoring of the two degree of freedom case. First assume that $M_{\dot\alpha} \simeq 0$ and γ_o = 0, then that the c.g. is at or near the neutral point so $M_\alpha \ll M_q Z_w$. Then, from Equation F22 (Appendix F) we have

$$\frac{\theta}{\delta_h} = \frac{M_{\delta_h} (s - Z_w)}{s[s^2 + (-Z_w - M_q)s + Z_w M_q]}$$

The characteristic equation factors exactly, so if $M_q > Z_w$ which is generally true, then

$$\lambda_{csp_1} = Z_w$$

$$\lambda_{csp_2} = M_q$$

For this case, q has the form of a first order response because of the pole-zero cancellation, but now $\lambda = \lambda_{csp}$.

Comparing $\theta/-\delta_h$ frequency responses in Figure B10 with the 3 DOF responses in Figure B7, it is readily apparent that addition of the speed degree of freedom and the phugoid mode affect primarily the lower frequency characteristics (i.e. $\omega < .4$ rad/sec). For the two extreme cases (c.g. at .35 and .506), adding the low-frequency θ zero ($Z_{\theta_1} \simeq -.07$) and the oscillatory phugoid mode ($\omega_p \simeq 0.2$ rad/sec) causes obvious additions to the 2 DOF responses. The amplitude breaks at $\omega \simeq .2$, from a zero slope at low frequencies. The phase has about 90^0 of lead added at $\omega = .01$, which increases with frequency due to the zero, and then shifts through the additional 180 degrees of lag, to come eventually to the 2 DOF value at $\omega = .2$ or $\omega = .4$ rad/sec. For the two intermediate cases, the picture is similar but more complex. For the c.g. at .434, the phugoid roots are real (see Table B4) and the effects are spread to much lower frequencies. For the c.g. at .451, though the phugoid is oscillatory, the smaller short-period real root goes from stable ($\lambda_{csp_1} = -.053$, Table B6) to unstable (λ_{sp_1} = +.11, Table B4) due to the added speed degree of freedom, so the phase curve for .451 shifts to one more like the .506 curve.

In summary, the comparison of constant-speed (2 DOF) and three-degree-of-freedom responses, in time and frequency domains, shows that for the range of frequencies of primary interest to the pilot in controlling attitude (0.3 to 6 rad/sec) there are essentially no differences. The differences at lower frequencies depend upon both the phugoid mode and associated zeros and upon the effects of speed on the short-period roots. The latter effect is generally to destabilize the lower frequency short-period root.

B.2.3 Steady-State Gradients

A number of flying qualities criteria are developed in terms of steady-state gradients, either with speed, or at constant speed in maneuvers. The foregoing development can be readily applied to assess the effect of relaxed static stability on these gradients, namely stick force with speed, fight path angle with speed, and stick force with normal acceleration.

Stick Force vs Speed

The stick position and force gradients with speed for unaugmented aircraft come directly from the u/δ_h transfer function. For $M_e = 0$ and $\gamma_0 = 0$, from Section 5.3 of Reference 50

$$\frac{du}{d\delta_h} = \frac{u(s)}{\delta_h(s)}\bigg|_{s \to 0} = \frac{D_u}{E} = \frac{g\,(M_\delta\,Z_w - Z_\delta\,M_w)}{g\,(Z_u\,M_w - M_u\,Z_w)}$$

$$\frac{F_s}{u} = \frac{F_s}{\delta_{ES}}\,\frac{\delta_{ES}}{\delta_h}\,\left(\frac{du}{d\delta_h}\right)^{-1} = \frac{F_s}{\delta_{ES}}\,\frac{\delta_{ES}}{\delta_h}\,\left(\frac{Z_u\,M_w - M_u\,Z_w}{M_\delta\,Z_w - Z_\delta\,M_w}\right)$$

From the data in Table B3 for the F-111A, it can be seen that D_u is relatively invariant of c.g. (from 30.3 to 30.2 for c.g. from .35 to .60). However, the numerator of F_s/u (note E above) is a direct measure of the static stability, so F_s/u will be negative for stability, zero for neutral stability, and positive for statically unstable aircraft.

For augmented aircraft with a rate command system such as the F-111A, or with a rate command/attitude hold system such as the YC-14, F_s/u will be zero but the augmented aircraft may have anywhere from neutral to strong static stability.

Flight Path Stability

Flight path stability is defined by the gradient of fight path angle with speed, $d\gamma/dV$, for constant throttle setting.

$$\frac{d\gamma}{dV} = \frac{d\gamma/d\delta_h}{du/d\delta_h} = \frac{\gamma(s)}{\delta_h(s)} \bigg/ \frac{u(s)}{\delta_h(s)} \bigg|_{s \to 0}$$

$$\frac{d\gamma}{dV} = \frac{D_\gamma}{E} \bigg/ \frac{D_u}{E} = \frac{D_\gamma}{D_u}$$

Since the zeros of the transfer functions for elevator inputs change negligibly with c.g., based on the F-111A data, it is clear that $d\gamma/dV$ is relatively insensitive to c.g. position and the effects of relaxed static stability. From Table B3, the results for the F-111A are as follows.

$d\gamma/dV$	$\overline{x}_{cg} = .35$	$\overline{x}_{cg} = .60$
rad/fps	-.00040	-.00052
deg/knot	-.039	-.050

Alternatively, the approximate expression given in Reference 2 is

$$\frac{d\gamma}{dV} = -\frac{1}{g}\frac{1}{T_{h_1}} = \frac{1}{g}Z_{h_1}$$

where Z_{h_1} is the small zero in the h/δ_h transfer function, and for $Z_{\delta_h}/M_{\delta_h}$ small,

$$\frac{d\gamma}{dV} = \frac{1}{g}\left[X_u - \left(X_w - \frac{g}{V}\right)\frac{Z_u}{Z_w}\right]$$

From the first expression and the data in Table B3, we see again that $d\gamma/dV$ does not change with c.g. location. Since the second expression contains only force derivatives, it shows no direct effect of c.g. shift or relaxed static stability.

Control Forces in Maneuvers (F_s /n)

The control forces in maneuvering flight important to longitudinal flying qualities are those at constant speed. The pitch control force per normal acceleration can be derived from the constant-speed equations in Appendix F, Section F.3, by making the following assumptions:

$$M_\theta = 0$$
$$\gamma_0 = 0$$
$$n = -n_z$$

where normal acceleration (n) is positive in a pullup.

$$\frac{F_s}{n} = \frac{F_s}{\delta_h} \left(\frac{g}{V}\right) \frac{Z_w M_q - M_\alpha}{M_w Z_\delta - Z_w M_\delta}$$

We note that

$$Z_w M_q - M_\alpha = \omega n_{csp}^2 = \lambda_{csp_1} \lambda_{csp_2}$$

where ωn_{csp}, λ_{csp_1}, and λ_{csp_2} are the constant-speed values. Also

$$Z_{\theta_2} = \frac{-1}{T_{\theta_2}} = \frac{Z_w M_\delta - M_w Z_\delta}{M_\delta + M_{\dot{w}} Z_\delta}$$

$$\frac{n}{\alpha} = \frac{-n_z/\delta_h}{\alpha/\delta_h} = - \left(\frac{V}{g}\right) \frac{Z_w M_\delta - M_w Z_\delta}{M_\delta - \frac{M_q}{V} Z_\delta}$$

Thus

$$\frac{F_s}{n} = \frac{F_s}{\delta_h} \left(\frac{g}{V}\right) \frac{\omega n_{csp}^2}{M_w Z_\delta - Z_w M_\delta}$$

or

$$\frac{F_s}{n} = \frac{F_s}{\delta_h} \left(\frac{g}{V}\right) \frac{\lambda_{csp_1} \lambda_{csp_2}}{M_w Z_\delta - Z_w M_\delta}$$

Normally $|M_\delta| \gg |M_{\dot{w}} Z_\delta|$ and $|M_\delta| \gg \left|\frac{M_q}{V} Z_\delta\right|$, so if the small terms are neglected and we define $M_{F_s} = (\delta_h/F_s) M_{\delta h}$,

then

$$\frac{F_s}{n} \approx \frac{\omega n_{csp}^2}{M_{F_s}(n/\alpha)} \text{ or } \frac{\lambda_{csp_1} \lambda_{csp_2}}{M_{F_s}(n/\alpha)}$$

and also

$$\frac{n}{\alpha} \approx - \frac{V}{g} Z_{\theta_2} = \frac{V}{g} \left(\frac{1}{T_{\theta_2}}\right)$$

63

The foregoing relationships show that c.g. position and relaxed static stability have a direct effect on control forces in maneuvers (F_S/n). In fact, F_S/n is directly proportional to the value of the smaller short period root (λ_{csp_1}) as obtained from the constant-speed equations. As described in Section B.2.4.3, the constant-speed root is more stable than the three-degree-of-freedom root,

$$\lambda_{csp_1} < \lambda_{sp_1}$$

and the effect is especially strong for small values of the root.

The stick-fixed maneuver point is defined as the c.g. position where the stick position gradient with normal acceleration is zero ($\delta_{ES}/n = 0$). Since for the feel systems under consideration, pitch control force is proportional to deflection, then $\delta_{ES}/n = 0$ is equivalent to $F_S/n = 0$ (stick-free maneuver point). Hence the condition

$$\lambda_{csp_1} = 0$$

corresponds to the stick-fixed maneuver point, for which there will generally be an unstable real root in three degrees of freedom

$$\lambda_{sp_1} > 0$$

B.3 Existing Flying Qualities Data on RSS

A search for flying qualities data pertinent to criteria for relaxed static stability reveals that there is not a large amount of data. The BIUG for MIL-F-8785B (Ref.2) lists five reports containing flight data on static instability, References 26, 28, 29, 30 and 31. The F-94 data by Chalk (Ref. 29) and the F-86 data by McFadden (30) were from fighter evaluations made at altitude, and neither used Cooper-Harper pilot ratings. The B-26 data by Bull (Ref. 28) was from landing approach evaluations covering a wide range of short-period frequencies and dampings, and even though it did not use the Cooper-Harper scale, the results are considered significant and useful. The T-33 data by Chalk in

64

Reference 31 contains only one unstable configuration, and that in Reference 26 contains only two unstable configurations, both phugoid instabilities.

Since publication of the BIUG (Ref. 2), two additional flight investigations have been reported containing significant data for the approach and landing, the work of Wasserman and Mitchell (Ref. 24) and that of Smith (Ref. 8). These, together with Bull's work (Ref. 28), comprise the bulk of the data on approach and landing flying qualities applicable to minimum stability requirements for airplanes with relaxed static stability.

Besides the flight data cited above, three airplane programs have involved the use of RSS: (1) the U.S. Supersonic Transport program with its initial Boeing SST development (cancelled) and subsequent NASA supported studies, (2) the Anglo-French (SNIA/BAC) Concorde SST, and (3) the YF-16 and F-16 airplanes. Results from the Boeing SST development are summarized by Kehrer (Ref. 14 and 15) and Tomlinson (Ref. 32). Much of the pertinent SST data from NASA studies and the Concorde are summarized by Chalk (Ref. 23). An SST simulation study performed by Sudderth et al. (Ref. 22) contains data on minimum stability and stall recovery requirements.

More recently Kehrer (Ref. 16) considers the application of RSS to advanced tactical aircraft and the requirements on stability, controllability and angle-of-attack limiting.

As for data with respect to the RSS requirements from the YF-16 and F-16 programs, since the airplanes are fly-by-wire and always have stability augmentation on, no data seems to have been generated concerning minimum stability levels. However, loss of control at extreme conditions was of great concern for the YF-16 and F-16, particularly high angle of attack conditions representative of stalls, departures, and spins. The YF-16 flight control system is described in detail in Reference 55. Lamers (Ref. 41) describes in depth the operation and flight testing of the YF-16 flight control system at high angles of attack, emphasizing its angle-of-attack limiting function. Buckner, et al. (Ref. 42) provide a similar treatment for the F-16 airplane and include descriptions of its departure prevention features, normal-

load-factor, angle-of-attack, roll-rate, and rudder limiting systems, and its automatic spin prevention feature.

Flying qualities data applicable to minimum requirements for RSS airplanes must essentially come from simulator investigations, either ground based or in-flight with variable stability airplanes where reversion to a non-catastrophic situation is possible.

B.3.1 Simulator Data

Criteria developed in past investigations for the minimum levels of allowable stability (maximum instability) for safe operation have mostly been in terms of the time to double amplitude of the airplane's response, usually calculated from the unstable root (λ_1) of the-three-degree-of-freedom characteristic equation as follows:

$$T_2 = \ln 2/\lambda_1 = .693/\lambda_1$$

Alternatively, boundaries have been drawn in the ω_n^2 vs $2\zeta\omega_n$ plane where ω_n^2 and $2\zeta\omega_n$ are the coefficients in the quadratic defining the short period mode as follows:

$$s^2 + bs + a = 0$$
$$b = 2\zeta_{sp}\,\omega_{n_{sp}}$$
$$a = \omega_n^2{}_{sp}$$

The unstable real root is often called a speed divergence root, though this name is in most cases a misnomer as is amply described in the previous Section B.2.5.

Kehrer (Ref. 15) presents the summary curve of pilot rating vs T_2 shown in Figure B11, based on various experiments on fixed-base simulators, moving-base simulators, and variable stability aircraft. He considers a 6.5 pilot rating as the minimum safe level for the Boeing SST and, in order to provide a comfortable safe margin, selects as criterion

$$T_2 > 6 \text{ seconds}$$

66
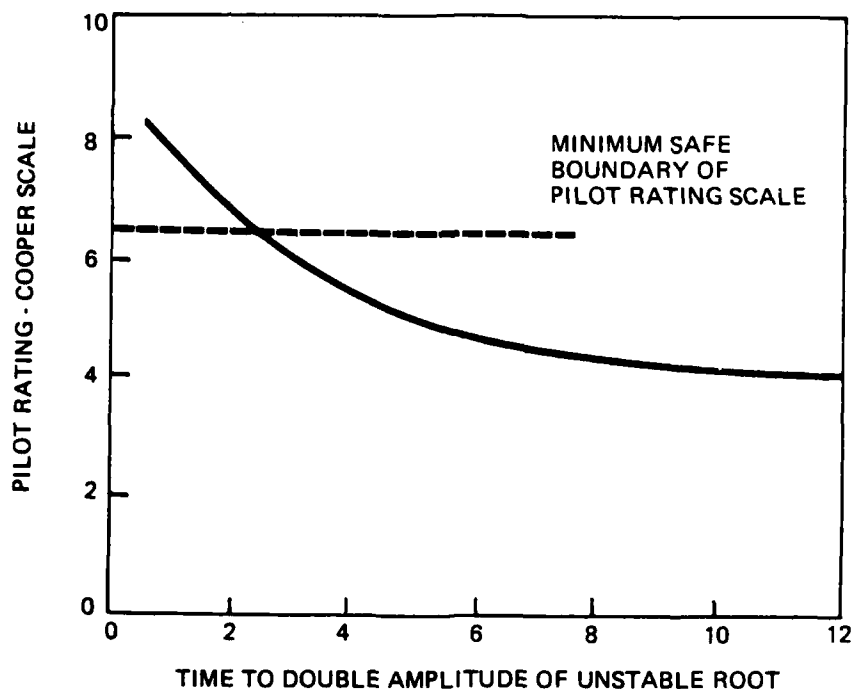
Note: Ref. 14 indicates that pilot rating scale is same as Cooper-Harper.

Figure B-11. Pilot Rating for Unstable Boeing SST (Ref. 15)

Sudderth, et al. (Ref. 22), recognizing that the value of T_2 measured from the response depends on both the variable selected and the direction of the input, used the time-to-double amplitude of pitch attitude $(T_{2\theta})$ for a small nose-up column pulse as the measure of longitudinal instability. From their moving-base ground simulations of landing approach in the NASA Ames FSAA, using the Boeing 2707-300PT Supersonic Transport model, they arrived at the criterion for $T_{2\theta}$ as a function of turbulence level shown in Figure B12. Since $\sigma_w = 4$ fps was selected as the requirement for the SST, then the corresponding stability criterion became $T_{2\theta} > 5.6$ seconds, very comparable to Kehrer's six second criteria.

The evaluation task in the Sudderth landing approach investigation consisted of an ILS approach including localizer and glide-slope acquisition, breakout at 200 feet altitude, short visual final, terminated with a flare and touchdown having the 1,000 ft. marker as objective. Approach speed was 144 knots.

67

MINIMUM-SAFE OPERATION
PILOT RATING = 6.5
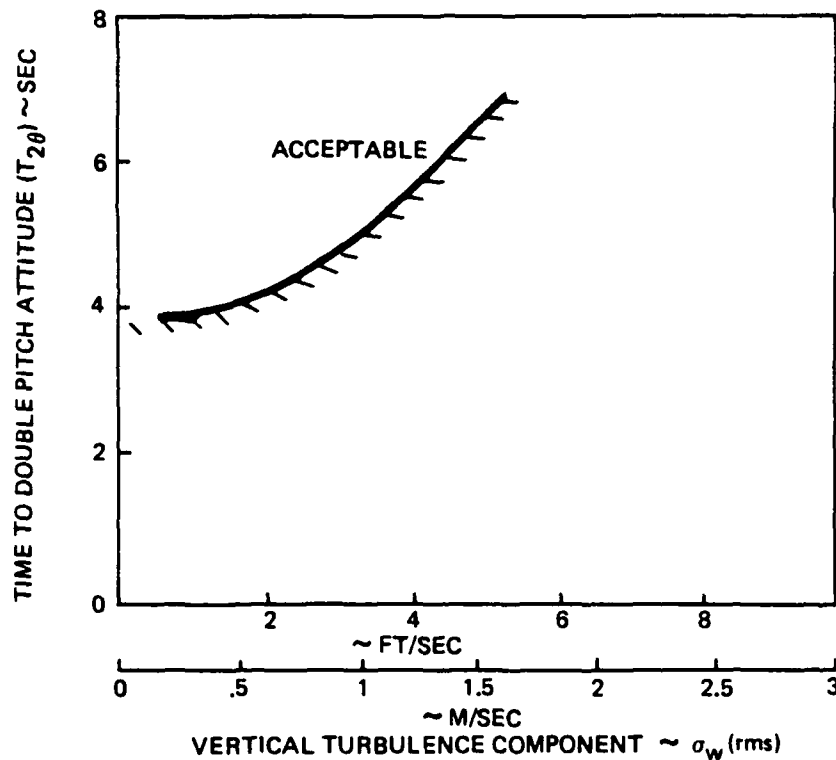
*Figure B-12. Landing Approach Minimum Safe Time to Double Pitch
Attitude as Function of Turbulence
(Ref. 22, p. 90, Boeing SST 2707-300 PT)*

The plot shown in Figure B12 was based on the pilot rating data shown in Figure B13. The method of varying $T_{2\theta}$ was to change the gain of the SST hard SAS (HSAS) which consisted of compensated pitch-rate feedback. Thus M_q was the primary parameter used to change $T_{2\theta}$. Data is not available in Reference 22 on either the specific transfer functions for the HSAS or the SST model. However, Reference 32 gives both the HSAS transfer function and the SST poles and zeros for θ/δ_h. Based on the data in Reference 19, it is clear that the airplane short period pole at $s = -1$ and the two HSAS feedback poles at $s = -.62$ all vary strongly with HSAS gain. Thus the variation of pilot rating shown in Figure B13 is not just due to the variation of $T_{2\theta}$, but also to the other poles in the total θ/F_s transfer function.

68

Included in Sudderth's evaluations (Reference 22) were cases of sudden degradation, simulating a SAS failure, but without any annunciation of the failure. Data points for two of these are indicated on Figure B13. In general, the pilots rated these sudden-degradation cases the same or better than when the degradation was present throughout, and the transition did not cause the pilots any particular difficulty. Also included on Figure B13 are cases where the FSAA motion system was turned off, and these show no significant difference in pilot rating due to the absence of the simulator motion cues. It is also noted in Reference 32 that no effect could be detected on pilot rating of pilot learning from experience with unstable configurations.

Test configuration
V_C = 144 KTS (74 M/sec)
G.W. = 415,000 Lbs (188,240 kg)
C.G. = .54 C_R
Flaps = 20 deg

SYM	PILOT
o	F
□	G

Sym shading	Wind $\bar{V}_{20}$	Vert gust σ_w (RMS)
Open ⊙	7 KTS H.W.	~ .8 FPS (.24 m/sec)
Half ◒	15 KTS C.W.	~ 2.3 FPS (.70 m/sec)
Solid ●	25 KTS C.W.	~ 4.0 FPS (1.22 m/sec)

Flags:
xO Fixed base
Q Sudden degredation from normal configuration

COOPER-HARPER PILOT RATING

TIME TO DOUBLE PITCH ATTITUDE
$T_{2\theta}$ ~ SEC
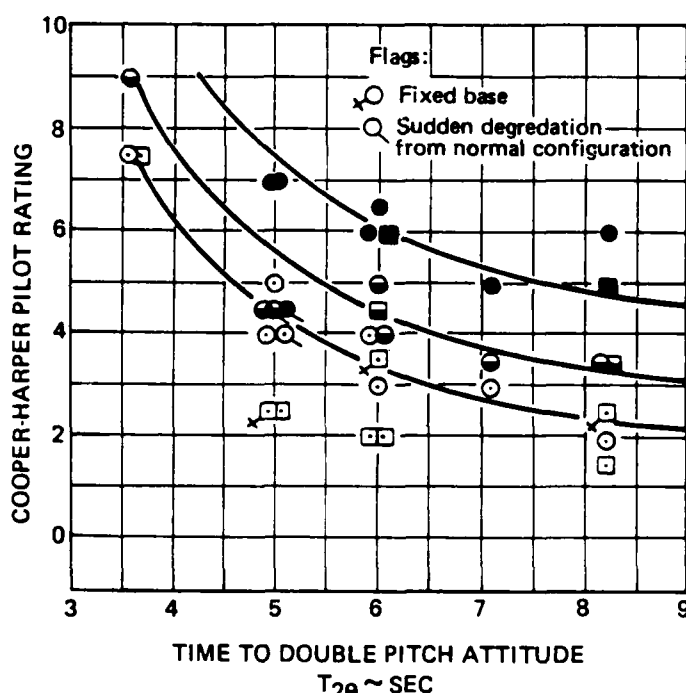
Figure B-13. Pilot Rating for Landing Approach Time-To-Double Pitch Attitude (Ref. 22, p. 88, Boeing SST 2707-300 PT)

B.3.2 Flight Data

Since the approach and landing data from the three variable-stability airplane flight test programs of References 8, 24, and 28 comprise the

bulk of the flight data on minimum stability levels applicable to RSS, they are analyzed in considerable detail. Acronyms (LAHOS, SST, B-26) are defined for each for ready reference, and a synopsis of the characteristics, limitations and procedures for each investigation follows.

LAHOS Data (Ref. 8). - The data in this reference have become widely known as the LAHOS data (Landing Approach Higher Order Systems). They are exceptionally high quality data, having been obtained in the USAF/Calspan variable stability T-33, are well documented and, unlike other similar data, the landings were carried through all the way to touchdown (except where safety required an earlier abort). The requirement for touchdown had recently been discovered while simulating prior to first flight the YF-16 and YF-17 prototype aircraft with the variable stability T-33 (Ref. 8 and 43). Included in the test configurations in the LAHOS data, which mostly are for high levels of augmentation, are three configurations with an unstable real root (T_2 = 2, 4, and 6 sec) obtained by using positive values of M_α so they represent an RSS airplane with failed augmentation. Approach speed used was 120 knots.

SST (TIFS) Data (Ref. 24). - An in-flight simulation of minimum longitudinal stability in landing approach using the Anglo/French Concorde as the baseline unaugmented airplane. The USAF/Calspan TIFS has six control degrees of freedom as well as a special simulation cockpit, and, because of this capability and the good documentation, the data in Reference 24 are exceptionally valuable. However the use of the Concorde SST baseline somewhat narrows the applicability of the data. Specifically, the simulated ground effect was significant and may be atypical, and the control sensitivity was low (.018 rad/sec^2/in) for the unstable configurations. Also, the TIFS airplane did not actually make touchdowns since its landing gear and wing tips were many feet in the air when the SST gear would have been on the ground (see Ref. 24), and knowledge of this fact may have affected the pilot and the precision of his performance in the touchdown task. The evaluation configurations included a stable case for reference and four configurations with unstable real roots (T_2 = 2, 4, 8, 60 seconds) obtained by varying C_{m_α}. Also included were

70

variations in $C_{m_q} + C_{m_{\dot{\alpha}}}$, $d\gamma/dV$, and a quadratic curvature in the pitch-up sense of C_m vs α.

The evaluation task consisted of an initial familiarization with the configuration, an IFR approach including a radar vectored track to the ILS course, localizer acquisition, glide slope acquisition, breakout at 300 feet altitude, and visual short final to a flare and simulated touchdown (indicator light, aural signal, "bump" from direct lift flaps at computed main gear touchdown). Three approaches were used for evaluation of the configurations: (A) straight-in approach ($\sigma_v \geq 0.5$ ft/sec), (B) glide slope error and 15 knot 90^0 crosswind ($\sigma_v \geq 0.5$ ft/sec), (C) localizer offset error and moderate turbulence ($\sigma_v \geq 3$ ft/sec). "Canned" turbulence was added to ambient turbulence, if needed, to achieve the minimum desired level.

B-26 Data (Ref. 28). - The investigation of minimum longitudinal flying qualities by Bull in a B-26 variable stability airplane covered a wide range of unstable configurations and provides the largest bulk of data applicable to RSS flying qualities requirements. Bull, finding that flying qualities are dependent not only on the value of the unstable real root but also on that of the stable real root, plots his short period data in the ω_n^2 vs $2\zeta\omega_n$ plane. Bull also found that variations in the low-frequency phugoid oscillation had little effect on flying qualities, whether it was the conventional phugoid or the "third mode", and that the range of C_{m_α} (equivalent to c.g. position) for which all roots were real was very small and concluded that this special case was not significant. Bull's investigation also compared the relative difficulty of the landing task and the enroute task, and determined that the landing approach was the more demanding.

The evaluation task was a VFR approach with the final portion made using a Navy Mirror Landing Aid System. A rectangular pattern was used, with the evaluation commencing on the downwind leg, and completed using the mirror system which made the final approach a demanding precision flight task. The airplane was flared and normally a waveoff was made at two to six feet altitude, but in some cases actual touchdowns were made. Approach speed was 117 knots.

71

Figure B-14. Flight Data on Minimum Longitudinal Stability, ω_n^2 vs $2\zeta\omega_n$

( ) No's in parentheses are configuration identifiers.

Numbers beside points are Cooper-Harper pilot ratings. B-26: A = Acceptable; AP = Acceptable Poor; U = Unacceptable.

Commas indicate a repeat. Range is shown (e.g., 6.5-10) for multiple rating or repeats.

Data Source	n_z/α Approach	Pilot Rating Scale
SST (TIFS)	5.20	Cooper-Harper
LAHOS (T-33)	4.65	Cooper-Harper
VS B-26 Rough Air	6.4 (Est.)	Special

72

variations in $C_{m_q} + C_{m_{\dot{\alpha}}}$, $d\gamma/dV$, and a quadratic curvature in the pitch-up sense of C_m vs α.

The evaluation task consisted of an initial familiarization with the configuration, an IFR approach including a radar vectored track to the ILS course, localizer acquisition, glide slope acquisition, breakout at 300 feet altitude, and visual short final to a flare and simulated touchdown (indicator light, aural signal, "bump" from direct lift flaps at computed main gear touchdown). Three approaches were used for evaluation of the configurations: (A) straight-in approach ($\sigma_v \geq 0.5$ ft/sec), (B) glide slope error and 15 knot 90^0 crosswind ($\sigma_v \geq 0.5$ ft/sec), (C) localizer offset error and moderate turbulence ($\sigma_v \geq 3$ ft/sec). "Canned" turbulence was added to ambient turbulence, if needed, to achieve the minimum desired level.

B-26 Data (Ref. 28). - The investigation of minimum longitudinal flying qualities by Bull in a B-26 variable stability airplane covered a wide range of unstable configurations and provides the largest bulk of data applicable to RSS flying qualities requirements. Bull, finding that flying qualities are dependent not only on the value of the unstable real root but also on that of the stable real root, plots his short period data in the ω_n^2 vs $2\zeta\omega_n$ plane. Bull also found that variations in the low-frequency phugoid oscillation had little effect on flying qualities, whether it was the conventional phugoid or the "third mode", and that the range of C_{m_α} (equivalent to c.g. position) for which all roots were real was very small and concluded that this special case was not significant. Bull's investigation also compared the relative difficulty of the landing task and the enroute task, and determined that the landing approach was the more demanding.

The evaluation task was a VFR approach with the final portion made using a Navy Mirror Landing Aid System. A rectangular pattern was used, with the evaluation commencing on the downwind leg, and completed using the mirror system which made the final approach a demanding precision flight task. The airplane was flared and normally a waveoff was made at two to six feet altitude, but in some cases actual touchdowns were made. Approach speed was 117 knots.

71

Unfortunately, documentation of the configurations is meager and incomplete. Also, Bull's investigation predated the Cooper-Harper scale, and the pilot ratings are given with adjectives: acceptable, acceptable poor, and unacceptable. These were considered to apply to making a landing in the emergency case with failed augmentation system. Based on the wording used in the Cooper-Harper scale (Ref. 51) and MIL-F-8785C (Ref. 5), the following equivalents are believed appropriate.

Adjective	Pilot Rating	Level
Acceptable	5-7 (or better)	2,3
Acceptable Poor	8-9	3
Unacceptable	10	3

The flights were conducted in moderate turbulence or in smooth air, with sets of data provided for each. Boundaries between acceptable and unacceptable are provided in the $\omega_n{}^2$ vs $2\zeta\omega_n$ plane, one for smooth air and one for rough air. The data points and the boundaries are found in Reference 2 as well as Reference 28.

To provide an overview of the flight data and various criteria, selected data points from the LAHOS, SST (TIFS), and B-26 flight test investigations have been plotted on the $\omega_n{}^2$ vs $2\zeta\omega_n$ plane in Figure B14, together with the B-26 rough air and smooth air boundaries, appropriate Level 1, 2, and 3 boundaries from MIL-F-8785B, and lines of constant time to double amplitude (T_2 = 2 and 6 sec). The B-26 configuration numbers are not from Reference 28, but were assigned for this analysis. It should be noted that all the data in Figure B14 refer to the short period roots of the three-degree-of-freedom longitudinal airplane (not constant speed), and there is generally an oscillatory phugoid with low frequency (ω_{n_p} < .2 rad/sec or $\omega_{n_p}{}^2$ < .04). In the few cases or small region where the modes are characterized by four real roots, the short period is defined by the most stable and least stable real root. In practicality, any mode combination approaching this four real-root condition may be considered to have neutral static stability. All data in Figure B14 are for an $n_z/\alpha \simeq 5$ except the B-26 data for which there is no value specified in Reference 28.

Figure B-15 Flight Data on Minimum Stability as Function of Short Period Roots

74
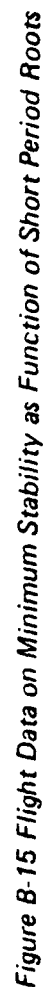
The SST stable configurations (1,13,20) support the Level 1 boundary, but SST configurations 14 and 15, and all three LAHOS configurations (7-1, -2, -3) indicate that the Level 2 boundary should be well below the $\omega_n^2 = 0$ axis, going somewhere between the $T_2 = 6$ sec. and 2 sec. lines for $2\zeta\omega_n$ larger than 1.0. SST configurations 2, 3, 4, 10, and 11 all have $PR \leq 9$ with the exception of flare and touchdown ratings of 10 for each of configurations 2 and 3. This suggests that near $\omega_n^2 = 0$, the B-26 rough air boundary (which goes through all these points) is about on the Level 3 boundary. However, SST configurations 5 and 12 (also on the B-26 rough air boundary) with $T_2 = 2$ sec have $PR = 10$, indicating the boundary should be above and to the right of these points.

If we except SST configuration 16 ($PR = 10$), there are three bands of data running parallel to the B-26 boundaries, (1) the B-26 rough air boundary with $PR \simeq 9.5$, (2) a line intercepting the $2\zeta\omega_n$ axis at 1.1 with $PR \simeq 6.5$, and (3) a line intercepting the $2\zeta\omega_n$ axis at 1.9 with $PR < 6$. Clearly, there is a strong gradient of PR along lines of constant T_2, with PR improving as $2\zeta\omega_n$ increases. In summary, the specification Level 2 boundary should be lower and the Level 3 boundary much lower than they currently are, allowing negative ω_n^2 for large amounts of damping ($2\zeta\omega_n$). Clearly, T_2 does not define the flying qualities for statically unstable aircraft as there is a strong gradient of pilot rating along lines of constant T_2.

The unstable data points and the B-26 rough air boundary from Figure B14 have been transformed to T_2 (for λ_{sp_1}) and λ_{sp_2} coordinates and are shown in Figure B15 with T_2 plotted on a logarithmic scale. The motivation comes from the strong gradient of pilot rating with $2\zeta\omega_n$, noting the following relationships

$$2\zeta\omega_{n_{sp}} = - (\lambda_{sp_1} + \lambda_{sp_2})$$
$$2\zeta\omega_{n_{sp}} \simeq - \lambda_{sp_2}, \text{ for } \lambda_{sp_1} \text{ small}$$

The scale of the coordinates now allows two additional points from the B-26 data to be plotted, configurations 5 and 6. The data points fall into three groups. Most points on the B-26 boundary have pilot ratings of 9 or 10. Points above the boundary have better ratings, with points farthest from the boundary and to the right (LAHOS data) having the best

ratings. SST configuration 16 stands out as an anomaly with its PR = 10. Also SST configuration 4 and 11, with PR $\simeq$ 6, are on the boundary. The arrangement of the points in the T_2 (logarithmic) vs λ_{sp_2} plane seems to correlate better with pilot rating than in the ω_n^2 vs $2\zeta\omega_n$ plane. For example, SST configuration 16 (PR = 10) is the closest point to the B-26 boundary, but not so in Figure B-14. The B-26 boundary for large T_2, corroborated by the other data, indicates there is a lower limit for λ_{sp_2} at -0.6. The data in Figure B-15 strongly indicate that flying qualities are directly related to λ_{sp_2}, the large, negative, real short-period root.

B.4   Simulation Experiment Design

Since analysis of existing data shows that flying qualities of airplanes with relaxed static stability are not defined by the value of the unstable root (λ_{sp_1} or T_2), additional parameters must be found upon which to base flying qualities prediction and criteria. Since the attitude response is probably of primary concern to the pilot, we look to the attitude transfer function for the needed parameters.

Airplane

$$\frac{\theta}{\delta_h}(s) = \frac{A_\theta(s - Z_{\theta_2})(s - Z_{\theta_1})}{(s - \lambda_{sp_1})(s - \lambda_{sp_2})(s^2 + 2\zeta_p\omega_{n_p}s + \omega_{n_p}^2)}$$

Control System

$$\frac{\delta_h}{F_s}(s) = \left[\frac{\delta_{ES}}{F_s}(s)\right]_{\substack{\text{Feel} \\ \text{System}}}\left[\frac{\delta_h}{\delta_{ES}}(s)\right]_{\text{Actuators}}$$

Gain

$$\frac{\theta}{F_s} = \frac{\delta_{ES}}{F_s}\frac{\delta_h}{\delta_{ES}}A_\theta \simeq \frac{\delta_{ES}}{F_s}\frac{\delta_h}{\delta_{ES}}M_{\delta_h}$$

$\dfrac{\delta_{ES}}{F_s}$ - stick force gradient, in/lb

$\dfrac{\delta_h}{\delta_{ES}}$ - gearing, rad/in

M_{δ_h} - pitch control effectiveness, rad/sec^2 per rad

The above transfer functions are in the form for the unaugmented airplane. However, most augmented airplane transfer functions can be recast into the above form by one of two techniques: 1) equivalent stability derivative approach, and (2) equivalent system approach. The first is suitable when simple response feedbacks are used (e.g., α, n_z, q...), without significant low-frequency compensation or feedback dynamics, so the feedback can be represented as the weighted sum of the airplane state variables. The second is suitable when significant compensation or control system dynamic elements are included so that the closed loop airplane response is of higher order than normal in the frequency range of interest (0.1 to 10 rad/sec). In this latter case, the higher-order closed-loop system is matched in the time and frequency domains with a lower-order normal (equivalent) airplane transfer function (e.g., Ref. 9). Thus by specifying response characteristics in the normal unaugmented form for an RSS airplane, criteria for two different conditions are developed:

(1) Unaugmented RSS airplane, following failure of normal FCS,
(2) RSS airplane augmented with backup FCS, following failure of normal FCS.

An alternative approach employing the closed-loop frequency-response analysis techniques of Neal and Smith (Ref. 7) is also available which does not depend on the specific form of the transfer functions. It may be presumed that if criteria for RSS airplanes can be developed using the normal form of the θ/F_S transfer function, then these criteria will apply to higher order systems as well. Of course, the assumption must be tested and proved valid. The beauty of the Neal-Smith approach is that it should be able to handle simultaneously the low frequency problems attributable to RSS and the high frequency problems associated with higher order responses and excessive control system lags.

77

The specific parameters in the θ/F_S transfer function selected for study were λ_{sp_1}, λ_{sp_2}, and Z_{θ_2} on the assumption that variations in ω_{n_p}, ζ_p and Z_{θ_1} would not be as important. Some investigation was also made of the control sensitivity, M_{F_S} or $M_{\delta_{ES}}$. In addition to the linear response characteristics defining minimum stability levels, the minimum requirements for control system rate and authority were investigated for both the augmented and unaugmented RSS airplane.

The general approach in the simulator investigation was as follows. First the characteristics of the baseline F-111A airplane were investigated on the simulator with respect to various augmentation systems, c.g. position, control authority, and linear versus nonlinear longitudinal aerodynamics. Then the LAHOS configurations of Reference 8 representing RSS airplanes were simulated to validate and calibrate the simulator. Finally, based on linear state models and pole-placement techniques, a matrix of airplane configurations was developed and evaluated to investigate λ_{sp_1}, λ_{sp_2} and Z_{θ_2} while holding all other characteristics constant.

Thus three basic groups of configurations were evaluated: the F-111A (F), the LAHOS (L), and the state model based (S) configurations. Data on control sensitivity, $M_{\delta_{ES}}$, was obtained because the F configurations used F-111A gearing which was a factor of four lower than the single value selected as optimum by the pilots for the S configurations. This latter was about the same as the LAHOS sensitivity. Feel system dynamics were those of the LAHOS configurations, and a single stick-force gradient of 7 lb/in was used (average of LAHOS 8 lb/in and F-111A 6 lb/in). The F-111A first order actuator was used for the F configurations, but the LAHOS second order actuator was used for the L and S configuration, with a few S configurations evaluated with the slower first order actuator for comparison. A more detailed description of the simulator and simulation configurations is found in Appendix C, together with the collected pilot rating data. Pilot comments are found in Appendix G. Summaries follow of the simulation program configurations, evaluation tasks, and procedures.

B.4.1   Simulation Configurations

A primary objective of the simulation program was to investigate the influence of λ_{sp_1}, λ_{sp_2} and Z_{θ_2} on the minimum-safe flying qualities in landing approach. Ranges for these parameters were selected based on what might be realized for actual airplanes and what was felt would exercise the flying qualities and give pilot ratings from good (PR < 3.5) to very bad (PR = 10). For λ_{sp_1} the possible range is very large, from large positive values to large negative ones, but it was felt that from neutral stability to T_2 = 2 seconds (λ_{sp_1} = +.347) would be adequate. For λ_{sp_2}, the least negative value would be set by total short period damping $2\zeta\omega_n > 0$, and since $-\lambda_{sp_2}$ = $2\zeta\omega_n + \lambda_{sp_1}$, it seemed that λ_{sp_2} = -0.3 would be reasonable for the small negative limit. For the large negative limit, λ_{sp_2} = -3.0 seemed adequate since it more than covered the available experimental data including the well-rated LAHOS cases. For Z_{θ_2}, the practical range based on the landing approach data in Reference 2 was -0.16 to -1.6, and the range selected for the experiment was from -0.3 (smallest negative value of λ_{sp_2}) to -2.0.

B.4.1.1   Configuration Identifier Codes

With the above guidelines in mind, the following code was defined for identifying the simulation configurations.

F-111A Configurations - Unaugmented

	$\overline{x}_{cg}$	
F0	= .35	Good stable airplane
F1	.440	Neutral but stable
F2	.505	T_2 = 2 sec
F4	.465	4 sec
F6	.453	6 sec

where F indicates unaugmented F-111A and the number following F indicates T_2 in sec, except 0 = stable, 1 = neutral.

LAHOS Configurations

L21	LAHOS Config. 2-1	Good stable airplane
L71	7-1	T_2 = 6 sec
L72	7-2	4 sec
L73	7-3	2 sec

State Model Configurations

$$\underset{T_2 \nearrow \quad \nwarrow \lambda_{sp_2}, \, Z_{\theta_2}}{SIJ}$$
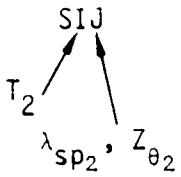
S indicates state model basis

I = 2, 4, 6: value of T_2

J = 0, 1, 2, 3, 4: index to λ_{sp_2} with Z_{θ_2} = -0.6

J = 5, 6, 7: index to Z_{θ_2} with λ_{sp_2} variable

J	λ_{sp_2}	J	Z_{θ_2}
0	-0.3	5	-0.3
1	-0.6	6	-1.2
2	-1.0	7	-2.0
3	-2.0		
4	-3.0		

Example: Configuration S23 has a state model basis, T_2 of 2 sec, λ_{sp_2} = -2.0, and Z_{θ_2} =-.6.

In the above tables, the values of T_2, λ_{sp_2} and Z_{θ_2} are nominal values. Actual values are mostly very close and are given in the configuration definition tables (Appendix C, Table C4 and C5) which also define the other airplane and flight control system characteristics associated with the use of the above identifiers. In addition, a capital letter suffix is added to the configuration identifier to indicate a variation in the flight control system from the baseline:

A,B suffix   Variation in FCS (e.g., S41A)

Changes or variations in a single parameter, such as control authority (e.g., $S_{h_{LIM}}$) are not indicated by changes in the configuration identifier but are given where needed to show the change from the baseline.

Besides the augmented or minimum-safe configurations, augmented F-111A configurations were used to provide a standard of good flying qualities and also to investigate minimum-safe control authority requirements (position and rate). The following codes identify these augmented configurations.

F-111A Augmented

F111   F-111A airplane simulation. Nonlinear longitudinal aerodynamics, linear lateral-directional aerodynamic coefficients (e.g., C_{l_β}), simplified F-111A FCS, c.g. as specified.

AFO, AF1   F configurations (FO, F1, F2, F4, F6) augmented with
AF2, AF4   generic FCS.
AF6

Augmentation Systems

F   Simplified F-111A FCS. Adaptive gains fixed, adaptive and structural mode filters omitted.

G   Generic FCS. Uncompensated feedbacks (α, $\dot{\alpha}$, n_z, q) and input (δ_{ES}). Same roll, yaw, and throttle FCS as F system.

U   Unaugmented, augmentation OFF or failed.

With the exception of the F111 configuration, all of the simulation configurations had linear longitudinal aerodynamic coefficients (i.e., constant C_{L_o}, C_{L_α}, C_{m_α}, etc) and $C_{D_{\delta_h}} = C_{L_{\delta_h}} = 0$. That $C_{L_{\delta_h}}$ was zero occurred inadvertently, but it is not believed to have affected the significance nor generality of the results. For example, the pilots could not see the difference between augmented configurations F111G (c.g. = .35) and AFO, which both had the same FCS, but the latter with $C_{L_{\delta_h}}$ = 0. It should be noted that though the simulation equations of motion had linear aerodynamic coefficients, they were in no other way linearized, and had full nonlinear representations of such quantities as gravitational forces, inertial terms, c.g. transformation, axis transformations, atmospheric quantities including dynamic pressure, ILS beam geometry, and the position of the airplane with respect to the earth, the landing field and the visual scene.

The configurations, F111 excepted, all have linear aerodynamic coefficients in order to fix the stability level, expecially with motion variables other than airspeed such as α, q, or control inputs. Without this linearity it would have been very difficult to assess or analyze the results, as the roots and transfer functions would have changed except for the smallest perturbations from trim conditions. Wasserman and Mitchell (Ref. 24) included deliberate nonlinearity of C_m vs α in some of their configurations as well as ground effect, and had substantial difficulty treating the effects. Their results, however, can be used to assess the effect of nonlinearity, especially pitch-up.

B.4.1.2 Primary Configuration Parameters

The primary characteristics of the evaluation configurations that were parametrically varied are presented in Tables B7, B8, and B9. The two baseline configurations (Table B7) are the F-111A with $\overline{x}_{cg}$ = .35 and the LAHOS 2-1 configuration of Reference 8. The matrix of real short period roots (Table B8) shows the values of λ_{sp_1} and λ_{sp_2} that were covered by the various F, L, and S configurations. The F configurations were derived on the simulator by varying the c.g. to achieve the desired T_2 of the pitch rate (q) response. The L configurations were derived from the state models given in the LAHOS

Table B-7. Baseline Configurations

Config.	$\omega_{n_{sp}}$ rad/sec	ζ_{sp}	Z_{θ_2}	$M_{\delta_{es}}$ rad/sec²/in
FO	.90	.57	−.59	.086
L21	2.29	.57	−.76	.434

Table B-8. Matrix of Real Root Configurations

λ_{sp_2} rad/sec	$T_2(T_{1/2})$ ~ sec λ_{sp_1} ~ rad/sec				
	(7) −.099	8 .087	6 .116	4 .173	2 .347
−0.3			S60		
−0.6			S61	S41	S21
−0.8	F1				
−1.0		F6	S62	S42,F4	S22
−1.25					F2
−2.0			S63,L71	S43,L72	S23
−2.5					L73
−3.0				S44	S24

Note: $Z_{\theta_2} \approx -0.6$ for all configurations in Table B8.
See Table B-10 for $M_{\delta_{es}}$

Table B-9. Matrix of Z_{θ_2} Configurations

Configuration Real Roots	$Z_{\theta_2} = -1/T_{\theta_2}$ rad/sec			
	$-.3$	$-.6$	-1.2	-2.0
$T_2 = 4, \lambda_{sp_2} = -1$	S45	S42[1]	S46	
$T_2 = 2, \lambda_{sp_2} = -2$	S25	S23[1]	S26	S27

Note: $M_{\delta_{ES}} = .341$ rad/sec^2/in.

(1) S23 and S42 also listed in Table B-8

Table B-10. Control Sensitivities and System Dynamics

Configuration	$M_{\delta_{ES}}$ rad/sec^2/in	M_{F_S} rad/sec^2/lb	Actuator No.
L71, L72, L73	.434	.062	2
S21–S27, S41–S46, S60–S63	.341	.049	2
S41A–S44A	.085	.012	1
S44B	.085	.012	2
F0, F1, F2, F4, F6	.086	.012	1

Actuator No. 1: First order, $1/\tau = 20$ rad/sec (FCS Config. G with pitch aug. OFF, Fig. C-10(a))

Actuator No. 2: Second order, $\zeta = .7, \omega_n = 75$ rad/sec (FCS Config. U, Fig C-11(a))

Feel System: $F_S/\delta_{ES} = 7$ lb/in, $\zeta_{FS} = .2, \omega_{n_{FS}} = 26$ rad/sec

84

Table B-11. Miscellaneous Configuration Characteristics

Config. Group	$V_{A_{pp}}$ Knots	ω_{n_p} rad/sec	ζ_p	Z_{θ_1} rad/sec	$d\gamma/dV$ deg/knot
F	145	.08 to .2	.01 to .6	−.08	−.054
L	120	.2 to .3	.15 to .8	−.08	−.012 to −.003
S	145	.2	.42 to .45	−.07 to −.14	−.023 to −.149

Table B-12. Nonlinear F-111A Simulation Configurations

Configuration	Aerodynamics (Coefficients)	$\bar{X}_{cg}$	FCS
AF111F	Nonlinear	.35	F-111A
AF111G	Nonlinear	.35	Generic
F111U	Nonlinear	.35	Aug. OFF

Table B-13. Linear Augmented F-111A Simulation Configurations

Configuration	Aerodynamic Coefficients	$\bar{X}_{cg}$	FCS	δ_h/a gain
AF0	Linear (FO)	.35	Generic	.7
AF1	Linear (F1)	.44	Generic	1.05
AF2	Linear (F2)	.505	Generic	1.55
AF4	Linear (F4)	.465	Generic	1.25
AF6	Linear (F6)	.453	Generic	1.20

report (Ref 8). The appropriate aerodynamic coefficients (C_{L_o}, etc.) were calculated for the F-111A geometry and mass but for the LAHOS 120 knot approach speed, so the coefficients are unusually large. The S configurations were derived from the F-111A by a pole placement technique, so the short period roots are essentially at the desired nominals and the phugoid roots are held fixed. The matrix of configurations shown in Table B8 was designed to define the independent effect of λ_{sp_1} and λ_{sp_2} on pilot rating (PR) as well as their interaction. Overlap with F-111A and LAHOS configurations was also desired. Configuration F1 was intended to provide comparison with neutral static stability, but resulted in somewhat more stability ($T_{1/2}$ = 7 sec). The value of $T_{1/2}$ or T_2 is very sensitive to c.g. position for values larger than six seconds (i.e., $-0.1 < \lambda_{sp_1} < +0.1$). This suggests that pilot rating may not be a significant function of T_2 or $T_{1/2}$ in this range.

The matrix of configurations displaying the variations of the large θ/F_s transfer function zero ($Z_{\theta_2} = -1/T_{\theta_2}$) is given in Table B9. The values of Z_{θ_2} were selected to explore the independent effects of Z_{θ_2} with respect to two of the configurations in the λ_{sp_1}, λ_{sp_2} set, S42 and S23. These two were selected because they had the same ratio of $\lambda_{sp_1} : \lambda_{sp_2}$.

B.4.1.3 Additional Configuration Parameters and Characteristics

The pitch control sensitivities and the control system dynamics are given in Table B10. The LAHOS baseline actuator (Ref. 8) was used as the baseline for the S configurations because it was faster than the F-111A actuator. The LAHOS feel system dynamics were used throughout, though the stick damping realized was about half that used in LAHOS. The pitch stick-force gradient (F_s/δ_{ES}), held fixed throughout at 7 lb/in, was a compromise between the LAHOS 8 lb/in and the F-111A 6 lb/in. The control sensitivity, $M_{\delta_{ES}}$, set by the gearing (δ_h/δ_{ES}), was selected to agree for the L configurations with the LAHOS value (nominal from Ref. 8), and for the F configurations with the F-111A augmentation off (mechanical) value. For the baseline S configurations, a single value of sensitivity $M_{\delta_{ES}}$ (actually δ_h/δ_{ES}) was used which was

selected by the pilots during preliminary evaluations as the optimum for the unstable configurations. Configurations S41A to S46A and S44B allow comparisons of the effect of the lowered sensitivity (one quarter) with both the first-order F-111A actuator and the second-order LAHOS actuator.

Certain configuration characteristics which were not viewed as simulator experiment parameters are listed in Table B11 for reference. Approach was decreased from 145 to 120 knots for the L configurations because these were intended to duplicate the LAHOS (Ref. 8) results in order to validate or calibrate the simulator. The phugoid characteristics were low-frequency oscillatory for all configurations, with the T_{θ_1} zero (Z_{θ_1}) small. Whereas the phugoid was fixed for the S configurations, the variation in the F configurations is a consequence of the c.g. shift and in the L configurations, a consequence of varying M_α (actually δ_{ES}/α gain). The values of $d\gamma/dV$ are all negative so the airplanes are all "front-side". As shown in Reference 2, Section 3.2.1.3, the following approximation is generally valid

$$\frac{d\gamma}{dV} \approx \frac{-1}{g} \frac{1}{T_{h_1}}$$

The Reference 2 data show that, for $1/T_{h_1} > 0$, pilot rating is essentially independent and invariant of $1/T_{h_1}$. So, for $d\gamma/dV < 0$, this parameter should have no significance to the results. Lateral-directional characteristics were held invariant throughout the simulation program.

B.4.1.4 <u>Augmented Configuration Characteristics</u>

Table B12 defines the augmented and unaugmented nonlinear F-111A evaluation configurations. The unaugmented configuration F111U (for C_L, C_D, C_m see Figures C6, C7, and C8 in Appendix C) was compared with F0 (Table B7) to determine the effect of the nonlinearities for these stable .35 cg configurations. For the evaluation tasks, the pilots detected no difference between the configurations. The augmented configurations AF111F and AF111G were used to compare the normal F-111A FCS as simulated to the "generic FCS" which was used as the baseline

augmentation system in the evaluation program. The pilots liked the Generic (G) FCS configuration somewhat better than the F-111A (F) FCS configuration, with pilot ratings about equal in smooth air (PR $\approx$ 2.5) but the Generic FCS was better in turbulence (2.5 for G, degraded to 4 for F).

The philosophy behind the design and use of the Generic FCS as the baseline augmentation system for the simulation program was to have a simple augmentation system which could be readily analyzed as apposed to the complex, higher order F-111A system with its feedback compensation and forward-loop filters. The structure of the two control systems is shown in Figures C9 and C10 of Appendix C.

The F-111A pitch system (Fig. C9(a)), as mechanized, uses q and n_z as primary feedbacks with α and $\dot{\alpha}$ feedbacks (air sensor) added for flaps extended (n_z is dropped in the actual system). The function of the feedback compensation or inverse model is to provide zeros which attract the short period poles to desirable locations. The α feedback, part of the F-111A "pitch trim compensation system", was found necessary to provide static stability at low speed, and $\dot{\alpha}$ compensates for lag in the system. The "lag" in the forward loop filters the pilot's input. The adaptive gain changer was set to 1.0 for the landing simulations. For roll control the airplane uses differential left and right horizontal tail deflection as well as spoilers, and as mechanized the F-111A FCS (Config F) had a left and right servo to mix pitch and roll inputs. The roll and yaw control systems are depicted in Figures C9(b) and C12, with roll and pitch mixing depicted in Figure C9(c). Failure of pitch augmentation leaves only the mechanical system with its reduced gain (-3.28 deg/in).

The structure of the generic pitch FCS is shown in Figure C10(a) in its most generalized form, but was mechanized with zero pitch rate (q) gain as the $\dot{\alpha}$ feedback, retained from the F configuration, provided all the necessary damping. The augmented short-period roots for configuration AF111G had

$$\omega_n \approx 1.4 \text{ rad/sec}$$

$$\zeta \approx 1.0$$

which is well within the Level 1 boundary for

$$n/\alpha \simeq \frac{V}{-g} Z_w = 4.8 \text{ g/rad}$$

Theoretically, it makes no difference what variables are fed back since any output (used for feedback) can be generated from any set of state variables to yield a desired pole-zero result. Practically, certain variables are more readily measured and lead to simpler feedback structure than others. Taking note of these facts, the Generic system used α feedback to provide conventional static stability and adjust short-period frequency, and $\dot{\alpha}$ feedback for short period damping. The α feedback was changed as a function of c.g. position (see Table B13) so that the same stability level was achieved for each c.g. The use of $\dot{\alpha}$ for damping does not affect steady states, so no washout is needed as with q feedback. Booth, et al. (Ref. 52) designed and evaluated in flight four augmentation systems of the generic type (n_z, q, α feedback) for an advanced fighter throughout its flight envelope. Their work provides design guides and shows that such systems can provide excellent flying qualities (PR = 1 and 2).

The generic system had separate pitch and roll servos (not left and right) whose outputs were each sent to left and right actuators (like the actual F-111A FCS). This scheme allows roll inputs to be limited to antisymmetric (equal left and right differential) inputs to the horizontal tail. Otherwise, as with the F configuration FCS, roll inputs could effectively produce pitch inputs which the pilots found objectionable. The roll system used with the generic pitch system, depicted in Figure C10(b), differs from the F configuration roll system only in the servo and pitch-roll mixing, depicted in Figure C10(c). Failure of the generic pitch augmentation system leaves only the mechanical system with reduced gain.

B.4.2 Evaluation Task

The pilots were asked to evaluate a given configuration for the overall task of making an ILS approach and precision landing under instrument conditions. Each configuration was evaluated in a sequence of

three separate, distinct approach and landings (A, B, C) which differed in starting point, turbulence level, and lateral offset from the runway at breakout.

Approach and Landing Run A.- The run started 5.5 miles out from runway threshold, at 1100 ft. altitude, with a lateral offset of 150 ft. from the localizer. The airplane was trimmed for level flight at approach speed, flaps and gear down (wing sweep at 16^0 for the F-111A), heading parallel to runway, and flight was on instruments. The pilot was asked to feel out the airplane, longitudinally and lateral-directionally, while flying toward glide-slope intercept at roughly constant altitude. The $\gamma = -3^0$ glide slope was acquired 3.5 miles out and maintained until breakout (airport and runway visual scene appeared) at 200 ft. altitude. The pilot was then asked to continue the approach visually (short final), flare to a low sink rate, and touchdown at the 1500 ft. mark. Touchdown was indicated by simulated "tire squeak". The glide slope intercepted the runway at the 1000 ft. marker. Turbulence was negligible, either none or at a very low level, so the air was smooth. There were no winds. There was no "hidden" offset of the localizer or glide slope.

Approach and Landing Run B. - The run started three miles out, at 900 ft, on glide slope and localizer. Turbulence was "moderate" (σ_w = 5.2 fps at 20 ft altitude) but there was no wind. There was a 150 ft hidden offset of the localizer, randomly selected to left or right, so if the airplane was on localizer at breakout, then the pilot had to execute a rapid lateral sidestep maneuver visually to get onto the correct approach path. Run B was a shortened version of Run A with added turbulence and hidden localizer offset.

Approach and Landing Run C. - This run was the same as Run B except the turbulence was "heavy" (σ_w = 7.0 fps), and there was no hidden localizer offset.

The above sequence of landing tasks was designed to allow the pilot to feel the airplane out at altitude, and provide at least three landings

for each configuration with ILS and visual approach tasks, and the flare and precision touchdown task which has been shown to be so important (Ref. 8 and 43). It also allowed the independent evaluation of the effects of turbulence, and included a fairly severe lateral maneuver to show up coupling problems. It particularly allowed the pilot to feel out the airplane by itself, free of the effects of turbulence, on the inbound portion of the A run.

Where the effects of control authority were being investigated, with no change in stability, the A run landing task with its negligible turbulence would have wasted valuable simulation time. Accordingly, for these type variations a combination of Run A and Run B, called Run D, was used, followed by a C run.

Approach and Landing Run D. - Run started 5.5 miles out and proceeded as in Run A. At 900 ft altitude, after glide slope acquisition, moderate turbulence was added, and the run proceeded as in Run B including the randomly selected right or left 150 ft hidden localizer offset on breakout.

B.4.3 Pilot Rating and Comments

After each run, the pilots were asked to make comments and assign Cooper-Harper pilot ratings (PR) for each of the subtasks in the run. These data were collected on a tape recorder. The pilots were provided a card which prompted them to answer specific questions and assign specific ratings. The pilot rating and comment card was revised, part way through the program. At the same time, the Cooper-Harper scale was interpreted with respect to the description of "Demands On The Pilot", and standards for desired performance, adequate performance, and controllability were defined. The bulk of the data collected used the revised card, pilot ratings, and rating scale interpretation.

The Cooper-Harper rating scale from Reference 51 is presented in Figure B16. In attempting to apply the Cooper-Harper scale to the approach and landing evaluations, some discrepancies in the description of the "Demands On The Pilot" (column four, Fig B16) were uncovered. The words "desired" and "adequate" are used to describe levels of perfor-

mance. Examining PR = 4 and 5, while performance goes from desired (4) to adequate (5), the pilot compensation required goes from moderate (4) to extensive (5). If these descriptions are taken literally, then there is a large difference between PR = 4 and 5: the work-load gets much heavier, while at the same time, the performance falls from desired to only adequate. The evaluation pilots, all highly experienced Boeing test pilots, agreed that some re-interpretation of the scale should be made and that the following approach should be adopted for the landing task. Adequate and desired performance were equated. Extensive and intensive, as applied to pilot compensation in describing PR = 6 and 9, were called maximum. The pilot rating scale as revised is shown in Figure B-17.

Three levels of performance are thus defined by the rating scale: desired performance which reflects a satisfactory landing, controllabilty or a controllable landing which reflects a safe landing, and loss of control in landing which reflects unsafe conditions with possible injury to the pilot or damage to the airplane. Table B14 shows explicitly how

Table B-14. Demands on Pilot in Landing Task

Pilot Rating	Pilot compensation required for	
	Desired Performance	Control
1	None	--
2	None	--
3	Minimal	--
4	Moderate	None
5	Considerable	None
6	Maximum	Minimal
7	Not Attainable	Moderate
8	--	Considerable
9	--	Maximum
10	--	Not Attainable

Definition

None:	— basic workload for task
Minimal	— noticeable increase in workload, not difficult
Moderate	— difficult workload, can be maintained for long periods
Considerable	— demanding workload, exceeds amount admissible for daily use, but does not require best effort
Maximum	— best effort is continuously required
Not Attainable	— exceeds pilot capability
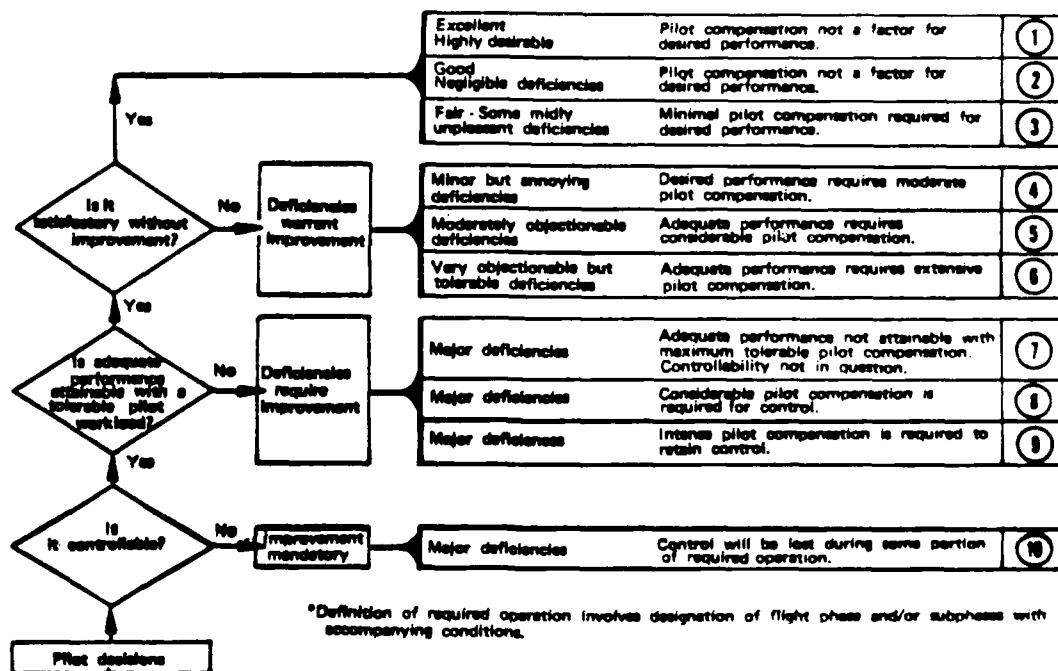
Figure B-16.   Cooper-Harper Pilot Rating Scale
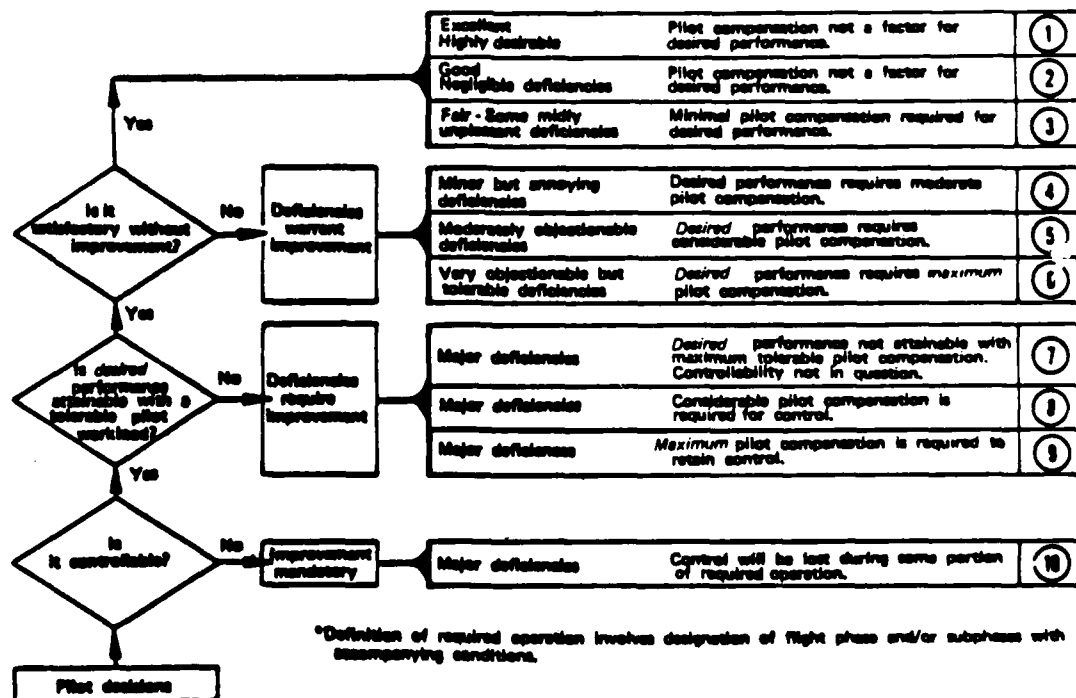
Figure B-17.   Cooper-Harper Scale as Modified for Approach and Landing Task

93

pilot workload varies with pilot rating for the performance levels. Table B15 quantifies the tasks in terms of approach and landing performance parameters. Controllability, explicitly loss of control, refers to any part of the landing task. For example, if the pilot loses control due to a divergent PIO while attempting to flare and touch down, but finds that he can regain and readily maintain control by waving off, this situation still reflects loss of control in landing, with a 10 the appropriate pilot rating.

The evaluation pilots were given an "Evaluation Card" to be used in tape recording pilot comments and assigning pilot ratings. The card used initially was revised part way through the program. The bulk of the evaluations used the revised card which is presented in Figure B18. The original evaluation card was different in that it asked for a pilot rating for the visual portion of the landing including flare and touchdown, plus an overall pilot rating. The two sets of pilot ratings as obtained with the original and revised evaluation cards are summarized below.

Pilot Ratings

Original Eval. Card	Revised Eval. Card
ILS	ILS
Visual, flare, touchdown	Visual short final
Overall	Flare, touchdown

Each card asked for three pilot ratings. It was noticed that the pilots gave an "overall" rating, using the original card, that was usually the same as the poorer rating of the "ILS" or "visual". The pilots felt that the overall rating was rather meaningless. At the same time, the pilots found the visual rating hard to arrive at because there were distinct flying qualities differences between the visual short final and the flare and touchdown maneuver. Accordingly, the "overall" rating was dropped, and the "visual" rating separated into one for the visual short final and one for the flare and touchdown.

Table B-15. Performance Standards for Landing Task

	Performance Level	
	Desired	Controllable
ILS		
Glide slope	1/2 dot	1-1/2 dots
Localizer	1 dot	2-1/2 dots, symbol not against stops
Airspeed, from target	+20 to 0 knots	+30 to -10 knots, no stall warning
Other		In position at visual transition where safe landing can be made
Landing		
TD dispersion:		
Longitudinal, down runway	1000 to 2000 ft	. 0 to 3000 ft
Lateral, from center	± 25 ft	±75 ft, inside white lines
TD airspeed, from target	+10 to -5 knots	+25 to -10 knots
TD sink rate	100 to 300 fpm	0 to 700 fpm, within structural limits
Other	Minimal lateral drift, steady attitude control in flare	Can stop safely on runway without damage or injury

Loss of control (PR = 10)

Refers to landing task, not wave off exclusively (i.e., if airplane has uncontrollable PIO in flare and touchdown, then PR = 10, even though it may be controllable in wave off).

Any unintentional pitch excursion greater than ±10°. Stall warning at any time. Inability to make landing within limits of controllable performance.

95

B.4.4 Simulation Procedures

The simulation was performed on the Boeing Visual Flight Simulator at the Kent Space Center. The simulation, described in detail in Appendix C, was fixed base. Though the baseline airplane was an F-111A, the simulation was of a single-engine single-seat fighter with variable sweep wings.

The right-hand seat of a transport cab was selected for the simulation because of its high quality flight instruments and center stick. The left-hand seat and unwanted flight instruments were blanked off with cardboard masks. The right-hand seat was used so the throttle would be on the left, normal for a single-seat fighter, and the throttles were ganged together to simulate a single-engine airplane. Gear, flaps, and wing-sweep handles were provided, though the landing evaluations were all made with gear and flaps down and wings forward.

The significant elements of the simulation consisted of the cockpit with flight instruments and controls, variable feel system, digital computer for solving the flight equations, and visual system which projected a view of the airport and runway on a screen in front of the pilot for visual flight. The visual system employed a large model of the airport and runway, viewed through a T.V. camera slaved to the pilot's eye position as computed by the digital computer, and projected onto a large flat screen located in front of the cab. Schematics and photos of the cockpit and visual scene are presented in Appendix C.

A preliminary evaluations program was conducted in order to familiarize the pilots with the simulator, various procedures, and the use of the evaluation card and Cooper-Harper pilot ratings. These preliminary evaluations also served to develop the simulator set-up, evaluation procedures, and to assist in selecting appropriate evaluation configurations.

Simulation evaluation sessions for collecting data were generally four hours in length and used one pilot. Actual evaluations were conducted in two 1 to 1-1/2 hour periods, separated by a half-hour break, with four to six configurations evaluated in each period. At the beginning and end of each session, standard check cases were run to ensure that the simulator was operating properly. Also, the evaluation

96

```
Run A - 5.5 mi out, no turbulence —
    Inbound
                Feel:  Forces - OK?
                        Sensitivity - OK?
                Lateral, directional:  OK?
                Pitch response:    Any problem
                                    PIO tendency
                                    Special inputs
                Airspeed control:  Any problems
    ILS
                Glide slope acquisition
                Maintaining glide slope
                Pilot rating
    Visual
                Pitch control
                Lateral maneuvers
                Difference from ILS:    Harder?
                                        Easier?
                Pilot rating
    Flare & touchdown
                Pilot rating
                Comments


Run B - 3 mi out, on glide slope, moderate turbulence
                Effect of turbulence:            Anything special
                Effect of lateral maneuver
                Pilot rating - change?


Run C - 3 mi out, on glide slope, heavy turbulence
                Effect of turbulence
                Pilot rating - change?
Summary
                Overall comments,  Runs A thru C
```

Figure B-18. Revised Pilot Evaluation Card

pilot was initially given one or more standard augmented airplane configurations (AF111F, AF111G or AF0, 1, 2, 4, or 6) to refamiliarize him with the simulation and to pick up any discrepancies or malfunctions.

A series of configurations was selected for each simulation session which included a range of flying qualities from good to bad. The order in which the pilot was given the configurations was somewhat random. The pilot was not told what the configurations were except for the augmentation warning lights which told him that pitch augmentation was ON or OFF (failure). Roll and yaw augmentation was always ON for evaluation configurations. Also, since some of the unaugmented configurations (e.g., L21 or LAHOS 2-1) had good flying qualities, the aug. OFF light did not necessarily clue the pilot that he could expect poor flying qualities. Repeat evaluations were included regularly, that is, the pilot was given configurations he had evaluated previously, earlier in the session or in a previous session, to check on the stability of his ratings and intra-pilot variability.

Each evaluation configuration was evaluated with the sequence of A, B, and C runs, except for the control authority investigations which used the D and C run sequence. After each run the pilot was asked to tape record his comments and pilot ratings, following the pilot evaluation card. Transcriptions of these tapes are found in Appendix G. The test engineer also took written notes on the pilot's comments and recorded the pilot ratings. The pilot was allowed to repeat any run he wished. Between runs A and B (or D and C), a calibration record of the configuration response to a test input was taken so the configuration could be subsequently checked to ensure its correctness. All evaluation runs were recorded on two 8-channel strip chart recorders, with each channel multiplexed so it could record two variables (details in Appendix C, Section 5.3).

B.4.5 Evaluation Pilot Background and Experience

Three evaluation pilots participated in the simulator flying qualities investigation. Their backgrounds are as follows.

Pilot A. - Boeing Production Test Pilot. Pilot A has been a production test pilot for six years, flying jet transport aircraft as well as a T-33 and light aircraft for special projects. Prior experience included 11 years as Naval Aviator flying combat carrier jet aircraft (including 200 carrier landings and 150 combat missions in F-4) and ASW aircraft, and 2-1/2 years as an aerodynamics engineer.

	Hours
Total flying time	4000
High-performance fighter and attack - jet	1800
Large multi-engine aircraft	1800
Light aircraft	300
Helicopter	100

Significant aircraft types: F-4, A-4, T-33, 727, 737, 747, P-2.

Education: BS - Mechanical Engineering
                    MS - Aeronautics and Astronautics

Pilot R. - Boeing Engineering Test Pilot. Pilot R has 29 years experience with Boeing as test pilot, starting on B-47 program and has flown on virtually all major Boeing flight test programs since then. Prior experience includes three years as aeronautical research pilot with NASA Ames, and four years in Army Air Corps which included two years flying B-17 and B-29 airplanes with 31 combat missions, and two years as Instructor Pilot in Advanced Twin-Engine Fighter School flying AT-6, AT-9, AT-17 and P-38 airplanes.

	Hours
Total flying time	10,800
Fighter time - jet	250
Fighter time - reciprocating	650
Bomber - jet	2,300
Bomber - reciprocating	1,100
Commercial - jet	4,500
Miscellaneous	2,000

Education: BS - Aeronautical Engineering

Pilot T. - Boeing Production Test Pilot. Pilot T has been a production test pilot for three years, flying jet transport aircraft as well as an F-86 on special projects and as chase, and before that for three years as an instructor flight engineer and simulator instructor pilot for Boeing. Prior experience includes five years with the U. S. Air Force flying high-performance T-38 jet aircraft as instructor pilot in aerobatics, formation, navigation, and instrument flight, and three years as aerodynamics and dynamics engineer.

	Hours
Total flying time	3100
High performance fighter - jet	1900
Large multi-engine - jet	900
Miscellaneous	300

Significant aircraft types: T-38, F-86, 727, 737, 747.

Education: BS - Aeronautical Engineering

MS - Aero/Astronautical Engineering

In the course of this experiment, Pilots A and R evaluated all configurations with very few exceptions. Pilot T evaluated all F-111 configurations (F and AF), all LAHOS configurations (L), and most configurations in the control authority investigation. The pilots made over 140 formal evaluations of the configurations including repeats, and probably as many preliminary evaluations.

Each pilot was distinctly different in the way he approached the flying task and in his performance as a controller, perhaps due to the distinct background and experience of each.

Pilot A. - Very smooth, moderately tight control. Used mostly very small inputs, kept errors moderate, frequency content of inputs was low. Technique was apt to cover up deficiencies in the airplane.

Pilot R. - Very loose control. Allowed errors to build before correcting. Used large infrequent inputs, with frequency content low. Techni-

que was apt to uncover deficiencies associated with larger amplitude excursions.

Pilot T. - Aggressive, tight controller. Used large frequent inputs, kept errors small, with frequency content of inputs high. Technique was apt to uncover deficiencies in closed loop stability, especially those associated with rapid, large inputs.

Each pilot also had, because of background, a different approach to flying qualities evaluations. Pilot R was an experienced research pilot, having participated in numerous flying qualities investigations, and was thoroughly familiar with the use of the Cooper-Harper rating scale. Pilot A had experience in military air-combat training programs, some experience in flying qualities, but was only minimally familiar with the Cooper-Harper rating scale. He was analytically minded, questioned critically, and was the primary impetus which lead to revising the wording in the Cooper-Harper scale and defining performance specifications for use of the scale in the landing task. Pilot T had no previous experience with flying qualities evaluations using the Cooper-Harper rating scale. The following characteristics were observed in the manner in which each pilot eva'·ated the various configurations.

Pilot A. - Because of his technique, Pilot A had less trouble with the unstable configurations and generally rated these better than the other two pilots. On the other hand, he usually tested for stability on the inbound portion of the A run, and if he thought the airplane was unstable, then he refused to give the configuration better than a PR = 4, in some cases downgrading an otherwise PR=3 airplane to 4.

Pilot R. - Because of background and technique, Pilot R tended to have more trouble than the other pilots with the more unstable configurations. Also he was somewhat less tolerant of poor handling qualities. For example, he was observed to downrate configurations (PR=8) due to high workload, though performance in the task appeared to be reasonably good.

101

Pilot T. - Because of his background, Pilot T tended to rate configurations numerically better than he should have, based on his performance and pilot comments and the test engineers observations of workload. Also, because of his technique, Pilot T had less difficulty with the effects of turbulence and downrated B and C runs less than the other pilots. On the other hand, also because of technique, he was more prone to low-frequency instability or PIO and on occasion lost control of a comparatively good configuration. For example, on separate occasions he rated F1 in heavy turbulence as a 5 and a 10, the latter due to a low-frequency PIO in which he lost control in the flare (configs. were carefully checked for correctness).

These noted differences in piloting background and technique tend to add validity to the results, but also tend to add to inter-pilot variability of ratings.

B.4.6 Simulation Validation

Besides direct check-out of the math model, the landing approach simulation was validated in two ways. First, and of lesser significance, the simulator was flown by three pilots currently familiar with the F-111A airplane, one from the Air Force and two from NASA Ames, who were all assigned to the AFTI-111 program. The three substantially agreed that, overall, the simulation was reasonably good. One discrepancy noted was that approach angle of attack (AOA) for the F-111A is 10 degrees, whereas the simulator approached at α = 4 degrees. It was concluded, after some checking, that the difference was probably due to position error in the AOA measured and displayed in the F-111A airplane.

The second method for validating the simulation, a very significant one, involved duplicating four configurations from the LAHOS experiment (Ref. 8), three unstable ones (7-1, 7-2, 7-3) and the baseline configuration for these (2-1). The four simulator configurations L71, L72, L73, and L21 duplicated the LAHOS configurations in longitudinal characteristics, including feel system, actuator, and aerodynamics (except the simulator had C_{L_δ} = 0). However, the propulsion model was the simplified F-111A one (single engine with twice F-111A thrust,

Table B-16. Comparison of Pilot Rating Data from LAHOS Flight Tests and Simulator

LAHOS Config	Turb. Level	Pilot Rating Ovr'l/App/FTD		Sim Config	Turb. Level	Pilot Rating ILS/Visual/FTD		
		Pilot A	Pilot B			Pilot A	Pilot R	Pilot T
2–1	N	2/–/–	2/–/–	L21	N	3/3/3	2/2/2	1.5/1.5/1.5
2–1	N	–/3/–		L21	N	3/3/3		
7–1	N	4/–/–		L71	N	4/3.5/3	4/3.5/3.5	4/4/4
7–2	N	3/–/–		L72	N	4/4/4	6/5/5	3/3/3
7–3	M	4/2/–	6/6/3	L73	M	6/5/5	7.5/7/7	4/4/4
				L73	M	6/6/6.5		

Turbulence Level: N — Negligible (None to light)
                             M — Moderate

including A/B), the feel system gradient was 7 lb/in instead of the 8 lb/in LAHOS value, and lateral-directional characteristics were those of the augmented F-111A, well liked by the pilots, as were those in the LAHOS flight test experiment. Comparative pilot ratings from this simulation experiment and the LAHOS flight test experiment are given in Table B16, with pilot comments summarized in the following Table B17.

Comparison of the pilot ratings (Table B16) shows that the average simulator ratings are very comparable to the ratings obtained in the LAHOS flight tests. The simulation ratings were selected for the level of turbulence corresponding to that encountered in flight test. The LAHOS "approach" rating is comparable to the simulator "ILS" and "Visual"" ratings combined. The LAHOS "flare and touchdown" rating is directly comparable to the similar simulator rating. The individual differences in pilots, described in Section B.4.5, may also be noted in the ratings in Table B16: Pilot T's high rating of L21 (PR=1.5) and L73 (PR=4), and Pilot R's low ratings for L72 (PR=6) and L73 (PR=7.5).

Comparison of the synopsized pilot comment data in Table B17 again indicates that the simulation of the LAHOS flight test configurations was reasonably correct. One difference in the conditioning of the pilots is worth noting. In the LAHOS experiment, the unstable cases (7-1, -2, -3) were the exception and the pilots were not conditioned to look for instability. Thus, they tended to be puzzled by the origins of

103

difficulties encountered. On the other hand, the simulator pilots were conditioned to look for instability and so were often well aware of the source of problems. These differences in conditioning are noticeable in the pilot comments in Table B17.

The pilot comments for the LAHOS configurations from flight test are comparable to those for their simulated configurations. The more unstable configurations are found easier to handle in visual flight, especially in flare and touchdown (B.5.5 amplifier on this). Pitch attitude requires constant attention. Inputs need to be small. The airplane can not be trimmed, airspeed wanders, and the work load is high. However, flight path control is fairly good, even in flare and touchdown. The airplanes are flyable, can be landed safely, though work load is high though tolerable.

The comparison of simulator results indicates that the simulator does provide a valid representation of the flying qualities in approach and landing, but if in error, the errors will tend to be conservative with pilot ratings worse than would actually be realized in flight.

B.5 Simulation Results - Parametric Analysis

Pilot rating data for all flying qualities evaluations are presented in Table C9 of Appendix C. The corresponding pilot comment data is presented in Appendix G. The pilot ratings are plotted in this section versus the various experiment parameters to show the effect of these parameters and to provide organized data on which to base the development of flying qualities criteria for airplanes with relaxed static stability.

In order to compact the amount of data to be dealt with, the following general policy has been adopted. Most of the data are plotted using one pilot rating to represent the overall landing flight phase. This pilot rating is taken to be the worst (largest) pilot rating for any of the three landing subtasks: ILS approach, visual short final approach, flare and touchdown. Then a separate analysis is made of the relationship of pilot rating for the individual subtasks. The adoption of the worst pilot rating as indicative of the overall rating is both conservative and rational, since the airplane must be able to land safely from either a visual or instrument approach on through flare and touchdown.

Table B17. Comparison of Pilot Comment Data From LAHOS Flight Tests With Simulator

CONFIG.	PILOT	PITCH ATTITUDE	AIRSPEED	APPROACH		FLARE, TOUCHDOWN
				ILS	VISUAL	
LAHOS 2-1	A	GOOD. NO PIO. SOME OVERSHOOT TENDENCY	EASY	GOOD	GOOD	EASY
LAHOS 2-1	B	GOOD. NO PIO	GOOD		OK	NO PROBLEM, SOME EFFORT TO HIT TD POINT.
SIM L21	A	FINE. BIT SPRINGY, BOUNCY	SOLID	PITCH WOBBLES. BOUNCY. GLIDE SLOPE GOOD.	SAME AS ILS	WELL CONTROLLED
SIM L21	R	SENSITIVITY A BIT HIGH. NO PIO.	GOOD	NO PROBLEM	NO PROBLEM	GOOD
SIM L21	T	RESPONSE IMMEDIATE. NO PROBLEM. NO PIO. TURBULENCE DISPLACES PITCH	NO PROBLEM	EASY	PITCH GOOD. EASIER THAN ILS	VERY GOOD
LAHOS 7-1	A	FUNNY RESPONSE. DRIFTS IN LONG TERM. NO PIO	WENT WELL	WENT WELL. LONG TERM DIFFICULTY	WENT WELL	WORKED HARDER THAN DESIRED. DON'T KNOW WHY
SIM L71	A	LITTLE BOUNCY. NO PIO TURBULENCE STIRS UP	SHADE SLUGGISH	DOES WELL ON GLIDE SLOPE PLOWS THRU TURBULENCE.	EASIER THAN ILS	EASIER THAN ILS
SIM L71	R	SLUGGISH. DAMPING LOW. WORK LOAD OK.		FOLLOWS INPUT CLOSELY	EASIER THAN ILS	CONTROLLABLE. BUT SLUGGISH
SIM L71	T	WANDERS, MORE STICK ACTIVITY. NO PIO. TURBULENCE DISPLACES PITCH.		HIGHER WORK TURBULENCE REQUIRES MORE EFFORT	PITCH WANDERS SOME EFFORT	SOME EFFORT
LAHOS 7-2	A	FAIRLY PREDICTABLE. SPONGY. NO PIO.	PRETTY GOOD	WENT WELL	WENT WELL	SPONGINESS BOTHER-SOME. NO OBVIOUS PROBLEM.
SIM L72	A	SLIGHT PIO TENDENCY.	REASONABLE. MORE STABLE (THAN L71)	OK. HOLDS FLIGHT PATH, PITCH RE-QUIRES EFFORT. TURBULENCE STIRS PITCH	SAME AS ILS	BIT OF PIO IN FLARE. DIDN'T GET AWAY.
	SUMMARY	PITCH INSTABILITY REQUIRES CONSTANT ATTENTION. FLIGHT PATH READILY MAINTAINABLE. AIRPLANE FLYABLE. CAN DO JOB YOU WANT, BUT HAVE TO WORK AT IT.				
SIM L72	R	UNSTABLE. CAN CONTROL IT, I HAVE TO SPIKE IT TO STOP PITCH.	FAIRLY DIFFICULT TO CONTROL	GOOD HOLDING GLIDE SLOPE WORKLOAD ON HIGH SIDE.	BETTER THAN ILS. CAN SMOOTH WITH SMALL INPUTS.	EASY TO HANDLE.
SIM L72	T	GREATER SENSITIVITY. WANDERS. HAVE TO BRING BACK AFTER INPUT. TURBU-LENCE MORE EFFORT. NO PIO		EASY	LITTLE HARDER THAN ILS	MORE EFFORT THAN NORMAL. MORE PITCH DUE TO TURBU-LENCE.
LAHOS 7-3	A	OK. NOT AS GOOD FOR AGGRESSIVE INPUTS. NO PIO	TURBULENCE AFFECTED.	GOOD	OK	WORKED HARD ON PITCH
LAHOS 7-3	B	INITIALLY SLOW. USE HIGH GAIN WELL. DITHER TYPE.	OK	VERY POOR. NOT GOOD ON INSTRU-MENTS	BETTER THAN ILS	NO BIG PROBLEM. USED TIGHT ATTITUDE CONTROL
SIM L73	A	QUITE UNSTABLE. MILD PIO. REQUIRES ATTENTION. PITCH AND INSTABILITY WORSE IN TURBULENCE.	HARDER. WANDERS. NO TRIM.	MORE DIFFICULT IN TURBULENCE	SIDE STEP CAUSED DIFFICULTY	A LITTLE HARDER.
SIM L73	R	UNSTABLE. DIVERGES. CAN'T TRIM. NO PORPOIS-ING. WORK LOAD HIGH.	DIFFICULT DUE TO PITCH DIVERGENCE	HOLD GLIDE SLOPE OK. WORK LOAD QUITE HIGH	NEED SMALL INPUTS, BIG INPUTS MAKE SINK RATE HARD TO CONTROL. EASIER THAN ILS.	HARD TO CONTROL SINK RATE. TROUBLE GETTING CONTROLLED TOUCHDOWN. HIGH WORK LOAD
SIM L73	T	MORE SENSITIVE THAN STABLE AIRPLANE. MORE CONTROL ACTIVITY TO CONTROL PITCH. TURBU-LENCE ACCENTUATES PITCH INSTABILITY. NO PIO.	NO PROBLEM.	MINIMAL COMPEN-SATION TO KEEP WHERE WANTED TURBULENCE MAKES HARDER.	PITCH CON-TROL GOOD TURBULENCE MAKES HARDER	GOOD CONTROL ON LANDING. TURBU-LENCE MAKES HARDER.

105

The data are generally presented for three levels of turbulence, negligible, moderate, and heavy, but these should be recognized as A, B, and C type runs. Turbulence is an important environmental parameter, and its effect on the flying qualities depends on the airplane characteristics and the tasks involved, so it must be treated as a separate parameter. It should be remembered that the simulator was fixed base, so the pilot saw accelerations due to turbulence as disturbances on his cockpit instruments and as accelerations of the visual scene when flying visually, but the proprioceptive cues were missing. The same applies to the pilot's perception of the acceleration response to control inputs or any other input or disturbance.

The primary characteristics of the various configurations for investigating the effect of stability level are presented in Table B18 for ready reference. These are the unaugmented (in pitch) configurations and they include the two stable baseline F-111A (F0) and LAHOS (L21) configurations.

B.5.1 Effect of c.g. Position (F Config's)

The effect of c.g. position was investigated using the F-111A as provided by the F configurations (F0, F1, F6, F4, F2). The pilot ratings for each pilot, separated by run type (A, B, C), are plotted in Figure B19, parts (a), (b), and (c). Curves have been faired through each set of data points, and these average curves have been combined in Figure B19, part (d). The pilot ratings have been plotted versus the value of the unstable root (λ_{sp_1}) rather than the time to double amplitude (T_2). Plotting PR vs λ_{sp_1} is much preferred because it eliminates the meaningless infinite discontinuity which arises as neutral stability is approached, and allows stable and unstable configurations to be plotted on a continuous scale. The values of T_2 and $T_{1/2}$ corresponding to λ_{sp_1} are given in Table B18.

The F configurations were baseline configurations, and as such were evaluated several times by each pilot. Some of these evaluations were performed very early, representing the first evaluations of unstable configurations the pilots were required to make, but the others were evaluated at various points through the program including well toward the

Table B-18. Primary Configuration Parameters

BASELINE CONFIGURATIONS:

CONF	$T_2(T_{1/2})$	λ_{SP_1}	λ_{SP_2}	Z_{θ_2}	$M_{\delta_{ES}}$	V_{app}	C.G.
FO	(1.346)	.903	.570	-.60	.086	145.	.35
L21	(.53)	2.29	.570	-.76	.434	120.	.45

UNSTABLE (OR NEUTRAL) CONFIGURATIONS:

CONF	$T_2(T_{1/2})$	λ_{SP_1}	λ_{SP_2}	Z_{θ_2}	$M_{\delta_{ES}}$	V_{app}	C.G.
F1	(6.9)	.100	-.82	-.59	.086	145.	.44
F6	7.6	.091	-.95	↓	↓	↓	.453
F4	4.5	.154	-1.04	↓	↓	↓	.465
F2	2.1	.331	-1.26	↓	↓	↓	.505
L71	7.4	.094	-2.02	-.69	.434	120.	.45
L72	4.3	.161	-2.18	↓	↓	↓	↓
L73	2.1	.330	-2.48	↓	↓	↓	↓
S60	6.0	.115	-0.30	-.58	.341	145.	.45
S61	↓	↓	-0.60	↓	↓	↓	↓
S62	↓	↓	-1.00	↓	↓	↓	↓
S63	↓	↓	-2.00	↓	↓	↓	↓
S41	4.1	.169	-0.60	-.58	.341	145.	.45
S42	4.0	.173	-1.00	↓	↓	↓	↓
S43	3.9	.178	-2.00	↓	↓	↓	↓
S44	3.9	.179	-3.00	↓	↓	↓	↓
S45	4.2	.165	-1.01	-.28	↓	↓	↓
S46	4.4	.156	↓	-1.18	↓	↓	↓
S21	2.0	.347	-.60	-.58	↓	↓	↓
S22	↓	↓	-1.00	↓	↓	↓	↓
S23	↓	↓	-2.00	↓	↓	↓	↓
S24	↓	↓	-3.00	↓	↓	↓	↓
S25	2.0	.347	-2.00	-.28	.341	145.	.45
S26	↓	↓	↓	-1.18	↓	↓	↓
S27	↓	↓	↓	-1.99	↓	↓	↓
S41A	4.1	.169	-.60	-.58	.085	145.	.45
S42A	4.0	.173	-1.00	↓	↓	↓	↓
S43A	3.9	.178	-2.00	↓	↓	↓	↓
S44A	↓	.179	-3.00	↓	↓	↓	↓
S44B	↓	.179	-3.00	↓	↓	↓	↓
S45A	4.2	.165	-1.01	-.28	↓	↓	↓
S46A	4.4	.156	↓	-1.18	↓	↓	↓

107
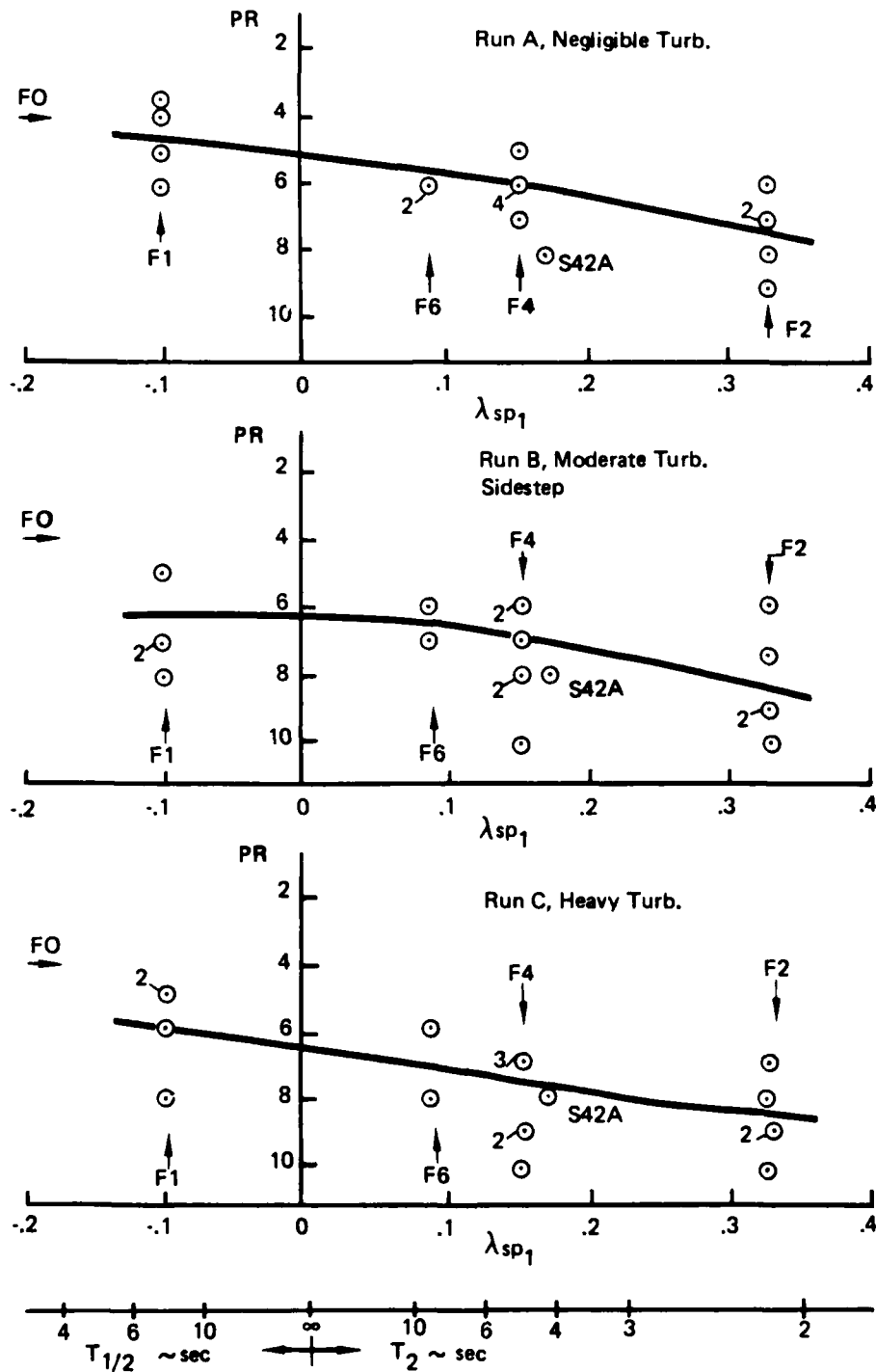
Figure B-19. *Effect of c.g. on Pilot Rating vs* λ_{sp_1} *– F, S42A Configurations*

(a) Pilot A

Figure B-19. Effect of c.g. on Pilot Rating vs λ_{sp_1} — F, S42A Configurations (Continued)
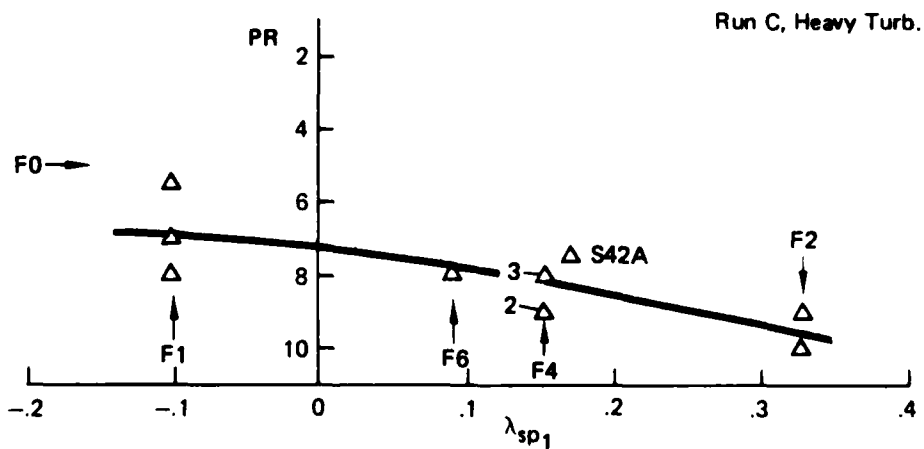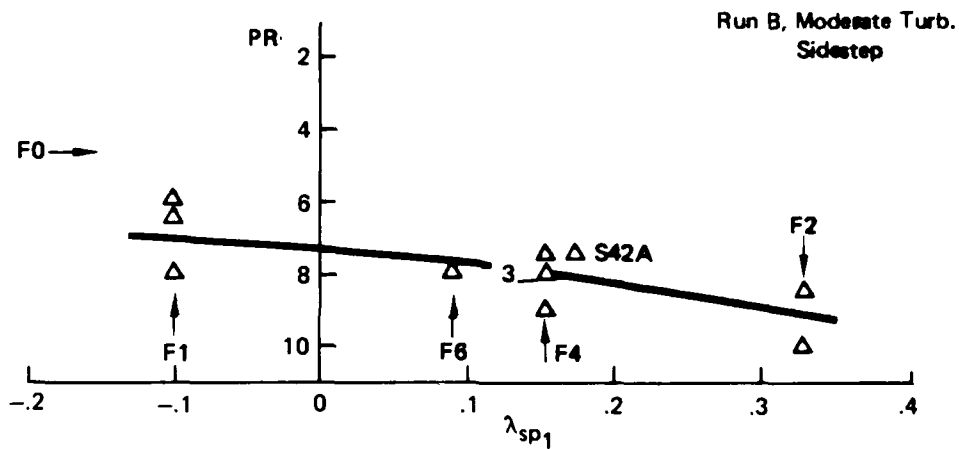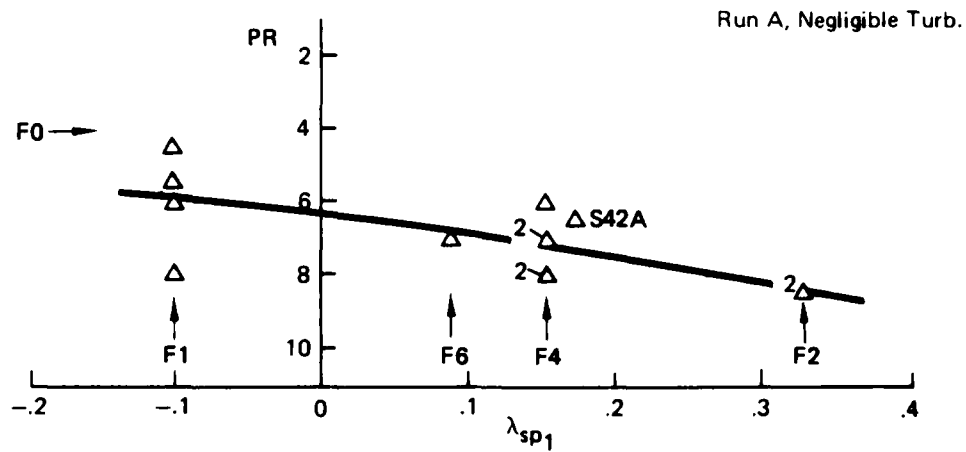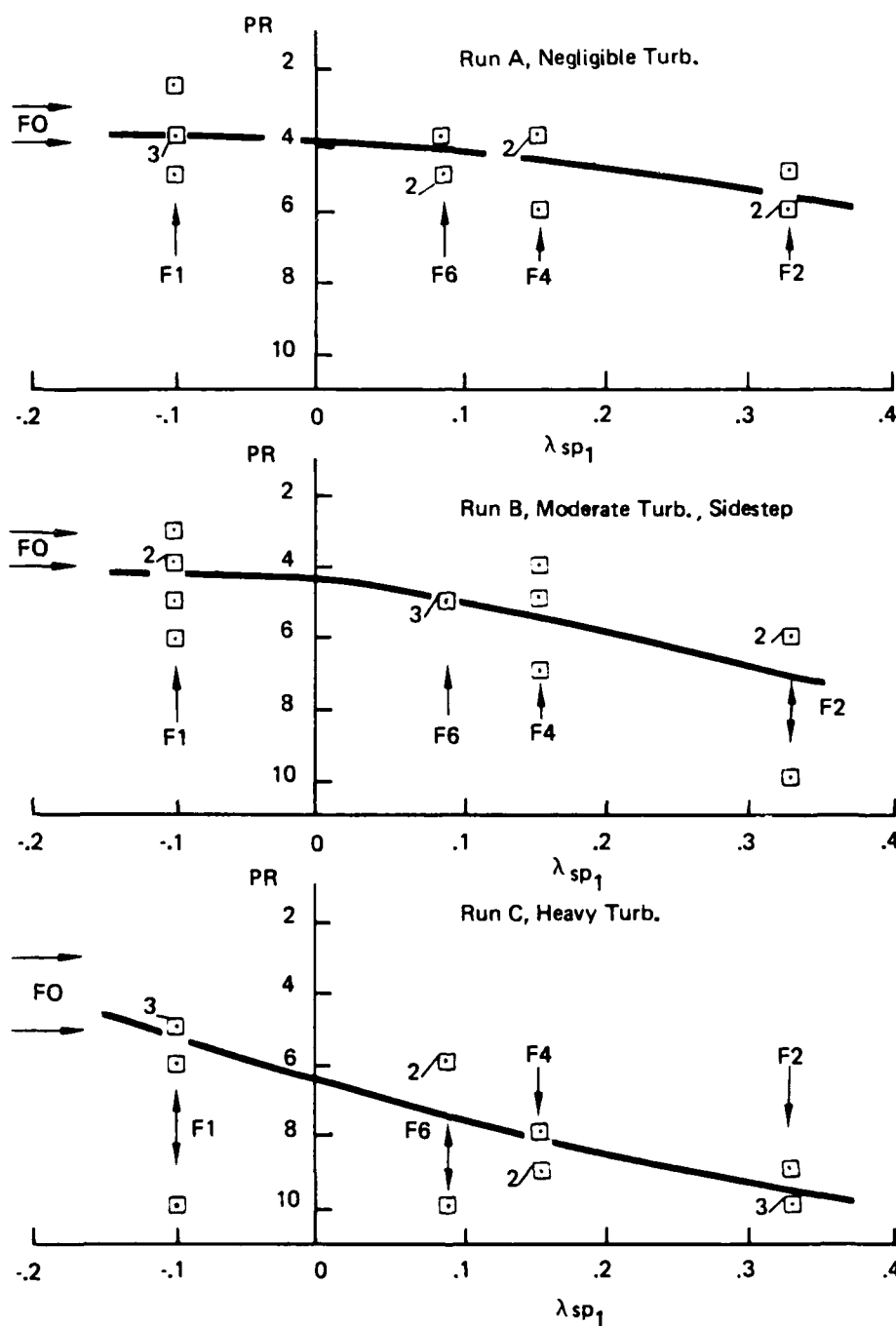
(b) Pilot R

Figure B-19. Effect of c.g. on Pilot Rating vs λ_{sp_1} — F, S42A Configurations (Continued)

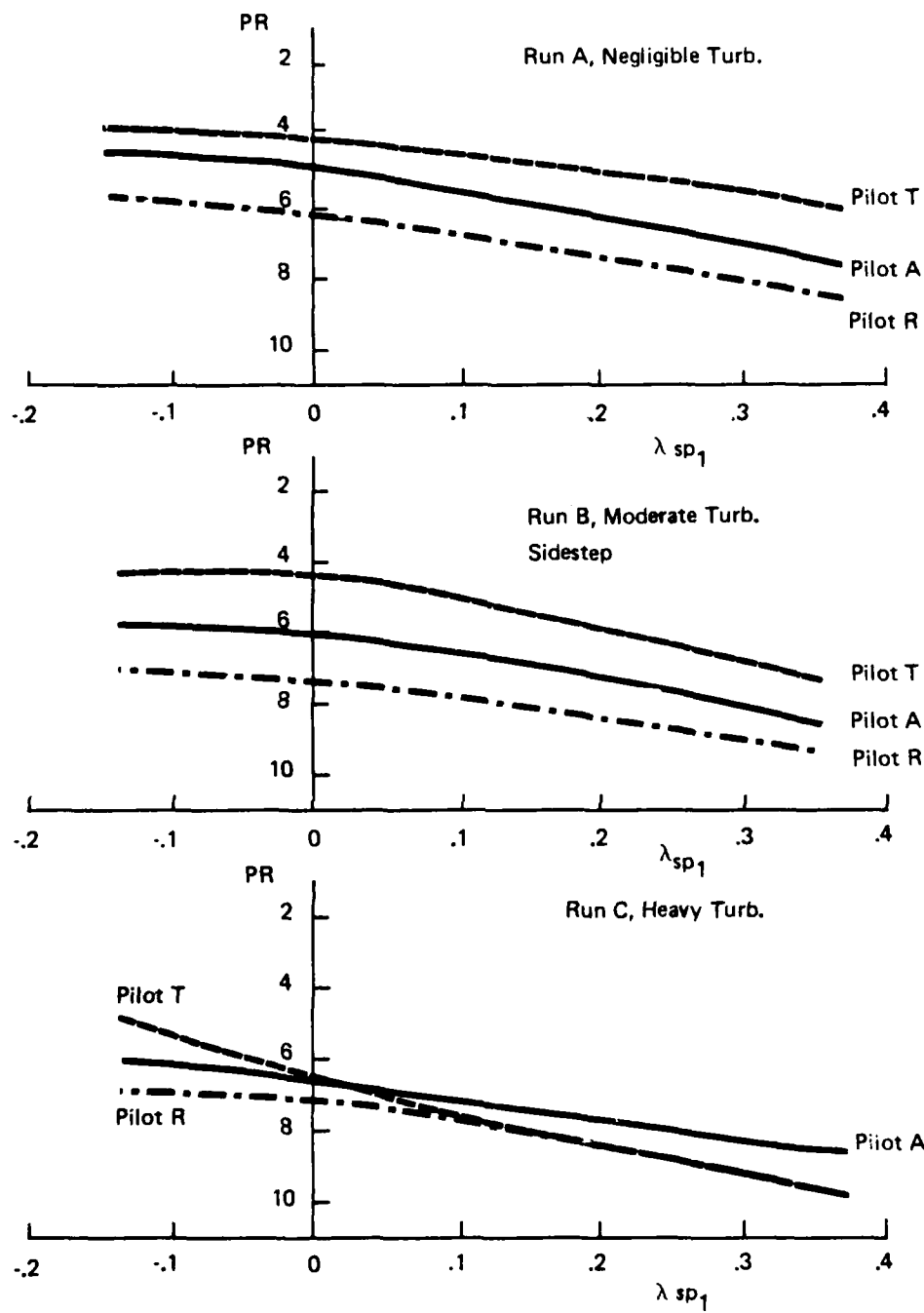(c) Pilot T

Pilot Rating: Worst of ILS, Visual, FTD

Figure B-19. Effect of c.g. on Pilot Rating vs λ_{sp_1} —F, S42A Configurations (Concluded)

(d) Faired Average for Pilots

111

end. Thus the pilot ratings in Figure B19 provide a basis for looking at intra-pilot and inter-pilot variabilility, including the effects of learning, as well as a description of the effect of aft c.g. location on the baseline F-111A airplane.

The curve of pilot rating (PR) with λ_{sp_1} is very flat. The decrease from F0, the stable case, to F1, which is near neutral stability but stable ($T_{1/2}$ = 6.9 sec), is not very much, about 1 pilot rating. There is even less change in pilot rating between F1 and F6 (T_2 = 7.6). The degradation with turbulence level is quite clear, and tends to affect the more unstable cases most. The pilot ratings deviate from the faired curve, with a few exceptions, by about 1 pilot rating at most.

Pilot T gave a 10 rating in one evaluation of F1 and also of F6, both with heavy turbulence. In the F1 case, he got into a low frequency PIO on attempting the visual flare and touchdown. He asked for a repeat, and the same thing happened. His comments say he was trying to "stair step" pitch attitude to get what he wanted. Four configurations later in the evaluation session, he was given F1 again (without his knowledge, of course) and he had no difficulty landing the airplane, and gave pilot ratings of 4/5/5 to the heavy turbulence (C) run. The configurations were carefully checked, and no difference or discrepancies could be found. Pilot T's 10 rating for F1 should probably be discounted.

The 10 rating for F6, Run C, by pilot T has a different origin: pitch-roll control interference effects. An examination of the F configuration FCS (Figure C9c) shows that the mechanical pitch input ($\delta_{ES\,mech}$, the only pitch input for F configs.) and the roll inputs ($\delta_{AS\,mech}$ and servo) sum to each actuator, and control deflection is limited at the actuator output (surface stops). Thus, if the pilot has full nose-down control and then adds a roll input or augmentation adds one, then one of the horizontal tails will come off the stop in response to the roll input, thus effectively putting in a nose-up pitch input. The pilots found this very disconcerting for the unstable cases. They did not understand what was happening, and generally ascribed the behavior to a large updraft (gust). Pilot T's comments indicate this type of behavior was why he downrated F6 to a 10 for this one C run.

The roll limiter and separate pitch and roll servos of the Generic FCS (Figure C10c) prevented this type of control coupling from

occurring. Examination of the available description of the F-111A FCS indicates this coupling can happen in the actual airplane, though not as severely as in the simulator. For aircraft with relaxed static stability this type of control coupling would be very undesirable, whether the augmentation is operative or failed.

A summary of the pilot rating data as well as the inter-pilot variability is shown by the curves in Figure B19d. The inter-pilot variation is about 1 pilot rating from the mean. Pilot A rates about 1 pilot rating better than Pilot R, for any turbulence level. Pilot T rates about 1 pilot rating above Pilot A for runs A and B. However, the heavy turbulence of run C apparently bothered Pilot T substantially more than the other pilots, and his ratings of unstable configurations degraded to those of Pilots A and R as indicated in Figure B19d. Pilot A's smooth, moderately tight control technique was most successful in dealing with the heavy turbulence for the more unstable configurations. The above comments and the trends shown in Figure B19 for the pilots can be used to help interpret the remainder of the pilot rating data.

An important fact to note about the data in Figure B19 is that the variations of λ_{sp_1} are not independent of other variations, as the data in Table B18 for λ_{sp_2} show, but are rather the consequence of aft c.g. movement for an airplane (F-111A) with λ_{sp_2}, Z_{θ_2}, and $M_{\delta_{ES}}$ (or M_{F_S}) as shown. The S configurations were specifically designed to investigate independent variations in these parameters. The data in Figure B19 is typical of what happens when an evaluation of aft c.g. locations is made for a given airplane in a given flight condition. However, the level of pilot rating or criteria for RSS airplanes can not be established by c.g. or C_{m_α} variations alone. This explains why different simulator and fight test investigations have produced such widely different results (e.g., Reference 8 and 24) based on T_2 (or λ_{sp_1}).

The pilot ratings for configuration S42A, rated only by pilots A and R, are included in Figure B19. The parameters for S42A and F4 are nearly identical, and the pilot ratings are very consistent except for Pilot A's evaluation in negligible turbulence (Run A) which appears low (too bad). The detailed ratings given in Table C9 show that Pilot A rated S42A low in flare and touchdown, and from pilot comments, found it much more

113

difficult than ILS or visual approach. The low (too bad) rating for S42A
by Pilot A is apparently just scatter, as are his 10 ratings for F4 in
moderate and heavy turbulance, also due to flare and touchdown problems.

B.5.2 Effect of Short Period Real Roots (λ_{sp_1} and λ_{sp_2})

The effect of the short-period real roots, λ_{sp_1} and λ_{sp_2}, was
investigated through the S configurations together with some F and L
configurations as outlined in the matrix of Table B8. However, the F
configurations have lower sensitivity ($M_{\delta_{ES}}$) and the L configurations
have a lower approach speed (120 knots) and can not be compared directly
with the S configurations.

The first series of plots, Figure B20a, b, and c, show the variation
of pilot rating with λ_{sp_1} for λ_{sp_2} = -0.6, -1, and -2, respect-
ively. Included in Figure B20c are LAHOS configurations L71 and L72. It
is important to recognize the difference between the variation with
λ_{sp_1} shown in these plots and those for the F configuration shown
previously (Figure B19). In Figure B20, the variation of λ_{sp_1} is
independent of λ_{sp_2}, Z_{θ_2}, or $M_{\delta_{ES}}$, which are held constant.
Note that for smaller λ_{sp_2} (-0.6 and -1), pilot rating gets worse,
increases, as λ_{sp_1} increases. But for λ_{sp_2} = -2 (Figure B19c),
there is essentially no variation of pilot rating with λ_{sp_1} in the
range tested (.115 to .347, or T_2 from 6 to 2 sec). Note that L71 and
L72 have pilot ratings that are very consistent with those for the S
configurations, which in themselves show minimum scatter. The constant
pilot rating with λ_{sp_1} or T_2 for λ_{sp_2} = -2 is at distinct
variance with most previously analyzed data, and strongly suggests that
any criteria based solely on T_2 will be quite inadequate.

Examination of the pilot comments for configurations S42 and S23 show
that they have close to Level 1 flying qualities. Of S43, Pilot A finds
"Noticeable instability - but didn't present any real problem - pitch
excursions were easily overcome - ILS a 4; visual was even easier - a 3;
FTD pretty much where I wanted it - a 3", but then "considering the
(instability) - both would have to be 4's but they are certainly good
4's"; in turbulence "effect was noticeable, more workload, pitch required
more attention, vertical speed seems less affected, (also) glide slope".
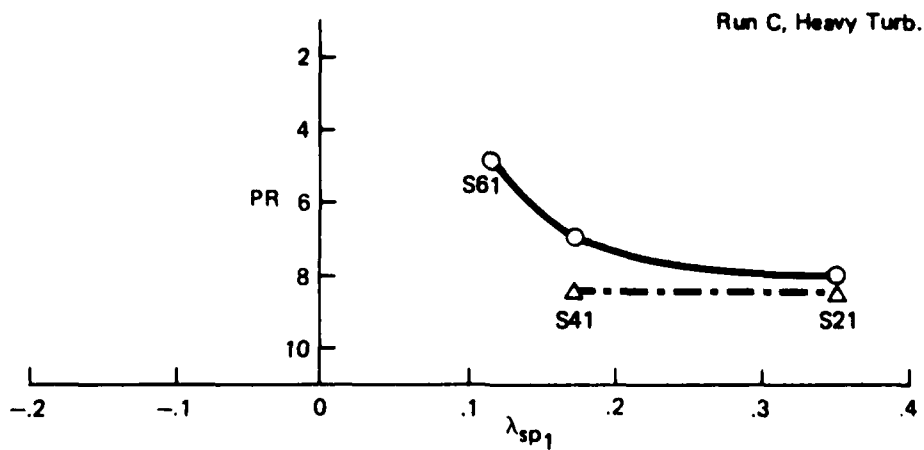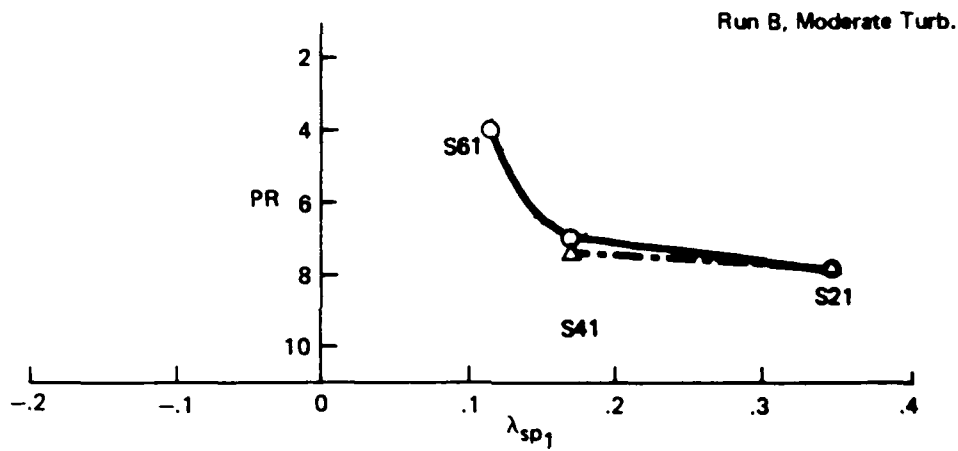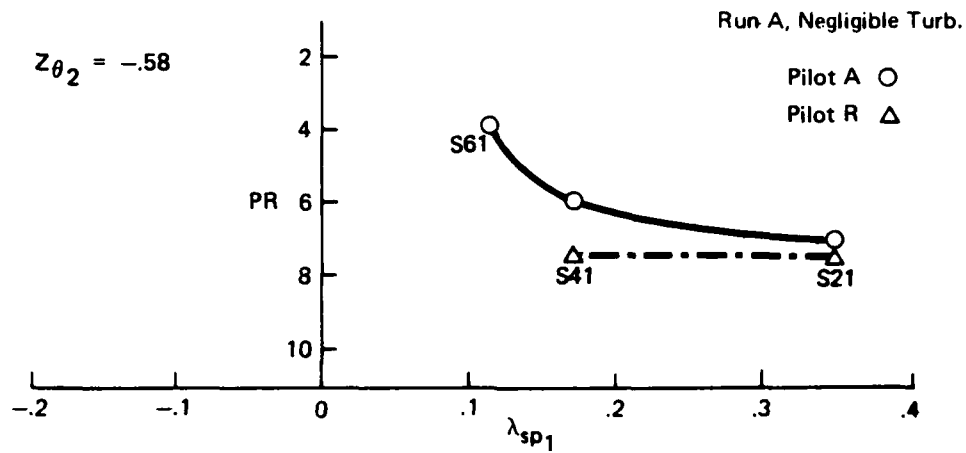
114

Figure B-20. *Pilot Rating vs Unstable Root* (λ_{sp_1})

(a) $\lambda_{sp_2} = -0.6$

115

Figure B-20.   *Pilot Rating vs Unstable Root* (λ_{sp_1}) *(Continued)*
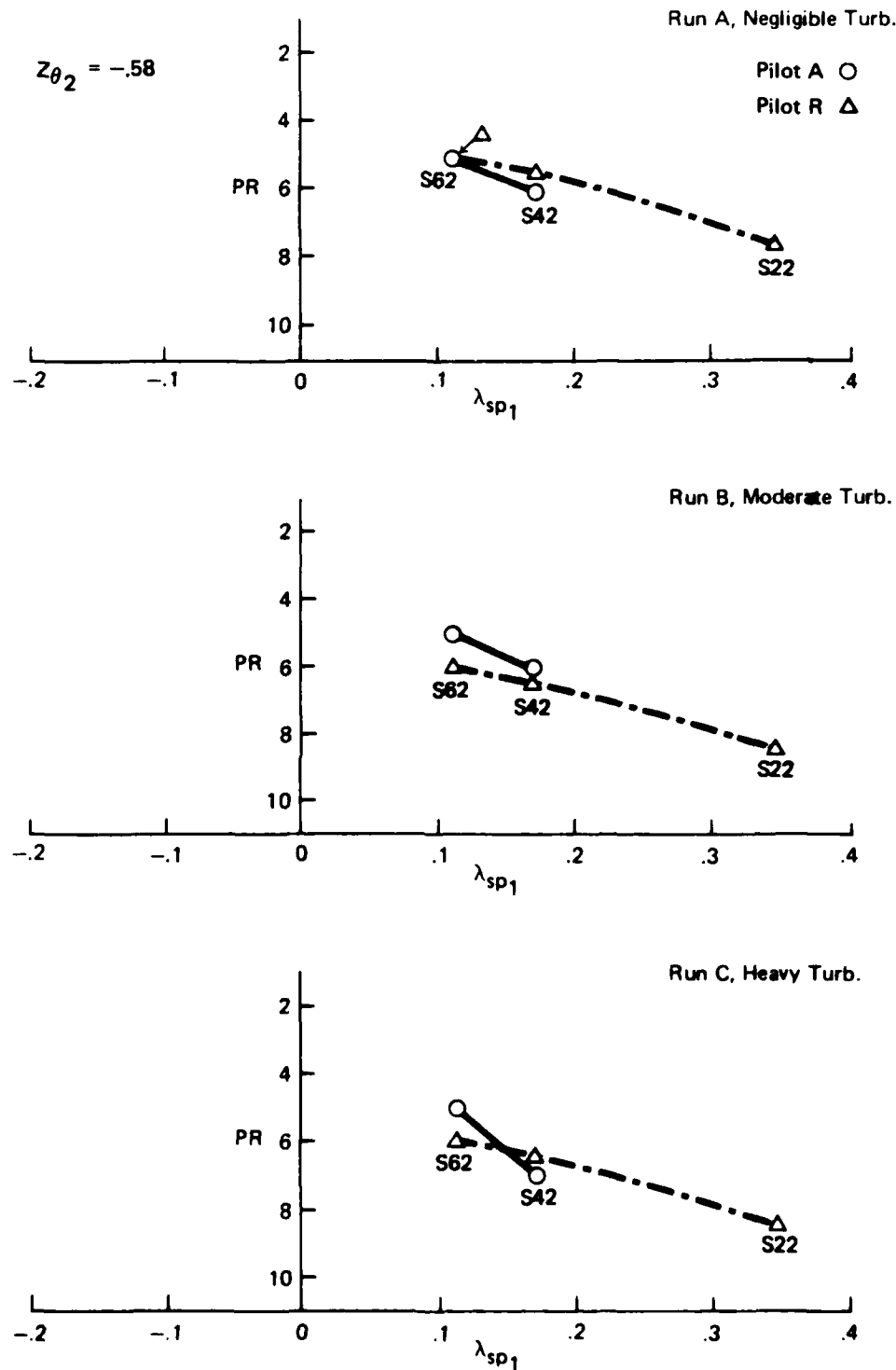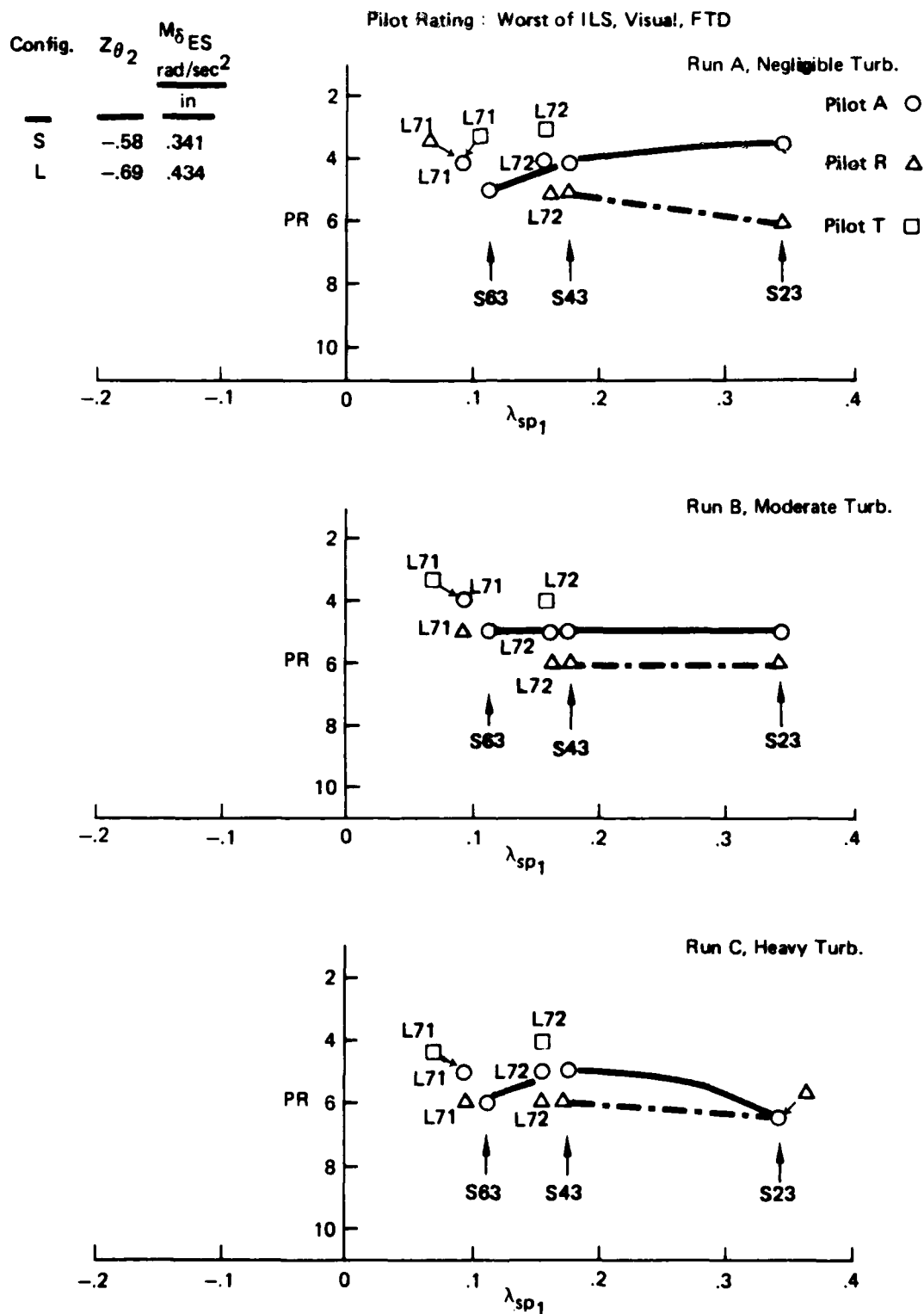
(b) $\lambda_{sp_2} = -1.0$

116

Figure B-20.   Pilot Rating vs. Unstable Root (λ_{sp_1}) (Concluded)

(c) $\lambda_{sp_2} = -2.0$

Pilot R finds S43 "unstable - but easy to handle - with heavy turbulence, didn't seem to create any problems".

Of S23, Pilot A says, "noticeable problem controlling pitch - instability or something going on there - but glide slope and airspeed, no real problem at all, a three for ILS, visual a 3.5 and FTD a 3.5 - no real problems". In turbulence, "effect noticeable, deteriorated ability to control airplane considerably - ILS is a five - visual didn't seem quite that bad but still call it five - FTD a five. Heavy turbulence made pitch attitude very difficult - everything degraded (6/6/6.5)". Pilot R finds S23 "tends to PIO more - tendency to over control - could stay reasonably close to glide slope - didn't give any particular problem particularly after breaking out - reasonably good landing characteristics even though unstable (5.5/6/6)". In turbulence, "work load went up - a little more trouble staying on glide slope - reasonably good response when I broke out - had good control of it (TD), surprised me that it worked out so well (6/6/6)". And heavy turbulence, "IFR and VFR still very satisfactory, didn't see any big change, PIO under visual more noticeable, ended up floating quite a ways (6/6.5/6.5)".

Clearly the pilots find S43 with its T_2 = 4 sec. and S23 with its T_2 = 2 sec. easy to fly, and even in severe turbulence they were able to obtain adequate performance without an excessive work load. They clearly saw the instability as a deficiency, but a tolerable one. Both airplanes are clearly Level 2 at worst.

The pilot ratings for the appropriate S and L configurations (Table B8) have been replotted in Figure B21 against the stable short period root (λ_{sp_2}) for λ_{sp_1} = .116, .173, and .347 (T_2 = 6, 4, and 2 sec respectively). The curves that have been faired through the three sets of data all have the same general characteristic shape: pilot rating remains constant with decreasing magnitude of λ_{sp_2} until a "critical value" is reached; below that, pilot rating drops off rapidly as the magnitude of λ_{sp_2} decreases further, heading for PR=10 or uncontrollable for λ_{sp_2} = 0 or positive. There are not enough data points, either for small negative or large negative values of λ_{sp_2}, to clearly define the curves drawn for each set of data. Not all S configurations were evaluated by both pilots A and R, and only the LAHOS configurations (L) were evaluated by Pilot T. However, if we use the
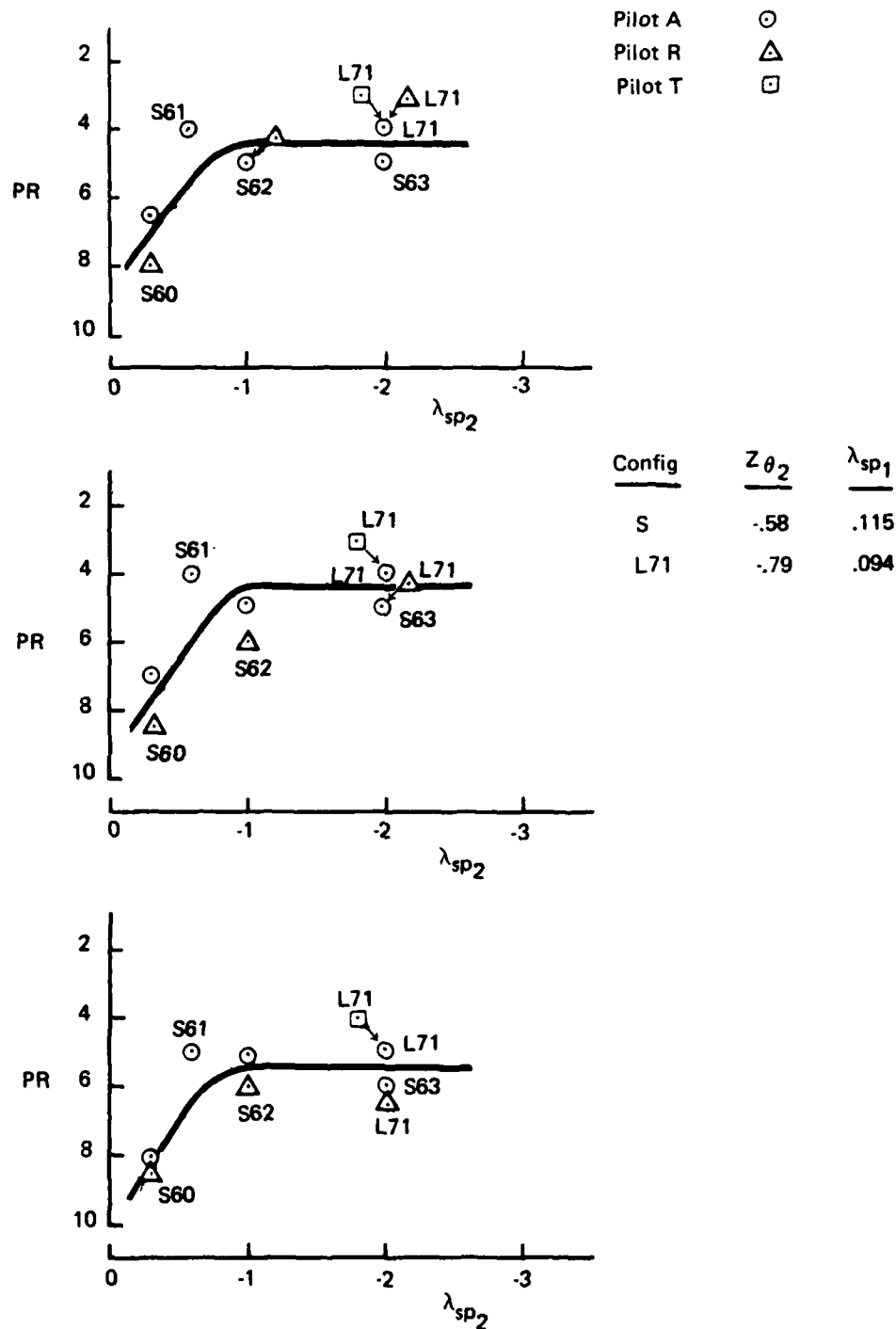
Figure B-21. Pilot Rating vs Stable Short-Period Root (λ_{sp_2})

(a) Nominal $T_2 = 6$ sec $(\lambda_{sp_1} = +.116)$

119

Pilot Rating: Worst of ILS, Visual, FTD

Run A, Negligible Turb.

Pilot A ○
Pilot R △
Pilot T □

Config	Z_{θ_2}	λ_{sp_1}
S	−.58	.169−.179
L72	−.69	.161

PR

L72
S43
L72
S43
L72
S44
S42
S41

λ_{sp_2}

Run B, Moderate Turb.

L72
S43
L72
S43
L72
S44
S42
S41

PR

λ_{sp_2}

Run C, Heavy Turb.

L72
S43
L72
S43
L72
S44
S42
S41

PR

λ_{sp_2}
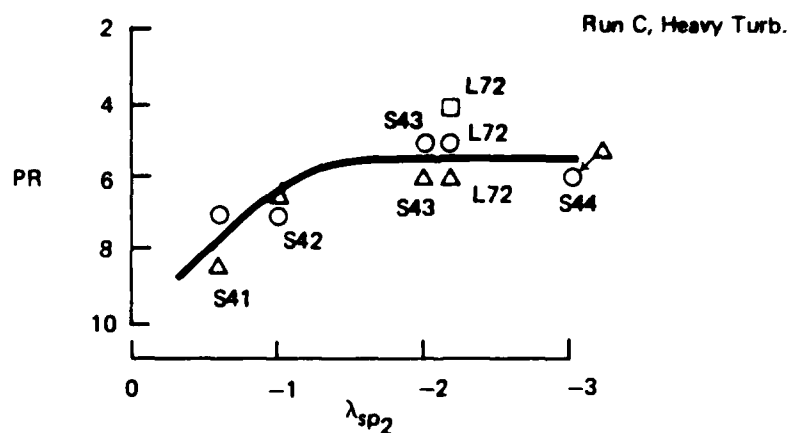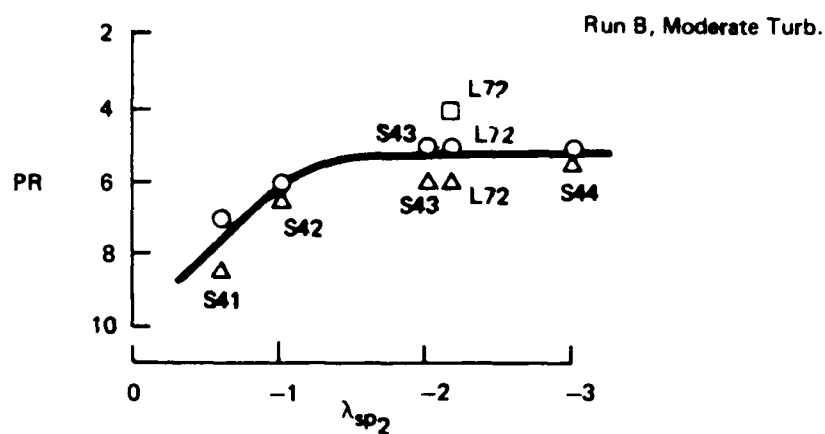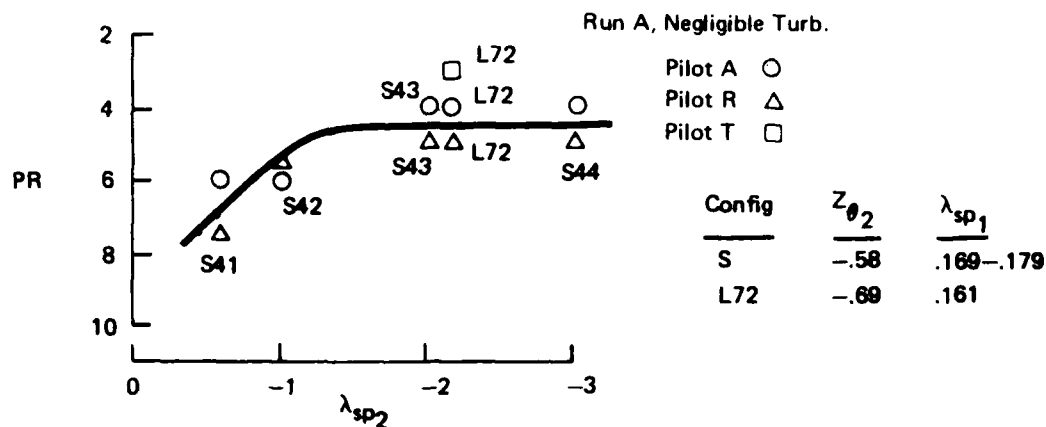
Figure B-21.   Pilot Rating vs Stable Short-Period Root (λ_{sp_2}) (Continued)

(b) Nominal $T_2 = 4\ sec\ (\lambda_{sp_1} = .173)$

Pilot Rating: Worst of ILS, Visual, FTD

Run A, Negligible Turb.

Pilot A ○
Pilot R △
Pilot T □

Config	Z_{θ_2}	λ_{sp_1}
S	−.58	.347
L73	−.69	.161

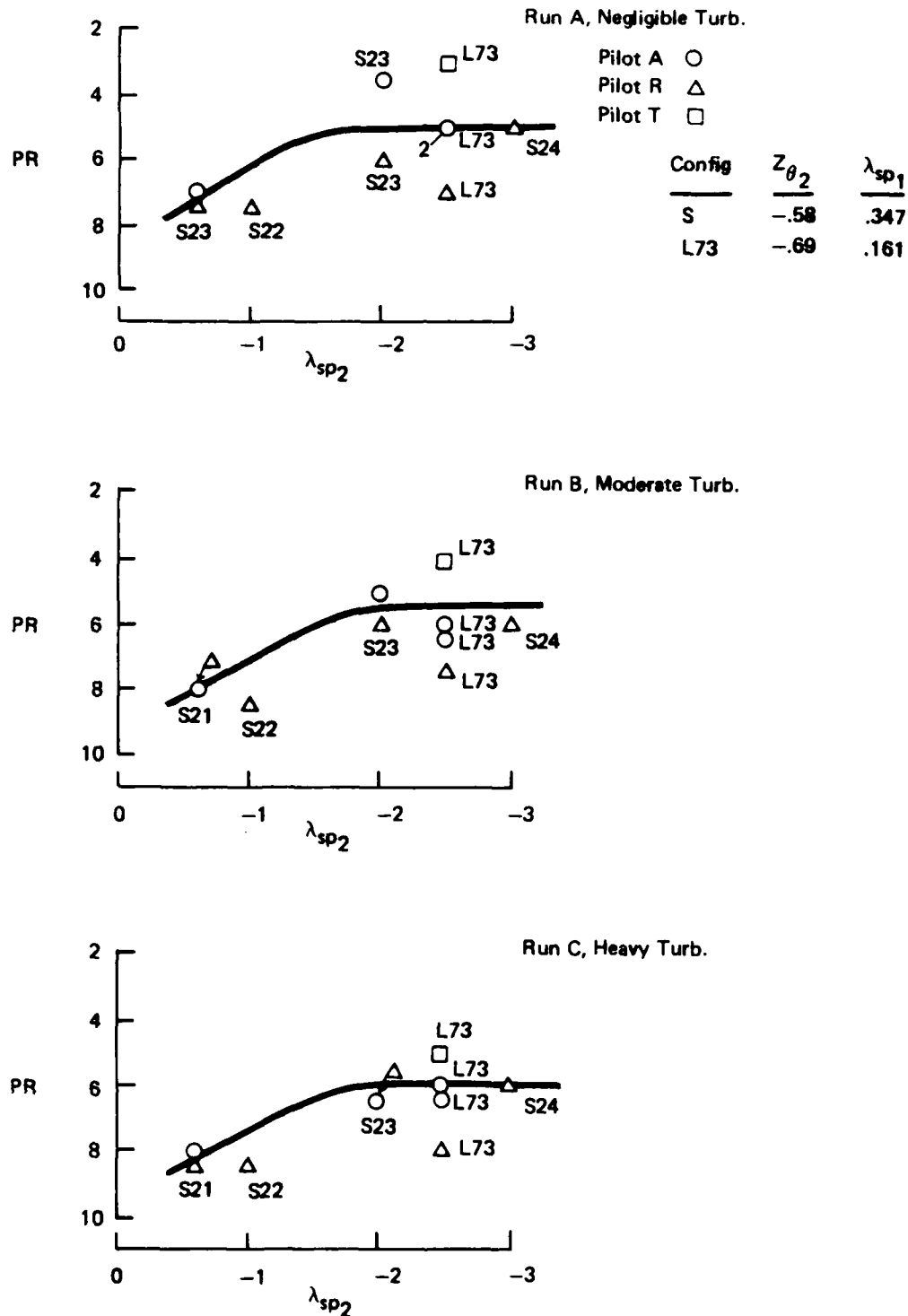Run B, Moderate Turb.

Run C, Heavy Turb.

Figure B-21. Pilot Rating vs Stable Short-Period Root (λ_{sp_2}) (Concluded)

(c) Nominal T_2 = 2 sec (λ_{sp_1} = .347)

121

knowledge that Pilot A tends to rate one pilot rating better than Pilot R (Fig. B19(d)), and assume that the shape of the curve for the three sets of data (for T_2 = 2, 4, 6 sec) is the same, then the faired curves shown in Figure B21 appear to be well founded. In Figure B21(c), Configuration S22 has a pilot rating that is too low for the curve as faired. However, the pilot comments do not support this low rating. Also the test conductor noted that Pilot R seemed particularly fatigued during his evaluation of S22, also S26, and neither looked as bad as he rated them.

Thus, the organization of the pilot rating data as a function of the two short-period roots (λ_{sp_1} and λ_{sp_2}) as presented in Figure B21 shows not only a consistent pattern but a clear functional relationship between pilot rating and these two roots. For a given value of the small or unstable root (λ_{sp_1}), pilot rating improves dramatically as the negative root (λ_{sp_2}) increases in magnitude until the root reaches a "critical value"; but beyond that, pilot rating approaches a constant asymptote for further negative increases in λ_{sp_2}. The pilot rating value of the asymptote depends weakly on the value of the unstable root in the tested range (.1 < λ_{sp_1} < .35). It is unfortunate that larger values of λ_{sp_i} were not included in the S configurations to see where pilot rating "blows up" (heads for PR = 10 as T_2 gets shorter), as it certainly must. The asymptote pilot rating also depends on the turbulence level, degrading about one pilot rating going from negligible to heavy turbulence. The critical value of λ_{sp_2}, at the knee of the curve, depends strongly on the value of the unstable root (λ_{sp_1}), as indicated in the table below.

λ_{sp_1}	T_2 sec	λ_{sp_2} at knee
.116	6	-.7
.173	4	-1.5
.347	2	-1.8

The changes in pilot ratings with λ_{sp_1} shown in Figures B20, parts (a) and (b), but lacking in part (c), can be attributed to the dependence of the knee or critical value of λ_{sp_2} on λ_{sp_1}.

122

The time histories, particularly of pitch rate (q), for the S config-urations found in Figures C20(a), C22(a) and C24(a) help in understanding the important effect of λ_{sp_2} on flying qualities for RSS airplanes. The pitch rate response is concave down in the first second or longer for all configurations with λ_{sp_2} above the knee (critical value). The time histories have a first-order-like response in q to a step input, with time constant related to λ_{sp_2} for the better rated configura-tions (not to λ_{sp_1} as hypothesized by Wasserman and Mitchell, Ref. 24).

A final item to note is that the LAHOS configurations have pilot ratings that agree with those of the S configurations in Figure B21, despite their (L configuration) 25 knot lower approach speeds. This strongly indicates that approach speed is not a major factor in flying qualities as related to criteria for relaxed static stability.

B.5.3 Effect of θ/F_s Zero ($Z_{\theta_2} = -1/T_{\theta_2}$)

Variations in the large zero of the θ/F_s transfer function were made about baseline configurations S42 and S23 as outlined in Table B9. The variation in Z_{θ_2} was produced by varying the derivative Z_w while holding the roots or poles invariant with the pole placement tech-nique. The result is that the w/F_s and θ/F_s transfer functions are invariant except for the Z_{θ_2} change, but of necessity, the zero in the u/F_s transfer function does change as it is proportional to Z_w.

The effect on pilot rating of changing Z_{θ_2} from the two baseline configurations, S42 and S23, is shown in Figure B22, parts (a) and (b) respectively. Again, curves have been faired through the data points recognizing the lower ratings that Pilot R assigns, and using the same shape of curve for all data sets.

There is a dramatic degradation in the pilot rating with negatively increasing Z_{θ_2}. The asymptotes (constant values of PR for large λ_{sp_2}) from Figures B21(b) and 21(c) are shown on Figure B22 to help in understanding the trends of pilot rating with Z_{θ_2}. Configuration S42, with λ_{sp_2} below critical (see Fig. B21(b)), has a pilot rating worse than the asymptotic value. As Z_{θ_2} decreases in magnitude, pilot rating improves, reaching the asymptotic value for S45. On the

123

other hand, S23 has a λ_{sp_2} above critical and pilot rating is at the asymptotic value. A further decrease in magnitude of Z_{θ_2} does not improve pilot rating. Apparently, the asymptote values for large negative λ_{sp_2} represent the best pilot ratings achievable as a function of λ_{sp_2} and Z_{θ_2}. As Z_{θ_2} increases negatively, pilot rating degrades about one rating point from the asymptote value for $Z_{\theta_2} = 1/2\ \lambda_{sp_2}$; beyond that, it degrades with a gradient of about -3. The condition that $Z_{\theta_2} = \lambda_{sp_2}$ corresponds to pole-zero cancellation in θ/F_s. This condition, or the closest data point to it, does have the worst (largest) pilot rating. However, there is insufficient data to warrant any conclusion that $Z_{\theta_2} = \lambda_{sp_2}$ is a worst case (maximum for PR). As will be demonstrated later through closed-loop analysis in the frequency domain, a large amount of pilot lead is required for attitude control with RSS. The zero, Z_{θ_2}, provides lead in θ/F_s, and this lead increases in the frequency range of interest as Z_{θ_2} decreases in magnitude. This is felt to be the primary factor in the extremely important role of Z_{θ_2} on flying qualities for RSS conditions.

A caveat: the variations in Z_{θ_2} were produced by changing Z_w, and the effect of these variations was investigated in a fixed-base simulator where the direct effect of normal acceleration (g's) on the pilot was not present. The results obtained for the effect of Z_{θ_2} need flight test corroboration. Also, the simulator investigation of the effects of Z_{θ_2} was very limited. More data points, over a wider range, for more baseline configurations should be investigated to define adequately the effect of Z_{θ_2} on landing flying qualities.

B.5.4 Effect of Control Sensitivity ($M_{\delta_{ES}}$)

Control sensitivity was not varied parametrically to determine its effect. Rather, it was found that the sensitivity for the baseline unaugmented F-111A was too low for RSS configurations, and a value four times that was selected as appropriate by the pilots. This value turned out to be similar to the sensitivities of the LAHOS configurations, also pilot selected. Thus evaluations were made using two values of sensitivity as determined by the pitch control gearing, plus the LAHOS
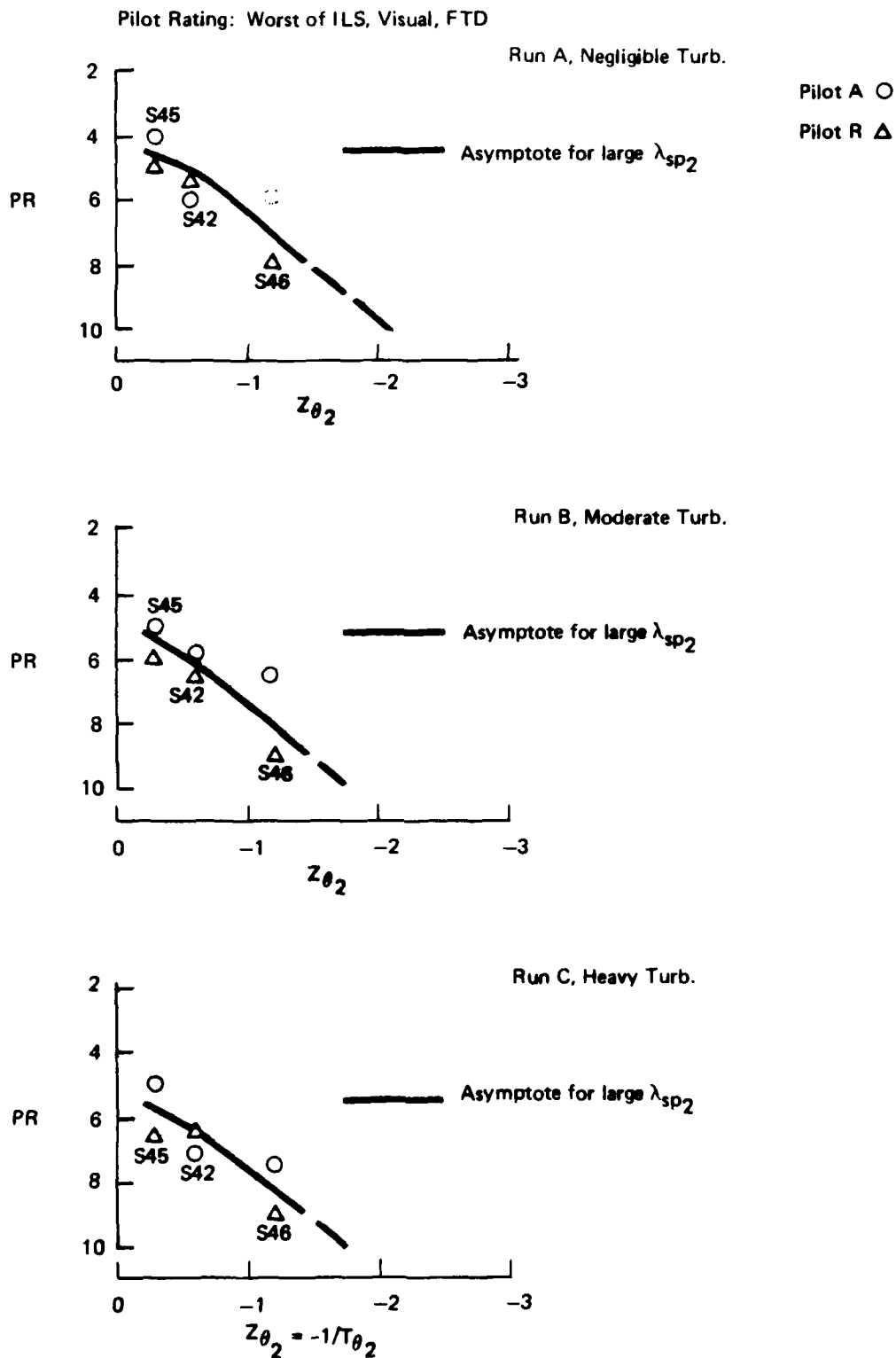
Figure B-22. Pilot Rating vs. Zero of θ/F_s Transfer Function

(a) $\lambda_{sp_2} = -1$, $T_2 = 4$ sec $(\lambda_{sp_1} = +.173)$
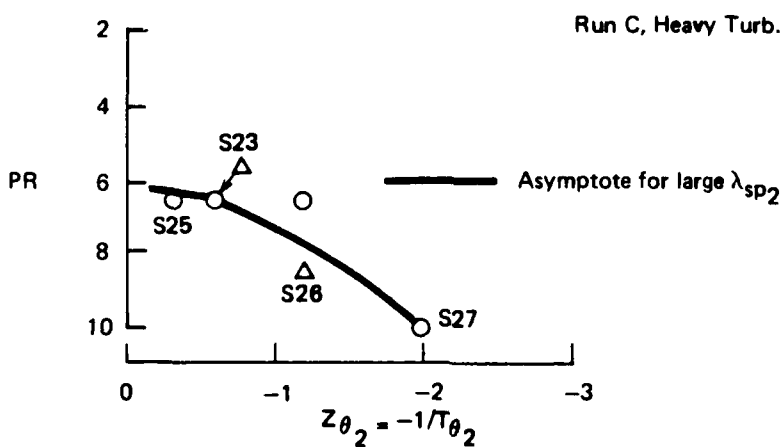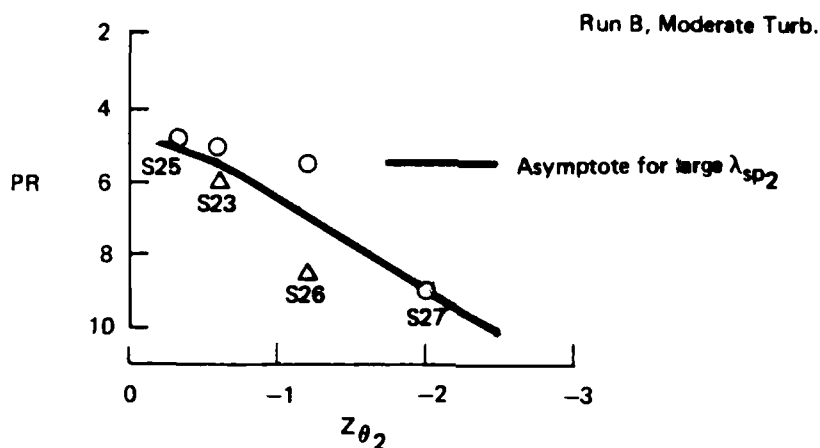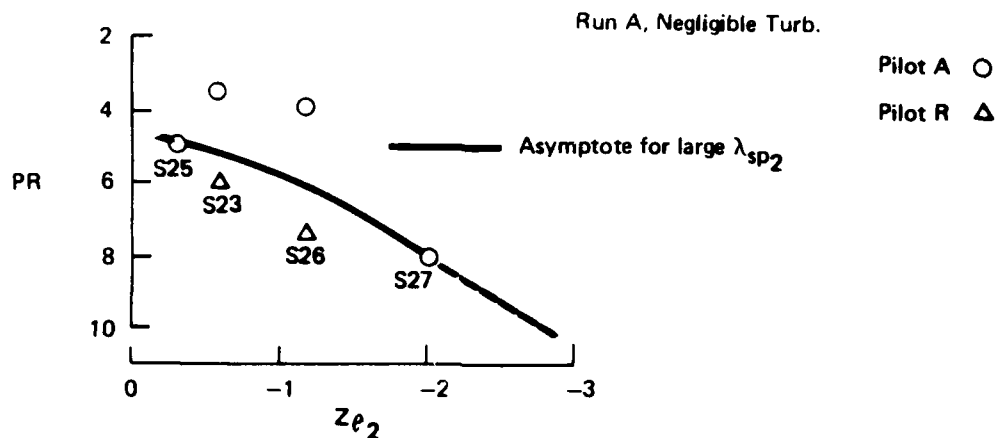
125

Figure B - 22. . Pilot Rating vs Zero of θ/F_s Transfer Function (Concluded)

(b) $\lambda_{sp_2} = -2$, $T_2 = 2$ sec $(\lambda_{sp_1} = +.347)$

sensitivity for the L configurations which had their own gearing and control effectiveness along with lower approach speed. The control sensitivities are listed in Table B18, and the separate values for gearing and effectiveness are listed below.

Configurations	δ_h/δ_{ES} deg/in	M_{δ_h} rad/sec² rad	$M_{\delta_{ES}}$ rad/sec²/in
S	-13.12	-1.489	.341
S-A,S-B	- 3.28	-1.489	.085
F	- 3.28	-1.505	.086
L	- 4.20	-5.92	.434

Note: All configurations had F_s/δ_{ES} = 7 lb/in.

Pilot ratings for the configurations with low sensitivity (S41A to S46A, S44B, and F4) have been plotted in Figure B23 in the same manner as for the corresponding high-sensitivity configurations in Figure B21b and B22a. The average curves from these latter two figures are shown as dashed lines in Figure B23. Note that F4 has essentially identical parameters as S42A (see Table B18). Also S44A and S44B differ only in actuator dynamics, which apparently had negligible effect as shown by the pilot ratings in Figure B23.

The pilot rating data in Figure B23 plotted versus λ_{sp_2} (left side) show several significant trends. First, there is a substantial degradation in pilot rating for the lower sensitivity (one-fourth the pilot selected value), from one to 3.5 rating points. For low values of λ_{sp_2} the degradation in pilot rating is about one pilot rating for all cases. However, as λ_{sp_2} increases negatively beyond the critical value (knee of the curve), there is a gradient of pilot rating with λ_{sp_2} which increases with the severity of the turbulence.

Examination of the pilot comments for configuration S43A shows that Pilot A has trouble, especially in turbulence, but doesn't identify why. Pilot R, however, says S43A "responds more slowly in pitch" on the A run, "more sluggish response than before, takes more stick" on the B run, "used full control because of sluggishness" on the C run. For configuration S44A, Pilot A says "it's kind of sluggish", and Pilot R says

127

"quite sluggishy, shows up even more (in turbulence), sluggishness shows up even worse VFR". For Configuration S44B, Pilot A says "very sluggish", Pilot R says "very sluggish, low sensitivity". The problem is clearly one of too low sensitivity, which appears to the pilot as sluggishness. For comparison, Pilot R evaluated S44 two configurations prior to S44B and said of S44, "impression of a little bit lower sensitivity, but still able to handle it reasonably well." Thus, the pilot comments verify the degradation with increasingly negative λ_{sp_2} for low $M_{\delta_{ES}}$, also that it is in fact due to the reduced sensitivity. As the short period convergence (λ_{sp_2}) increases, the pilot clearly wants more sensitivity to control it.

The data points in Figure B23 (right side) show a constant degradation in pilot rating with Z_{θ_2} from the higher sensitivity data, 1 to 1-1/2 rating points. The data points in Figure B23 clearly support the trends in pilot rating with Z_{θ_2} shown in Figure B22. Also, since the pilot rating degradation due to low sensitivity does not vary with Z_{θ_2}, desirable levels of sensitivity $(M_{\delta_{ES}}$ or $M_{F_S})$ are probably just a function of λ_{sp_2} for RSS configurations. Additional investigations of the effects of sensitivity are clearly needed.

B.5.5 Effect of Landing Subtask - ILS, Visual, Flare and Touchdown

As part of the evaluation procedure, the pilot was asked to give a separate pilot rating for each of three subtasks performed during each approach and landing: 1) ILS, the part of the approach on instruments; 2) Visual, the visual "short final" from break-out to start of flare; 3) FTD, the flare and touchdown. However, during the early part of the simulation program the three ratings asked for were: 1) ILS, 2) Visual, the whole visual part including short final, flare and touchdown; 3) Overall, an overall rating for the whole approach and landing. The pilot rating data for all the evaluations are presented in Table C9 of Appendix C. Most of the pilot ratings are given in sets of three for the three subtasks, ILS/Visual/FTD. The rating data for the early evaluations are given in sets of two, ILS/Visual and FTD/N, with the N in the third place distinguishing these earlier evaluations and replacing the overall rating which has been omitted as essentially meaningless.
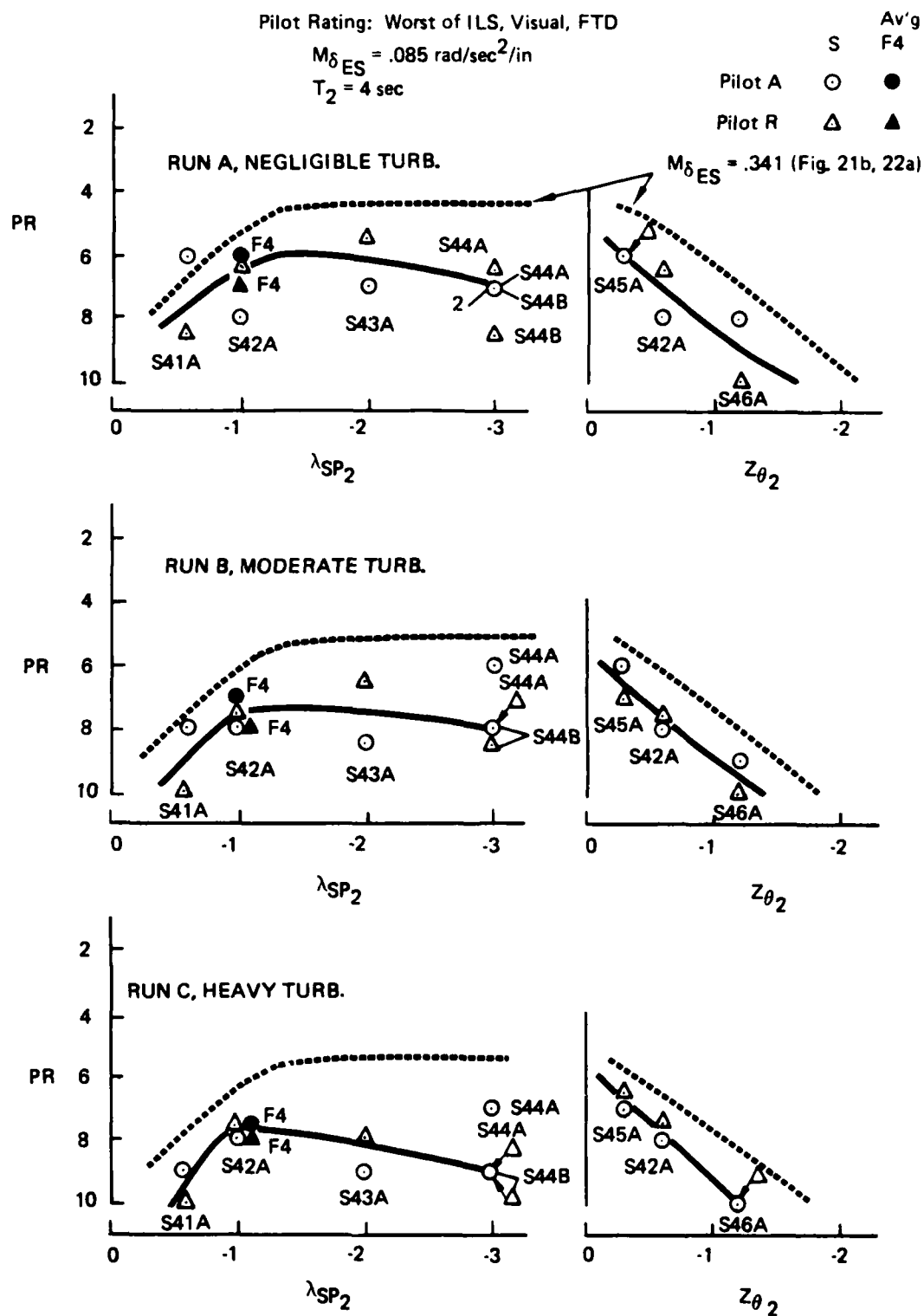
Figure B23. Effect of Control Sensitivity ($M_{\delta_{ES}}$) on Pilot Rating
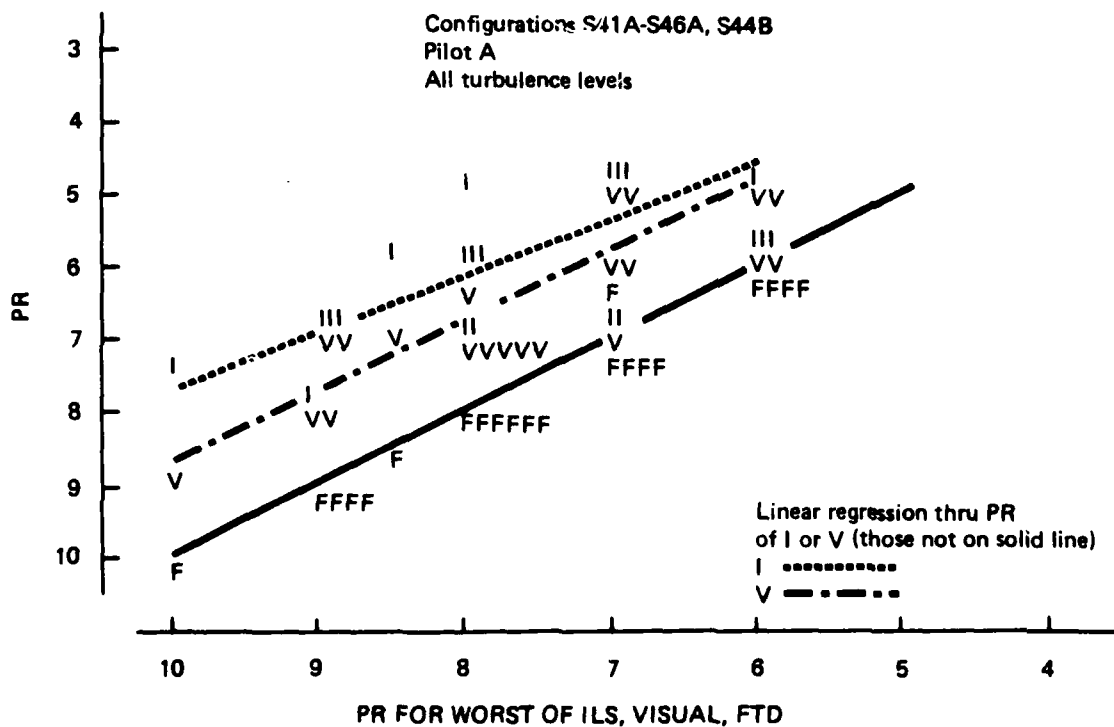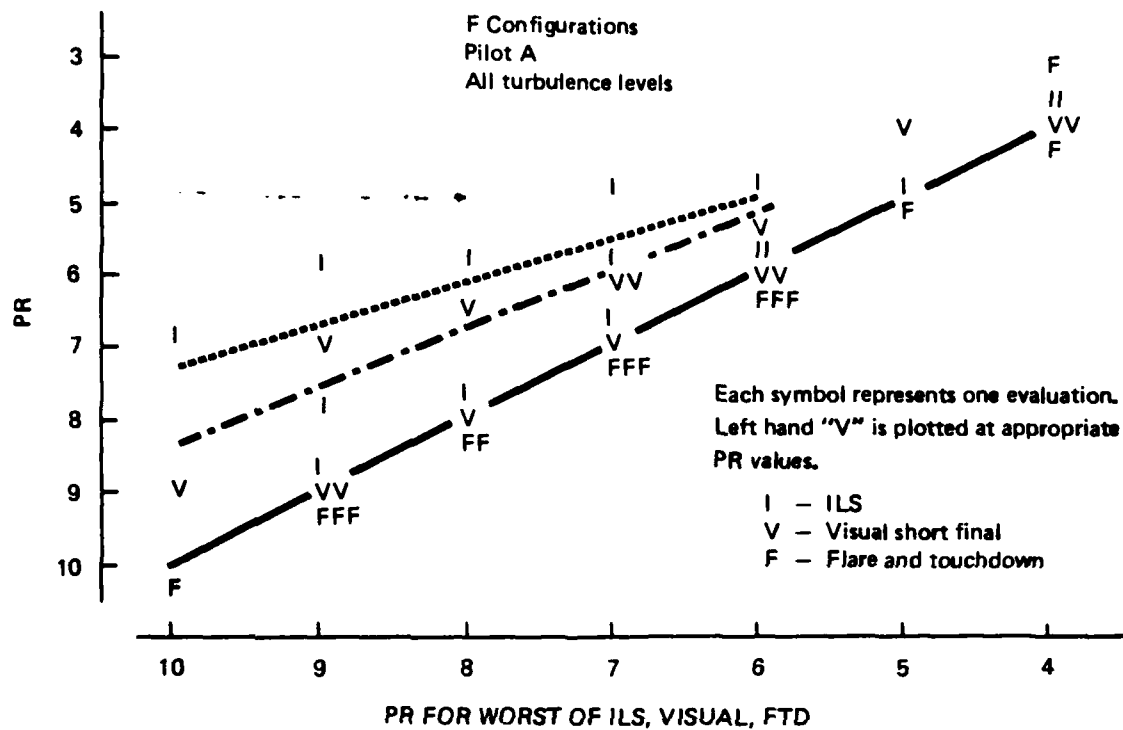
Figure B24. Effect of Task on Pilot Rating — ILS, Visual, FTD

In the previously presented analyses, the pilot rating considered to represent each evaluation was the worst rating of the three given (or of the two, in the case of the earlier evaluations). Examination of the data in Table C9 shows that for all the higher control-sensitivity configurations, the pilot ratings do not deviate by more than one rating point for the ILS, Visual, and FTD subtasks with two exceptions (S60 and S27 by Pilot A for the heavy turbulence or C run). On the other hand, the majority of the evaluations for the low-sensitivity configurations (F and S41A through S46B) have pilot rating deviations of more than one rating point for at least one of the runs. Analysis of the rating data shows that to a great extent the deviation in rating is proportional to the rating value, that is, the worse the rating the more the deviation. To illustrate this trend, all the pilot ratings from Pilot A for S41A through S46B and all F configurations with three ratings (not the earlier evaluations with two ratings) have been plotted in Figure B24. The individual ratings for each subtask (ILS, Visual, FTD) are plotted against the worst pilot rating of the three (adopted as indicative of the overall rating).

The data in Figure B24 clearly show that the flare and touchdown task was critical. With but two exceptions, the pilot ratings for flare and touchdown (F) all lie on the PR (subtask) = PR (worst) line. Examination of the data suggests that there are two populations, one where the subtask ratings in any one approach and landing were equal, and those where the instrument approach (I) and visual approach (V) portions were rated definitely better than the flare and touchdown (F). Accordingly, lines are shown on Figure B24 through the ILS (I) and visual (V) ratings in the second of the above populations, calculated from a least square fit. Though not shown, Pilot A's ratings of configurations S41 to S46 and S27 and S60 (all with the higher sensitivity) when similarly plotted show the same trends, as do the ratings of Pilot R though they tend to have less deviation between ILS, Visual, and FTD. These trends are:

1) For PR_w = 6 or better, the deviation with subtask (I, V, F) has ΔPR = 1.

2) For $PR_W > 6$, the deviation increases with PR_W, reaching $\Delta PR \simeq 2.5$ at $PR_W = 10$.

3) For $PR_W > 6$, the flare and touchdown subtask is the most difficult and critical.

The L configurations show a somewhat different characteristic which can probably be attributed to the lower approach speed (see Table C9).

1) The deviation with subtask has $\Delta PR \leq 1$ for all landings.

2) Pilot A and Pilot R found, for configurations L71 and L72, the ILS subtask to be most difficult in eight out of the nine landings for which they rated subtasks differently. For L73, the ILS was worse in five out of eight cases.

Apparently the slower approach speed made the visual short final and particularly the flare and touchdown easier. Thus the three subtasks tended to have uniform pilot ratings (16 out of 42 landings by the three pilots with the L configurations had equal I, V, F ratings). However, where differences in ratings occurred, they strongly indicated that visual flight was easier than instrument flight. Pilots A and R found visual flight "easier, a little easier, or definitely easier" than ILS. Pilot T generally saw them as "about the same". The LAHOS Pilot A found "not much difference", but LAHOS Pilot B found configuration 7-3, "landing much better than approaches. ILS approach was very demanding, high workload." He gave approach PR = 6, overall PR = 6, flare and touchdown PR = 3.

In summary, for unstable airplanes (RSS) there is not much difference in the difficulty of the various parts of the overall landing task. However, for higher landing speeds and poor handling qualities (PR $\geq$ 7), the flare and touchdown task appears critical.

B.5.6 Effect of Turbulence Intensity

There were three intensities of turbulence used in the simulation:

1) Negligible, 0 or $\sigma_{w_{20}}$ = 1.8 ft/sec
2) Moderate, $\sigma_{w_{20}}$ = 5.4 ft/sec
3) Heavy, $\sigma_{w_{20}}$ = 7.2 ft/sec

where $\sigma_{w_{20}}$ is the rms vertical component at 20 ft. of altitude. The turbulence model is described in Section C.2.5.1. Negligible turbulence was generally smooth air ($\sigma_{w_{20}}$ = 0), but on occasion a very low intensity of turbulence was inadvertently present ($\sigma_{w_{20}}$ = 1.8 ft/sec) which was barely noticeable to the pilots and did not affect their performance or pilot ratings.

All configuration evaluations (those for control authority excepted) involved three approaches and landings at the three intensities of turbulence:

Run A, Negligible turbulence

Run B, Moderate turbulence plus sidestep

Run C, Heavy turbulence.

In almost every evaluation, the pilot rating was either unchanged or degraded by the addition of turbulence. No meaningful relationship between the degradation due to turulence and the various experiment parameters could be found (again excepting the control authority variations). Accordingly, a simple statistical analysis of all the unaugmented cases was made and the results are presented in Figure B25, part (a). The upper set of figures show the probability of occurrence, $p_{1/2}$, of an amount of degradation due to turbulence as obtained by subtracting the pilot rating in negligible turbulence, PR (A), from the pilot rating in moderate, PR(B), or heavy, PR(C), turbulence. The pilots used both whole- and half-rating values, but they clearly avoided half-ratings, hence the low values for $p_{1/2}$ for half-rating decrements. Accordingly, the half-rating decrements were assigned in equal amounts to the whole-rating decrements on either side, resulting in

133

the probability density, p_1, shown in the lower set of figures. The most probable degradation is one rating point, for either moderate or heavy turbulence. However the next most probably degradation for moderate turbulence is none, while for heavy turbulence it is two pilot ratings.

The obvious small second peak, centered around a pilot rating decrement of 4, was examined and found to be peculiar to Pilot T and the F configurations. The frequency of occurrence of decrements in pilot rating due to turbulence are shown in Figure B-25(b) for the F configurations, separated by pilot. The distributions for Pilots A and R are similar, and show no second peak at ΔPR of 4. However the distributions for Pilot T are clearly different. For Run B with moderate turbulence, the decrement distribution centers around ΔPR $\simeq$ 1/2. However, for Run C with heavy turbulence, there appear to be two nearly equal distributions, the first centering on ΔPR $\simeq$ 1, the second, on ΔPR $\simeq$ 4. This second distribution is almost completely responsible for the secondary peak in p_1 shown in part (a) of Figure B25.

One half of Pilot T's rating decrements in heavy turbulence for the F configurations were three rating points or larger. These large values are felt to be due to two factors: the too low sensitivity, and Pilot T's control technique. Pilot T flew aggressively, controlled errors tightly, and used large high-frequency inputs in this process. The low sensitivity of the F configurations required Pilot T to make much larger stick inputs and exert much heavier forces than for the L configurations. (Pilot T evaluated no S configurations). In the heavy turblence of Run C, the physical workload apparently became excessive about 50% of the time and degraded the effectiveness of Pilot T's control technique, perhaps adding lag, and precipitated loss of control or near loss of control. Analysis of the pilot rating data shows that in most cases where the degradation in Pilot T's rating due to turbulence was three or more, the degradation was from six or better in smooth air to nine or ten in heavy turbulence.

134

PR = Worst of ILS, Visual, FTD
Lower figures have half-rating values
added in equal parts to full rating
values on either side

MODERATE TURBULENCE
σ_w = 5.4 ft/sec
SIDESTEP

HEAVY TURBULENCE
σ_w = 7.2 ft/sec

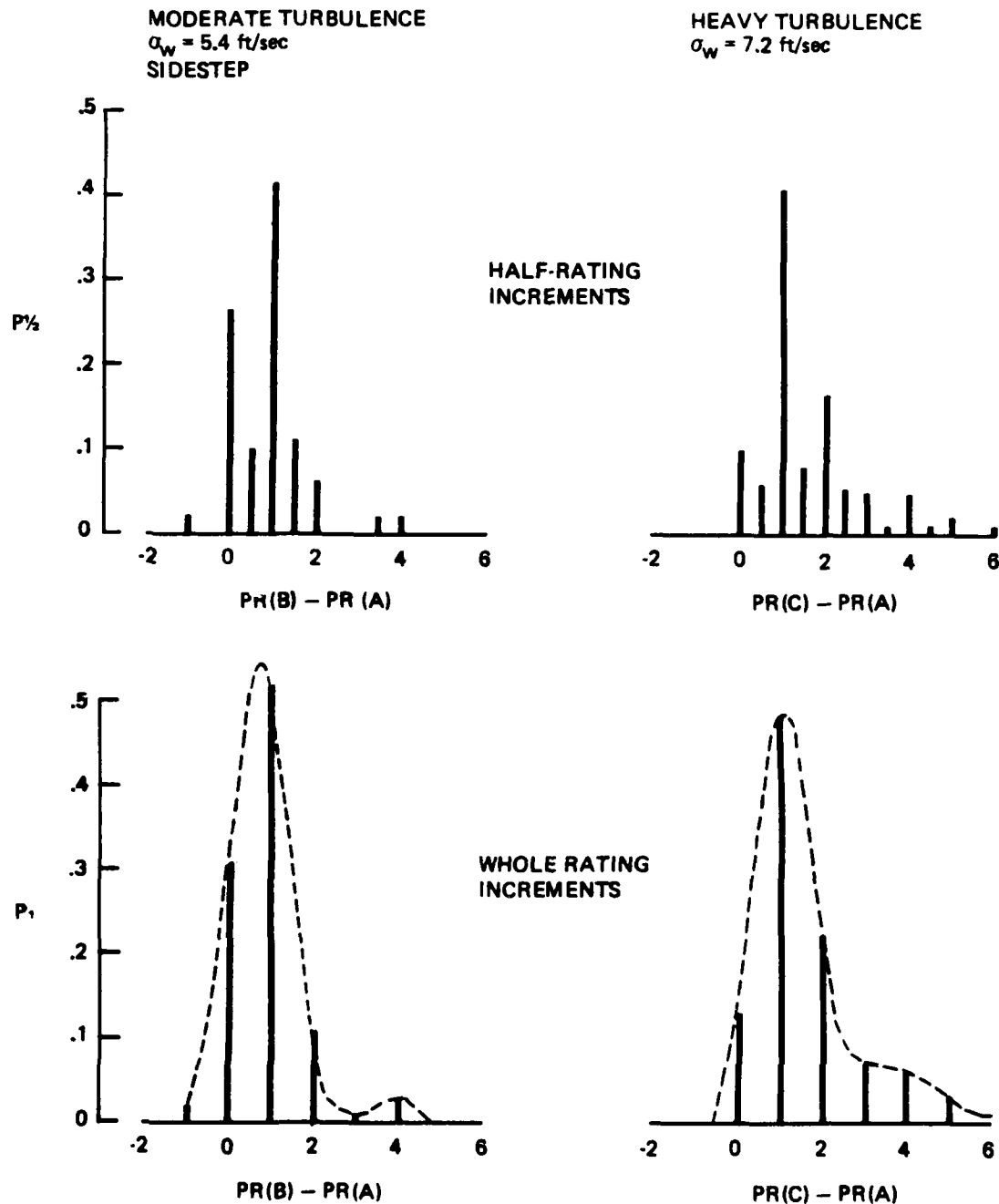HALF-RATING
INCREMENTS

WHOLE RATING
INCREMENTS

Figure B-25. Degradation in Pilot Rating Due to Turbulence
(a) All F, L, S Configurations and All Pilots
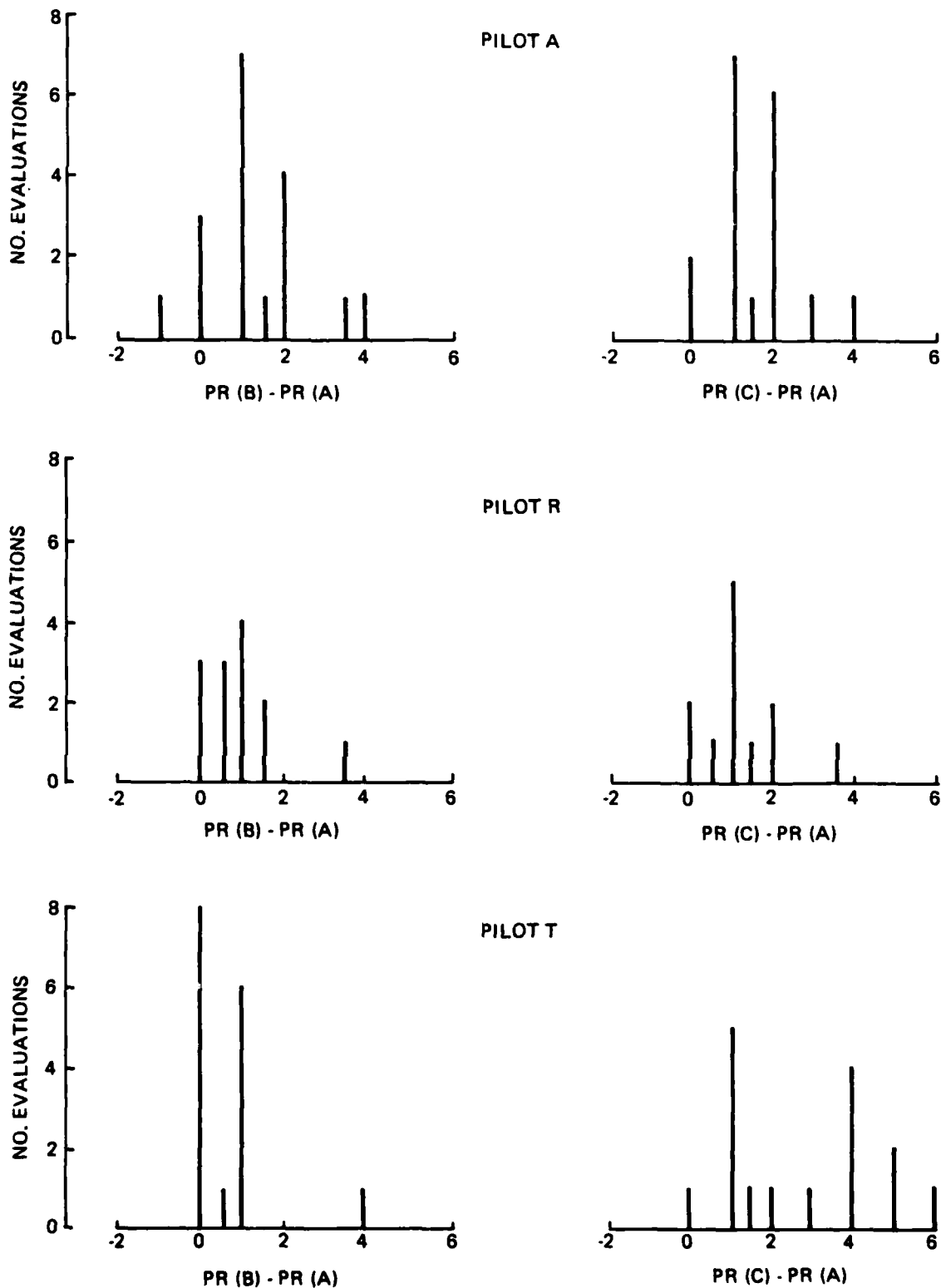
135

PR = WORST OF ILS, VISUAL, FTD

Figure B-25. Degradation in Pilot Rating Due to Turbulence
(b) F Configurations

136

In summary, the degradation in pilot rating due to moderate or heavy turbulence for RSS configurations had the following statistics:

		Moderate Turbulence	Heavy Turbulence
Mean	$\overline{\Delta PR}$	.9	1.6
Std. Dev.	$\sigma_{\Delta PR}$	.9	1.1

However, approximately 50% of F configurations evaluated by Pilot T in heavy turbulence had a different pilot rating distribution:

$$\text{Mean} \qquad \overline{\Delta PR} = 4.4$$
$$\text{Std. Dev.} \qquad \sigma_{\Delta PR} = .8$$

On these runs the combination of heavy turbulence, low control sensitivity of the F configurations, and Pilot T's aggressive control technique resulted in loss, or near loss, of control.

B.5.7 Augmented Airplane Flying Qualities

The primary use of the flight control augmentation system in the ground simulator evaluation program was to investigate control system authority and rate requirements. A lesser use was to serve as a standard of good flying qualities. The pilots felt that all the augmented configurations (with full control authority) had generally good flying qualities, and pilot ratings usually ranged from 2 to 3 depending on turbulence level.

Flying qualities for the three baseline augmented F-111A airplanes are presented in Table B-19. The pilot ratings are those of Pilot A, made on three consecutive runs, so the relative ranking of the three configurations should be especially consistent. Configuration AF-111F has the nonlinear F-111A aerodynamics and the F-111A flight control system. AF-111G has the generic FCS instead, and AFO has both the generic FCS and linearized aerodynamic coefficients. As can be seen, the

pilot ratings are not materially different between the three configura-
tions, and degradation due to turbulence is relatively minor.

TABLE B-19

COMPARISON OF PILOT RATINGS FOR AUGMENTED F-111A CONFIGURATIONS
WITH DIFFERING AERODYNAMICS AND FCS

Config.	Pilot	Run A (Negligible Turbulence)	Run B (Moderate Turbulence)	Run C (Heavy Turbulence)	Run No.
AF-111F	A	2.5	4	4	10/31/79-13
AF-111G	A	3	3.5	3.5	10/31/79-14
AFO	A	3	3	3	10/31/79-15

TABLE B-20

EFFECT OF C.G. ON PILOT RATINGS FOR AUGMENTED
F-111A CONFIGURATIONS

(PR: Worst of ILS, Visual, FTD averaged for
each pilot, then averaged over three pilots)

Config.	Pilot	Run A	Run B	Run C
AFO	Avg.	2.1	2.5	2.7
AF4	Avg.	2.0	2.7	$3.5^{(1)}$
AF2	Avg.	2.1	2.9	3.1

(1) Pilot rating for Run 5/7/80-90C seemed unjustifiably low (PR of
5/6/7), and listed average does not include this 7 rating.

138

The baseline augmented configurations used for investigation of control authority requirements were AF0 and its derivatives AF4 and AF2, formed by moving the c.g. aft from .35 to .465 and .505, where the airplane with augmentation OFF would have T_2 = 4 and 2 secs, respectively. The flying qualities for these configurations are summarized in Table B-20. The ratings by each pilot were first averaged, and then the three pilots' average ratings were averaged to provide the data in Table B-20. Degradation of PR with turbulence is less than that for the unaugmented airplane. There is essentially no change in pilot rating as the c.g. moves aft. This invariance was intended, since the α feedback was varied with c.g. to keep constant static stability.

B.5.8 Control Authority and Rate Variations

A specific investigation was made of the effects of parametrically reducing the position limits and the rate limits of the left and right horizontal tails. The horizontal tails provide both pitch (symmetric deflection) and roll (antisymmetric deflection) control. However, since in the landing configuration the spoilers provide the primary roll control except for very small inputs, limiting the horizontal tail deflection only minimally affects roll control. Thus limiting position and rate of the horizontal tail effectively limits only pitch control power and rate.

Position limit variations were performed only for the augmented airplane, taking the most aft c.g. or worst case (Configuration AF2). Rate limit variations were performed both for unaugmented airplanes and for augmented airplanes for several c.g. values. The pilot rating data is found at the end of Table C-9, Appendix C.

The evaluation of parametric changes in horizontal tail position limits was performed in the early or first simulation program, using A, B, and C runs with negligible, moderate and heavy turbulence, respectively. The evaluation of rate limits was performed in the later or
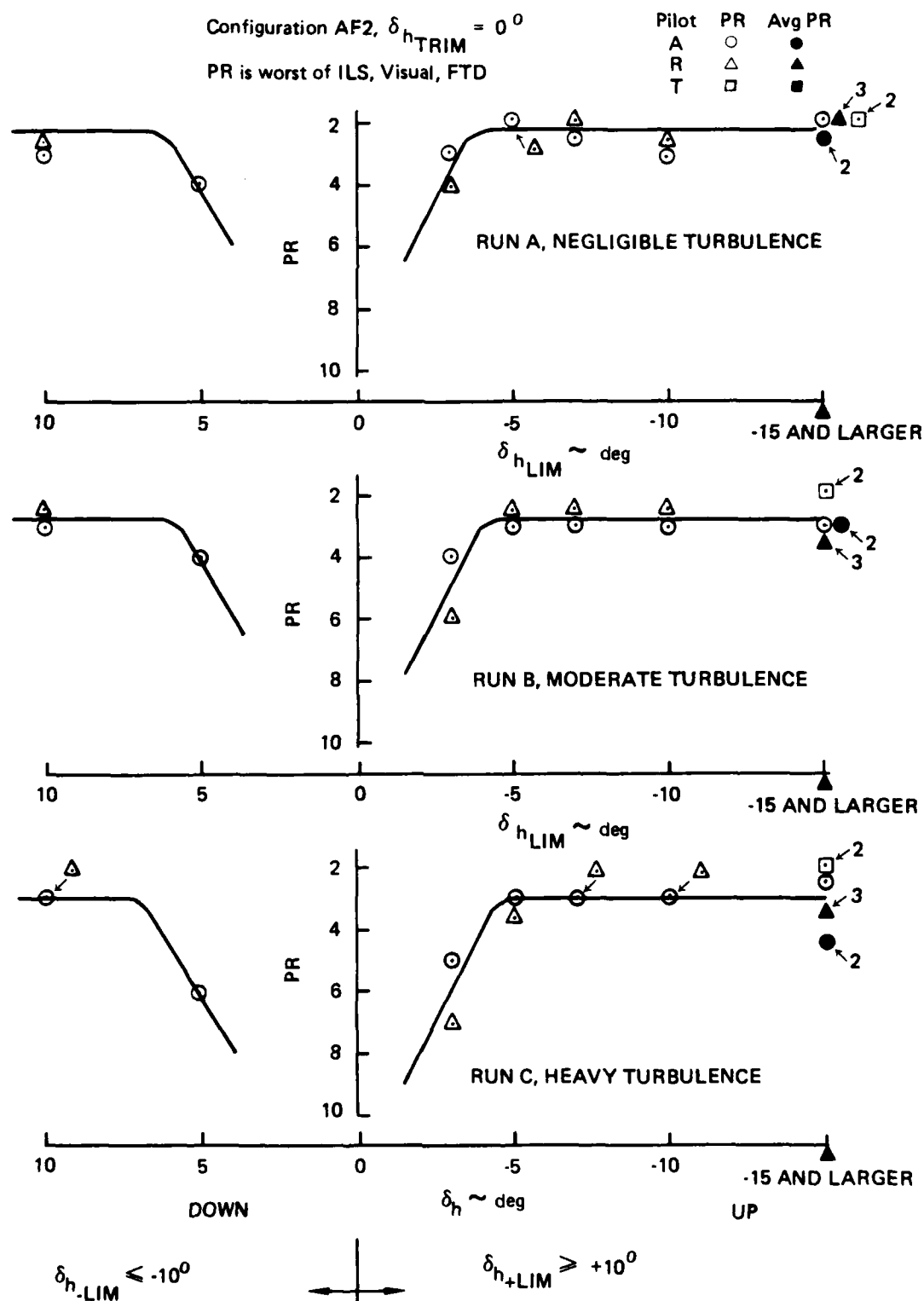
139

Figure B-26. Effect of Horizontal Tail Position Limits for Augmented Airplane

140

second simulation program, using D and C runs. The D run combined the smooth-air of the A run in level-flight and ILS acquisition with the moderate turbulence and sidestep of the B run in ILS and visual approach and landing. As can be seen in Table C-9 of Appendix C, the initial pilot rating for the D run with no turbulence is not degraded by restricted position or rate limits. The remaining three ratings of the D run correspond to those of the B run, vis., ILS approach, short visual final with sidestep, and visual flare and touchdown, all in moderate turbulence.

Coupling of roll inputs into pitch can cause serious piloting difficulties, especially for relaxed static stability and restricted control authority. In the simulated F-111A flight control system, this coupling occurs when the horizontal tail is against the stop due to a pitch input, and a roll command is added. One horizontal tail leaves the stop, to produce a roll input, but in the process the mean tail position changes thus producing a pitch input. In the actual F-111A this occurs as described for nose-down inputs (max surface = 15°, max pitch command = 15°, max roll command = $\pm 8^O$), but for nose-up inputs only after roll command exceeds $\pm 5^O$ (max surface = -30°, max pitch command = -25°, max roll command = $\pm 8^O$). In the earlier simulator evaluations, this type of coupling occurred occasionally on the B and C runs, and the pilots found it extremely disconcerting. To the pilots the airplane appeared to have encountered a large gust, up or down draft, as the airplane pitched without apparent command input, or failed to respond in pitch to a full pitch-stick input. To avoid this problem, the approach taken in other than the control authority studies was to increase the horizontal tail deflection limits to $+20^O$ and -30°. For the investigation of position limits, the traces were monitored for pitch inputs due to roll, and if they occurred sufficiently to affect the evaluation, the condition was re-run. For the investigation of rate limits, a limiter was incorporated into the FCS so that roll commands to the horizontal tail actuators were limited to maintain anti-symmetry ($\Delta\delta_{h_L}$ = $-\Delta\delta_{h_R}$, where $\Delta\delta_{h_L}$ and $\Delta\delta_{h_R}$ are due to roll command), thus eliminating pitch due to roll inputs.

The effects of varying the pitch control effectiveness (horizontal tail position limits) are presented in Figure B-26 for the augmented

141

airplane with most aft c.g. location (AF2). It should be noted that C_{m_0} was adjusted so that trim horizontal tail deflection was zero at the reference landing flight condition. The data show that the pilot is surprisingly tolerant of restricted control effectiveness. Degradation in pilot rating did not occur until horizontal tail deflection was limited to 3° up, or 5° down, even in heavy turbulence. Data points are sparse, so the data are faired using the shape of curve found applicable by Hall and Booth (Ref. 34). Using these faired data, it appears that 5° nose up and 7° nose down were required to provide the pilot with sufficient control effectiveness. The following table translates control deflection into control effectiveness units appropriate for criteria.

δ_h deg	$M_{\delta_h} \delta_{h_{max}}$ rad/sec^2	Requirement for Landing
3	.08	
5	.13	Nose-up minimum
7	.18	Nose-down minimum
10	.26	

The indicated need for larger nose-down than nose-up control authority was generally borne out throughout this simulator investigation of landing, and is probably peculiar to relaxed static stability. The data of Figure B-26 is for the airplane with augmentation ON. However, based on the data on effect of rate limits, the augmented case is the critical one, and providing adequate authority for the augmented case will assure there is adequate authority for augmentation OFF as well.

The effects of varying the horizontal-tail actuator rate limits are presented in Figure B-27 for both unaugmented and augmented configurations. The unaugmented evaluations were performed primarily for the F6 configuration (Figure B-27, part (a)). The data indicate that a rate of at least 20 deg/sec is required to avoid degradation in pilot rating. Pilot A accommodated a rate limit of 10 deg/sec in moderate turbulence without degradation, but Pilot T found 10 deg/sec unflyable for F6, also F1, and F0. This difference is explainable in terms of piloting

PR: Worst of ILS, Visual, FTD
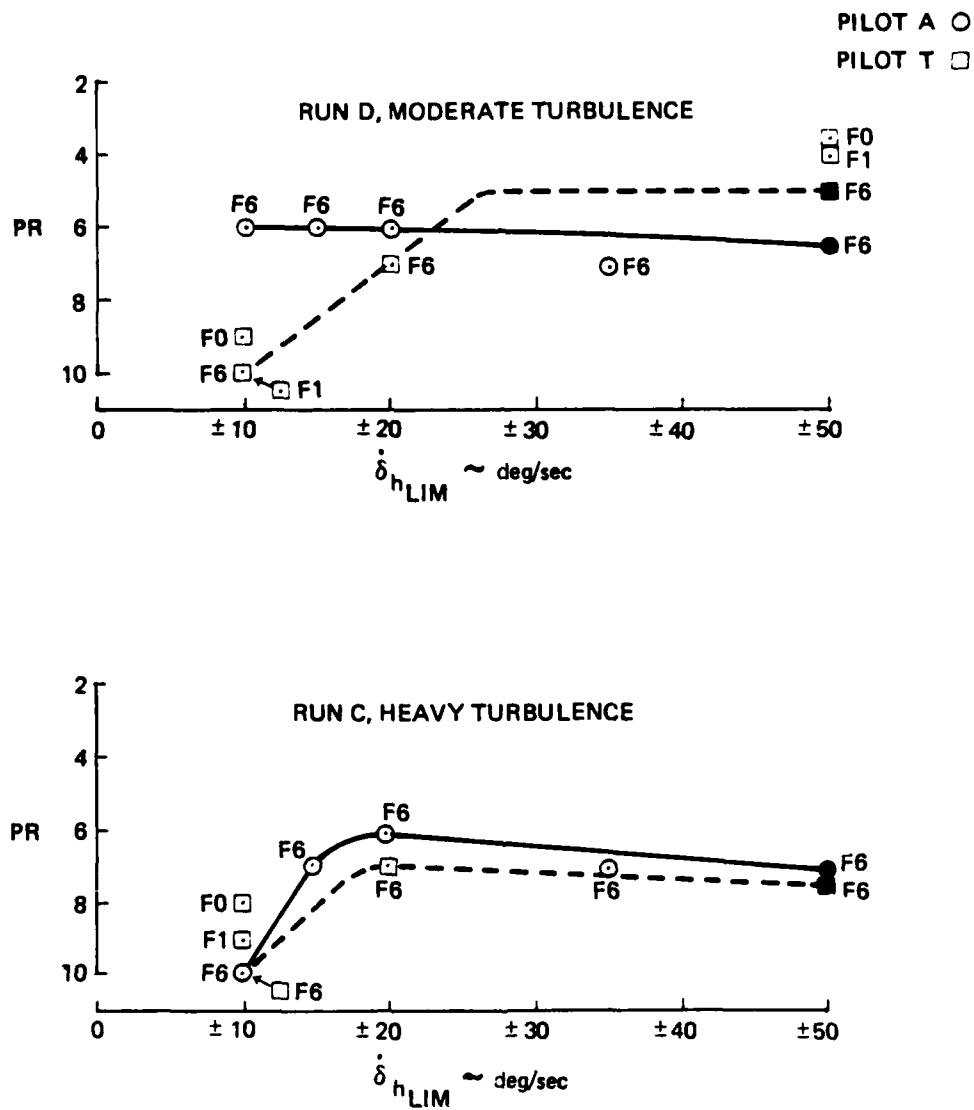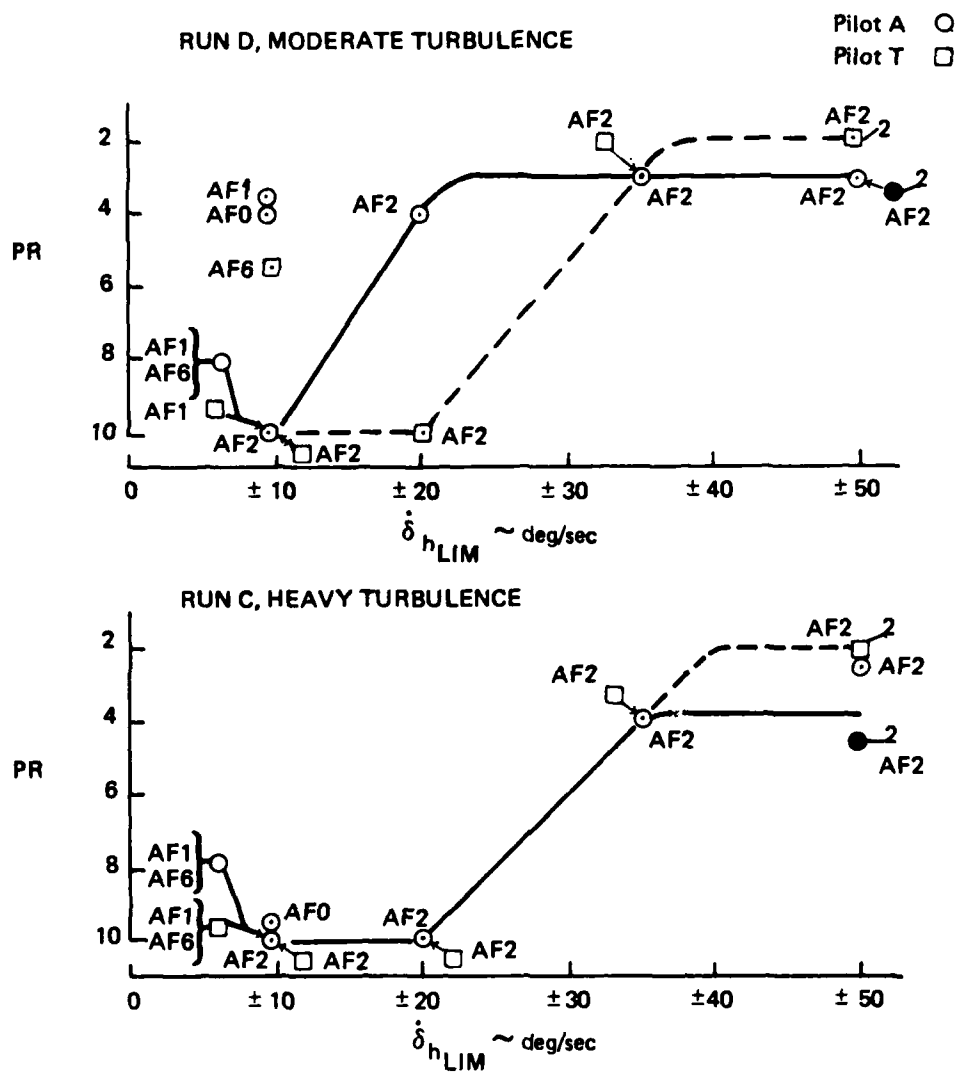
Solid PR (●■) are faired averages from Figure B-19

PILOT A ○
PILOT T ▫

Figure B-27. Effect of Horizontal Tail Rate Limits
(a) Unaugmented Configurations (F)

143

Figure B-27. Effect of Horizontal Tail Rate Limits
(b) Augmented Configurations (AF)

144

technique: Pilot A flew very smoothly using continual small inputs; Pilot T was very aggressive and used rapid large inputs. In heavy turbulence, the data from the two pilots agrees closely. The pilot ratings for F1 and F6 at 10 deg/sec are essentially the same, so going from $T_2 = 6$ sec to $T_{1/2} = 7$ sec does not relax the rate limit requirement. However, F0 with its fairly good short period does rate better (PR = 8).

The effect of rate limit for augmented configurations is shown in Figure B-27, part (b), for the full range of F configuration (AF0 to AF2) though the bulk of the data are for AF2, the most severe case. The variation between pilots, and with turbulence level, is similar to that for the unaugmented configurations (Figure 27(a)): Pilot A does better at the lower rate limits for moderate turbulence, but in heavy turbulence the two agree closely. The data for heavy turbulence indicates no variation in control rate requirements, either with stability level or with pilot technique. It appears that a control rate of 35 deg/sec is necessary to ensure that there will be no degradation in flying qualities. This value is that of the baseline F-111A airplane. Translated into angular acceleration units, the requirement becomes

$$\left| M_{\delta_h} \dot{\delta}_{h_{max}} \right| \geq 0.9 \ \text{rad/sec}^2/\text{sec}$$

In summary, though the control authority reqirements for relaxed static stability are modest, the control rate requirements are not. For approach and landing in fighter or attack airplanes, the minimum control authority margins required, in pitch angular acceleration units, are

0.13 rad/sec^2	nose up
0.18 rad/sec^2	nose down

These margins are over and above trim, and are for maneuvering and to stabilize the airplane in turbulence (moderate or severe). The similar minimum requirements for control rate, in terms of pitch acceleration per sec, are

$$\pm \ 0.9 \ \text{rad/sec}^2/\text{sec}$$

Significant degradation below these values may make the airplane unflyable.

Though the above summarized requirements are based on approach and landing, they probably can be applied throughout the flight envelope since approach and landing in turbulence is usually critical for control rate, and is probably critical for control authority for RSS airplanes. This control authority margin must be the margin over and above that required for trim, steady maneuvers, and specific transients such as configuration changes or failure transients. The requirements apply to both augmented and unaugmented states. They can also probably be applied to stall, though stall and departure require additional consideration.

B.5.9 Summary Analysis and Criteria

Based on the results of the fixed-base simulation, four parameters in the pitch-attitude response to pitch control input (θ/F_s) have been found highly significant to flying qualities of airplanes with relaxed static stability in the landing tasks:

λ_{sp_1} unstable or small short-period real root

λ_{sp_2} large stable short-period real root

Z_{θ_2} larger zero in θ/F_s transfer function

$M_{\delta_{ES}}$, M_{F_S} control sensitivity

An additional factor of significance to the flying qualities is the turbulence level, quantified by the following parameter:

$\sigma_{w_{20}}$ rms vertical component of turbulence at 20 ft altitude

In addition, minimum levels of control authoriity and rate were determined which would avoid serious degradation of flying qualities.

$$M_{c_{max}} = M_{\delta_h} \, \delta_{h_{max}} \qquad \text{control authority}$$

$$\dot{M}_{c_{max}} = M_{\delta_h} \, \dot{\delta}_{h_{max}} \qquad \text{control rate}$$

146

The simulator data pertinent to the above parameters and factors are *organized and summarized in* this section in a form suitable for use in criteria development.

B.5.9.1 <u>Real Short-Period Roots $(\lambda_{sp_1}, \lambda_{sp_2})$</u>

The simulator pilot rating data for all unaugmented configurations with real roots and $Z_{\theta_2} \simeq -0.6$ are plotted in Figure B-28 on the real root plane (λ_{sp_2} vs λ_{sp_1}). The ratings from each pilot are separated by slashes. The high sensitivity data in Figure B-28(a) are ratings from individual evaluations, with repeats separated by commas. The low sensitivity data in Figure B-28(b) are average ratings from one or more (often many) evaluations of the configuration made by each pilot.

The high sensitivity data of Figure B-28(a) reveals the fundamental relationship of flying qualities to the real roots, uncontaminated by the degradation due to inadequate control sensitivity (Figure B-28(b). Iso-rating boundaries for PR = 6.5 and 8.5 shown on the figure are felt to reflect the Level 2 and Level 3 boundaries for flying qualities in each level of turbulence. It has been conventional to consider PR = 9.5 as the Level 3 boundary. But the definition of Level 3 (Ref. 5) states that "the airplane can be controlled safely", which translates for the landing task to "the airplane can be landed safely". The definitions of a controllable landing (Table B-15) and the workload for a PR = 9.5 (Table B-14) clearly indicate that a 9.5 pilot rating is not safe, and with PR = 9 there is no margin at all, hence safety appears questionable. Hence, for the landing task, PR = 8.5 as the Level 3 boundary appears *much more* consistent with the Level 3 definition.

The values of λ_{sp_2} for the "knee" of the curve from Figure B-21 (where PR reaches an asymptotic value as λ_{sp_2} becomes more negative) have been plotted in Figure B-28(a), labeled with the asymptote values of pilot rating, and a dashed line faired through the points. Therefore, as λ_{sp_2} goes above this line at constant λ_{sp_1}, no change in pilot rating is expected. Very clearly, as λ_{sp_1} decreases and approaches 0.1 ($T_2 = 7$ sec), the magnitude of λ_{sp_2} needed to help stabilize the airplane decreases.

147

The low sensitivity data on Figure B-28(b) also has iso-rating boundaries plotted, with the dashed part of the boundary indicating extrapolation based on less than sufficient data points. A cursory view suggests that these boundaries are very different from those for the high sensitivity cases (Fig. B-28(a)), but in fact this is not the case. Before the boundaries curve up sharply, in the $\lambda_{sp_1} = .1$ to $.2$ region, the boundaries for low and high sensitivity are similar, except the corresponding low sensitivity boundaries have pilot ratings one to two rating points lower.

The low sensitivity data in Figure B-28(b) are important because they cover a wider range of conditions than the high sensitivity data. The boundaries, primarily the 6.5 one, are relatively flat in the range $-.1 < \lambda_{sp_1} < .1$. They indicate there is a lower floor or limit on λ_{sp_2}. The boundaries for large λ_{sp_1} clearly curve up, though there are too few data points to more than suggest trends. However, this trend must surely exist for the high sensitivities too, but λ_{sp_1} was not made large enough in the tests to uncover it.

B.5.9.2 Zero in θ/F_s Transfer Function (Z_{θ_2})

Variations in Z_{θ_2} were investigated on the simulator for only two combinations of λ_{sp_1} and λ_{sp_2} (Config's S23 and S42). For one combination, Z_{θ_2} variations were made with the low control sensitivity (S42A) as well as the high one. All the data are contained in Figures B-22 and B-23 (right half).

Despite the very limited number of data points, some general conclusions were drawn in Section B.5.3, and these are used to develop a method for determining the effect of Z_{θ_2} on pilot rating. The baseline data for the functional dependence of pilot rating on short period roots $(\lambda_{sp_1}, \lambda_{sp_2})$ is for $Z_{\theta_2} \simeq .6$. Accordingly, the increment in pilot rating due to variations of Z_{θ_2} from the baseline needs to be determined.

The increment in pilot rating has been plotted in Figure B-29 for all the simulator evaluations of variations in Z_{θ_2}. However, the baseline pilot ratings were obtained in various ways depending on the data set involved. For the data from Figure B-22(b) for variations from
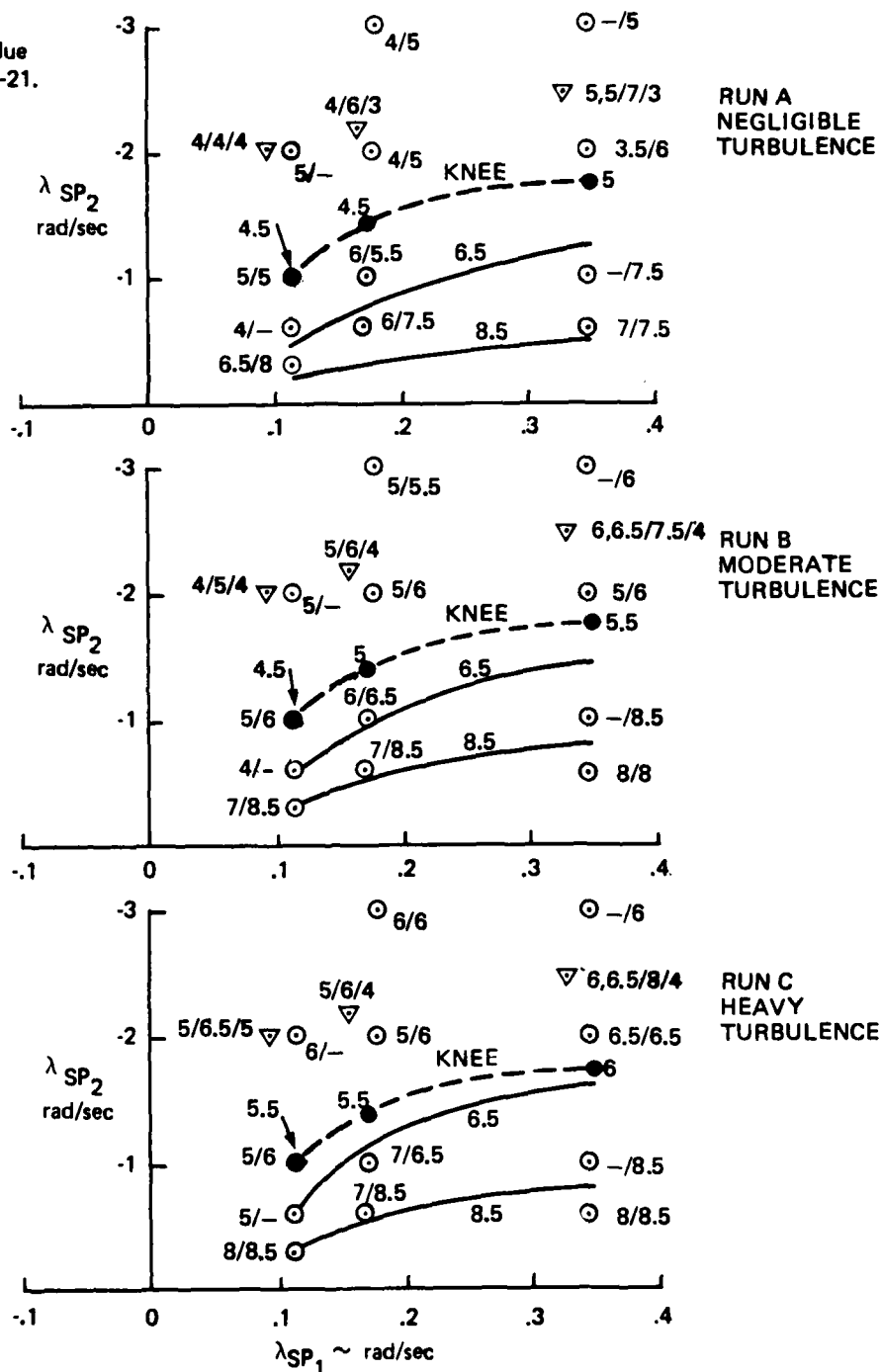
Figure B-28. Pilot Rating as Function of Real Roots (λ_{SP_1}, λ_{SP_2})
(a) High Sensitivities; $Z_{\theta_2} \cong -.6$

Configuration S23, the baseline pilot rating (PR_B) at the appropriate turbulence intensity was taken as the asymptotic (KNEE) value from the dashed line in Figure B-28(a), as S23 falls above this line. For the data from Figure B-22(a) for variations about S42, the baseline ratings were interpolated from Figure B-28(a) using the iso-rating lines. For the low sensitivity data from Figure B-23, the baseline rating was taken as the average rating for Configuration S42A. The baseline ratings are tabulated below and were used to calculate the increments plotted in Figure B-29.

Configuration	Run A Negligible Turbulence	Run B Moderate Turbulence	Run C Heavy Turbulence
S23	5	5.5	6
S42	6	6.5	7
S42A	7.25	7.75	7.75

The data points in part (b) of Figure B-29 are well fit by a straight line with slope of -3.5 passing through $\Delta PR = 0$ at $Z_{\theta_2} = -.6$. Since these cases have λ_{sp_2} less than critical (below the dashed line in Figure B-28(a)), this fairing is appropriate. The decrease in ΔPR is limited at the asymptotic value from Figure B-28(a), and turns out to be a $\Delta PR = -1.5$ for all three turbulence levels.

The data points in part(a) of Figure B-29 are also reasonably fit by a straight line with slope of -3.5, but the $\Delta PR = 0$ intercept is at a larger value of Z_{θ_2} than -.6. We have no solid basis for generalizing where this intercept should be. However, to fit the data the intercept must be at about $Z_{\theta_2} = -.85$ so that Z_{θ_2} (intercept) - Z_{θ_2} (baseline) = -.25. Noting that $\lambda_{sp_2} - \lambda_{sp_2crit} = -.25$, we conclude these two quantities may be equal and fit the data accordingly.

To support the foregoing hypothesis, we recall the previous conclusion that the primary effect of Z_{θ_2} is felt through phase angle.

Symbol	$M_{\delta_{ES}}$	Z_{θ_2}	Configs
◇	.086	-.59	F1, F6, F4, F2
⊙	.085	-.58	S41A - 44A, S44B

Ratings
Pilot A/R/T
Pilot A/R

Pilot ratings are average worst (of ILS, Visual, FTD) rating
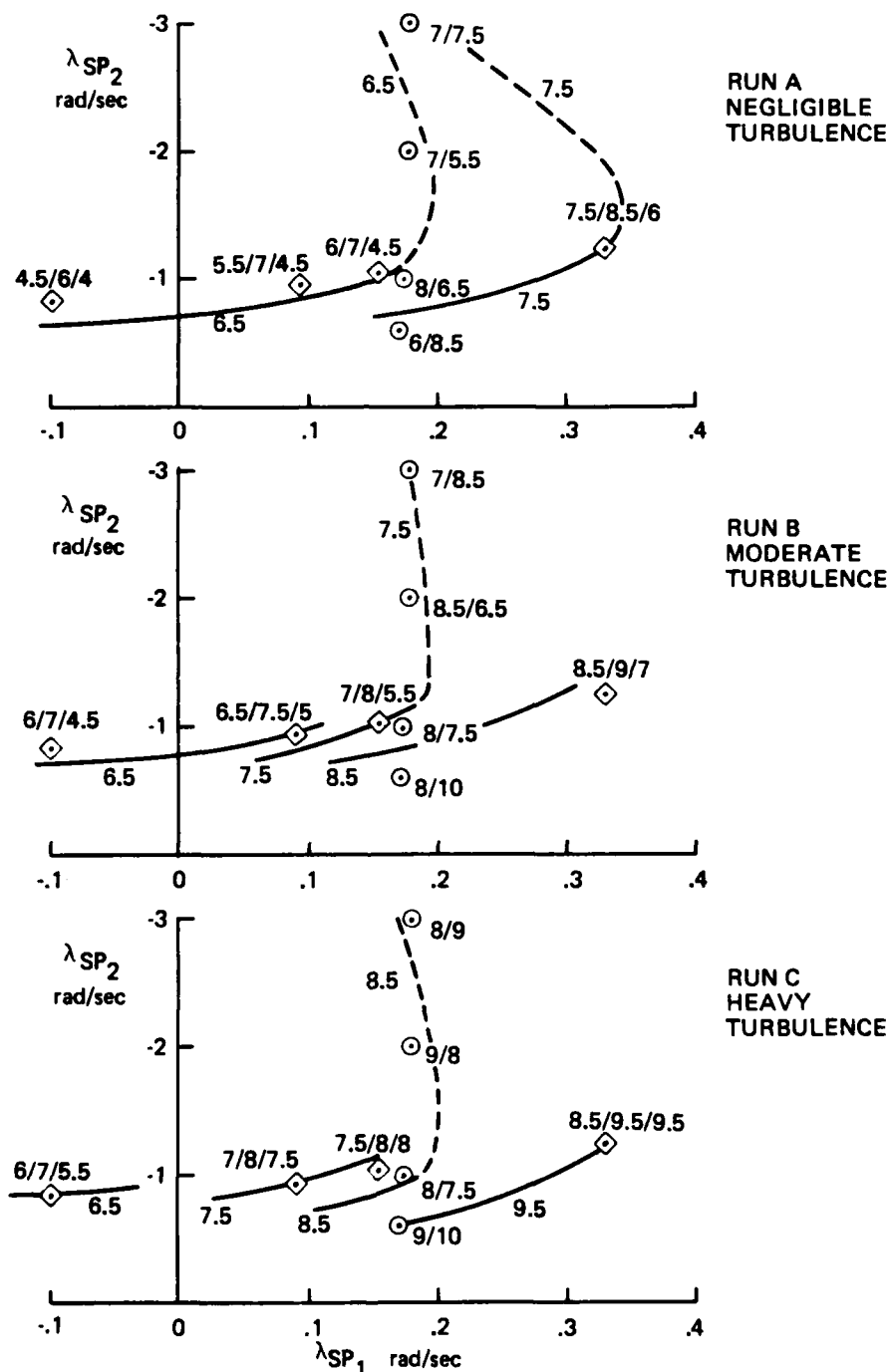
Figure B-28. Pilot Rating as Function of Real Roots $(\lambda_{SP_1}, \lambda_{SP_2})$ - Concluded
(b) Low Sensitivities; $Z_{\theta_2} \cong -.6$

Since phase is approximately linear with frequency (below the break frequency of first order factors), then phase angle would be held roughly constant at low frequencies if Z_{θ_2} (lead) and λ_{sp_2} (lag) were increased equal increments. On this basis, the effect of Z_{θ_2} on pilot rating, in terms of the increment to be added to the data of Figure B-28(a), would be

$$\Delta PR = -3.5 \, (Z_{\theta_2} - Z_{\theta_2 \, int}) \qquad \text{for } Z_{\theta_2} < Z_{\theta_2 \, int}$$

$$\Delta PR = 0 \qquad\qquad\qquad \text{for } Z_{\theta_2} \geq Z_{\theta_2 \, int}$$

where

$$Z_{\theta_2 \, int} = \lambda_{sp_2} - \lambda_{sp_2 crit} \quad -0.6$$

and

$$\lambda_{sp_2} < \lambda_{sp_2 crit}$$

Until the above relations describing the interactions between Z_{θ_2} and λ_{sp_2} are verified, a more conservative approach is indicated, namely, to assume that Z_{θ_2} has the effect on pilot rating indicated in Figure B-29(a) for all λ_{sp_2} above critical:

$$\Delta PR = -3.5 \, (Z_{\theta_2} + .85) \qquad \text{for } Z_{\theta_2} < -.85$$

$$\Delta PR = 0 \qquad\qquad\qquad \text{for } Z_{\theta_2} > -.85$$

B.5.9.3 Control Sensitivity ($M_{\delta_{ES}}$, M_{F_S})

Only a meager amount of data on control sensitivity was obtained in the course of the simulator investigation, not enough to develop any general criteria. The best that can be done is to specify a range of sensitivity within which no degradation in flying qualities should occur due to inadequate (too low or high) sensitivity, at least for approach and landing.

152
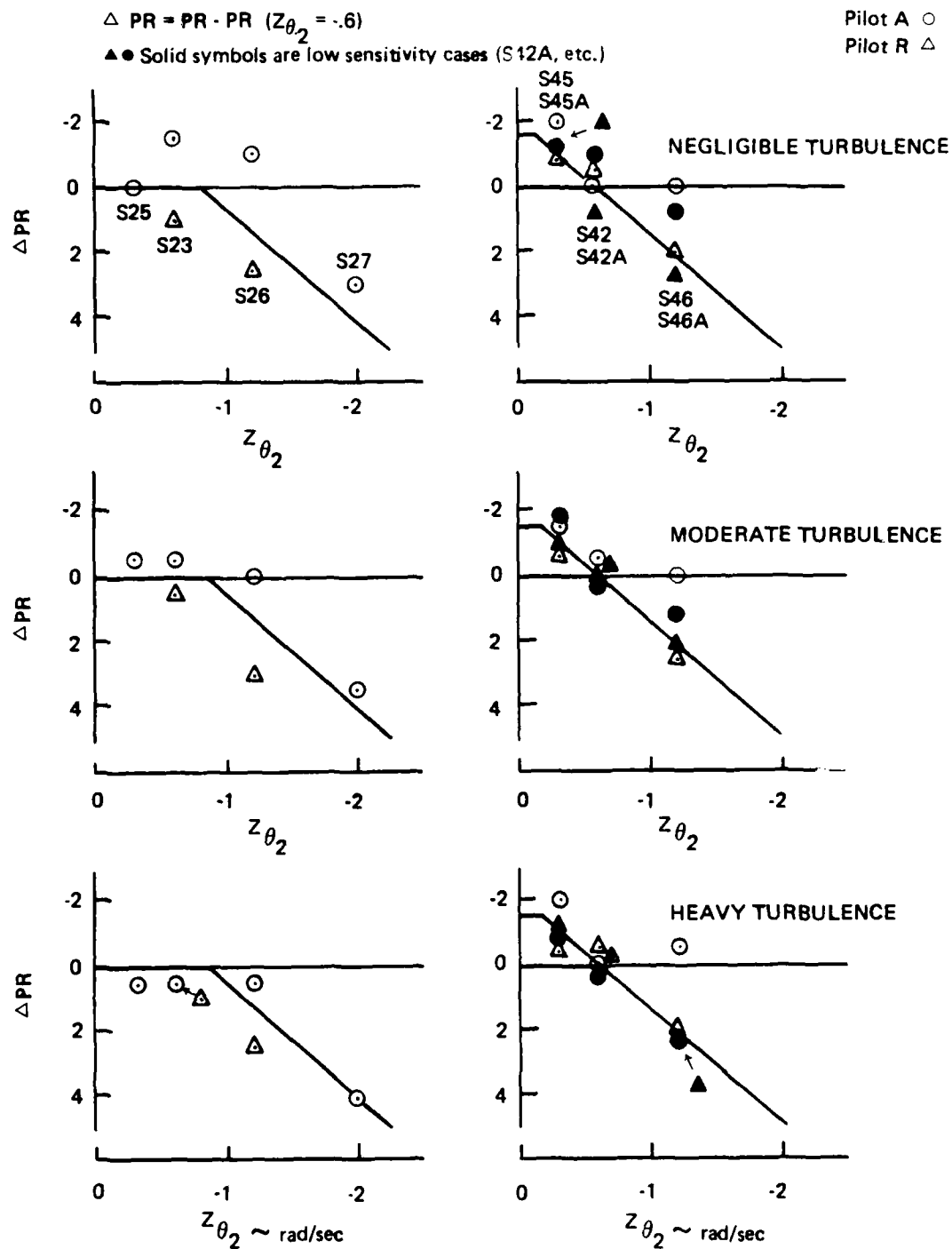
Figure B-29. Increment in Pilot Rating Due to Z_{θ_2} Zero

	$M_{\delta_{ES}}$ rad/sec^2/in	M_{F_S} (Stick) deg sec^2 lb	M_{F_W} (Wheel) deg sec^2 lb
Maximum	.55	4.5	9
Minimum	.25	2	4

The above values of $M_{\delta_{ES}}$ were obtained by adding 20% to the LAHOS value and subtracting 20% from the S configuration value of this experiment. The values of M_{F_S} were obtained by using the 7 lb/in stick force gradient used throughout this experiment, and doubling it for wheel controllers. The force gradient is given in deg/sec^2 units to avoid small decimal numbers.

$$\triangle PR = PR\ (M_{\delta_{ES}} = .085) - PR\ (M_{\delta_{ES}} = .341)$$

Based on data of Figure B-23
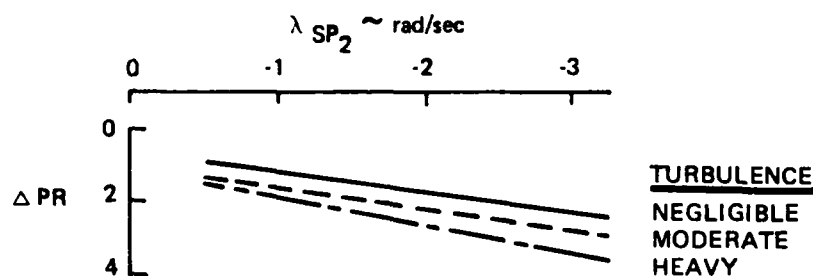
Figure B-30. Degradation in Pilot Rating Due to Low Control Sensitivity as Function of λ_{SP_2}

One trend uncovered by the simulator experiment is the need for increased sensitivity as λ_{sp_2} becomes more negative (see Figure B-23). The pilot rating increments between the solid ($M_{\delta_{ES}} = .085$) and dashed ($M_{\delta_{ES}} = .341$) curves of Figure B-23 were plotted and straight fairings, which very closely represent the increments, are found

154

in Figure B-30. The increase in ΔPR with λ_{sp_2} strongly suggests the need for higher sensitivity as λ_{sp_2} becomes more negative.

B.5.9.4 Control Authority and Rate

Control authority and rate requirements were investigated on the simulator, for the augmented as well as the unaugmented airplane, in various turbulence intensities for approach and landing. The requirements for the augmented airplane were similar but more severe than for the unaugmented airplane. The authority requirements were found modest, but rate requirements were substantial.

For fighter aircraft in landing approach, the following minimum angular acceleration authority and rate, over and above trim, were required to handle moderate to heavy turbulence.

$$M_{c_{max}} = M_{\delta_h} \delta_{h_{max}} \begin{cases} .13 \text{ rad/sec}^2 & \text{nose-up} \\ -.19 \text{ rad/sec}^2 & \text{nose-down} \end{cases}$$

$$\dot{M}_{max} = M_h \dot{\delta}_{h_{max}} \qquad \pm.9 \text{ rad/sec}^2/\text{sec}$$

Though the above requirements are based on approach and landing, they probably apply to the whole flight envelope including the nose-down requirement for stall, provided they are treated as the control margin required over and above that required for trim, steady maneuvers, and specific transients such as those due to configuration changes or failures.

B.5.9.5 Turbulence Intensity

The turbulence intensity was an important part of the simulation task in landing, and most of the results are presented as a function of the three levels of turbulence tested. The turbulence model used is described in detail in Appendix C, but its characteristics are very close to those of the model in MIL-F-8785C (Ref. 5). The index used to quantify the turbulence is the rms value of the vertical component measured at 20 feet altitude above the ground.

In general, there was a degradation in pilot rating due to turbulence of the following magnitudes for the configurations with standard control position and rate limits.

Turbulence Intensity	$\sigma_{w_{20}}$ ft/sec	ΔPR (mean)
Moderate	5.2	.9
Heavy	7.2	1.6

However, for configurations with severely limited control position and rate, the degradation in pilot rating due to turbulence was much larger, ranging anywhere from 3 to 8 rating points. For the rate-limit cases, the degradation was usually to a PR = 10, reflecting loss of control. Turbulence represents a primary disturbance the pilot must contend with.

One of the pilots (Pilot T) used an aggressive control technique employing large rapid inputs with much high-frequency content. Given configurations with too low a control sensitivity (F configurations), Pilot T often downrated them 4 to 5 rating points in heavy turbulence, reflecting loss or near loss of control. Similarly, Pilot T required a higher control-surface rate limit in turbulence than the other pilots.

Turbulence intensity thus represents a primary driving function which can push an apparently safe, but underlying unsafe, configuration over the "edge" or "cliff".

B.5.9.6 Criteria

The criteria presented here are based directly on the fixed-base ground simulator investigation of approach and landing, and are not meant to be all encompassing. Some extrapolation has been used to broaden the applicability of the criteria.

Criteria for relaxed static stability are based on the following equivalence between Level and pilot rating (PR):

Level 1	$1 \leq PR \leq 3.5$
Level 2	$3.5 < PR \leq 6.5$
Level 3	$6.5 < PR \leq 8.5$

$$-.5 > z_{\theta_2} = -1/T_{\theta_2} > -.7$$

Satisfactory level of control sensitivity
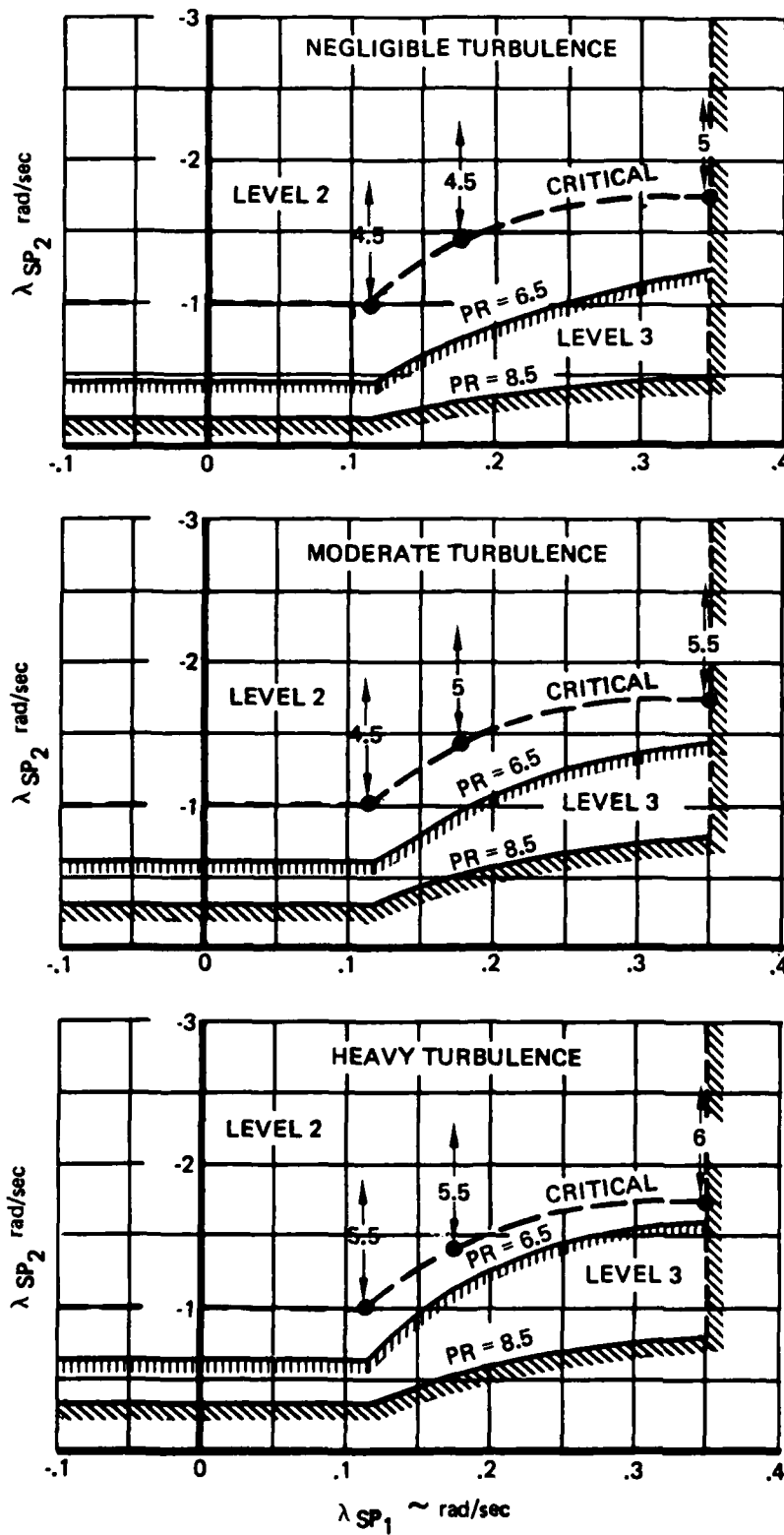
Figure B-31. RSS Criteria for Short-Period Roots (λ_{SP_1}, λ_{SP_2}) in Approach and Landing

157

Satisfactory level of control sensitivity

λ_{SP_2} Above Critical

$(\lambda_{SP_2} < \lambda_{SP_{2_{CRIT}}})$

$Z_{\theta_2} = -/T_{\theta_2} \sim$ rad/sec
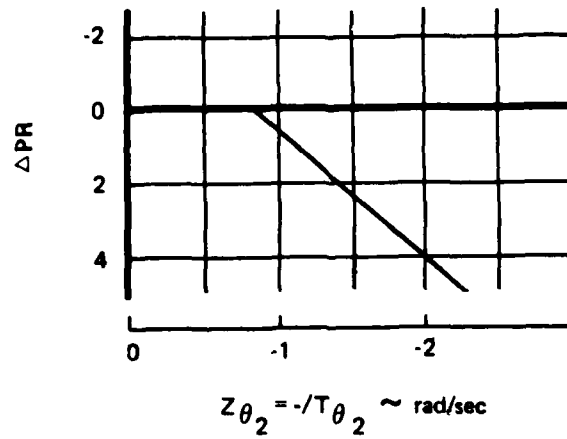
λ_{SP_2} Below critical

$(\lambda_{SP_2} > \lambda_{SP_{2_{CRIT}}})$

$Z_{\theta_2} = -1/T_{\theta_2} \sim$ rad/sec
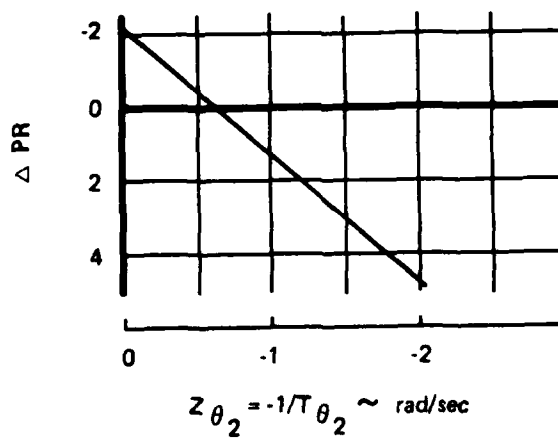
PR = PR (Figure B-31) + $\triangle$ PR ; but PR limited to no better (less) than PR$_{CRIT}$ at λ_{SP_1}

Figure B-32. Correction for Z_{θ_2} to RSS Criteria for Approach and Landing

158

The Level 3 boundary, conventionally considered equivalent to PR = 9.5, has been chosen at PR = 8.5 as being more consistent with the definition of Level 3 for the landing task.

Criteria for the short-period roots $(\lambda_{sp_1}, \lambda_{sp_2})$ are presented in Figure B-31 for a restricted range of $Z_{\theta_2} = -1/T_{\theta_2}$ (large zero of the θ/F_s transfer function) and desirable levels of control sensitivity, defined as follows:

$$.25 < M_{\delta_{ES}} < .55 \quad \text{rad/sec}^2/\text{in}$$
$$2 \leqslant M_{F_S} \leqslant 4.5 \quad \text{deg/sec}^2/\text{lb – stick controller}$$
$$4 \leqslant M_{F_W} \leqslant 9 \quad \text{deg/sec}^2/\text{lb – wheel controller}$$

The dashed line labeled "critical" in Figure B-31 separates the λ_{sp_1}, λ_{sp_2} plane into two regions. Above the critical line, PR does not vary as the magnitude of λ_{sp_2} increases at constant λ_{sp_1}. Below the line, PR decreases sharply with the magnitude of λ_{sp_2}.

The criteria in Figure B-31 are specified at three different intensities of turbulence which correspond closely to the values specified in MIL-F-8785C (Ref 5) for low-altitude turbulence.

Turbulence Intensity (Simulation)	$\sigma_{w_{20}}$ ft/sec	Turbulence Intensity (MIL-F-8785C)	σ_w ft/sec	Exceedence Probability
Negligible	2.5	Light	2.5	10^{-1}
Moderate	5.2	Moderate	5.1	10^{-3}
Heavy	7.2	Severe	7.6	10^{-5}

The right-hand boundary in Figure B-31 at $\lambda_{sp_1} = .35$ ($T_2 = 2$ sec) is not based on any specific data. Rather, it reflects the lack of any data for larger λ_{sp_1}, the rapidity of a two-second divergence, and the certainty that such a boundary does exist for some λ_{sp_1} larger than .35.

A correction for Z_{θ_2} not in the range specified in Figure B-31 is given in Figure B-32. The correction is given as a pilot rating increment (ΔPR), with its value dependent on whether λ_{sp_2} is above

or below the critical value $(\lambda_{SP2_{crit}})$. The net pilot rating is the sum of the interpolated value from Figure B-31 plus the increment from Figure B-32. It should be noted that the net PR is limited to no better (less) than $PR_{crit} = PR(\lambda_{SP_1}, \lambda_{SP2_{crit}})$. The Flying Qualities Level is then obtained by applying the previously given equivalence.

A correction for low control sensitivity is given in Figure B-33. This correction is to be added, as a pilot rating increment (ΔPR), to the pilot rating interpolated from Figure B-31 (corrected for Z_{θ_2}). Thereafter, the resultant pilot rating is converted to the equivalent Flying Qualities Level. The control sensitivity correction is actually the average increment in pilot rating going from $M_{\delta_{ES}}$ = .341 to .085, a 75% reduction, and reflects all the data obtained on sensitivity. Applying a flat correction to all cases in the indicated range is dictated by the lack of data and a need for caution. No data is available on too high sensitivities.

Apply correction for $.08 \leqslant M_{\delta_{ES}} < .25$

Average ΔPR for all turbulence levels

PR = PR (Figure B-31 & B-32) + ΔPR (Low M_δ)
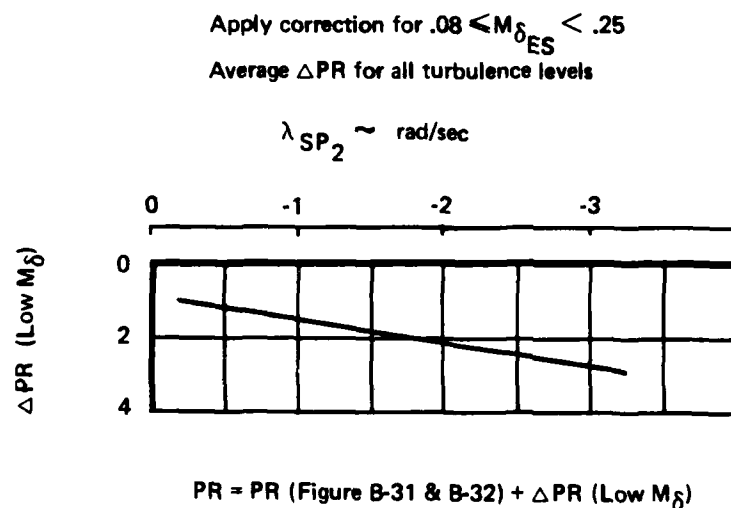
Figure B-33. Correction for Low Control Sensitivity to RSS Criteria for Approach and Landing

Data on control authority indicate the following criteria apply to all degrees of relaxed static stability, for both augmented and unaugmented airplanes, and are valid for both moderate and heavy turbulence.

$$M_{c_{max}} = M_{\delta_h} \delta_{h_{max}} \qquad \begin{cases} .13 \text{ rad/sec}^2 & \text{nose-up} \\ .18 \text{ rad.sec}^2 & \text{nose-down} \end{cases}$$

$$\dot{M}_{c_{max}} = M_{\delta_h} \dot{\delta}_{h_{max}} \qquad \pm.9 \text{ rad/sec}^2/\text{sec}$$

The above requirements are for the control margins over and above control required for trim, steady maneuvers, and specific transients such as configuration changes or failures. The requirements are specifically for approach and landing, but should be applicable over the flight envelope, including stall (nose down only).

Additional characteristics that are implicit in the above criteria have to do with phugoid stability, flight-path stability, lateral-directional characteristics, and control system dynamics. The simulation had Level 1 characteristics for all of the above except for phugoid damping which was as low as $\zeta_p = .01$. Degrading them to Level 2 would probably not affect the results, but the following characteristics would best be met to avoid difficulty:

$$\omega_{n_p} < .3 \text{ rad/sec}$$
$$\zeta_p < 0$$
$$d\gamma/dV < 0$$

Pitch control system dynamics were Level 1, clearly adequate for the task. Specifically, the delay in pitch acceleration response ($\dot{q}$) to pitch control input (MIL-F-8785C, par. 3.5.3) does not exceed 0.1 seconds.

The basis for the above criteria is largely the fixed-base simulation, validated to a degree by repeating LAHOS (Ref 8) flight test results. The criteria of Figure B-31 are well supported by the simulator data. The trends indicated for the effect of Z_{θ_2} in Figure B-32 are also clearly supported by the simulator data, but there were insufficient data to fully define the interaction with other parameters (λ_{sp_1}, λ_{sp_2}). The criteria for the effect of control sensitivity presented in Figure B-33, or the force levels specified in the text for M_{F_s}, clearly fail to treat the requirements adequately.

B.6 Simulation Results - Closed-Loop Analysis

The parametric analysis of the simulator flying qualities data developed in the Section B.5, though appealing because of its simplicity, leaves much to be desired. The approach can take into account only those parameters which were systematically varied in the experiment, only for the range of the parameters investigated, and only for the baseline conditions and values of other characteristics and parameters that were present in the simulator. For example, there is nothing in the parametric approach that would predict or tell what the effect would be of changes in the control system or feel system dynamics or phugoid characteristics. A more general approach is needed, one which is capable of dealing not only with the effects of RSS investigated on the simulator, but also which has been successfully used to analyze and predict the effects of other characteristic changes. More specifically, an approach is needed which can take into account, at a minimum, the attitude response of the airplane over the pertinent frequency range, about from 0.1 to 10 radians per second for pilot control of attitude. The approach should allow inclusion in the treatment of RSS characteristics of the higher frequency (above 0.1 rad/sec) effects of speed change and phugoid dynamics, and the higher order effects of the flight control system including feel system, servo and actuator dynamics, and possible feedforward or feedback control system elements. Given a generalized approach which can accommodate RSS within its framework, it should be possible to extrapolate the results of the current investigation to much broader range of parameters and conditions.

The closed-loop frequency response approach of Neal and Smith (Ref. 7) provides such a more generalized approach. Originally developed to analyze and predict longitudinal flying qualities in up and away flight based on pilot-airplane closed-loop performance in pitch attitude tracking tasks, the Neal-Smith approach incorporates most of the above described necessary features. Accordingly, the Neal-Smith approach and criteria have been applied to the simulator flying qualities data, and with some modification and adaptation of the approach, the results look justifiable and promising.

B.6.1 Adaptation and Justification of Neal-Smith Criterion

This section describes the original Neal-Smith criterion as developed
in Reference 7. It then describes the results of applying the criterion
to airplanes with a range of static stability and shows the problems
encountered with relaxed static stability. Finally, a modified Neal-
Smith approach is developed and justified based on the simulator pilot
rating data and comments and quantitative measurements from simulator
time histories of pilot evaluations.

B.6.1.1 Original Neal-Smith Criterion

The following description of the Neal-Smith criterion is taken from
Reference 7, Section VIII, but with some changes made for simplicity and
clarity.

The basic Neal-Smith premise was as follows. The acceptability to
the pilot of an airplane's maneuvering dynamics in the performance of a
given task can be defined in terms of the pilot compensation required to
achieve some minimum "performance standard" with the least possible
tendency to oscillate or PIO. The performance standard is dictated
primarily by the requirements of the task. For the combat phase of a
fighter's mission, precise control of pitch attitude is fundamental and
critical. Hence the pilot compensation and closed-loop performance in
pitch attitude tracking will be a defining factor in longitudinal flying
qualities.

Implementing this basic premise for pitch attitude control in the
frequency domain, Neal and Smith defined the model shown in Figure
B-34(a) for the closed-loop pilot-airplane combination. The following
terms are defined.

> Bandwidth (BW): The frequency for which the closed-loop phase angle,
> ϕ_{θ/θ_c}, is -90 deg.

> Droop: The minimum value of closed-loop amplitude, A_{θ/θ_c}, below
> 0 db (or < 1) for frequencies less than BW, illustrated in Figure
> B-34(b).

<u>Performance Standard</u>: A minimum bandwidth, $(BW)_{min}$, of 3.5 rad/sec, and a maximum droop of 3 db. Stated mathematically

$$\left. \begin{array}{l} \phi_{\theta/\theta_c} > -90^{o} \\[2ex] A_{\theta/\theta_c} > -3 \text{ db} \end{array} \right\} \qquad \text{for } \omega < 3.5 \text{ rad/sec}$$

The performance standard is depicted in Figure B-34(b).

<u>Resonant Amplitude (RA)</u>: Magnitude of any closed-loop resonant peak, $|\theta/\theta_c|_{max}$, that results from meeting the performance standard, illustrated in Figure B34(b).

<u>Pilot Compensation (ϕ_{PL})</u>: The phase angle of the pilot lead or lag compensation evaluated at $\omega = (BW)_{min}$, not including the time delay $(e^{-0.3s})$.

$$\phi_{PL} = \sphericalangle \left(\frac{\tau_{p_1} s + 1}{\tau_{p_2} s + 1} \right) \quad s = j\omega = j(BW)_{min}$$

The Neal-Smith Criterion is stated as follows.

<u>Neal-Smith Criterion</u>: Find values of K_p, τ_{p_1}, and τ_{p_2} which will minimize the resonant amplitude RA while maintaining a minimum bandwidth of 3.5 rad/sec and a maximum droop of -3 db. The values of ϕ_{PL} and RA corresponding to this condition are plotted on the criterion of Figure B-35 to define the flying qualities or acceptability of the airplane's maneuvering characteristics (PR or Level).

Though Neal and Smith state their criteria with a $(BW)_{min}$ = 3.5 rad/sec, they used 3.0 rad/sec to correlate some of their data and 2.5 rad/sec to correlate the data from Reference 6. As reasons for using these lower bandwidths, they cite (in Ref. 7) airplane deficiencies for each case which kept the pilot from flying as aggressively as he did without the deficiency and led to his accepting a lower level of performance.
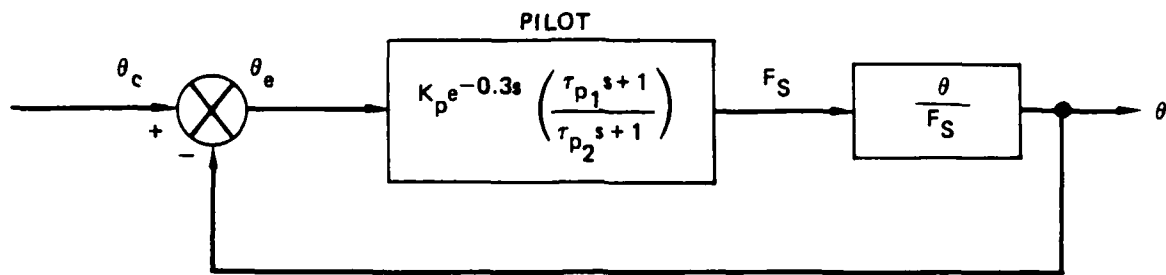
(a) MODEL OF CLOSED-LOOP PILOT-AIRPLANE COMBINATION
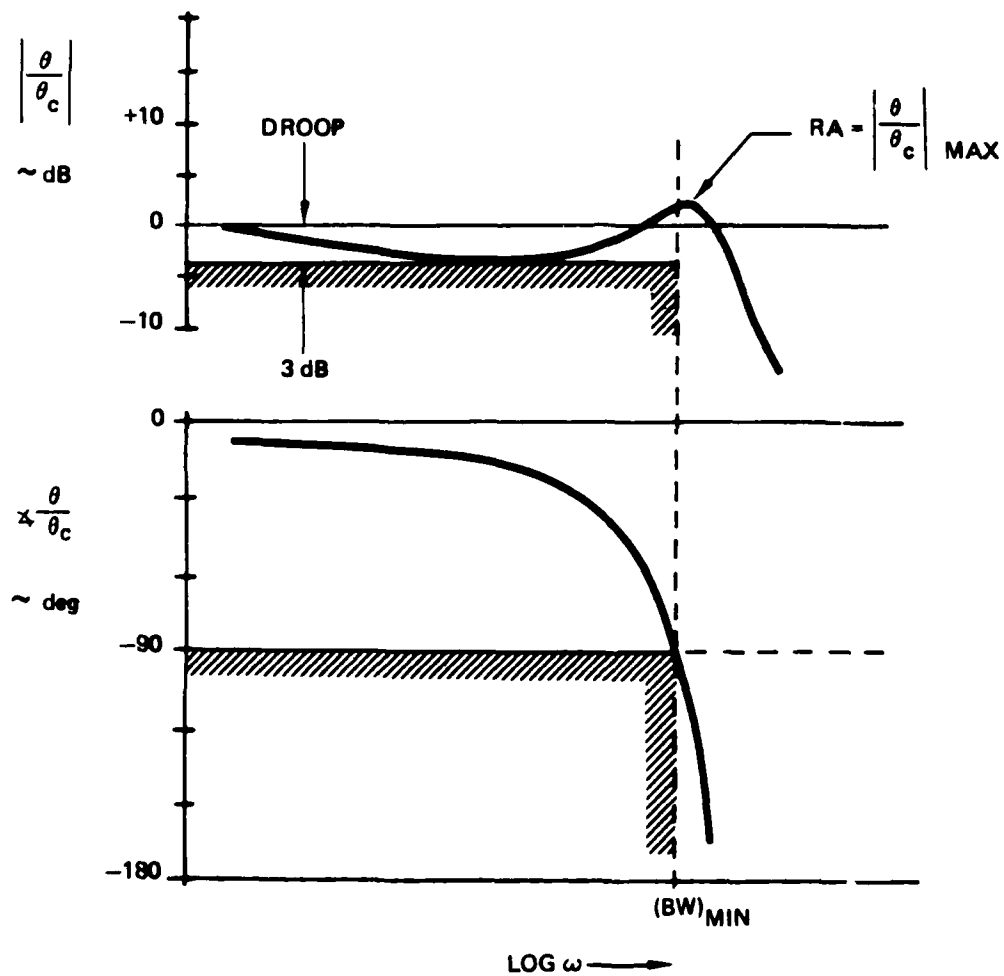
(b) PERFORMANCE STANDARD FOR PITCH ATTITUDE TRACKING

Figure B-34. Model and Performance Standard for Neal-Smith Criteria

165
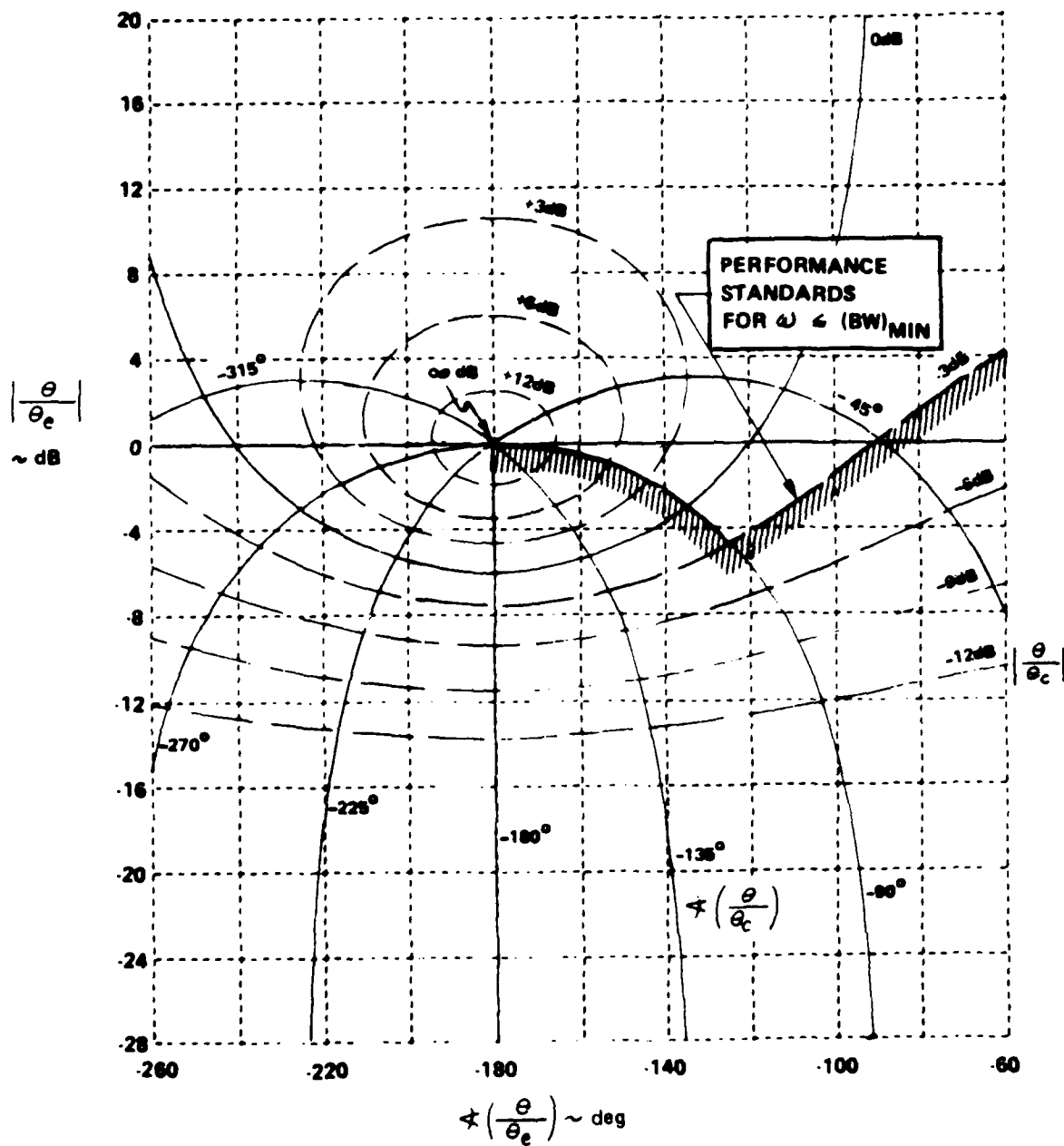
Figure B-34. Model and Performance Standards of Neal-Smith Criterion
(c) Nichols chart

166
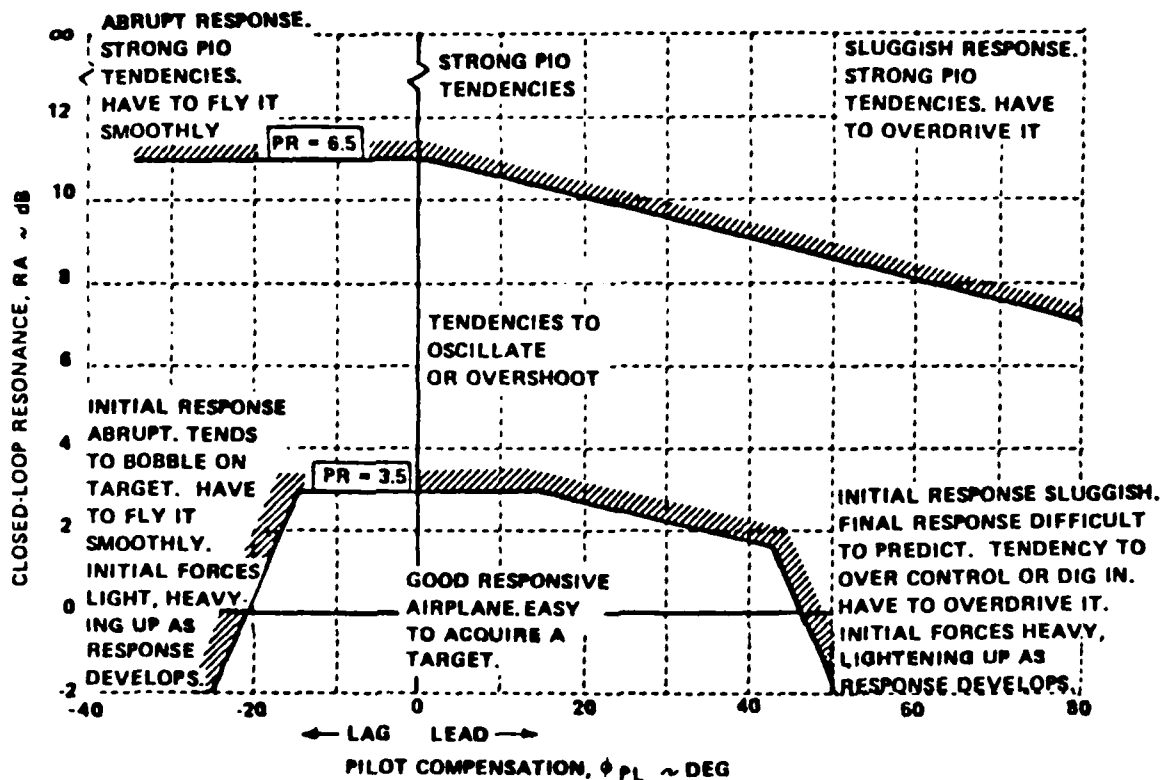
Figure B-35. Neal-Smith Criterion for Fighter Maneuvering Dynamics

Neal and Smith (Ref. 7) interpret the bandwidth as a measure of how quickly the pilot can move the airplane nose toward the target, the droop as a measure of how slowly the nose settles on target (supposing no large oscillations), the resonant amplitude as a measure of the tendency to oscillate or PIO, and the pilot lead or lag as a measure of the pilot's physical and mental workload. The time delay represents both the reaction-time delay (neural synaptic, nerve conduction, and central processing times) and the neuromuscular lag. The pilot model, with its gain, delay, and lead-lag elements, is not meant to be an accurate representation of the pilot. Rather, it is a compensation element which can be used to examine the closed-loop attitude performance and assess flying qualities of the airplane based on the parameters of the required compensation and the performance realized.

167

It is intuitively appealing that parameters in the pilot model or compensation element correspond to physical characteristics of the pilot, and that performance parameters such as bandwidth and resonant amplitude correspond to physical characteristics found in the time response of the airplane flying under pilot control. The higher the degree of this correspondence, the more likely are we to accept the results and criteria based on the results.

Neal and Smith implemented the criterion with graphical techniques based on the use of "Nichols charts", illustrated in Figure B-34(c), which relate open- and closed-loop frequency response (see for example, Ref. 53). The ordinate and abscissa in Figure B-34(c) are the open-loop amplitude and phase while the curvilinear coordinates are closed-loop amplitude and phase. The symbols on Figure B-34(c) correspond to those in the diagram of Figure B-34(a). The Neal-Smith criterion bounds for phase and droop are indicated on Figure B-34(c).

The graphical technique of Neal and Smith (Ref. 7) is tedious and time consuming. Mayhew (Ref. 27) developed a digital computer program to perform the calculations. The Mayhew program does not minimize the resonant amplitude, but rather, solves the relations for a given bandwidth (BW) and "DROOP". Normally the minimum resonant amplitude is obtained with BW = $(BW)_{min}$ and "DROOP" = -3 db, so the Mayhew program directly calculates the Neal-Smith criterion parameters, pilot lead (ϕ_{PL}) and resonant amplitude (RA). A Calspan Corp. modified version of the Mayhew program has been used to perform the Neal-Smith computations in this report.

Though the Neal-Smith computer program eliminates the need for the Nichols charts for computational purposes, this form of presentation is most valuable for understanding and interpreting the results of Neal-Smith analyses, and accordingly, is used extensively for this purpose.

B.6.1.2 Problems in Applying Neal-Smith Criterion to RSS

Direct application of the Neal-Smith criterion to airplanes with relaxed static stability immediately uncovers difficulties which show that some modification to the approach is necessary. To illustrate,

168

three configurations with progressively less stability have been selected for example application of the Neal-Smith criterion:

Configuration	Stability Level
L21	Good ($1.5 < PR < 6$; $\overline{PR_0} = 2$)
FO	Marginal ($3 < PR < 5$; $\overline{PR_0} = 4$)
S42	Unstable ($5.5 < PR < 7$; $\overline{PR_0} = 6$)

The pilot rating range indicated includes the best and worst ratings given by any pilot for all turbulence levels evaluated; $\overline{PR_0}$ is the mean overall (worst of ILS, visual, FTD) rating of all pilots for negligible turbulence, rounded to the nearest half rating. Configuration L21, the simulation of LAHOS 2-1, is near the center of the MIL-F-8785C short-period requirements and should exhibit excellent flying qualities. Configuration FO, the unaugmented F-111A with cg at 35%, has $\omega n_{sp} = 0.90$ rad/sec and $n/\alpha = 4.5$ g/rad at the 145 knot landing speed, which places its short period on the lower Level 1 boundary. Configuration S42, statically unstable with time to double amplitude of 4 seconds, does not meet even the MIL-F-8785C Level 3 requirements, but is clearly Level 2 based on pilot ratings.

For approach and landing, bandwidths (BW) from 1 to 3 rad/sec have been applied using the Neal-Smith criterion. Smith (Ref. 8) applies BW from 1.5 to 3 in 0.5 increments, and notes that the change in resonance (RA) with BW is indicative of pilot rating, a large gradient indicating poor flying qualities. Radford and Smith (Ref. 46) further examine the LAHOS data for the relationship of pilot rating to various gradients resulting from Neal-Smith analysis. They find the gradients $\partial\phi_{PL}/\partial BW$, $\partial RA/\partial BW$, and $\partial RA/\partial\phi_{PL}$ very important, and that landing is a high bandwidth task. There is considerable evidence that pilot gain and bandwidth are only moderate for ILS or visual approaches, but as the airplane approaches the ground and the pilot has to make a flare and touchdown, pilot gain and bandwidth increase substantially. The consensus appears to be that in the approach the pilot is satisfied to achieve a BW = 1, but in the final flare and touchdown, below 50 ft. altitude, he tries to achieve a BW = 3.

Configuration	BW rad/sec	ϕ_{PL} deg	RA dB	ω_{RA} rad/sec
L21	.5	−42.5	0.9	.30
$\left(\dfrac{Stable}{\overline{PR}_o = 2}\right)$	1.0	−34.7	0.2	.40
	1.5	−16.0	−1.5	1.90
↓	2.0	0	3.4	2.40
	2.5	26.9	2.8	2.80
	3.0	45.3	5.0	3.40
	3.5	58.8	8.3	3.95
FO	.5	−16.0	0.6	.25
$\left(\dfrac{Stable}{\overline{PR}_o = 4}\right)$	1.0	31.3	−2.6	.85
	1.5	64.6	−2.0	1.15
↓	2.0	79.2	−0.8	1.65
	2.5	$\phi_{PL} > 90°$ (and higher BW)		
S42	.5	55.7	2.0	.30
$\left(\dfrac{Unstable}{\overline{PR}_o = 6}\right)$	1.0	64.5	3.3	.40
	1.5	76.7	2.1	.40
↓	2.0	88.2	−0.3	.35
	2.5	$\phi_{PL} > 90°$ (and higher BW)		

Note: Pilot model of Figure B-34(a) with −0.3 second delay and −3 dB droop

With the foregoing in mind, the three selected configurations have been analyzed for BW from .5 to 3.5 using the standard Neal-Smith approach (pilot model of Figure B-34(a), -3 db droop) and the results are presented in Table B-21.

For the good stable configuration (L21) the pilot compensation is moderate ($42°$ lag to $59°$ lead), resonance varies slowly (-1.5 to 8.3 db), and for BW = 1.5 to 2.5 rad/sec the configuration would have PR < 3.5 on the Neal-Smith criterion (Fig. B-35). Comparing the results for L21 with Smith's (Ref. 8) for LAHOS 2-1, we see that they are similar (e.g., Smith obtains for BW = 1.5, ϕ_{PL} = -25$°$ and RA = 3 db; for BW = 3, ϕ_{PL} = 42$°$ and RA = 6 db).

170

For configuration FO, the pilot lead is greater than 90° for BW greater than two, so the pilot model is incapable of closing the loop any tighter than BW ≃ 2. However, the resonance is negligible for all achievable BW. For Configuration S42 the maximum BW is also 2 rad/sec and resonance is small (RA < 3.3 db) for all achievable BW, but ϕ_{PL} is larger than for FO, particularly at the low BW. Viewing the gradients Smith and Radford (Ref. 46) find important, for FO and S42 the gradient $\partial RA/\partial BW$ is roughly zero and much less than that for L21, similarly for $\partial RA/\partial\phi_{PL}$. For $\partial\phi_{PL}/\partial BW$ the gradients are similar for all three configurations. By these measures, pilot rating for S42 and FO ought to be as good or better than for L21. Only one characteristic stands out in Table B-21 as varying with flying qualities, the amount of pilot compensation or pilot lead (ϕ_{PL}), which increases in proportion to the pilot rating at any given bandwidth. Recent trends have been to downrate pilot lead as an indicator of flying qualities (e.g. Chalk's criteria, Ref. 23, Section 3.5.7, involve only the resonant amplitude and place no constraint on phase). Emphasis on pilot lead would go back to the original Neal-Smith criteria (Fig. B-35) which show a strong effect of ϕ_{PL} on the Level 1 (PR = 3.5) boundary though only a minor effect on the Level 2 (PR = 6.5) boundary. The primary conclusion to be drawn from Table B-21 is that the pilot model must be changed to allow larger pilot lead so higher bandwidths may be realized. A second important conclusion is that though FO is stable, its marginal stability makes its characteristics not unlike those of unstable S42.

To examine further and illustrate the results of Neal-Smith analysis for the three example configurations, the various steps in the analysis are depicted graphically in Figure B-36, parts (a) through (e). The open-loop frequency response for the three configurations (L21, FO, and S42) are presented in Figure B-36(a). These are for the airplane alone and do not include the pilot model. L21 has a conventional frequency response representative of a good airplane, with obvious resonance and phase shift due to the phugoid at ω = 0.2 rad/sec, and with break in amplitude and concomitant phase shift above ω = 2.0 rad/sec due to the well-damped short period ($\omega_{n_{sp}}$ = 2.3 rad/sec). FO, similar in amplitude to L21 up to ω = 1 rad/sec, shows the effect on amplitude and phase of the low short-period frequency ($\omega_{n_{sp}}$ = 0.9 rad/sec) above 1

rad/sec. S42 shows the 180° lag at low frequencies typical of unstable RSS configurations, and the heavier damping of the "third mode" type of phugoid. However, above ω = 2 rad/sec, S42 and FO are equal in phase, all three are equal in slope of amplitude with frequency, but FO has a quarter the sensitivity of S42 (12 db lower). Clearly, the increasing phase lag in the .3 < ω < 1 rad/sec range must be indicative of the stability and pilot rating.

Nichols charts showing the results of Neal-Smith loop closures for the three example configurations are presented in Fig. B-36, L21 and FO in part (b) and S42 separately in part (c) to avoid confusion. The frequency response curves include the pilot model, gain, delay, and compensation, and are for DROOP = -3 db and BW = 2 rad/sec, the highest bandwidth achievable for all three configurations. L21 and FO have the typical low-frequency loop caused by the phugoid, and the knee below the bandwidth at the criterion -3 db droop (ω = .5 for FO, 1.0 for L21). The Neal-Smith computer program used normally includes frequencies from 0.1 BW to 10 rad/sec. So for BW = 2, the lowest frequency considered for droop was 0.2 rad/sec, thus omitting the greater than -3 db droop of L21 and FO for ω < 0.1 rad/sec. A 0.2 rad/sec frequency has a period of 31 seconds, and any such low frequency must be below the effective frequency band for the pilot's attitude loop closure with pitch control, and would be more subject to altitude-rate or speed loop closures with throttle (possibly also pitch control). Though L21 has a typical resonance of about 3 db at a frequency above the bandwidth, FO has a maximum of about -1 db, so a better Neal-Smith closure would be with less droop, hence less pilot lead, and a unity (0 db) closed-loop gain near bandwidth frequency.

The characteristics displayed in Figure B-36(c) for S42 are different. The phugoid loop has collapsed, with closed-loop lag approaching -180 deg at low frequency. There is no knee, -3 db droop and bandwidth are coincident, and maximum closed loop gain (< 0db) is at a low ω = .3 rad/sec. The required pilot lead of 88.2 deg (Table B-21) requires a $1/\tau_{p_1}$ = .063 rad/sec, so the upward break in magnitude of the lead is more than a decade below the bandwidth. This low break frequency results in low loop-gain at low frequencies as gain is set by the criterion at bandwidth. Wasserman, et al. (Ref. 54) uncovered this same behavior for

172
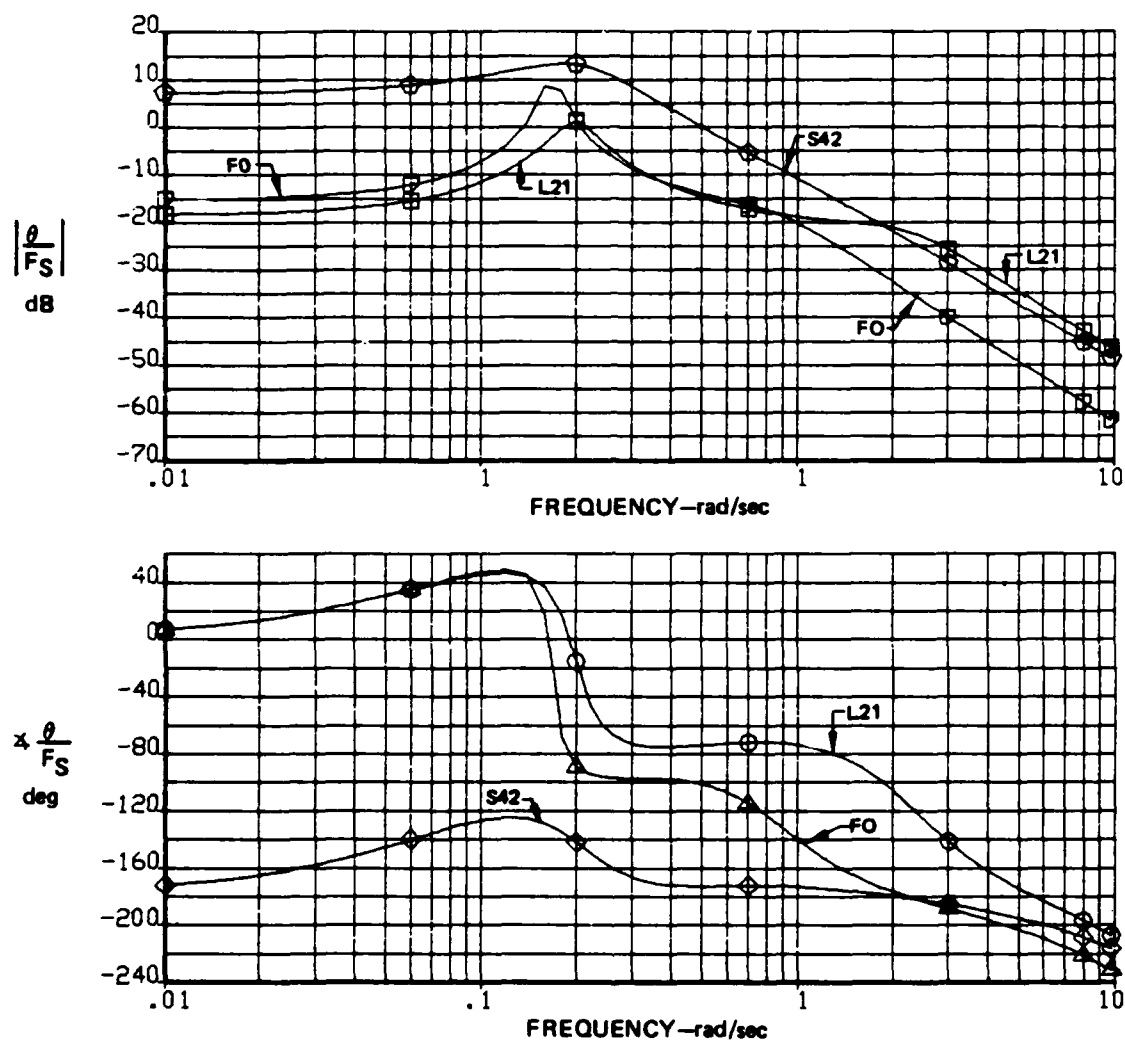
Figure B-36. Neal-Smith Analyses—Configurations L21, FO, and S42
(a) Open-loop Frequency Response of Airplane

BW = 2 rad/sec
Droop = −3dB
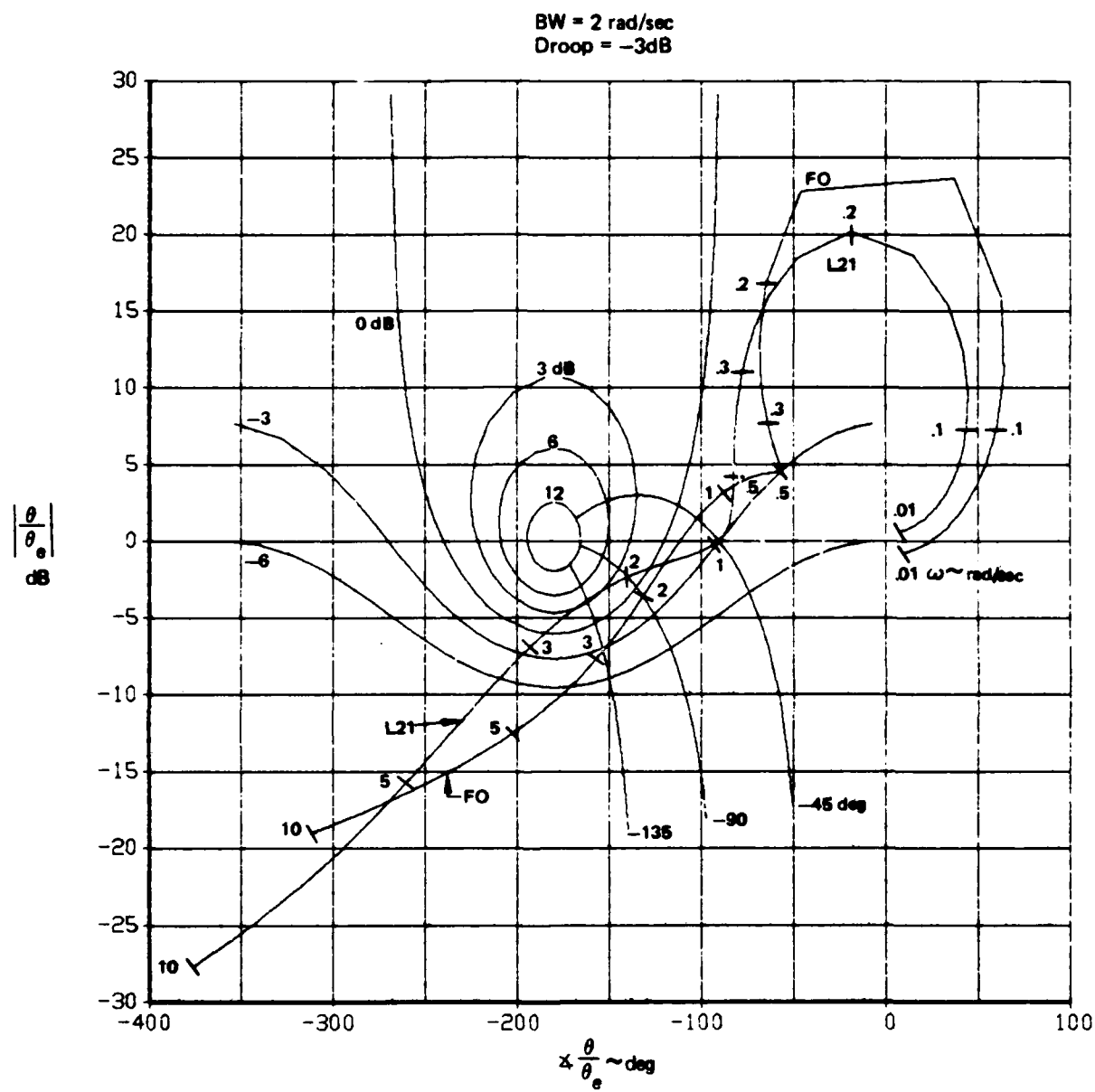
Figure B-36. Neal-Smith Analyses—Configurations L21, FO, S42
(b) Nichols Chart for L21 and FO

174
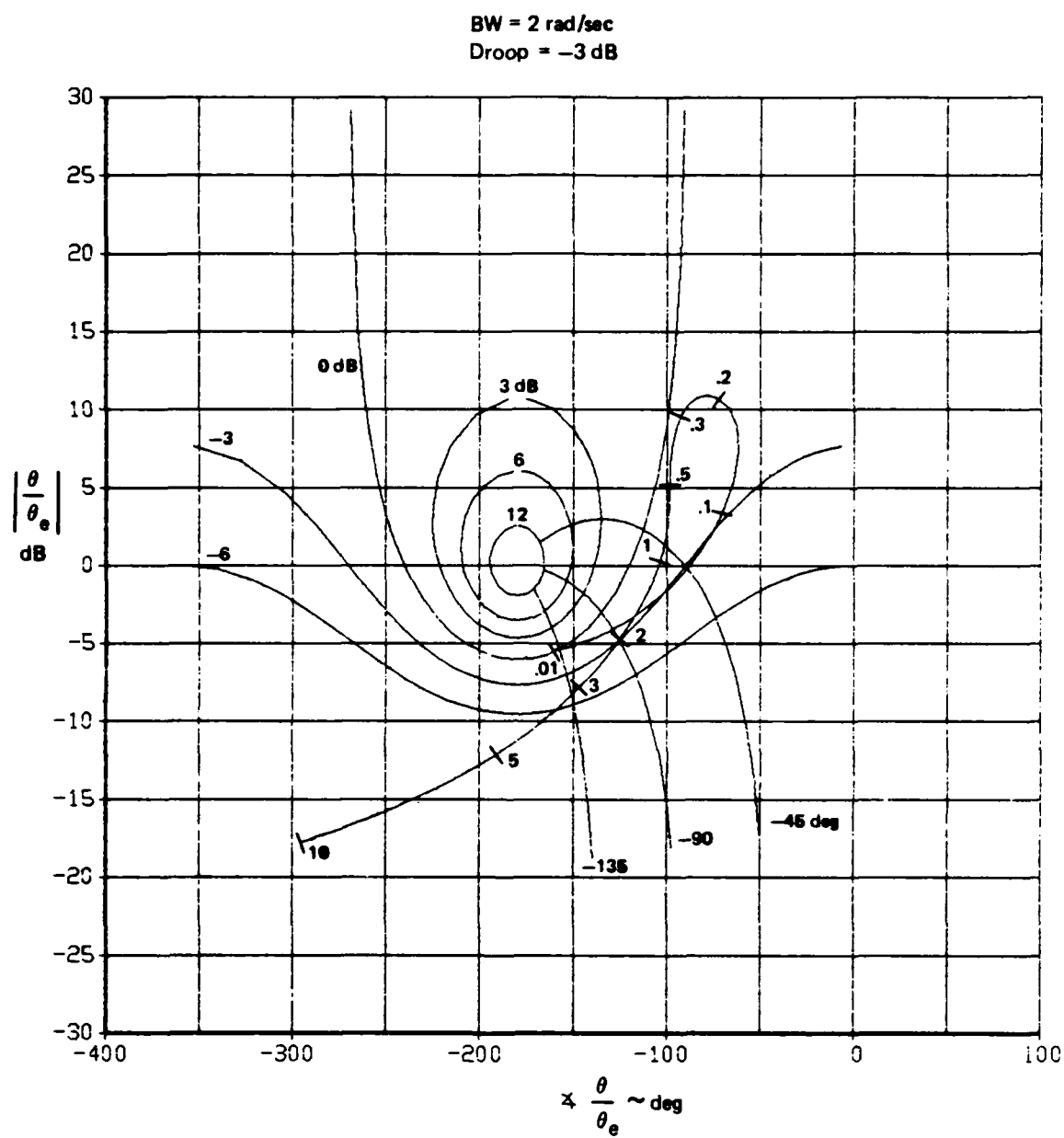
Figure B-36. Neal Smith Analyses—Configurations L21, FO, S42
(c) Nichols Chart for S42

175

their unstable SST configurations. They used bandwidths of 1.2 and 1.1 rad/sec., found too much lead required (> 90°) for some configurations, and found poor discrimination and poor correlation of pilot rating with lead and resonant amplitude for the worse cases.

To complete the picture for the standard Neal-Smith analysis of the three example configurations, the compensated (pilot gain, delay, and lead-lag) open-loop frequency responses are presented in Figure B-36(d), and the closed-loop responses in Figure B-36(e). The pilot compensated open loop curves, part (d), show that the three configurations have very similar magnitude and phase from $\omega = 0.3$ to 3.0 rad/sec. However, unstable S42 has a lag approaching -180° as frequency decreases. Also, despite its 7 db higher uncompensated low-frequency gain, its compensated low-frequency gain is 5 db lower than either L21 or FO. The closed-loop frequency responses (e) show the criterion to be met ($\phi = -90$ degrees at BW = 2; droop = -3 db) for $\omega > .2$ rad/sec. However, droop is greater for L21 and FO for $\omega < .08$ rad/sec, and phase is greater for S42 for $\omega < .035$ rad/sec. But, these frequencies are considered to be too low to be pertinent to the attitude loop closure as explained earlier. In the closed loop, FO and S42 look much alike for $\omega > .2$ rad/sec. However, the magnitude of S42 shows no sign of resonance near the bandwidth, dropping off steadily from near 0 db at $\omega = .3$ rad/sec to -3 db at the bandwidth, behavior typical of the unstable cases. The approach of closed-loop phase to -180 degrees with decreasing frequency suggests there is an unstable root near the origin ($\lambda \simeq +.03$).

To summarize the problems encountered with application of the standard Neal-Smith analysis to RSS configurations, the major problem is the pilot model can not generate enough pilot lead ($\phi_{PL} > 90^\circ$) to achieve the high bandwidths (BW $\simeq$ 3 or 3.5 rad/sec) known to be characteristic of close-in visual flight and flare and touchdown. Other problems are the lack of resonance near bandwidth frequencies which should be there to reflect the PIO tendencies found for poor RSS configurations, and the low-frequency phase lag ($\phi \rightarrow -180^\circ$ as $\omega \rightarrow 0$) in the closed loop. A modified approach is needed, an RSS Neal-Smith criterion, which will correct these deficiencies and provide correlation with pilot rating data for RSS configurations.

BW = 2 rad/sec
Droop = −3dB
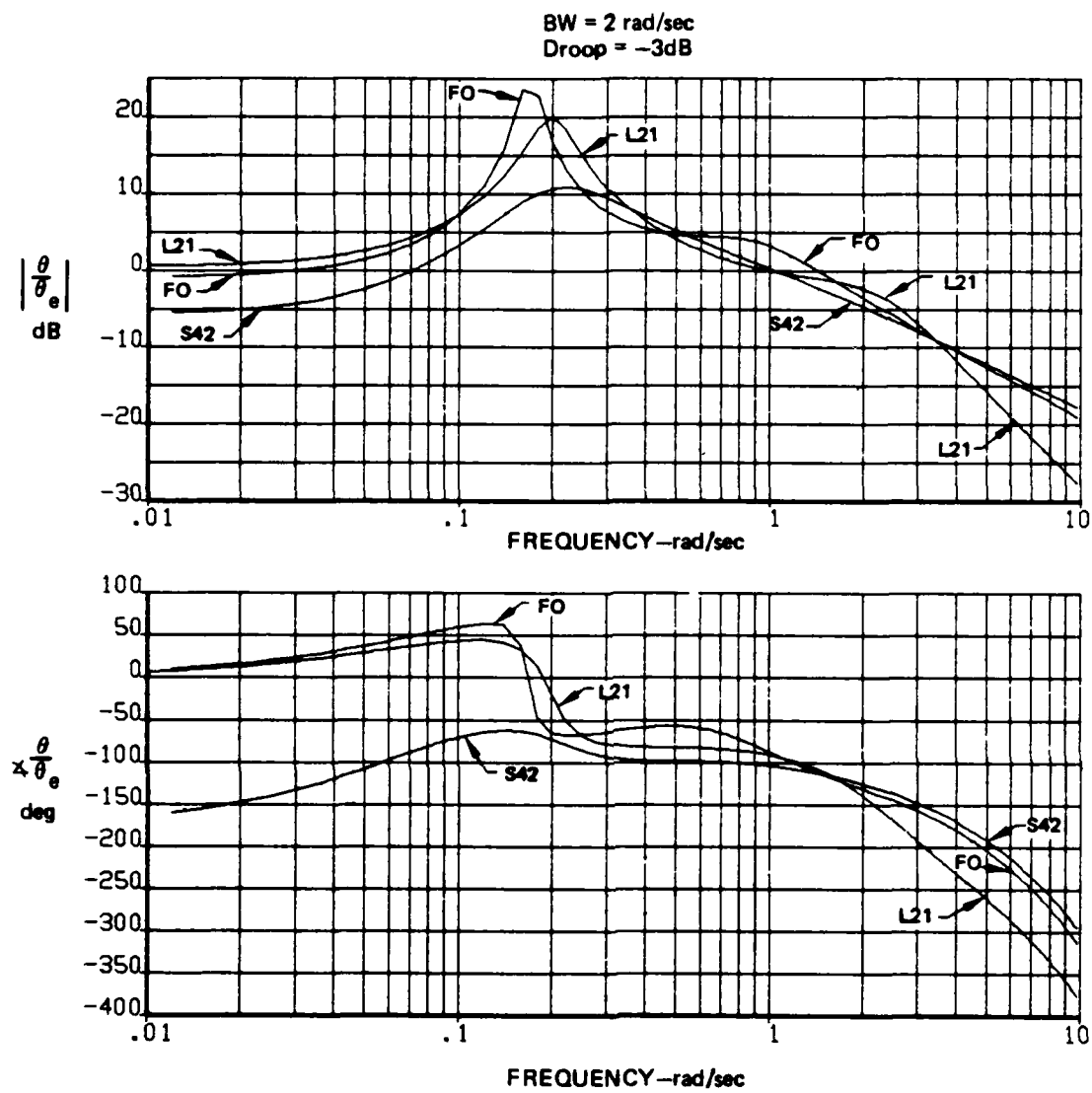
Figure B-36. Neal-Smith Analyses—Configurations L21, FO, and S42
(d) Pilot-compensated Open-Loop Frequency Responses

177

BW = 2 rad/sec
Droop = −3dB
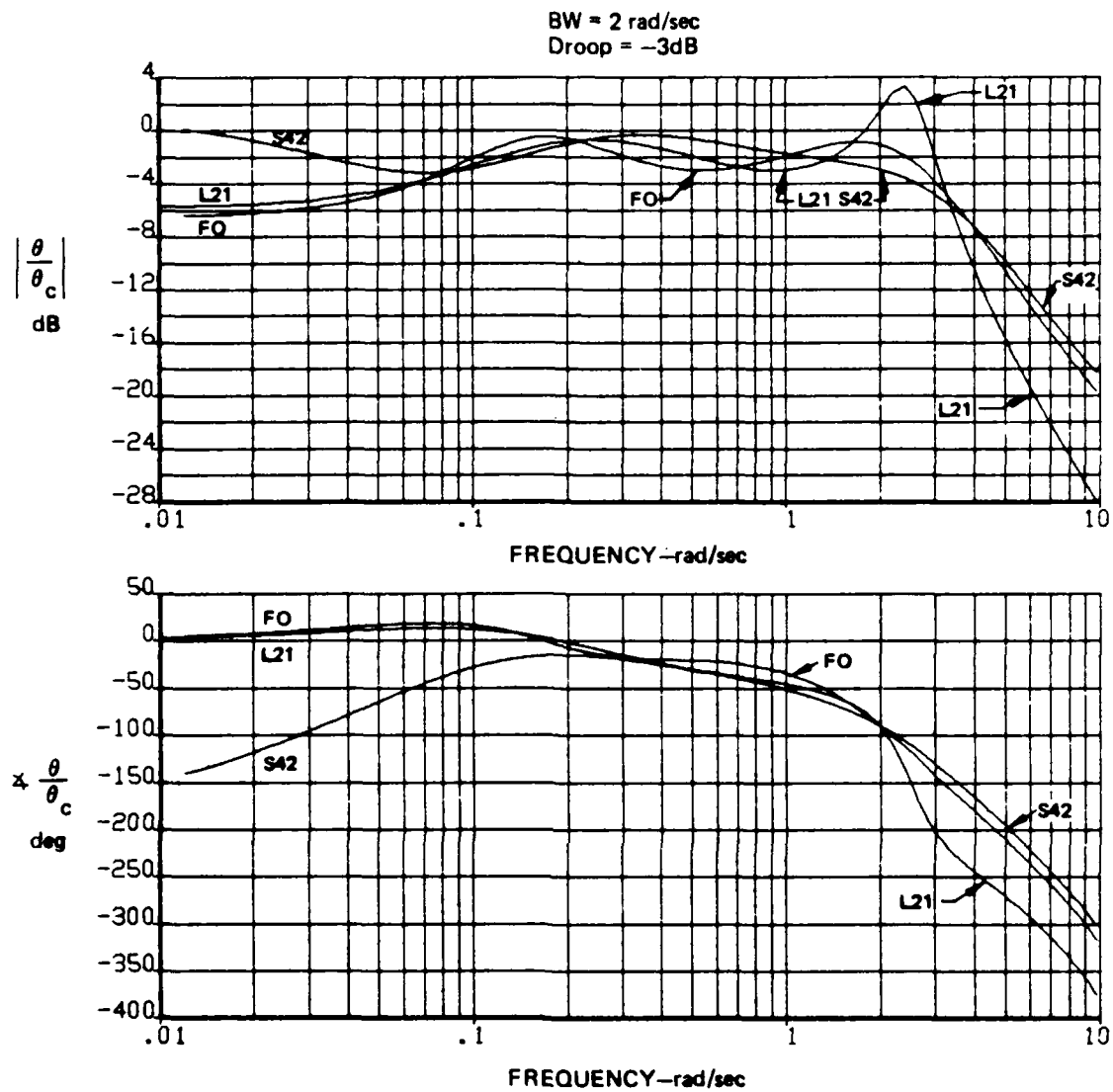
Figure B-36. Neal-Smith Analyses—Configurations L21, FO, S42
(e) Closed-Loop Frequency Response

178

B.6.1.3 Development of RSS Neal-Smith Criterion

The primary problem is to incorporate in the pilot model means for generating substantial additional lead above 90°. Examination of the pilot comments, especially of Pilot R, shows repeated reference to "overdriving" and to "spiking" the control, that is, applying a pulse to initiate the response, and then applying an opposite pulse to stop the response at the desired value (Appendix G, Runs 5/6/80-91-R and 5/8/80-91-R, of configurations S42A and S42, respectively). If the pilot flies stable airplanes with steps (a simplified view), then the derivative of these steps would be pulses (spiking). This suggests that the pilot incorporates differentiation in his output when dealing with less stable or unstable aircraft, i.e., an additional lead. Sudderth, et al. (Ref. 22) extracted amplitude and phase of the pilot from experimental data, then matched the data with analytical expressions. In some cases they found phase lead approaching 180 deg, and positive slopes of 40 db/decade in the 1 to 5 rad/sec range, indicative of two orders of lead. Based on the above, it is concluded that adding a second lead term to the pilot model $(\tau_{p_3} s+1)$ is a reasonable way to achieve the desired additional lead.

Accordingly, a new pilot model is proposed as follows for application to RSS or cases with low static stability where pilot lead above 85 deg is needed to achieve the higher bandwidths.

$$Y_p(s) = K_p e^{-0.3s} \frac{(\tau_{p_1} s + 1)(\tau_{p_3} s + 1)}{(\tau_{p_2} s + 1)}$$

$$1/\tau_{p_3} = BW$$

$$BW = 1 \text{ and } 3 \text{ rad/sec}$$

$$Droop = 0db$$

The selection of zero droop follows directly from the thesis that minimization of pilot lead is a primary objective. The selection of $1/\tau_{p_3} = BW$, and criterion based on two bandwidths, 1 and 3 rad/sec, were arrived at as follows.

Examination of the frequency responses for the various configurations in Appendix C shows that the effect of the unstable real root, λ_{sp_1}, on phase angle occurs primarily in the range $\omega = .2$ to 2 rad/sec (see Fig. C-15, -17, and -19). The effects of the negative real root, λ_{sp_2}, and the large θ/F_s zero, Z_{θ_2}, though extending to higher frequencies, are still predominant around $\omega = 1$ rad/sec (see Fig C-21, -23, -25, -27, and -29). Thus if a closed-loop frequency-response approach is going to be able to discriminate among the levels of pilot rating, it must take this phase shift around $\omega = 1$ rad/sec into account. If a Neal-Smith approach based on pilot lead at the bandwidth is to work, then BW = 1 seems necessary. This bandwidth is consistent with what has been found characteristic of ILS or visual approaches. On the other hand, the last part of the landing, the flare and touchdown, is a high bandwidth task, BW $\simeq 3$ rad/sec. Thus, it appears that in landing the pilot starts out using a low bandwidth (BW = 1) but increases this to a high value (BW = 3) later. Thus it makes sense that the airplane should meet criteria based on two bandwidths simultaneously. BW = 1 will effectively provide a criterion for RSS while BW = 3 will provide a criterion for higher order control system effects.

Examination of the effect of τ_{p_3} shows some very interesting properties for the RSS configurations. The table at the top of the following page shows the effect of varying τ_{p_3} for BW = 1 and 3 rad/sec, droop = 0 db, for configuration S42. <u>Pilot lead is invariant of</u> τ_{p_3}!

For BW = 1 rad/sec, the cases for $1/\tau_{p_3} = 1$ and 5 are the same since $1/\tau_{p_1}$ and $1/\tau_{p_3}$ are just exchanged. For BW = 3, the same is true of 1 and 5, also .2 and 10.

$1/\tau_{p_3}$ rad/sec	$1/\tau_{p_1}$ rad/sec	ϕ_{PL} deg	RA db	ω_{RA} rad/sec
BW = 1 rad/sec				
0.2	$1.52^{(1)}$	55	2.5	.55
1.0	5.78	55	4.7	.60
3.0	1.34	55	4.9	.60
5.0	1.04	55	4.7	.60
10.0	.86	55	4.6	.60

(1) lead-lag: $1/\tau_{p_2} = .66$

$1/\tau_{p_3}$ rad/sec	$1/\tau_{p_1}$ rad/sec	ϕ_{PL} deg	RA db	ω_{RA} rad/sec
BW = 3 rad/sec				
0.2	12.8	99	.7	3.30
1.0	5.21	102	2.4	1.10
3.0	1.98	102	3.5	1.35
5.0	1.06	102	2.5	1.15
10.0	.28	101	.1	2.75

The effects of τ_{p_3} on the shape of the response curves is most readily seen in the Nichols charts of Figure B-37, BW = 1 in part (a) and BW = 3 in part (b). For BW = 1, below the bandwidth the curves for $1/\tau_{p_3}$ from 1 to 10 are similar with 1 and 5 indistinguishable. Only the curve for $1/\tau_{p_3}$ = 0.2 is different, reflecting the lead-lag compensation. Above the bandwidth, τ_{p_3} strongly affects the shape of the curves. For BW = 3, the close resemblance of the curves with exchanged values of τ_{p_1} and τ_{p_3} is readily apparent. Closed loop resonance is about maximized with $1/\tau_{p_3}$ = BW for both bandwidths, a sought for result to bring the analysis into agreement with simulator results.

The major problems are clearly resolved by the new pilot model for RSS Neal-Smith analysis. Adequate pilot lead is available, there is potential for closed-loop resonance in the vicinity of the bandwidth frequency, and the closed-loop response at very low frequencies ($\omega \to 0$) approaches zero phase lag and indicates stability and moderate gain.

Configuration S42

$1/\tau_{P_3}$ = 0.2, 1, 3, 5, 10 rad/sec

BW = 1 rad/sec

Droop = 0 dB
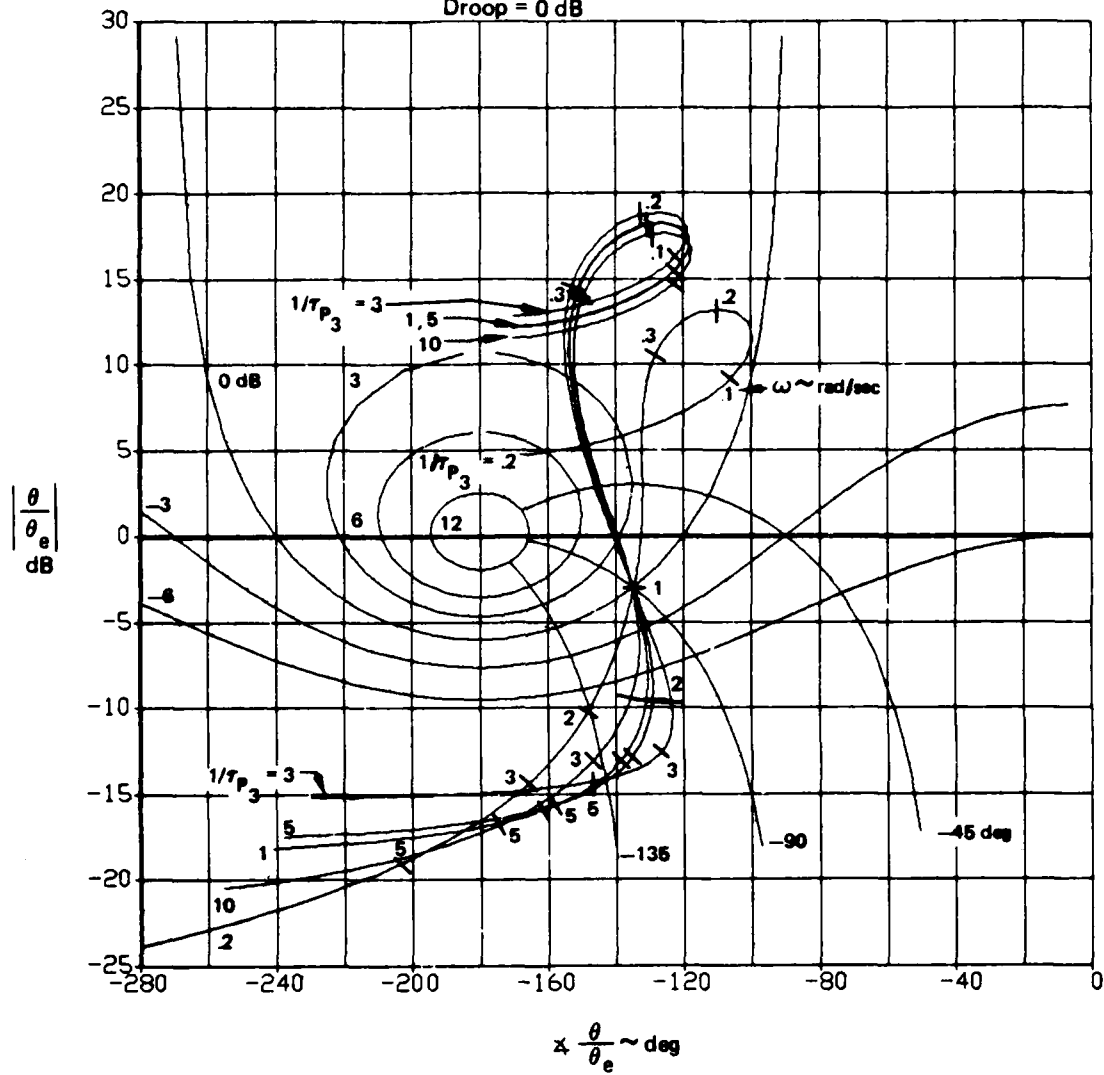
Figure B-37. RSS Neal-Smith Analysis Varying $1/\tau_{P_3}$

(a) BW = 1 rad/sec

182

Configuration S42
$1/\tau_{P_3}$ = 0.2, 1, 3, 5, 10 rad/sec
BW = 3 rad/sec
Droop = 0 dB
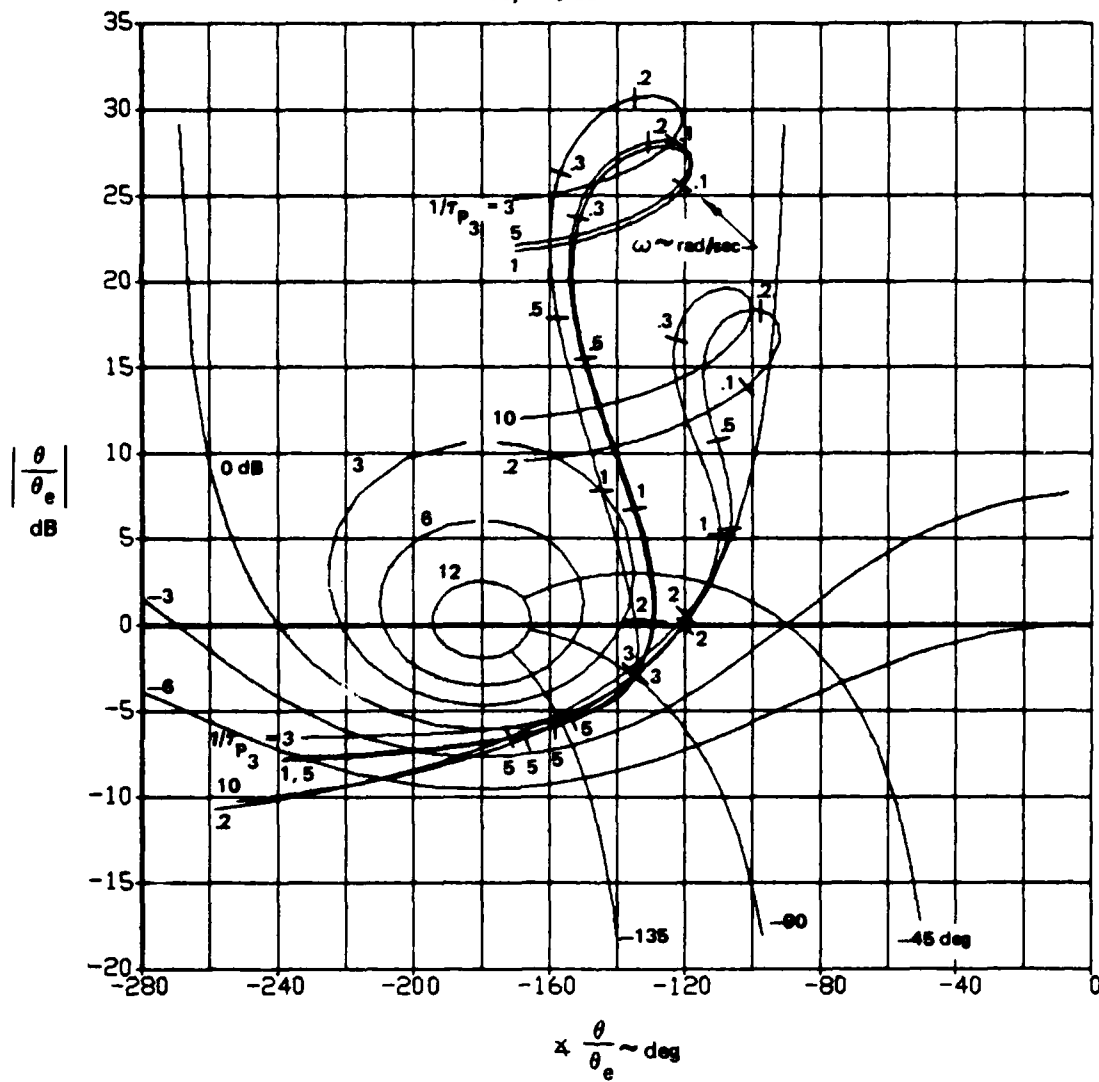
Figure B-37. RSS Neal-Smith Analysis Varying $1/\tau_{P_3}$
(b) BW = 3 rad/sec

B.6.1.4 Correlation of RSS Neal-Smith Analysis with Simulator Time Histories

Three simulator configurations are analyzed with the proposed RSS Neal-Smith approach and the results compared with time histories from the simulator. The three configurations include the previous example unstable case, S42, which is intermediate in characteristics, and two rapidly divergent cases, S21, with a small negative real root (λ_{sp_2}), and S24, with a large one. Nichols charts and closed-loop frequency responses are presented for BW = 1, 2, 3, and 4 rad/sec, together with the simulator time histories.

Configurations S42 and S42A

For configuration S42, the Nichols chart and closed-loop frequency response are found in Figure B-38, part (a) and (b) respectively. By comparison with Figure B-36, it is readily apparent that for this unstable configuration, the RSS Neal-Smith approach produces a more satisfactory closure of attitude (Fig. B38(a)) and closed loop performance (Fig. B38(b)). From the Nichols chart for S42 it is apparent that there are two possibilities for resonance, a lower frequency one (RA_1) around 1 rad/sec and a higher frequency one (RA_2) around 6 rad/sec. RA_1 is primarily associated with the phase lag due to the unstable root or negative static stability. RA_2 is associated with the combined phase lag from the negative real root (λ_{sp_2}), the actuator, and the feel system. The resonances themselves are most apparent in the closed-loop responses (Fig. B-38(b)). The values of pilot lead required to achieve the various bandwidths, together with the resonant amplitude and frequency thereof, are tabulated in Table B-22 on page 186.

A time history of configuration S42A (low sensitivity) with Pilot R (Fig. B-39) and two time histories of configuration S42, one with Pilot R and one with Pilot A (Figures B-40, (a) and (b)), are presented for comparison with the RSS Neal-Smith analysis. The time histories are, in each case, of the A run with negligible turbulence, and include most of the approach from glide-slope acquisition to touchdown. Note that Figures B-39 and B-40(b) have twice as large a time scale as Figure

BW = 1,2,3,4 rad/sec
Droop = 0 dB
$1/\tau_{P_3} = BW$
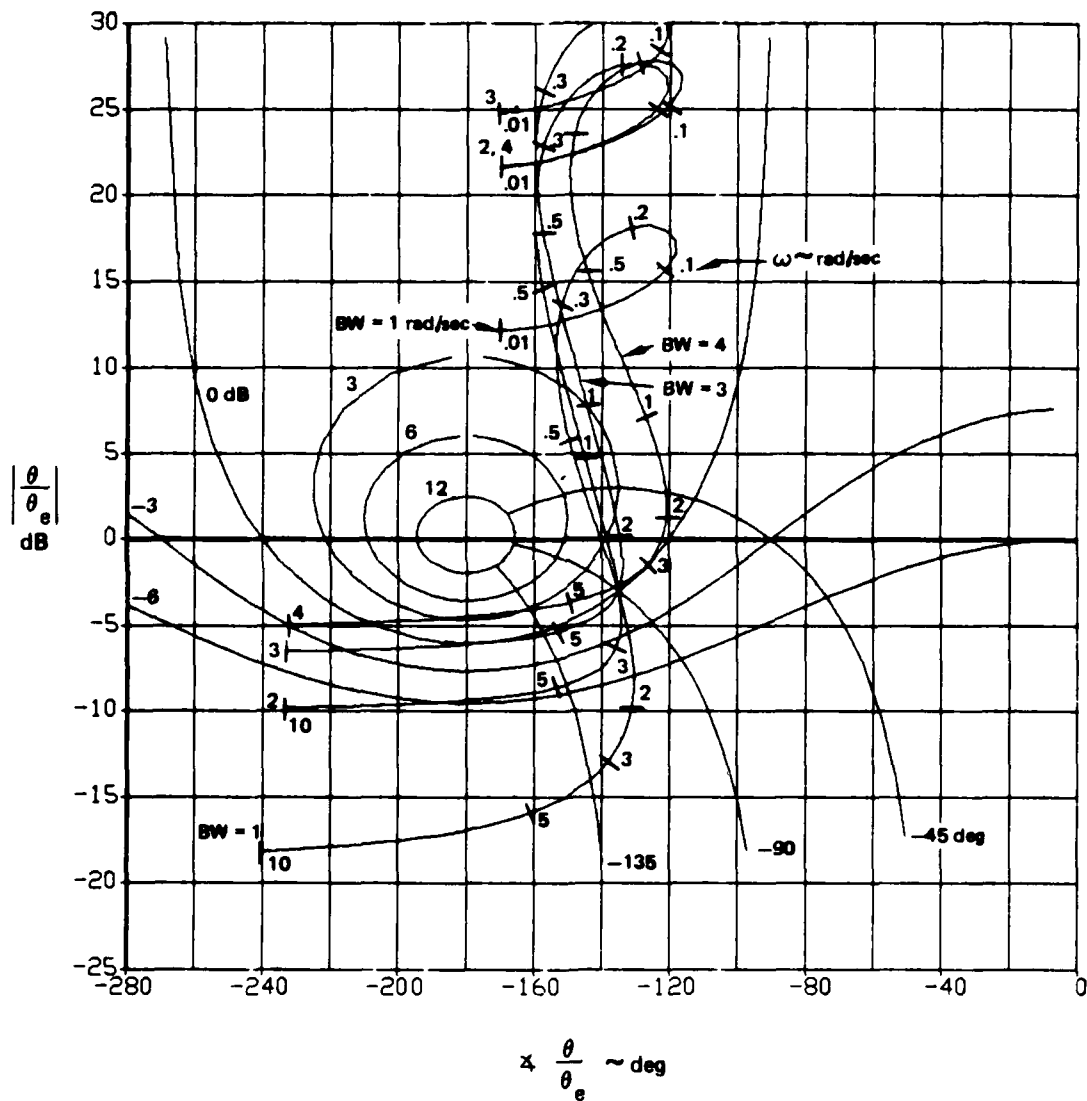
Figure B-38. RSS Neal-Smith Analysis of S42
(a) Nichols Chart

185

PILOT LEAD AND RESONANCE vs BANDWIDTH, CONFIGURATION S42

BW rad/sec	ϕ_{PL} deg	RA_1 db	ω_{RA_1} rad/sec	RA_2 db	ω_{RA_2} rad/sec
1	54.8	4.7	.6	--	--
2	78.6	4.2	1.1	--	--
3	101.6	3.5	1.4	0.0	6.3
4	122.6	2.8	1.3	1.8	6.6

B-40(a). Also, though not shown, RSS Neal-Smith computations and Nichols charts for S42A with its 20 rad/sec first-order actuator were compared with those for S42 for BW = 1 and 3 rad/sec, and no significant differences were found (only minor numerical differences, except for the factor of 4 in gain). Accordingly, the RSS Neal-Smith analytical results in Figure B-38 and the associated tabular data may be considered applicable to S42A as well as S42.

The characteristics in approach and landing for S42A as depicted in Figure 39 are considered first, as they show particularly clean oscillations and seem to correlate most easily with the RSS Neal-Smith closed-loop analysis. Viewing the overall motions, there is an obviously dominant oscillation (e.g., α, θ, $\dot{h}$) which speeds up in frequency following breakout to visual at 200 ft altitude. There is also a much higher-frequency oscillation, visible in stick force (F_{ES}) and horizontal tail position (δ_{h_L} and δ_{h_R}), and to a lesser extent in pitch rate (q). Note that because S42 was generated on the simulator by changes in aerodynamics rather than feedback, the symmetrical tail deflections ($\delta_{h_L} = \delta_{h_R}$) are from pilot pitch control alone, though antisymmetrical deflections ($\delta_{h_L} = -\delta_{h_R}$) include both pilot input and FCS augmentation.

The frequencies of oscillation as estimated by hand measurements from the approach time history are compared with resonant frequencies obtainable from the RSS Neal-Smith closures in the following Table B-23.

BW = 1,2,3,4, rad/sec
Droop = 0dB
$1/\tau_{P_3}$ = BW
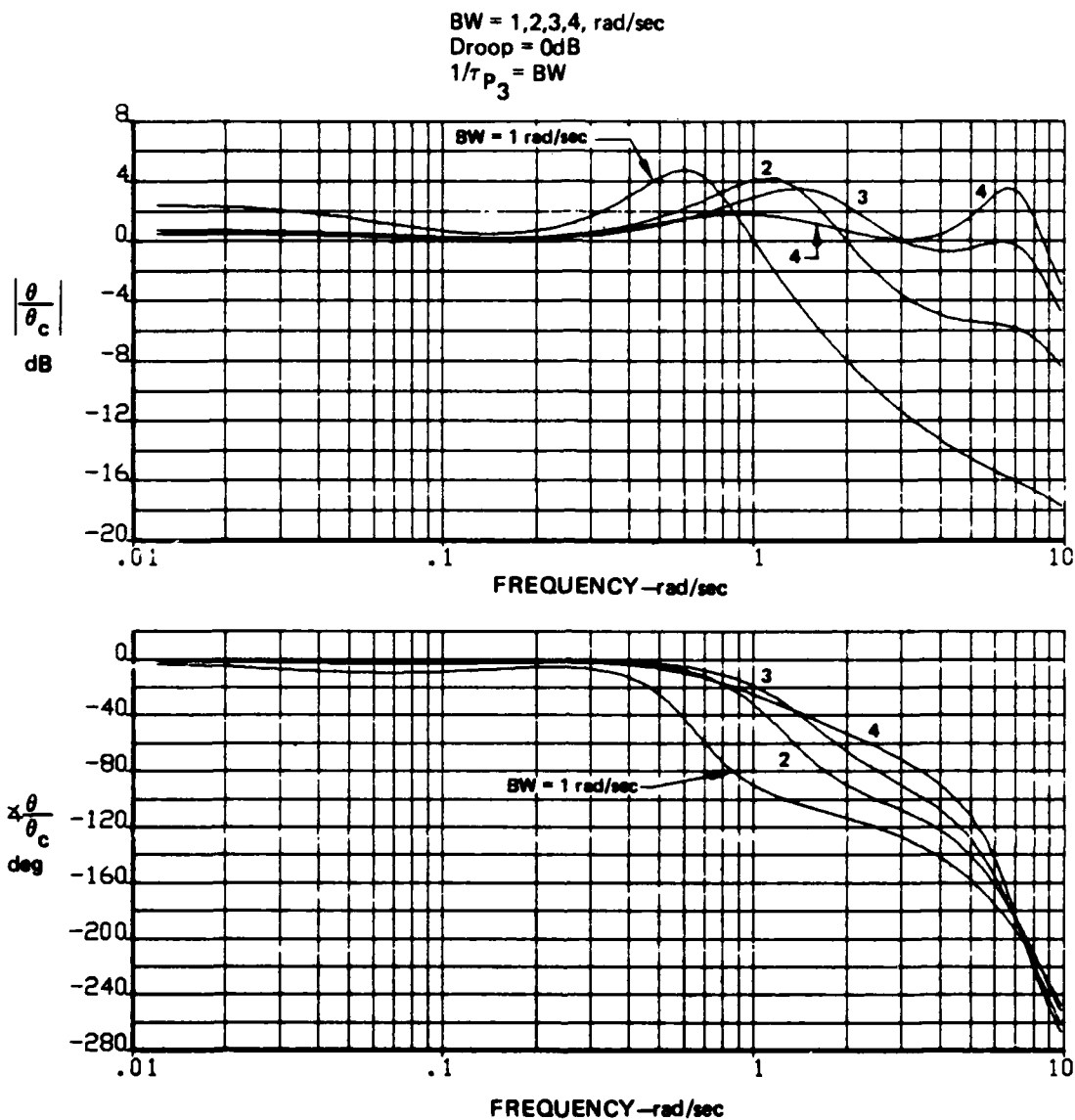
Figure B-38. RSS Neal-Smith Analysis of S42
(b) Closed-Loop Frequency Response

TABLE B-23
RESONANT FREQUENCIES FROM TIME HISTORIES AND ANALYSIS, CONFIGURATION S42A, PILOT R

Measured (Fig. B-39):	$\omega_1(\alpha,\theta,\dot{h})$	$\omega_2(q,F_{ES})$	$\omega_3(F_{ES})$
ILS	0.6	1.3	4.8
Visual, FTD	1.0	--	6.3
RSS Neal-Smith:			
$\omega_{RA}(BW)$	0.6(1.0)	1.3(2.5)	?
$\omega_{RA}(BW)$	1.0(1.8)	--	6.3(3.0)

The three measured frequencies are the primary oscillation (ω_1), a secondary oscillation (ω_2) visible with sufficient clarity only in the IFR portion, and a high frequency oscillation (ω_3). Variables used for estimation of frequency are in parentheses. The RSS Neal-Smith bandwidths (BW) are interpolated from Table B-22 by selecting resonant frequency (ω_{RA}) equal to measured frequency. Where no corresponding ω_{RA} exists, a (?) denotes this. For S42A, the IFR bandwidth range is 1.0 to 2.5 rad/sec while for visual flight, flare and touchdown the bandwidths increase, ranging from 1.8 to 3.0 rad/sec.

To characterize the time history in Figure B-39 from the pilot's point of view, we refer to the pilot comments. Briefly, Pilot R says, "I had to spike it - just a spike on it seemed to stop it in one overshoot or less. Didn't create what I call PIO tendencies." Basically, the pilot saw no oscillatory tendency, either slow or fast.

Configuration S42 is considered next, with again Pilot R flying the approach and landing (Fig. B-40(a)), but still in the context of the preceding RSS Neal-Smith analysis (Fig. B-38). The shortened time scale allows the complete evaluation to be viewed, including the initial level-flight portion where the pilot feels out the configuration. There is a dominant oscillation apparent in the initial level-flight portion, which then speeds up as glide-slope acquisition is approached and is then roughly maintained throughout the approach and through flare and touchdown. The oscillation, however, becomes more obvious and regular during the last 100 ft. of altitude before touchdown. The amplitudes of the oscillations are clearly less for S42 than the previous S42A. The
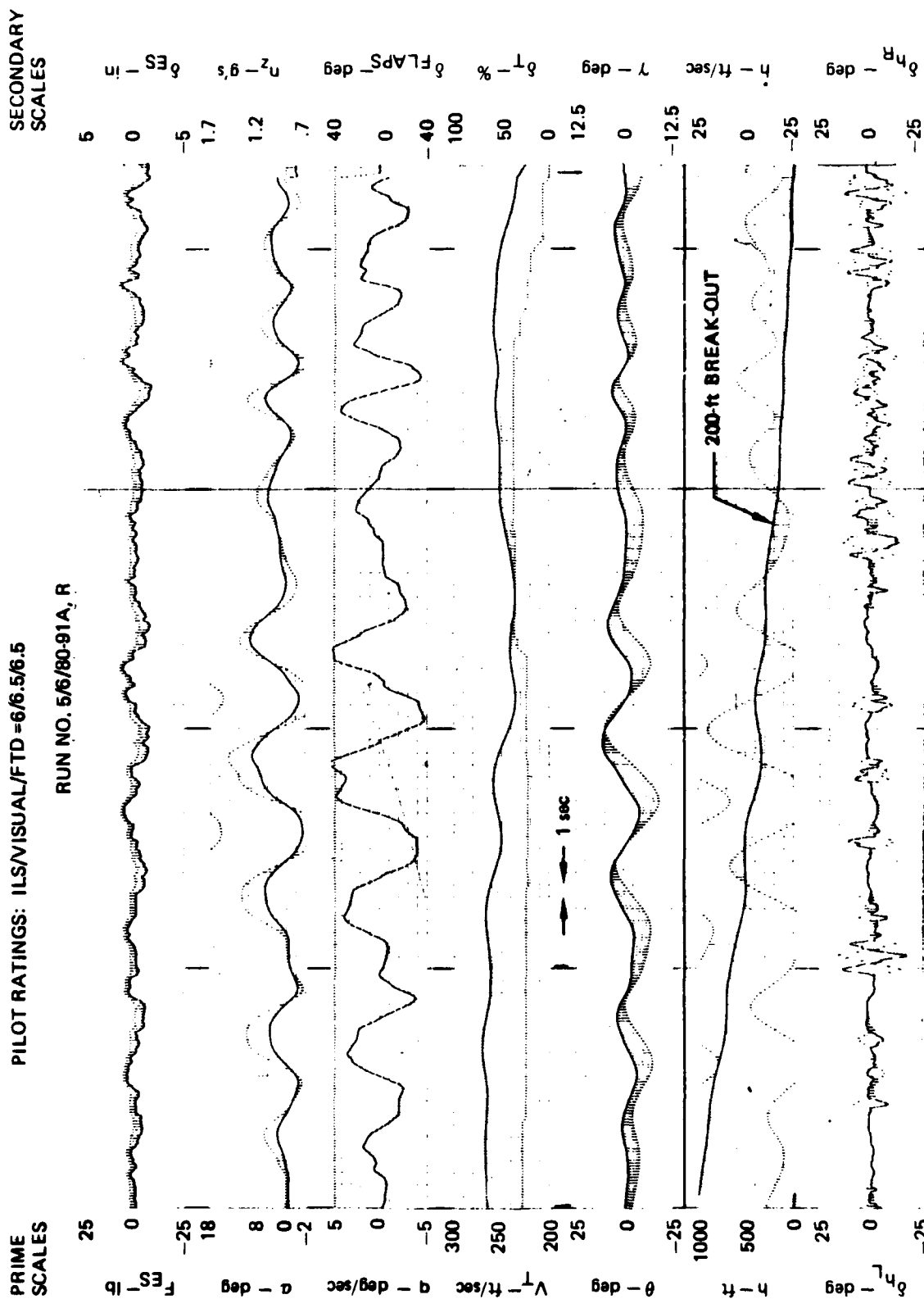
Figure B-39. Time History of Approach and Landing, Configuration S42A, Pilot R

189

various frequencies of oscillation are again estimated and compared with RSS Neal-Smith results.

<div align="center">

TABLE B-24

RESONANT FREQUENCIES FROM TIME HISTORIES AND ANALYSIS,
CONFIGURATION S42, PILOT R

</div>

Measured (Fig. B-40(a)):	$\omega_1(\alpha,q,\theta)$	$\omega_2(\dot{h},V,\theta)$	$\omega_3(F_{ES})$
ILS	1.3	0.6	3.0
Visual, FTD	1.6	--	5.2
RSS Neal-Smith:			
$\omega_{RA}(BW)$	1.3(2.5)	0.6(1.0)	?
$\omega_{RA}(BW)$	1.4(3.0)	--	6.0(2.5)

The RSS Neal-Smith bandwidths required to match the primary time-history frequencies (ω_1) for Pilot R for S42 are BW = 2.5 rad/sec for the ILS approach and 3.0 rad/sec for final visual flight, flare and touchdown. However, oscillations indicative of a BW = 1.0 rad/sec are also present in the IFR approach.

From Pilot R's point of view, "Sensitivity good - some negative static stability. Slight PIO tendency easily damped by spiking the pitch. Easy to control it. Touchdown good but did notice tendency for porpoising." Pilot R clearly saw some oscillatory tendencies.

Continuing to Pilot A's evaluations of Configuration S42, depicted in part (b) of Figure B-40 with the longer time scale, we find the same overall pattern of a dominant oscillation which increases in frequency for visual flight in the final part of the landing. The oscillations appear to be smaller in amplitude than for Pilot R, and control motions smoother. Frequency estimates and comparable RSS Neal-Smith results are found in Table B-25. Only one RSS Neal-Smith resonant frequency will match the observed frequencies in the time history, that for a bandwidth BW=3 rad/sec for the IFR approach. The other two frequencies cannot be realized. No resonances are possible between 1.5 and 6 rad/sec from the RSS Neal-Smith closure on attitude. The pilot's comments are not very illuminating, "Very noticeable instability."

<div align="center">

190

</div>

Figure B-40. Time History of Approach and Landing, Configuration S42 Run A

(a) Evaluation by Pilot R

TABLE B-25

RESONANT FREQUENCIES FROM TIME HISTORIES AND ANALYSIS,

CONFIGURATION S42, PILOT A

| Measured (Fig. B-40(b)):	$\omega_1(\alpha,q,\theta)$	$\omega_2(F_{ES})$
ILS	1.4	--
Visual, FTD	2.3	5.2
RSS Neal-Smith:		
$\omega_{RA}(BW)$	1.4(3.0)	--
$\omega_{RA}(BW)$	?	6.0(2.5)

Configuration S21

For configuration S21, the Nichols charts and closed-loop frequency responses for BW = 1, 2, 3, and 4 rad/sec are found in Figure B-41 and the time history of Pilot R's evaluation of an A run with negligible turbulence in Figure B-42. Pilot lead, closed-loop resonances and the frequencies thereof are tabulated below in Table B-26.

TABLE B-26

PILOT LEAD AND RESONANCE vs BANDWIDTH FOR CONFIGURATION S21

BW rad/sec	ϕ_{PL} deg	RA_1 db	ω_{RA_1} rad/sec	RA_2 db	ω_{RA_2} rad/sec
1	78.6	7.4	0.6	-7.4	7.6
2	93.3	6.3	1.1	-3.1	6.8
3	111.6	4.8	1.3	0.8	6.6
4	131.0	1.8	0.7	3.4	6.7

The characteristics of S21, a fast divergence (T_2 = 2 sec, λ_{sp_1} = +.347) and a small negative real root (λ_{sp_2} = -.6), mean that its flying qualities (PR = 7.3, Run A) are distinctly worse than S42's ($\overline{PR}$ = 5.8, Run A). This degradation is reflected in the larger pilot leads required and the higher resonance, especially at BW = 1. The time histories for S21 (Fig. B-42) are much more oscillatory than those for S42 (Fig. B-40(a)), especially in control input (F_{ES}). During the ILS

Figure B-40. Time History of Approach and Landing, Configuration S42, Run A

(b) Evaluation by Pilot A

193
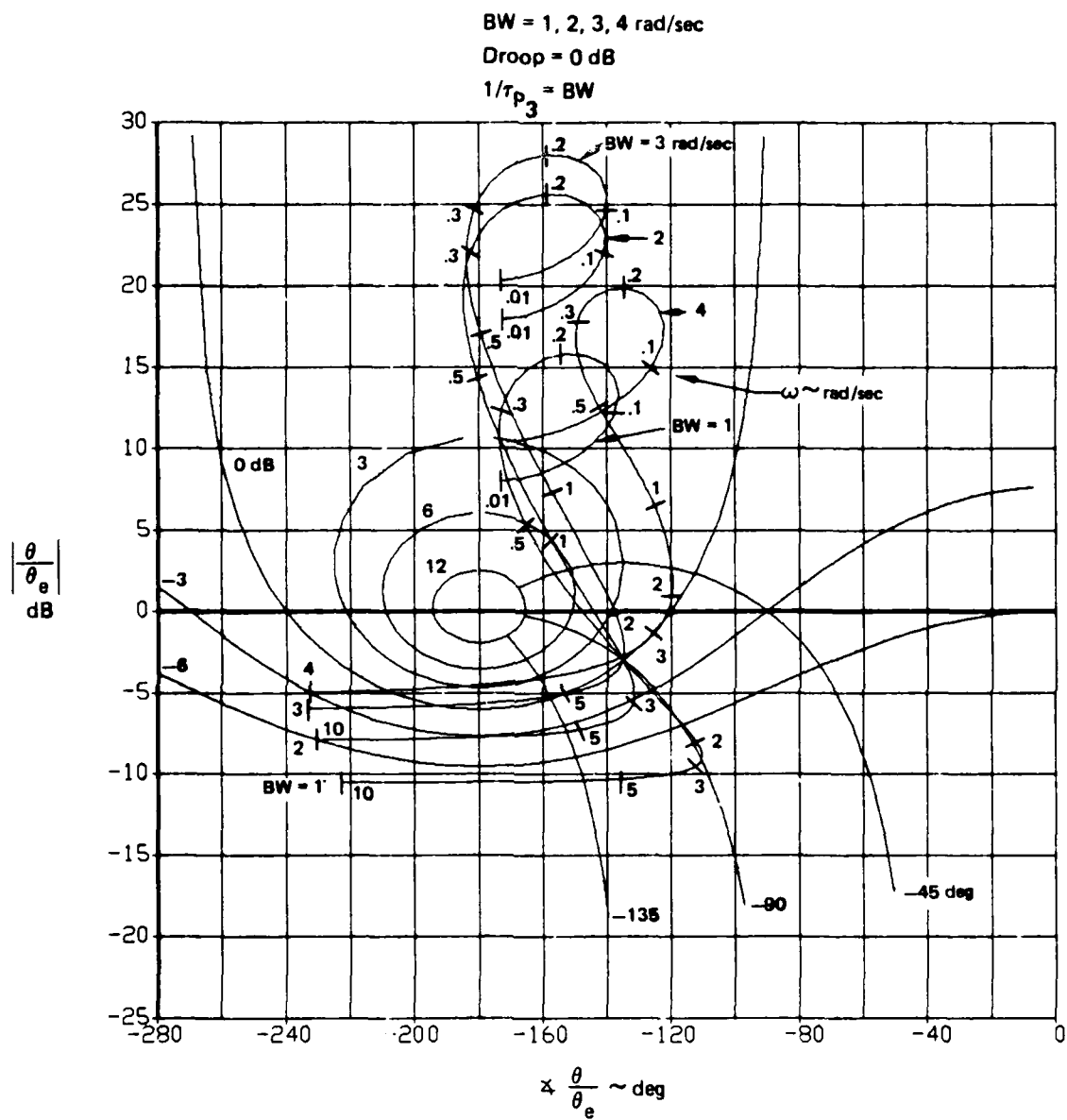
Figure B-41. Neal-Smith Analysis of S21
(a) Nichols Chart

194

BW = 1, 2, 3, 4 rad/sec

Droop = 0 dB

$1/\tau_{P_3}$ = BW
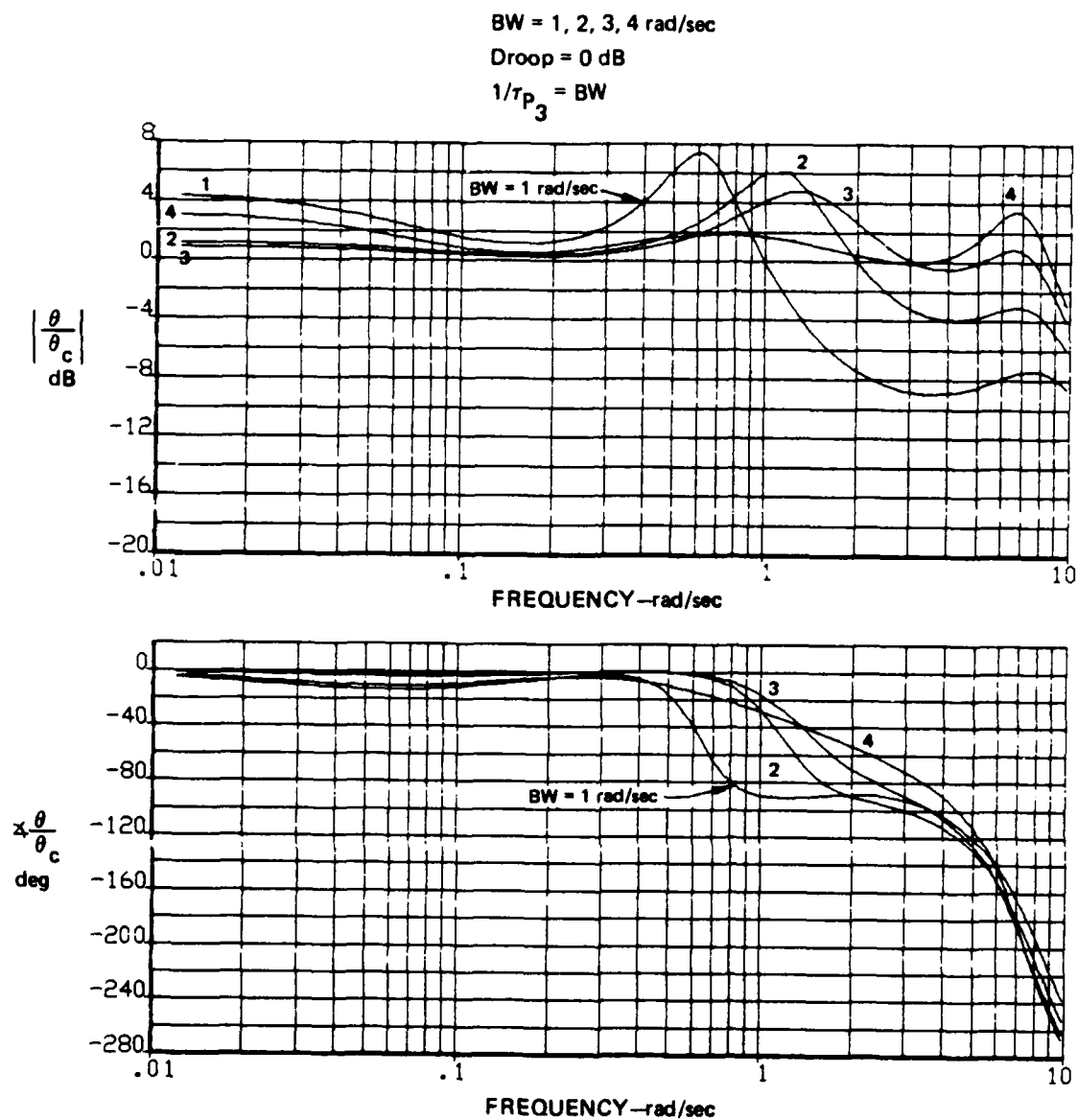
Figure B-41. RSS Neal-Smith Analysis of S21
(b) Closed-Loop Frequency Response

approach a dominant oscillation persists with shifting frequency. The RSS Neal-Smith predicted resonant frequencies can only match the low end of the frequency range measured on ILS, and not the frequencies measured for the final visual portion as shown in Figure B-41 and indicated in Table B-27 as follows.

TABLE B-27

RESONANT FREQUENCIES FROM TIME HISTORIES AND ANALYSIS,
CONFIGURATION S21, PILOT R

	$\omega_1(\theta)$	$\omega_2(F_{ES})$
Measured (Fig. B-42):		
ILS	1.4 - 2.2	--
Visual, FTD	2.6	5.7
RSS Neal-Smith:		
$\omega_{RA}(BW)$	1.3(3.0)	--
$\omega_{RA}(BW)$	?	6.6(3.0)

The measured and RSS Neal-Smith predicted frequencies in the above table have a pattern very similar to that shown for Pilot A's evaluation of S42 (Table B-25).

Pilot R's description of the response is, "There is a very noticeable tendency for PIO. Very difficult to hold pitch attitude because of unstable condition. Under VFR a bit easier but still porpoising." Clearly, the pilot found Configuration S21 very oscillatory and PIO prone.

Configuration S24

For Configuration S24, the Nichols chart and closed-loop frequency responses for BW = 1, 2, 3, and 4 rad/sec are found in Figure B-43 and the time history of Pilot R's evaluation of an A run in Figure B-44. Pilot lead, closed-loop resonances, and frequencies thereof are tabulated in Table B-28 on the following page.

196
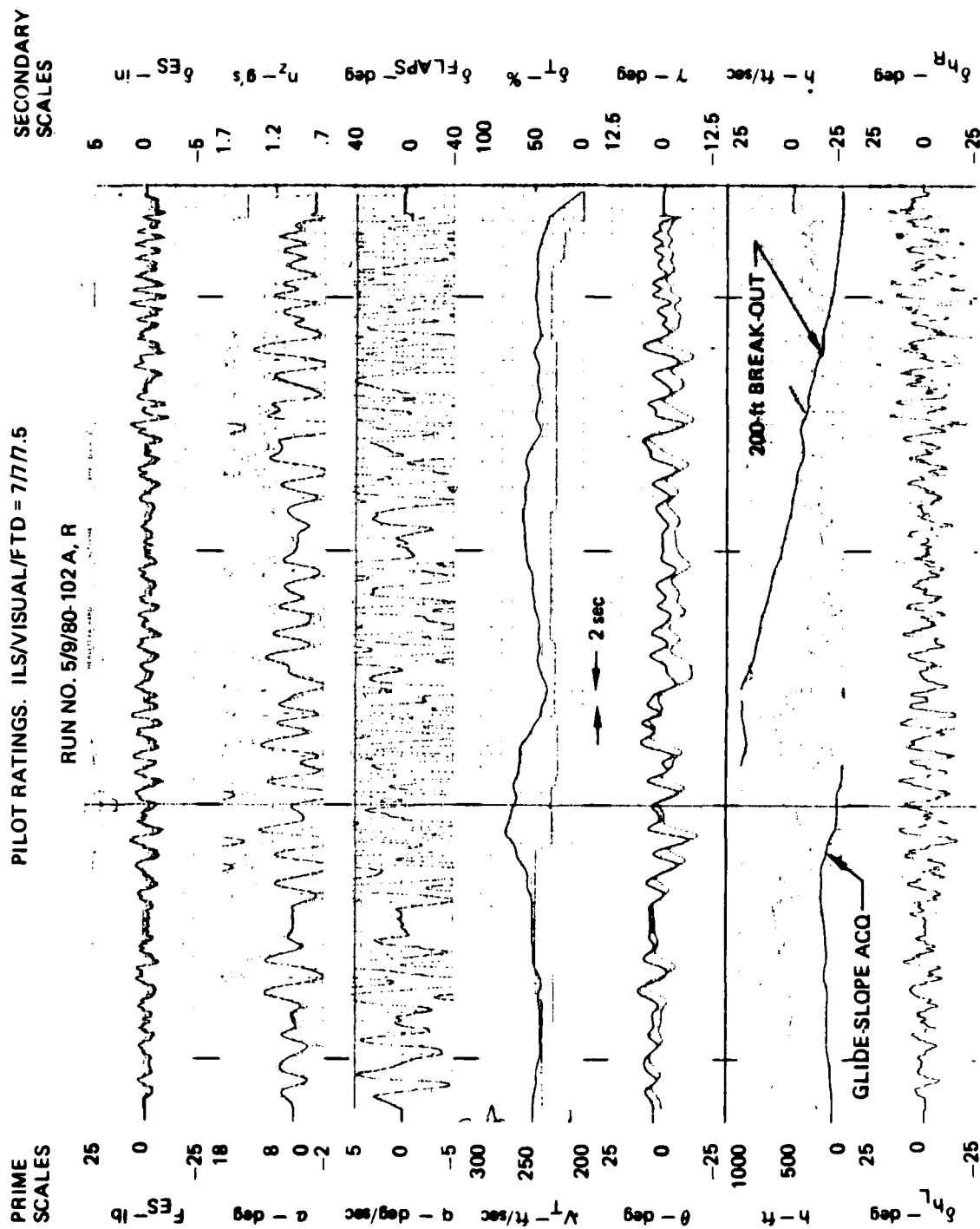
Figure B-42. Time History of Approach and Landing, Configuration S21, Run A, Pilot R

197
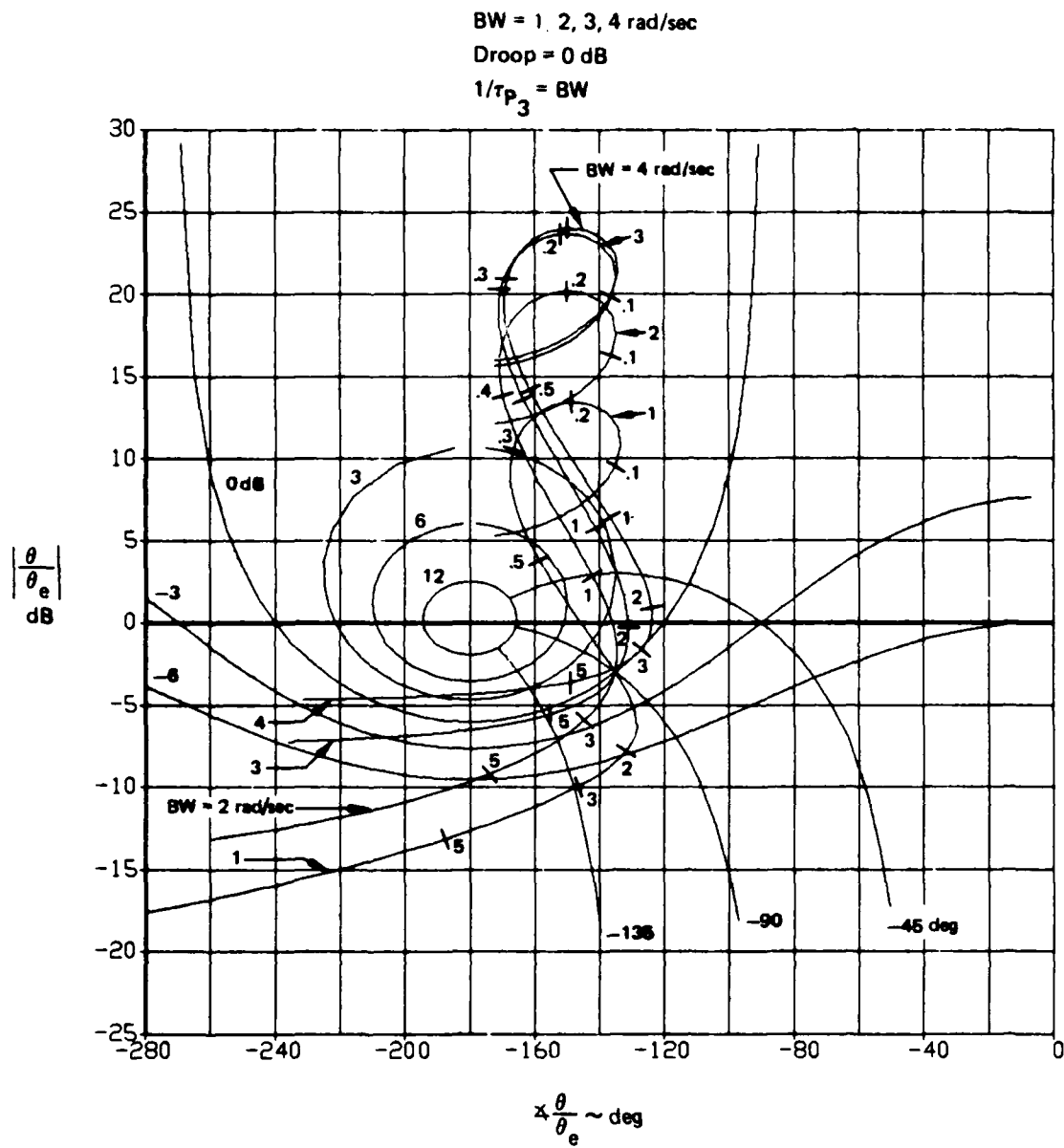
Figure B-43. RSS Neal-Smith Analysis of S24
(a) Nichols Chart

BW = 1, 2, 3, 4 rad/sec

Droop = 0 dB

$1/\tau_{P_3}$ = BW
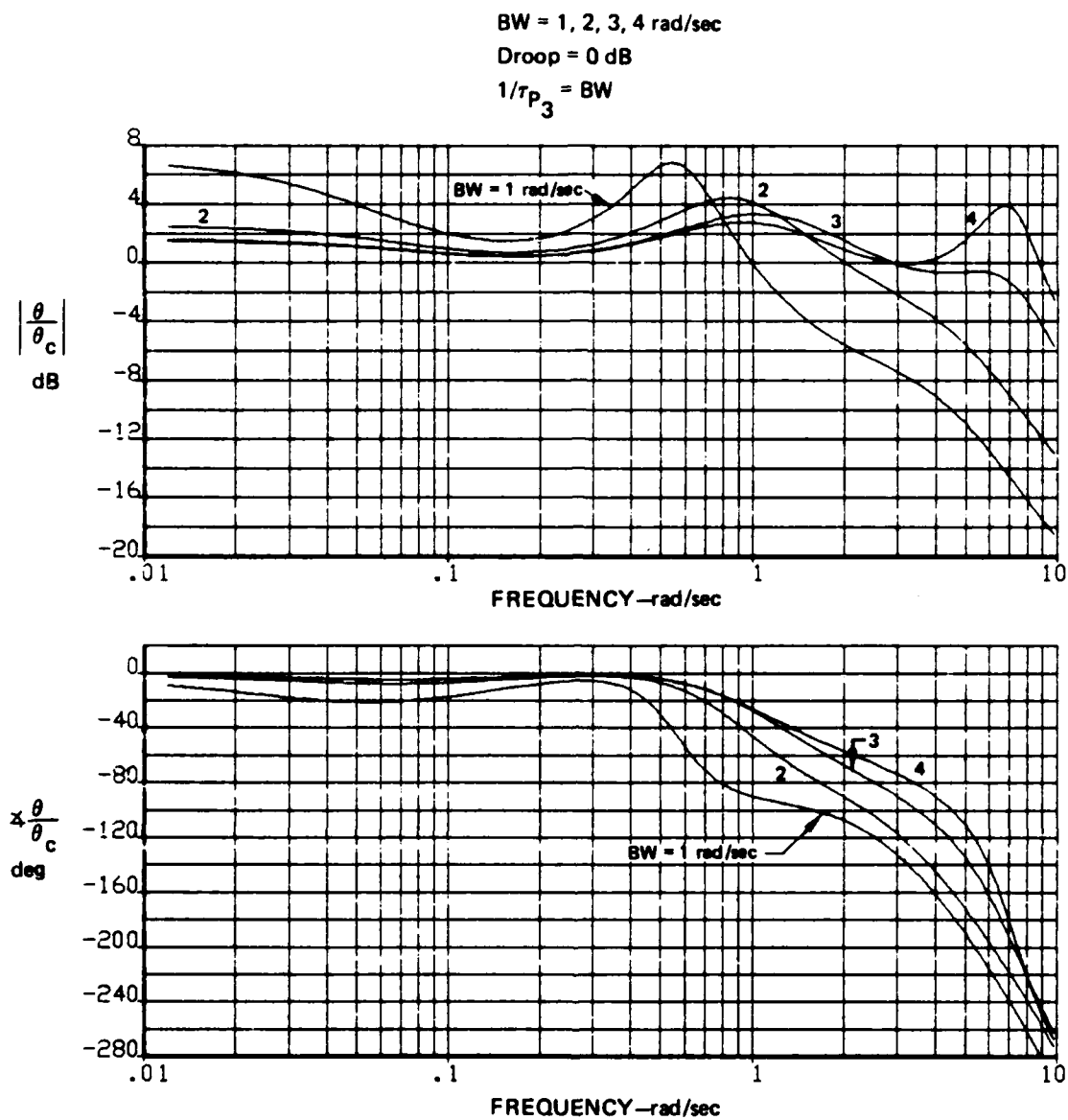
Figure B-43. RSS Neal-Smith Analysis of S24
(b) Closed-Loop Frequency Response

TABLE B-28
PILOT LEAD AND RESONANCE vs BANDWIDTH, CONFIGURATION S24

BW rad/sec	ϕ_{PL} deg	RA_1 db	ω_{RA_1} rad/sec	RA_2 db	ω_{RA_2} rad/sec
1	38.0	6.8	0.6	--	--
2	53.6	4.4	0.8	--	--
3	78.8	3.3	1.0	-0.6	5.5
4	102.7	2.8	1.0	3.9	6.8

The characteristics of S24, a fast divergence but with a larger negative real root (λ_{sp_2} = -3), mean that it should obtain a better pilot rating than S21, as it does (PR = 5). The Nichols chart plots and closed loop responses are not significantly different between S21 and S24. The significant differences are in the pilot lead which is much lower for S24, and in the time history which has much less oscillation for S24. The comparison (Table B-29) of frequencies measured from the time history and calculated from RSS Neal-Smith analysis show correlation for a BW = 2 during the ILS approach for the lower of the two discernible frequencies. For the higher frequency, found in both ILS and visual portions, there is no corresponding closed-loop analytical condition.

TABLE B-29
RESONANT FREQUENCIES FROM TIME HISTORIES AND ANALYSIS, CONFIGURATION S24, PILOT R

Measured (Fig. B-44):	$\omega_1(\theta,\dot{h})$	$\omega_2(q)$
ILS	0.8	2.4
Visual, FTD	2.6	--
RSS Neal-Smith:		
ω_{RA}(BW)	0.8(2.0)	?
ω_{RA}(BW)	?	--
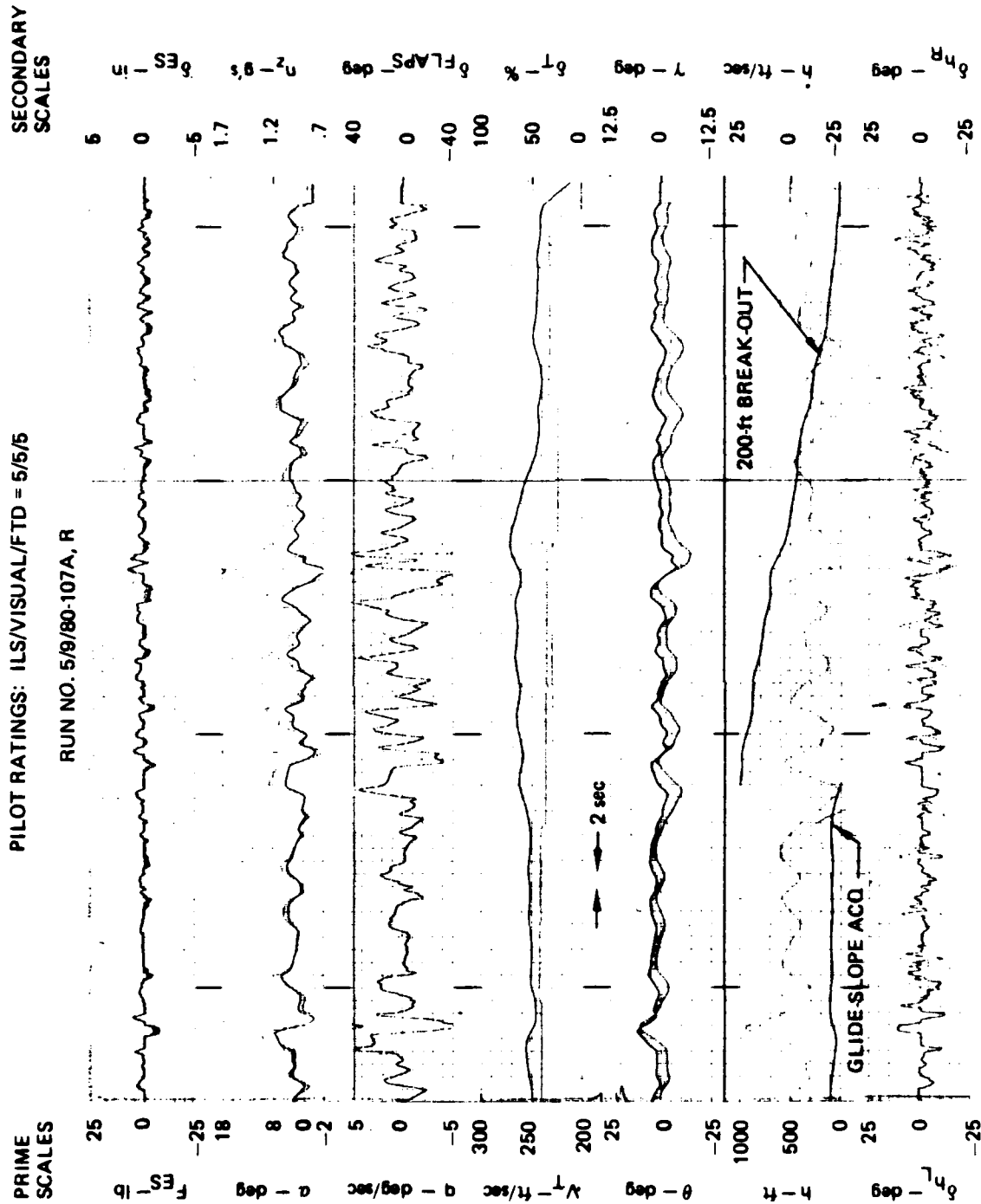
Figure B-44. Time History of Approach and Landing, Configuration S24, Run A, Pilot R

201

Pilot R's view of S24 on the A run was, "Airplane was unstable - but sensitivity and all, such that it wasn't too difficult to fly. Wasn't any real tendency for PIO. Forces were quite light and response, fairly good. VFR no problem. Didn't see any tendency to porpoise. Didn't see any big trouble, other than fact it was unstable." Pilot R clearly saw no oscillations to speak of, and found S24 relatively easy to fly.

Summary

Correspondence has been found between the frequencies of oscillations measured from simulator time histories and determined from the proposed RSS Neal-Smith closed-loop analysis procedure. The correspondence is best for the low sensitivity configurations, e.g. S42A, with bandwidths of 1 to 2 rad/sec representing the ILS portion of the approach and 2 to 3 rad/sec representing the visual short final, flare, and touchdown. The correlation of frequencies for the higher sensitivity cases, e.g. S42, S21, and S24, is only fair. The primary frequencies ($0.8 < \omega < 1.4$ rad/sec) found in the ILS portion can be matched with bandwidths from 2 to 3 rad/sec in the RSS Neal-Smith closure process, but the higher frequencies found in the visual portion ($2.3 < \omega < 2.6$ rad/sec) have no direct counterpart in the resonances predicted by the analysis. Apparently the pilot model and the assumed feedback (θ) do not represent the physical situation with sufficient accuracy to provide one-to-one correspondence of resonant conditions. Thus a semi-empirical approach to an RSS Neal-Smith criterion must be used, with emphasis on pilot lead (ϕ_{PL}) as the parameter that best correlates with pilot rating.

B.6.2 Correlation of Pilot Rating with Closed-Loop Parameters

The Neal-Smith computer program was used together with what is termed the RSS Neal-Smith approach to calculate the closed loop characteristics for all configurations evaluated with the ground simulator. The pilot model and the parameters for the closure process were as follows for all RSS configurations, unstable or near neutral stability.

$$Y_p(s) = K_p e^{\tau_d s} \frac{\tau_{p_1} s + 1}{\tau_{p_2} s + 1} (\tau_{p_3} s + 1)$$

$$\tau_d = -0.3 \text{ sec}$$

$$1/\tau_{p_3} = BW$$

Droop = 0 db

BW = 1 and 3 rad/sec

The zero droop condition derives from the criterion of minimum pilot lead, replacing the standard Neal-Smith minimum resonant amplitude criterion. The bandwidths of 1 and 3 derive from the concept that the pilot closes the attitude loop over a range of bandwidths in the landing task, roughly spanned by these two values, with the lower one dealing primarily with the problems posed by relaxed static stability (RSS).

Results of the RSS Neal-Smith calculations of pilot lead and resonant amplitude and frequency are presented in Table B-30. It will be noted that L21, a good stable configuration, was closed with the standard Neal-Smith approach. Also, both the RSS and standard approach were used for configuration FO which has low (marginal Level 1) stability. For FO at BW = 3, more than 90° of pilot lead is required for a standard Neal-Smith closure with -3 db, so a -2 db closure is used instead. For BW = 1, the pilot lead is slightly less for the RSS than the standard closure of FO.

B.6.2.1 Pilot Lead

The pilot ratings (PR) for all the high-sensitivity RSS configurations have been plotted versus pilot lead (ϕ_{PL}) for a bandwidth of 1 rad/sec in Figure B-45, part (a) for Pilot A and part (b) for Pilot R. It can be seen that there is a strong correlation of PR with ϕ_{PL}. Pilot rating tends to hold constant at its best value (for a given turbulence level and pilot) for $\phi_{PL} < 50^\circ$, and to degrade strongly as ϕ_{PL} goes from 50° to 80°.

To better assess the existence of this correlation of PR with the single parameter, ϕ_{PL}, the pilot ratings from the average curves of Figures B-21 and B-22 were used to plot PR vs ϕ_{PL} in Figure B-46. With few exceptions the pilot ratings fall within a very narrow band of a single curve of PR v.s. ϕ_{PL} for each turbulence level, regardless of the values of the three parameters, λ_{sp_1}, λ_{sp_2}, Z_{θ_2}. That the curve for the S60 series configurations with moderate turbulence plots significantly high in Figure B-46 suggests that this fairing of the data points is too high in Figure B-21(a), Run B. The extra-low pilot ratings for large negative values of Z_{θ_2} (Fig. B-22(b), S26 and S27), since they are present for both the higher turbulence levels, is probably more than just scatter in the data and probably reflects an actual degradation in PR as Z_{θ_2} takes on large negative values.

The mean lines from the narrow bands of Figure B-46 have been plotted on Figure B-45, along with the lines for large negative Z_{θ_2}. As can be seen, these lines provide a good fairing of the data (Fig. B-45), on the low side for Pilot A and high side for Pilot R, reflecting their average one-rating differential.

To attempt to assess the scatter found in the data, the known high or low data points from pilot or test engineer comments have been flagged with arrows indicating which direction the point should probably move. As can be seen, most of the points far from the average line would be moved in the right direction to reduce the scatter.

Pilot rating is plotted versus pilot lead for a bandwidth of 3 rad/sec in Figure B-47, again separated by pilot. The trends are very similar to those for a bandwidth of 1 rad/sec, but much larger values of lead are required and the range is now much less ($75^0 < \phi_{PL} < 115^0$). Average curves have been faired through each set of data points, with the direction of probable change indicated for questionable pilot rating values. The single-valued functional relationship of PR upon ϕ_{PL} is again maintained for BW = 3 rad/sec, with PR relativ.ely invariant of ϕ_{PL} for ϕ_{PL} < 100 deg.

Table B-30. Pilot Lead, Resonant Amplitude and Frequency
$1/\tau_{p_3}$ *= BW and Droop = 0 dB except as noted*

Config	BW = 1 rad/sec			BW = 3 rad/sec		
	ϕ_{PL} deg	RA dB	ω_{RA} rad/sec	ϕ_{PL} deg	RA dB	ω_{RA} rad/sec
F0[1]	19.5	0.7	1.00	86.8	7.1	3.45
F0[2]	15.7	1.9	0.95	105.0	1.7	1.70
F1	51.4	3.2	0.60	106.6	2.7	1.30
F2	64.0	7.8	0.55	107.7	4.0	1.10
F4	56.5	4.9	0.60	107.1	3.2	1.20
F6	54.0	4.1	0.60	106.9	2.9	1.25
L21[3]	−34.3	0.1	0.40	45.3	5.0	3.40
L71	21.4	2.6	0.65	81.6	1.7	1.40
L72	27.6	3.2	0.65	82.5	2.1	1.30
L73	41.5	5.4	0.60	85.0	3.3	1.15
S21	78.6	7.4	0.60	112.0	4.8	1.30
S22	64.2	6.7	0.60	105.3	4.2	1.25
S23	45.6	6.7	0.55	90.1	3.5	1.15
S24	38.0	6.8	0.55	78.8	3.3	1.05
S25	34.2	5.8	0.50	85.3	2.6	1.05
S26	64.7	7.1	0.60	99.9	4.7	1.30
S27	77.9	7.1	0.60	111.7	4.8	1.30
S41	69.4	5.4	0.65	108.7	4.2	1.35
S42	54.8	4.8	0.60	101.6	3.5	1.35
S43	36.4	4.7	0.60	86.8	2.7	1.20
S44	28.7	5.0	0.60	75.5	2.5	1.05
S45	42.1	3.7	0.55	97.0	2.8	1.40
S46	73.2	5.3	0.65	111.9	4.2	1.35
S60	80.4	6.1	0.65	113.7	4.6	1.34
S61	65.7	4.9	0.65	107.6	4.0	1.40
S62	51.7	4.2	0.60	100.6	3.3	1.40
S63	33.6	4.2	0.60	85.4	2.5	1.25

Notes: (1) Standard Neal-Smith: BW = 1, droop = −1 dB. Minimum RA > 0.

BW = 3, droop = −2 dB. ϕ_{PL} > 90° for droop = −3 dB.

(2) RSS Neal-Smith: BW = 1, $1/\tau_{p_3}$ = 1, droop = 0 dB. Minimum ϕ_{PL}.

BW = 3, $1/\tau_{p_3}$ = 3, droop = 0 dB. Minimum ϕ_{PL}.

(3) Standard Neal-Smith: BW = 1, droop = −3 dB.

BW = 3, droop = −3 dB.

PILOT LEAD (ϕ_{PL}) CALCULATED FROM RSS NEAL-SMITH, $1/\tau_{P_3}$ = BW, DROOP = 0 dB
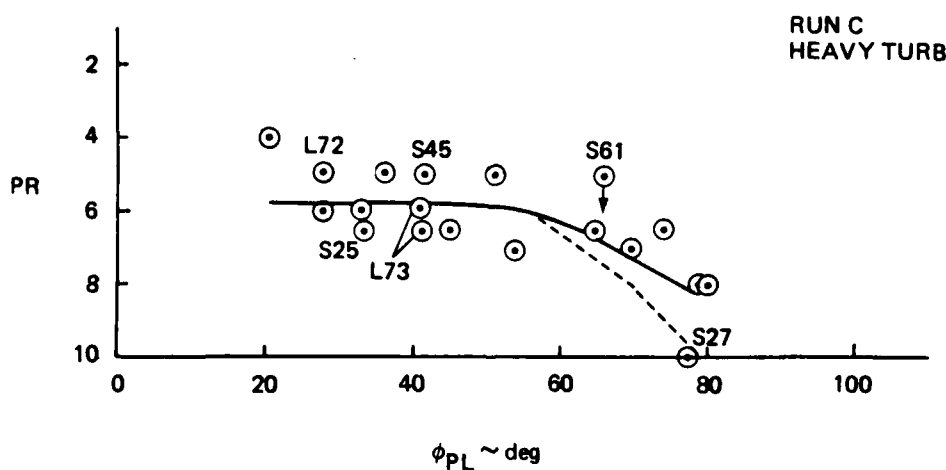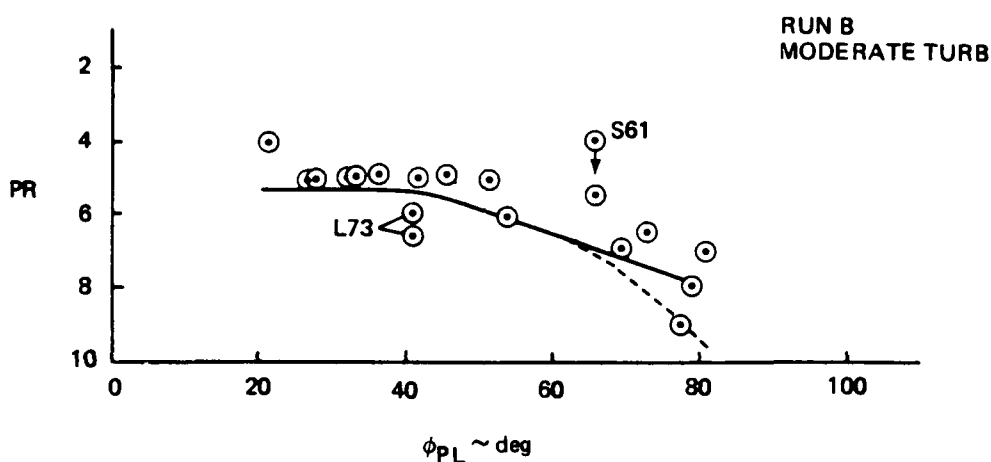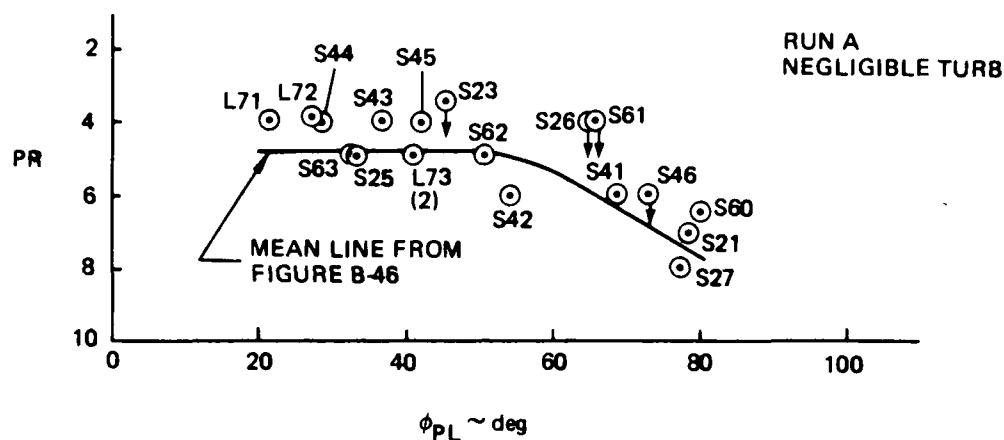
Figure B-45 Pilot Rating vs Pilot Lead, BW = 1 rad/sec
(a) Pilot A
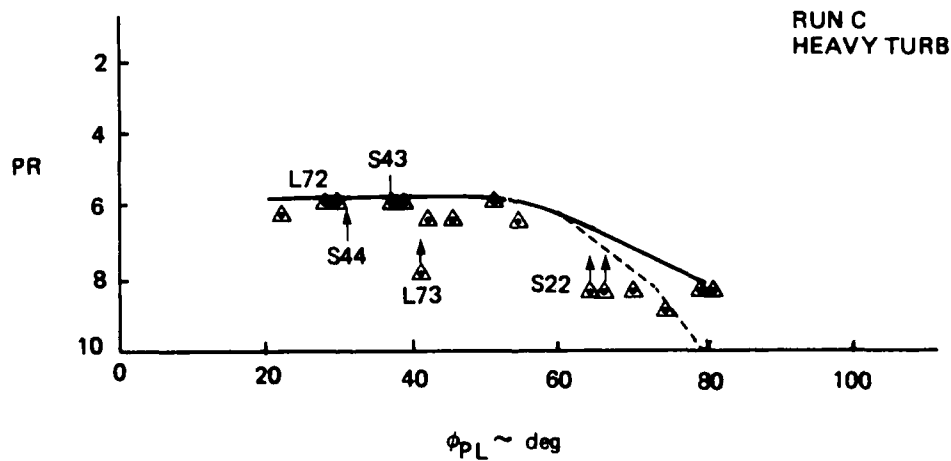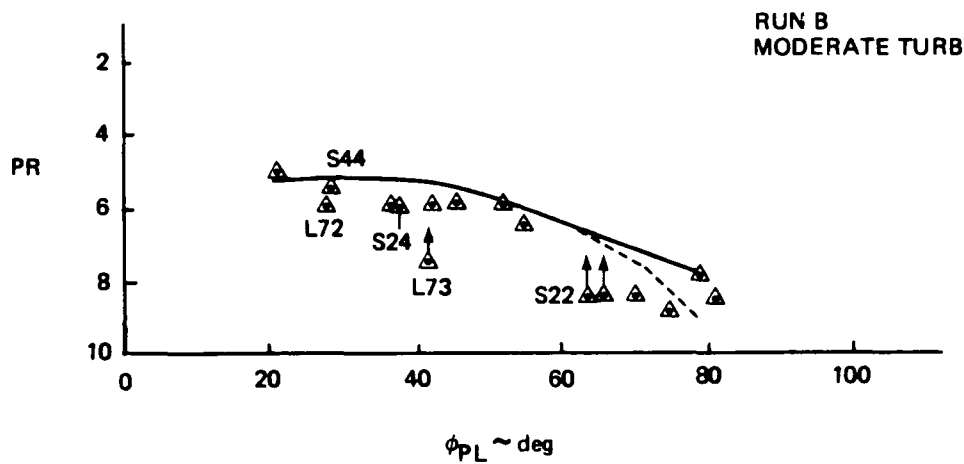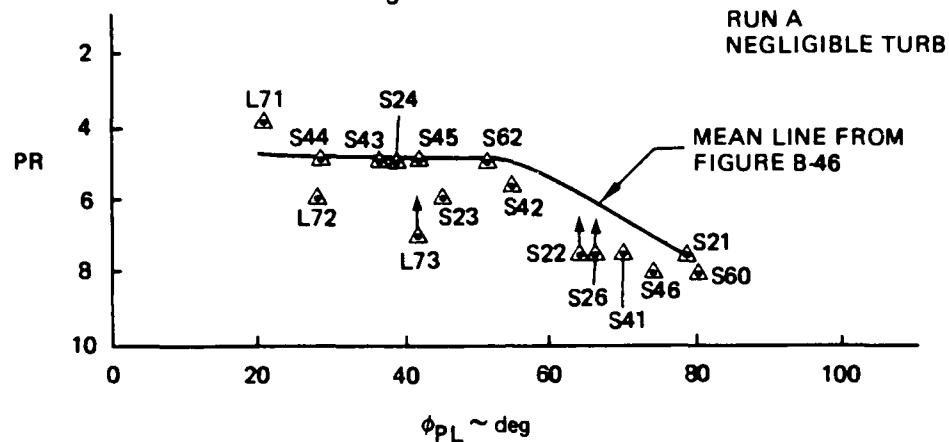
Figure B-45. Pilot Rating vs Pilot Lead, BW:1 Rad/Sec
(b) Pilot R

207

PILOT LEAD (ϕ_{PL}) CALCULATED FROM RSS NEAL-SMITH, BW = 1 rad/sec
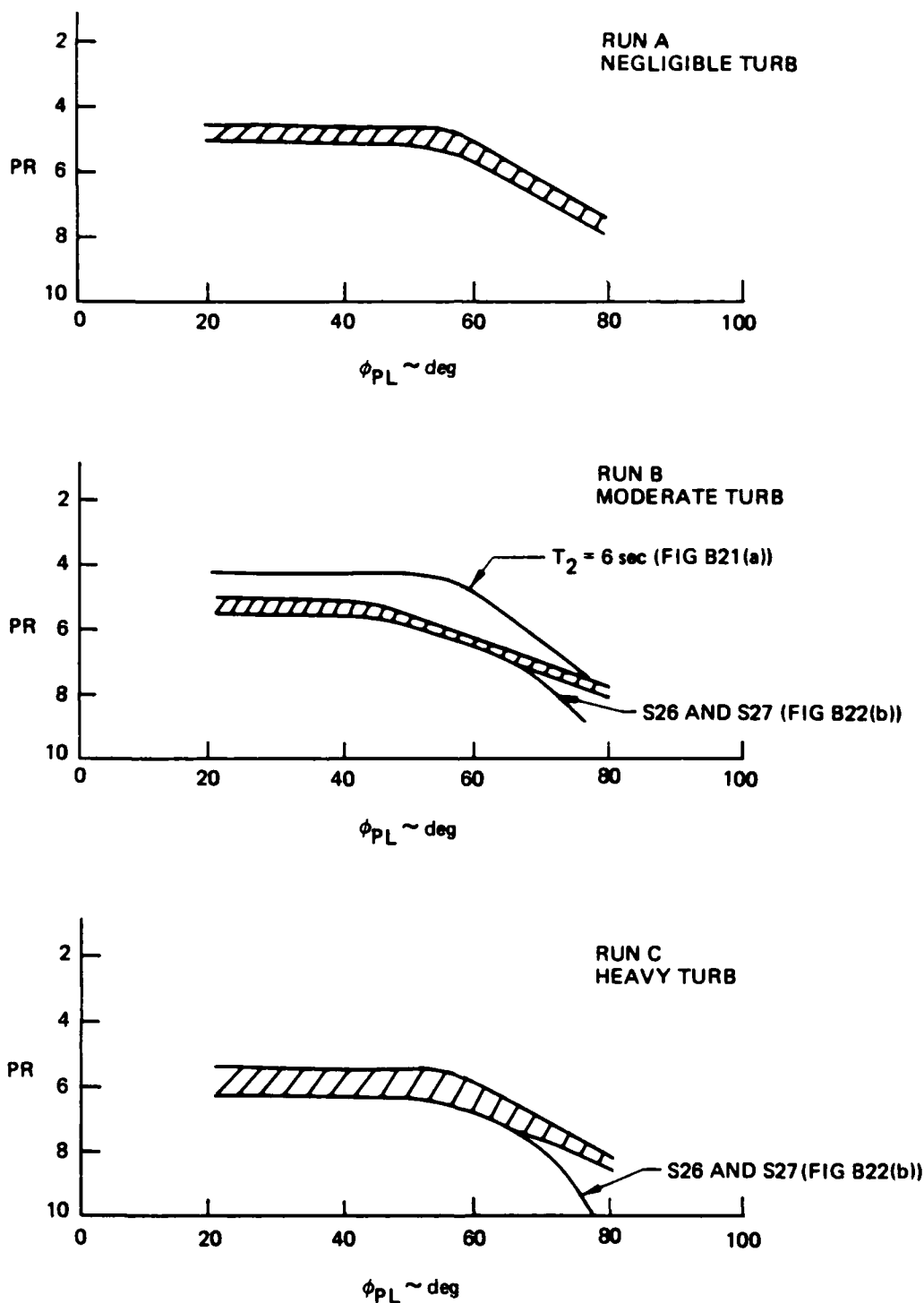
Figure B-46. Pilot Rating vs Pilot Lead From Faired Curves of Figures B-21 and B-22

208

PILOT LEAD (ϕ_{PL}) CALCULATED FROM RSS NEAL-SMITH, $1/\tau_{P_3}$ = BW, DROOP = 0 dB
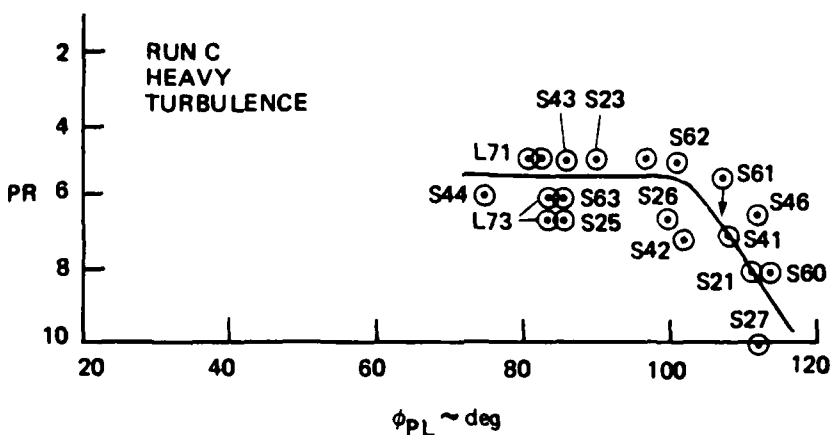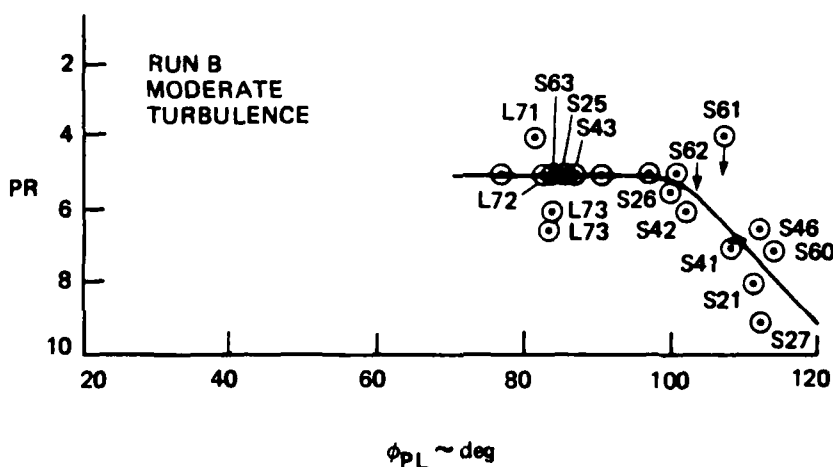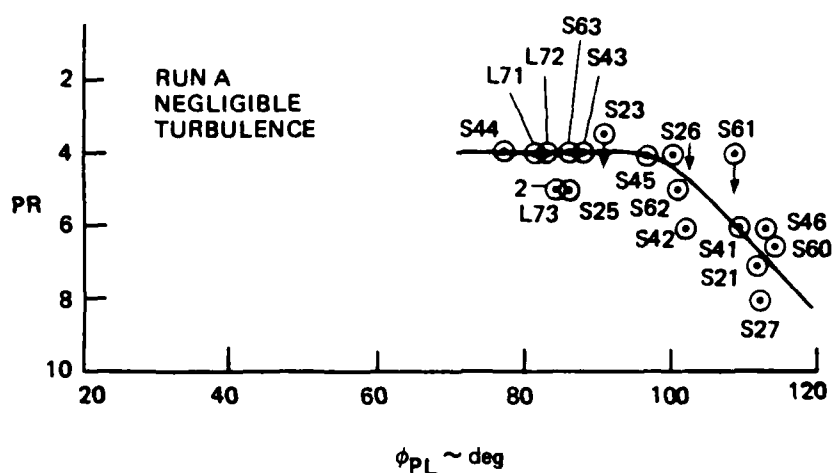
Figure B-47. Pilot Rating vs Pilot Lead, BW = 3 rad/sec
(a) Pilot A

209
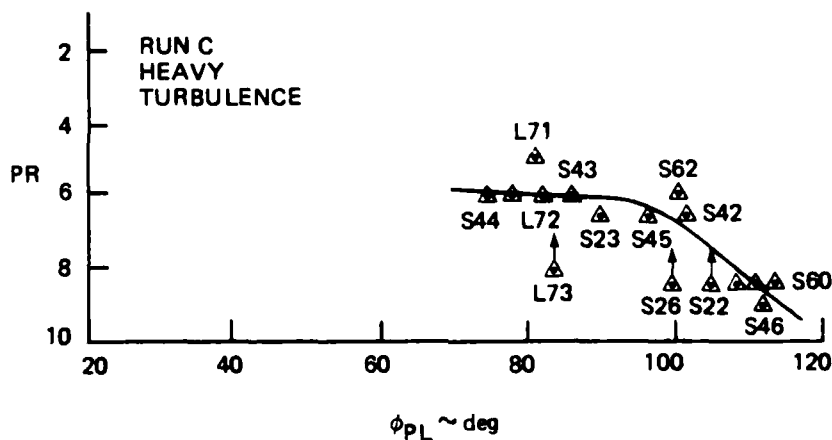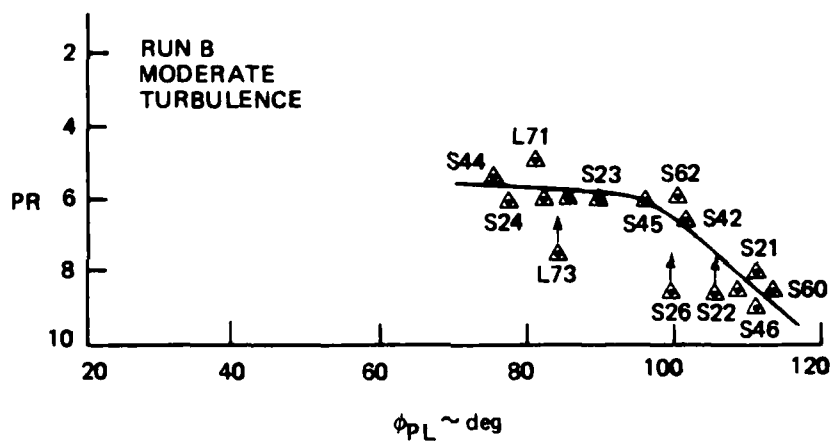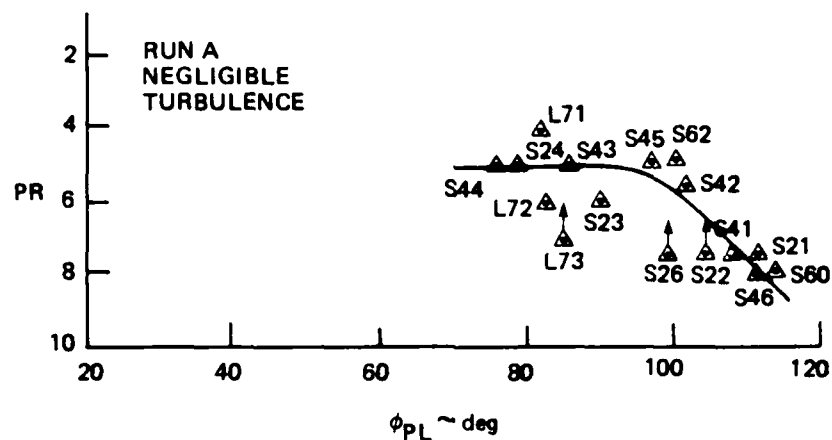
Figure B-47. Pilot Rating vs Pilot Lead, BW = 3 rad/sec
(b) Pilot R

210

Though the one-to-one correlation of pilot rating (PR) with pilot lead (ϕ_{PL}) shown in Figure B-45 and B-47 looks very strong, suggesting that a criterion for flying qualities could be based on pilot lead alone, the fact that PR is invariant with ϕ_{PL} for nearly half the range (e.g., $20^0 < \phi_{PL} < 50^0$ for BW = 1) begs for further consideration. When PR is invariant with a parameter, it says the parameter has no effect, or else there is another compensating parameter.

B.6.2.2 Pilot Lead and Resonant Amplitude

Since correlation of pilot ratings with pilot lead alone seems not to account for all factors, the ratings are analyzed as a function of both pilot lead and resonant amplitude. Resonant amplitude (RA) and pilot lead (ϕ_{PL}) for all unaugmented configurations are shown plotted for BW = 1 and 3 rad/sec in Figure B-48. Variations of the parameters λ_{sp_1} (or T_2), λ_{sp_2}, Z_{θ_2}, M_α (L series), and c.g. location (F series) are indicated on Figure B-48 and are most significant for BW = 1 rad/sec. The unstable root affects primarily resonant amplitude. The negative real root affects primarly pilot lead. The Z_{θ_2} zero affects both. The LAHOS cases parallel the S configurations with λ_{sp_2} = -2 (S63, S43, S23), but have correspondingly much lower resonant amplitude. This lower value is primarily due to the more heavily damped phugoid, most easily seen by comparing Nichols charts (not shown) but also seen by comparing frequency responses in Appendix C. The F configurations, created by c.g. variations of the F-111, have less variation of pilot lead and larger variation of resonant amplitude than is shown for any other variation of a single parameter.

It is significant that the variations of RA and ϕ_{PL} are much less for BW = 3 rad/sec than 1 rad/sec. Also, the variations that do exist in RA are grossly one-to-one with ϕ_{PL}; that is, a single line can be drawn through the points that has most of the points fairly near it.

Besides the configuration points, standard Neal-Smith criterion boundaries are shown on Figure B-48, but only on the BW = 3 rad/sec part to avoid a confusion of plots on the BW = 1 rad/sec part.

<u>BW = 1 rad/sec</u>

The pilot ratings for the high sensitivity configurations are plotted in Figure B-49 at the appropriate resonant amplitude and pilot lead, separately for each turbulence level. Lines of constant pilot rating (iso-ratings) have been drawn on these figures. Average values of the pilot ratings and cross plots helped to establish the iso-ratings. The correlation of pilot rating as a function of RA and ϕ_{PL} is very good and accounts for all parametric variations with the exception of control sensitivity. There are very few anomalous points. The few there are have already been noted to have suspect ratings, and these are identified with a + or - on Figure B-49 to indicate the trend thought appropriate. S61, evaluated only by Pilot A, is rated too good by about two rating points. S26 as evaluated by Pilot A is rated too good for the A run, but is counterbalanced by Pilot R's overly poor rating. Pilot R's rating of L73 at PR = 7 is also counterbalanced by Pilot T's PR = 3. The Neal-Smith PR = 3.5 boundary, where it approaches the RSS data, unexpectedly appears to agree with it. In short, the correlation of the simulator data shown in Figure B-49 for BW = 1 rad/sec with RA and ϕ_{PL} is excellent, and the iso-rating lines appear to provide a good foundation upon which to base criteria.

Continuing to the low sensitivity data, the ratings for these configurations, when plotted on the RA vs ϕ_{PL} plane for BW = 1 rad/sec, showed a substantially different pattern. Accordingly, the ratings were adjusted from low to high sensitivity by the increment developed in Figure B-30 which accounts for the need for higher sensitivity with increasingly negative λ_{sp_2}. The adjusted data are plotted in Figure B-50, which also has the iso-rating lines from Figure B-49. The adjusted pilot rating data correlates well with the iso-rating lines, with the possible exception of configuration F2 which rates a little too good, especially for Run A. The point for F0 uses the RSS Neal-Smith values of RA and ϕ_{PL}, with which its ratings fit well into the pattern. The good correlation shown in Figure B-50 further corroborates the results shown in Figure B-49, and also that the degradation in pilot rating due to low sensitivity is correctly represented as a function of λ_{sp_2} as in Figure B-30.
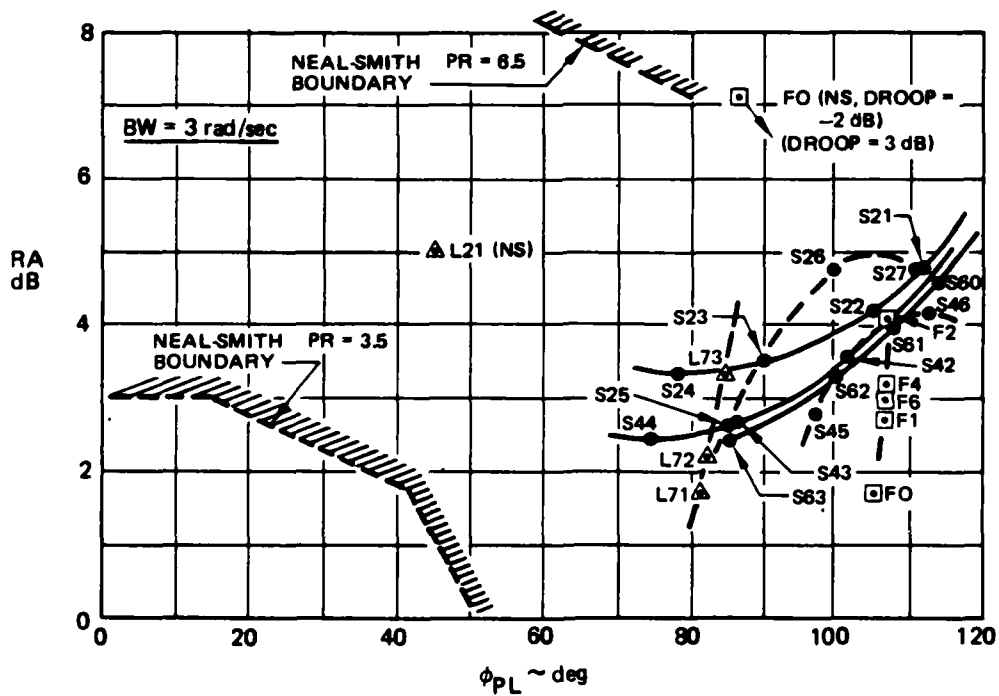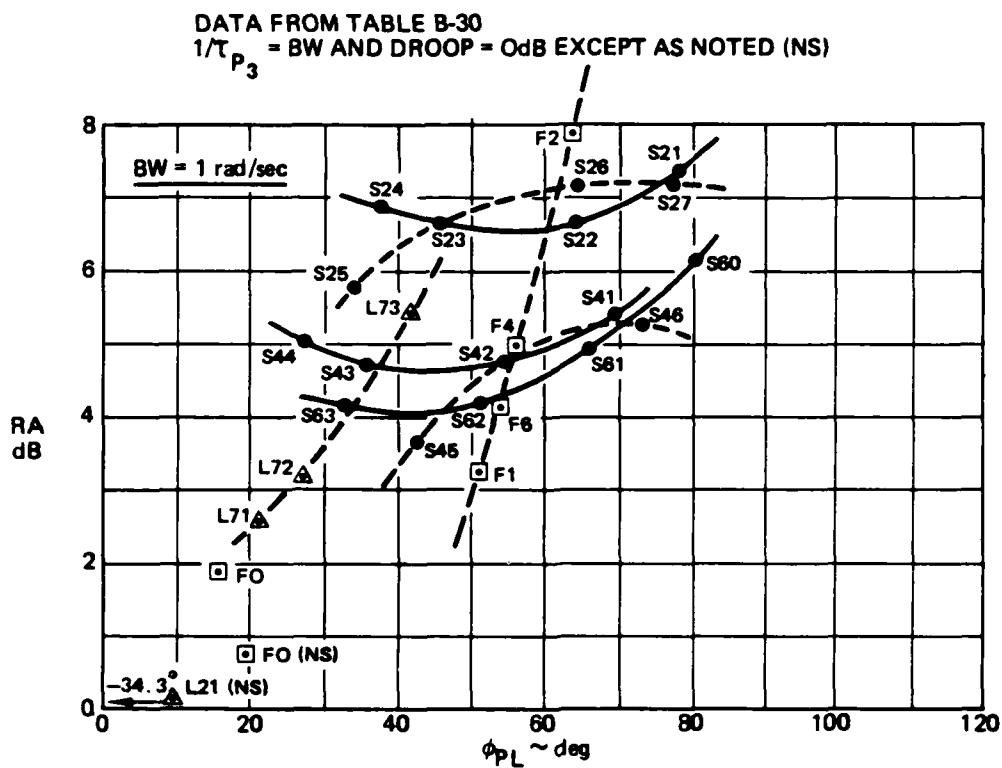
Figure B-48. Resonant Amplitude and Pilot Lead for All Simulator Configurations
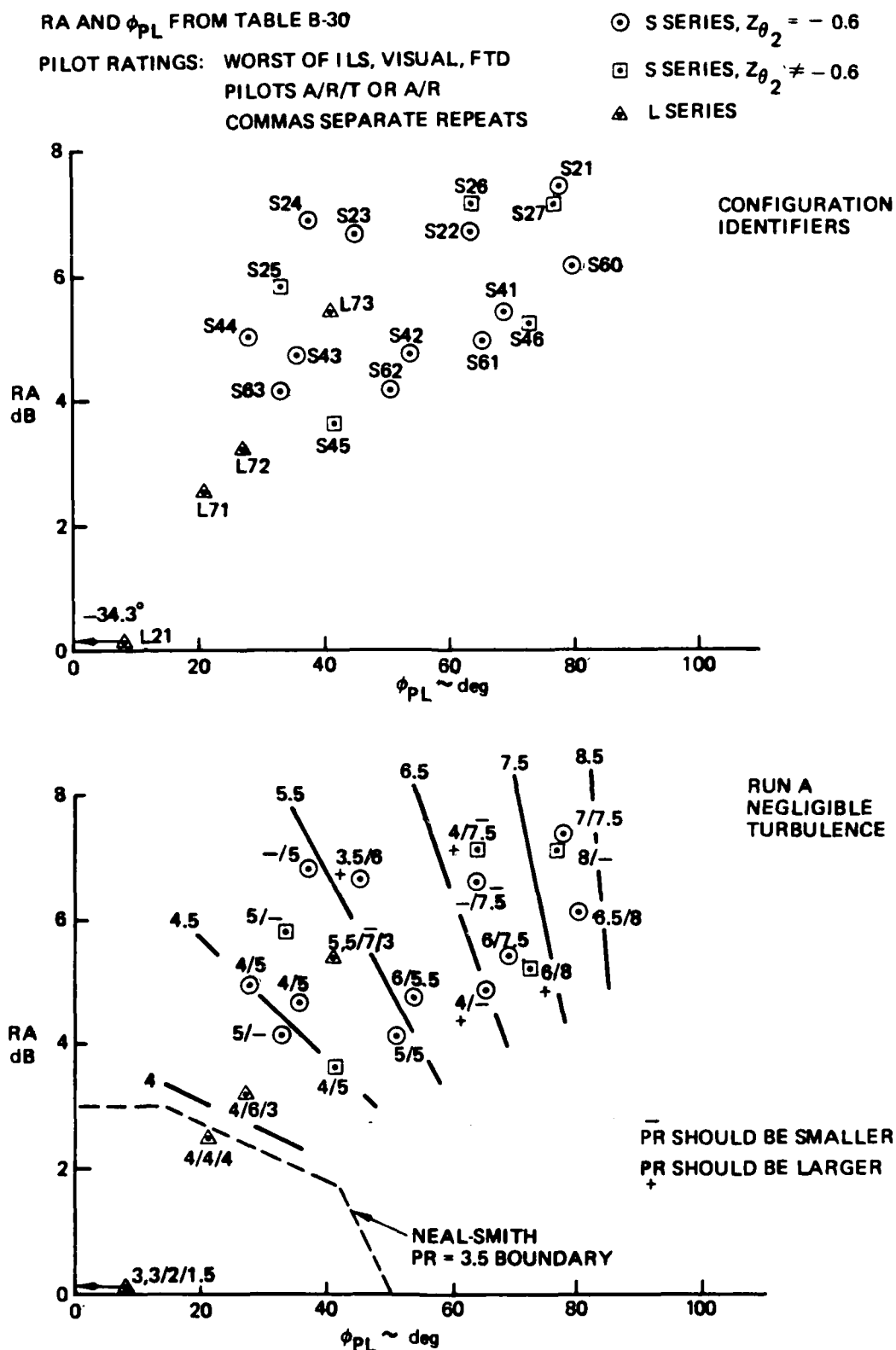
213

PILOT RATINGS: WORST OF ILS, VISUAL, FTD
PILOTS A/R/T OR A/R
COMMAS SEPARATE REPEATS

⊙ S SERIES, $Z_{\theta_2} = -0.6$

⊡ S SERIES, $Z_{\theta_2} \neq -0.6$

△ L SERIES

Figure B-49. Pilot Rating vs RA and ϕ_{PL}, High Sensitivity, BW = 1 rad/sec
(a) Configuration Identifiers and Run A

214

Figure B-49. Pilot Rating vs RA and ϕ_{PL}, High Sensitivity, BW = 1 rad/sec
(b) Run B and Run C

215

Figure B-50. PR vs RA and ϕ_{PL}, Adjusted Low Sensitivity, BW = 1 rad/sec

(a) Configuration Identifiers and Run A

216

Figure B-50. PR vs RA and ϕ_{PL}, Adjusted Low Sensitivity, BW = 1 rad/sec
(b) Run B and Run C

217
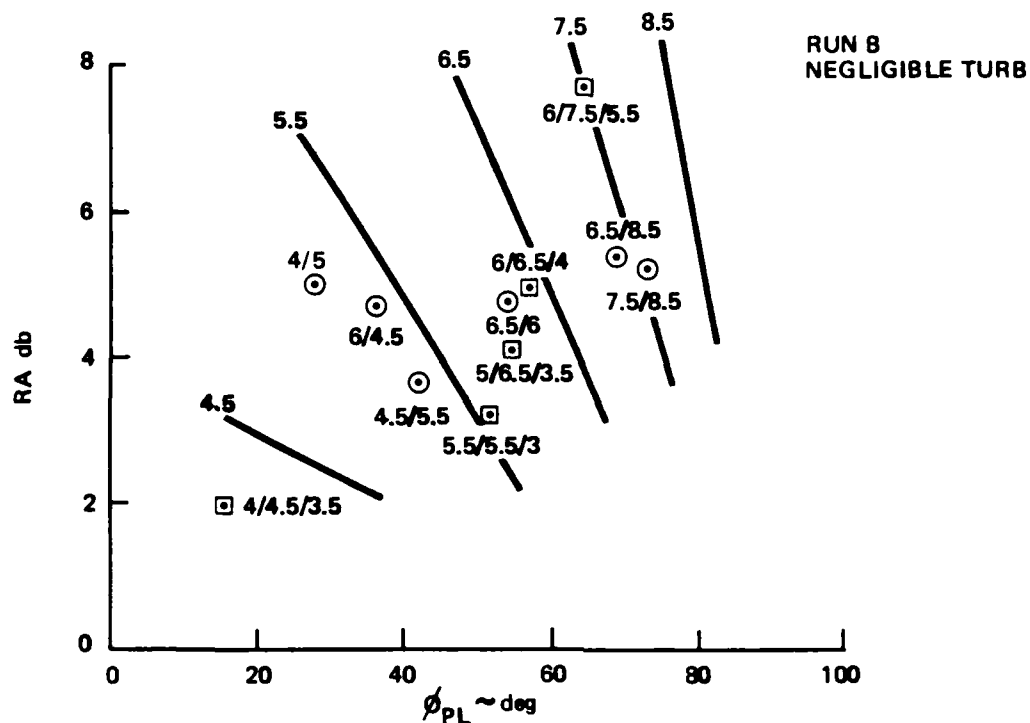
BW = 3 rad/sec

For analysis of the pilot rating data as a function of resonant amplitude and pilot lead, at a bandwidth of 3 rad/sec, average pilot ratings for each configuration for each turbulence level are presented in Table B-31. Since the range of RA and ϕ_{PL} covered is so small (Fig. B-48), expanded scales (2.5 times) have been used to plot the data in Figure B-51. All points have RA and ϕ_{PL} from RSS Neal-Smith (computer program) calculations performed with $1/\tau_{p_3}$ = BW and droop = 0 db, except for L21. The L21 point comes from a standard Neal-Smith calculation with τ_{p_3} = 0 and droop = -3 db.

All average pilot ratings are plotted in Figure B-51 at the appropriate RA and ϕ_{PL} for BW = 3. The ratings in parentheses are those which have been adjusted from low to high control sensitivity values, and there is close correspondence between the adjusted average ratings and high-sensitivity ratings. Iso-rating lines have been drawn where their values seem to be established by the data. The iso-ratings show a very different pattern from BW = 1 rad/sec data. The iso-ratings are primarily horizontal and show dependence of pilot rating primarily on resonant amplitude. It is noted that the slope of the iso-rating lines at large RA and ϕ_{PL} (upper right) is largely set by the ratings for S26, and these ratings are suspected to be too low (good). Perhaps the 6.5 to 8 iso-rating lines should be more nearly level.

Because RA and ϕ_{PL} for the configurations at BW = 3 cover such a small range and lie in a comparatively narrow band, the value of the pilot rating points and iso-ratings as criteria seems questionable. On the other hand, it is clear that the flare and touchdown was the determining factor in the poorer ratings (see Section B.5.5 and Figure B-24), and it is clear (Section B.6.1.4) that the pilot increases bandwidth in the flare and touchdown. Accordingly, the higher bandwidth data (BW = 3 rad/sec) cannot be dismissed and must be included as part of the criteria. Perhaps a different way of closing the loop or selecting the pilot model, specifically a different selection of $1/\tau_{p_3}$, would produce a more satisfactory result. Selecting $1/\tau_{p_3}$ = BW tends to place a knee at BW, which tends to reduce RA in the vicinity of BW. Only the criterion of minimizing pilot lead, which leads to droop = 0 db, is

Table B-31. Average Pilot Ratings with Adjustment for Low Control Sensitivities

Configuration	Run A Heavy Turbulence	Run B Negligible Turbulence	Run C Moderate Turbulence
F0	3.8	4.0	4.7
F1	3.8	4.6	4.8
F2	5.3	6.3	7.2
F4	5.0	5.5	6.3
F6	4.8	5.0	5.5
L21	2.2	3.7	5.3
L71	4.0	4.3	5.5
L72	4.3	5.0	5.0
L73	5.0	6.0	6.4
S21	7.3	8.0	8.3
S22	7.5	8.5	8.5
S23	4.8	5.5	6.5
S24	5.0	6.0	6.0
S25	5.0	5.0	6.0
S26	5.8	7.0	7.5
S27	8.0	9.0	10.0
S41	6.8	7.8	7.8
S42	5.8	6.3	6.8
S43	4.5	5.5	5.5
S44	4.5	5.3	6.0
S45	4.5	5.5	5.8
S46	7.0	7.8	7.8
S60	7.3	7.8	8.3
S61	4.0	4.0	5.0
S62	5.0	5.5	5.5
S63	5.0	5.0	6.0
S41A	6.3	7.5	8.0
S42A	6.3	6.3	6.0
S43A	4.3	5.3	6.0
S44A	4.3	4.0	4.5
S44B	5.3	5.3	5.5
S45A	5.0	5.5	4.8
S46A	8.0	7.8	8.0

Pilot ratings: Worst of ILS, Visual, FTD.
Averaging: Three pilot average of average rating for each pilot.
Sensitivity Adjustment: F (except F0), S-A, S-B series have pilot ratings decreased by increment from Figure B-30.

ALL PILOT RATINGS ARE AVERAGES FROM TABLE B-31. ( ) INDICATE RATINGS
ADJUSTED FOR LOW SENSITIVITY. RA AND ϕ_{PL} FROM TABLE B-30.

⊙ S SERIES
▲ L SERIES
⊡ F SERIES

CONFIGURATION
IDENTIFIERS

RA
dB

45.3° ← ▲ L21
S27 ⊙ S21
S26 ⊙
⊙ S60
S22 ⊙
S41 ⊙ S46 ⊙
F2 ⊡ ⊙ S61
S23 ⊙
⊙ S42
S24 ⊙
▲ L73
⊙ S62
⊡ F4
⊡ F6
⊙ S45
⊡ F1
S25 ⊙ ⊙ S43
S44 ⊙
⊙ S63
▲ L72
▲ L71
⊡ F0

$\phi_{PL} \sim$ deg

70   80   90   100   110

RA
dB

← ▲ 2.2
5.8 ⊙
7.5
8 ⊙ 7.3
⊙ 7.3
6.5
7.5 ⊙
6.8 ⊙
7 ⊙ (8)
(6.3) ⊡ ⊙ 4
(5.3)
RUN A
NEGLIGIBLE
TURBULENCE
5.5
5.8 ⊙
⊙ (6.3)
5 ⊙
▲ 5
⊙ 4.8
⊙ 5
⊡ (5)
4.5 ⊙
⊙ 4.5
⊡ (4.8)
4.5 ⊙
⊙ (5)
⊡ (3.8)
4.5
(4.3) (5.3)
A   B
5 ⊙
⊙ (4.3)
⊙ 5
▲ 4.3
▲ 4
⊡ 3.8

70   80   90   100   110

$\phi_{PL} \sim$ deg
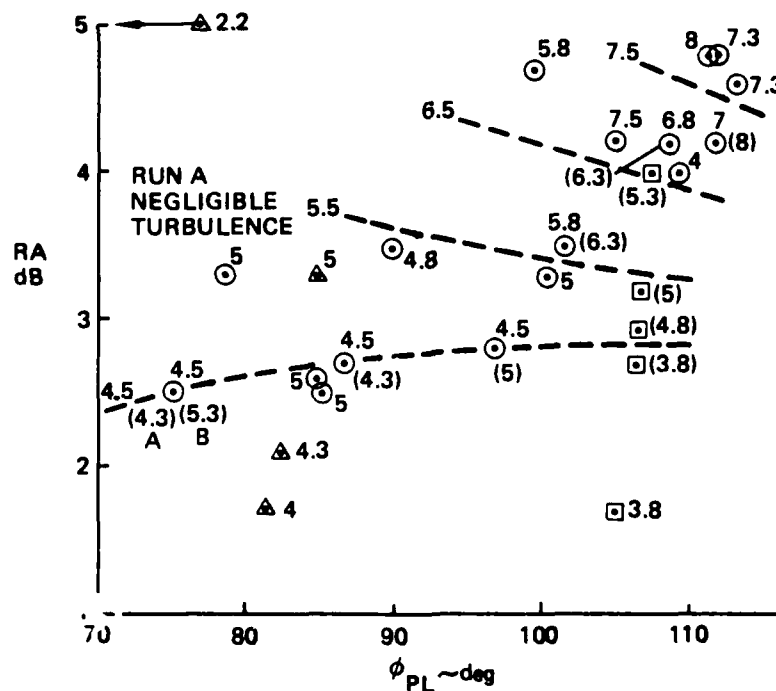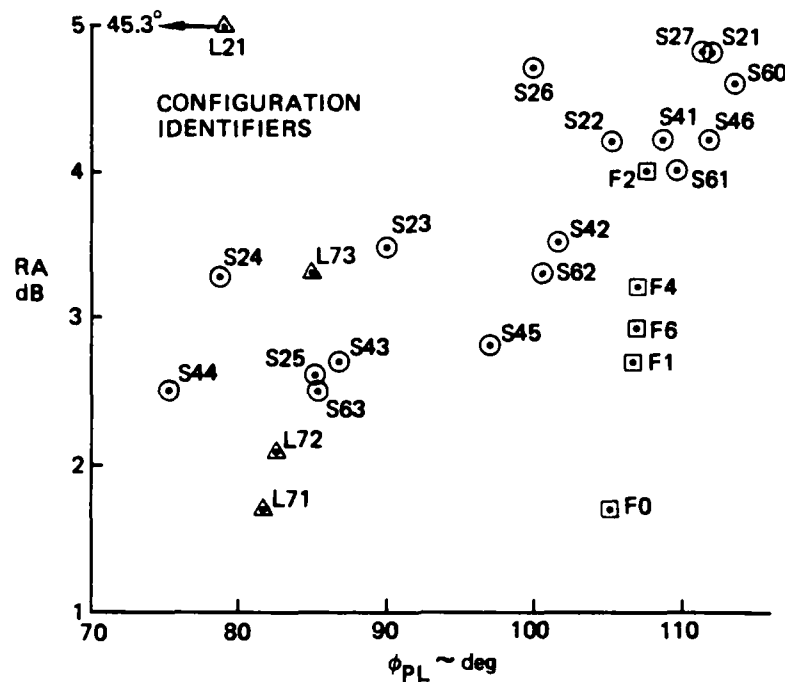
Figure B-51. Pilot Rating vs Resonant Amplitude and Pilot Lead, BW = 3 rad/sec
(a) Configuration Identifiers and Run A

220
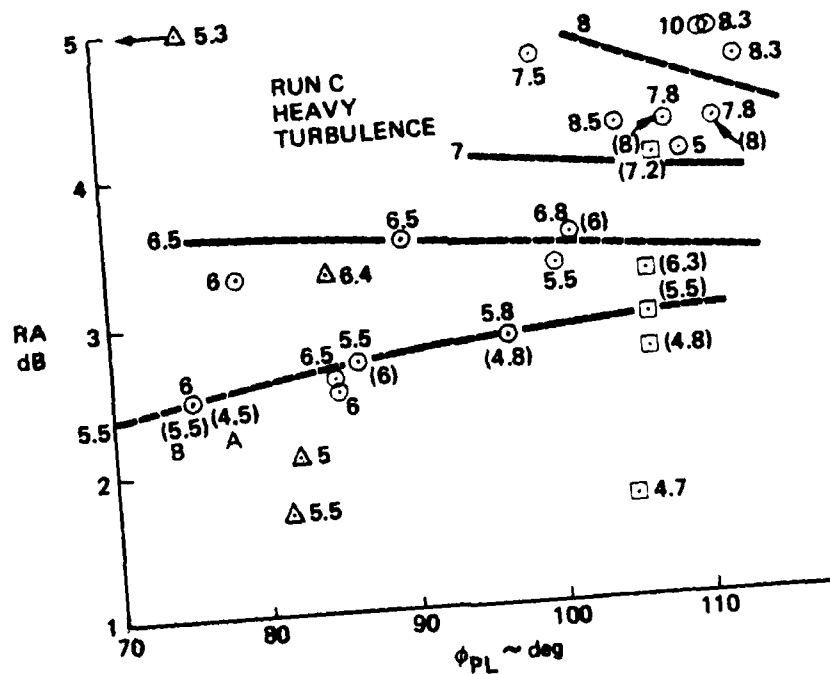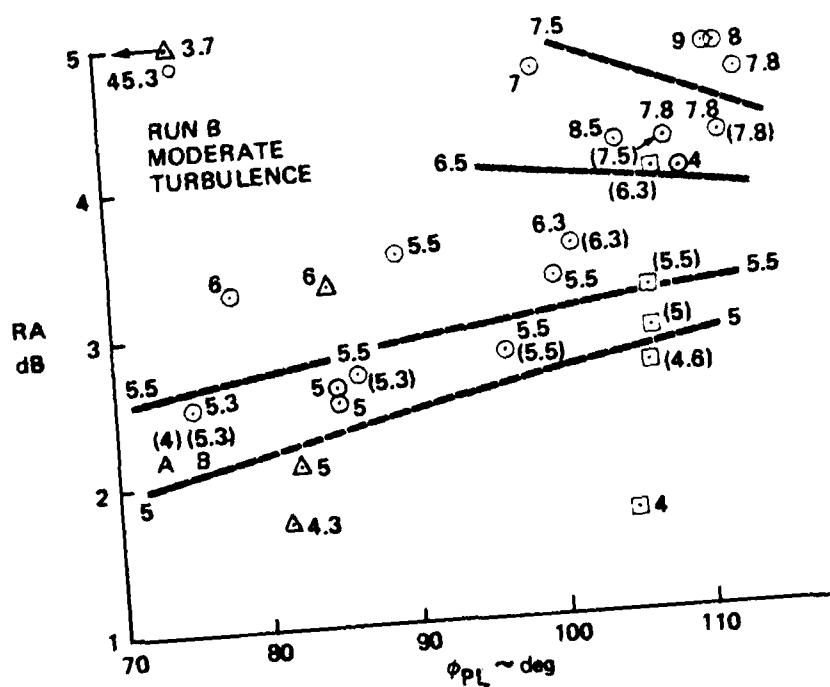
Figure B-51. *Pilot Rating vs Resonant Amplitude and Pilot Lead, BW = 3 rad/sec*
(b) Run B and Run C

221

responsible for producing any significant resonance. One of the bothersome points is that the primary frequencies measured from the simulator time histories are so much higher than the resonant frequencies predicted by the analytical loop closure. Since the data are well correlated in Figure B-51, and until a more satisfactory method of loop closure is derived, the BW = 3 data from the specified RSS Neal-Smith method will be considered appropriate for developing criteria for the higher bandwidths.

B.6.3 RSS Neal-Smith Criteria

The criterion of Neal and Smith (Ref.7) has been modified to make it applicable to the assessment of flying qualities for airplanes with relaxed static stability. The criteria presented here are based directly on the fixed-base ground simulator investigation of approach and landing, with some extrapolation made to broaden the applicability of the criteria. The criteria are for pitch dynamics with pilot in the loop, and are based on modelling the pilot-airplane pitch attitude closed loop with a simple pilot model. To paraphrase Chalk (Ref. 23), the design criteria are based on the hypothesis that if a specific level of closed-loop dynamic performance can be achieved with an autopilot of the form described by the assumed pilot model, then the human pilot will also be able to achieve a comparable level of performance. Thus it is not necessary for the pilot model to be an exact analog of the human pilot. The criteria, as modified for application to conditions of relaxed static stability, are called the RSS Neal-Smith Criteria.

The criteria are based on the following conceptual block diagram of the airplane and pilot model.
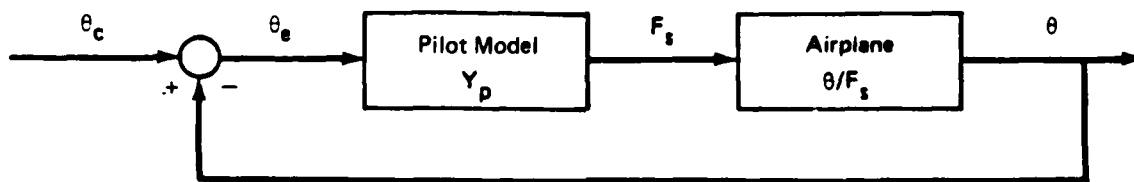
$$\frac{\theta}{F_s}(s)$$ Transfer function of pitch attitude response to stick force input for airplane and flight control system.

$$Y_p = K_p e^{-0.3s} \frac{(\tau_{p_1} s + 1)}{(\tau_{p_2} s + 1)} (\tau_{p_3} s + 1)$$

Criterion

The criterion is that the resonant amplitude (RA) and the pilot lead (ϕ_{PL}) shall fall within the boundaries shown in Figure B-52 for the appropriate Level of Flying Qualities when K_p, τ_{p_1}, τ_{p_2} and τ_{p_3}, subject to specified conditions, are adjusted to meet the specified closed-loop performance standards with minimum pilot lead.

Definitions

RA   Resonant amplitude: $\left|\frac{\theta}{\theta_c}\right|_{max}$ for $0.1 < \omega < 10$ rad/sec

ϕ_{PL} Pilot compensation, lead or lag (not including time delay, $e^{-0.3s}$):

$$\measuredangle \left[\frac{(\tau_{p_1} s + 1)}{(\tau_{p_2} s + 1)} (\tau_{p_3} s + 1) \right]_{s = j\omega = jBW}$$

BW   Bandwidth: ω for $\measuredangle \frac{\theta}{\theta_c} = -90^\circ$

Droop $\left|\frac{\theta}{\theta_c}\right|_{min}$ for $\omega < BW$

Performance Standard

For a BW = 1 and 3 rad/sec, the pilot gain (K_p) and compensation (τ_{p_1} and τ_{p_2}) shall be adjusted to yield the minimum pilot compensation (lead or lag) while maintaining the following closed loop characteristics:

Droop $\geq$ -3 db $0.1 < \omega < BW$ rad/sec

Droop $\leq$ 0 db $0.1 BW < \omega < BW$

Conditions

There are no constraints on K_p, τ_{p_1}, or τ_{p_2}. However τ_{p_3} must be set so that

$$1/\tau_{p_3} = BW \text{ in rad/sec.}$$

Applicability

The intent of the criteria is to provide safe levels of flying qualities for airplanes with relaxed static stability, either unaugmented or augmented with a back-up or hard SAS. To this intent, the criteria should be applicable if the following conditions are met (i.e., in a standard Neal-Smith loop closure).

$$\phi_{PL} > 80^o$$

. when: $\tau_{p_3} = 0$, $BW = 3$ rad/sec, minimum RA instead of ϕ_{PL} (i.e., normally droop = -3 db).

The criteria should be applicable to any airplane with static instability, or near neutral static stability, or any airplane that fails to meet the Level 1 short-period requirements for Category C Flight Phases of MIL-F-8785C because the short-period frequency is too low.

Discussion

The droop criterion requires some additional explanation and discussion with respect to both the original Neal-Smith criterion and the new RSS criterion. The original Neal-Smith criterion (Ref. 7) called for minimizing, down to zero db (unity gain), the resonant amplitude by use of pilot lead and/or lag, subject to a minimum droop of -3 db. The criterion did not require a -3 db droop, only that is should not go below that. The frequency range specified for the overall criteria was from 0.5 to 10 rad/sec, with the droop criterion only applicable below BW. Though Neal and Smith (Ref. 7) state that no pilot compensation is required for $|\theta/\theta_c|_{max} = 0$ db, apparently in their applications they always used a -3 db droop (except where it led to $\phi_{PL} > 80^o$, Ref. 7, Vol. II, p. 3), not recognizing that cases could exist where less droop than 3 db was called for (i.e., droop > -3 db).

CRITERION ASSUMES A SATISFACTORY LEVEL OF CONTROL SENSITIVITY.
DATA BASED ON FIXED-BASE GROUND SIMULATION OF APPROACH AND LANDING
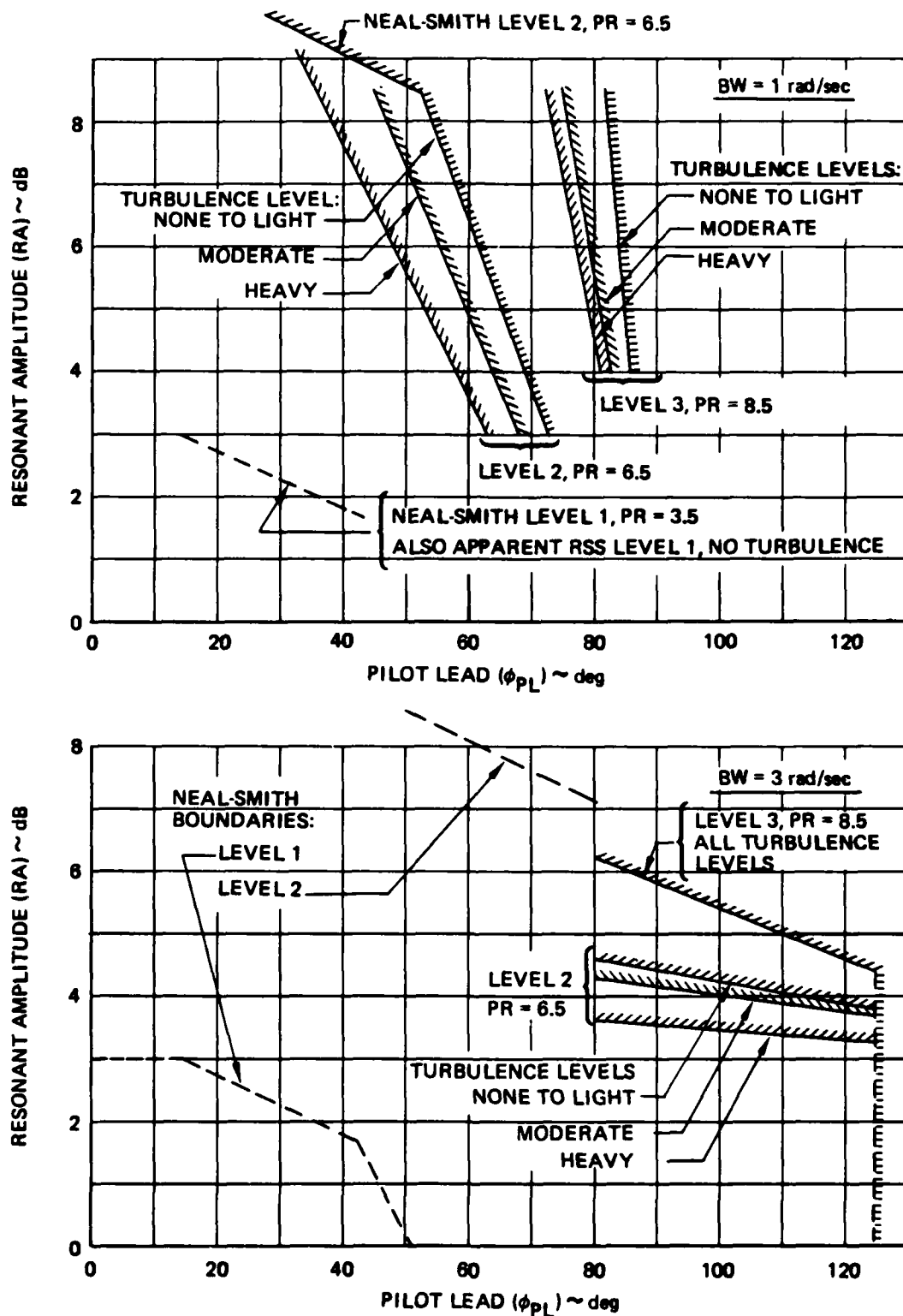
Figure B-52. Criterion for Pitch Attitude Dynamics of RSS Airplanes

The new RSS criterion calls for minimizing pilot lead without specifying a constraint on resonant amplitude, but subject to two droop constraints. The general constraint of minimum droop of -3 db (i.e., $|\theta/\theta_c|_{min} \geq$ -3 db) is the same as the Neal-Smith one, except the applicable frequency range has been extended from BW down to 0.1 rad/sec. The RSS-specific constraint of a droop not more positive than 0 db (i.e., $|\theta/\theta_c|_{min} \leq$ 0 db) provides the limit for minimizing pilot lead, and applies to the narrower frequency range from BW down to 0.1 BW. The concept allows oscillations or resonances to develop below BW in order to minimize pilot lead, while still maintaining unity gain (0 db) at or near BW. Since the closed-loop frequency response must have amplitude > 0 db over the whole frequency band applicable to the 0 db droop constraint, this band does not need to be very wide. A band from BW down to 0.1 BW was selected, but it is noted that it probably could be further narrowed from BW to only 0.3 BW. There is no intent to keep phugoid or lower frequency dynamics f om producing droop down to the -3 db limit at lower frequencies. However, a droop constraint at any positive value above 0 db does not appear rational, since this would tend to force the low-frequency closed-loop response toward infinite amplitude and -180^0 phase (the center of the Nichols chart), and apparent closed-loop instability. Although all RSS cases examined so far have the minimum pilot lead occuring for a 0 db droop, this combination may not always occur.

The terminology and notation requires some amplification. The term "droop" has been retained from Neal and Smith (Ref. 7) because it is well established not only by them, but also in previous literature. Droop specifically means $|\theta/\theta_c|_{min}$, and in this text a value for droop (e.g. -3 db) means the closed-loop reponse has a minimum of -3 db (which is 3 db down from 0 db). In Reference 7, a 3 db droop is sometimes used to mean the same thing, and care must be exercized. Note also that in Figure 5 (3.2.1.3) of Volume I, the cross-hatched curves are boundaries for θ/θ_e in open-loop coordinates and θ/θ_c in closed-loop coordinates. They are not meant to be the droop limits (0 db to -3 db). The terminology and presentation has been formulated so the Neal/Smith computer program (Ref. 27), or updated versions, can be as readily used for the RSS criteria calculations as the standard Neal-Smith ones.

The criteria boundaries in Figure B-52 come primarily from the PR = 6.5 and 8.5 iso-rating lines from Figure B-49 and B-51. The Neal-Smith PR = 6.5 boundary has been somewhat arbitrarily used as a cut-off of resonant amplitude for the Level 2 boundaries at BW = 1 rad/sec. The Neal-Smith Level 1 boundary is used to indicate potential approach to Level 1 flying qualities for relaxed static stability, though caution should certainly be used in allowing any airplane with marginal, neutral, or a lack of longitudinal static stability to be considered Level 1.

For BW = 3 rad/sec, the boundaries have been extended from 80° to 125° of pilot lead. The Level 2, heavy turbulence boundary is reasonably well established by the simulator data. The remaining boundaries involve substantial extrapolation, especially the Level 3 boundary. This Level 3 boundary passes through the PR = 8.5 data for moderate turbulence at ϕ_{PL} = 110°, with a slope judged consistent with the rest of the data. The PR = 8.5 data for heavy turbulence has almost the same iso-rating as that for moderate turbulence, and extrapolation indicates the same for negligible turbulence. The boundaries are drawn to ϕ_{PL} = 80° to indicate that this is an appropriate value at which to shift from the standard Neal-Smith approach to the RSS approach with its additional pilot lead term. However, with the RSS approach, a pilot lead of less than 80° is readily obtainable. The boundaries are extended to 125°, with a cut-off indicated, because this is near the limit of pilot lead (absolute limit is 135°) obtainable from the pilot model used in the RSS approach. There certainly must be an upper limit to pilot lead. Since no cases were investigated with more than 114°, it is unwise to allow much more. Furthermore, as the absolute limit of lead is approached, τ_{p_1} becomes very small and distorts the relationship of amplitude and lead, hence the 10° margin and the 125° cut-off.

In summary, the analysis of the simulator pilot rating data with the proposed RSS Neal-Smith approach using a resonant amplitude vs. pilot lead criterion provides excellent correlation of the data for a bandwidth of 1 rad/sec. The results appear to provide a good basis for developing criteria for flying qualities of airplanes with relaxed static stability. On the other hand, the results of the analysis for a bandwidth of 3 rad/sec are not as satisfactory. The range of resonant amplitude and phase covered by the data are small, and the resonant frequencies do not

227

agree well with the experimental time history data. Some modification to the approach seems indicated, even though there is good correlation of the pilot rating data with resonant amplitude and pilot lead for a bandwidth of 3 rad/sec. From the experimental data it is clearly apparent that the pilot varies bandwidth during the course of an approach and landing, and criteria for both high and low bandwidths are necessary.

APPENDIX C

SIMULATION AND DATA

C.1 Introduction

The simulation experiment design including simulation configurations, evaluation tasks, procedures, background of the evaluation pilots, and the method of validating the simulation are all described in Appendix B, Section B.4. The purpose of this appendix is to document in detail for reference use the characteristics of the simulation and the simulation configurations.

Details of the simulation are described in Section C.2. Additional aspects of the conduct of the experiment not covered in Section B.4 are given in Section C.3. The longitudinal characteristics of the evaluation configurations are documented in considerable detail in Section C.4 to facilitate further analysis and interpretation of the pilot rating data. The characteristics include the following for each of the unaugmented configurations:

> aerodynamic coefficients
> coefficients in equations of motion
> state models
> transfer function poles and zeros for u, w and θ
> time histories of q, α, θ, n_z, and u for step pitch input
> frequency responses (amplitude and phase vs frequency)

The primary simulation program data, the pilot ratings from each formal evaluation performed, are given in Section C.5 along with some information concerning the pilot rating data and strip chart recorded data. The pilot comments themselves are found in Appendix G which comprises Volume III.

C.1.1 Overall Simulation Description

The baseline airplane used for the simulation was the F-111A airplane, but since only generic characteristics were of interest, considerable liberties were taken to simplify the aerodynamics and flight controls. The evaluation program simulations were of approach and landing, all performed at a fixed wing-sweep and landing-flap settings, and there was no concern for post-stall behavior. Primary concern was centered on determining the effects of relaxed static longitudinal stability on fighter and attack airplane characteristics and flying qualities. Accordingly, the baseline F-111A simulation aerodynamic data are for a fixed 16° wing sweep and 37.5^O flap settings, go from below zero to stall angles of attack, and are at a fixed Mach number of 0.2. Lift, drag, and pitching moment for the baseline F-111A were closely represented with table look-ups. However, lateral directional characteristics were simplified to constant stability derivatives (i.e., C_{n_β}, etc), with no dependence on angle of attack or control deflection, as the object here was simply to have good lateral-directional characteristics.

The baseline F-111A flight control system was also simplified by omitting the self-adaptive gain changer and all filters associated with structural modes. The self-adaptive gain was set at an appropriate fixed value. On the other hand, feel system and actuator dynamics were carefully represented since they affect the overall airplane response in the frequency range of interest to the pilot (10 rad/sec or less).

The F-111A has two P&W TF30 turbofan engines with multi-stage of afterburners (A/B). The propulsion system was greatly simplified. First, the two engines were treated as one to effectively produce a single-engine airplane. Then, static thrust was represented as a straight-line function of throttle handle position, including A/B, with a detent delineating entry into A/B.

For most of the evaluations performed, further simplifications were made in the longitudinal aerodynamics and in the flight control augmentation system, primarily to enable more ready set-up of the evaluation configurations and interpretation and analysis of the data.

230

The longitudinal aerodynamic coefficients were linearized (i.e., table look-ups replaced by constant C_{L_α}, C_{D_α}, etc.). The F-111A pitch augmentation feedbacks with their complex compensation were replaced by simple α, $\dot{\alpha}$, n_z and q feedbacks. These simplifications allowed the airplane including its flight control system to be represented, for small changes in airspeed, by linearized equations and straight-forward state models. This was an important advantage in analyzing the data from the simulator evaluations since frequencies, dampings, roots, etc., could be calculated with certainty that they accurately represented the simulation.

The simulation was performed on the Boeing Visual Flight Simulator (VFS) facility at the Kent Space Flight Center, Seattle, Wa. An overview of the simulator is provided in Figure C-1 which emphasizes the software programmed on the Varian V74/75 computers that were used to solve the flight equations as well as control all the various elements of the simulator. The cockpit was provided by the right-hand pilot station of a widebody cab, selected because of its high-quality flight instruments and center stick with variable feel system. With left-hand pilot station appropriately masked off with cardboard, the cockpit well represented a single-place fighter or attack airplane with throttle handle on the left. For visual flight a TV camera, slaved to airplane motion, picked up the image from a 150th scale model of a large airport runway which was then back-projected on a flat screen infront of the pilot.

The arrangement of the simulator cab and back-projected visual scene is shown in the line drawing of Figure C-2. The landing field is shown in the photograph in Figure C-3, taken from well above the approach path to more clearly show the runway markings, buildings, taxi-ways, and parked airplanes. The visual scene as viewed from the cockpit on final approach is shown in the photograph of Figure C-4, which also shows the cockpit instruments and controls. A wider field of view than depicted was seen by the pilot as the camera taking the photo was back of the pilot's seat.

231
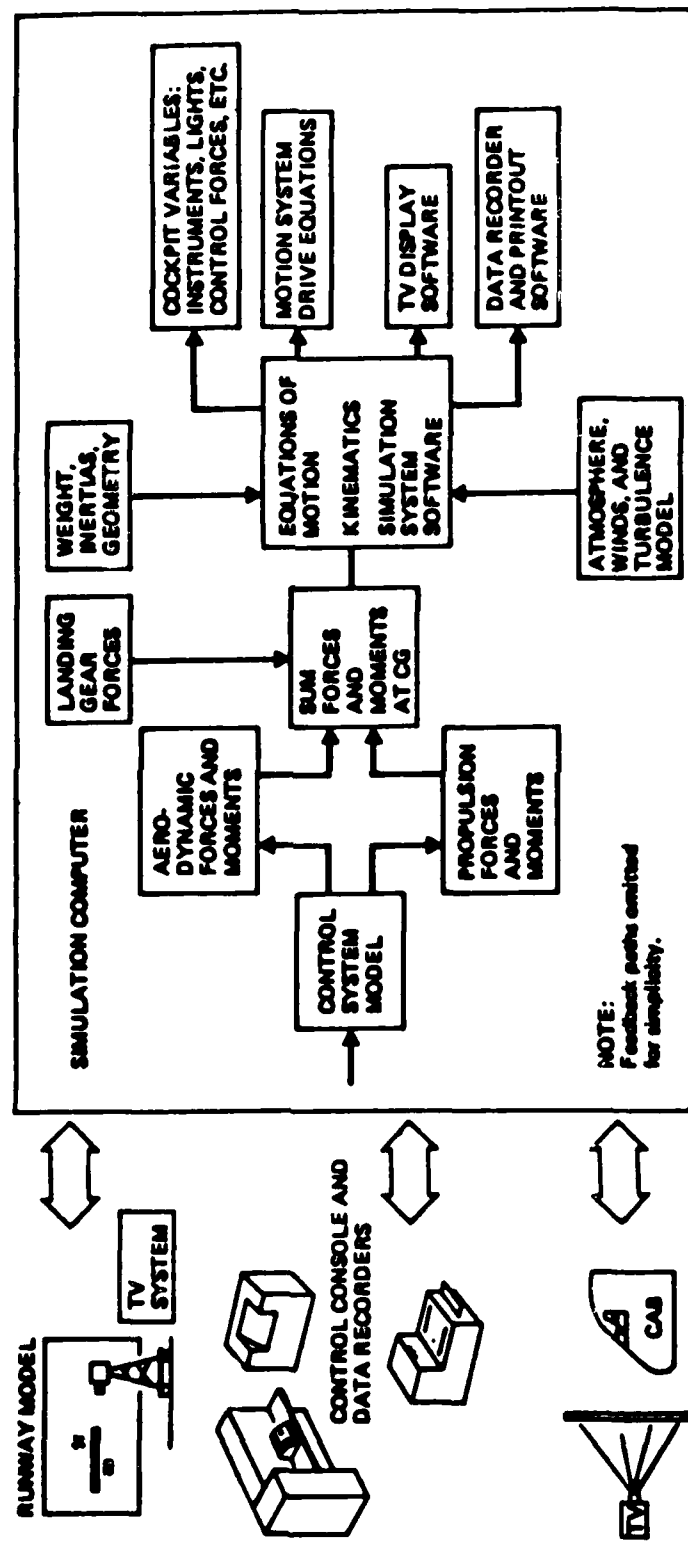
Figure C-1. Simulator Schematic
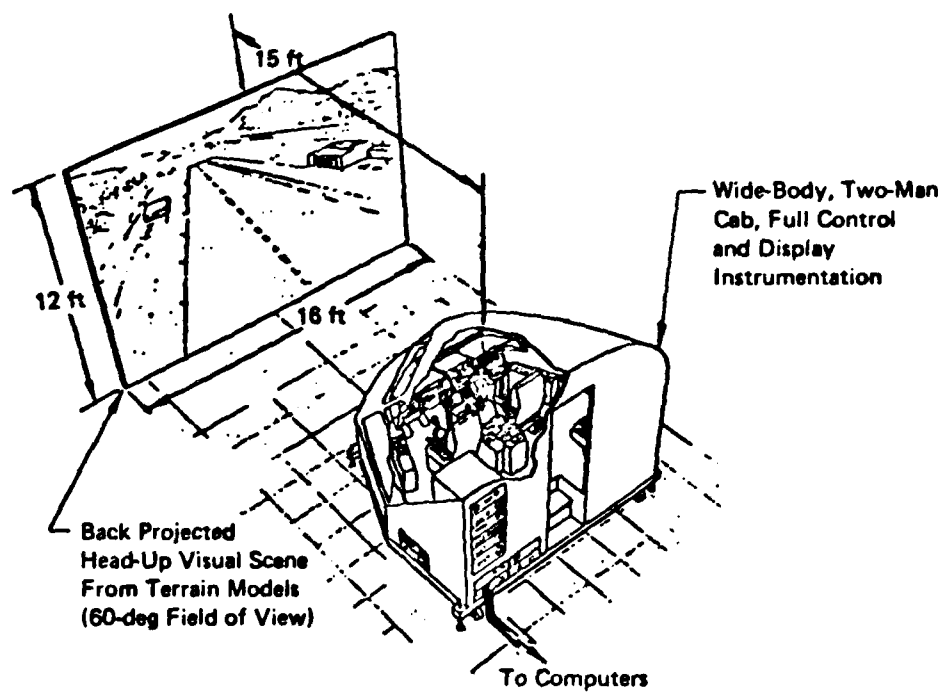
Figure C-2. Wide-Body Cab and Visual Scene

Figure C-3. Landing Field Model

Figure C-4. Cockpit Controls, Instruments, and Landing
Visual Scene

234

C.1.2 Overall Simulation Program

The simulation program was run in two parts. The first part, performed under Air Force contract, included the initial check-out and validation of the baseline F-111A simulation, the preliminary evaluation program, and the formal evaluations of the augmented and unaugmented F-111A as a function of c.g. position and the investigation of control authority requirements. The second part of the simulation program, performed under IR&D funding as a separate Boeing program, was based on the results of the first simulation program. The later program investigated the independent effects of parameters in the pitch attitude transfer function for the airplane, validated the simulation by direct comparison with flight test results from Reference 8, and also included the investigation of control rate requirements. The results of both simulation programs are included in this report, generally without distinguishing between them, but the run numbers include the date and those in '79 were from the first program, those in '80, from the second.

C.2 Simulator Description

C.2.1 Equations of Motion

The reference coordinate system for determining aircraft location and orientation is an earth-fixed inertial system. The origin is at the inbound edge of the runway, with the X-axis down the center of the runway, positive in the direction of landing. The Y-axis is perpendicular to and is positive to the right of the positive X direction. The Z-axis points downward, so is the negative of altitude (h). The body axis system is related to the earth fixed system by the Euler angles ψ (heading), θ (attitude) and ϕ (bank angle). The geometric reference point on the aircraft is normally at the 25% reference chord, but for the F-111A in the approach condition, it was at the 45% chord. The airplane body axes for the equations of motion have as origin the c.g.

A block diagram of the equations of motion and all associated computations is shown in Figure C-5, which represents standard library software of the VFS (Ref. 57). Data for the various standard blocks, plus special blocks for this simulation, are as follows:

o The aero, propulsion, and wind/atmosphere models are described in sections C.2.2, C.2.3, and C.2.5, respectively.

o There was no gear model as such in the simulation. Once the airplane "touched down" (height $\leq$ 11 ft.), the computer took control and brought the airplane to a pre-programmed stop. It decelerated the airplane at a reasonable level and brought it to the center of the runaway. Therefore the variables L_G, M_G, N_G, F_{GX}, F_{GY} and F_{GZ}, coming from the aero and gear model, were irrelevant. This simplified approach was used since the roll-out following touchdown was not material to the evaluation, and it was desired to simplify the simulation as much as possible but still retain a modicum of reality for the pilot.

o The cockpit/crew station block included the feel system described in C.2.4.1 and the cockpit displays and controls described in C.2.7. It also contained the kinematic relations for calculating the pilot's eye position and line of sight in order to position and orient the TV camera viewing the runway model, also the transformation of motions at the c.g. to pilot's location for cockpit instruments.

o The c.g. transformations are based on a reference moment center at $\overline{x}_{cg}$ = .45, and are indicated in the "Body-axis moment" block.

o All aircraft configurations had a constant mass or weight.

236
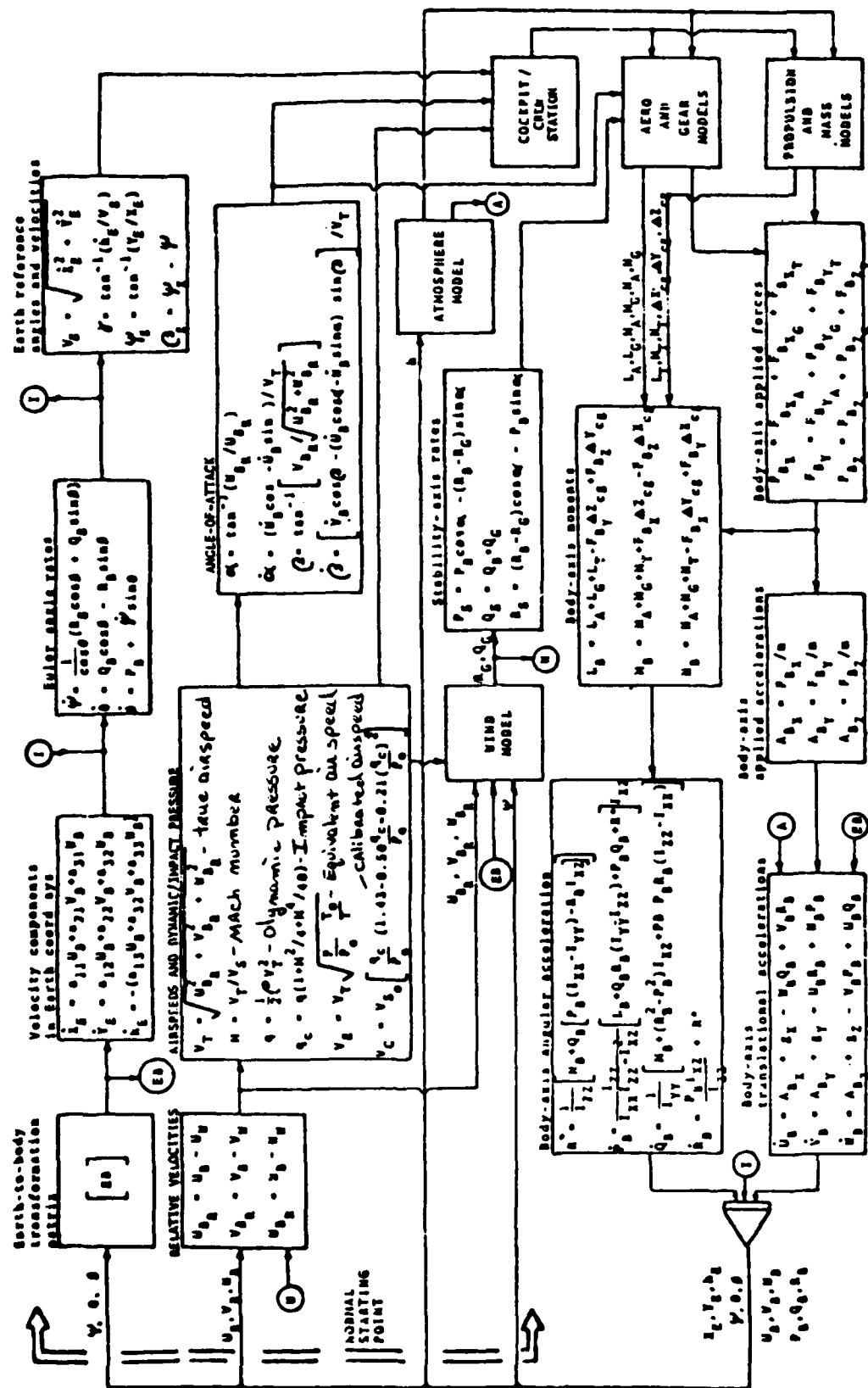
Figure C-5. Equations of Motion for VFS Simulator

237

o   In the "Body-axis applied forces" block and "--moment" block, the A subscript stands for aerodynamic, the G for landing gear, and the T for thrust. The "body axes" for the equations of motion are aligned with the airplane reference axis with origin at the airplane center of gravity (c.g.).

o   In the "Body axis translational accel." block g_x, g_y and g_z are the normalized components of the gravitational force.

o   The "Atmosphere model" block calculated atmospheric pressure, density, temperature, speed of sound, and gravitational constant as a function of altitude for the standard atmosphere (Ref. 58). It also allowed an off-standard temperature.

o   The "Wind model" block calculated the body axis velocity components due to winds and turbulence, also the yaw and pitch angular components of turbulence R_G and Q_G. Inputs, for low-altitude, were the wind velocity and direction at 20 ft altitude, and surface roughness. The wind and turbulence model was that of Reference 56. The simulation used three intensities of tubulence but, for simplicity, had the corresponding steady wind set to zero as well as R_G and Q_G. The turbulence model is defined in C.2.5.

o   In the "Earth reference angles and velocities" block: V_g is the ground velocity, γ is the inertial flight path angle, ψ_g is the ground track angle, and β_g is the airplane crab angle.

C.2.2 Aerodynamics

There were two aerodynamic routines, FQAERO and FQAERX, which differ only in longitudinal characteristics.

The FQAERO subroutine contained the nonlinear F-111A longitudinal aerodynamic data from Reference 49. It was originally intended to represent the data as a function of angle of attack, horizontal tail deflection, flap deflection, and wing sweep, at several values of Mach number as indicated in the following equations in C.2.2.1. Some exploratory simulation was done with variable sweep and flaps. However, since all the formal simulation evaluations which generated pilot rating data were made with fixed sweep and flaps, gear down, in approach and landing, only the pertinent data is included in C.2.2.1.

The FQAERX subroutine contained the fixed linear aerodynamic coefficients or stability derivatives as indicated by the equation in C.2.2.2. The $C_{D_\alpha}{}^2$ term is nonlinear, but it was set to zero for all evaluation configurations that used FQAERX.

The lateral-directional aerodynamic equations and values given in C.2.2.3 were used, with both FQAERO and FQAERX, for all simulation configurations.

The aerodynamics coefficients C_D and C_L are defined to be in the stability axis system while C_y, C_l, C_m, and C_n are defined to be in body axes, both axes with origin at the reference moment center (.45c for F-111A). Thus C_D is in the plane of symmetry (x_B-z_B plane) and C_y normal to it. The forces and moments are calculated by the standard equations, including transformation of C_L and C_D from stability to body axes (see C.2.2.4), for inclusion in the "Body-axis applied forces" block in Figure C-5. Transformation of moments from reference moment center to c.g. occurs in the "Body-axis moments" block of Figure C-5.

C.2.2.1 FQAERO

Subroutine FQAERO calculated C_D, C_L and C_m by linearly interpolating on tables whose indendent variables were angle of attack and horizontal tail deflection. The tables could also interpolate for
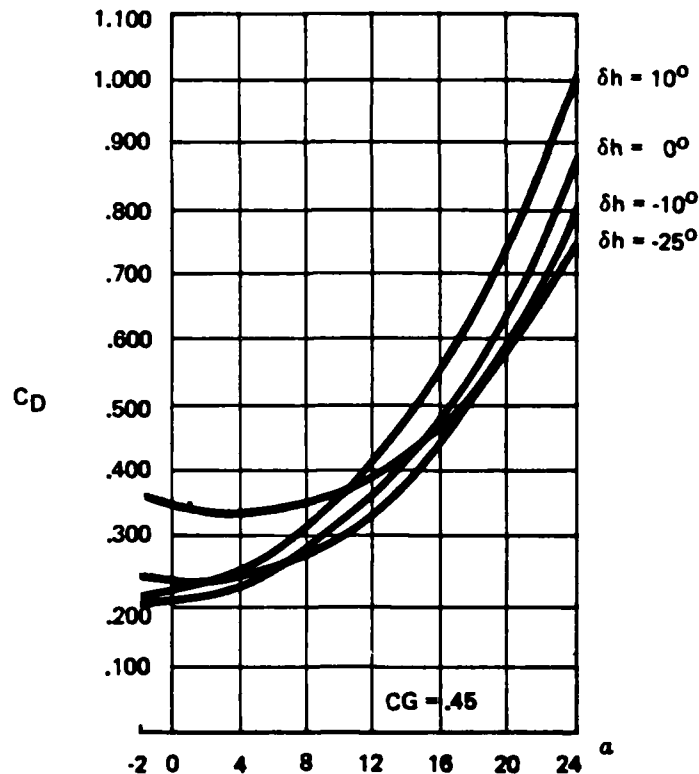
Figure C-6. Drag Coefficient Used in "FQAERO", Sweep = 16°, Flaps Down

flap position, wing sweep position and Mach number. The form of the equations is as follows:

$$C_L = C_L (\alpha, \delta_h, \delta_F, \Lambda, M) + \frac{c}{2V_a} [C_{L_{\dot{\alpha}}}(M)\dot{\alpha} + C_{L_q}(\alpha,M)q] + \Delta C_{L_G}$$

$$C_D = C_D (\alpha, \delta_h, \delta_F, \Lambda, M) + \Delta C_{D_G}$$

$$C_m = C_m (\alpha, \delta_h, \delta_h, \Lambda, M) + \frac{c}{2V_a} [C_{m_q}(\alpha,M)q + C_{m_{\dot{\alpha}}}(\alpha,M)\dot{\alpha}] + \Delta C_{m_G}$$

Graphs of the tables defining C_L, C_D and C_m as functions of α and δ_h are shown in Figures C6, C7, and C8, respectively. (All simulator configurations in this report have: Flaps = 37.5°, wing sweep = 16° and Mach = .2).
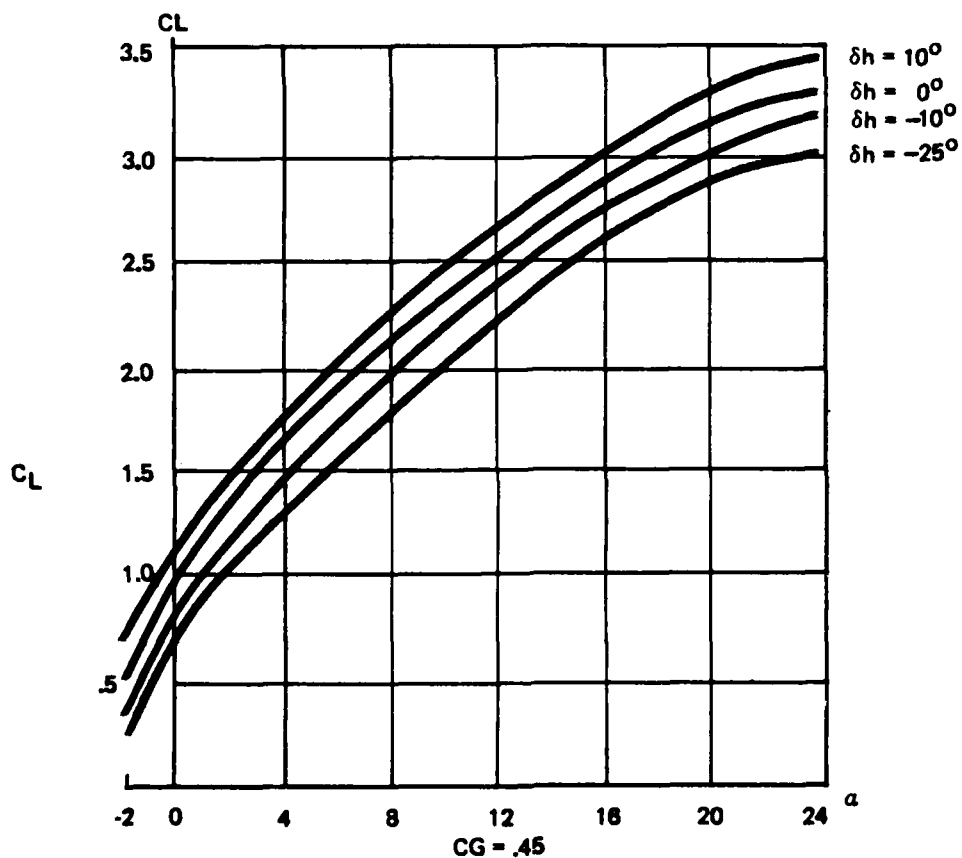
Figure C-7. Lift Coefficient Used in "FQAERO", Sweep = 16°, Flaps Down

The dynamic derivatives $C_{L_{\dot{\alpha}}}$, C_{L_q} and $C_{m_{\dot{\alpha}}}$ are given as follows (α in radians):

$$C_{L_{\dot{\alpha}}} = 2.65$$

$$C_{L_q} = C_{L_{q_0}} + C_{L_{q_\alpha}} \alpha$$

where $C_{L_{q_0}} = +5.68$, $C_{L_{q_\alpha}} = +0.86$

$$C_{m_{\dot{\alpha}}} = C_{m_{\dot{\alpha}_0}} + C_{m_{\dot{\alpha}_\alpha}} \alpha$$

where $C_{m_{\dot{\alpha}_0}} = -4.5$, $C_{m_{\dot{\alpha}_\alpha}} = -0.86$
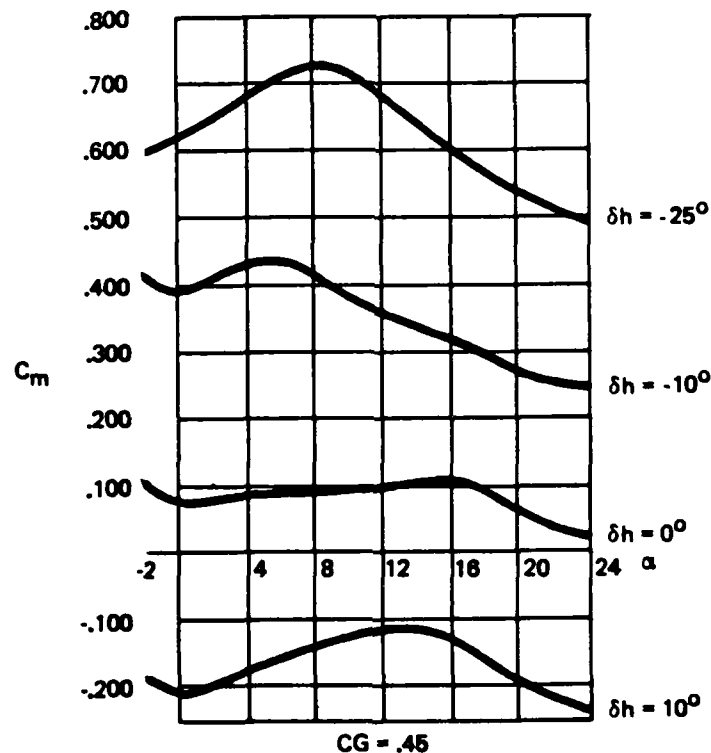
Figure C-8. Pitch Moment Coefficient used in "FQAERO", Sweep = 16°, Flaps Down

The derivative C_{m_q} is given by the following table, with linear interpolation used for intermediate values:

α	0.0°	2°	4°	6°	8°	10° or greater
C_{m_q}	-16.2	-14.2	-13.8	-19.2	-22.1	-22.3

Increments ΔC_D, ΔC_L and ΔC_m are added for the effects of landing gear as follows. The gear increments varied linearly with time when the gear handle was moved up or down. Gear rotation took 15 seconds. However, the gear was down for all the evaluation configurations.

$$\Delta C_{D_G} = +.100$$

$$\Delta C_{L_G} = +.005$$

$$\Delta C_{m_G} = +.025$$

C.2.2.2 FQAERX

Subroutine FQAERX used fixed linear aerodynamic coefficients, but otherwise had full non-linear kinematics and aerodynamics. The aerodynamics coefficients were accessed or changed through "patch" files which allowed configuration changes to be made quickly. The values of the coefficients for the various configurations are found in Table C-6 of C.4.2.

C_D, C_m and C_L were expressed as follows, but the $\Delta\alpha^2$ term in C_D was set to zero in all evaluation configurations to preserve linearity.

$$C_D = C_{D_{ref}} + C_{D_\alpha} \Delta\alpha + C_{D_{\alpha^2}} (\Delta\alpha)^2 + C_{D_{\delta_h}} \Delta\delta_h + \frac{2}{V_a} C_{D_u} \Delta u$$

$$C_L = C_{L_{ref}} + C_{L_\alpha} \Delta\alpha + C_{L_{\delta_h}} \Delta\delta_h + \frac{c}{2V_a} (C_{L_{\dot\alpha}}\dot\alpha + C_{L_q} q) + \frac{2}{V_\alpha} C_{L_u} \Delta u$$

$$C_m = C_{m_{ref}} + C_{m_\alpha} \Delta\alpha + C_{m_{\delta_h}} \delta_h + \frac{c}{2V_a} (C_{m_{\dot\alpha}}\dot\alpha + C_{m_q} q) + \frac{2}{V_a} C_{m_u} \Delta u + C_{m_\theta} \Delta\theta$$

(Reference moment center at $.45\bar{c}$)

where:

$\Delta\alpha$	$= \alpha - \alpha_1$	α_1	$= 4.1^0$
$\Delta\delta_h$	$= \delta_h - \delta_{h_1}$	δ_{h_1}	$= 2.1^0$
Δu	$= u - u_1$	u_1	$= 145$ knots (120 knots for L configurations)
$\Delta\theta$	$= \theta - \theta_1$	θ_1	$= 0$

and:

$$C_{L_{\dot\alpha}} = \partial C_L / \partial \left(\frac{\dot\alpha c}{2V_a}\right)$$

$$C_{L_q} = \partial C_L / \partial \left(\frac{qc}{2V_a}\right)$$

$$C_{m_{\dot{\alpha}}} = \partial C_m / \partial \left(\frac{\dot{\alpha}c}{2V_a}\right)$$

$$C_{m_q} = \partial C_m / \partial \left(\frac{qc}{2V_a}\right)$$

$$C_{D_u} = \frac{V_a}{2} \cdot \frac{\partial C_D}{\partial u}$$

$$C_{L_u} = \frac{V_a}{2} \cdot \frac{\partial C_L}{\partial u}$$

$$C_{m_u} = \frac{V_a}{2} \cdot \frac{\partial C_m}{\partial u}$$

C.2.2.3 Lateral-Directional Coefficients

C_y, C_l and C_n are expressed as follows:

$$C_y = C_{y_\beta}\beta + \frac{b}{2V_a}(C_{y_{\dot{\beta}}}\dot{\beta} + C_{y_r}r + C_{y_p}p) + C_{y_{\delta_a}}\delta_a + C_{y_{\delta_{sp}}}\delta_{sp} + C_{y_{\delta_r}}\delta_r$$

$$C_l = C_{l_\beta}\beta + \frac{b}{2V_a}(C_{l_{\dot{\beta}}}\dot{\beta} + C_{l_r}r + C_{l_p}p) + C_{l_{\delta_a}}\delta_a + C_{l_{\delta_{sp}}}\delta_{sp} + C_{l_{\delta_r}}\delta_r$$

$$C_n = C_{n_\beta}\beta + \frac{b}{2V_a}(C_{n_{\dot{\beta}}}\dot{\beta} + C_{n_r}r + C_{n_p}p) + C_{n_{\delta_a}}\delta_a + C_{n_{\delta_{sp}}}\delta_{sp} + C_{n_{\delta_r}}\delta_r$$

Where:

$$\delta_h = .5(\delta_{h_L} + \delta_{h_R}), \quad \delta_{sp} = \delta_{sp_L} - \delta_{sp_R}, \quad \delta_a = .5(\delta_{a_L} - \delta_{a_R})$$

and:

$$C_{y_{\dot{\beta}}} = \partial C_y / \partial \left(\frac{\dot{\beta}b}{2V_a}\right), \quad C_{y_r} = \partial C_y / \partial \left(\frac{rb}{2V_a}\right), \quad C_{y_p} = \partial C_y / \partial \left(\frac{pb}{2V_a}\right)$$

and similarly for the n and l derivatives.

The values used for the lateral coefficients in all cases were:

C_{y_β}	= -1.198	C_{n_β}	= 0.093	C_{l_β}	= -.080
$C_{y_{\dot{\beta}}}$	= -.122	$C_{n_{\dot{\beta}}}$	= 0.038	$C_{l_{\dot{\beta}}}$	= -.009

$$C_{y_r} = 0.280 \qquad C_{n_r} = -.200 \qquad C_{l_r} = 0.065$$

$$C_{y_p} = 0.100 \qquad C_{n_p} = 0.004 \qquad C_{l_p} = -.415$$

$$C_{y_{\delta_a}} = 0.00 \qquad C_{n_{\delta_a}} = 0.033 \qquad C_{l_{\delta_a}} = 0.072$$

$$C_{y_{\delta_{sp}}} = 0.00 \qquad C_{n_{\delta_{sp}}} = -.011 \qquad C_{l_{\delta_{sp}}} = -.112$$

$$C_{y_{\delta_r}} = 0.298 \qquad C_{n_{\delta_r}} = -.108 \qquad C_{l_{\delta_r}} = 0.010$$

C.2.2.4 Aero Forces and Moments

The outputs of the aero programs (FQAERO and FQAERX), in body axes with moments about the reference moment center, were $F_{B_{x_a}}$, $F_{B_{z_a}}$, $F_{B_{y_a}}$, M_a, L_a and N_a.

Let $T = \rho V_a^2 S/2$, $V_a = V_{a_1} + \Delta V_a = V_T$

then:

$$F_{B_{x_a}} = (C_L \sin \alpha - C_D \cos \alpha)\, T$$

$$F_{B_{y_a}} = C_y T$$

$$F_{B_{z_a}} = -(C_L \cos \alpha + C_D \sin \alpha)\, T$$

$$M_a = C_m Tc$$

$$L_a = C_l Tb$$

$$N_a = C_n Tb$$

C.2.3 Propulsion

The basis for the engine model was Pratt & Whitney data on engine thrust for the Pratt & Whitney TF30-P-412A turbofan engine.

The propulsion subroutine simulated engine dynamics with a first order time lag with time constant = 2 sec and a rate limit of ±3,500

lb/sec. Steady state thrust at sea level was given by the following graph. The afterburners came on after throttle position reached 70% of full throttle travel. The thrust shown in the graph below was doubled for the two engines of the F-111A. The two throttle handles in the simulator cab were ganged together, so the airplane appeared as a single-engine airplane to the pilot.

PERCENT THROTTLE TRAVEL
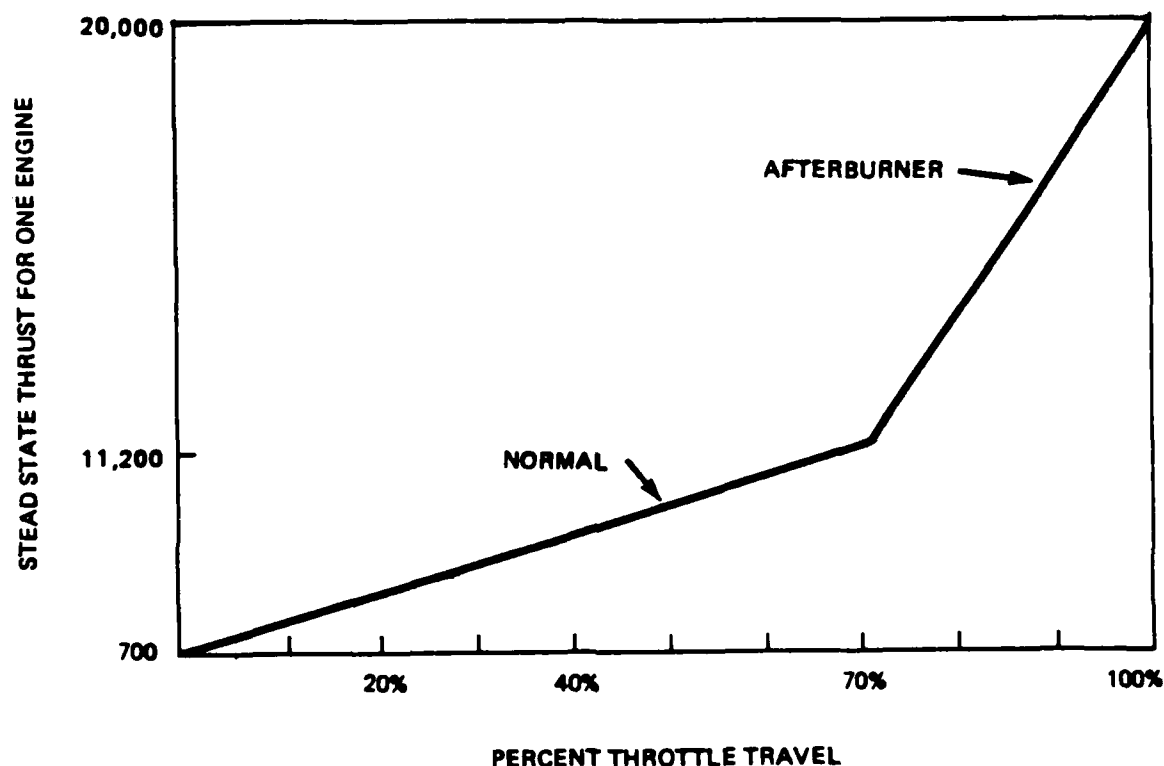
C.2.4 Flight Control Systems

There were three basic types of Flight Control Systems used in the simulation: F (simplification of the F-111 flight control system), G (generic flight control system), and U (strictly unaugmented in pitch, with a fast actuator). The options for each flight control system included: pitch augmentation failure, roll augmentation failure, yaw augmentation failure, and ability to turn off the spoilers and series trim servo(s). Time constants, transfer function gains, software

246

position and rate limits, inputs, etc. for each flight control system could be quickly changed, even during a simulation run, by using "patch" files.

The differences between the G and F systems were:

1. Types of longitudinal feedback.
2. The method in which roll and pitch were mixed prior to actuation of the left and right horizontal tails.
3. The G system had an optional roll limiter that ensured antisymmetrical (left = - right) actuator roll commands. Problems arose when a combined pitch and roll command exceeded one of the stops, which, without the roll limiter, caused unwanted pitch deflections in the horizontal tail. This uncommanded pitch control deflection was very objectionable to the pilots.

The U system was derived from the G system by replacing the pitch and roll servos and first-order horizontal tail actuators with second-order integrated actuators, by eliminating (failing) the pitch augmentation feedbacks, and by combining electrical and mechanical pitch stick inputs. The second order actuator were needed to duplicate the actuator of the LAHOS configurations.

All three systems are shown in Figures C-9 through C-12. For F and G systems (Figures C-9 and C-10), three diagrams for each system are given: (a) pitch system, (b) roll system, (c) pitch roll mixing. The U system (C-11) has only two diagrams: (a) pitch, and (b) roll. The yaw system (C-12) is identical for the F, G and U systems. Double arrows and boxes indicate where two elements are used for separate control of left and right horizontal tails.

The baseline (simulator software) limits for the various system parameters are given in Table C-1. The physical limits of the stick and rudder pedals are given in Table C-2 together with other feel system characteristics (C.2.4.1).

C.2.4.1 Feel System

The stick feel system was electro-hydraulic with adjustable dynamics. The rudder pedals used a mechanical spring. The trim system had a rate trim for pitch and roll, and a proportional trim for yaw. Trim for pitch and roll was controlled by a stick mounted "hat" button. Trim for the rudder was controlled by a knob on the left console. The transfer functions and parameters defining the feel system characteristics are listed in Table C-2. The breakout force (FBO) in pitch was .8 lb for the L configurations, 1.2 lb otherwise. The feel-system or stick natural frequencies in pitch and roll were the same as for the LAHOS configurations (Ref. 8), but the damping was somewhat less (LAHOS had $\zeta = 0.6$).

248
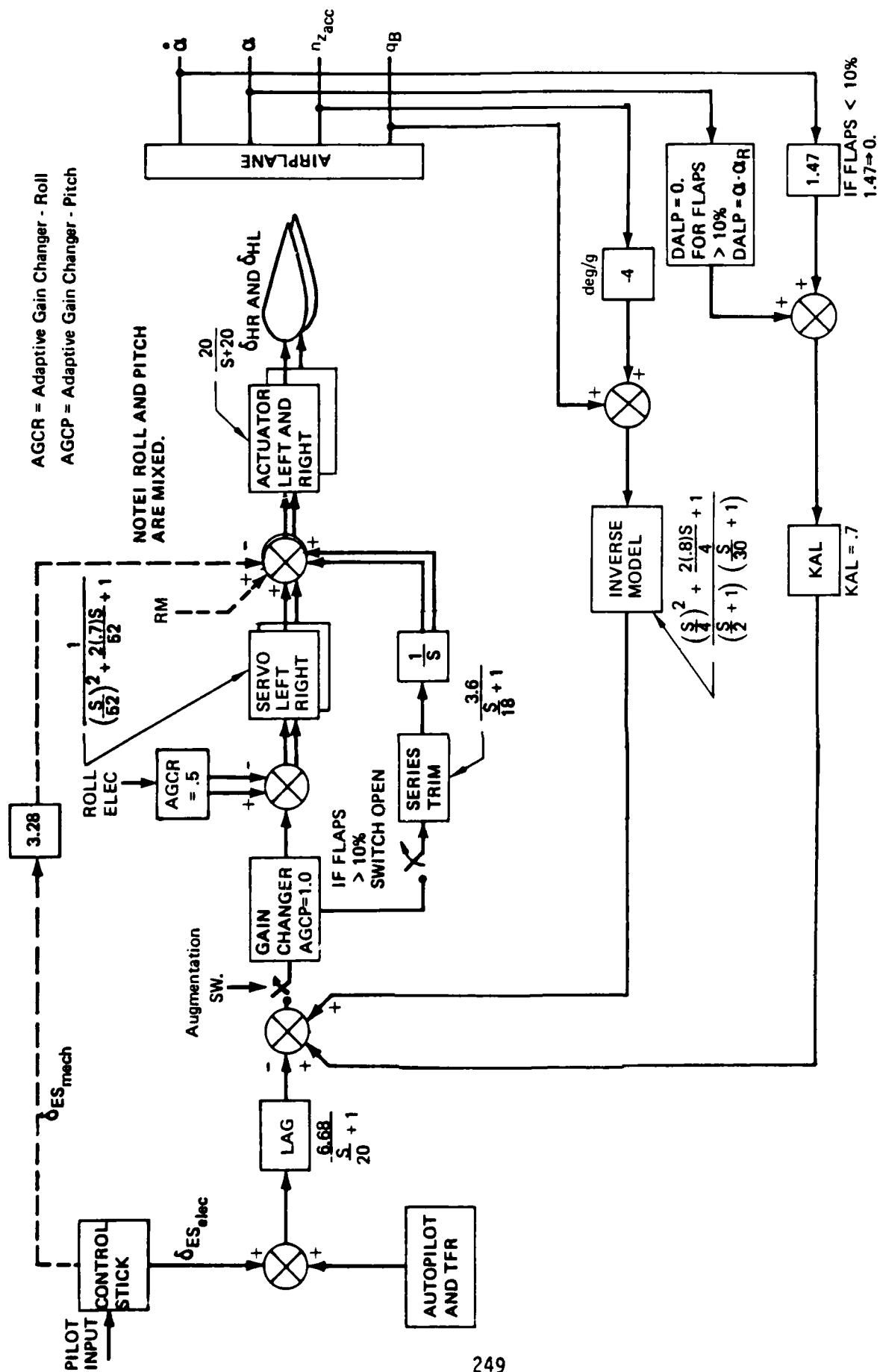
Figure C-9. Flight Control System, Configuration F
(a) Pitch System)

249
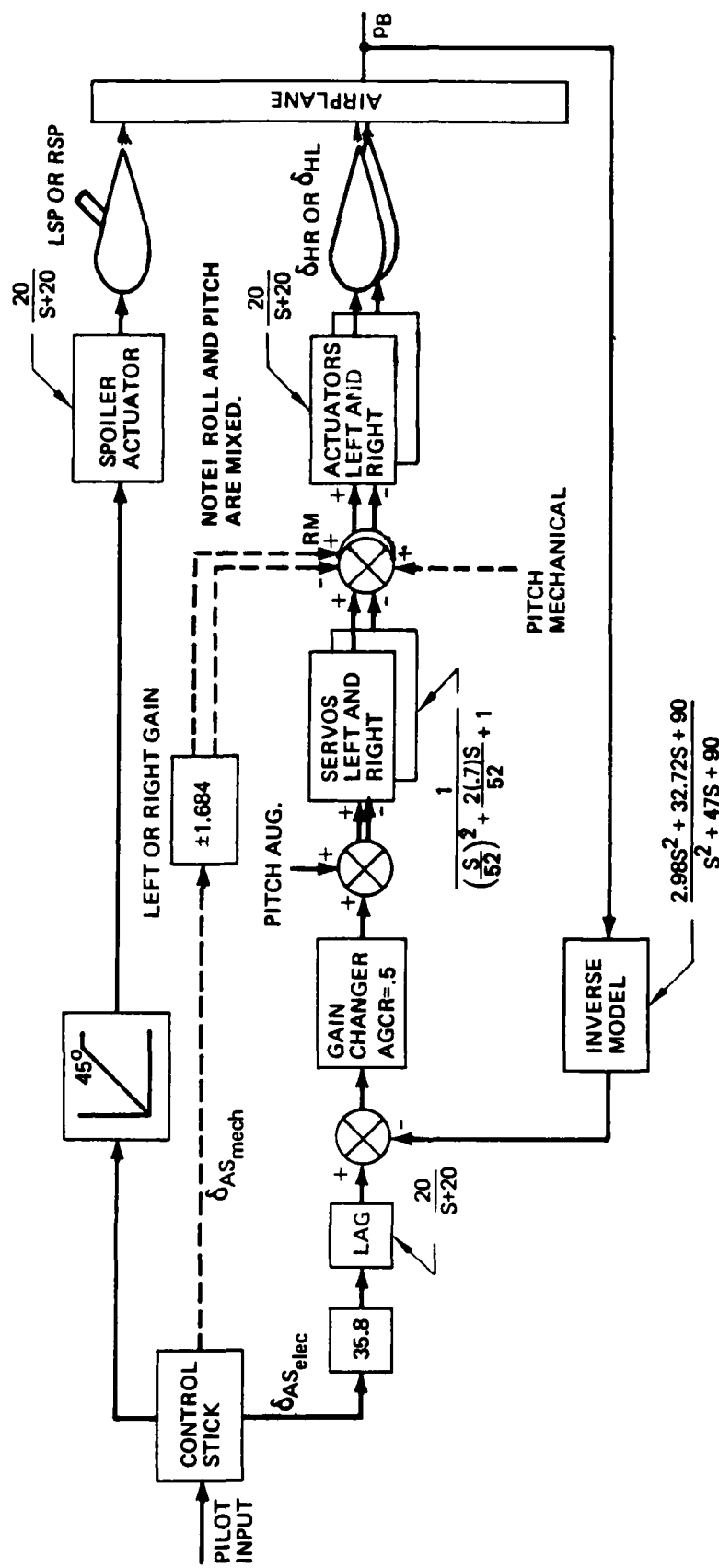
Figure C-9. Flight Control System, Configuration F (Cont'd)
(b) Roll System

250
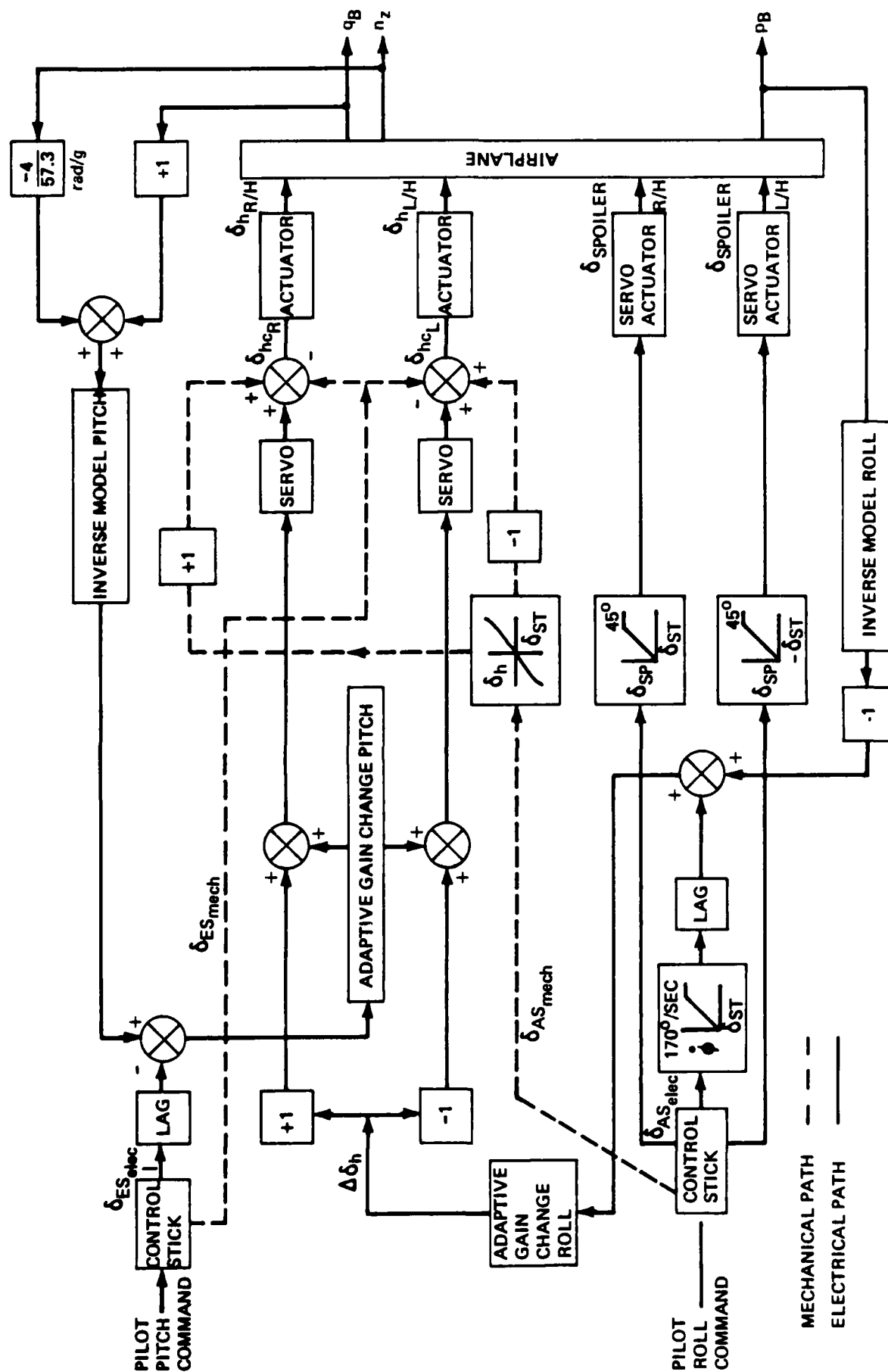
Figure C-9. Flight Control System, Configuration F (Concluded)
(c) Pitch-Roll Mixing (Trim Not Shown)

251
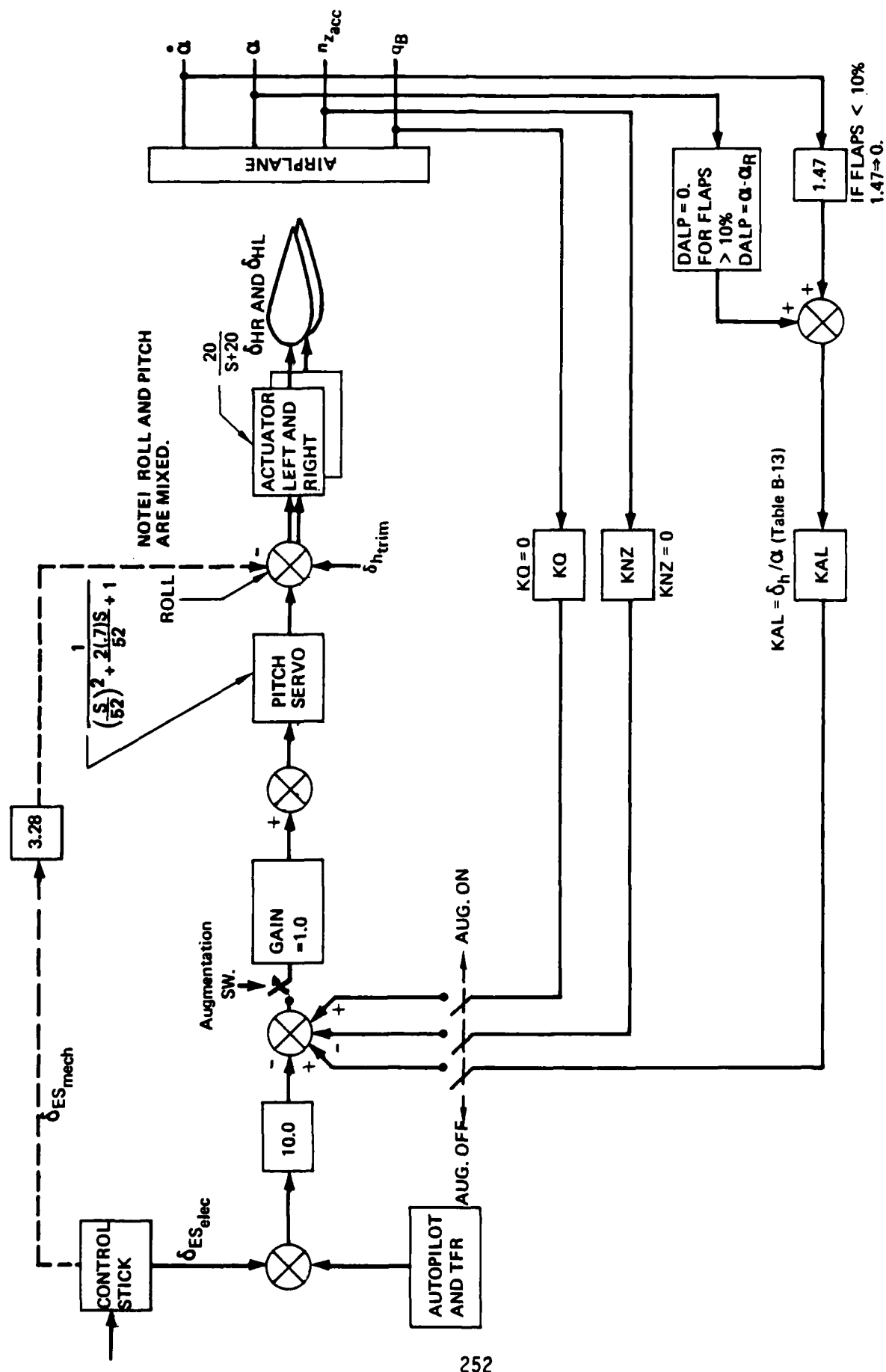
Figure C-10. Flight Control System, Configuration G
(a) Pitch System

252
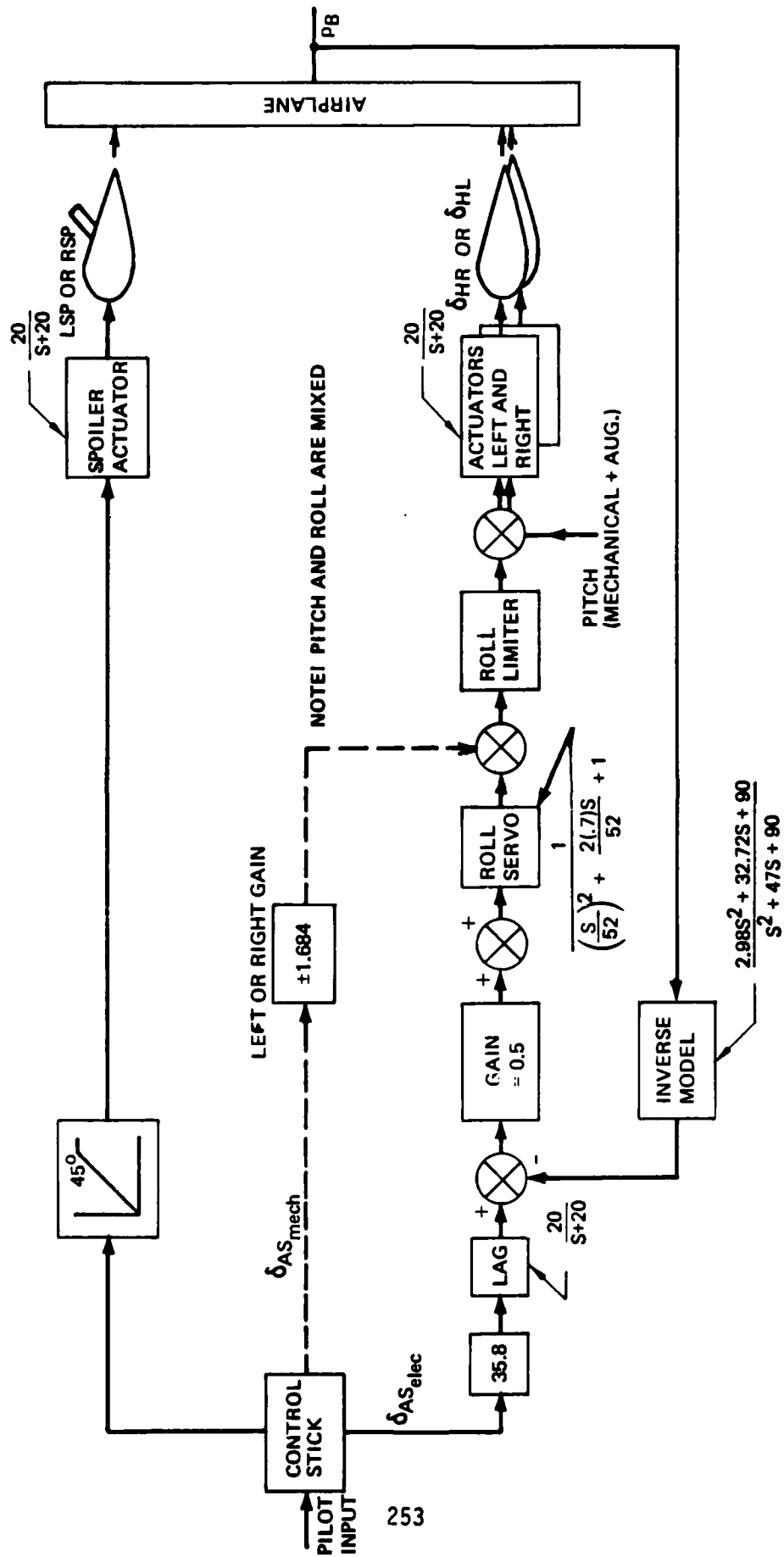
Figure C-10. Flight Control System, Configuration G (Cont'd)
(b) Roll System

253
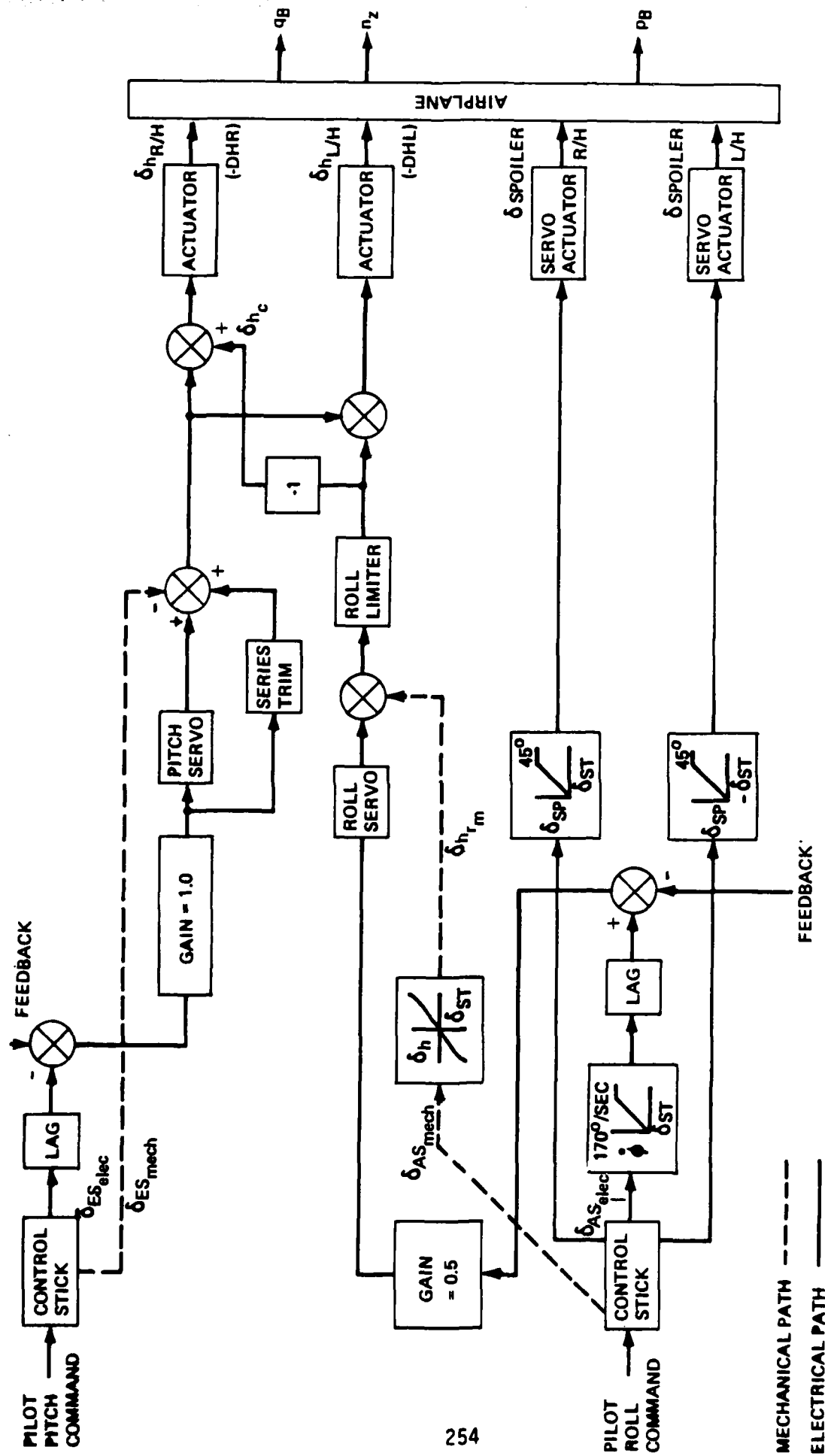
Figure C-10. Flight Control System, Configuration G (Concluded)
(c) Pitch-Roll Mixing (No Details of Feedbacks or Series Trim Shown)

254
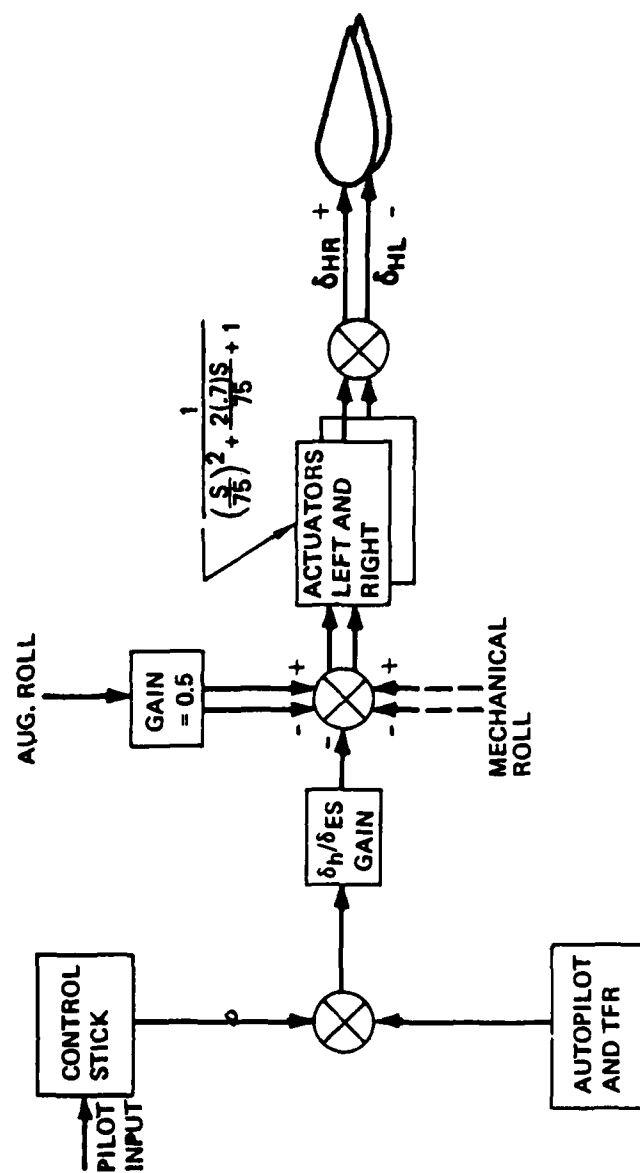
Figure C-11. Flight Control System, Configuration U
(a) Pitch System
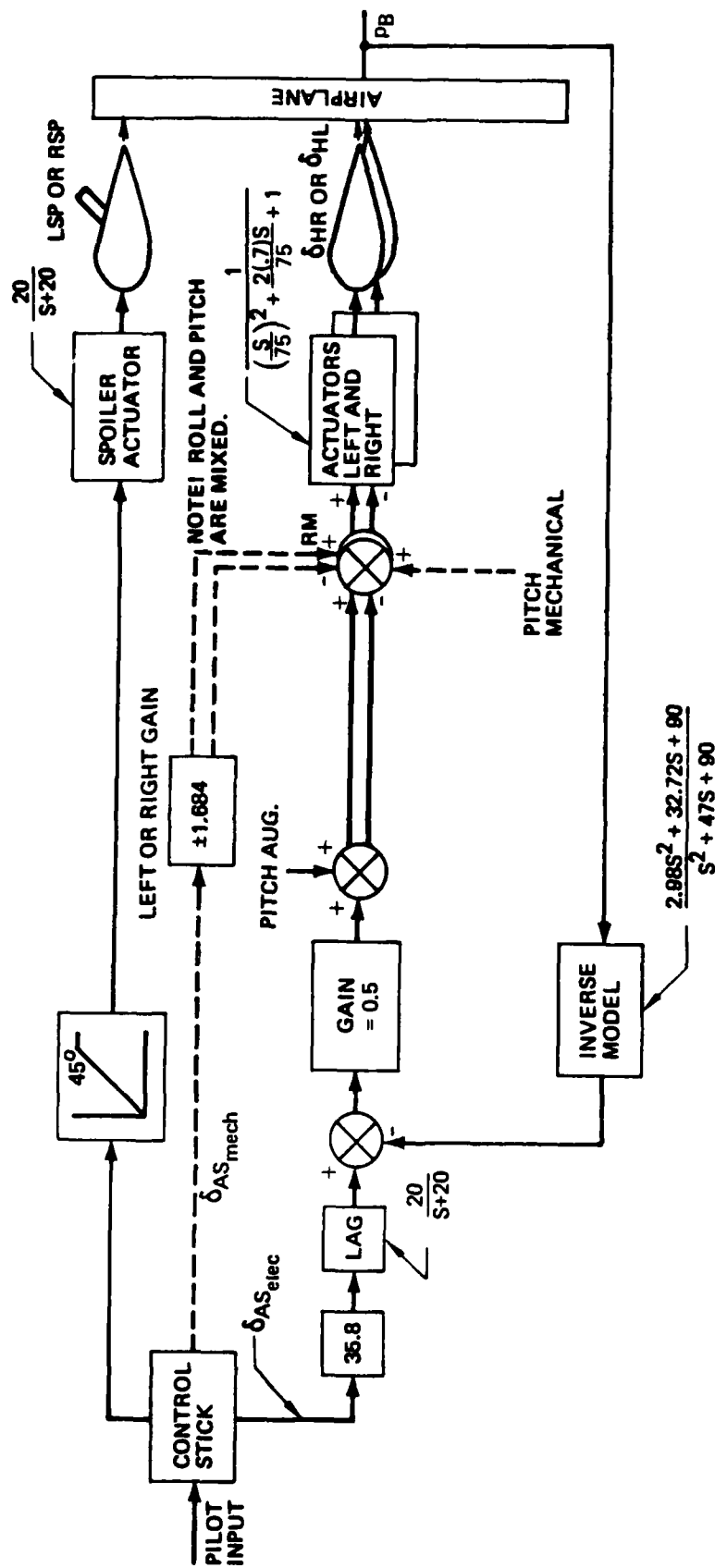
Figure C-11. Flight Control System, Configuration U (Concluded)
(b) Roll System

256

Figure C-12. Yaw Control Systems for Configurations F, G, and U

257

Table C-1. Baseline Actuator Software Limits

Symbol	Max Value	Min Value	Description
δ_h (deg)	+15	-25	Horizontal stabilizer actuator position limits (for both Left and Right)
$\dot{\delta}_h$	50	-50	Horizontal stabilizer actuator rate limits (for both left and right). Does not apply to the U FCS.
$\delta_{ES_{mech}}$	6.7 in	-4.26 in	Mechanical pitch control stick limits (Aft is positive)
$\delta_{ES_{elec}}$	6.6 in	-4 in	Electrical pitch control stick limits (Aft is positive)
$\delta_{AS_{mech}}$	4.75	-4.75	Mechanical roll control stick limits
$\delta_{AS_{elec}}$	4.75	-4.75	Electrical roll control stick limits
δ_{serv}	30 deg	-30 deg	Horizontal stabilizer servo position limits (left and right for the F FCS, pitch and roll for the G FCS, does not apply to the U FCS)
δ_{sp}	45 deg	0 deg	Spoiler position limits
δ_R	30 deg	-30 deg	Rudder position limit ($\pm 11.25^\circ$ for flaps up)

Table C-2. Feel System Characteristics

Parameter	Pitch	Roll	Yaw
K (lb/in)	7.0	4.5	16.0
ω_n (Radions/sec)	26.0	26.0	—
ζ	.3	.36	—
FBO (lb)	1.2 or .8	0.6	6.0
δ physical limits (in)	-5 fwd/7 aft	±7.0	± 3.5

C.2.5 Wind and Turbulence Model

The simulation of concern to this report did not use steady state winds but only continuous turbulence. The wind was omitted to simplify analysis and minimize the number of independent parameters. The turbulence model was found to occasionally produce large low-frequency components, which appeared to the pilots to be large discrete gusts or wind shears. No other discrete gusts were produced. The wind and turbulence model used was essentially that of Barr, Gangsaas, and Schaeffer (Ref. 56), and the assumptions used in the atmospheric model are as follows:

- Turbulence intensities vary with altitude (inhomogeneous) and are only isotropic $(\sigma_u = \sigma_v = \sigma_w)$ for altitudes greater than 1,000 ft.

- Turbulence scale lengths are inhomogeneous and nonisotropic for altitudes less than 1,000 feet but are both homogeneous and isotropic at higher altitudes.

- The atmosphere is neutrally stable.

- The statistical properties of atmospheric turbulence are independent of time.

- The Von Karman power spectra are used.

- The atmosphere and its related parameters (temperature, pressure, density etc.) was defined from Reference 58 (Standard Atmosphere).

C.2.5.1 The Turbulence Model

The turbulence model used is described here and compared to the standards set in MIL-F-8785C (Reference 5). The simulator standard

software manual (Reference 57) describes the model's implementation. A concise description of the model is given by Carlson (Reference 59).

Random turbulence velocities are generated from filtered white noise (unity rms) using a Gaussian noise generator. (It repeats itself approximately every 32,000 iterations). The filters used to produce the velocity components are an approximation to a Von Karman power spectrum and match it for $\omega < 10$ rad/sec. The approximation is given by the following transfer functions for use with a digital noise generator. The turbulence components are with respect to an axis system aligned (x_t axis) with the projection of the airplane's relative velocity vector (airspeed vector) on the earth's surface.

$$F_{u_t}(s) = \sigma_u \sqrt{\frac{2L_u}{\Delta T \ V_{RW}}} \ \frac{(1 + 0.25 \frac{L_u}{V_{RW}} s)}{(1 + 119 \frac{L_u}{V_{RW}} s)(1 + 0.167 \frac{L_u}{V_{RW}} s)}$$

$$F_{v_t}(s) = \sigma_v \sqrt{\frac{L_v}{\Delta T \ V_{RW}}} \ \frac{(1 + 2.618 \frac{L_v}{V_{RW}} s)(1 + 0.1298 \frac{L_v}{V_{RW}} s)}{(1 + 2.083 \frac{L_v}{V_{RW}} s)(1 + 0.823 \frac{L_v}{V_{RW}} s)(1 + 0.898 \frac{L_v}{V_{RW}} s)}$$

$$F_{w_t}(s) = \sigma_w \sqrt{\frac{L_w}{\Delta T \ V_{RW}}} \ \frac{(1 + 2.618 \frac{L_w}{V_{RW}} s)(1 + 0.1298 \frac{L_w}{V_{RW}} s)}{(1 + 2.083 \frac{L_w}{V_{RW}} s)(1 + 0.823 \frac{L_w}{V_{RW}} s)(1 + 0.898 \frac{L_w}{V_{RW}} s)}$$

where

ΔT is the computer frame time, = .04 seconds in simulation

$V_{RW} = \sqrt{u_a^2 + v_a^2 + w_a^2}$, relative airspeed

The magnitude of the horizontal components of turbulence, σ_u, and σ_w, are derived from the vertical components, σ_w, using the following relations.

$$\frac{\sigma_u}{\sigma_w} = \frac{\sigma_v}{\sigma_w} = (0.177 + .000823\, h)^{-0.4} \qquad ; \text{ for } h < 1000 \text{ ft}$$
$$= 1.0 \qquad\qquad\qquad\qquad ; \text{ for } h \geq 1000 \text{ ft}$$

The scale lengths are given by the following relations.

$$L_w = h$$
$$L_u = L_v = \left(\frac{\sigma_u}{\sigma_w}\right)^3 h \qquad\qquad \text{for } h < 1000 \text{ ft}$$
$$L_u = L_w = L_v = 1000 \text{ ft} \qquad ; \quad \text{for } h \geq 1000 \text{ ft}$$

The above relations are the same as those in MIL-F-8785c (Ref 5).

The magnitude of σ_w is given by the following relationship.

$$\sigma_w = \frac{.52\,(V_{20})}{\ln\left(\frac{20 + z}{20}\right)} - \frac{L_w}{1538}$$

where V_{20} is the mean wind speed at 20 ft altitude (in ft/sec) and z is the surface roughness factor. A value of z = 0.15 was used for the simulation and reflects average airport conditions. The above value of σ_w is different from that of MIL-F-8785c (which uses σ_w = 0.1 V_{20}), but for z = 0.15 and h < 150 ft, the two σ_w's are nearly equal. The value of σ_w used decreased about 6% going from 20 ft to 1000 ft altitude.

The wind model also specifies the mean wind as a function of altitude and surface roughness, but this is not pertinent to the simulation results since mean wind was set to zero to minimize the number of parameters and hence simplify the simulation program. Though wind speed was zero, this only affected the final resulting velocity components applied to the airplane, and the turbulence characteristics (intensity, etc.) were computed in terms of a specified wind magnitude (V_{20}) and direction (head-wind along runway, u_t).

261

Table C-3. Turbulence Model Characteristics and Comparison with MIL-F-8785C

SIMULATION		LIGHT	MODERATE	HEAVY
σ_u, σ_v	(ft/sec)	4.8	10.0	13.9
σ_w	(ft/sec)	2.5	5.2	7.2
MIL-F-8785C		LIGHT	MODERATE	SEVERE
σ_w	(ft/sec)	2.5	5.1	7.6
V_{20}	(knots)	15	30	45
Exceedence Probability		10^{-1}	10^{-3}	10^{-3}

Note: $\sigma_u, \sigma_v, \sigma_w$ are at 20 ft altitude.

The simulations were confined to altitudes of near 1100 ft., or less, so there is no need for other than the low-altitude turbulence model. The simulation used principally two intensities of turbulence, "moderate" turbulence corresponding to V_{20} = 30 knots, and "heavy" tubulence corresponding to V_{20} = 40 knots. Occasionally, a default turbulence intensity corresponding to V_{20} = 15 knots, called "light", was present instead of smooth air. The pilots noticed this light turbulence on the airspeed indicator, but otherwise saw no difference from flight in smooth air.

The turbulence intensities for light, moderate, and heavy turbulence as used in the simulation are listed in Table C-3 for an altitude of 20 ft. The values of σ_w for light, moderate, and severe turbulence for the MIL-F-8785c model, listed for comparison in Table C-3, show negligible difference between the two sets at 20 ft altitude. To 1000 feet altitude and above, while the MIL-F-8785c value of σ_w holds constant, the simulator σ_w decreased only about 6%. Clearly, the three turbulence environments used in the simulator investigation can be considered identical to the light, moderate, and severe environments of the MIL-F-8785C low-altitude turbulence model for Category C flight phases.

262

C.2.6 Landing Systems

The landing systems consisted of the model of the airport and runway, the visual TV display system, together with the ILS system and cockpit instruments which displayed the ILS signals to the pilot. Figures C-2 shows the simulator cab and arrangement for the visual scene. Figure C-3 depicts the runway while Figure C-4 shows the view of the runway on approach, from slightly behind the pilot. Figure C-13 shows a close-up of the cockpit instrument together with a line drawing indicating instrument functions. Detailed characteristics follow.

ILS System

Glide slope:

Glide slope	3^0
Beam height	$\pm 0.7^0$
Transmitter located 1000 ft down runway from threshold	
ADI indicator sensitivity	$.35^0$ per dot
ADI maximum deflection	± 2 dots

Localizer:

Beam width	$\pm 2^0$
Transmitter located 10,000 ft down runway from threshold	
HSI indicator sensitivity	1^0 per dot
HSI maximum deflection	± 2 dots
ADI indicator sensitivity	1^0 per dot
ADI maximum deflection	± 1 dot

Visual System

Runway:

Length	7500 ft
Width (between white lines)	150 ft
Width (pavement)	200 ft
Threshold ($S_x = 0$) markers	4 wide bars
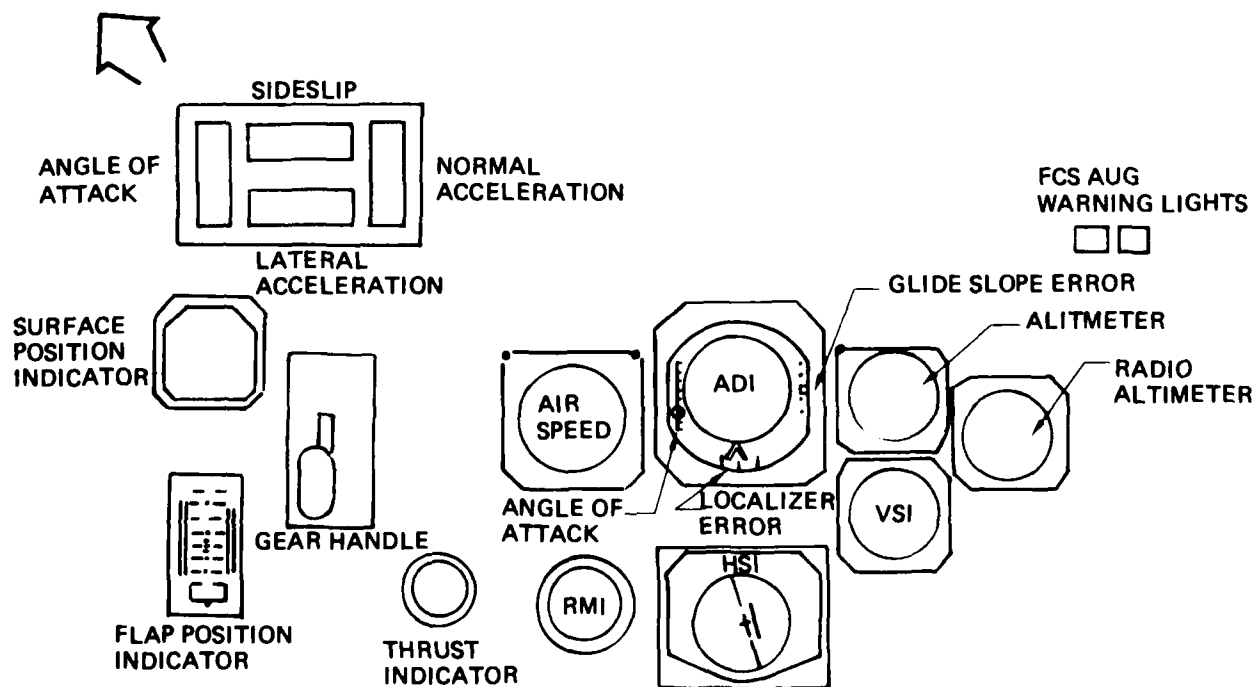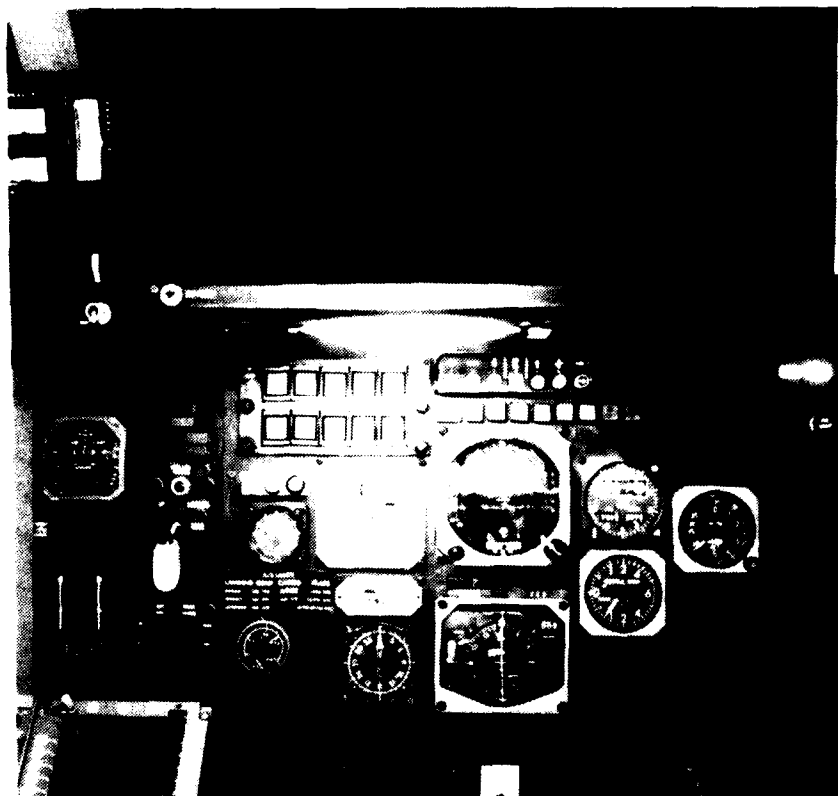
Figure C-13. Cockpit Instrument Panel Layout

500 ft markers	4 bars
1000 ft markers	3 bars
1500 ft markers	2 bars
2000 ft markers	1 bar

Visual scene:

Vertical field of view	45°
Horizontal field of view	60°

Model scale	1 : 150
Pilot location ahead of reference (.45$\bar{c}$)	9 ft

C.2.7 Cockpit Displays and Controls

The cockpit instrument panel and the labeled layout of the instruments is shown in Figure C-13. The primary instruments on the panel were standard instruments with the following particulars and exceptions. The ADI had an indicator for angle of attack as well as glide slope and localizer. Distance to runway threshold (DME) and airspeed had digital readouts under the ADI. The rate of climb indicator (VSI) was "instantaneous" (lag small). The radar altimeter displayed altitude below 1000 feet. The thrust indicator was not in % RPM, but rather, actual thrust was displayed for both normal and augmented (afterburner) operation. The surface position indicators displayed both left and right horizontal tail position, left and right aileron position, left and right spoiler position, and rudder position as well as flap position. A special instrument was mounted above the panel, to the left on top of the glare shield, which displayed angle of attack, normal acceleration, sideslip, and lateral acceleration with indicators on linear scale instruments. Warning lights were provided to indicate failure of the pitch augmentation system (used in simulation) and the total augmentation system (used only for testing and check-out). Stall warning was indicated by a flag on the ADI as well as with an aural warning. Touchdown was indicated by an aural "squeals" simulating tire noise at touchdown.

265

The cockpit controls can be seen, though somewhat indistinctly, in Figure C-4. These consisted of a normal fighter center-stick with "hat" button for pitch and roll trim, rudder pedals with yaw trim on the left console, and a single throttle lever for control of engine thrust. Feel system characteristics are described in Section C.2.4.1 for pitch, roll and yaw. The two throttle levers in the simulator were bolted together to simulate a single-engine airplane, with a friction detent provided to tell the pilot when he was going from normal to afterburner operation. Levers for gear, flaps, and wing sweep were also provided though they were not used in the evaluation program.

The cockpit interior and exterior were darkened completely for evaluation flight operation, so the only light came from lights on the instrument panel (as in night flight) and the visual scene. With no visual scene projected, as in flight above the 200 foot breakout altitude, the screen gave the appearance of flight in dense clouds. The scene, when projected in black and white below 200 ft, gave the appearance of flight under a heavy cloud cover with some obscuration. Thus breakout appeared quite realistic, and when the airplane oscillated through 200 ft, the appearance was not unlike flight through cloud patches.

The measured frequency response characteristics of the visual scene are defined in the following table for ω = 1 and 3 rad/sec. The lag is primarily due to the mechanical carriage and gimbals supporting the TV camera. The frequency responses have flat amplitude and slowly increasing phase lag to the frequency where rate and acceleration limits affect the response. Above that frequency, the phase lag increases sharply and amplitude distorts. So, in the following table, the maximum distortion-free amplitude (zero to peak) is given for each frequency and degree of freedom as well as the phase lag for lower amplitudes.

	Phase Lag		Max Linear Amplitude	
	$\phi_{\omega=1}$ deg	$\phi_{\omega=3}$ deg	$A_{\omega=1}$	$A_{\omega=3}$
Roll	1	3	$\gg 25°$	$> 25°$
Pitch	4	12	$> 10°$	$7°$
Yaw	2	5	$\gg 10°$	$> 10°$
Vertical	4	12	40'	8'
Side	2	7	80'	9'

The amplitudes in the above table are full scale, not model scale. At 1 rad/sec, the amplitude per second is indicative of the rate limits. The side-velocity rate limit (40 ft/sec) is probably the most severe one. These lags were not taken into account in the closed-loop analysis in Appendix B. The $12°$ lag in pitch at 3 rad/sec may have affected flying qualities some in visual flight.

C.3 Conduct of Experiment

Overall, the simulator experiment was conducted in two distinct parts. The first part, done under Air Force contract in the fall of 1979, investigated through formal evaluations the effect of c.g. position and control authority on the baseline F-111A with pitch augmentation both on and off, also the effect of different types of pitch augmentation systems. Preliminary informal evaluations included validation of the F-111A simulation (see B.4.6), evaluations in the air-combat configuration (M $\simeq$ .8, h = 35,000 ft, see B.2) but only on instruments, and terminal area flight including operation of wing sweep, flaps, and landing gear. The final evaluation procedures (pilot rating and comment and excepted, see B.4.3) were developed during these preliminary evaluations with the objective of maximizing the amount of data produced in the formal evaluations, for the given available simulation time, while still retaining credibility of the data. The data for the first part of the simulation program can be identified by the number 79 in the run numbers.

The second part of the simulation program, performed in 1980 under Boeing IR and D funds and benefiting from the experience gained in the first part, produced the most significant data. The investigation was primarily for the effect of independent variations in the pitch attitude transfer function (θ/δ_{ES}), but also included variation of control-surface rate limits in pitch for both the augmented and unaugmented airplane. Also included was validation of the simulation by comparison with flight test results of Reference 8 (see B.4.6). These data can be identified by the number 80 in the run numbers.

C.3.1 Simulation Procedures

The simulation procedures are described in considerable detail in Appendix B in the sections on the evaluation task (B.4.2), pilot ratings and comments (B.4.3), and simulation procedures (B.4.4). Only additional information is provided here.

The preliminary evaluations had as objectives to develop and validate the approach and landing simulation, to indoctrinate the pilots into the purpose of the program and to obtain their help in developing the simulation and procedures to be used, to insure that the pilots fully understood the Cooper-Harper pilot rating scale and its use, and to insure that the evaluation task was adequately defined and clearly understood by both the pilots and the test engineers. Pilots A and R participated fully in these efforts as well as during the course of the evaluations. Pilot T, unable to participate as much, received less indoctrination and evaluated only a portion of the configurations. To some extent this explains the larger variation in pilot ratings of Pilot T as compared to Pilots A and R.

Simulations were conducted with as much realism as the simulator would provide. The room exterior to the simulator was carefully darkened so the pilot could see only the visual scene outside the cockpit, which on instruments in non-visual flight showed a dim murky white similar to flight in dense clouds. In visual flight the scene was realistic of a landing with somewhat obscured vision, and the transient between was quite representative of breakout. The cab and scene were properly lined up so the pilots felt the visual cues were correct and had no distracting

aberrations. The pilots were more than satisfied that, with the masking used to hide the left-hand seat and instruments, the cab represented a single-seat airplane. They also felt that the lack of all-around vision d'd not significantly affect the illusion of a single-seat fighter in the approach and landing task.

Evaluations were conducted with the pilot in the right-hand seat and the test engineer sitting behind him in a jump seat. The dim light at the back of the cab allowed the test engineer to make notes during the course of the evaluations, and to record pilot comments and ratings to provide an instant check on the progress of the experiment.

Besides recording a test configuration at the start and end of each evaluation session, a calibration run was made of each configuration after the first approach and landing while the evaluation pilot was tape recording his comments and pilot ratings. These comments and rating were recorded after each approach and landing, by pilot preference, instead of during the evaluation itself. However, the pilots tended to make comments during the approach and landing which the test engineer jotted down, but conversation was avoided until after the landing was completed and the pilot had recorded his comments and ratings. The pilots were allowed as many repeats of an evaluation run (configuration, turbulence level, and starting point) as they desired, but not many were requested. The use of the "reset" button was limited to computer or simulator malfunctions (if one occurred during an evaluation run, it was scratched) and for re-initializing after landing rollout, waveoff, or occasional "crash".

All evaluations were continuously monitored and recorded using two 8-channel strip chart recorders. With time sharing, this allowed 32 variables to be recorded. The pilots were not informed of what configuration they were evaluating, and repeat configurations were included regularly to test the stability of the pilot ratings. Each evaluation session usually include a range of configurations from good to bad, arranged somewhat randomly, to keep the pilots calibrated.

The pilot rating scale including specialized interpretation for the landing task, the performance standards used by the pilots, the pilot comment card used as a prompt, and the specific pilot ratings requested, are all adequately covered in Appendix B (B.4.3).

269

C.3.2 Pilot Experience and Simulation Validation

The pilot background and experience are adequately treated in Appendix B (B.4.5), as is the method of validating the simulation (B.4.6).

C.4 Configuration Characteristics

This section describes and defines the longitudinal characteristics of the major configurations used in the visual flight simulator experiments. The description is in terms of: state models, aerodynamic coefficients, equations of motion coefficients, transfer-function poles of the state matrix, transfer-functions zeros for the u, w and θ states to a δ_h control input, and open loop frequency responses of θ/F_s.

Each configuration is characterised by its aerodynamics and flight control system. All configurations used the same lateral directional aerodynamics, which are found in Section C.2.2.3.

An overview of the configurations using the linear aerodynamics package (FQAERX, see C.2.2.2) is given in Table C-4 for the configurations without augmentation. The table shows the relationships between configurations by listing the primary experiment parameters (λ_{sp_1}, λ_{sp_2}, Z_{θ_2}, and $M_{\delta_{ES}}$) as well as the controlled secondary parameters (ω_{np}, ζ_p, and Z_{θ_1}). Complete configuration definitions are provided in the next section (C.4.1) and Table C-5.

The rest of Section C.4 is concerned with the tabular characteristics, time-histories, and frequency responses of the various configurations. These tables and figures are all grouped together at the end of this section (tables first, figures next), with explanatory text preceding them. These characteristics are based on a linear system representation of the airplane using equations of motion defined in "stability-body" axes. These axes have the c.g. as origin, and the x-axis is coincident with the projection of the airspeed vector into the plane of symmetry ($x_B - z_B$) in the reference flight conditions (in this case, approach at $\gamma = -3^0$). These axes are body-fixed and are sometimes called "stability axes", a confusing name since it is generally used for axes that align (x_s) with the projection of the airspeed vector in the plane of symmetry at all times and hence rotate in the body. Transformation of characteristics from the simulator body axes to the stability-body axes have been carefully attended to as described in Appendix F.

271

C.4.1 Complete Configuration Definition Table

The purpose of this section is to provide means of completely defining every configuration. Table C-5 gives access to all defining configuration parameters by either explicity listing them or giving the appropriate reference to the location elsewhere in the report where they are defined.

The following explains the column headings in Table C-5.

"Configuration": Name associated with specified parameters.

"Aero Eq": Specifies longitudinal aero program used. See C.2.2.

"Aero Coeff": Name of aero coefficients in Table C-6. See Section C.4.2.

"FCS": Flight control system used. See C.2.4.

"Aug": Flight control system augmentation status for pitch.

"$\delta_{h_{Lim}}$": The baseline value for horizontal stabilizer position limits in deg.

"$\dot{\delta}_{h_{Lim}}$": The baseline value for horizontal stabilizer rate limits in deg/sec.

"δ_h/δ_{ES}": Pitch stick gear ratio in deg/inch.

"FBO": Pitch stick breakout force in lbs. For a complete definition of the feel system, see C.2.4.1.

"$\bar{x}_{cg}$": Distance of c.g. aft of the m.a.c. leading edge in fractions of m.a.c. or $\bar{c}$.

"K_α": Value of angle-of-attack feedback (δ_n/α), varied with c.g. position for AF configurations. See Figures C-9a through C-10a and B.4.1.4.

"C_{m_o}": Reference value of C_m in approach condition varied with c.g. shift for F configurations to maintain reference $\delta_h = 2.1^o$, or reference $\delta_h = 0^o$ for control authority and rate variations (see B.5.8).

"V_{app}": Approach airspeed in knots.

The terms F, L and S are used throughout this report to refer to general groups of configurations, ᵌe B.4 aᵣ B.4.1.

Table C-4. Configuration Overview

Config	$T_2 (T_{1/2})$	λ_{sp_1}	λ_{sp_2}	Z_{θ_2}	ω_p	ζ_p	Z_{θ_1}	$M_{\delta_{ES}}$
S60	6.0	.115	-.30	-.58	.210	.450	-.091	.341
S61			-.60					
S62			-1.00					
S63	↓	↓	-2.00	↓	↓	↓	↓	↓
S41	4.1	.169	-.60	-.58	.208	.435	-.088	.341
S42	4.0	.173	-1.00		.210	.446		
S43	3.9	.178	-2.00		.210	.453		
S44	3.9	.179	-3.00	↓	.210	.456	↓	↓
S45	4.2	.165	-1.01	-.28	.210	.445	-.131	.341
S46	4.4	.156	↓	-1.18	.208	.422	-.071	↓
S21	2.0	.347	-.60	-.58	.210	.450	-.09	.341
S22			-1.00					
S23			-2.00					
S24	↓	↓	-3.00	↓	↓	↓	↓	↓
S25	2.0	.347	-2.00	-.28	.210	.450	-.136	.341
S26				-1.18			-.073	
S27	↓	↓	↓	-1.99	↓	↓	-.067	
L71	7.4	.094	-2.02	-.69	.275	.803	-.076	.434
L72	4.3	.161	-2.18		.286	.621		
L73	2.1	.330	-2.48	↓	.280	.40	-.075	↓
F1	(6.9)	-.100	-.82	-.59	.082	.714	-.079	.086
F6	7.6	.091	-.95		.178	.50		
F4	4.5	.154	-1.04		.190	.40		
F2	2.1	.331	-1.26	↓	.195	.254	↓	↓
S41A	4.1	.169	-.60	-.58	.208	.435	-.088	.085
S42A	4.0	.173	-1.00		.210	.446		
S43A	3.9	.178	-2.00			.453		
S44A		.179	-3.00			.456		
S44B	↓	.179	-3.00	↓	↓	.456	↓	↓

Stable cases	$T_{1/2}$	$\omega_{n_{sp}}$	ζ_{sp}	Z_{θ_2}	ω_p	ζ_p	Z_{θ_1}	$M_{\delta_{ES}}$
F0	1.346	.903	.57	-.6	.169	.06	-.079	.086
L21	.53	2.29	.57	-.76	.20	.15	-.076	.434

273

Table C5. Complete Configuration Definition

CONFIG	AERO EQ	AERO COEFF.	FCS	AUG.	$\delta_{h_{Lim}}$	$\dot{\delta}_{h_{Lim}}$	δ_h/δ_{ES}	FBO	X_{cg}	K_α	C_{m_α}	V_{app}
S21	FQAERX	S21	U	OFF	-30/20	±50	-13.12	±1.2 lb	.45	0.	0.	145 kn
S22		S22										
S23		S23										
S24		S24										
S25		S25										
S26		S26										
S27		S27										
S41		S41										
S41A		S41	G				-3.28					
S42		S42	U				-13.12					
S42A		S42	G				-3.28					
S43		S43	U				-13.12					
S43A		S43	G				-3.28					
S44		S44	U				-13.12					
S44A		S44	G				-3.28					
S44B		S44	U									
S45		S45					-13.12					
S45A		S45					-3.28					
S46		S46					-13.12					
S46A		S46					-3.28					
S60		S60					-13.12					
S61		S61										
S62		S62										
S63		S63										
L21		L21	U		-25/15		-4.2	+.8 lb				120 kn
L71		L71										
L72		L72										
L73		L73										
AF0		F0	G	ON	-25/15	+50.0	-13.28	±1.2 lb	.35	.7	.16	145 kn
AF1		F1							.44	1.05	.0709	
AF2		F2							.505	1.55	-.0336	
AF4		F4							.465	1.25	.0307	
AF6		F6							.453	1.2	.05	
F0		F0		OFF			-3.28		.35	.0	.16	
F1		F1							.44		.0709	
F2		F2							.505		-.0336	
F4		F4							.465		.0307	
F6		F6							.453		.05	
		SEE FIG.										
AF111-F	FQAERO	C6-C8	F	ON	-25/15	+50.0	-9.96	±1.2 lb	.35	.7	See Fig. C8	145 kn
F111-F			F	OFF								
AF111-G			G	ON								

C.4.2 Tabulated Characteristics

A description of the equational forms used to define the various types of coefficients given in this Appendix is found in Appendix F.

The aerodynamic coefficients in Table C6 are described in Sections F.2.1 and F.2.2, as are the equation of motion Coefficients in Table C7. Both types of Coefficients are in stability body axes (i.e., body axes aligned with stability axes in the reference conditions).

To help describe the matrix format of these tables, the following is given: CD-REF $= C_{D_1}$, CD-ALPHA $= C_{D_\alpha}$, CD-ALPHAD $= C_{D_{\dot\alpha}}$, CD-Q $= C_{D_q}$, CD-U $= C_{D_u}$, CD-THETA $= C_{D_\theta}$ and CD-DELTA $= C_{D_\delta}$; also X-u $= X_u$, X-w $= X_w$, X-WD $= X_{\dot w}$, X-Q $= X_q$, X-THETA $= X_\theta$, X-DE $= X_{\delta_e}$ and X-DT $= X_{\delta_t}$. In addition, ALPHAO $= \alpha_0$, XR $= \bar{X}_{cg}$ and RO $= \rho$.

The state models in Table C8 correspond to the A_s and B_s matrices described in Section F.1.2, Equation F7. These were derived from the aerodynamic coefficients, see Section C.4.4. They are in stability-body axes. The numerator polynomial for the zeros is in normalized form with unity as the coefficient of the highest power of "s". The numerator gain is given separately.

The ordering of the configurations for Table C8 is F1 through F6, L21, L71 through L73, S21 through S27, S41 through S46, and S60 through S63.

Note that for the S configurations $C_{m_{\delta_e}}$ in the aero coefficient table (C-6) and M_{δ_e} in the equation of motion table (C-7) vary slightly. This is due to the effect of $M_{\dot w}$ on $C_{m_{\delta_e}}$ in the original calculation of the aero coefficients from state models. See Appendix C.4.4 for a further description of the derivation of configurations.

It should be noted that for all configurations using FQAERX (see Table C-5), $C_{L_{\delta_e}}$ and Z_{δ_e} are zero. This occurred because in the simulator program $C_{L_{\delta_h}}$ was inadvertently set to zero. In effect, the center of rotation was at the reference moment center ($.45\bar{c}$) rather than ahead of it. It is not felt that this caused a significant difference in results of the simulation (see comments near end of B.4.1.1).

For ready reference, the state equation and states for the state models of Table C-8 are repeated from Appendix F.

$$[\dot{x}] = [A][x] + [B][u]$$

$$[x] = [u \ w \ q \ \theta]^T$$

$$[u] = [\delta_e]$$

Note that δ_e (for elevator) in the linearized equations has the same significance as δ_h (for horizontal tail) in the simulator equations.

C.4.3 Time Histories and Frequency Responses

The time histories and frequency responses are grouped together in sets of configurations with like parameter variations. The configuration ordering can be found from the list of figures since the configuration identifies are included in the title.

Each time history figure includes responses, α, q, θ, n_z, u, and δ_e to a step input in δ_{ec}, where δ_{ec} is the command to the elevator (horizontal tail) actuator and δ_e is the elevator output. The time histories used the state models of Table C-8, corresponding to Equation F7 given in Section F.1.2 (not including gust inputs).

The time histories are for the unaugmented airframe with an actuator for δ_e which has no rate or position limits. Two types of actuators are used. For the S and L configurations, the actuator has second-order dynamics described by the transfer function in the Laplace domain $(\frac{s^2}{\omega_n^2} + \frac{2\zeta s}{\omega_n} + 1)^{-1}$ where $\omega_n = 75$ and $\zeta = 0.7$. For the F configurations, the actuator has first-order dynamics, $20 (s + 20)^{-1}$.

The step size (at $t = 0.1$ sec) was gauged to keep $q_{0.1+}$ (q just after the step) the same for all configurations. Since M_{δ_E} of the F and S configurations (see state models in Table C-8) are approximately the same and both are 1/4 the size of M_{δ_E} for the L configurations, the step size is -2.0^O for the F and S configurations whereas it is $-.5^O$ for the L configurations. All steps are input to the actuator.

The integration technique was fourth-order Runge Kutta, with an integration frame time of .01 seconds.

The frequency responses are in the form of open-loop θ/F_s Bode plots, and include the dynamics for the actuators used in computing the time histories described above. Also feel system dynamics are included. The feel system transfer function is given by $(\frac{s^2}{\omega_n^2} + \frac{2\zeta s}{\omega_n} + 1)^{-1}$ where $\omega_n = 26.$ and $\zeta = .6$.

The Bode plots shown do not incorporate the δ_h/δ_{ES} gain. Also the stick force gradient used was 8 lb/in. In the ground simulator a stick force gradient of 7 lb/in was used. Therefore, the notation "θ'/F_s" is used to describe the Bode plots. Then "θ/F_s" corresponding to the simulator configurations is computed from $\theta/F_s = (8/7)(\delta_h/\delta_{ES})(\theta'/F_s)$ as noted above each Bode.

C.4.4 Notes on Derivation of Characteristics

The state models given in Table C8 come from the aero coefficients in Table C6 which were used in the longitudinal equations in the simulator (see Appendix C.2.2.2, "FQAERX", which describes the equations). The equations for obtaining state models in stability-body axes from the aero coefficients can be found in Appendix F, Sections F.1.1 through F.2.2. The following describes how the aero coefficients were derived.

The aero coefficients for the F configurations come from Table B1, Appendix B, after a c.g. transformation. The c.g. transformation is described in the last part of Appendix F.2.2.

The aero coefficients for both L and S configurations came from state models. The L configurations came from the state models for Configurations 2-1, 7-1, 7-2 and 7-3, given in body axis, found in Reference 8 (the "LAHOS Report"). The coefficients for the S configurations were derived from the state model for the F111-A with $\bar{x}_{cg} = .465$ by using pole placement. The pole placing technique only changed the M derivatives of the A matrix.

Note: Pole placement was done using total state feedback to δ_e. X_{δ_e} and Z_{δ_e} were set to zero so that only the M derivatives changed.

277

For the L and S configurations, the transformation from the state models described above to the aero coefficients for the simulator required a two step process: (1) transformation from state model coefficients to equations of motion coefficients, (2) calculation of aero coefficients from equation of motion coefficients. Also, since the L configuration state models were given in body axes (Ref. 8), these first had to be transformed to stability-body axes. For the latter process, the equation in Section F.1.2 were used to obtain $[A_s]$ and $[B_s]$ from $[A]$ and $[B]$.

To go from state models to equations of motion, the reverse of the process described in Section F.1.1 was used (with $\dot{w}_0 = 0$). Since the reverse equations are indeterminate in M_w and M_q, the following relations and assumption were used.

$$M_{\dot{w}} = \frac{1}{U_0} \left(\frac{K_4}{1 + K_4}\right) (M_q + U_0 M_{\dot{w}})$$

where in the $[A]$ matrix

$$U_0 = A_{23}$$
$$M_q + U_0 M_{\dot{w}} = A_{33}$$

and

$$K_4 = \frac{M_{\dot{\alpha}}}{M_q} = \frac{C_{m_{\dot{\alpha}}}}{C_{m_q}} = 0.3$$

The ratio of $C_{m_{\dot{\alpha}}}$ to C_{m_q} (approximately $d\epsilon/d\alpha$) for the F-111A in landing approach, $K_4 = 0.3$, was assumed applicable to all configurations for this calculation.

To go from equations of motion to aero coefficients, the equations in Section F.2.2 were used. To remove the indeterminacy here, the following additional assumption were made:

$$C_{m_1} = 0, \ C_{D_u} = 0, \ C_{L_u} = 0, \ z_T = 0, \ \text{and} \ T_V = 0$$

278

TABLE C6   AERODYNAMIC COEFFICIENTS FOR F, S AND L CONFIGURATIONS

AERO COEFF DATA

VO(FT.)	ALPHAO	ALPHAO(DEG)	XR	IT	GAMMA	GAMMA(DEG)
206.52	0.00000	0.0000	0.45000	0.00000	-.42894E-1	-2.4576
AREA		CHORD	MASS	IY	RO	
525.00		9.0170	1864.9	0.33500E+06	0.23780E-02	

CONFIG.	REF.	ALPHA	ALPHAD	Q	U	THETA	DELTA
	CD 0.50738	2.2207	0.00000	0.00000	0.00000	0.00000	+.16800
	CL 2.2860	10.644	0.00000	0.00000	0.00000	0.00000	0.00000
L21	CM 0.00000	-6.6152	-27.195	-69.982	0.00000	0.00000	-8.2630
	CD 0.49283	2.0408	0.00000	0.00000	0.00000	0.00000	0.16800
	CL 2.2860	8.6605	0.00000	0.00000	0.00000	0.00000	0.00000
L71	CM 0.00000	0.40402	-23.777	-78.673	0.00000	0.00000	-8.2630
L72	CM 0.00000	0.81024	-23.777	-78.673	0.00000	0.00000	-8.2630
L73	CM 0.00000	1.80290	-23.777	-78.673	0.00000	0.00000	-8.2630

VO(FT.)	ALPHAO	ALPHAO(DEG)	XR	IT	GAMMA	GAMMA(DEG)
244.72	0.00000	0.00000	0.45000	0.00000	0.00000	0.00000
AREA		CHORD	MASS	IY	RO	
525.00		9.0170	1864.9	0.33500E+06	0.23780E-02	

	REF.	ALPHA	ALPHAD	Q	U	THETA	DELTA
	CD 0.34100	0.77740	0.00000	0.00000	-.61180E-01	0.00000	0.00000
	CL 1.5900	7.3100	2.5000	5.7500	0.61180E-01	0.00000	0.00000
F0	CM 0.10000E-02	-.61600	-4.8200	-15.572	0.68520E-02	0.00000	-1.4960
F1	CM 0.55000E-01	0.41900E-01	-4.5950	-15.057	0.12358E-01	0.00000	-1.4960
F6	CM 0.54770E-01	0.13083	-4.5625	-14.983	0.13154E-01	0.00000	-1.4960
F4	CM 0.54550E-01	0.22465	-4.5325	-14.914	0.13888E-01	0.00000	-1.4960
F2	CM 0.53850E-01	0.51705	-4.4325	-14.685	0.16335E-01	0.00000	-1.4960

279

TABLE C6 AERODYNAMIC COEFFICIENTS FOR F, S AND L CONFIGURATIONS

(CONCLUDED)

AERO COEFF DATA

VO(FT.)	ALPHAO	ALPHAO(DEG)	XR	IT	GAMMA	GAMMA(DEG)
241.75	0.00000	0.00000	0.45000	0.00000	0.00000	0.00000
AREA	CHORD	MASS	IY	RO		
525.00	9.0170	1864.9	0.35500E+06	0.23780E-02		

CONFIG.	REF.	ALPHA	ALPHAD	Q	U	THETA	DELTA
	CD 0.35837	0.77851	0.00000	0.00000	0.00000	0.00000	0.00000
	CL 1.6065	7.2616	0.00000	0.00000	0.00000	0.00000	0.00000
S21	CM 0.00000	0.32750E-01	2.9242	9.7474	-.45670E-01	0.13642E-01	-1.5120
S22	CM 0.00000	0.28853	-2.1162	-7.0541	-.21574E-01	0.38820E-01	-1.5187
S23	CM 0.00000	0.92799	-14.717	-49.060	0.38664E-01	0.10178	-1.5354
S24	CM 0.00000	1.5674	-27.319	-91.062	0.98902E-01	0.16474	-1.5520
S60	CM 0.00000	-.13225	3.7925	12.842	-.44492E-01	-.21924E-01	-1.5109
S61	CM 0.00000	-.34796E-02	0.12138E-01	0.40460E-01	-.23949E-01	-.17530E-01	-1.5159
S62	CM 0.00000	0.18445	-5.0283	-16.761	-.34428E-02	-.11660E-01	-1.5225
S63	CM 0.00000	0.63686	-17.630	-58.765	0.71921E-01	0.29990E-02	-1.5393
	CD 0.34100	0.77851	0.00000	0.00000	0.00000	0.00000	0.00000
	CL 1.6065	7.3666	0.00000	0.00000	0.00000	0.00000	0.00000
S41	CM 0.00000	0.10726E-01	0.75630	2.5211	-.28615E-01	-.11281E-01	-1.5149
S42	CM 0.00000	0.20944	-4.2842	-14.281	-.29311E-02	-.24100E-03	-1.5216
S43	CM 0.00000	0.70622	-16.885	-56.285	0.61278E-01	0.29050E-01	-1.5383
S44	CM 0.00000	1.2030	-29.483	-98.276	0.12550	0.57850E-01	-1.5550
S45	CD 0.34100	0.77851	0.00000	0.00000	0.00000	0.00000	0.00000
	CL 1.6065	4.1954	0.00000	0.00000	0.00000	0.00000	0.00000
	CM 0.00000	0.19658	-7.7497	-25.832	-.24441E-02	0.12588E-01	-1.5262
S46	CD 0.34100	0.77851	0.00000	0.00000	0.00000	0.00000	0.00000
	CL 1.6065	14.576	0.00000	0.00000	0.00000	0.00000	0.00000
	CM 0.00000	-.15638	2.8353	9.4509	-.43568E-01	-.18018E-01	-1.5121
S25	CD 0.35837	0.77851	0.00000	0.00000	0.00000	0.00000	0.00000
	CL 1.6065	4.0903	0.00000	0.00000	0.00000	0.00000	0.00000
	CM 0.00000	0.69365	-17.951	-59.837	-.54402E-02	0.17371	-1.5397
S26	CD 0.35837	0.77851	0.00000	0.00000	0.00000	0.00000	0.00000
	CL 1.6065	14.471	0.00000	0.00000	0.00000	0.00000	0.00000
	CM 0.00000	0.97558	-7.3662	-24.554	0.18840E-01	0.39543E-01	-1.5256
S27	CD 0.35837	0.77851	0.00000	0.00000	0.00000	0.00000	0.00000
	CL 1.6065	24.357	0.00000	0.00000	0.00000	0.00000	0.00000
	CM 0.00000	0.11751	2.7147	9.0490	-.48284E-01	0.10596E-01	-1.5123

TABLE C7 EQUATION OF MOTION COEFFICIENTS FOR F,L, AND S CONFIGURATIONS.

VO(FT.) 206.52	ALPHAO 0.00000	ALPHAO(DEG) 0.00000	XR 0.45000	IT 0.00000	GAMMA -.42894E-01	GAMMA(DEG) -2.4576
AREA 525.00	CHORD 9.0170	MASS 1864.9	IY 0.33500E+06	RO 0.23780E-02		

CONFIG.		U	W	WD	Q	THETA	DE	DT
L21	X	-.70147E-01	0.45140E-02	0.00000	0.00000	0.00000	-2.3984	0.00000
	Z	-.31605	-.77086	0.00000	0.00000	0.00000	0.00000	0.00000
	M	0.00000	-.20178E-01	-.20601E-02	-1.4077	0.00000	-5.9213	0.00000
	X	-.68136E-01	0.16950E-01	0.00000	0.00000	0.00000	-2.3984	0.00000
	Z	-.31605	-.70187	0.00000	0.00000	0.00000	0.00000	0.00000
L71	M	0.00000	0.14019E-02	-.18011E-02	-1.2308	0.00000	-5.9213	0.00000
L72	M	0.00000	0.28115E-02	-.18011E-02	-1.2308	0.00000	-5.9213	0.00000
L73	M	0.00000	0.62559E-02	-.18011E-02	-1.2308	0.00000	-5.9213	0.00000

VO(FT.) 244.72	ALPHAO 0.00000	ALPHAO(DEG) 0.00000	XR 0.45000	IT 0.00000	GAMMA 0.00000	GAMMA(DEG) 0.00000
AREA 525.00	CHORD 9.0170	MASS 1864.9	IY 0.33500E+06	RO 0.23780E-02		

		U	W	WD	Q	THETA	DE	DT
F0	X	-.45842E-01	0.66563E-01	0.00000	0.00000	0.00000	0.00000	0.00000
	Z	-.27051	-.62672	-.37727E-02	-2.1124	0.00000	0.00000	0.00000
F0	M	0.56343E-04	-.25328E-02	-.36512E-03	-.28867	0.00000	-1.5053	0.00000
F1	M	0.10163E-03	0.17228E-03	-.34608E-03	-.27913	0.00000	-1.5053	0.00000
I3	M	0.10817E-03	0.56302E-03	-.34502E-03	-.27775	0.00000	-1.5053	0.00000
F4	M	0.11421E-03	0.92371E-03	-.34334E-03	-.27648	0.00000	-1.5053	0.00000
F2	M	0.13433E-03	0.21260E-02	-.33577E-03	-.27224	0.00000	-1.5053	0.00000

TABLE C7   EQUATIONS OF MOTION COEFFICIENTS FOR F,L, AND S CONFIGURATIONS - CONCLUDED.

VO(FT.)	ALPHAO	ALPHAO(DEG)	XR	IT	GAMMA	GAMMA(DEG)
241.75	0.00000	0.0000	0.45000	0.00000	0.00000	0.00000
AREA	CHORD	MASS	IY	RO		
525.00	9.0170	1864.9	0.33500E+06	0.23780E-02		

EOM DATA

		U	W	WD	Q	THETA	DE	DT
	X	-.57998E-01	0.67000E-01	0.00000	0.00000	0.00000	0.00000	0.00000
	Z	-.25999	-.61660	0.00000	0.00000	0.00000	0.00000	0.00000
S21	M	-.37101E-03	0.13303E-03	0.22151E-03	0.17850	0.13396E-01	-1.4847	0.00000
S22	M	-.17526E-03	0.11720E-02	-.16031E-03	-.12918	0.38119E-01	-1.4913	0.00000
S23	M	0.31410E-03	0.37694E-02	-.11148E-02	-.89843	0.99943E-01	-1.5077	0.00000
S24	M	0.80345E-03	0.63666E-02	-.20695E-02	-1.6676	0.16177	-1.5240	0.00000
S60	M	-.36144E-03	-.53718E-03	0.28729E-03	0.23151	-.21528E-01	-1.4836	0.00000
S61	M	-.19455E-03	0.14134E-04	0.91947E-06	0.74094E-03	-.17214E-01	-1.4885	0.00000
S62	M	0.27968E-04	0.74921E-03	-.38090E-03	-.30694	-.11450E-01	-1.4950	0.00000
S63	M	0.58427E-03	0.25868E-02	-.13355E-02	-1.0762	0.29449E-02	-1.5115	0.00000
	X	-.55187E-01	0.67000E-01	0.00000	0.00000	0.00000	0.00000	0.00000
	Z	-.25999	-.62369	0.00000	0.00000	0.00000	0.00000	0.00000
S41	M	-.23246E-03	0.43568E-04	0.57291E-04	0.46169E-01	-.11077E-01	-1.4876	0.00000
S42	M	-.23811E-03	0.85072E-03	-.32453E-03	-.26153	0.23665E-03	-1.4941	0.00000
S43	M	0.49781E-03	0.28686E-02	-.12791E-02	-1.0307	0.28526E-01	-1.5105	0.00000
S44	M	0.10195E-02	0.48864E-02	-.22334E-02	-1.7997	0.56806E-01	-1.5269	0.00000
	X	-.55187E-01	0.67000E-01	0.00000	0.00000	0.00000	0.00000	0.00000
	Z	-.25999	-.36708	0.00000	0.00000	0.00000	0.00000	0.00000
S45	M	-.19855E-04	0.79848E-03	-.58705E-03	-.47306	0.12361E-01	-1.4987	0.00000
	X	-.55187E-01	0.67000E-01	0.00000	0.00000	0.00000	0.00000	0.00000
	Z	-.25999	-1.2071	0.00000	0.00000	0.00000	0.00000	0.00000
S46	M	-.35393E-03	-.63519E-03	0.21478E-03	0.17307	-.17693E-01	-1.4848	0.00000
	X	-.57998E-01	0.67000E-01	0.00000	0.00000	0.00000	0.00000	0.00000
	Z	-.25999	-.35998	0.00000	0.00000	0.00000	0.00000	0.00000
S25	M	-.44195E-04	0.28175E-02	-.13598E-02	-1.0958	0.17058	-1.5119	0.00000
	X	-.57998E-01	0.67000E-01	0.00000	0.00000	0.00000	0.00000	0.00000
	Z	-.25999	-1.2000	0.00000	0.00000	0.00000	0.00000	0.00000
S26	M	0.15305E-03	0.39627E-02	-.55800E-03	-.44965	0.38829E-01	-1.4981	0.00000
	X	-.57998E-01	0.67000E-01	0.00000	0.00000	0.00000	0.00000	0.00000
	Z	-.25999	-2.0000	0.00000	0.00000	0.00000	0.00000	0.00000
S27	M	-.39225E-03	0.47731E-03	0.20564E-03	0.16571	0.10405E-01	-1.4850	0.00000

TABLE C 8 STATE MODELS, POLES AND ZEROS - ALL CONFIGURATIONS

STATE MODEL F0

A =

-0.458420E-01	0.665630E-01	0.000000E+00	-0.321700E+02
-0.270510E+00	-0.626720E+00	0.244720E+03	0.000000E+00
0.155120E-03	-0.230400E-02	-0.378020E+00	0.000000E+00
0.000000E+00	0.000000E+00	0.100000E+01	0.000000E+00

B =

0.000000E+00
0.000000E+00
-0.150530E+01
0.000000E+00

POLES

REAL	IMAG	TAU	OMEGA	ZETA	T1/2,2
-0.51505000	0.74163000	--------	0.90293497	0.57041760	1.3457862
-0.51505000	-0.74163000	--------	0.90293497	0.57041760	1.3457862
-0.01023800	0.16830000	--------	0.16861111	0.06071960	67.703378
-0.01023800	-0.16830000	--------	0.16861111	0.06071960	67.703378

CHARACTERISTIC POLYNOMIAL:
1.00   1.05060   0.98983G   0.459780E-01   0.231780E-01

ZEROS OF u/δ_h

REAL	IMAG	TAU	OMEGA	ZETA	T1/2,2
-1.27000000	0.00000000	0.78740157	--------	--------	0.54578510

NUMERATOR POLNOMIAL: GAIN = 23.90000000
1.00   1.27000

ZEROS OF w/δ_h

REAL	IMAG	TAU	OMEGA	ZETA	T1/2,2
-0.02291300	0.18714000	--------	0.18853749	0.12153021	30.251263
-0.02291300	-0.18714000	--------	0.18853749	0.12153021	30.251263

NUMERATOR POLNOMIAL: GAIN = -368.502100
1.00   0.458260E-01   0.355480E-01

ZEROS OF θ/δ_h

REAL	IMAG	TAU	OMEGA	ZETA	T1/2,2
-0.59400000	0.00000000	1.68350168	--------	--------	1.1669144
-0.07870000	0.00000000	12.70648030	--------	--------	8.8074610

NUMERATOR POLNOMIAL: GAIN = -1.51000000
1.00   0.668670   0.466230E-01

DATE: (7/31/80) = 213   TIME: 16:1

TABLE C 8 STATE MODELS, POLES AND ZEROS - ALL CONFIGURATIONS (CONTINUED)

STATE MODEL F1

A =

-0.458420E-01	0.665630E-01	0.000000E+00	-0.321700E+02
-0.270510E+00	-0.626720E+00	0.244720E+03	0.000000E+00
0.195790E-03	0.390430E-03	-0.364310E+00	0.000000E+00
0.000000E+00	0.000000E+00	0.100000E+01	0.000000E+00

B =

0.000000E+00
0.000000E+00
-0.150530E+01
0.000000E+00

POLES

REAL	IMAG	TAU	OMEGA	ZETA	T1/2,2
-0.82003000	0.00000000	1.21946758	--------	--------	0.84527052
-0.05849300	0.05738500	--------	0.08194187	0.71383535	11.850088
-0.05849300	-0.05738500	--------	0.08194187	0.71383535	11.850088
-0.09985200	-0.00000000	10.01482194	--------	--------	6.9417456

CHARACTERISTIC POLYNOMIAL:
1.00   1.03690   0.196210   0.157560E-01   0.549800E-03

ZEROS OF u/δ_h

REAL	IMAG	TAU	OMEGA	ZETA	T1/2,2
-1.26960000	0.00000000	0.78764965	--------	--------	0.54595714

NUMERATOR POLNOMIAL: GAIN = 23.9052400
1.00   1.26960

ZEROS OF w/δ_h

REAL	IMAG	TAU	OMEGA	ZETA	T1/2,2
-0.02292100	0.18718000	--------	0.18857817	0.12154641	30.240704
-0.02292100	-0.18718000	--------	0.18857817	0.12154641	30.240704

NUMERATOR POLNOMIAL: GAIN = -368.377000
1.00   0.458420E-01   0.355600E-01

ZEROS OF θ/δ_h

REAL	IMAG	TAU	OMEGA	ZETA	T1/2,2
-0.59386000	0.00000000	1.68389856	--------	--------	1.1671895
-0.07869800	0.00000000	12.70680322	--------	--------	8.8076649

NUMERATOR POLNOMIAL: GAIN = -1.50530100
1.00   0.672560   0.467360E-01

284

TABLE C 8   STATE MODELS, POLES AND ZEROS - ALL CONFIGURATIONS (CONTINUED)

STATE MODEL F2

A =

-0.458420E-01	0.665630E-01	0.000000E+00	-0.321700E+02
-0.270510E+00	-0.626720E+00	0.244720E+03	0.000000E+00
0.225160E-03	0.233640E-02	-0.354410E+00	0.000000E+00
0.000000E+00	0.000000E+00	0.100000E+01	0.000000E+00

B =

0.000000E+00
0.000000E+00
-0.150530E+01
0.000000E+00

POLES

REAL	IMAG	TAU	OMEGA	ZETA	T1/2,2
-1.25880000	0.00000000	0.79440737	-------	-------	0.55064123
-0.33087000	0.00000000	-3.02233506	-------	-------	2.0949230
-0.04952700	0.18832000	-------	0.19472377	0.25434491	13.995340
-0.04952700	-0.18832000	-------	0.19472377	0.25434491	13.995340

CHARACTERISTIC POLYNOMIAL:
1.00   1.02700   -0.286670   -0.607140E-02   -0.157920E-01

ZEROS OF u/δ_h

REAL	IMAG	TAU	OMEGA	ZETA	T1/2,2
-1.2696000	0.00000000	0.78764965	-------	------	0.54595714
		23.9052700			

NUMERATOR POLNOMIAL: GAIN =
1.00   1.26960

ZEROS OF w/δ_h

REAL	IMAG	TAU	OMEGA	ZETA	T1/2,2
-0.02292100	0.18718000	--------	0.18857817	0.12154641	30.240704
-0.02292100	-0.18718000	--------	0.18857817	0.12154641	30.240704

NUMERATOR POLNOMIAL: GAIN =   -368.377100
1.00   0.458420E-01   0.355600E-01

ZEROS OF θ/δ_h

REAL	IMAG	TAU	OMEGA	ZETA	T1/2,2
-0.59386000	0.00000000	1.68389856	-------	-------	1.1671895
-0.07869800	0.00000000	12.70680322	-------	-------	8.8070849

NUMERATOR POLNOMIAL: GAIN =   -1.51000000
1.00   0.672560   0.467360E-01

TABLE C 8 STATE MODELS, POLES AND ZEROS - ALL CONFIGURATIONS (CONTINUED)

STATE MODEL F4

A =

-0.458420E-01	0.665630E-01	0.000000E+00	-0.321700E+02
-0.270510E+00	-0.626720E+00	0.244720E+03	0.000000E+00
0.207090E-03	0.113890E-02	-0.360500E+00	0.000000E+00
0.000000E+00	0.000000E+00	0.100000E+01	0.000000E+00

B =

0.000000E+00
0.000000E+00
-0.150530E+01
0.000000E+00

POLES

REAL	IMAG	TAU	OMEGA	ZETA	T1/2,2
-1.03500000	0.00000000	0.96618357	---------	---------	0.66970742
-0.07613400	0.17363000	---------	0.18958840	0.40157519	9.1043053
-0.07613400	-0.17363000	---------	0.18958840	0.40157519	9.1043053
0.15418000	0.00000000C	-6.48592554	---------	---------	4.4957010

CHARACTERISTIC POLYNOMIAL:
1.00 1.03310 0.104830E-01 0.736040E-02 -0.573580E-02

ZEROS OF u/δ_h

REAL	IMAG	TAU	OMEGA	ZETA	T1/2,2
-1.26960000	0.00000000	0.78764965	---------	---------	0.54595714

NUMERATOR POLNOMIAL: GAIN = 23.9052400
1.00 1.26960

ZEROS OF w/δ_h

REAL	IMAG	TAU	OMEGA	ZETA	T1/2,2
-0.02292100	0.18718000	---------	0.18857817	0.12154641	30.240704
-0.02292100	-0.18718000	---------	0.18857817	0.12154641	30.240704

NUMERATOR POLNOMIAL: GAIN = -368.377100
1.00 0.458420E-01 0.355600E-01

ZEROS OF θ/δ_h

REAL	IMAG	TAU	OMEGA	ZETA	T1/2,2
-0.59386000	0.00000000	1.68389856	---------	---------	1.1671895
-0.07869800	0.00000000	12.70680322	---------	---------	8.8076849

NUMERATOR POLNOMIAL: GAIN = -1.50530000
1.00 0.672560 0.467360E-01

TABLE C 8 STATE MODELS, POLES AND ZEROS - ALL CONFIGURATIONS (CONTINUED)

STATE MODEL F6

A =

-0.458420E-01	0.665630E-01	0.000000E+00	-0.321700E+02
-0.270510E+00	-0.626720E+00	0.244720E+03	0.000000E+00
-0.201660E-03	0.779630E-03	-0.362330E+00	0.000000E+00
0.000000E+00	0.000000E+00	0.100000E+01	0.000000E+00

B =

0.000000E+00
0.000000E+00
-0.150530E+01
0.000000E+00

POLES

REAL	IMAG	TAU	OMEGA	ZETA	T1/2,2
-0.94547000	0.00000000	1.05767502	-------	-------	0.73312446
-0.09028600	0.15296000	-------	0.17761848	0.50831423	7.6772388
-0.09028600	-0.15296000	-------	0.17761848	0.50831423	7.6772388
-0.09115100	0.00000000	-10.97080668	-------	-------	7.6043837

CHARACTERISTIC POLYNOMIAL:
1.00   1.03490   0.996340E-01   0.113900E-01   -0.271880E-02

ZEROS OF u/δ_h

REAL	IMAG	TAU	OMEGA	ZETA	T1/2,2
-1.26960000	0.00000000	0.78764965	-------	-------	0.54595714

NUMERATOR POLNOMIAL: GAIN = 23.9052400
1.00   1.26960

ZEROS OF w/δ_h

REAL	IMAG	TAU	OMEGA	ZETA	T1/2,2
-0.02292100	0.18718000	-------	0.18857817	0.12154641	30.240704
-0.02292100	-0.18718000	-------	0.18857817	0.12154641	30.240704

NUMERATOR POLNOMIAL: GAIN = -368.376900
1.00   0.458420E-01   0.355600E-01

ZEROS OF θ/δ_h

REAL	IMAG	TAU	OMEGA	ZETA	T1/2,2
-0.59386000	0.00000000	1.68389856	-------	-------	1.1671895
-0.07869800	0.00000000	12.70680322	-------	-------	8.8076849

NUMERATOR POLNOMIAL: GAIN = 0.467360E-01
1.00   0.672560   -1.50530100

287

TABLE C8   STATE MODELS, POLES AND ZEROS - ALL CONFIGURATIONS (CONTINUED)

STATE MODEL L21

A =

-0.701470E-01	0.451400E-02	0.000000E+00	-0.321400E+02
-0.316050E+00	-0.770860E+00	0.206520E+03	0.137950E+01
0.651090E-03	-0.185900E-01	-0.183320E-01	-0.284190E-02
0.000000E+00	0.000000E+00	0.100000E+01	0.000000E+00

B =

-0.239840E+01
0.000000E+00
-0.592130E+01
0.000000E+00

POLES

REAL	IMAG	TAU	OMEGA	ZETA	T1/2,2
-1.30690000	1.87990000	-------	2.28954398	0.57081236	0.53037507
-1.30690000	-1.87990000	-------	2.28954398	0.57081236	0.53037507
-0.03016200	0.19637000	-------	0.19867290	0.15181738	22.980810
-0.03016200	-0.19637000	-------	0.19867290	0.15181738	22.980810

CHARACTERISTIC POLYNOMIAL:
1.00   2.67420   5.43830   0.419410   0.206920

ZEROS OF u/δ_h

REAL	IMAG	TAU	OMEGA	ZETA	T1/2,2
-8.49020000	0.00000000	0.10537186	-------	-------	0.73038206E-01
-0.83424000	0.00000000	1.19869582	-------	-------	0.83087263
-7.72040000	0.00000000	-0.12952697	-------	-------	0.89781253E-01
		-2.39840000			

NUMERATOR POLYNOMIAL: GAIN = -71.7920
1.00   2.60410   -61.1240

ZEROS OF w/δ_h

REAL	IMAG	TAU	OMEGA	ZETA	T1/2,2
-0.03800100	0.21964000	-------	0.22290313	0.17048213	18.240235
-0.03800100	-0.21964000	-------	0.22290313	0.17048213	18.240235

NUMERATOR POLYNOMIAL: GAIN = -1222.10886
1.00   0.760010E-01   0.496850E-01

ZEROS OF θ/δ_h

REAL	IMAG	TAU	OMEGA	ZETA	T1/2,2
-0.76538000	0.00000000	1.30654054	-------	-------	0.90562490
-0.07588800	0.00000000	13.17731394	-------	-------	9.1338180

NUMERATOR POLYNOMIAL: GAIN = 0.580830E-01
1.00   0.841270   -5.92130000

288

TABLE C8   STATE MODELS, POLES AND ZEROS - ALL CONFIGURATIONS (CONTINUED)

STATE MODEL L71

A =

```
-0.681360E-01   0.169500E-01   0.000000E+00  -0.321400E+02
-0.316050E+00  -0.701870E+00   0.206520E+03   0.137950E+01
 0.569240E-03   0.266600E-02  -0.160280E+01  -0.248460E-02
 0.000000E+00   0.000000E+00   0.100000E+01   0.000000E+00
```

B =

```
-0.239840E+01
 0.000000E+00
-0.592130E+01
 0.000000E+00
```

POLES

REAL	IMAG	TAU	OMEGA	ZETA	T1/2,2
-2.17840000	0.00000000	0.45905252	--------	--------	0.31819096
-0.17785000	0.22450000	--------	0.28641032	0.62096226	3.8973696
-0.17785000	-0.22450000	--------	0.28641032	0.62096226	3.8973696
-0.16130000	-0.00000000	-6.19962802	--------	--------	4.2972547

CHARACTERISTIC POLYNOMIAL:
1.00   2.37280   0.448140   0.404800E-01 -0.288230E-01

ZEROS OF u/δ_h

REAL	IMAG	TAU	OMEGA	ZETA	T1/2,2
-9.24170000	0.00000000	0.10820520	--------	--------	0.75002130E-01
-0.78011000	0.00000000	1.28187051	--------	--------	0.88852493
7.71710000	0.00000000	-0.12958236	--------	--------	0.89819645E-01

NUMERATOR POLNOMIAL: GAIN = -70.1300
1.00   2.30470   -2.39840000   -55.6370

ZEROS OF w/δ_h

REAL	IMAG	TAU	OMEGA	ZETA	T1/2,2
-0.03704900	0.21977000	--------	0.22287100	0.16623518	18.708931
-0.03704900	-0.21977000	--------	0.22287100	0.16623518	18.708931

NUMERATOR POLNOMIAL: GAIN = 0.496720E-01
1.00   0.740990E-01   -1222.10886

ZEROS OF θ/δ_h

REAL	IMAG	TAU	OMEGA	ZETA	T1/2,2
-0.69365000	0.00000000	1.44123370	--------	--------	0.99898708
-0.07638600	0.00000000	13.09140418	--------	--------	9.0742699

NUMERATOR POLNOMIAL: GAIN = 0.530000E-01
1.00   0.770240   -5.92130000

289

TABLE C8 STATE MODELS, POLES AND ZEROS - ALL CONFIGURATIONS (CONTINUED)

STATE MODEL L72

A =

```
-0.681360E-01   0.169500E-01   0.000000E+00  -0.321400E+02
-0.316050E+00  -0.701870E+00   0.206520E+03   0.137950E+01
 0.569240E-03   0.407560E-02  -0.160280E+01  -0.248460E-02
 0.000000E+00   0.000000E+00   0.100000E+01   0.000000E+00
```

B =

```
-0.239840E+01
 0.000000E+00
-0.592130E+01
 0.000000E+00
```

POLES

REAL	IMAG	TAU	OMEGA	ZETA	T1/2,2
-2.17840000	0.00000000	0.45905252	--------	--------	0.31819096
-0.17785000	0.22450000	--------	0.28641032	0.62096226	3.8973696
-0.17785000	-0.22450000	--------	0.28641032	0.62096226	3.8973696
-0.16130000	0.00000000	-6.19962802	--------	--------	4.2972547

CHARACTERISTIC POLYNOMIAL:

1.00   2.37280   0.448140   0.404800E-01   -0.288230E-01

ZEROS OF u/δ_h

REAL	IMAG	TAU	OMEGA	ZETA	T1/2,2
-9.26040000	0.00000000	0.10798670	--------	--------	0.74850674E-01
-0.77699000	0.00000000	1.28701785	--------	--------	0.89209280
7.73270000	0.00000000	-0.12932094	--------	--------	0.89638442E-01
		-2.39840000	-55.6390		

NUMERATOR POLNOMIAL: GAIN = -70.4210

1.00   2.30470

ZEROS OF w/δ_h

REAL	IMAG	TAU	OMEGA	ZETA	T1/2,2
-0.03704900	0.21977000	--------	0.22287100	0.16623518	18.708931
-0.03704900	-0.21977000	--------	0.22287100	0.16623518	18.708931

NUMERATOR POLNOMIAL: GAIN = -1222.10896

1.00   0.740990E-01   0.496720E-01

ZEROS OF θ/δ_h

REAL	IMAG	TAU	OMEGA	ZETA	T1/2,2
-0.69414000	0.00000000	1.44063157	--------	--------	0.99856972
-0.07609300	0.00000000	13.14181331	--------	--------	9.1092109
		-5.92130000			

NUMERATOR POLNOMIAL: GAIN = 0.528200E-01

1.00   0.770240

TABLE C3 STATE MODELS, POLES AND ZEROS - ALL CONFIGURATIONS (CONTINUED)

STATE MODEL L73

A =

-0.681360E-01	0.169500E-01	0.000000E+00	-0.321400E+02
-0.316050E+00	-0.701870E+00	0.206520E+03	-0.137950E+01
-0.569240E-03	0.752000E-02	-0.160280E+01	-0.248480E-02
0.000000E+00	0.000000E+00	0.100000E+01	0.000000E+00

B =

-0.239840E+01
0.000000E+00
-0.592130E+01
0.000000E+00

POLES

REAL	IMAG	TAU	OMEGA	ZETA	T1/2,2
-2.48100000	0.00000000	0.40306328	-------	-------	0.27938218
0.32982000	0.00000000	-3.03195662	-------	-------	2.1015923
-0.11080000	0.25708000	--------	0.27984983	0.39578520	6.2558410
-0.11080000	-0.25708000	--------	0.27984983	0.39578520	6.2558410

CHARACTERISTIC POLYNOMIAL:
1.00   2.37280   -0.263200   -0.127390E-01   -0.641340E-01

ZEROS OF u/δ_h

REAL	IMAG	TAU	OMEGA	ZETA	T1/2,2
-9.30590000	0.00000000	0.10745871	-------	-------	0.74484701E-01
-0.76948000	0.00000000	1.29957884	-------	-------	0.90079948
7.77070000	0.00000000	-0.12868854	-------	-------	0.89200096E-01
		-2.39840000			

NUMERATOR POLYNOMIAL: GAIN = -71.1320
1.00   2.30470   -55.6440

ZEROS OF w/δ_h

REAL	IMAG	TAU	OMEGA	ZETA	T1/2,2
-0.03704900	0.21977000	--------	0.22287100	0.16623518	18.708931
-0.03704900	-0.21977000	--------	0.22287100	0.16623518	18.708931

NUMERATOR POLYNOMIAL: GAIN = -1222.10886
1.00   0.740990E-01   0.496720E-01

ZEROS OF θ/δ_h

REAL	IMAG	TAU	OMEGA	ZETA	T1/2,2
-0.69486000	0.00000000	1.43913882	-------	-------	0.99753502
-0.07536100	0.00000000	13.26594235	-------	-------	9.1952506

NUMERATOR POLYNOMIAL: GAIN = -5.921300000
1.00   0.770240   0.523790E-01

Table C8. State Models, Poles and Zeros — All Configurations (continued)

STATE MODEL S21

A =
```
-0.380000E-01    0.670000E-01    0.000000E+00   -0.321300E+02
-0.299999E+00   -0.616626E+00    0.241755E+03    0.000000E+00
-0.428610E-03   -0.351183E-05    0.232058E+00    0.133967E-01
 0.000000E+00    0.000000E+00    0.100000E+01    0.000000E+00
```

B =
```
 0.000000E+00
 0.000000E+00
-0.148859E+01
 0.000000E+00
```

POLES

REAL	IMAG	TAU	OMEGA	ZETA	T1/2,2
0.34660000	0.00000000	-2.88517023	----------	----------	1.9998476
-0.09458200	0.18754000	----------	0.21004049	0.45030366	7.3285317
-0.09458200	-0.18754000	----------	0.21004049	0.45030366	7.3285317
-0.60000000	0.00000000	1.66666667	----------	----------	1.1552453

CHARACTERISTIC POLYNOMIAL:
1.00   0.442570   -0.115910   -0.281590E-01   -0.917450E-02

ZEROS OF u/δ_h

REAL	IMAG	TAU	OMEGA	ZETA	T1/2,2
-1.24350000	0.00000000	0.80418175	----------	----------	0.55741031

NUMERATOR POLNOMIAL: GAIN = 23.7000000
1.00   1.24350

ZEROS OF w/δ_h

REAL	IMAG	TAU	OMEGA	ZETA	T1/2,2
-0.02900000	0.18361000	----------	0.18588607	0.15600954	23.901627
-0.02900000	-0.18361000	----------	0.18588607	0.15600954	23.901827

NUMERATOR POLNOMIAL: GAIN = -360.000000
1.00   0.580000E-01   0.345550E-01

ZEROS OF θ/δ_h

REAL	IMAG	TAU	OMEGA	ZETA	T1/2,2
-0.58348000	0.00000000	1.71385480	----------	----------	1.1879536
-0.09115100	0.00000000	10.97080668	----------	----------	7.6043837

NUMERATOR POLNOMIAL: GAIN = -1.49000000
1.00   0.674630   0.531840E-01

Table C8. State Models, Poles and Zeros — All Configurations (continued)

STATE MODEL S22

A =
```
-0.580000E-01   0.670000E-01   0.000000E+00   -0.321300E+02
-0.259999E+00  -0.616626E+00   0.241755E+03    0.000000E+00
-0.133587E-03   0.127086E-02  -0.167938E+00    0.381263E-01
 0.000000E+00   0.000000E+00   0.100000E+01    0.000000E+00
```

B =
```
 0.000000E+00
 0.000000E+00
-0.148859E+01
 0.000000E+00
```

POLES

REAL	IMAG	TAU	OMEGA	ZETA	T1/2,2
-1.00000000	0.00000000	1.00000000	--------	--------	0.69314718
-0.34660000	0.00000000	-2.88517023	--------	--------	1.9998476
-0.09458100	0.18754000	--------	0.21004004	0.45029986	7.3286092
-0.09458100	-0.18754000	--------	0.21004004	0.45029986	7.3286092

CHARACTERISTIC POLYNOMIAL:
1.00 0.842560 -0.178880 -0.367370E-01 -0.152810E-01

ZEROS OF u/δ_h

REAL	IMAG	TAU	OMEGA	ZETA	T1/2,2
-1.24350000	0.00000000	0.80418175	--------	--------	0.55741631
		23.7000000			

NUMERATOR POLNOMIAL: GAIN = 1.24350

ZEROS OF w/δ_h

REAL	IMAG	TAU	OMEGA	ZETA	T1/2,2
-0.02900000	0.18361000	--------	0.18588607	0.15600954	23.901627
-0.02900000	-0.18361000	--------	0.18588607	0.15600954	23.901627

NUMERATOR POLNOMIAL: GAIN = -360.090000
1.00 0.580000E-01 0.345550E-01

ZEROS OF θ/δ_h

REAL	IMAG	TAU	OMEGA	ZETA	T1/2,2
-0.58348000	0.00000000	1.71385480	--------	--------	1.1879536
-0.09115100	0.00000000	10.97080668	--------	--------	7.6043837

NUMERATOR POLNOMIAL: GAIN = -1.49000000
1.00 0.674630 0.531840E-01

Table C8. State Models, Poles and Zeros — All Configurations (continued)

STATE MODEL S23

A =
```
-0.580000E-01    0.670000E-01    0.000000E+00   -0.321300E+02
-0.259999E+00   -0.616626E+00    0.241755E+03    0.000000E+00
 0.603966E-03    0.445689E-02   -0.116794E+01   -0.999499E-01
 0.000000E+00    0.000000E+00    0.100000E+01    0.000000E+00
```

B =
```
 0.000000E+00
 0.000000E+00
-0.148859E+01
 0.000000E+00
```

POLES

REAL	IMAG	TAU	OMEGA	ZETA	T1/2,2
-2.00000000	0.00000000	0.50000000	---------	-------	0.34657359
-0.09458100	0.18754000	---------	0.21004004	0.45029986	7.3286092
-0.09458100	-0.18754000	---------	0.21004004	0.45029986	7.3286092
-0.34660000	0.00000000	-2.88517023	-0.305820E-01	-------	1.9998476

CHARACTERISTIC POLYNOMIAL:
1.00   1.84260   -0.336320   -0.581840E-01   -0.305820E-01

ZEROS OF u/δ_h

REAL	IMAG	TAU	OMEGA	ZETA	T1/2,2
-1.24350000	0.00000000	0.80418176	---------	-------	0.55741631
		23.70000000			

NUMERATOR POLNOMIAL: GAIN =
1.00   1.24350

ZEROS OF w/δ_h

REAL	IMAG	TAU	OMEGA	ZETA	T1/2,2
-0.02900000	0.18361000	---------	0.18588607	0.15600954	23.901627
-0.02900000	-0.18361000	---------	0.18588607	0.15600954	23.901627
		-360.000000			

NUMERATOR POLNOMIAL: GAIN =   0.580000E-01   0.345550E-01
1.00

ZEROS OF θ/δ_h

REAL	IMAG	TAU	OMEGA	ZETA	T1/2,2
-0.58348000	0.00000000	1.71385480	----------	---------	1.1679536
-0.09115100	0.00000000	10.97080668	----------	---------	7.6043037

NUMERATOR POLNOMIAL: GAIN =   -1.49000000
1.00   0.674030   0.531840E-01

Table C8. State Models, Poles and Zeros — All Configurations (continued)

STATE MODEL S24

A =

-0.580000E-01	0.670000E-01	0.000000E+00	-0.321300E+02
-0.259999E+00	-0.816626E+00	0.241755E+03	0.000000E+00
-0.134152E-02	0.764292E-02	-0.216794E+01	0.161774E+00
0.000000E+00	0.000000E+00	0.100000E+01	0.000000E+00

B =

0.000000E+00
0.000000E+00
-0.148859E+01
0.000000E+00

POLES

REAL	IMAG	TAU	OMEGA	ZETA	T1/2,2
-3.00000000	0.00000000	0.33333333	--------	--------	0.23104906
-0.09458100	0.18754000	--------	0.21004004	0.45029986	7.3286092
-0.09458100	-0.18754000	--------	0.21004004	0.45029986	7.3286092
0.34660000	0.00000000	-2.88517023	--------	--------	1.9998476

CHARACTERISTIC POLYNOMIAL:
1.00   2.84260   -0.483780   -0.796300E-01   -0.458730E-01

ZEROS OF u/δ_h

REAL	IMAG	TAU	OMEGA	ZETA	T1/2,2
-1.24350000	0.00000000	0.80418175	--------	--------	0.55741631
		23.7000000			

NUMERATOR POLYNOMIAL: GAIN =
1.00   1.24350

ZEROS OF w/δ_h

REAL	IMAG	TAU	OMEGA	ZETA	T1/2,2
-0.02900000	0.18361000	--------	0.18588607	0.15600954	23.901627
-0.02900000	-0.18361000	--------	0.18588607	0.15600954	23.901627
		-360.000000			

NUMERATOR POLYNOMIAL: GAIN = 0.580000E-01   0.345550E-01
1.00   0.580000E-01

ZEROS OF θ/δ_h

REAL	IMAG	TAU	OMEGA	ZETA	T1/2,2
-0.58348000	0.00000000	1.71385480	--------	--------	1.1879536
-0.09115100	0.00000000	10.97080668	--------	--------	7.6043837
		-1.49000000			

NUMERATOR POLYNOMIAL: GAIN = 0.631840E-01
1.00   0.674630

295

Table C8. State Models, Poles and Zeros — All Configurations (continued)

STATE MODEL S25

A =
```
-0.580000E-01   0.670000E-01   0.000000E+00   -0.321300E+02
-0.259999E+00  -0.360000E+00   0.241755E+03    0.170578E+00
-0.309358E-03   0.330711E-02  -0.142458E+01    0.000000E+00
 0.000000E+00   0.000000E+00   0.100000E+01    0.000000E+00
```

B =
```
 0.000000E+00
 0.000000E+00
-0.148658E+01
 0.000000E+00
```

POLES

REAL	IMAG	TAU	OMEGA	ZETA	T1/2,2
-2.00000000	0.00000000	0.50000000	----------	----------	0.34657359
-0.09458100	0.18754000	----------	0.21004004	0.45029986	7.3286092
-0.09458100	-0.18754000	----------	0.21004004	0.45029986	7.3286092
0.34660000	0.00000000	-2.88517023	----------	----------	1.9998476

CHARACTERISTIC POLYNOMIAL:
1.00   1.84260   -0.336320   -0.581840E-01   -0.305820E-01

ZEROS OF u/δ_h

REAL	IMAG	TAU	OMEGA	ZETA	T1/2,2
-0.72599000	0.00000000	1.37742944	----------	----------	0.95478134
		23.7000000			

NUMERATOR POLNOMIAL: GAIN =
1.00   0.725980

ZEROS OF w/δ_h

REAL	IMAG	TAU	OMEGA	ZETA	T1/2,2
-0.02900000	0.18361000	-------	0.18588607	0.15600954	23.901627
-0.02900000	-0.18361000	-------	0.18588607	0.15600954	23.901627
		-380.000000			

NUMERATOR POLNOMIAL: GAIN = 0.345550E-01
1.00   0.580000E-01   0.345550E-01

ZEROS OF θ/δ_h

REAL	IMAG	TAU	OMEGA	ZETA	T1/2,2
-0.28236000	0.00000000	3.54157813	----------	----------	2.4548349
-0.13564000	0.00000000	7.37245650	----------	----------	5.1101975
		-1.49000000			

NUMERATOR POLNOMIAL: GAIN =
1.00   0.418000   0.383000E-01

296

Table C8. State Models, Poles and Zeros — All Configurations (continued)

STATE MODEL S26

A =

-0.580000E-01	0.670000E-01	0.000000E+00	-0.321300E+02
-0.259999E+00	-0.120000E+01	0.241755E+03	0.000000E+00
0.298131E-03	0.463233E-02	-0.584560E+00	0.388309E-01
0.000000E+00	0.000000E+00	0.100000E+01	0.000000E+00

B =

0.000000E+00
0.000000E+00
-0.148859E+01
0.000000E+00

POLES

REAL	IMAG	TAU	OMEGA	ZETA	T1/2,2
-2.00000000	0.00000000	0.50000000	----------	-------	0.34657359
-0.34660000	0.00000000	-2.88517023	----------	-------	1.9998476
-0.09458100	0.18754000	----------	0.21004004	0.45029986	7.3286092
-0.09458100	-0.18754000	----------	0.21004004	0.45029986	7.3286092

CHARACTERISTIC POLYNOMIAL:
1.00   1.84260   -0.336320   -0.581050E-01   -0.305020E-01

ZEROS OF u/δ_h

REAL	IMAG	TAU	OMEGA	ZETA	T1/2,2
-2.42190000	0.00000000	0.41288896	------	-------	0.28619975
		23.7000000			

NUMERATOR POLNOMIAL: GAIN = 2.42190
1.00   2.42190

ZEROS OF w/δ_h

REAL	IMAG	TAU	OMEGA	ZETA	T1/2,2
-0.02900000	0.18361000	----------	0.18588607	0.15600954	23.901627
-0.02900000	-0.18361000	----------	0.18588607	0.15600954	23.901627
		-360.000000			

NUMERATOR POLNOMIAL: GAIN = 0.580000E-01   0.345550E-01
1.00   0.580000E-01   0.345550E-01

ZEROS OF θ/δ_h

REAL	IMAG	TAU	OMEGA	ZETA	T1/2,2
-1.18450000	0.00000000	0.84423808	------	---------	0.58518124
-0.07346300	0.00000000	13.61229462			9.4353237

NUMERATOR POLNOMIAL: GAIN = 0.870200E-01
1.00   1.25800   -1.49000000

Table C8. State Models, Poles and Zeros – All Configurations (continued)

STATE MODEL S27

A =

```
-0.580000E-01    0.670000E-01    0.000000E+00   -0.321300E+02
-0.259999E+00   -0.200000E+01    0.241755E+03    0.000000E+00
-0.445718E-03    0.660399E-04    0.215431E+00    0.104049E-01
-0.000000E+00    0.000000E+00    0.100000E+01    0.000000E+00
```

B =

```
 0.000000E+00
 0.000000E+00
-0.148859E+01
 0.000000E+00
```

POLES

REAL	IMAG	TAU	OMEGA	ZETA	T1/2,2
0.346600000	0.00000000	-2.88517023	--------	--------	1.9998476
-0.09458200	0.18754000	--------	0.21004049	0.45030366	7.3285317
-0.09458200	-0.18754000	--------	0.21004049	0.45030366	7.3285317
-2.00000000	0.00000000	0.50000000	--------	--------	0.34657359

CHARACTERISTIC POLYNOMIAL:

1.00   1.84260   -0.336310   -0.581830E-01   -0.305820E-01

ZEROS OF u/δ_h

REAL	IMAG	TAU	OMEGA	ZETA	T1/2,2
-4.03790000	0.00000000	0.24765348	--------	--------	0.17186031
		23.7000000			

NUMERATOR POLNOMIAL: GAIN =

1.00   4.03790

ZEROS OF w/δ_h

REAL	IMAG	TAU	OMEGA	ZETA	T1/2,2
-0.02900000	0.18361000	--------	0.18588607	0.15600954	23.901627
-0.02900000	-0.18361000	--------	0.18588607	0.15600954	23.901627
		-360.000000			

NUMERATOR POLNOMIAL: GAIN = 0.345550E-01

1.00   0.580000E-01   0.345550E-01

ZEROS OF θ/δ_h

REAL	IMAG	TAU	OMEGA	ZETA	T1/2,2
-1.99100000	0.00000000	0.50226017	--------	--------	0.34814022
-0.06701200	0.00000000	14.92270041	--------	--------	10.343628
		-1.49000000			

NUMERATOR POLNOMIAL: GAIN =

1.00   2.05400   0.133420

Table C8. State Models, Poles and Zeros – All Configurations (continued)

STATE MODEL S41, S41A

A =
```
-0.551880E-01    0.670000E-01    0.000000E+00   -0.321300E+02
-0.259999E+00   -0.616626E+00    0.241755E+03    0.000000E+00
-0.247359E-03    0.824221E-05    0.600195E-01   -0.111741E-01
-0.000000E+00    0.000000E+00    0.100000E+01    0.000000E+00
```

B =
```
 0.000000E+00
 0.000000E+00
-0.148859E+01
 0.000000E+00
```

POLES

REAL	IMAG	TAU	OMEGA	ZETA	T1/2,2
0.16879000	0.00000000	-5.92452159	-------	-------	4.1065655
-0.09062200	0.18769000		0.20842237	0.43479078	7.6487738
-0.09062200	-0.18769000		0.20842237	0.43479078	7.6487738
-0.59934000	-0.00000000	1.66850202	-------	-------	1.1565175

CHARACTERISTIC POLYNOMIAL:
1.00 0.611790 0.203100E-01 0.367890E-03 -0.439470E-02

ZEROS OF u/δ_h

REAL	IMAG	TAU	OMEGA	ZETA	T1/2,2
-1.24350000	0.00000000	0.80418175	-------	-------	0.55741631

NUMERATOR POLNOMIAL: GAIN = 23.7000000
1.00 1.24350

ZEROS OF w/δ_h

REAL	IMAG	TAU	OMEGA	ZETA	T1/2,2
-0.02759400	0.18383000	-------	0.18588948	0.14844304	25.119489
-0.02759400	-0.18383000	-------	0.18588948	0.14844304	25.119489

NUMERATOR POLNOMIAL: GAIN = -360.000000
1.00 0.551880E-01 0.345550E-01

ZEROS OF ϑ/δ_h

REAL	IMAG	TAU	OMEGA	ZETA	T1/2,2
-0.58366000	0.00000000	1.71332625	-------	-------	1.1875873
-0.08815100	0.00000000	11.34417080			7.8631800

NUMERATOR POLNOMIAL: GAIN = -1.49000000
1.00 0.671810 0.514500E-01

299

Table C8. State Models, Poles and Zeros — All Configurations (continued)

STATE MODEL S42

A =

-0.551880E-01	0.670000E-01	0.000000E+00	-0.321300E+02
-0.259999E+00	-0.616626E+00	0.241755E+03	0.000000E+00
-0.605659E-04	0.105084E-02	-0.339980E+00	0.780962E-03
0.000000E+00	0.000000E+00	0.100000E+01	0.000000E+00

B =

0.000000E+00
0.000000E+00
-0.148859E+01
0.000000E+00

POLES

REAL	IMAG	TAU	OMEGA	ZETA	T1/2,2
-0.99831000	0.00000000	1.00169286	--------	--------	0.09432058
0.17347000	0.00000000	-5.76468554	--------	--------	3.9957755
-0.09347800	0.18777000	-------	0.20975154	0.44566061	7.4150836
-0.09347800	-0.18777000	-------	0.20975154	0.44566061	7.4150836

CHARACTERISTIC POLYNOMIAL:
1.00   1.01180   0.250270E-01   0.391210E-02   -0.761870E-02

ZEROS OF u/δ_h

REAL	IMAG	TAU	OMEGA	ZETA	T1/2,2
-1.24350000	0.00000000	0.80418175	--------	--------	0.55741631

NUMERATOR POLNOMIAL: GAIN =   23.7000000
1.00   1.24350

ZEROS OF w/δ_h

REAL	IMAG	TAU	OMEGA	ZETA	T1/2,2
-0.02759400	0.18383000	-------	0.18588948	0.14844304	25.119489
-0.02759400	-0.18383000	-------	0.18588948	0.14844304	25.119489

NUMERATOR POLNOMIAL: GAIN = -360.000000
1.00   0.551880E-01   0.345650E-01

ZEROS OF θ/δ_h

REAL	IMAG	TAU	OMEGA	ZETA	T1/2,2
-0.58366000	0.00000000	1.71332625	--------	--------	1.1875873
-0.08815100	0.00000000	11.34417080	--------	--------	7.8631800

NUMERATOR POLNOMIAL: GAIN = -1.49000000
1.00   0.871810   0.514500E-01

Table C8. State Models, Poles and Zeros — All Configurations (continued)

STATE MODEL S43,S43A

A =

```
-0.551880E-01   0.670000E-01   0.000000E+00  -0.321300E+02
-0.259999E+00  -0.616626E+00   0.241755E+03   0.000000E+00
 0.830377E-03   0.365733E-02  -0.133900E+01   0.306685E-01
 0.000000E+00   0.000000E+00   0.100000E+01   0.000000E+00
```

B =

```
 0.000000E+00
 0.000000E+00
-0.148859E+01
 0.000000E+00
```

POLES

REAL	IMAG	TAU	OMEGA	ZETA	T1/2,2
-1.99850000	0.00000000	0.50037528	--------	-------	0.34663372
-0.09539800	0.18732000		0.21021313	0.45381561	7.2658461
-0.09539800	-0.18732000		0.21021313	0.45381561	7.2658461
0.17753000	0.00000000	-5.63285079			3.9043947

CHARACTERISTIC POLYNOMIAL:
1.00   2.01180   0.368220E-01   0.127730E-01   -0.156790E-01

ZEROS OF u/δ_h

REAL	IMAG	TAU	OMEGA	ZETA	T1/2,2
-1.24350000	0.00000000	0.80418175	------	------	0.55741631
		23.7000000			

NUMERATOR POLNOMIAL: GAIN =
1.00   1.24350

ZEROS OF w/δ_h

REAL	IMAG	TAU	OMEGA	ZETA	T1/2,2
-0.02759400	0.18383000		0.18588948	0.14844304	25.119489
-0.02759400	-0.18383000		0.18588948	0.14844304	25.119489
		-360.000000			

NUMERATOR POLNOMIAL: GAIN = 0.345550E-01
1.00   0.551880E-01

ZEROS OF θ/δ_h

REAL	IMAG	TAU	OMEGA	ZETA	T1/2,2
-0.58366000	0.00000000	1.71332625	------	------	1.1875873
-0.08815100	0.00000000	11.34417080		------	7.8631800

NUMERATOR POLNOMIAL: GAIN = -1.49000000
1.00   0.671810   0.614500E-01

301

Table C8. State Models, Poles and Zeros — All Configurations (continued)

STATE MODEL S44,S44A,S44B

A =

```
-0.551880E-01    0.670000E-01    0.000000E+00   -0.321300E+02
-0.259999E+00   -0.616626E+00    0.241755E+03    0.000000E+00
 0.160018E-02    0.626382E-02   -0.233967E+01    0.605561E-01
 0.000000E+00    0.000000E+00    0.100000E+01    0.000000E+00
```

B =

```
 0.000000E+00
 0.000000E+00
-0.148859E+01
 0.000000E+00
```

POLES

REAL	IMAG	TAU	OMEGA	ZETA	T1/2,2
-2.99860000	0.00000000	0.33348896	--------	--------	0.23115693
-0.09595800	0.18710000	--------	0.21027208	0.45635160	7.2234434
-0.09595800	-0.18710000	--------	0.21027208	0.45635160	7.2234434
-0.17906000	0.00000000	-5.58472021	--------	--------	3.87103331

CHARACTERISTIC POLYNOMIAL:
1.00   3.01150   0.484070E-01   0.216170E-01   -0.237390E-01

ZEROS OF u/δ_h

REAL	IMAG	TAU	OMEGA	ZETA	T1/2,2
-1.24350000	0.00000000	0.80418175	--------	--------	0.55741631

NUMERATOR POLNOMIAL: GAIN = 23.7000000
1.00   1.24350

ZEROS OF w/δ_h

REAL	IMAG	TAU	OMEGA	ZETA	T1/2,2
-0.02759400	0.18383000	--------	0.18588940	0.14844304	25.119489
-0.02759400	-0.18383000	--------	0.18588940	0.14844304	25.119489

NUMERATOR POLNOMIAL: GAIN = -360.000000
1.00   0.551880E-01   0.345550E-01

ZEROS OF θ/δ_h

REAL	IMAG	TAU	OMEGA	ZETA	T1/2,2
-0.58366000	0.00000000	1.71332625	--------	--------	1.1875873
-0.08812100	0.00000000	11.34417080	--------	--------	7.8631800

NUMERATOR POLNOMIAL: GAIN = -1.49000000
1.00   0.671810   0.514500E-01

Table C8. State Models, Poles and Zeros — All Configurations (continued)

STATE MODEL   S45, S45A

A =

-0.551880E-01	0.670000E-01	0.000000E+00	-0.321300E+02
-0.258998E+00	-0.360000E+00	0.241755E+03	0.000000E+00
0.132778E-03	0.100982E-02	-0.615000E+00	0.133459E-01
0.000000E+00	0.000000E+00	0.100000E+01	0.000000E+00

B =

0.000000E+00
0.000000E+00
-0.148850E+01
0.000000E+00

POLES

REAL	IMAG	TAU	OMEGA	ZETA	T1/2,2
-1.00850000	0.00000000	0.99157104	---------	---------	0.68730509
-0.09367300	0.18845000	---------	0.21044722	0.44511398	7.3996475
-0.09367300	-0.18845000	---------	0.21044722	0.44511398	7.3996475
0.16563000	0.00000000	-6.03755358	-0.739760E-02	---------	4.1849133

CHARACTERISTIC POLYNOMIAL:
1.00   1.03020   0.351530E-01   0.603330E-02   -0.739760E-02

ZEROS OF u/δ_h

REAL	IMAG	TAU	OMEGA	ZETA	T1/2,2
-0.72599000	0.00000000	1.37742944	---------	---------	0.95476134
		23.7000000			

NUMERATOR POLNOMIAL: GAIN = 0.725990
1.00   0.725990

ZEROS OF w/δ_h

REAL	IMAG	TAU	OMEGA	ZETA	T1/2,2
-0.02759400	0.18383000	---------	0.18588948	0.14844304	25.119480
-0.02759400	-0.18383000	---------	0.18588948	0.14844304	25.119480
		-360.000000			

NUMERATOR POLNOMIAL: GAIN = 0.345550E-01
1.00   0.551880E-01   0.345550E-01

ZEROS OF θ/δ_h

REAL	IMAG	TAU	OMEGA	ZETA	T1/2,2
-0.28380000	0.00000000	3.52360817	---------	---------	2.4423791
-0.13139000	0.00000000	7.61092829	---------	---------	5.2754942

NUMERATOR POLNOMIAL: GAIN = -1.49000000
1.00   0.415190   0.372880E-01

303

Table C8. State Models, Poles and Zeros — All Configurations (continued)

STATE MODEL   S46, S46A

A =

-0.551880E-01	0.670000E-01	0.000000E+00	-0.321300E+02
-0.259999E+00	-0.120000E+01	0.241755E+03	0.000000E+00
-0.409787E-03	-0.892930E-03	0.225000E+00	-0.180517E-01
0.000000E+00	0.000000E+00	0.100000E+01	0.000000E+00

B =

| 0.000000E+00 |
| 0.000000E+00 |
| -0.148859E+01 |
| 0.000000E+00 |

POLES

REAL	IMAG	TAU	OMEGA	ZETA	T1/2,2
-1.01110000	0.00000000	0.98902186	-------	-------	0.99953771
0.15629000	0.00000000	-6.39836202	-------	-------	4.4350066
-0.08771400	0.18850000	-------	0.20790862	0.42108726	7.9023552
-0.08771400	-0.18850000	-------	0.20790862	0.42108726	7.9023552

CHARACTERISTIC POLYNOMIAL:
1.00 1.03020 0.561520E-01 0.922510E-02 -0.683030E-02

ZEROS OF u/δ_h

REAL	IMAG	TAU	OMEGA	ZETA	T1/2,2
-2.42000000	0.00000000	0.41322314	-------	-------	0.28642446

NUMERATOR POLNOMIAL: GAIN = 23.70000000
1.00 2.42200

ZEROS OF w/δ_h

REAL	IMAG	TAU	OMEGA	ZETA	T1/2,2
-0.02759400	0.18383000	-------	0.18588948	0.14844304	25.119489
-0.02759400	-0.18383000	-------	0.18588948	0.14844304	25.119489

NUMERATOR POLNOMIAL: GAIN = -360.000000
1.00 0.551880E-01 0.345550E-01

ZEROS OF θ/δ_n

REAL	IMAG	TAU	OMEGA	ZETA	T1/2,2
-1.18460000	0.00000000	0.84416681	-------	-------	0.58513184
-0.07061200	0.00000000	14.16189883	-------	-------	9.8162803

NUMERATOR POLNOMIAL: GAIN = -1.49000000
1.00 1.25520 0.836460E-01

304

Table C8. State Models, Poles and Zeros – All Configurations (continued)

STATE MODEL S60

A =
```
-0.580000E-01   0.670000E-01   0.000000E+00  -0.321300E+02
-0.259999E+00  -0.816626E+00   0.241755E+03   0.000000E+00
-0.436142E-03  -0.714324E-03   0.300965E+00  -0.215294E-01
 0.000000E+00   0.000000E+00   0.100000E+01   0.000000E+00
```

B =
```
 0.000000E+00
 0.000000E+00
-0.148859E+01
 0.000000E+00
```

POLES

REAL	IMAG	TAU	OMEGA	ZETA	T1/2,2
-0.09458000	0.18754000	-------	0.21003959	0.45029607	7.3286866
-0.09458000	-0.18754000	-------	0.21003959	0.45029607	7.3286866
-0.11550000	0.00000000	-8.65800866	----------	----------	6.0012743
-0.30000000	0.00000000	-3.33333333	----------	----------	2.3104906

CHARACTERISTIC POLYNOMIAL:
1.00 0.373660 0.443660E-01 0.168500E-02 -0.152860E-02

ZEROS OF u/δ_h

REAL	IMAG	TAU	OMEGA	ZETA	T1/2,2
-1.24350000	0.00000000	0.80418175	----------	----------	0.55741631

NUMERATOR POLNOMIAL: GAIN = 23.7000000
1.00   1.24350

ZEROS OF w/δ_h

REAL	IMAG	TAU	OMEGA	ZETA	T1/2,2
-0.02900000	0.18361000	-------	0.18588607	0.15600954	23.901627
-0.02900000	-0.18361000	-------	0.18588607	0.15600954	23.901627

NUMERATOR POLNOMIAL: GAIN = -360.000000
1.00 0.580000E-01 0.345550E-01

ZEROS OF θ/δ_h

REAL	IMAG	TAU	OMEGA	ZETA	T1/2,2
-0.58348000	0.00000000	1.71385480	----------	----------	1.1879536
-0.09115100	0.00000000	10.97080668	----------	----------	7.6043837

NUMERATOR POLNOMIAL: GAIN = -1.49000000
1.00 0.674630 0.531840E-01

Table C8. State Models, Poles and Zeros — All Configurations (continued)

STATE MODEL S61

A =

```
-0.580000E-01    0.670000E-01    0.000000E+00   -0.321300E+02
-0.259999E+00   -0.616826E+00    0.241755E+03    0.000000E+00
-0.194795E-03    0.135668E-04    0.963211E-03   -0.172105E-01
-0.000000E+00    0.000000E+00    0.100000E+01    0.000000E+00
```

B =

```
 0.000000E+00
 0.000000E+00
-0.148859E+01
 0.000000E+00
```

POLES

REAL	IMAG	TAU	OMEGA	ZETA	T1/2,2
-0.09458100	0.18754000	---------	0.21004004	0.45029986	7.3286092
-0.09458100	-0.18754000	---------	0.21004004	0.45029986	7.3286092
-0.11550000	0.00000000	-8.65800866	---------	---------	6.0012743
-0.60000000	0.00000000	1.66666667	---------	---------	1.1552453

CHARACTERISTIC POLYNOMIAL:
1.00 0.673660 0.664650E-01 0.826660E-02 -0.305730E-02

ZEROS OF u/δ_h

REAL	IMAG	TAU	OMEGA	ZETA	T1/2,2
-1.24350000	0.00000000	0.80418175	---------	---------	0.55741631
		23.7000000			

NUMERATOR POLNOMIAL: GAIN = 1.24350
1.00   1.24350

ZEROS OF w/δ_h

REAL	IMAG	TAU	OMEGA	ZETA	T1/2,2
-0.02900000	0.18361000	---------	0.18588607	0.156009954	23.901627
-0.02900000	-0.18361000	---------	0.18588607	0.156009954	23.901627

NUMERATOR POLNOMIAL: GAIN = -360.000000
1.00   0.580000E-01   0.345550E-01

ZEROS OF θ/δ_h

REAL	IMAG	TAU	OMEGA	ZETA	T1/2,2
-0.58348000	0.00000000	1.71385480	---------	---------	1.1879536
-0.09115100	0.00000000	10.97080668	---------	---------	7.6043837

NUMERATOR POLNOMIAL: GAIN = -1.49000000
1.00   0.674630   0.531840E-01

Table C8. State Models, Poles and Zeros — All Configurations (continued)

STATE MODEL S62

A =

-0.580000E-01	0.670000E-01	0.000000E+00	-0.321300E+02
-0.259999E+00	-0.616626E+00	0.241755E+03	0.000000E+00
0.127004E-03	0.984083E-03	-0.399037E+00	-0.114519E-01
0.000000E+00	0.000000E+00	0.100000E+01	0.000000E+00

B =

0.000000E+00
0.000000E+00
-0.148859E+01
0.000000E+00

POLES

REAL	IMAG	TAU	OMEGA	ZETA	T1/2,2
-1.00000000	0.00000000	1.00000000	--------	--------	0.69314718
-0.11550000	0.00000000	-8.65800866	--------	--------	6.00012743
-0.09458100	0.18754000	--------	0.21004004	0.45029986	7.3286092
-0.09458100	-0.18754000	--------	0.21004004	0.45029986	7.3286092

CHARACTERISTIC POLYNOMIAL:
1.00   1.07370   0.959300E-01   0.171730E-01   -0.509550E-02

ZEROS OF u/δ_h

REAL	IMAG	TAU	OMEGA	ZETA	T1/2,2
-1.24350000	0.0000000	0.80418175	--------	--------	0.55741631

NUMERATOR POLNOMIAL: GAIN = 23.7000000
1.00   1.24350

ZEROS OF w/δ_h

REAL	IMAG	TAU	OMEGA	ZETA	T1/2,2
-0.02900000	0.18361000	--------	0.18588607	0.15600954	23.901627
-0.02900000	-0.18361000	--------	0.18588607	0.15600954	23.901627

NUMERATOR POLNOMIAL: GAIN = -360.000000
1.00   0.580000E-01   0.345550E-01

ZEROS OF θ/δ_h

REAL	IMAG	TAU	OMEGA	ZETA	T1/2,2
-0.58348000	0.00000000	1.71385480	--------	--------	1.1879536
-0.09115100	0.00000000	10.97080668	--------	--------	7.6043837

NUMERATOR POLNOMIAL: GAIN = -1.49000000
1.00   0.674630   0.531840E-01

307

Table C8. State Models, Poles and Zeros — All Configurations (concluded)

STATE MODEL S63

```
A =
  -0.580000E-01    0.670000E-01    0.000000E+00   -0.321300E+02
  -0.259999E+00   -0.616626E+00    0.241755E+03    0.000000E+00
   0.931497E-03    0.341037E-02   -0.139904E+01    0.204467E-02
   0.000000E+00    0.000000E+00    0.100000E+01    0.000000E+00
B =
   0.000000E+00
   0.000000E+00
  -0.148859E+01
   0.000000E+00
```

POLES

REAL	IMAG	TAU	OMEGA	ZETA	T1/2,2
-2.00000000	0.00000000	0.50000000	--------	--------	0.34657359
-0.09458100	0.18754000		0.21004004	0.45029986	7.3286092
-0.09458100	-0.18754000		0.21004004	0.45029986	7.3286092
0.11550000	0.00000000	-8.65000868	--------	--------	6.0012743

CHARACTERISTIC POLYNOMIAL:
1.00   2.07370   0.168590   0.394420E-01   -0.101910E-01

ZEROS OF u/δ_h

REAL	IMAG	TAU	OMEGA	ZETA	T1/2,2
-1.24350000	0.00000000	0.80418175	--------	--------	0.55741631

NUMERATOR POLNOMIAL: GAIN = 23.7000000
1.00   1.24350

ZEROS OF w/δ_h

REAL	IMAG	TAU	OMEGA	ZETA	T1/2,2
-0.02900000	0.18361000	--------	0.18588607	0.15600954	23.901627
-0.02900000	-0.18361000	-360.000000	0.18588607	0.15600954	23.901627

NUMERATOR POLNOMIAL: GAIN = -0.345550E-01
1.00   0.580000E-01   0.345550E-01

ZEROS OF θ/δ_h

REAL	IMAG	TAU	OMEGA	ZETA	T1/2,2
-0.58348000	0.00000000	1.71385480	--------	--------	1.1879536
-0.09115100	0.00000000	10.97080668	--------	--------	7.6043837

NUMERATOR POLNOMIAL: GAIN = -1.49000000
1.00   0.674630   0.531640E-01

Figure C-14. Time History for Step δ_h Command - Configuration F0, F1, F6, F4, F2

(a) α and q

309

$M_{\delta_{ES}}$	T_2	λ_{sp_2}	Z_{θ_2}
rad/sec²/in	sec	rad/sec	rad/sec
.086	Varies	Varies	-.59

δ_{hc} = -2.0 deg. step at t = 0.1 sec

$\dot{q}_{0.1+}$ = .0416 rad/sec²

Figure C-14. Time History for Step δ_h Command — Configuration F0, F1, F6, F4, F2 (Continued)
(b) N_Z and θ

310

$M\delta_{ES}$	T_2	λ_{sp_2}	Z_{θ_2}
rad/sec²/in	sec	rad/sec	rad/sec
.086	Varies	Varies	-.59

δ_{hc} = -2.0 deg. step at t = 0.1 sec

$\dot{q}_{0.1+}$ = .0416 rad/sec²
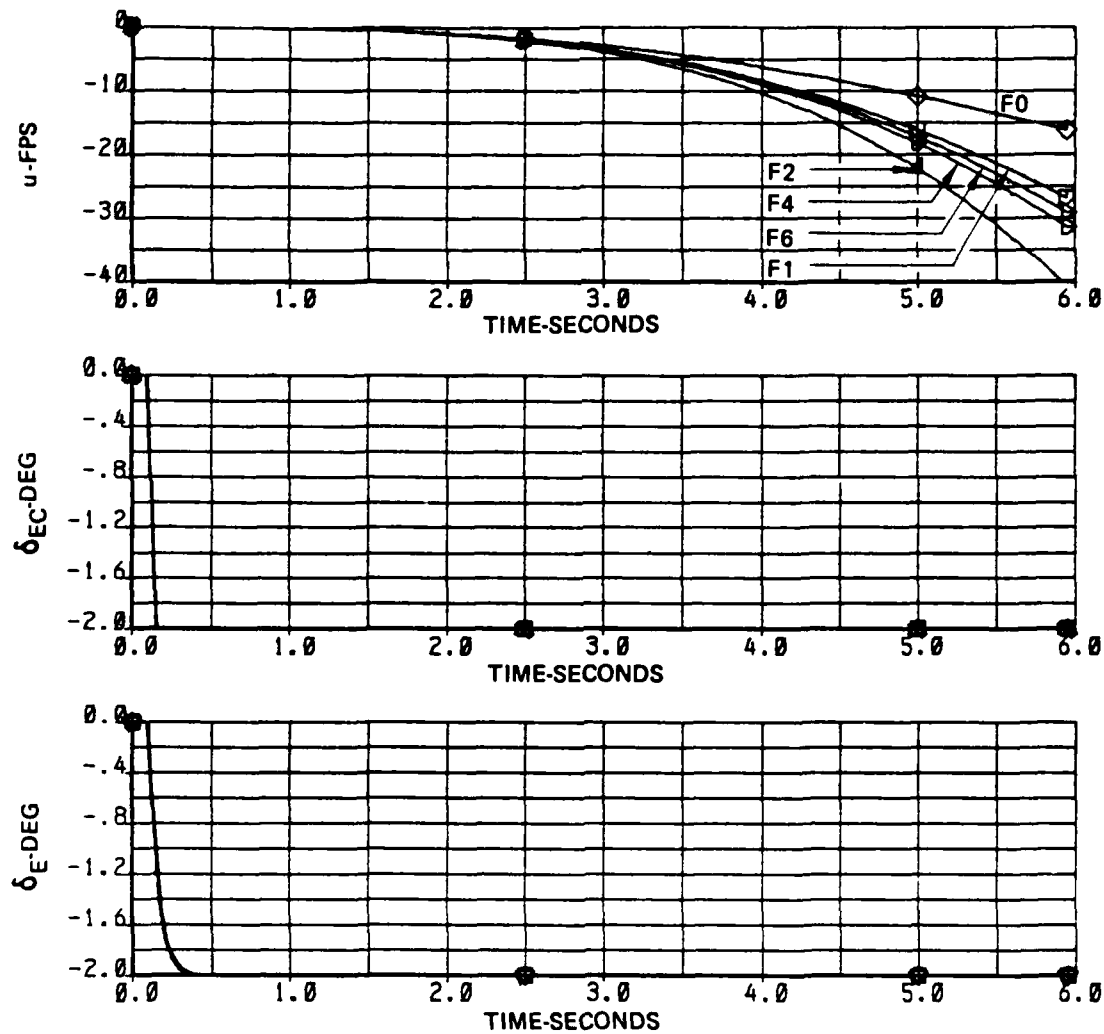
Figure C-14. Time Histroy for Step δ_h Command — Configuration F0, F1, F6, F4, F2 — Concluded
(c) δ_E, δ_{EC}, and u

311

Note: $\theta/F_s = 1.143(\frac{\delta_h}{\delta_{ES}})\,\theta'/F_s$ rad/lb

$$\frac{\delta_h}{\delta_{ES}} = -3.28/57.3 \text{ rad/in}$$
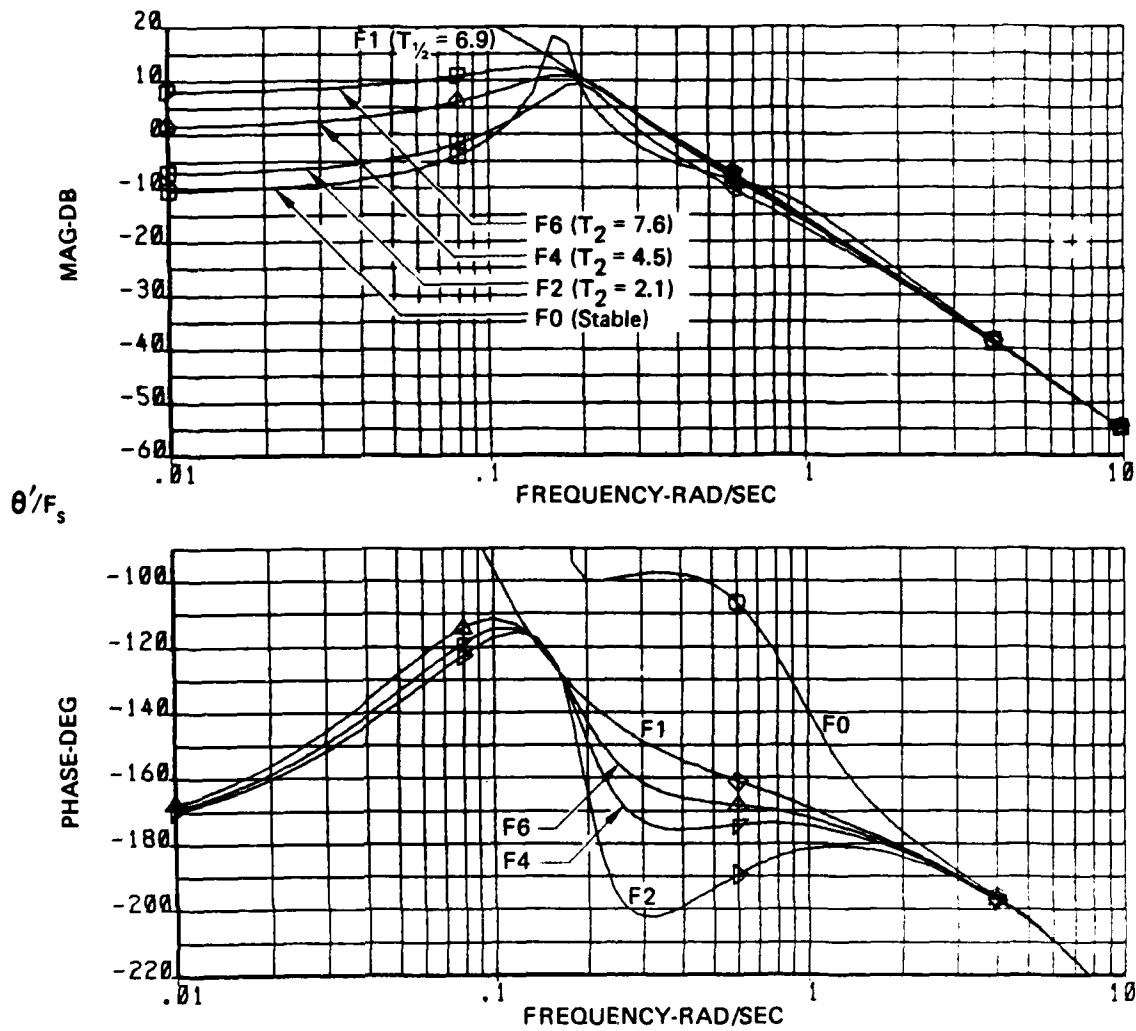
Figure C-15. Frequency Response of θ/F_s — Configuration F0, F1, F6, F4, F2

$M_{\delta_{ES}}$	T_2	λ_{sp_2}	Z_{θ_2}
rad/sec^2/in	sec	rad/sec	rad/sec
.434	Varies	Varies	-.67

δ_{hc} = -0.5 deg. step at t = 0.1 sec

$\dot{q}_{0.1+}$ = .0416 rad/sec^2

Figure C-16.   Time History for Step δ_h Command — Configuration L21, L71, L72, L73

(a) α and q

313

$M\delta_{ES}$	T_2	λ_{sp_2}	Z_{θ_2}
rad/sec^2/in	sec	rad/sec	rad/sec
.434	Varies	Varies	-.87

δ_{hc} = -0.5 deg. step at t = 0.1 sec

$\dot{q}_{0.1+}$ = .0416 rad/sec^2

Figure C-16. Time History for Step δ_h Command — Configuration L21, L71, L72, L73 (Continued)

(b) θ and N_Z

314

$M_{\delta_{ES}}$	T_2	λ_{sp_2}	Z_{θ_2}
rad/sec^2/in	sec	rad/sec	rad/sec
.434	Varies	Varies	-.67

δ_{hc} = -0.5 deg. step at t = 0.1 sec

$\dot{q}_{0.1+}$ = .0416 rad/sec^2

u-FPS

L21

L71
L72
L73

TIME-SECONDS

δ_{EC}-DEG

TIME-SECONDS

δ_E-DEG

TIME-SECONDS

Figure C-16. Time History for Step δ_h Command — Configuration L21, L71, L72, L73 — Concluded

(c) δ_E, δ_{EC}, and u

315

Note: $\theta/F_s = 1.143\left(\dfrac{\delta_h}{\delta_{ES}}\right)\theta'/F_s$ rad/lb

$\dfrac{\delta_h}{\delta_{ES}} = -4.2/57.3$ rad/in

θ/F_s

Figure C-17.   Frequency Response of θ/F_s – Configuration L21, L71, L72, L73

316

$M_{\delta_{ES}}$	T_2	λ_{sp_2}	Z_{θ_2}
rad/sec^2/in	sec	rad/sec	rad/sec
.341	Varies	-1.0	-.58

δ_{hc} = -2 deg. step at t = 0.1 sec

$\dot{q}_{0.1+}$ = .0416 rad/sec^2

Figure C-18.   Time History for Step δ_h Command — Configuration S22, S42, S62

(a) α and q

317

$M_{\delta_{ES}}$	T_2	λ_{sp_2}	Z_{θ_2}
rad/sec^2/in	sec	rad/sec	rad/sec
.341	Varies	-1.0	-.58

δ_{hc} = -2 deg. step at t = 0.1 sec

$\dot{q}_{0.1+}$ = .0416 rad/sec^2

Figure C-18. Time History for Step δ_h Command — Configuration S22, S42, S62 — Concluded

(b) δ_E, δ_{EC} and u

318

Note: $\theta/F_s = 1.143\left(\dfrac{\delta_h}{\delta_{ES}}\right)\theta'/F_s$ rad/lb

$\dfrac{\delta_h}{\delta_{ES}} = -13.12/57.3$ rad/in

Figure C-19. Frequency Response of θ/F_s — Configuration S22, S42, S62

319

$M_{\delta_{ES}}$	T_2	λ_{sp_2}	Z_{θ_2}
rad/sec²/in	sec	rad/sec	rad/sec
.341	2.0	Varies	-.58

δ_{hc} = -2 deg. step at t = 0.1 sec
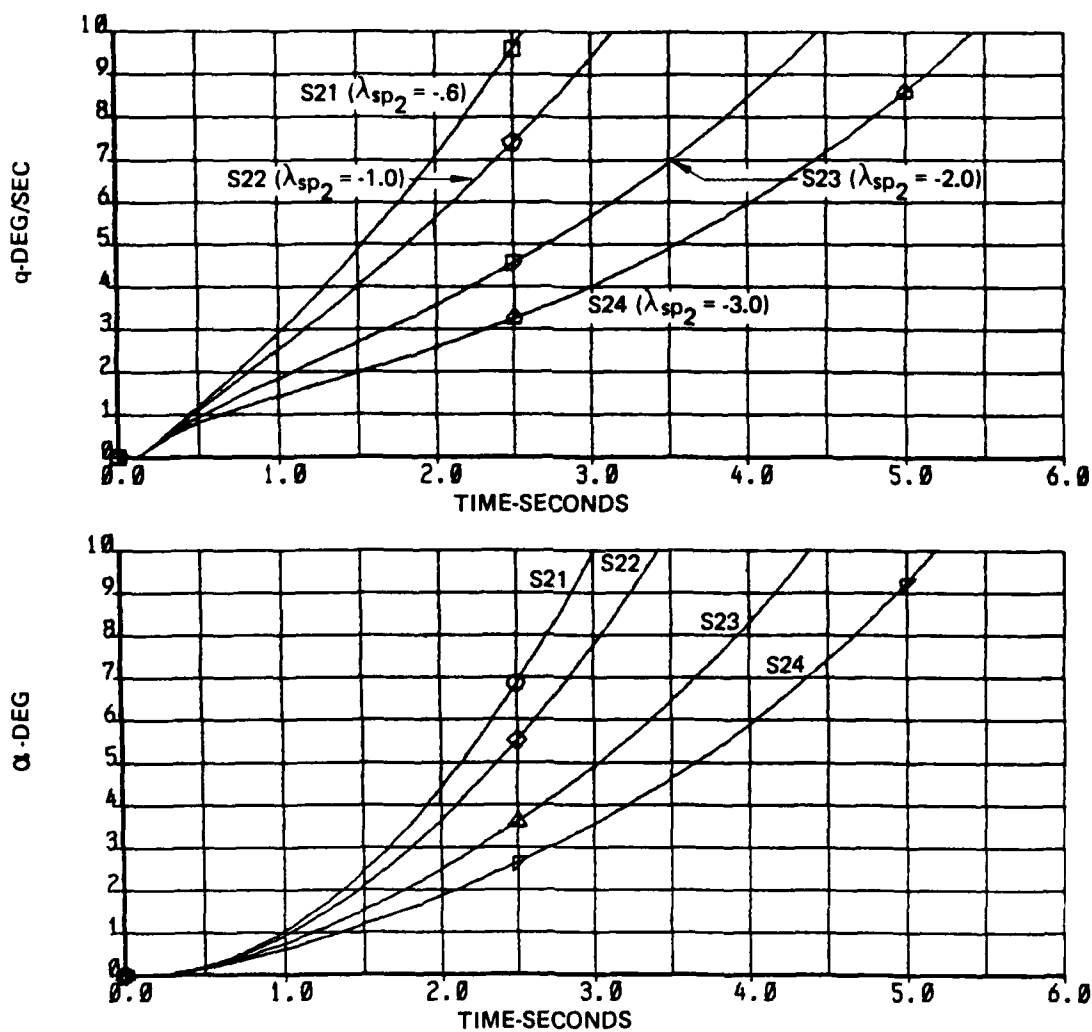
$\dot{q}_{0.1+}$ = .0416 rad/sec²

Figure C-20. Time History for Step δ_h Command — Configuration S21, S22, S23, S24

(a) α and q

320

$M\delta_{ES}$	T_2	λ_{sp_2}	Z_{θ_2}
rad/sec²/in	sec	rad/sec	rad/sec
.341	2.0	Varies	-.58

δ_{hc} = -2 deg. step at t = 0.1 sec

$\dot{q}_{0.1+}$ = .0416 rad/sec²

Figure C-20: Time History for Step δ_h Command — Configuration S21, S22, S23, S24 — Continued

(b) θ and n_z

321

$M_{\delta_{ES}}$	T_2	λ_{sp_2}	Z_{θ_2}
rad/sec²/in	sec	rad/sec	rad/sec
.341	2.0	Varies	-.58

δ_{hc} = -2 deg. step at t = 0.1 sec

$\dot{q}_{0.1+}$ = .0416 rad/sec²
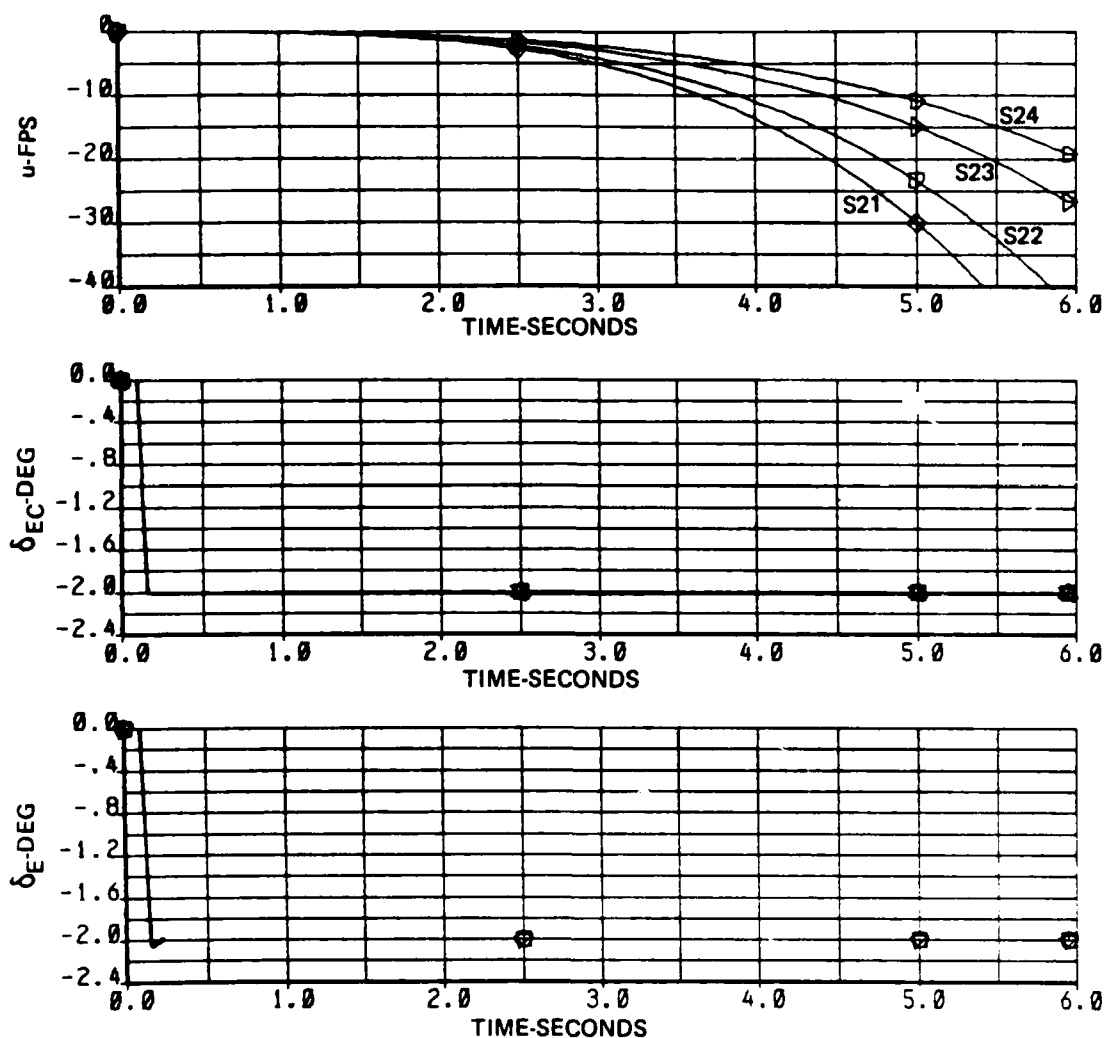
Figure C-20. *Time History for Step δ_h Command — Configuration S21, S22, S23, S24 — Concluded*
(c) δ_E, δ_{EC}, and u

322

Note: $\theta/F_s = 1.143 \left(\dfrac{\delta_h}{\delta_{ES}}\right) \theta'/F_s$ rad/lb

$\dfrac{\delta_h}{\delta_{ES}} = -13.12/57.3$ rad/in
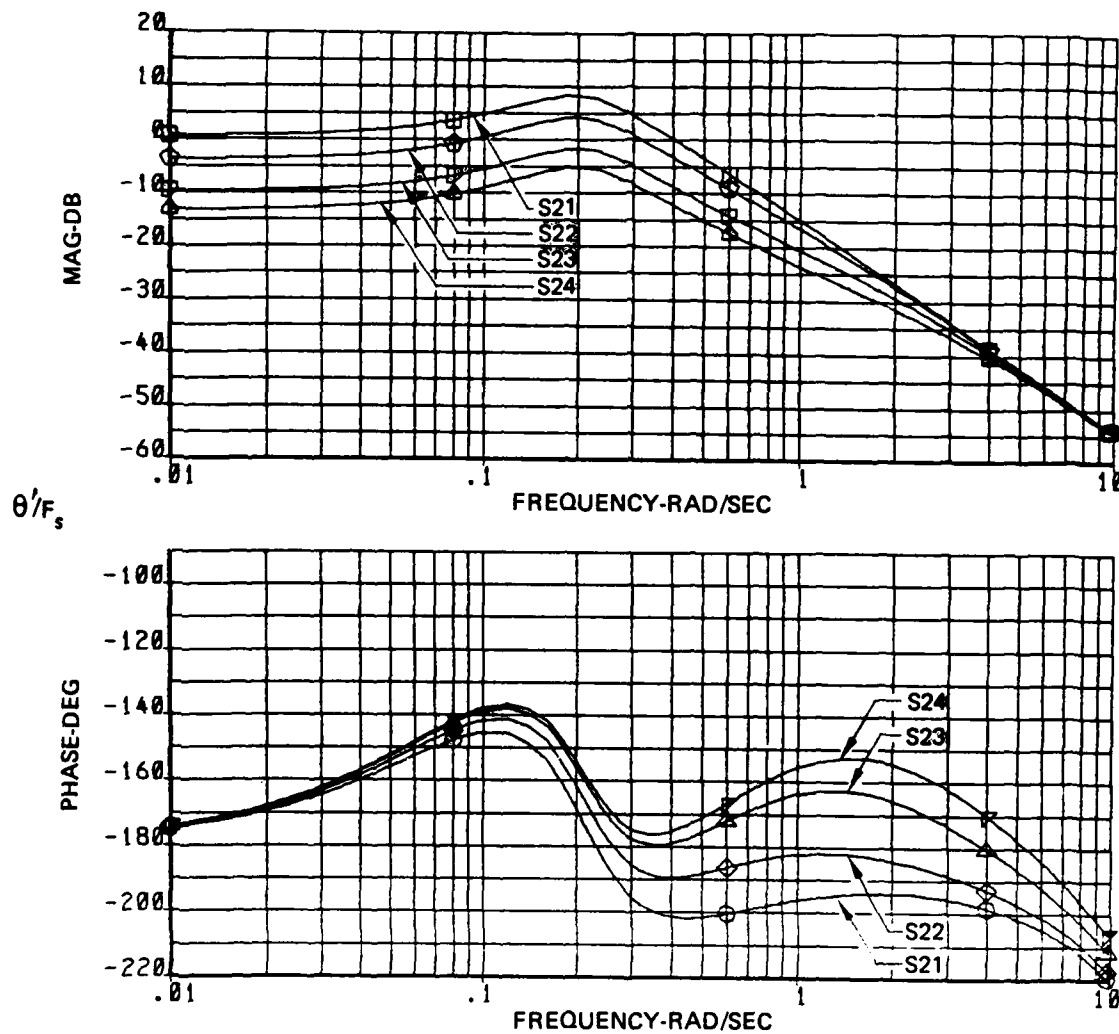
Figure C-21. Frequency Response of θ/F_s — Configuration S21, S22, S23, S24

$M\delta_{ES}$	T_2	λ_{sp_2}	Z_{θ_2}
rad/sec^2/in	sec	rad/sec	rad/sec
.341	~4.0	Varies	-.58

δ_{hc} = -2 deg. step at t = 0.1 sec

$\dot{q}_{0.1+}$ = .0416 rad/sec^2

Figure C-22.   Time History for Step δ_h Command — Configuration S41, S42, S43, S44

(a) α and q

324
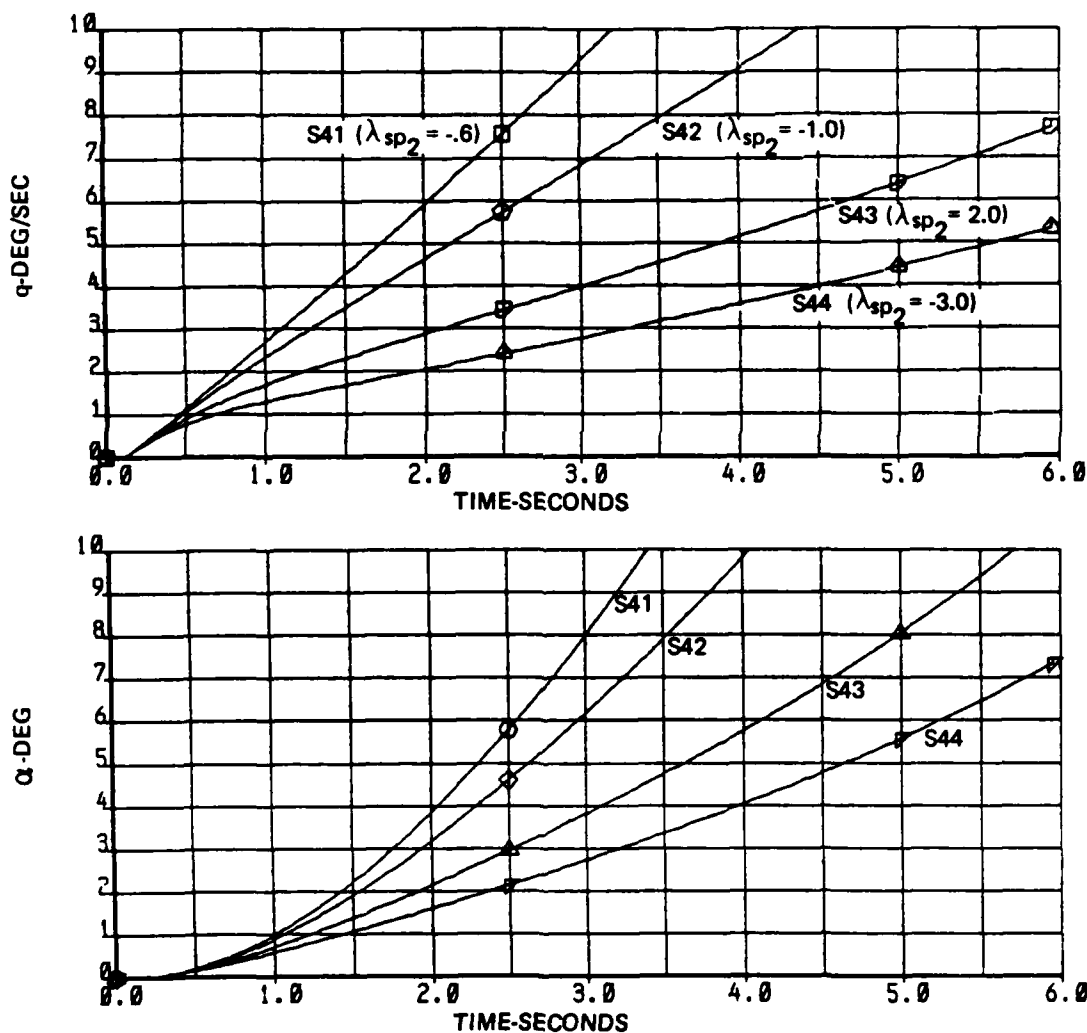
Figure C-22. Time History for Step δ_h Command — Configuration S41, S42, S43, S44 — Continued (b) θ and n_z

325

$M_{\delta_{ES}}$	T_2	λ_{sp_2}	Z_{θ_2}
rad/sec^2/in	sec	rad/sec	rad/sec
.341	~4.0	Varies	-.58

δ_{hc} = -2 deg. step at t = 0.1 sec

$\dot{q}_{0.1+}$ = .0416 rad/sec^2
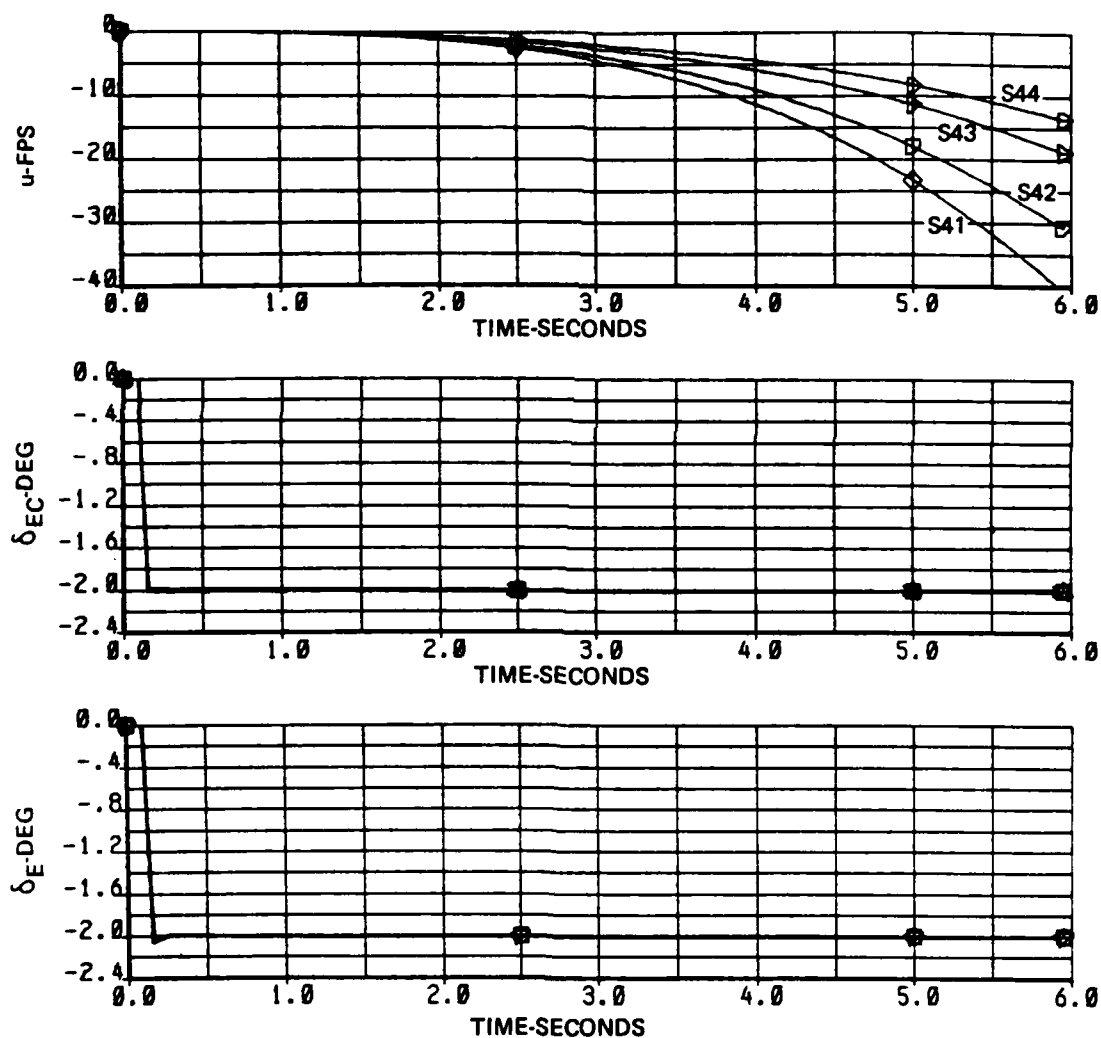
Figure C-22. Time History for Step δ_h Command —Configuration S41, S42, S43, S44 — Concluded

(c) δ_E, δ_{EC}, and u

326

Note: $\theta/F_s = 1.143 \left(\dfrac{\delta_h}{\delta_{ES}}\right) \theta'/F_s$ rad/lb

$\dfrac{\delta_h}{\delta_{ES}} = -13.12/57.3$ rad/in
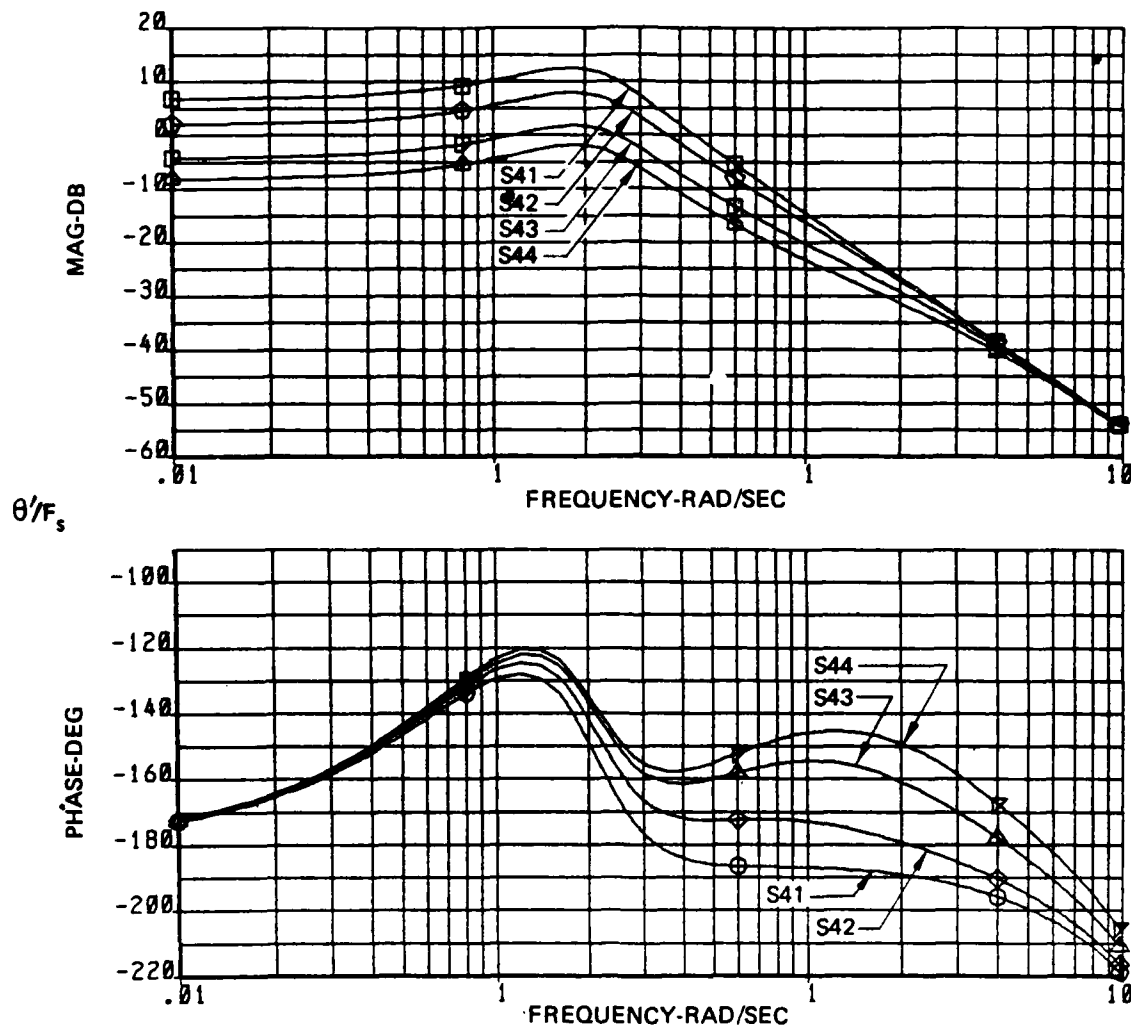
Figure C-23. Frequency Response of θ/F_s — Configuration S41, S42, S43, S44

$M\delta_{ES}$	T_2	λ_{sp_2}	Z_{θ_2}
rad/sec^2/in	sec	rad/sec	rad/sec
.341	6.0	Varies	-.58

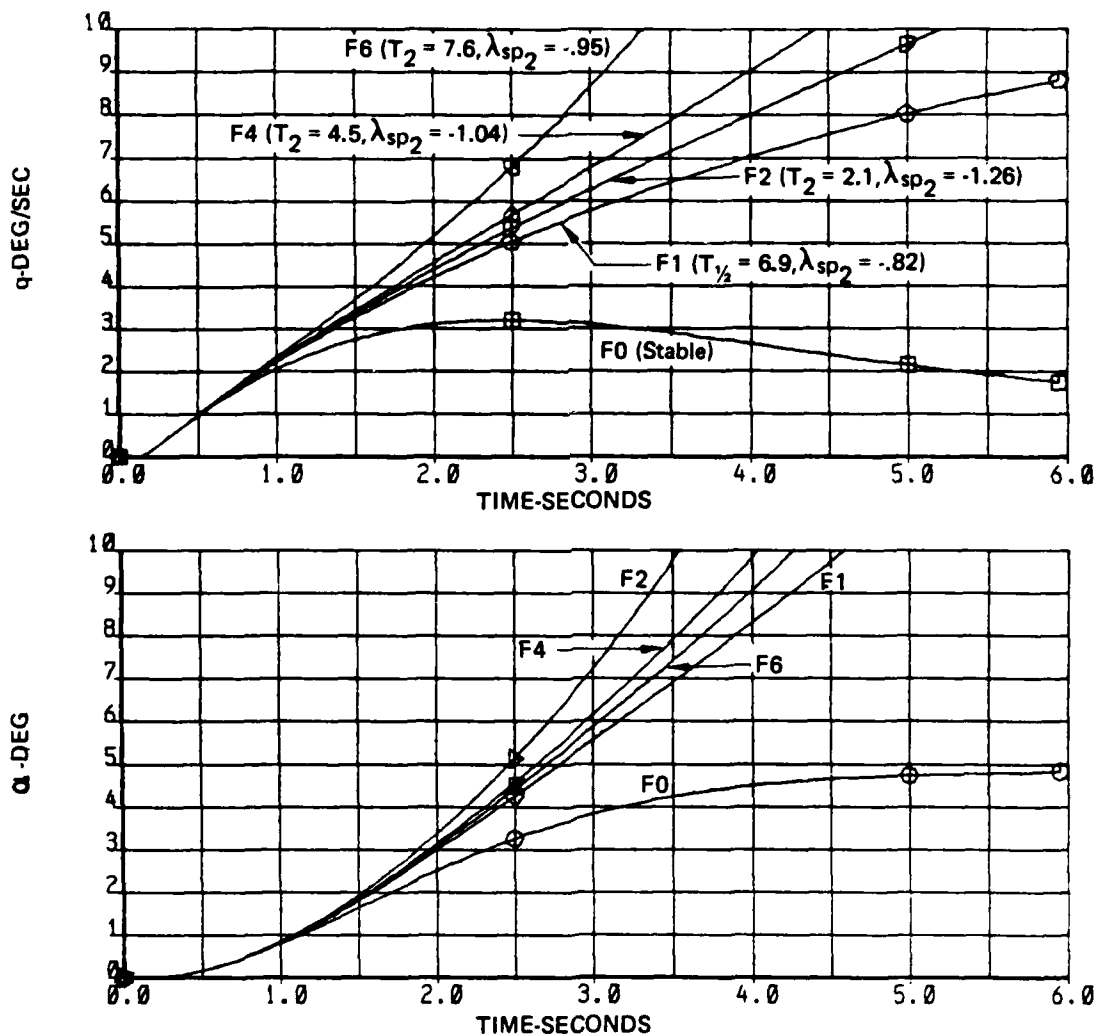$\delta_{hc} = -2$ deg. step at t = 0.1 sec
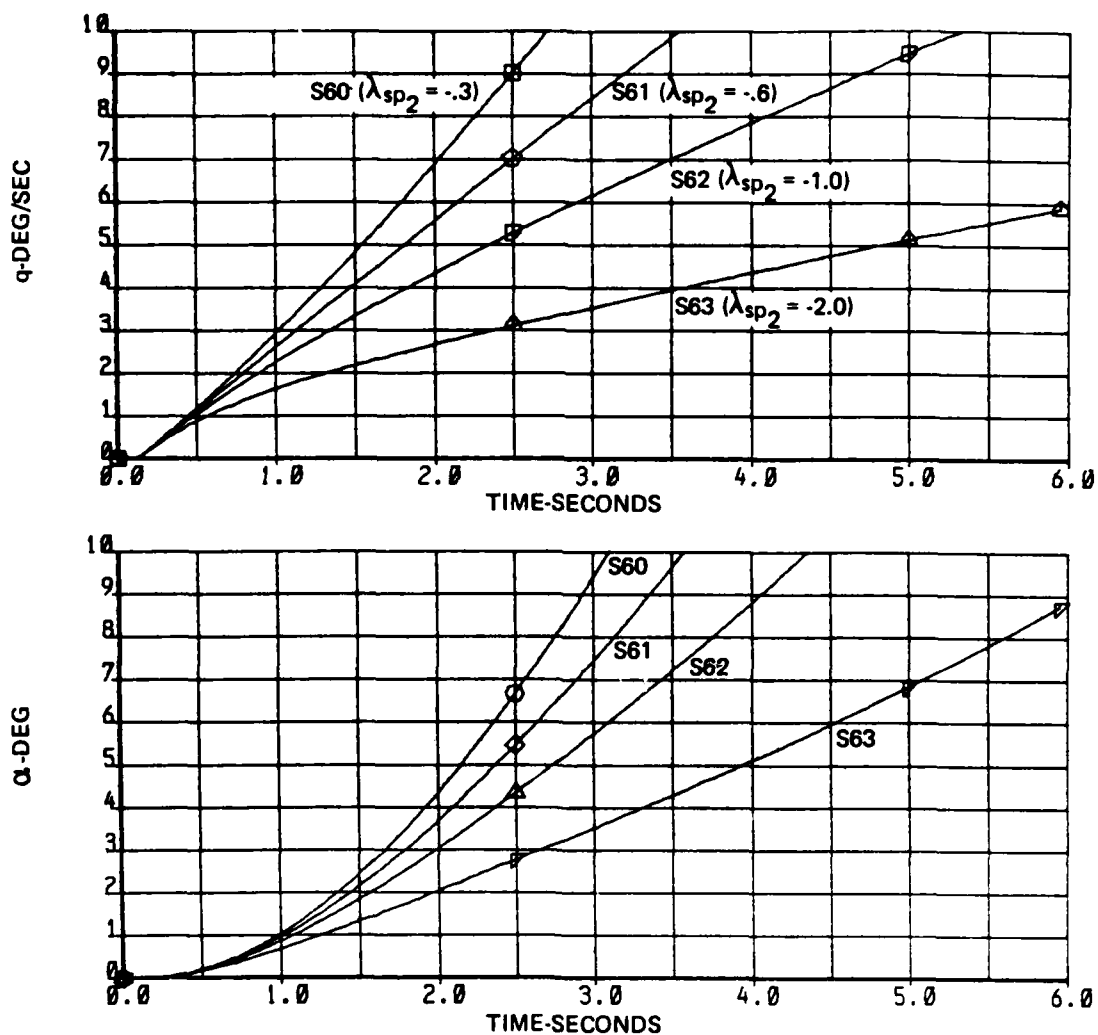
$\dot{q}_{0.1+} = .0416$ rad/sec^2

Figure C-24.   Time History for Step δ_h Command — Configuration S60, S61, S62, S63

(a) α and q

328

$M\delta_{ES}$	T_2	λ_{sp_2}	Z_{θ_2}
rad/sec^2/in	sec	rad/sec	rad/sec
.341	6.0	Varies	-.58

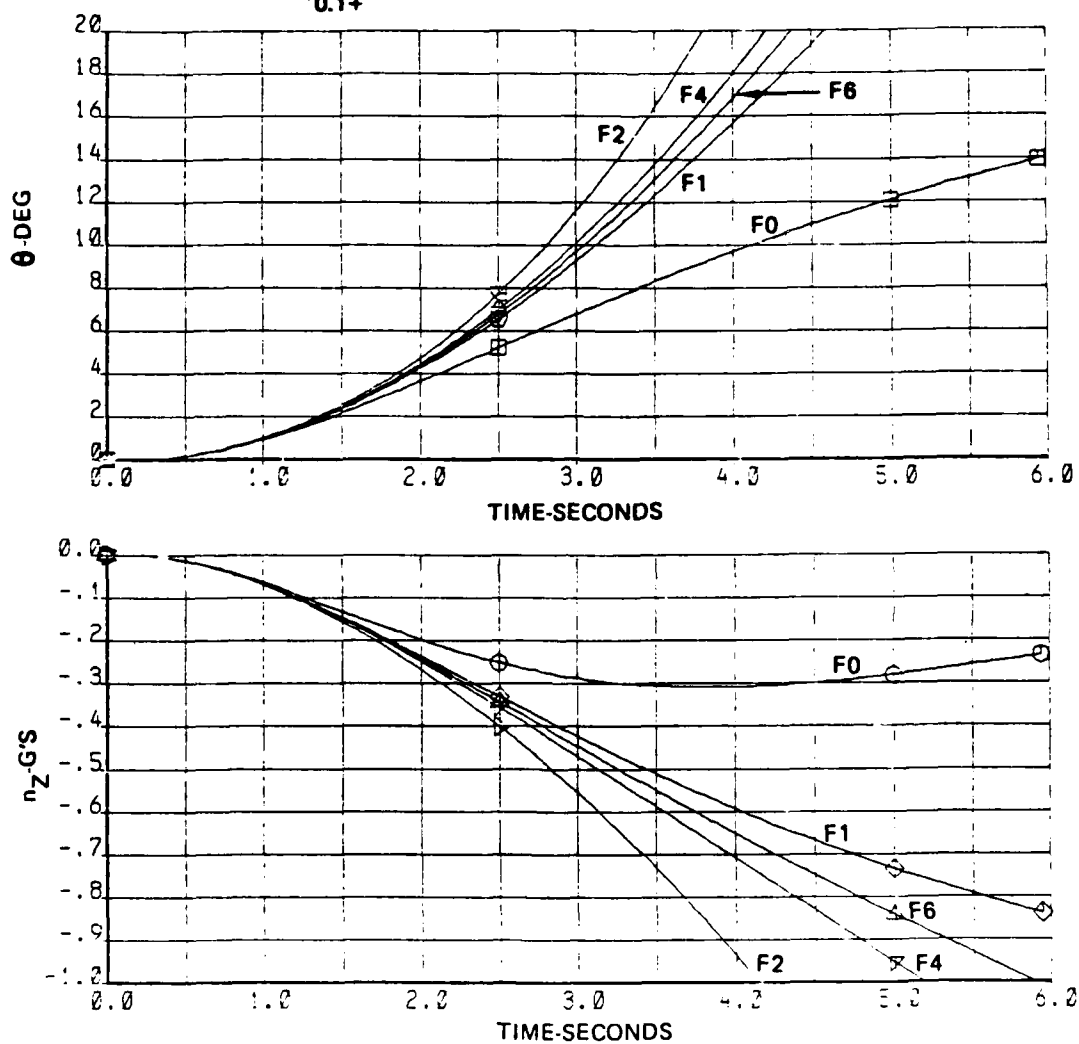δ_{hc} = -2 deg. step at t = 0.1 sec

$\dot{q}_{0.1+}$ = .0416 rad/sec^2

Figure C-24. Time History for Step δ_h Command – Configuration S60, S61, S62, S63 – Continued

(b) θ and n_z

329

$M_{\delta_{ES}}$	T_2	λ_{sp_2}	Z_{θ_2}
rad/sec^2/in	sec	rad/sec	rad/sec
.341	6.0	Varies	-.58

$\delta_{hc} = -2$ deg. step at $t = 0.1$ sec

$\dot{q}_{0.1+} = .0416$ rad/sec^2
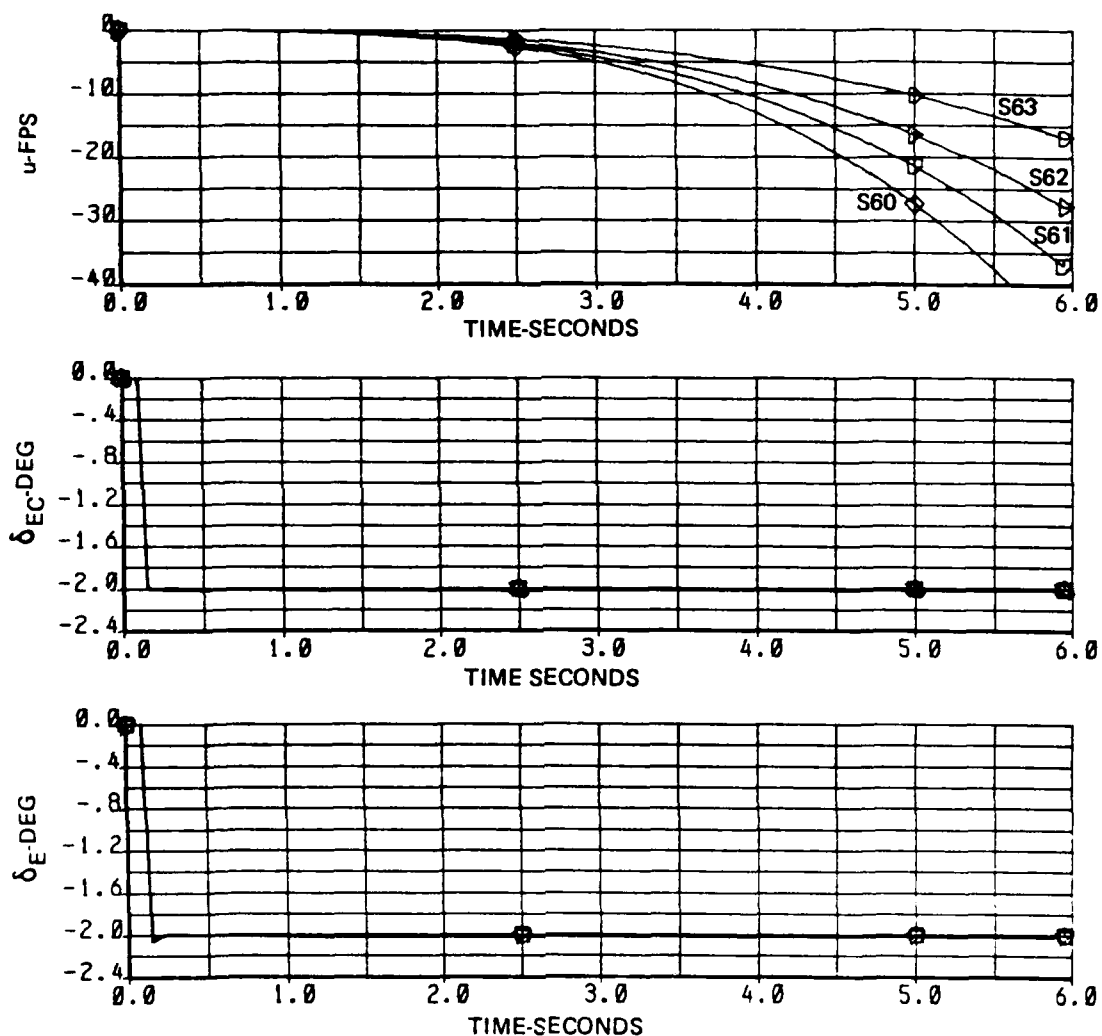
Figure C-24.   Time History for Step δ_h Command — Configuration S60, S61, S62, S63 — Concluded

(c) δ_E, δ_{EC}, and u

330

Note: $\theta/F_s = 1.143 \left(\dfrac{\delta_h}{\delta_{ES}} \right) \theta'/F_s$ rad/lb

$\dfrac{\delta_h}{\delta_{ES}} = -13.12/57.3$ rad/in

θ'/F_s
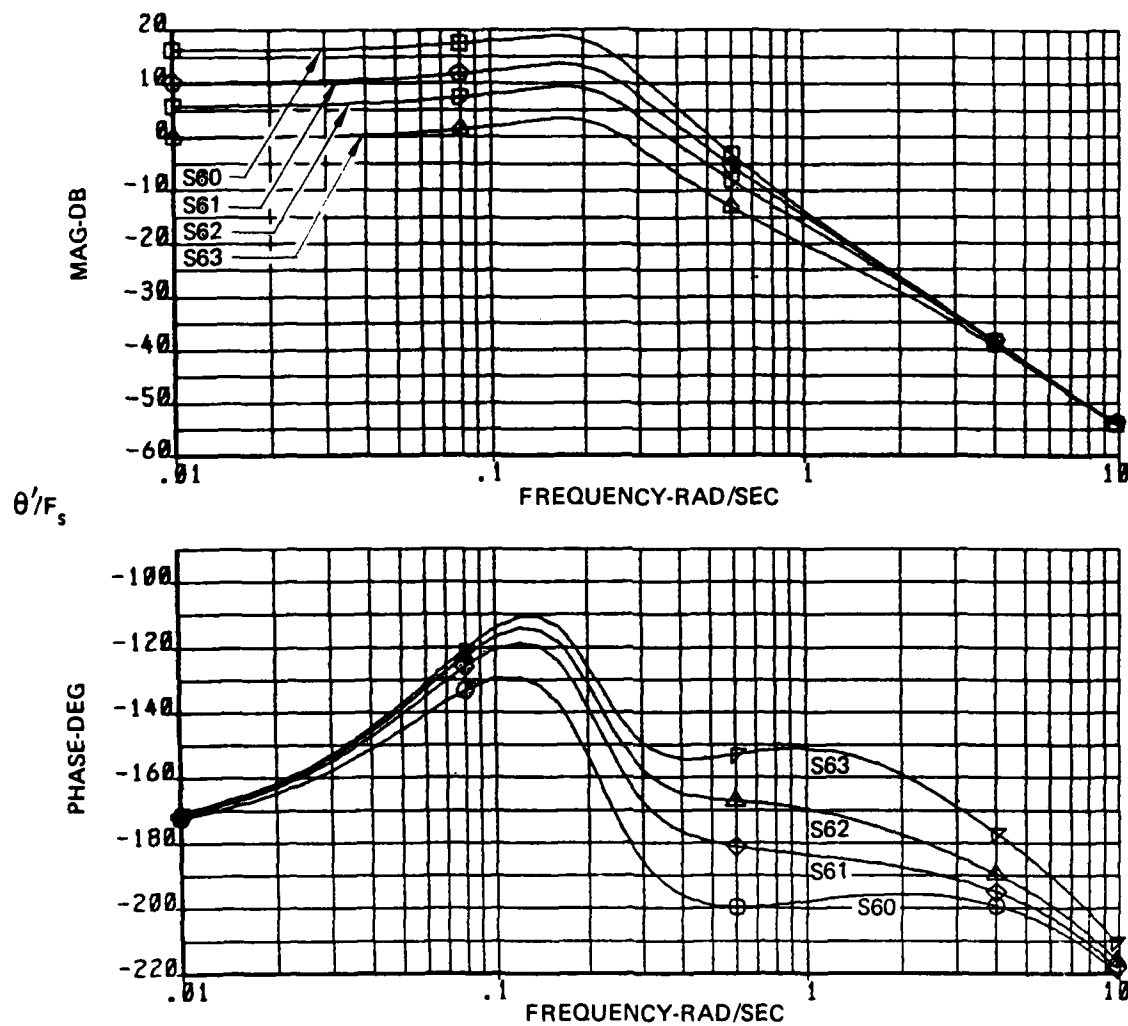
Figure C-25. Frequency Response of θ/F_s — Configuration S60, S61, S62, S63

331

$M_{\delta_{ES}}$	T_2	λ_{sp_2}	Z_{θ_2}
rad/sec^2/in	sec	rad/sec	rad/sec
.341	2.0	-2.0	Varies

δ_{hc} = -2 deg. step at t = 0.1 sec
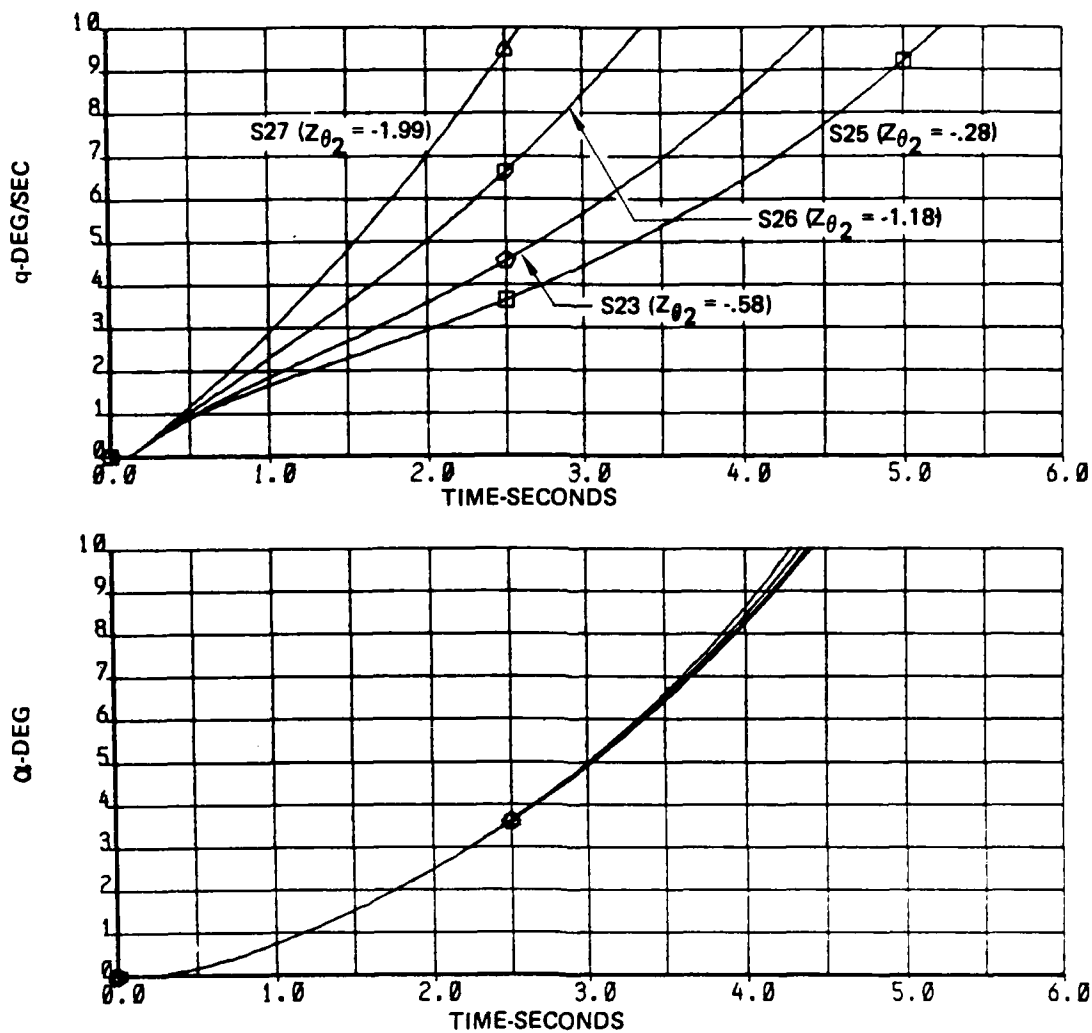
$\dot{q}_{0.1+}$ = .0416 rad/sec^2

Figure C-26.   Time History for Step δ_h Command — Configuration S23, S25, S26, S27

(a) α and q

332

$M_{\delta_{ES}}$	τ_2	λ_{sp_2}	Z_{θ_2}
rad/sec²/in	sec	rad/sec	rad/sec
.341	2.0	-2.0	Varies

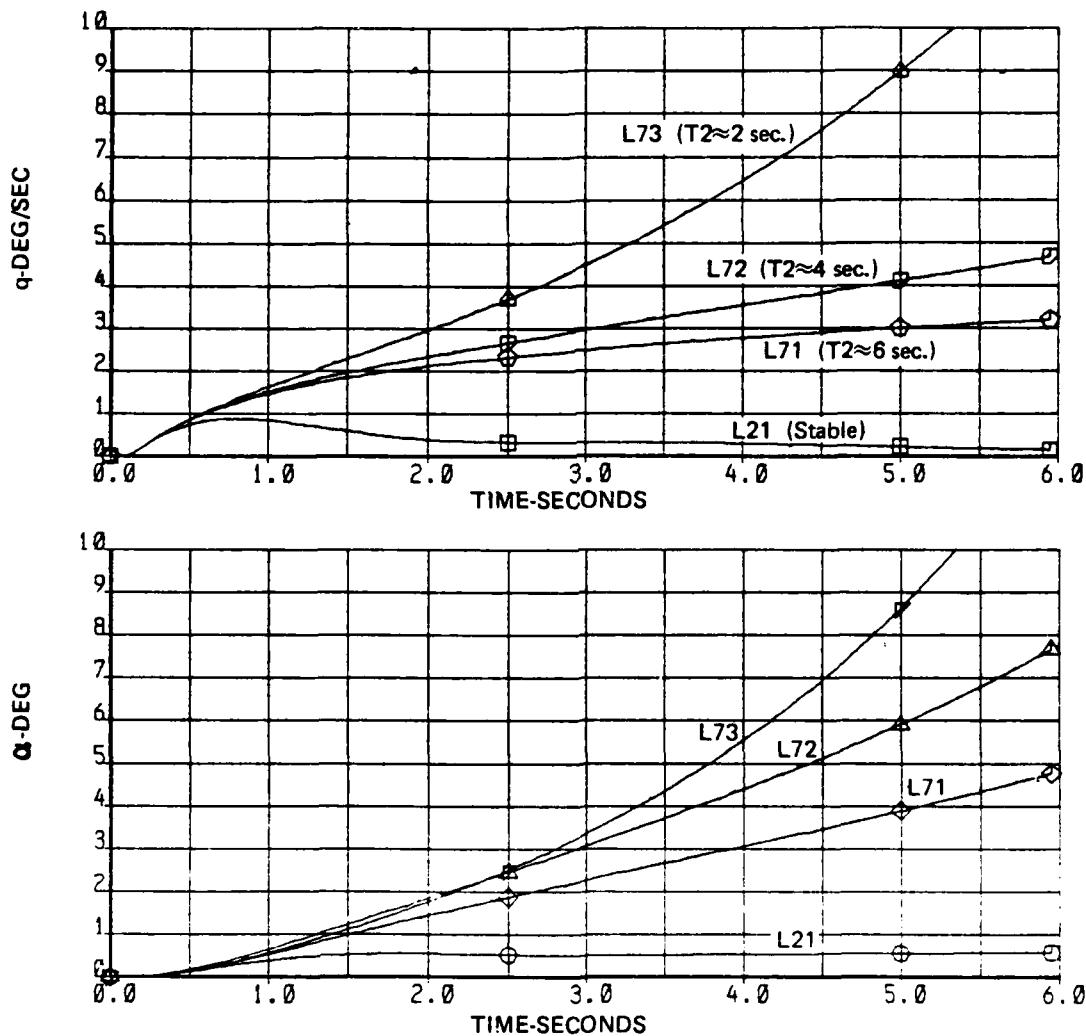δ_{hc} = -2 deg. step at t = 0.1 sec

$\dot{q}_{0.1+}$ = .0416 rad/sec²

Figure C-26. Time History for Step δ_h Command — Configuration S23, S25, S26, S27, — Continued

(b) θ and n_z

333

$M_{\delta_{ES}}$	T_2	λ_{sp_2}	Z_{θ_2}
rad/sec^2/in	sec	rad/sec	rad/sec
.341	2.0	-2.0	Varies

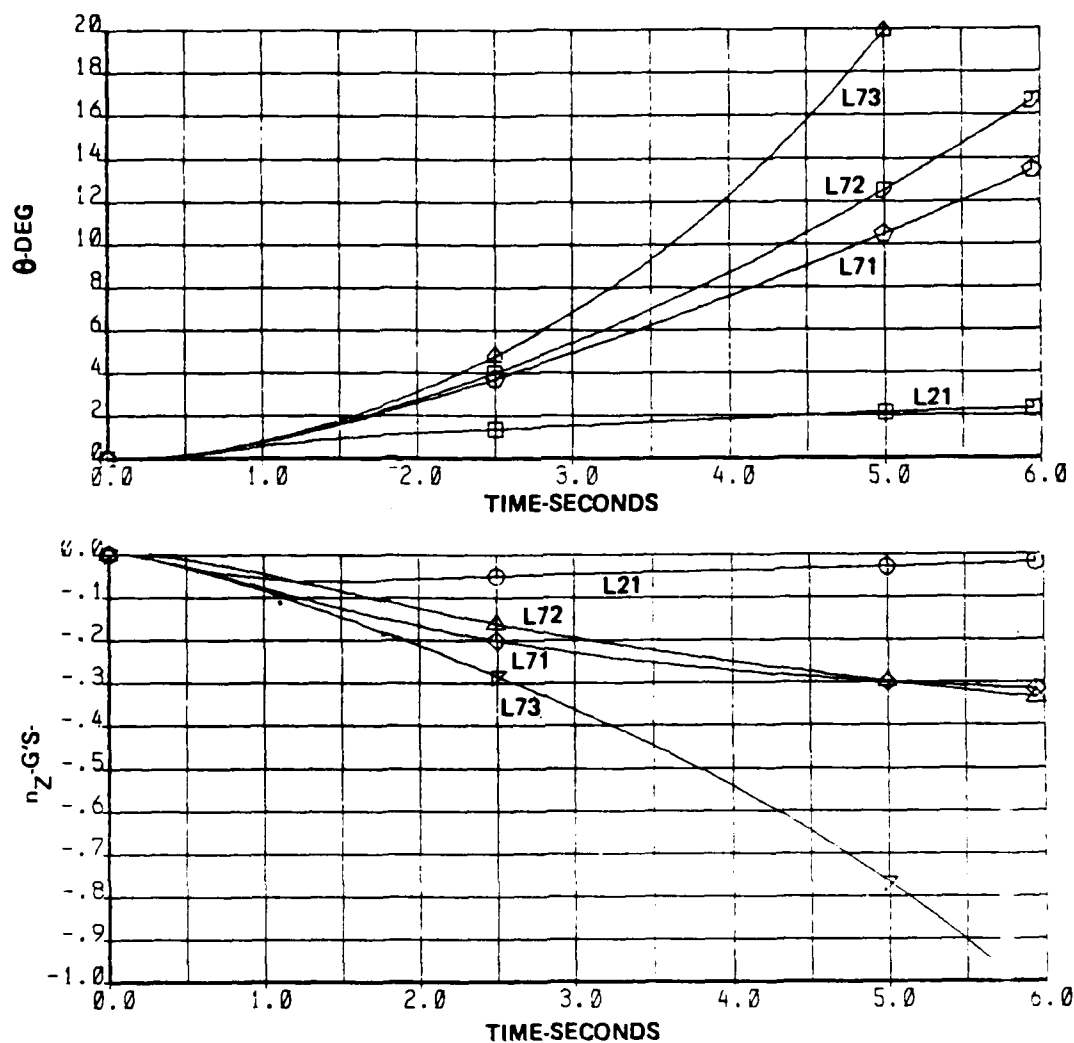δ_{hc} = -2 deg. step at t = 0.1 sec

$\dot{q}_{0.1+}$ = .0416 rad/sec^2

u-FPS

S25

S26   S23

S27

TIME-SECONDS

δ_{EC}-DEG

TIME-SECONDS

δ_E-DEG

TIME-SECONDS
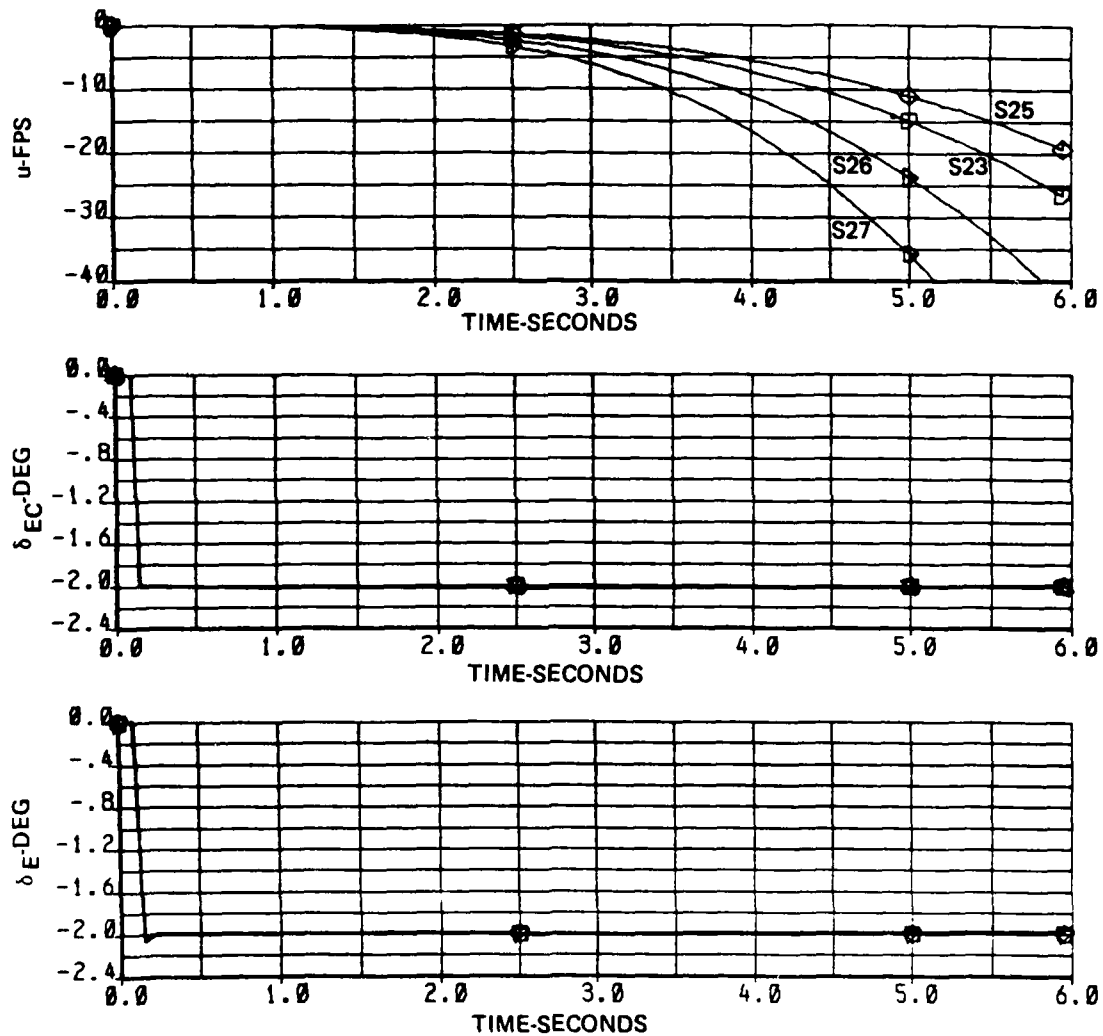
Figure C-26.   Time History for Step δ_h Command — Configuation S23, S25, S26, S27 — Concluded

(c) δ_E, δ_{EC}, and u

334

Note: $\theta/F_s = 1.143 \left(\dfrac{\delta_h}{\delta_{ES}} \right) \theta'/F_s$ rad/lb

$\dfrac{\delta_h}{\delta_{ES}} = -13.12/57.3$ rad/in
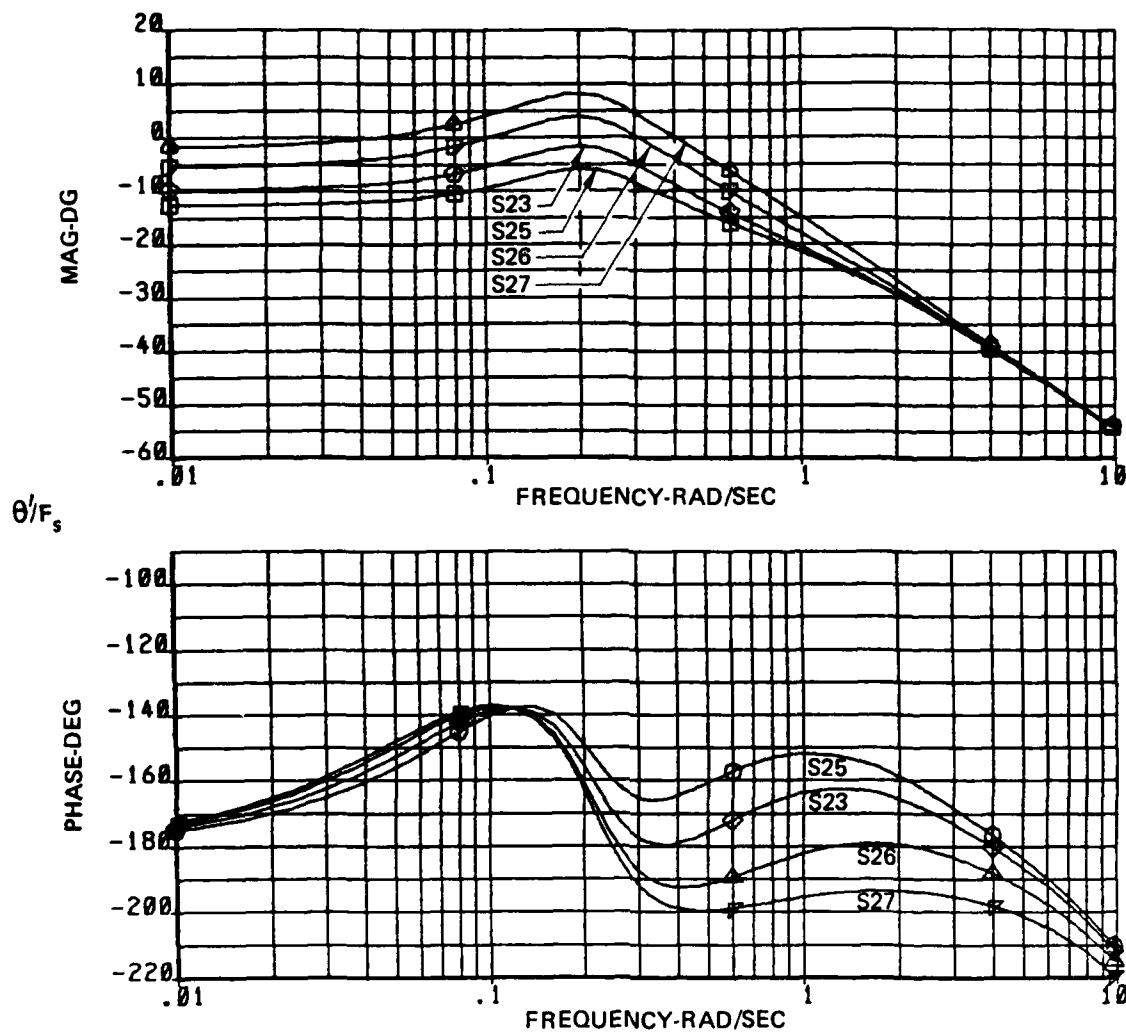
Figure C-27.   Frequency Response of θ/F_s — Configuration S23, S25, S26, S27

335

$M_{\delta_{ES}}$	T_2	λ_{sp_2}	Z_{θ_2}
rad/sec^2/in	sec	rad/sec	rad/sec
.341	~4.0	-1.01	Varies

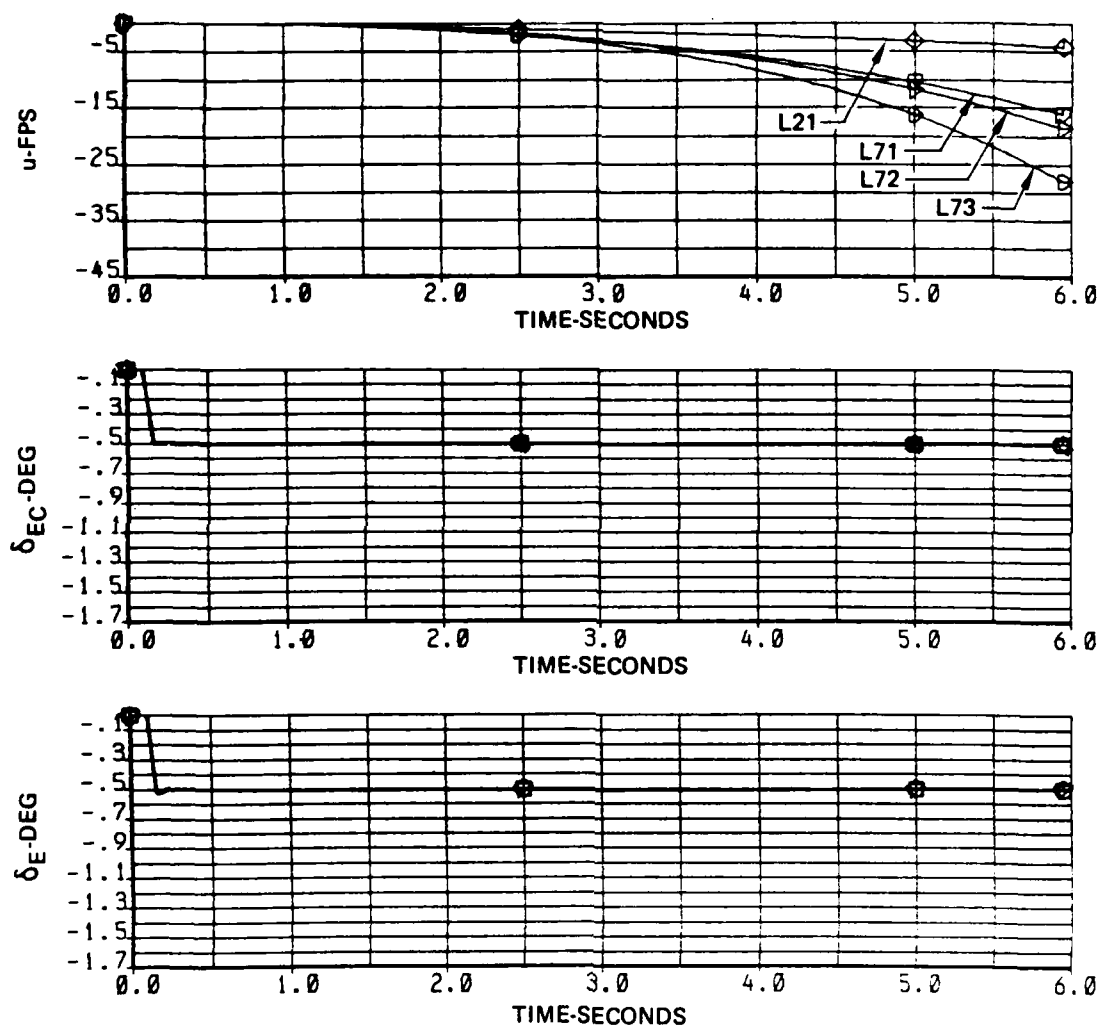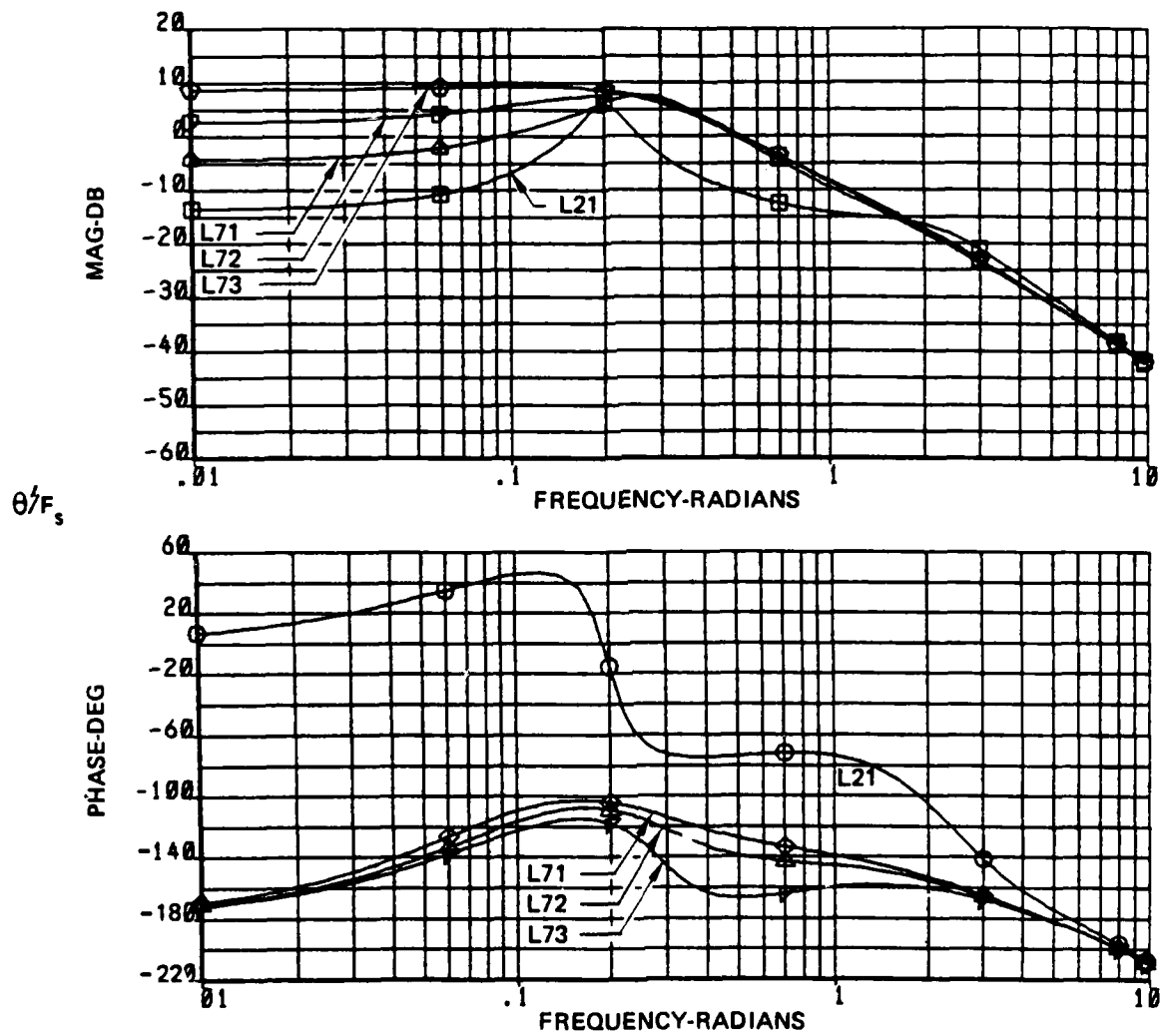δ_{hc} = -2 deg. step at t = 0.1 sec

$\dot{q}_{0.1+}$ = .0416 rad/sec^2

Figure C-28.   Time History for Step δ_h Command — Configuarion S42, S45, S46

(a) α and q

336

$M_{\delta_{ES}}$	T_2	λ_{sp_2}	Z_{θ_2}
rad/sec²/in	sec	rad/sec	rad/sec
.341	~4.0	-1.01	Varies
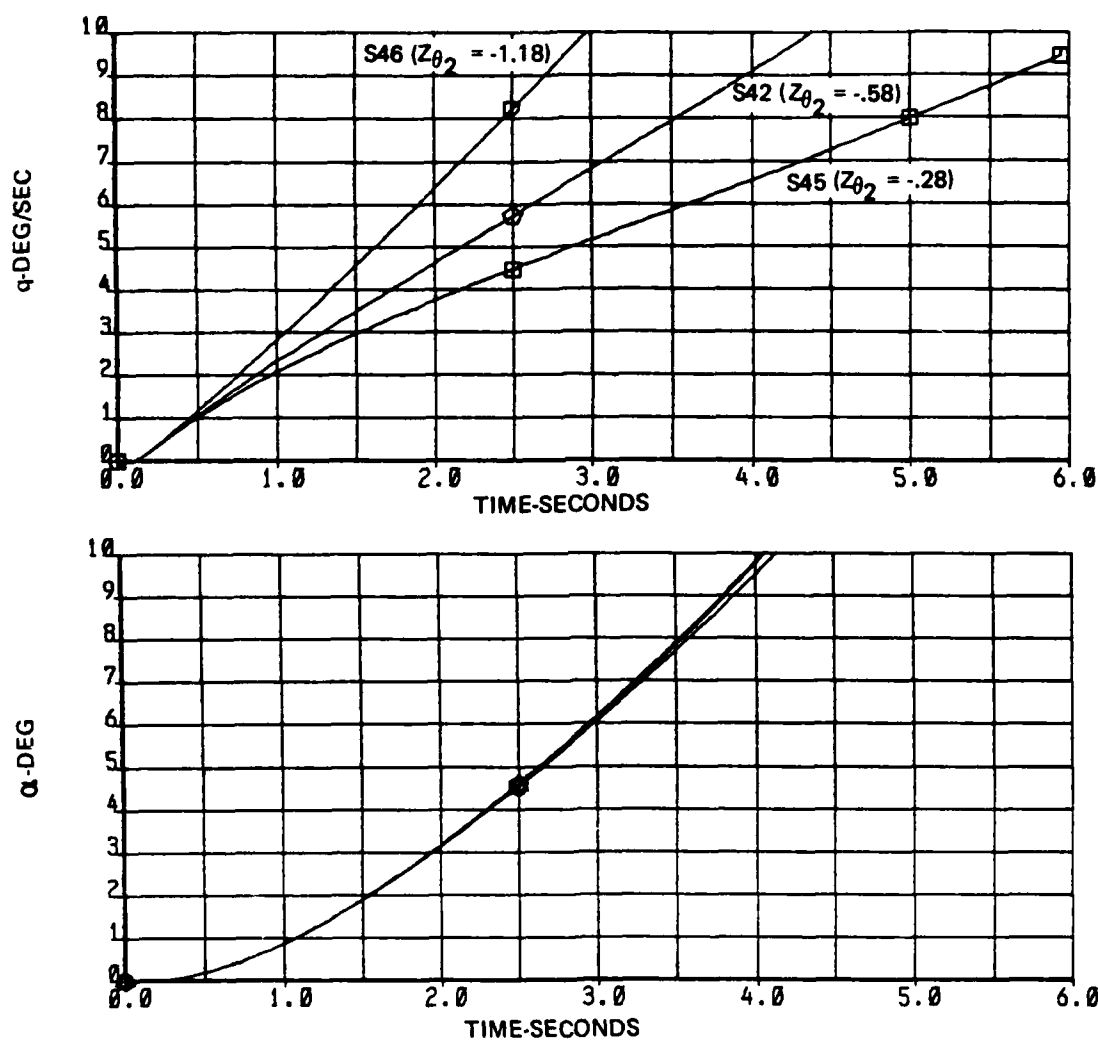
δ_{hc} = -2 deg. step at t = 0.1 sec

$\dot{q}_{0.1+}$ = .0416 rad/sec²

Figure C-28. Time History for Step δ_h Command — Configuration S42, S45, S46 — Continued

(b) θ and n_z

337

$M_{\delta_{ES}}$	T_2	λ_{sp_2}	Z_{θ_2}
rad/sec^2/in	sec	rad/sec	rad/sec
.341	~4.0	-1.01	Varies

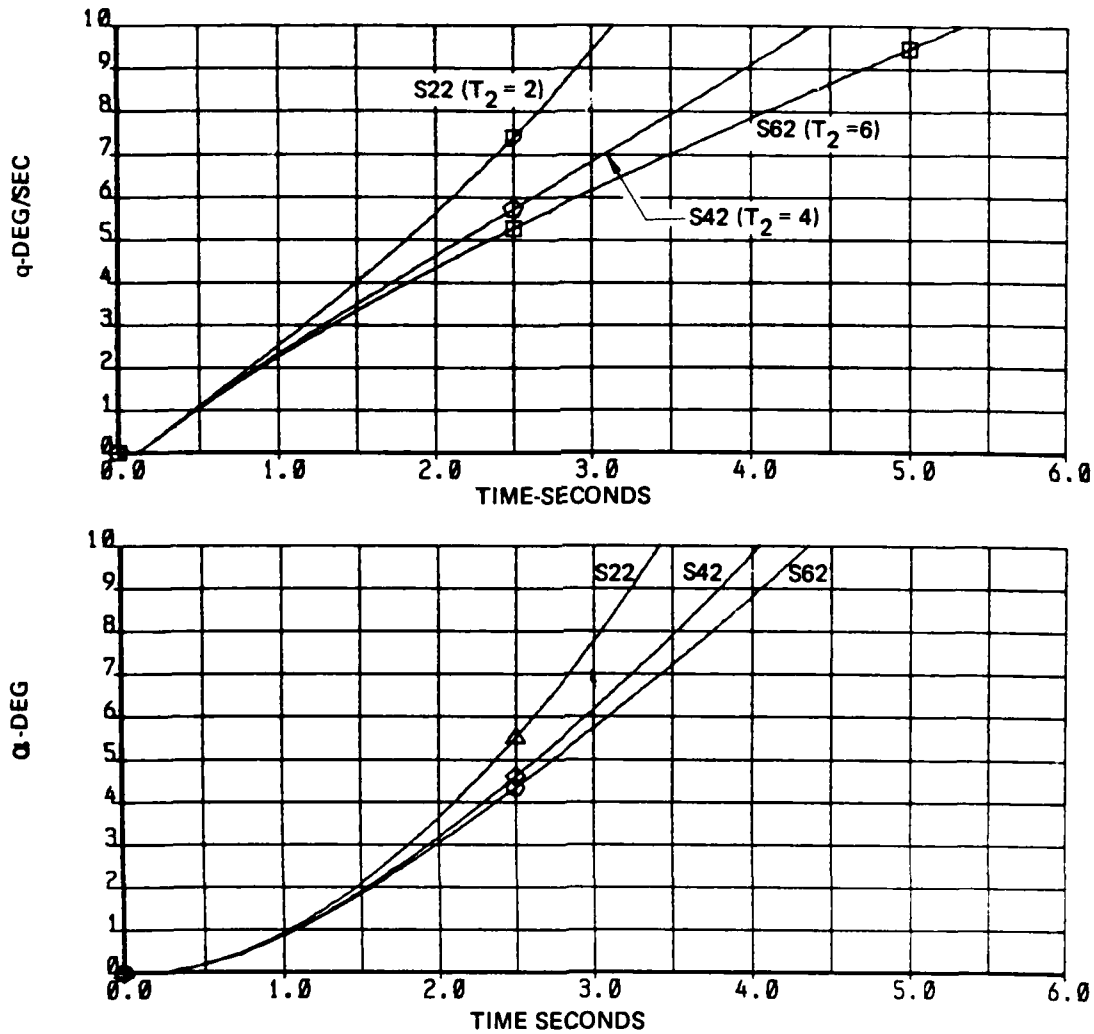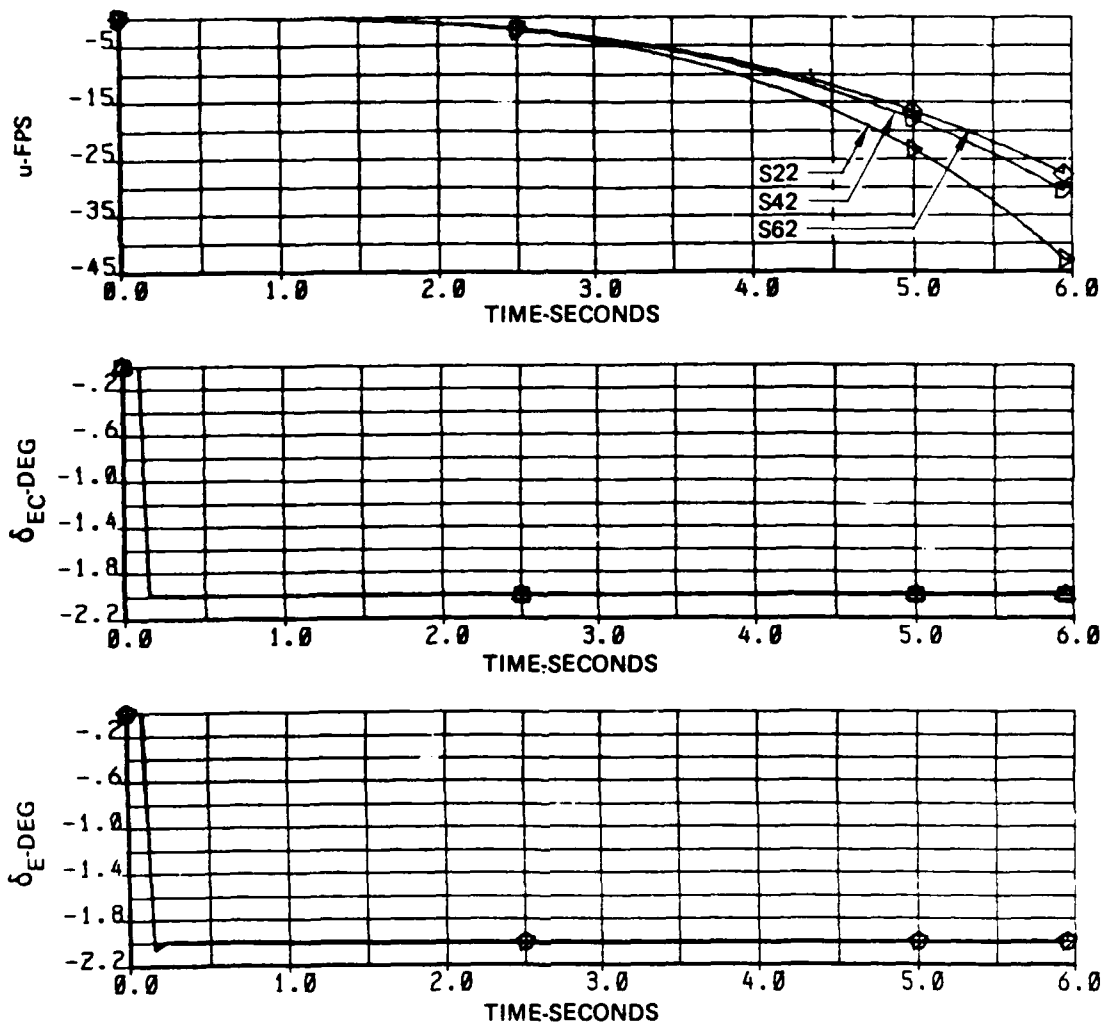δ_{hc} = -2 deg. step at t = 0.1 sec

$\dot{q}_{0.1+}$ = .0416 rad/sec^2
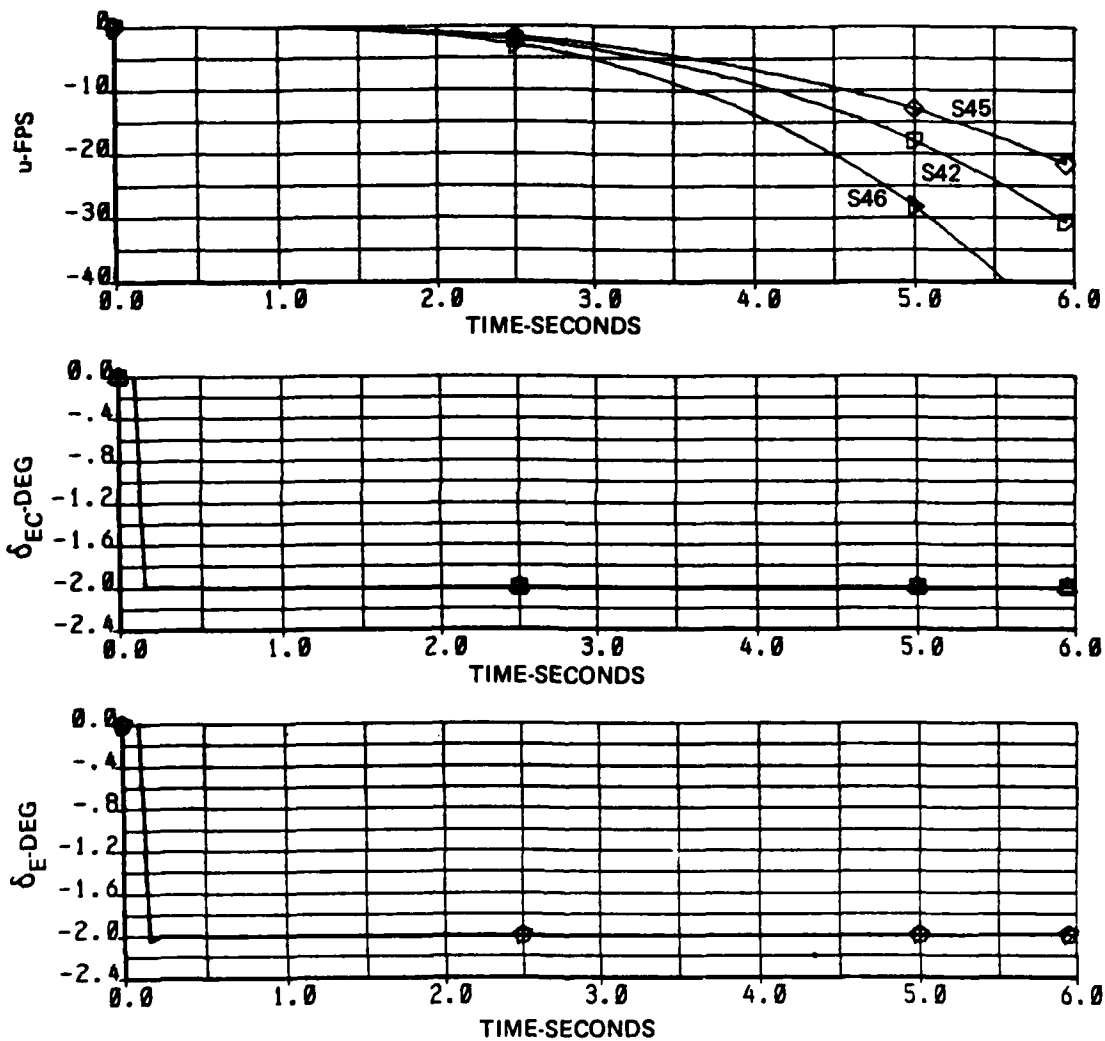
Figure C-28. Time History for Step δ_h Command — Configuration S42, S45, S46 — Concluded

(c) δ_E, δ_{EC}, and u

338

Note: $\theta/F_s = 1.143 \left(\dfrac{\delta_h}{\delta_{ES}} \right) \theta'/F_s$ rad/lb

$\dfrac{\delta_h}{\delta_{ES}} = -13.12/57.3$ rad/in

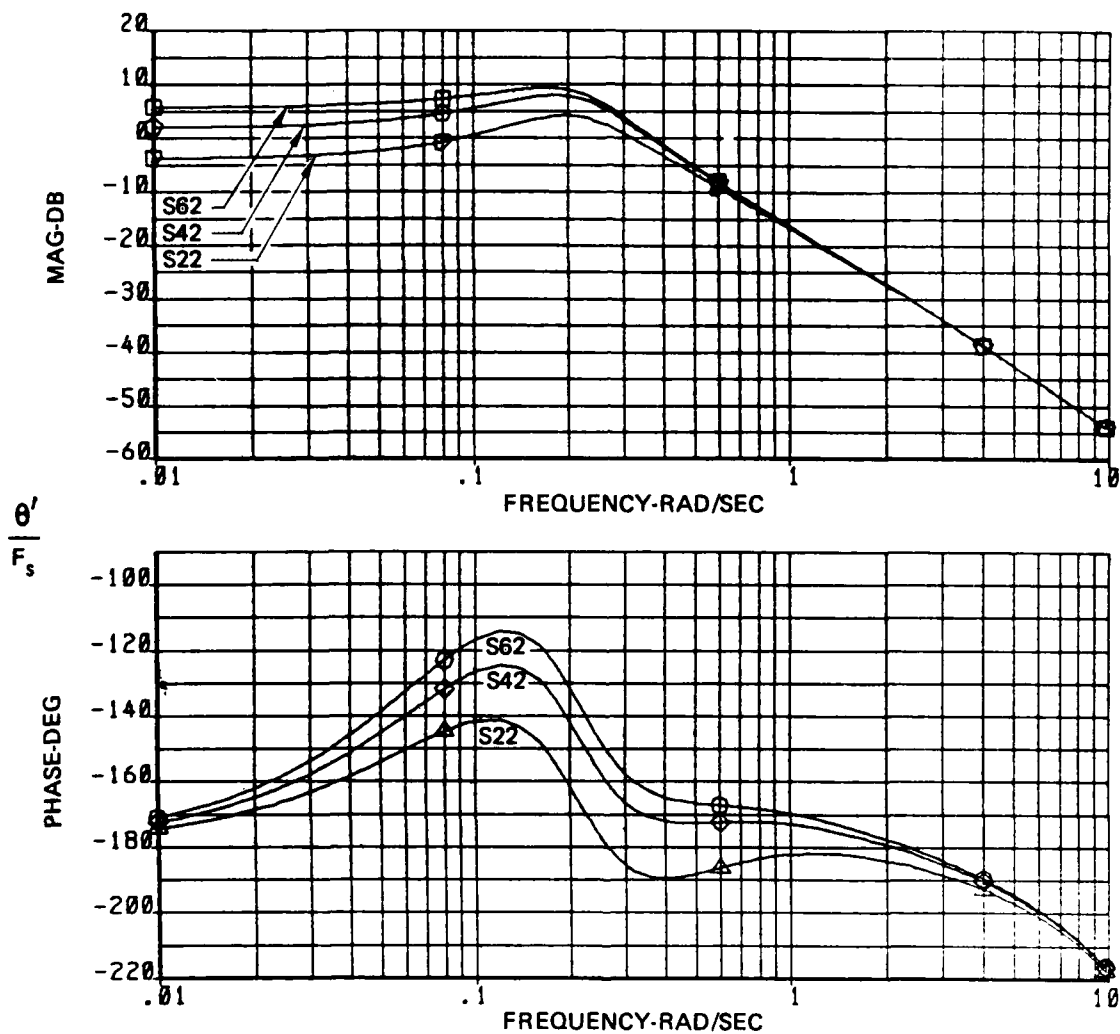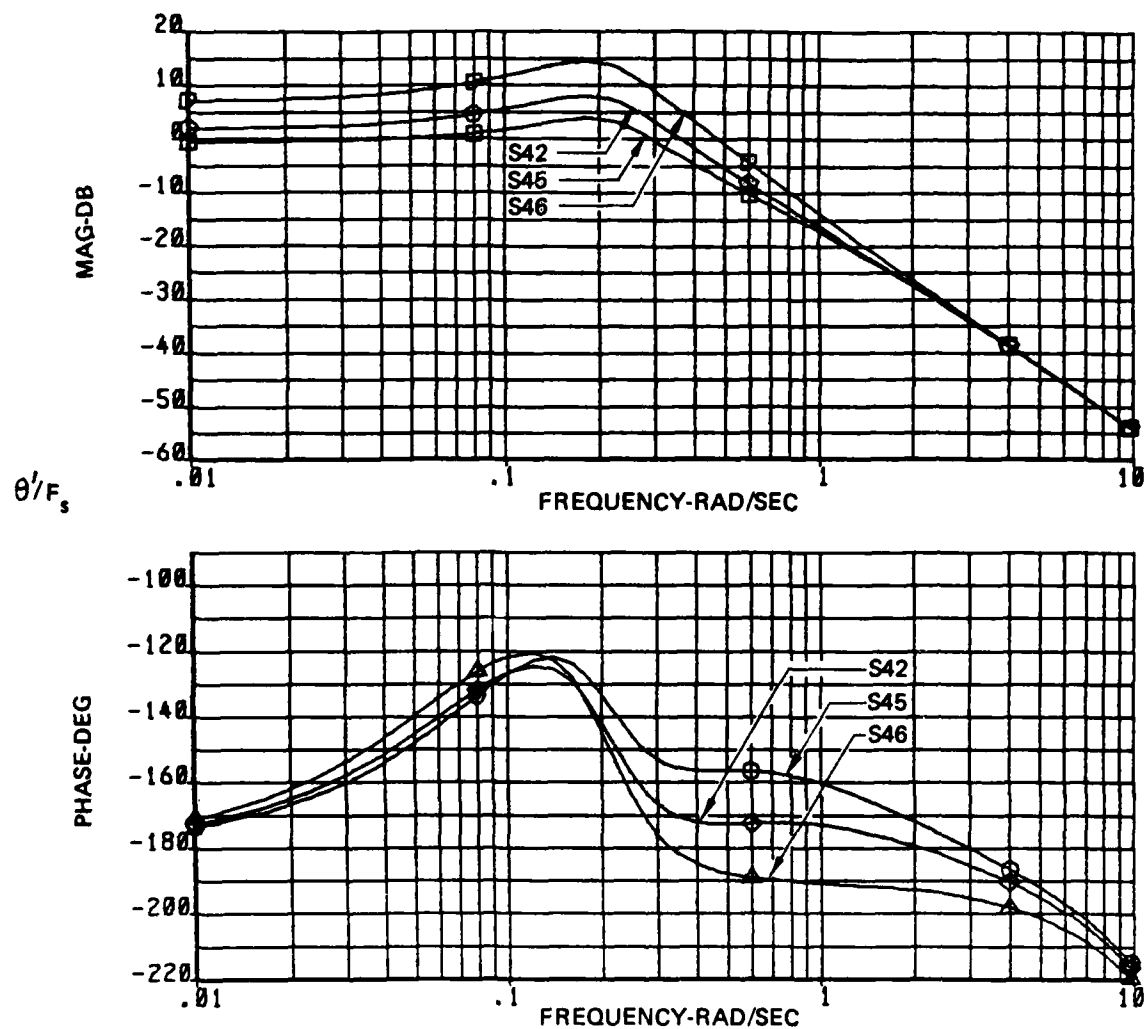Figure C-29. Frequency Response of θ/F_s — Configuration S42, S45, S46

C.5 Simulation Data

C.5.1 Pilot Rating Data

All pilot ratings for every evaluation configuration flown in the simulation program are given in this section in Table C-9. The configuration identifiers are defined in B.4.1.1 and their primary and secondary characteristics are described in B.4.1.2 through B.4.1.4 and are also summarized in Table C-4 of C.4. The configurations are fully defined by Table C-5 in C.4.1. The experience and background of the three evaluation pilots (A, R, and T), who were all Boeing test pilots, are given in B.4.5. The evaluation tasks (A through D) are described in B.4.2. The Cooper-Harper pilot rating scale, re-interpreted slightly, was used to obtain quantitative data. The basis for the ratings and the quantitative performance measures used by the pilots in assigning a pilot rating are given in B.4.3. The run number is composed of the date followed by the daily run number, and their are a very few run numbers that are the same except for the pilot.

Three different sets of pilot ratings are found in the data in Table C-9, with the alpha-numerics in each defined as follows.

x/y/N (used primarily in '79 simulation program)

- x - pilot rating for ILS portion of task
- y - pilot rating for visual portion of task (below 200 ft. altitude) including flare and touchdown
- N - denotes "not applicable" and is included to more clearly identify this set.

x/y/z (used in '80 simulation program)

- x - pilot rating for ILS portion of task (same as above)
- y - pilot rating for visual portion of approach but excluding flare and touchdown
- z - pilot rating for flare and touchdown only.

w/x/y/z (used for D run only)

- w – Pilot rating for inbound and glide-slope acquisition portions of ILS approach task, flown in smooth air, down to 900 ft. altitude
- x – pilot rating for final portion of ILS approach task, flown in moderate turbulence, below 900 ft. altitude (same as x in x/y/z for Run B)
- y – pilot rating for visual portion of approach excluding flare and touchdown (same as y in x/y/z for B run)
- z – pilot rating for flare and touchdown only (same as z in x/y/z for B run)

The first set of data (x/y/N) used the earlier evaluation card while the second set of data (x/y/z) used the later evaluation card, as described in section B.4.3, for Runs A, B, and C as described in section B.4.2. The third set of data (w,x,y,z) was from the evaluations performed with varying elevator (horizontal tail) rate limit, and applies only to Run D which, as defined and explained in section B.4.2, replaced Runs A and B in these evaluations.

Ratings for the position and rate control authority variations are found at the end of Table C-9.

TABLE C-9
PILOT RATINGS

CONF	PILOT	TASK			RUN NO.	$\delta_{h_{LIM}}$ deg
		A	B	C		
F0	A	4/4/3	4/4/4	5/4/5	5/5/80-63	-25/15
F0	R	4/3.5/3.5	4.5/4/4	5/5/5	5/2/80-63	-25/15
F0	T	3/3/N	3/3/N	3/3/N	11/12/79-9	-25/15
F0	T	4/4/N	4/4/N	5/5/N	11/14/79-16	-25/10
F1	A	5/6/N	6/8/N	6/8/N	10/31/79-16	-25/10
F1	A	4/4/N	4/5/N	4/5/N	10/31/79-16A	-25/10
F1	A	4/5/N	5.5/7/N	6/6/N	4/19/80-54	-25/10
F1	A	3.5/2.5/N	4/7/N	4/5/N	11/5/79-23	-25/10
F1	R	4/4.5/N	4.5/8/N	4.5/8/N	10/12/79-15	-25/10
F1	R	4/6/N	5/6.5/N	6/7/N	4/19/80-57	-25/15
F1	R	6/8/N	7/8/N		4/18/80-54	-25/10
F1	R	5/5.5/N	5.5/6/N	5.5/5.5/N	4/19/80-58	-25/20
F1	T	4/4/N	4/4/N	5/5/N	11/12/79-6	-25/10
F1	T	5/5/N	5/6/N	5/6/N	11/12/79-10	-25/10
F1	T	4/4/N	4/5/N	4/5/N	11/14/79-14	-25/10
F1	T	2.5/2.5/2.5	3/3/3	4/5/5	5/8/80-55	-30/20
F1	T	3/4/4	4/4/4	7/10/10	5/8/80-51	-30/20
F2	A	9/9/N	9/10/N	9/10/N	10/31/79-17	-25/10
F2	A	6/5/N	6/7.5/N	7/8/N	11/5/79-24	-25/10
F2	A	5/7/N	6/6/N	6/7/N	11/5/79-25	-25/15
F2	A	7/7/7	7/8/9	8/9/9	5/5/80-75	-25/15
F2	A	8/8/8	9/9/9	9/9/9	5/5/80-77	-30/28
F2	R	8/8.5/N	8.5/8.5/N	9/9/N	10/23/79-2	-25/10
F2	R	8/8.5/N	8.5/10/N	8.5/10/N	10/12/79-20	-25/10
F2	T	6/6/N	8/10/N	9/10/N	11/12/79-7	-25/15
F2	T	6/6/N	6/6/N	6/10/N	11/14/79-18	-25/10
F2	T	5/5/5	6/6/6	7/9/9	5/8/80-53	-30/20
F4	A	5/5/N	6/6/N	6/7/N	10/31/79-18	-25/10
F4	A	5/5.5/6	6/6/7	6/6/7	5/6/80-81	-30/20
F4	A	5/6/7	5/6/8	6/7/9	5/5/80-76	-25/15
F4	A	6/6/6	7/9/10	7/9/10	5/5/80-64	-25/15

342

TABLE C-9
PILOT RATINGS

CONF	PILOT	TASK			RUN NO.	$\delta_{h_{LIM}}$ deg
		A	B	C		
F4	A	5/6/N	6/8/N	6/9/N	4/19/80-55	-25/10
F4	A	5/6/N	5/6/N	5/7/N	4/19/80-56	-25/15
F4	R	7/8/N	7/8/N	8/8/N	10/23/79-1	-25/10
F4	R	7/7/N	7/8/N	7/8/N	10/12/79-19	-25/10
F4	R	7/7/8	8/8/9	8/8/9	5/2/80-64	-25/15
F4	R	7/7/7	7.5/7.5/8	8/8/9	5/8/80-98	-30/20
F4	R	6/6/N	6.5/7.5/N	6.5/8/N	4/19/80-59	-25/20
F4	T	4/4/N	4/4/N	5/8/N	11/12/79-8	-25/15
F4	T	5/6/N	6/7/N	7/9/N	11/14/79-15	-25/10
F4	T	4/4/4	5/5/5	7/9/9	5/8/80-52	-30/20
F6	A	6/6/N	6/6/N	6/6/N	10/31/79-19	-25/10
F6	A	6/6/6	6/6/7	6/6.5/8	5/5/80-74	-25/15
F6	R	7/7/N	7.5/8/N	7.5/8/N	10/23/79-18	-25/10
F6	T	4/5/N	5/5/N	8/10/N	11/12/79-5	-25/10
F6	T	5/5/N	5/5/N	5/6/N	11/14/79-17	-25/10
F6	T	4/4/4	5/5/5	5/5/6	5/8/80-54	-30/20
L21	A	3/3/3	4/5/5	5/5/5	5/5/80-65	-25/15
L21	A	3/3/3	4/3.5/3	5/5/4	5/5/80-73	-25/15
L21	R	2/2/2	3/3.5/3.5	4/4/5	5/2/80-66	-25/15
L21	T	1.5/1.5/1.5	3/3/3	5/6/6	5/8/80-56	-30/20
L71	A	4/3.5/3	4/3/3	5/4/4	5/5/80-68	-25/15
L71	R	4/3.5/3.5	5/4/5	6.5/6/6	5/2/80-68	-25/15
L71	T	4/4/4	4/4/4	5/5/5	5/8/80-57	-30/20
L72	A	4/4/4	5/5/5	5/5/5	5/5/80-69	-25/15
L72	R	6/5/5	6/5.5/5.5	6/5.5/5.5	5/2/80-69	-25/15
L72	T	3/3/3	3/4/4	3/4/4	5/8/80-58	-30/20
L73	A	5/4/4	6/5/5	6/5/5	5/5/80-66&66R	-25/15
L73	A	5/4/4	6/6/6.5	6/6.5/6	5/5/80-70&72	-30/20
L73	R	7/6/7	7.5/7/7	8/8/8	5/2/80-70	-30/20
L73	T	3/3/3	4/4/4	5/5/5	5/8/80-59	-30/20

343

TABLE C-9
PILOT RATINGS

CONF	PILOT	TASK A	TASK B	TASK C	RUN NO.	δh_{LIM} deg
S21	A	7/6/6	8/8/8	8/8/8	5/9/80-102	-30/20
S21	R	7/7/7.5	8/8/8	8/8/8.5	5/9/80-102	-30/20
S22	R	7.5/7.5/7.5	8.5/7.5/7.5	8.5/8/8	5/9/80-108	-30/20
S23	A	3/3.5/3.5	5/5/5	6/6.5/6.5	5/9/80-101	-30/20
S23	R	5.5/6/6	6/6/6	6/6.5/6.5	5/9/80-101	-30/20
S24	R	5/5/5	5.5/6/6	5.5/6/6	5/9/80-107	-30/20
S25	A	5/4/4	5/4/4	6.5/6/6	5/9/80-109	-30/20
S26	A	4/4/4	5/5/5.5	6/6/6.5	5/9/80-110	-30/20
S26	R	7.5/7.5/7.5	8.5/8/8	8.5/8.5/8.5	5/9/80-110	-30/20
S27	A	8/7/7	8/8/9	8/9/10	5/9/80-111	-30/20
S41	A	6/6/6	7/6/6	7/7/7	5/7/80-94	-30/20
S41	R	7/7/7.5	8/8/8.5	8/8/8.5	5/8/80-94	-30/20
S42	A	6/5/5	6/5/5	7/6/6	5/7/80-91	-30/20
S42	R	5/5/5.5	6/6/6.5	6/6/6.5	5/8/80-91	-30/20
S43	A	4/4/4	5/5/5	5/5/5	5/7/80-92	-30/20
S43	R	5/5/5	5.5/5.5/6	6/6/6	5/8/80-92	-30/20
S44	A	3/4/4	4/5/5	5/6/6	5/7/80-93	-30/20
S44	R	5/5/5	5.5/5.5/5.5	5.5/5.5/6	5/8/80-93	-30/20
S45	A	4/3.5/4	5/4/4	5/4/4	5/7/80-96	-30/20
S45	R	5/5/5	6/6/6	6.5/6.5/6.5	5/8/80-96	-30/20
S46	A	6/6/6	6/6/6.5	6/6/6.5	5/7/80-97	-30/20
S46	R	7.5/7.5/8	8/8/9	8/8/9	5/8/80-97	-30/20
S60	A	5/6/6.5	7/6/6	8/6.5/6	5/9/80-105	-30/20
S60	R	8/7/7	8.5/7.5/7.5	8.5/8.5/8.5	5/9/80-105	-30/20
S61	A	4/3/3	4/4/4	5/4/4	5/9/80-106	-30/20
S61	A	4/3/3	4/4/4	5/4/4	5/9/80-106	-30/20
S62	A	5/4/4	5/4/4	5/4/4	5/9/80-104	-30/20
S62	R	5/5/5	6/5.5/5.5	6/6/6	5/9/80-104	-30/20
S63	A	4/4/5	4.5/4.5/5	5/5/6	5/9/80-100	-30/20

344

TABLE C-9
PILOT RATINGS

CONF	PILOT	TASK			RUN NO.	$\delta_{h_{LIM}}$ deg
		A	B	C		
S41A	A	6/5/6	7/7/8	8/7/9	5/6/80-85	-30/20
S41A	R	8/8.5/6.5	8.5/10/10	9/10/10	5/6/80-94	-30/20
S42A	R	6/6.5/8	6/7/8	7/7/8	5/6/80-82	-30/20
S42A	R	6/6.5/8.5	7/7.5/7.5	7/7.5/7.5	5/6/80-91	-30/20
S43A	A	5/5/7	6/7/8.5	7/7/9	5/6/80-83	-30/20
S43A	R	5.5/5.5/5.5	6.5/6.5/6.5	6.5/7/8	5/6/80-92	-30/20
S44A	A	5/5/7	6/6/6	7/6/6	5/6/80-84	-30/20
S44A	R	6.5/6.5/6.5	7.5/8/8	7.5/8.5/9	5/6/80-93	-30/20
S44B	A	5/6/7	5/7/8	7/8/9	5/7/80-95	-30/20
S44B	R	8/8/8.5	8/8/8.5	8/8/9	5/8/80-95	-30/20
S45A	A	5/5/6	6/6/6	7/7/7	5/6/80-86	-30/20
S45A	R	6/6/6	6.5/6.5/7	6.5/6.5/6.5	5/6/80-95	-30/20
S46A	A	6/7/8	7/8/9	7.5/9/10	5/6/80-87	-30/20
S46A	R	9/10/10	9.5/10/10	10/10/10	5/6/80-96	-30/20
AF111-G	A	2/3/N	2/3.5/N	2/3.5/N	10/31/79-14	-25/10
AF111-G	A	2/2/N	2/2/N	2/2/N	4/19/80-51	-25/10
AF111-G	R	2.5/2.5/N	3/3/N	3/3/N	4/18/80-51	-25/10
AF111-F	A	2.5/2.5/N	4/4/N	4/4/N	10/31/79-13	-25/10
AFO	A	2.5/2.5/N	2.5/2.5/N	3/3/N	11/14/79-35	-25/15
AFO	A	3/3/N	3/3/N	3/3/N	10/31/79-15	-25/10
AFO	A	2/2/N	2/2/N	2/2/N	11/5/79-21	-25/10
AFO	A	2/2/N	2/2/N	3/3/N	4/19/80-50	-25/10
AFO	A	2/2/N	2/2.5/N	2/2.5/N	4/19/80-52	-25/10
AFO	A	3/3/3	3/3/4	4/4/5	5/5/80-62	-25/15
AFO	A	1/1/1	3/3/3.5	5/5/5	5/9/80-103	-30/20
AFO	R	2/2/N	2.5/2.5/N	2.5/3/N	10/23/79-4	-25/10
AFO	R	2/2/N	2.5/2.5/N	2.5/2.5/N	4/18/80-50	-25/10
AFO	R	2/2/N	2.5/2.5/N	2.5/2.5/N	4/19/80-55	-25/10
AFO	R	2.5/2.5/N	3/3/N	3/3/N	4/18/80-52	-25/10
AFO	R	2/2/N	2.5/2.5/N	2.5/2.5/N	10/30/79-3	-25/10

TABLE C-9
PILOT RATINGS

CONF	PILOT	TASK			RUN NO.	$\delta_{h_{LIM}}$ deg
		A	B	C		
AFO	R	2/2/2	2/2/2	2.5/2.5/2.5	5/2/80-62	-25/15
AFO	R	3/3/3	3.5/3.5/3.5	3.5/3.5/3.5	5/9/80-103	-30/20
AFO	T	2/2/N	2/2/N	2/2/N	11/12/79-4	-25/10
AFO	T	2/2/N	2/2/N	2/2/N	11/14/79-12	-25/10
AFO	T	2/2/2	2/2/2	2/2/2	5/08/80-49	-30/20
AF2	A	2/2/N	2.5/3/N	2.5/2.5/N	11/14/79-34	-25/15
AF2	A	3/2/N	3/2/N	5/5/N	10/31/79-20	-25/10
AF2	A	1.5/2/N	3/4/N	4/4/N	4/19/80-53	-25/10
AF2	R	2/2/N	2.5/2.5/N	3/3/N	10/30/79-4	-25/10
AF2	R	2/2/N	2.5/2.5/N	2.5/2.5/N	4/18/80-53	-25/10
AF2	R	2/2/N	3/5/N	4/5/N	4/19/80-56	-25/10
AF2	T	2/2/N	2/2/N	2/2/N	11/14/79-13	-25/10
AF2	T	2/2/N	2/2/N	2/2/N	11/14/79-19	-25/10
AF4	A	3/3/3	3/4/4	5/6/7	5/7/80-90	-30/20
AF4	A	2/2/2	3/3/4	4/4/4.5	5/6/80-80	-30/20
AF4	F	2/2/2	2.5/2.5/2.5	3/3/3	5/8/80-90	-30/20
AF4	R	2/2/2	2.5/2.5/2.5	2.5/3/3	5/6/80-90	-30/20
AF4	T	1.5/1.5/1.5	2/2/2	2/3/3	4/8/80-50	-30/20

TABLE C-9
PILOT RATINGS

CONTROL AUTHORITY VARIATIONS - δ_h POSITION LIMITS

CONF	PILOT	TASK A	TASK B	TASK C	δ_h LIM deg	RUN NO.
AF2	A	2/2/N	2.5/3/N	2.5/2.5/N	-25/15	11/14/79-34
AF2	A	2.5/2/N	3/3/N	4.5/4.5/N	-25/10	(Avg. rating of 2)
AF2	R	2/2/N	2.5/3.5/N	3/3.5/N	-25/10	(Avg. rating of 3)
AF2	T	2/2/N	2/2/N	2/2/N	-25/10	(Rating for 2)
AF2	A	2.5/2/N	3/3/N	3/3/N	-7/15	11/12/79-26
AF2	A	2/2/N	3/3/N	3/3/N	-5/15	11/12/79-27
AF2	A	3/3/N	3/4/N	5/5/N	-3/15	11/12/79-28
AF2	A	3/3/N	3/3/N	3/3/N	-10/10	11/12/79-29
AF2	R	2/2.5/N	2.5/2.5/N	3/3/N	-10/10	10/23/79-4
AF2	R	2/2/N	2.5/2.5/N	2.5/3/N	-7/10	10/30/79-5
AF2	R	2/2/N	2.5/2.5/N	3/3.5/N	-5/10	10/30/79-6
AF2	R	4/4/N	4.5/6/N	5/7/N	-3/10	10/3/79-7
AF2	A	4/4/N	4/4/N	5/6/N	-10/5	11/12/79-30

TABLE C-9
PILOT RATINGS

CONTROL AUTHORITY VARIATIONS - δ_h RATE LIMITS

CONF	PILOT	TASK C	TASK D	RUN NO.	$\dot{\delta}_{h_{LIM}}$ deg/sec	$\delta_{h_{LIM}}$ deg
F0	T	6/8/8	4/7/9/9	5/17/80-1126	±10	-25/15
F1	T	8/9/9	4/7/10/10	5/17/80-1125	±10	-25/15
F6	A	5/6/7	4/4.5/7/7	5/17/80-127	±35	-25/15
F6	A	6/5/5	4/6/6/6	5/17/80-128	±20	-25/15
F6	T	6/7/7	3/5/7/7	5/17/80-128	±20	-25/15
F6	A	7/6/7	4/5/6/6	5/17/80-129	±15	-25/15
F6	A	8/10/10	3.5/6/6/6	5/17/80-30	±10	-25/15
F6	T	8/10/10	4/6/9/10	5/17/80-130	±10	-25/15
AF0	A	4.5/7.5/9	3/3/4/4	5/17/80-126	±10	-25/15
AF1	A	4/10/10	2.5/3.5/3.5/3	5/17/80-125	±10	-25/15
AF1	T	8/10/10	3/5/10/10	5/17/80-125	±10	-25/15
AF2	A	4/4/3	2/3/3/3	5/17/80-121	±35	-25/15
AF2	T	3/4/4	2/3/3/3	5/17/80-121	±35	-25/15
AF2	A	5/8/10	2/3/4/3	5/17/80-122	±20	-25/15
AF2	T	5/10/10	2/3/10/10	5/17/80-122	±20	-25/15
AF2	A	5.5/10/10	3/3/10/10	5/17/80-123	±10	-25/15
AF2	T	5/10/10	2/4.5/10/10	5/17/80-123	±10	-25/15
AF6	T	5/10/10	2/3/5/5	5/17/80-124	±10	-25/15
AF6	A	7/10/10	3/4/10/10	5/17/80-124	±10	-25/15

C.5.2 Strip Chart Recorders

For every simulation flight discussed in this report, a "hard copy" time history record was made of pertinent variables. The recordings were made on two 18-channel, multiplexed, Brush, pen, strip-chart recorders; or alternately, two similar recorders using heat-sensitive paper.

The variables recorded included airplane orientation angles (θ, α, γ, ϕ, ψ, β), rates (q, V_T, h, p, r), surface deflections (δ_{h_L}, δ_{h_R}, δ_{sp_L}, δ_{sp_R}, δ_{Flaps}), pilot inputs (δ_T, F_{ES}, δ_{ES}, F_{AS}, δ_{AS}, δ_{RP}) and the accelerations n_z and n_y. Also variables giving reference to the ILS approach path and runway were recorded: LOCE (localizer error), GSE (glide slope error), h (height), Sx (distance from approach end of runway, negative on approach) and Sy (offset from runway center, positive to right). For a complete description of the coordinate system used for these last two variables, see the first paragraph in C.2.1.

Figures C28 and C29 show the variables assigned to each recorder (C28 has basically longitudinal parameters and C29 lateral-directional). The scaling is also described. The figures show ouputs for about 40 seconds of I.L.S. flying with configuration F1, pilot A. GSE and LOCE were not recorded (zero) in the example.

Note that as shown in the trace for height in figure C28, if the scale limits of a trace are exceeded, the pen shifts to the opposite side of the trace and continues. So the range of the traces are not limited to the values shown.

Each trace has two variables multiplexed to it. One variable is shown as a solid curve and the other as a dashed curve that is filled in to the solid curve (the amount of detail in the figures may not make this easily apparent).

349

Solid	Dashed
25	5
F_{ES} –lb	δ_{ES} –In
–25	–5
18	1.7
a –deg	n_z –g's
–2	.7
5	40
$q \frac{deg}{sec}$	δ_{FLAPS} –deg
–5	–40
200	1
$V_T - \frac{ft}{sec}$	δ_T –percent
100	0
	ticks=seconds
25	12.5
θ –deg	γ –deg
–25	–12.5
1,000	25
H-ft	$\overset{\bullet}{H} - \frac{ft}{sec}$
0	–25
25	25
δ_{h_L} –deg	δ_{h_R} –deg
–25	–25
1	5,000
GSE–deg	S_x –ft
(Not on)	
–1	–45,000
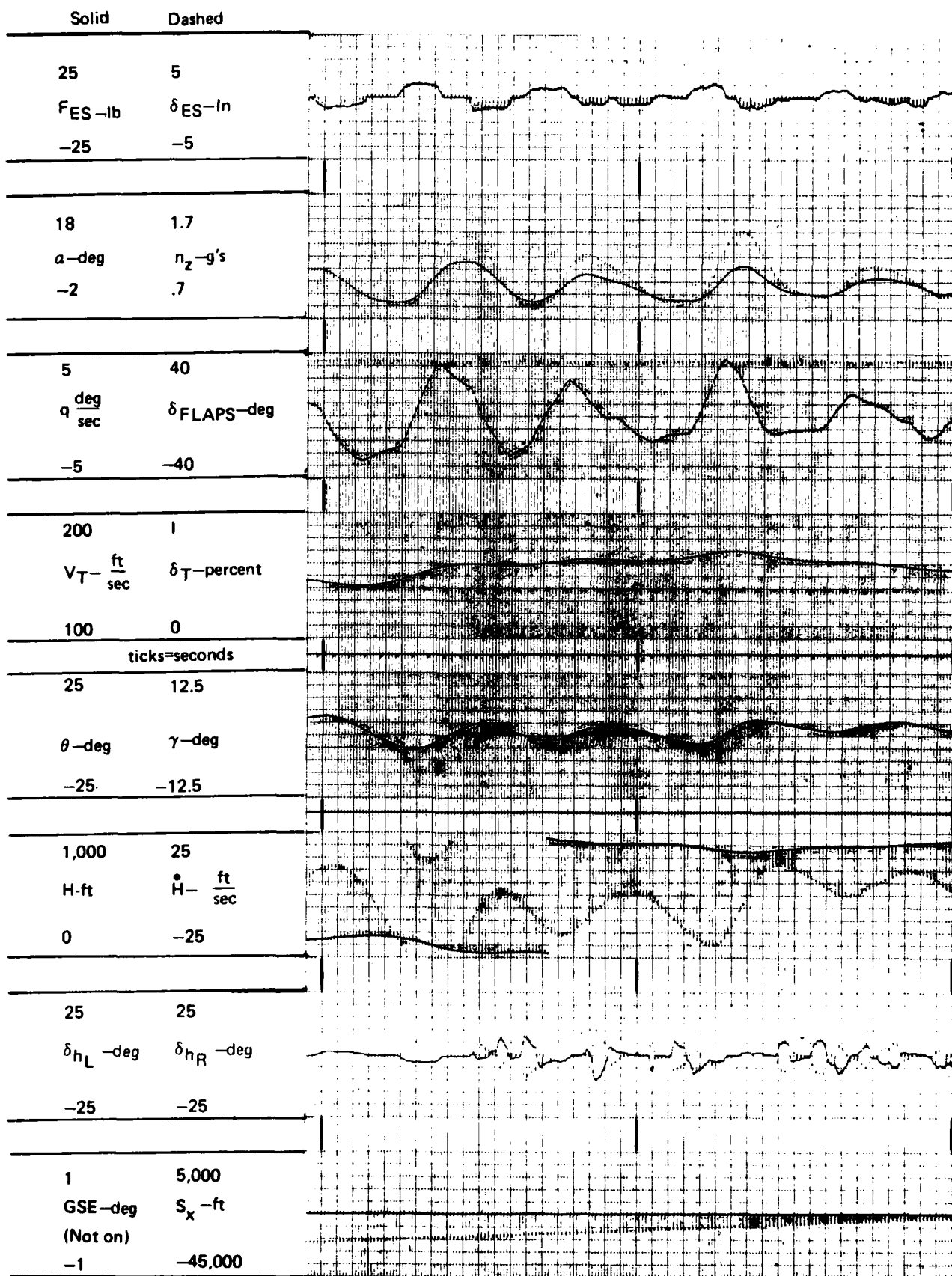
Figure C-30.   Strip Chart Output – Longitudinal

350

Solid	Dashed
25	5
F_{AS-lb}	δ_{AS-in}
−25	5

10	1
β−deg	n_y−g's
−10	−1

50	25
ϕ−deg	$P-\dfrac{deg}{sec}$
−50	−25

5	5
$r-\dfrac{deg}{sec}$	δ_{RP-in}
−5	−5

50	50
δ_{sp_L-deg}	δ_{sp_R-deg}
0	0

NOT USED

ticks=seconds

25	50
δ_r−deg	ψ−deg
−25	−50

5	500
LOCE−deg	S_y−ft
(not on)	
−5	−500
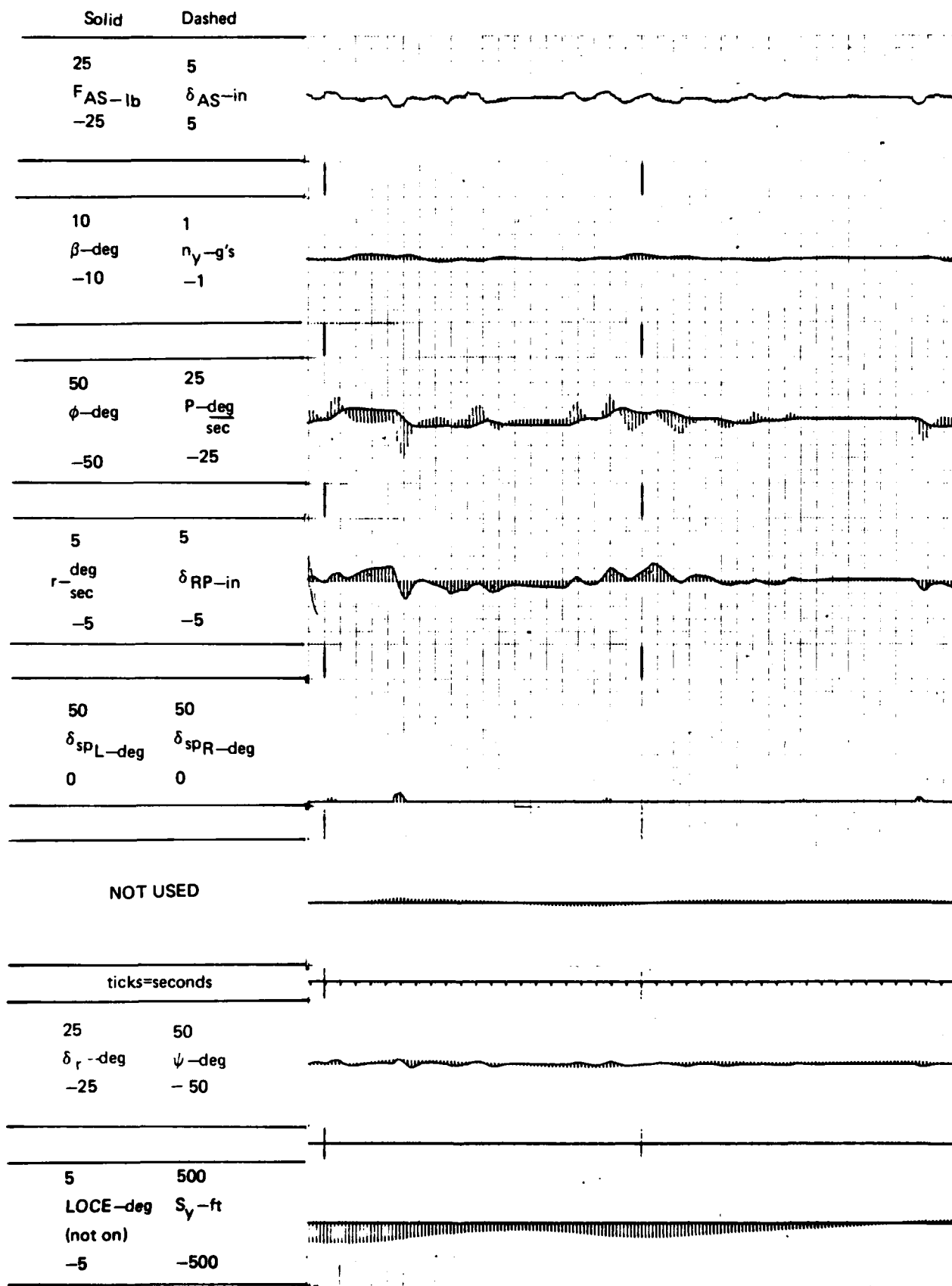
Figure C-31. Strip Chart Output − Lateral-directional

351

APPENDIX D

YC-14 FLIGHT TEST EXPERIENCE

Bernard F. Ray
Boeing Seattle

The Boeing YC-14 Advanced Medium STOL Transport (AMST) prototype used upper surface blown (USB) flaps and two high by-pass ratio engines to developed powered lift for STOL flight. It had a three-channel digital flight control system with mechanical back-up. Two airplanes were built and accumulated over 600 flight hours in the joint Air Force, NASA, and Boeing flight test program. A concise summary of the overall character-istics and capabilities of the YC-14 and the flight test results are provided in Reference 60. The flight control system characteristics and capabilities are summarized by Lee in Reference 61. The pilot assessment and flight test experience with the rate-command/attitude-hold feature of the flight control system are summarized below.

The YC-14 electrical flight control system had rate command and attitude hold control logic in pitch and roll. When a force was applied to the pilot's controller, a pitch or roll rate was commanded proportional to that force, and when the force was released the airplane held the attitude it had attained. This appeared to the pilot as a well damped, neutrally stable airplane since no stick force was required to fly coordinated turns or to change and hold a new airspeed. This control logic was selected because it reduces pilot workload in addition to providing excellent handling characteristics. The system allows the pilot to "point" the aircraft and release it, and eliminates the need to correct trim changes due to speed changes, landing gear, flaps, speed brakes, etc. The rate-command/attitude-hold feature was not, as commonly incorporated in the past, an autopilot type mode but was rather an integral part of the normal flight control augmentation system, and thus was normally used by the pilots in flying the airplane.

The handling characteristics of the YC-14 were evaluated by many test pilots, including Boeing, Air Force, and NASA pilots, during the flight test program. General agreement among the pilots was never reached as to the acceptability of the pitch attitude hold concept. Those pilots who preferred the system as designed felt it eased the piloting task considerably. It relieved the pilot of the requirement to continuously fly the airplane and allowed him to divert his attention to other duties. The attitude hold feature was also beneficial in turbulence and crosswinds in that it held attitude during disturbances.

Those pilots objecting to the system liked the benefits mentioned above, but were concerned about the lack of stick force in turns. Since it was possible to maneuver by merely rolling to the desired bank angle, they felt that it was possible to over-"g" the airplane.

In an attempt to alleviate these concerns, modifications were made to the control logic to provide stick force in turns while retaining the attitude hold features during other flight conditions. Bugs appeared in the modified logic, giving rise to annoying control characteristics in a few instances. Due to schedule pressures, the bugs were not exterminated. Instead, the system was returned to its original configuration for the remainder of the flight test program.

YC-14 experience with the rate-command/attitude-hold concept is inconclusive. Some pilots liked it and some didn't. Attempts to eliminate objections failed, but they failed for lack of time, not for some fundamental physical reason.

APPENDIX E
STUDY OF MIL-F-8785B AND MIL-F-9490D INTERFACE
Olen Visor and Don Nordwall
Boeing Wichita

E.1 Introduction

This appendix presents suggestions resulting from the study to identify incompatibilities and define proposed revisions to the subject specifications. Review of the specifications indicated several areas of inconsistencies in classifications and requirements. Although the primary task was to identify and document areas that need revision in MIL-F-8785B, a general consensus of the personnel reviewing the interface was that simultaneous revisions of both specifications were desirable, if not necessary, to remove inconsistencies and areas of incompatibility.

Specific suggested changes to MIL-F-8785B and any corresponding impact on MIL-F-9490D are presented in Section E.2. Items which should be considered in a general revision of MIL-F-8785B, for which no specific requirements could be established in this limited study, are presented in Section E.3. Section E.4 contains comments and suggestions on FCS classification inconsistencies in the specifications.

E.2 Specific Suggested Changes to MIL-F-8785B

E.2.1 Paragraph 1.5 Levels of Flying Qualities

Level 3

Flying qualities such that the airplane can be controlled safely, but pilot workload is excessive or mission effectiveness is inadequate, or both. The primary missions can be terminated safely and the airplane can continue to the mission terminal destination and land safely.

Paragraph 1.5   Background

Level 3 is made more general to allow some Category B phases to be recognized as primary mission functions to which mission failure probabilities apply.

E.2.2   Paragraph 3.1.10.2   Requirements for Airplane Failure States

Paragraph 3.1.10.2.1   Flying Qualities - Mission Reliability

When airplane failure states exist (3.1.6.2), a degradation in flying qualities or loss of mission effectiveness is permitted only if the probability of encountering a lower level than specified in 3.1.10.1 is sufficiently small.

At intervals established by the procuring activity, the contractor shall determine, based on the most accurate available data, the probability of occurrence of each Airplane Failure State per flight and the effect of that Failure State on the flying qualities within the Operational and Service Flight Envelopes. These determinations shall be based on MIL-STD-756 except that (a) all airplane components and systems are assumed to be operating for a time period, per flight, equal to the longest operational mission time to be considered by the contractor in designing the airplane and (b) each specific failure is assumed to be present at whichever point in the Flight Envelope being considered is the most critical (in the flying qualities sense). From these Failure State probabilities and effects, the contractor shall determine the overall probability, per flight, that one or more flying qualities are degraded to Level 2 because of one or more failures. Within the Operational Flight Envelope the probability of Level 2 after failure shall be less than 10^{-2} per flight.

The contractor shall also determine the probability that one or more failures affecting flying qualities results in mission failures. The probability of mission failure per flight due to degradation in flying qualities shall not exceed the applicable limits specified below. Representative mission to which this requirement applies shall be

355

established and defined by the Contractor, subject to approval of the procuring activity.

a. Where the overall aircraft mission accomplishment reliability is specified by the procuring activity:

$$Q_{M(fq)} \leq (1 - R_M) \, A_{M(fq)}$$

b. Where overall aircraft mission accomplishment reliability is not specified,

$$Q_{M(fq)} \leq 1 \times 10^{-3}$$

where $Q_{M(fq)}$ = mission unreliability due to failure affecting flying qualities

R_M = specified overall aircraft mission accomplishment reliability

$A_{M(fq)}$ = mission accomplishment allocation factor for flying qualities (chosen by the contractor)

Paragraph 3.1.10.2 Background

The paragraph is rewritten to relate failures more critical than Level 2 to mission reliability. The corresponding requirement in MIL-F-9490D, Paragraph 3.1.6, should be deleted. MIL-F-9490D or MIL-F-8785B should indicate that all control system failures relate to handling qualities even though no concrete relationship exists, such as flight restriction due to flutter system failure or maneuver or gust restrictions with load alleviation failure.

Paragraph 3.1.10.2.2 Quantitative Flight Safety

The probability of aircraft loss per flight, defined as extremely remote, due to failures affecting flying qualities shall not exceed:

$$Q_{S(fq)} \leq (1 - R_S) A_{S(fq)}$$

356

where $Q_{S(fq)}$ = aircraft loss rate per flight due to failures affecting aircraft controllability

$A_{S(fq)}$ = flight safety allocation factor for aircraft controllability

R_S = overall aircraft flight safety requirements as specified by the procuring activity

Failures in power supplies or other subsystems that do not otherwise cause aircraft loss shall be considered where pertinent. A representative mission to which this requirement applies shall be established and defined by the contractor subject to approval of the procuring activity. Special failures states of Paragraph 3.1.6.2.1 need not be considered in meeting this requirement.

E.2.3 Paragraph 3.2.2.1.3 Residual Oscillations

For Levels 1 and 2, vertical sustained residual oscillations at the pilot's station shall be less than the level shown in Figure E-1 for any flight phase. Pitch attitude oscillations greater than ±0.05 degrees will be considered excessive for Category A flight phases requiring precision control of attitude.

Paragraph 3.2.2.1.3 (and 3.3.1.5) Background

The vertical (and lateral) acceleration levels versus frequency represent 80 percent of mean perceptible levels from Reference 21.

Paragraph 3.3.1.5 Residual Oscillations

For Levels 1 and 2, lateral sustained residual oscillations at the pilot's station shall be less than the level shown in Figure E-2 for any flight phase. Residual oscillations in roll and yaw attitude at the pilot's station shall not exceed ±0.3 degrees for flight phases requiring precision control of attitude.
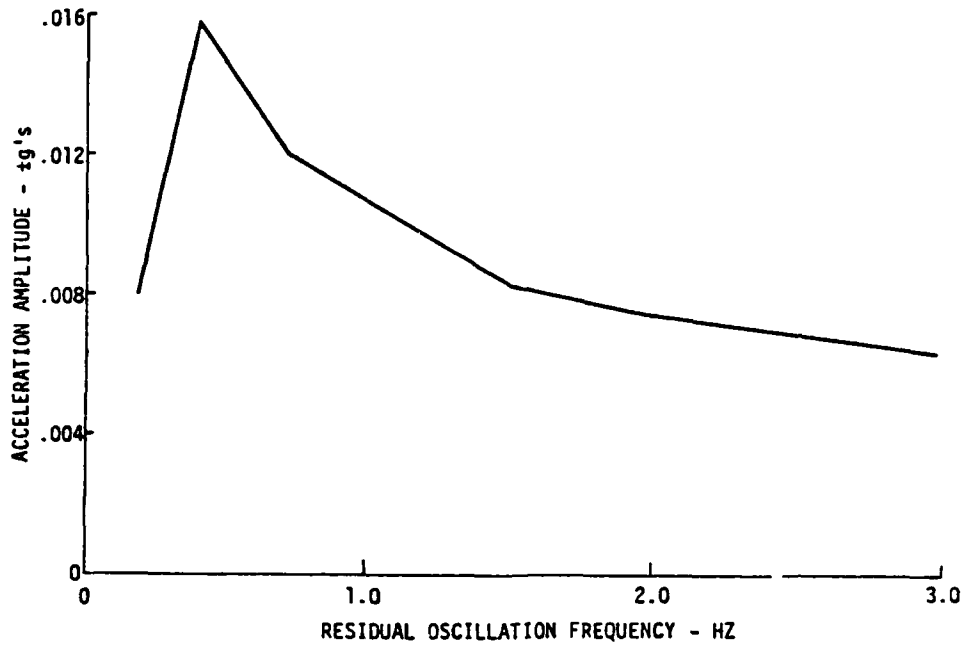
Figure E-1. Vertical Sustained Residual Oscillation Limitation
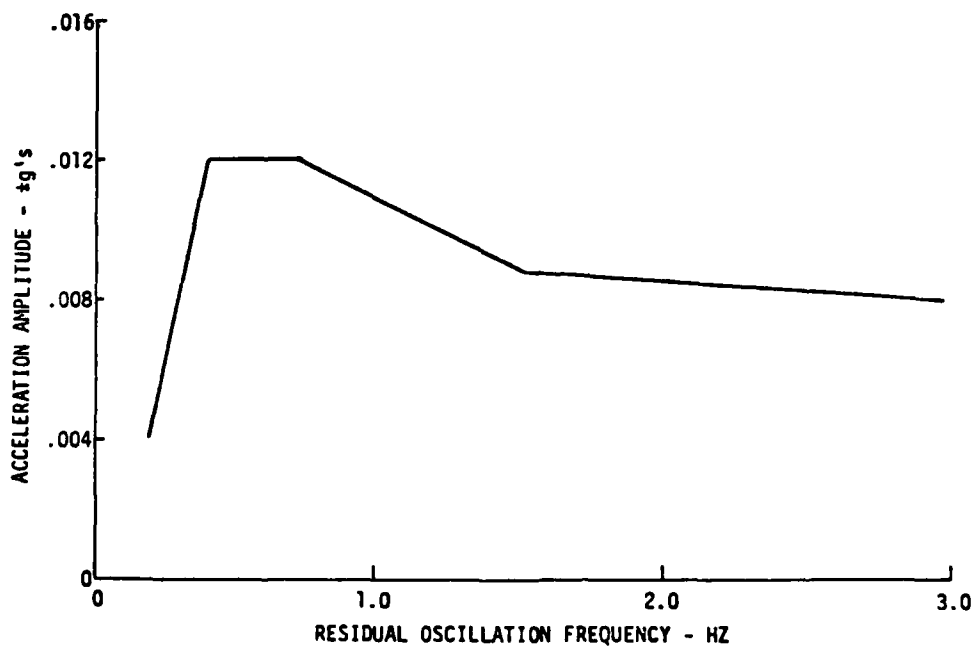
Figure E-2. Lateral Sustained Residual Oscillation Limitation

358
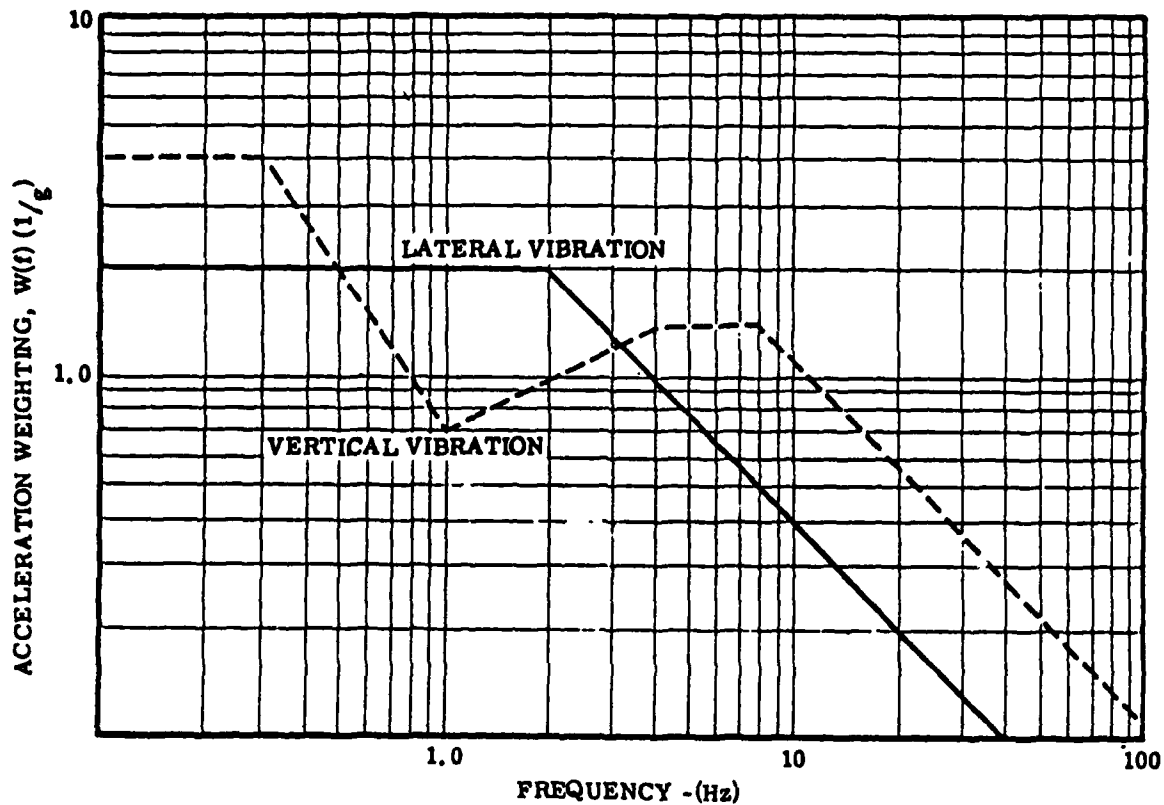
Figure E-3. Acceleration Weighting Functions.

E.2.4 Paragraph XXXX Ride Qualities

For Levels 1 and 2, the ride quality index, D_i, evaluated at the pilot's station, shall not exceed 0.28 at the most critical condition of Table I within the operational envelope. The ride quality index is defined as:

$$D_i = \left[\int_{0.1}^{f_t} [W(f)]^2 [T_{cs}(f)]^2 \, \phi_u(f) df \right]^{1/2}$$

D_i = Ride discomfort index (vertical or lateral)

$W(f)$ = acceleration weighting function (vertical or lateral), 1/g, defined in Figure E-3

359

$T_{cs}(f)$ = transmissability, at crew station, g/ft/sec

$\phi_u(f)$ = Von Karman gust power spectral density, defined in 3.7.2.1

f = frequency, Hz

f_t = truncation frequency (frequency beyond which aeroelastic responses are no longer significant in turbulence)

Unless otherwise specified by the procuring agency, the RMS gust levels of Table E-1 will apply.

TABLE E-1

RMS TURBULENCE INTENSITIES FOR RIDE QUALITIES EVALUATION

Altitude ft	RMS Turbulence ft/sec
500	6.6
1750	6.9
3750	7.4
7500	6.7
15000	4.6
25000	2.7
35000	0.4

Terrain following mission (up to 1000 ft alt.):

Lateral turbulence intensity = 10.2 ft/sec

Vertical turbulence intensity = 8.9 ft/sec

Paragraph XXXX   Ride Qualities Background

The critical ride quality criteria from MIL-F-9490D is proposed for inclusion in MIL-F-8785B as a flight safety requirement for all aircraft. The corresponding section in MIL-F-9490D, Paragraph 3.1.2.12, could be revised to address ride smoothing control systems, with a reference to the MIL-F-8785B criteria to eliminate duplication. Ride criteria are recommended over any requirements that attempt to relate flying quality levels to turbulence.

E.2.5 Paragraph 3.5.3 Dynamic Characteristics

The response of the control surfaces in flight shall not lag the cockpit control force inputs by more than the angles shown in Table E-2 for frequencies equal to or less than the frequencies shown in Table E-2. The allowable lags of Table E-2 exclude any contribution from augmentation devices and flight control systems.

TABLE E-2
ALLOWABLE CONTROL SURFACE LAGS

	Allowable Lag deg			Control	Upper Frequency rad/sec
Level	Category A and C Flight Phases	Category B Flight Phases		pitch	$\omega_{n_{sp}}$ or highest frequency for a higher-order longitudinal system
1 & 2	30	45			
3	60			yaw and roll	ω_{n_d}, $1/\tau_R$ or highest frequency for a higher-order lateral system

Paragraph 3.5.3 Background

This paragraph is revised to exclude the effects of feedback control systems which may drastically alter the phase of surface response due to control. Revision also specifies lag evaluation frequency for an airplane which has higher order characteristics resulting from the use of feedback control systems.

E.2.6 Paragraph 3.5.5 Failures

If the flying qualities with any or all the augmentation devices and flight control systems inoperative are dangerous or intolerable, special provisions shall be incorporated to preclude a failure jeopardizing

flight safety. Failure induced transient motion and trim changes resulting either immediately after failure or upon subsequent transfer to alternate control modes shall be small and gradual enough that dangerous flying qualities never result.

Paragraph 3.5.5 Background

This paragraph is revised to include all systems covered in MIL-F-8785 and MIL-F-9490 and to include multiple failures which produce a critical condition.

Paragraph 3.5.5.1 Failure Transients

With controls free, the airplane motion due to failures described in 3.5.5 shall not exceed the following limits for at least two seconds following the failure, as a function of the level of flying qualities after the failure transient has subsided:

Level 1 and 2
(after failure)

$\pm$ 0.5g incremental normal or lateral acceleration at the pilot's station or $\pm$ 10 degrees/second roll rate. With the airplane operating within the operational flight envelope, the failure transient shall not result in operation exceeding the service flight envelope.

Level 3
(after failure)

No dangerous attitude or structural limit is reached, and no dangerous alteration of the flight path results from which recovery is impossible. With the airplane operating within the operational envelope, the failure transient shall not result in operation exceeding the permissible flight envelope.

Paragraph 3.5.5.1 Background

The transient effects for Level 1 and 2 operation (after failure) have been increased to be more compatible with MIL-F-9490D requirements which were set considering safety needs and nuisance disengagement characteristics of redundant system. The flight envelope restrictions are applied for safety assurance covering transients during non-steady flight.

With this revision, MIL-F-8785 will still not be completely compatible with MIL-F-9490. Lateral acceleration at the c.g. in MIL-F-9490D does not cover the effects of yawing motion transients on the pilot.

E.3 General Recommended Changes to MIL-F-8785

E.3.1 Paragraphs Pertaining to Longitudinal and Lateral Maneuvering Characterisitics

It is recommended that these paragraphs address the following items:

a. Response requirements of higher-order systems

b. Exemption of fully automatic (non-piloted) response from requirements of MIL-F-8785B but meeting the requirements for the appropriate systems in MIL-F-9490D.

c. Specifying requirements for "steering modes" of AFCS.

E.3.2 Paragraph 3.7 Atmospheric Disturbances

MIL-F-8785B is not consistent with MIL-F-8861A which specifies gusts for aircraft strength and loads; whereas MIL-F-9490D is. The gust requirements of MIL-F-9490D are broader and more conservative in terms of safety. MIL-F-8785B is vague on longitudinal controllability requirement in gusts. A common atmospheric disturbance model for all aircraft specifications would be desirable, perhaps in a self-contained specification.

363

E.3.3 Paragraph 3.3.9.1 Thrust Loss During Takeoff Run

An automatic control system which normally operates in the event of a thrust failure should be addressed in terms of failure of the automatic device and the impact on airplane flying qualities and mission reliability. Classification of this type system should be consistent with other similiar systems, i.e., an automatic control system which provides pilot assistance.

E.3.4 Paragraph 3.6.5 Direct Normal-Force Control

It may be advantageous to utilize direct force for primary control. This type of system for primary control will need to be addressed in terms of the impact on maneuvering characteristics.

E.4 MIL-F-8785B/MIL-F-9490D FCS Classification

The control system classification and requirements should be compatible between the two specifications. It appears that the exisiting classifications in MIL-F-9490D are more ambiguous when compared with MIL-F-8785B. One example is the B-52 yaw stabilty augumentation system. Functionally, this system was designed for gust load alleviation and, therefore, would be classified as an AFCS in MIL-F-9490D. Operationally this system damps the Dutch roll mode and would then be classified as a MFCS.

A possibility for classifications would be categories of control systems associated with piloted and nonpiloted usage. The piloted control systems would have to meet the flying qualities requirements of MIL-F-8785B and the nonpiloted controls would meet the requirements of MIL-F-9490D. The piloted controls would include all systems that are engaged when the pilot is flying the airplane. This would include rigid body mode dampers (pitch, roll, yaw), ride control systems, gust load alleviation systems, flutter suppression systems, maneuver load alleviation system, stick steeing, etc.

The non-piloted classification would include hands off autopilot operation, automatic terrain following, etc.

LINEARIZED LONGITUDINAL EQUATIONS OF MOTION

F.1 Equations of Motion and State Models

F.1.1 Body Axes

The longitudinal equation of motion (from Ref. 50, p. 256) in body axes, assuming wings-level flight, are written for perturbations u, w, q, θ, and δ from reference conditions U_o, w_o, θ_o and δ_o which are trimmed, steady, level flight conditions. The assumption is made (from Ref. 50, p. 298) that $X_{\dot{u}}$, $Z_{\dot{u}}$, $M_{\dot{u}}$, $X_{\dot{w}}$, $Z_{\dot{w}}$, X_q, and Z_q can be neglected.

$$\left.\begin{array}{l} \dot{u} + w_o\,q + g\cos\theta_o\,\theta = X_u\,u_a + X_w\,w_a + \Sigma\,X_\delta\,\delta \\[2mm] \dot{w} - U_o\,q + g\sin\theta_o\,\theta = Z_u\,u_a + Z_w\,w_a + \Sigma Z_\delta\,\delta \\[2mm] \dot{q} = M_u\,u_a + M_{\dot{w}}\dot{w}_a + M_w\,w_a + M_q\,q + \Sigma\,M_\delta\,\delta + \dfrac{1}{U_o}\,M_q\,\dot{w}_g \end{array}\right\} \qquad (F1)$$

where

$$u_a = u - u_g \qquad q = \dot{\theta}$$
$$w_a = w - w_g \qquad \gamma = \theta - a$$
$$a = \tan^{-1}\!\left(\frac{w_o + w_a}{U_o + u_a}\right) \approx (w_o + w_a)/U_o$$

The gust velocities, u_g, and w_g, are measured positively in the direction of the body axes, so a positive u_g reduces u_a and a positive w_g reduces α.

In matrix form, the equations can be written as

$$[M][\dot{x}] = [A'][x] + [B'][u] + [B'_g][u_g] \qquad \text{(F2)}$$

where

$$[M] = \begin{bmatrix} 1 & 0 & 0 & 0 \\ 0 & 1 & 0 & 0 \\ 0 & -M_{\dot{w}} & 1 & 0 \\ 0 & 0 & 0 & 1 \end{bmatrix} \qquad [A'] = \begin{bmatrix} X_u & X_w & -w_o & -g\cos\theta_o \\ Z_u & Z_w & U_o & -g\sin\theta_o \\ M_u & M_w & M_q & 0 \\ 0 & 0 & 1 & 0 \end{bmatrix}$$

$$[B'] = \begin{bmatrix} X_\delta \\ Z_\delta \\ M_\delta \\ 0 \end{bmatrix} \qquad [B'_g] = \begin{bmatrix} -X_u & -X_w & 0 \\ -Z_u & -Z_w & 0 \\ -M_u & -M_w & (-M_{\dot{w}} + M_q/U_o) \\ 0 & 0 & 0 \end{bmatrix}$$

$$[x] = [u\ w\ q\ \theta]^T, \quad [u] = [\delta], \quad [u_g] = [u_g\ w_g\ \dot{w}_g]^T$$

The equations in body axes can be written in state model form as follows, together with their relation to the equations of motion form.

$$[\dot{x}] = [A][x] + [B][u] + [B_g][u_g] \qquad \text{(F3)}$$

where

$$[A] = [M]^{-1}[A'] \ , \ [B] = [M]^{-1}[B'] \ , [B_g] = [M]^{-1}[B'_g]$$

$$[A] = \begin{bmatrix} X_u & X_w & -w_o & -g\cos\theta_o \\ Z_u & Z_w & U_o & -g\sin\theta_o \\ M_u + M_{\dot{w}}Z_u & M_w + M_{\dot{w}}Z_w & M_q + U_o M_{\dot{w}} & -M_{\dot{w}}\,g\sin\theta_o \\ 0 & 0 & 1 & 0 \end{bmatrix}$$

$$[B] = \begin{bmatrix} X_\delta \\ Z_\delta \\ M_\delta + M_{\dot{w}}Z_\delta \\ 0 \end{bmatrix} \qquad [B_g] = \text{Same as } [B'_g] \text{ except:}$$

$$B_{g_{31}} = -(M_u + M_{\dot{w}}Z_u)$$
$$B_{g_{32}} = -(M_w + M_{\dot{w}}Z_w)$$

$$[M]^{-1} = \begin{bmatrix} 1 & 0 & 0 & 0 \\ 0 & 1 & 0 & 0 \\ 0 & +M_{\dot{w}} & 1 & 0 \\ 0 & 0 & 0 & 1 \end{bmatrix}$$

F.1.2 Stability - Body Axes

The equations of motion can be converted to stability-body[1] axes by transforming through the reference angle of attack, α_0. We define the transformation $[\alpha]$ as follows and depicted below:

$$[\alpha] = \begin{bmatrix} \cos\alpha_0 & \sin\alpha_0 & 0 & 0 \\ -\sin\alpha_0 & \cos\alpha_0 & 0 & 0 \\ 0 & 0 & 1 & 0 \\ 0 & 0 & 0 & 1 \end{bmatrix} \qquad (F4)$$

Then the equations of motion in stability-body axes are, in matrix form,

$$[M_s]\,[\dot{x}_s] = [A'_s]\,[x_s] + [B'_s]\,[u] + [B'_{gs}]\,[u_{gs}] \qquad (F5)$$

where

$$[M_s] = [\alpha]\,[M]\,[\alpha]^T = \begin{bmatrix} 1 & 0 & 0 & 0 \\ 0 & 1 & 0 & 0 \\ -M_{\dot{w}}\sin\alpha_0 & -M_{\dot{w}}\cos\alpha_0 & 1 & 0 \\ 0 & 0 & 0 & 1 \end{bmatrix}$$

$$[A'_s] = [\alpha]\,[A']\,[\alpha]^T = \begin{bmatrix} X_{u_s} & X_{w_s} & 0 & -g\cos\gamma_0 \\ Z_{u_s} & Z_{w_s} & V_0 & -g\sin\gamma_0 \\ M_{u_s} & M_{w_s} & M_q & 0 \\ 0 & 0 & 1 & 0 \end{bmatrix}$$

$$[B'_s] = [\alpha]\,[B'] = \begin{bmatrix} X_{\delta_s} \\ Z_{\delta_s} \\ M_{\delta_s} \\ 0 \end{bmatrix} \qquad [B'_{gs}] = [\alpha]\,[B'_g]\,[\alpha]^T$$

---

[1]We use the term "stability-body" to emphasize that these axes are a special case of body axes where $w_0 = 0$, and not true stability axes which move in the body with their x-axis aligned with the projection of the relative wind in the plane of symmetry.

Note that θ_0 transforms to γ_0, u_0 to V_0, and w_0 to 0. M_q remains unchanged. But, whereas $M_{\dot{u}}$ is zero in body axes by assumption, clearly it will be non-zero in any other axis system. Because of the imprecision of estimates for $M_{\dot{w}}$, it may be assumed that

$$[M] = [M_s] \qquad (F6)$$

from

$$M_{\dot{w}_s} = M_{\dot{w}} \cong M_{\dot{w}} \cos a_0$$

$$M_{\dot{u}_s} = 0 \cong M_{\dot{w}} \sin a_0$$

The state model form of the equations in stability-body axes are then

$$[\dot{x}_s] = [A_s]\,[x_s] + [B_s]\,[u] + [B_{g_s}]\,[u_{g_s}] \qquad (F7)$$

$$[A_s] = [M]^{-1}\,[A'_s]$$

$$[B_s] = [M]^{-1}\,[B'_s]$$

$$[B_{g_s}] = [M]^{-1}\,[B'_{g_s}]$$

where

$$[A_s] = \begin{bmatrix} X_{u_s} & X_{w_s} & 0 & -g\cos\gamma_0 \\ Z_{u_s} & Z_{w_s} & V_0 & -g\sin\gamma_0 \\ M_{u_s} + M_{\dot{w}}\,Z_{u_s} & M_{w_s} + M_{\dot{w}}\,Z_{w_s} & M_g + V_0\,M_{\dot{w}} & -M_{\dot{w}}\,g\sin\gamma_0 \\ 0 & 0 & 1 & 0 \end{bmatrix}$$

$$[B_s] = \begin{bmatrix} X_{\delta_s} \\ Z_{\delta_s} \\ M_{\delta_s} + M_{\dot{w}}\,Z_{\delta_s} \\ 0 \end{bmatrix} \qquad [B_{g_s}] = \begin{bmatrix} -X_{u_s} & -Z_{u_s} & 0 \\ -Z_{u_s} & -Z_{w_s} & 0 \\ -M_{u_s} - M_{\dot{w}}\,Z_{u_s} & -M_{w_s} - M_{\dot{w}}\,Z_{w_s} & -M_{\dot{w}} + \dfrac{M_q}{V_0} \\ 0 & 0 & 0 \end{bmatrix}$$

F.1.3 Transformation from Body to Stability-Body Axes

The transformations indicated in Equation F5 are carried out and the results summarized below, where α_o is the angle of attack of the body axes.

$$X_{u_s} = X_u \cos^2 \alpha_o + (Z_u + X_w) \cos \alpha_o \sin \alpha_o + Z_w \sin^2 \alpha_o$$

$$X_{w_s} = X_w \cos^2 \alpha_o + (Z_w - X_u) \cos \alpha_o \sin \alpha_o - Z_u \sin^2 \alpha_o$$

$$Z_{u_s} = Z_u \cos^2 \alpha_o + (Z_w - X_u) \cos \alpha_o \sin \alpha_o - X_w \sin^2 \alpha_o$$

$$Z_{w_s} = Z_w \cos^2 \alpha_o - (Z_u + X_w) \cos \alpha_o \sin \alpha_o + X_u \sin^2 \alpha_o$$

$$M_{u_s} = M_u \cos \alpha_o + M_w \sin \alpha_o$$

$$M_{w_s} = M_w \cos \alpha_o - M_u \sin \alpha_o$$

$$M_{q_s} = M_q$$

$$X_{\delta_s} = X_\delta \cos \alpha_o + Z_\delta \sin \alpha_o$$

$$Z_{\delta_s} = Z_\delta \cos \alpha_o - X_\delta \sin \alpha_o$$

$$M_{\theta_s} = M_\theta \text{ if } M_\theta \neq 0$$

The $\dot{u}$ and $\dot{w}$ derivatives transform in the same manner as the u and w derivatives; the q ones, as the δ derivatives. However, the force derivatives due to $\dot{u}$, $\dot{w}$ and q normally have a negligible effect on the airplane dynamics and can be assumed zero. Also, from Equation F6, we assume[1]

$$M_{\dot{u}_s} = M_{\dot{u}} = 0$$

$$M_{\dot{w}_s} = M_{\dot{w}}$$

Only the u and w state variables are different in the two axis systems.

$$u_s = u \cos \alpha_o + w \sin \alpha_o$$

$$w_s = w \cos \alpha_o - u \sin \alpha_o$$

---

[1]If an accurate numerical check of the transformation is being made, from body to stability-body axes, then $M_{\dot{u}_s}$ and $M_{\dot{w}_s}$ from the $[M_s]$ matrix of Equation 5 should be used. Otherwise the eigenvalues will be slightly different in the two axis systems.

F.2 Equations of Motion in Stability-Body Axes

The equations of motion, definition of coefficients in the equations, and transfer functions are defined in this section.

F.2.1 Equations of Motion

Most of the analytical work in this report uses the equations of motion in stability axes. These are written out as follows, including $Z_{\dot{w}}$, Z_q, M_θ, and the gust terms, where all derivatives and the velocites u and w are in stability-body axes, and all variables (u, w, θ, q, γ, α, n_z) are perturbation from reference values.

$$
\begin{bmatrix}
s - X_u & -X_w & g\cos\gamma_o \\
-Z_u & (1 - Z_{\dot{w}})s - Z_w & -(V_o + Z_q)s + g\sin\gamma_o \\
-M_u & -M_{\dot{w}}s - M_w & (s - M_q)s - M_\theta
\end{bmatrix}
\begin{bmatrix} u \\ w \\ \theta \end{bmatrix} =
$$

$$
\begin{bmatrix}
X_{\delta_e} & X_{\delta_T} \\
Z_{\delta_e} & Z_{\delta_T} \\
M_{\delta_e} & M_{\delta_T}
\end{bmatrix}
\begin{bmatrix} \delta_e \\ \delta_T \end{bmatrix}
+
\begin{bmatrix}
-X_u & -X_w & 0 \\
-Z_u & -Z_w & -Z_{\dot{w}} + \dfrac{Z_q}{V_o} \\
-M_u & -M_w & -M_{\dot{w}} + \dfrac{M_q}{V_o}
\end{bmatrix}
\begin{bmatrix} u_g \\ w_g \\ \dot{w}_g \end{bmatrix}
\qquad\text{(F8)}
$$

$$q = s\theta \qquad\qquad\text{(F9)}$$

$$\gamma = \theta - a_l = \theta - \frac{\dot{w}}{V_o} \qquad\text{(F10)}$$

$$a = (w - w_g)/V_o \qquad\text{(F11)}$$

$$a_z = \dot{w} - V_o q = -V_o \dot{\gamma} = -\ddot{h} \ , \ \text{inertial acceleration} \qquad\text{(F12)}$$

$$n_z = \frac{1}{g}(\dot{w} - V_o q) + \sin\gamma_o \theta \ , \ \text{c.g. accelerometer} \qquad\text{(F13)}$$

$$n_{z_x} = n_z - x_a \dot{q} \qquad\qquad , \ \text{accelerometer } x_a \text{ ft ahead of c.g.} \qquad\text{(F14)}$$

The coefficients in the equation are related to the aerodynamic coefficients as follows, where the s subscript denotes stability-body axes. All reference values are denoted by the zero subscript (e.g., V_o, α_o, δ_o) with the exception of the aerodynamic coefficients where the unit subscript (i.e., C_{D_l}, C_{L_l}, C_{m_l}) is used to avoid confusion with zero lift or angle-of-attack values.

F.2.2 Coefficients in Equations of Motion

$$X_{u_s} = \frac{\rho S V}{m} \left(-C_{D_1} - C_{D_u} \right) + \frac{\cos a_T}{m} T_V$$

$$X_{w_s} = \frac{\rho S V}{2m} \left(C_{L_1} - C_{D_a} \right)$$

$$X_{\dot{w}_s} = \frac{\rho S C}{4m} \left(-C_{D_{\dot{a}}} \right) \quad \approx 0$$

$$X_{q_s} = \frac{\rho S c V}{4m} \left(-C_{D_q} \right) \quad \approx 0$$

$$X_{\delta_{e_s}} = \frac{\rho S V^2}{2m} \left(-C_{D_{\delta_e}} \right)$$

$$X_{\delta_{T_s}} = \frac{\cos a_T}{m} T_{\delta_T}$$

$$Z_{u_s} = \frac{\rho S V}{m} \left(-C_{L_1} - C_{L_u} \right) - \frac{\sin a_T}{m} T_V$$

$$Z_{w_s} = \frac{\rho S V}{2m} \left(-C_{D_1} - C_{L_a} \right)$$

$$Z_{\dot{w}_s} = \frac{\rho S c}{4m} \left(-C_{L_{\dot{a}}} \right) \sim \text{normally negligible}$$

$$Z_{q_s} = \frac{\rho S c V}{4m} \left(-C_{L_q} \right) \sim \text{normally negligible}$$

$$Z_{\delta_{e_s}} = \frac{\rho S V^2}{2m} \left(-C_{L_{\delta_e}} \right)$$

$$Z_{\delta_{T_s}} = \frac{\sin a_T}{m} T_{\delta_T}$$

$$M_{u_s} = \frac{\rho S V c}{I_y} \left(C_{m_1} + C_{m_u} \right) + \frac{z_T}{I_y} T_V$$

$$M_{w_s} = \frac{\rho S V c}{2 I_y} C_{m_a}$$

$$M_{\dot{w}_s} = \frac{\rho S c^2}{4 I_y} C_{m_{\dot{a}}}$$

$$M_{q_s} = \frac{\rho S V c^2}{4 I_y} C_{m_q}$$

$$M_{\delta_{e_s}} = \frac{\rho S V^2 c}{2 I_y} C_{m_{\delta_e}}$$

$$M_{\delta_{T_s}} = \frac{z_T}{I_y} T_{\delta_T}$$

where

$$C_{D_u} = \frac{V}{2} \frac{\partial C_D}{\partial u} \qquad C_{D_{\dot{a}}} = \partial C_D / \partial \frac{\dot{a} c}{2V} \qquad C_{D_q} = \partial C_D / \partial \frac{q c}{2V}$$

$$C_{L_u} = \frac{V}{2} \frac{\partial C_L}{\partial u} \qquad C_{L_{\dot{a}}} = \partial C_L / \partial \frac{\dot{a} c}{2V} \qquad C_{L_q} = \partial C_L / \partial \frac{q c}{2V}$$

$$C_{m_u} = \frac{V}{2} \frac{\partial C_m}{\partial u} \qquad C_{m_{\dot{a}}} = \partial C_m / \partial \frac{\dot{a} c}{2V} \qquad C_{m_q} = \partial C_m / \partial \frac{q c}{2V}$$

$$T_V = \partial T / \partial V \qquad z_T \sim \text{distance of thrust line (pos.) below c.g.}$$

$$T_{\delta_T} = \partial T / \partial \delta_T \qquad a_T = a_0 + i_T , \quad i_T \sim \text{incidence of thrust line}$$

The values of C_{D_1}, C_{L_1}, T_o, α_o, V_o, and γ_o are given or must be obtained from the equilibrium equations for trimmed straight unaccelerated flight

$$\tfrac{1}{2} \rho V_o^2 S C_{D_1} - T_o \cos \alpha_T + mg \sin \gamma_o = 0$$

$$\tfrac{1}{2} \rho V_o^2 S C_{L_1} + T_o \sin \alpha_T - mg \cos \gamma_o = 0 \qquad \text{(F15)}$$

$$\tfrac{1}{2} \rho V_o^2 Sc\, C_{m_1} + z_T T_o = 0$$

where

$$C_{m_1} \sim C_m \text{ at reference condition to balance direct}$$
$$\text{thrust moment}$$

so

$$C_{m_1} = \frac{-2\, z_T T_o}{\rho V_o^2 S c} \qquad \text{(F16)}$$

Auxilliary relations of use, in the notation of Ref. 50, are

$$X_\alpha = V X_w$$
$$Z_\alpha = V Z_w \qquad \text{(F17)}$$
$$M_\alpha = V M_w$$

The derivative M_θ is included to allow consideration of attitude stabilization, and because it was found necessary for the pole-placement technique used in configuration selection and definition for the simulation program. Interpreted as attitude stabilization,

$$C_{m_\theta} = C_{m_{\delta_e}} K_\theta$$

$$K_\theta = \delta_e/\theta$$

The use of the "e" subscript stands for a generic "elevator". For airplanes with an all movable horizontal tail,
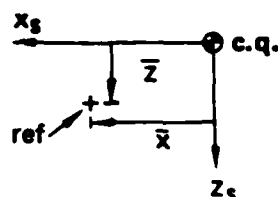
$$\delta_e = \delta_h$$

The aerodynamic data are normally given with respect to some nominal reference moment center. To obtain the aerodynamic coefficients with respect to the center of gravity, a transfer is required as follows:

$$C_{m_x} = C_{m_{x_{ref}}} + \bar{x}\, C_{L_x} - \bar{z}\, C_{D_x}$$

$$x = u, a, \dot{a}, q, \delta e, \delta_T, etc.$$

(F18)

where $\bar{x}$ and $\bar{z}$ are the coordinates (in chord lengths) of the reference moment center in stability axes with c.g. as origin. For small angles of attack and small $\bar{z}$, $\bar{x}$ is defined as follows:

$$\bar{x} \cong \left(\frac{x_{cg} - x_R}{c} \right)$$

where x_{cg} and x_R are the distance aft of the leading edge of the mean aerodynamic chord.

The reference value for C_{m_I} is not obtained from the moment center transfer but from the thrust moment (Eq. F16). The elevator must trim the pitching moments to zero at each c.g. Generally the trim equations (Eq. F15) must be solved for trim δ_e and α with C_D, C_L, and C_m functions of α and δ_e. However, if $C_{L_{\delta_e}}$ and $C_{D_{\delta_e}}$ are small, $z = 0$, and α small, then the following approximations can be used:

$$C_{m_o} = C_{m_{o_{ref}}} + \bar{x}\, C_{L_1}$$

$$\delta_{e_o} = \frac{C_{m_1} - C_{m_o}}{C_{m_{\delta_e}}} + \delta_{e_{ref}}$$

(F19)

where C_{m_I} balances the thrust moment (Eq. F16).

F.2.3 Transfer Functions

The transfer functions for all variables are presented in condiderable detail in Ref. 50 for the equations as given by Equation F8, but with $Z_{\dot{w}} = Z_q = 0$, $\gamma_0 = 0$, and $M_\theta = 0$. The first is no loss, level flight is the most useful special case, and the additional terms required to include M_θ are listed below. The equations of motion are given on p. 298 (Ref. 50), the transfer function factor forms on p. 299, and the characteristic equation and numerator polynomials in terms of the derivatives in Table 5-1 on p. 300. In addition, Table 5-5 on p. 336 gives approximate factors for the poles and zeros in terms of the derivatives. However, these approximate factors should be used with caution since relaxed static stability may violate implicit assumptions as well as those given explicitly.

The following additions are required to Table 5-1, p. 300 (Ref. 50). to account for M_θ.

	C	D	E
Δ	$-M_\theta$	$(X_u + Z_w) M_\theta$	$-M_\theta (X_u Z_w - Z_u X_w)$
N_δ^θ	0		
N_δ^w	$-Z_\delta M_\theta$	$(X_u Z_\delta - Z_u X_\delta) M_\theta$	
N_δ^u	$-X_\delta M_\theta$	$(Z_w X_\delta - X_w Z_\delta) M_\theta$	
sN_δ^h	$Z_\delta M_\theta$	$(Z_u X_\delta - X_u Z_\delta) M_\theta$	

No additions need be made to A or B in the polynomials. The factor forms are unaffected by the addition of M_θ. No attempt is made to incorporate M_θ in the approximate factors in Table 5-5 (Ref. 50).

F.3 Constant Speed Equations

The constant speed equations of motion in stability-body axes are obtained by setting $u = 0$ in the three-degree-of-freedom longitudinal equations. Implicit in the constraint u = constant is that $\dot{u} = 0$, so the equation for $\dot{u}$ is deleted along with the thrust control which may be presumed to provide the constraint. Also, $Z_{\dot{w}}$ and Z_q are set to zero. The u_g inputs are retained.

$$
\begin{bmatrix} s - Z_w & -V_o s + g\sin\gamma_o \\ -M_{\dot{w}}s - M_w & s^2 - M_q s - M_\theta \end{bmatrix} \begin{bmatrix} w \\ \theta \end{bmatrix} = \begin{bmatrix} Z_{\delta_e} \\ M_{\delta_e} \end{bmatrix} \begin{bmatrix} \delta_e \end{bmatrix}
$$

$$
+ \begin{bmatrix} -Z_u & -Z_w & 0 \\ -M_u & -M_w & -M_{\dot{w}} + M_q/U_o \end{bmatrix} \begin{bmatrix} u_g \\ w_g \\ \dot{w}_g \end{bmatrix} \tag{F20}
$$

The characteristic equation is obtained as

$$
\Delta = s^3 + (-Z_w - M_q - M_{\dot{\alpha}})s^2 + (-M_\alpha + Z_w M_q + M_{\dot{w}}\, g \sin\gamma_o - M_\theta)s
$$
$$
+ (M_w\, g \sin\gamma_o + Z_w M_\theta) \tag{F21}
$$

and the transfer functions for elevator inputs are

$$
\frac{\theta}{\delta_e} = \frac{(M_{\delta_e} + M_{\dot{w}} Z_{\delta_e})\, s + (-Z_w M_{\delta_e} + M_w Z_{\delta_e})}{\Delta} \tag{F22}
$$

$$
\frac{w}{\delta_e} = \frac{Z_{\delta_e} s^2 + (V_o M_{\delta_e} - M_q Z_{\delta_e})\, s + (-g \sin\gamma_o M_{\delta_e} - M_\theta Z_{\delta_e})}{\Delta} \tag{F23}
$$

$$
\frac{\gamma}{\delta_e} = \frac{1}{V_o} \frac{-Z_{\delta_e} s^2 + (M_q + M_{\dot{\alpha}}) Z_{\delta_e} s + (-Z_\alpha M_{\delta_e} + g \sin\gamma_o M_{\delta_e} + M_\alpha Z_{\delta_e} + M_\theta Z_{\delta_e})}{\Delta}
$$
$$
\tag{F24}
$$

The constant speed equations are third order rather than the conventional second order. The third root, for $M_\theta = 0$, is a degenerate phugoid with sign dependent on γ_o. For $\gamma_o = 0$ the third root collapses into the origin, leaving a conventional second-order short period mode.

If we assume level flight ($\gamma_0 = 0$) and further simplify by setting $Z_{\delta_e} = 0$, then the transfer functions substantially simplify.

$$\Delta = s^3 + (-Z_w - M_q - M_{\dot{\alpha}})s^2 + (-M_\alpha - M_\theta + Z_w M_q)s + Z_w M_\theta \qquad \text{(F25)}$$

$$\frac{\theta}{\delta_e} = \frac{M_{\delta_e}(s - Z_w)}{\Delta} \qquad \text{(F26)}$$

$$\frac{\alpha}{\delta_e} = \frac{1}{V_0}\left(\frac{w}{\delta_e}\right) = \frac{M_{\delta_e}s}{\Delta} \qquad \text{(F27)}$$

$$\frac{\gamma}{\delta_e} = \frac{-Z_w M_{\delta_e}}{\Delta} \qquad \text{(F28)}$$

$$\frac{n_z}{\delta_e} = \frac{1}{g}\left(\frac{Z_\alpha M_{\delta_e}s}{\Delta}\right) \qquad \text{(F29)}$$

F.3.1 Attitude Hold/Rate Command

Consider an attitude-hold/rate-command type of augmentation system, with attitude hold engaged only when the stick force is within detent ($F_s \sim 0$). Then in detent the response is third order and the system will hold attitude (θ) and flight path angle (γ). Out of detent, $M_\theta = 0$ and the system will provide a conventional short period response. In this case, the free "s" in the denominator will cancel the "s" in the numerator of α and n_z transfer functions, and steady state α and n_z will result from a steady δ_e input.

F.3.2 Weak Attitude Stability (M_θ or γ_0)

The simulator state model configurations (S21 through S63) were determined by a pole placement technique which resulted in a small M_θ derivative (incorporated into the simulator as C_{m_θ}). As demonstrated by Equations F20 through F24, this leads to a third-order response for the constant-speed equations, analogous to the effect of flight path angle ($\gamma_0 = 0$). To find an equivalent second-order short period response, two possibilities seem appropriate:

1)   Let $M_\theta = 0$

In this case Equation F20 reverts to the standard short-period approximation if $\gamma_0 = 0$.

376

2)   Let $M_\alpha' = M_\alpha + M_\theta$; replace M_α with M_α'.
        Let $M_\theta = 0$.

In this case Equation F17 is the standard short-period approximation form, but M_α and hence $\omega_{n_{sp}}^2$ are now corrected for the effect of the small M_θ.

Numerical results show that the constant-speed equations produce a large negative real root together with either two small real roots or a complex pair. The large real root from the constant speed equations, or from Method 1 or Method 2 above, all match the three degree of freedom root. Method 2 above more accurately approximates the larger of the two small real roots of the constant speed equations. However, the constant speed equations and Method 1, and Method 2, all predict a more stable small real root than the three degree of freedom equations. Examples for configurations S22, S42, and S62 follow together with L72 presented for comparison.

Config	Method	λ_{SP_2}	λ_{SP_1}	λ_{SP_0}	Phugoid
S22	3 DOF	-1.00	.347		$-.095 \pm .188j$
	u=const.	-1.00	.279	-.048	
	Method 2	-1.02	.247	0	
	Method 1	-.99	.231	0	
S42	3 DOF	-1.00	.173		$-.093 \pm .188j$
	u=const.	-1.00	.054	-.009	
	Method 2	-1.00	.045	0	
	Method 1	-1.00	.044	0	
S62	3 DOF	-1.00	.116		$-.095 \pm .187j$
	u=const.	-1.00	$(-.006 \pm .084)$		
	Method 2	-1.00	-.020	0	
	Method 1	-1.01	-.008	0	
L72	3 DOF	-2.18	.161		$-.178 \pm .225j$
	u=const.	-2.17	-.145	.012	
	Method 2	-2.17	-.131	0	
	Method 1	-2.17	-.130	0	

The state models for all F and L configurations have $M_\theta = 0$ but the L cases have the A_{34} element non-zero since $\gamma_0 \approx -2.5^\circ$ (see $[A_s]$ in Eq. F7). In the example for L72, $M_\alpha' = M_\alpha - M_w g \sin \gamma_0$ for Method 2, and we must take $\gamma_0 = 0$ for both Methods 1 and 2 to eliminate the third root. By comparison, the effect of flight path angle (L72) is similar to the effect of M_θ (S cases).

If we define stability in terms of the roots, then a primary conclusion is that for relaxed static stability, the instability from the constant speed equations is less than from the three degree of freedom equation.

If weak attitude stability (or instability) exists, either from an M_θ derivative or from a non-zero flight path angle ($\gamma_0 \neq 0$), then the constant-speed equation will be third order (three non-zero roots). To obtain a conventional second-order short period representation, M_α should be modified to M_α' and γ_0 set to zero. ($g \sin \gamma_0 = 0$ in Eq. F20).

$$M_\alpha' = M_\alpha + M_\theta - M_w g \sin \gamma_0 \qquad (F30)$$

The results will not, however, be much different than simply setting all θ coefficients to zero in Eq. F20.

If M_θ is not weak and has a large value, then the constant-speed equations will be third order as will the short period response. This third-order response is inherent in attitude stabilization, and effectively mixes conventional short period and phugoid modes.

378

REFERENCES

1. Anon, <u>Military Specification, Flying Qualities of Piloted Airplanes:</u> <u>MIL-F-8785B(ASG)</u>, August 1969

2. Chalk, C. R., et al., <u>Background Information and User Guide for</u> <u>MIL-F-8785B(ASG), "Military Specification - Flying Qualities of</u> <u>Piloted Airplanes"</u>, AFFDL-TR-69-72, August 1969.

3. Chalk, C. R., et al., <u>Revisions to MIL-F-8785B(ASG) Proposed by</u> <u>Cornell Aeronautical Laboratory under Contract F33615-71-C-1254</u>, AFFDL-TR-72-41, April 1973.

4. Ashkenas, I. L., et al., <u>Recommended Revisions to Selected Portions</u> <u>of MIL-F-8785B(ASG) and Background Data</u>, AFFDL-TR-73-75, August 1973.

5. Anon, <u>Military Specification, Flying Qualities of Piloted Airplanes</u>, MIL-F-8785C, 5 November 1980.

6. DiFranco, D. A., <u>In-Flight Investigation of the Effect of Higher</u> <u>Order System Dynamics on Longitudinal Handling Qualities</u>, AFFDL-TR-68-90, August 1968.

7. Neal, T. P. and R. E. Smith, <u>An In-Flight Investigation to Develop</u> <u>Control Systems Design Criteria for Fighter Airplanes</u>, AFFDL-TR-70-74, December 1970.

8. Smith, R. E., <u>Effects of Control System Dynamics on Fighter Approach</u> <u>and Landing Longitudinal Flying Qualities</u>, AFFDL-TR-78-122, March 1978.

9. Hodgkinson, J., et al., "Handling Qualities Analysis of Aircraft with Stability and Control Augmentation Systems - A Fundamental Approach", <u>Journal R.Ae.S.</u>, February 1976.

10. Bihrle, W., _A Study of Longitudinal Control Surface Pumping During Landing Flare-Outs_, EAR 313, Republic Aviation, 15 December 1956.

11. Bihrle, W. Jr., _A Handling Qualities Theory for Precise Flight-Path Control_, AFFDL-TR-65-198, June 1966.

12. Anon, _Military Specification, Flight Control Systems - Design, Installation and Test of Piloted Aircraft, General Specification for_, MIL-F-9490D (USAF), 6 June 1975.

13. Moorhouse, David J. and Michael W. M. Jenkins, "Use of Short Period Frequency Requirements in Horizontal Tail Sizing," AIAA _Journal of Aircraft_, June, 1975.

14. Kehrer, W. T., _The Performance Benefits Derived for the Supersonic Transport Through a New Approach to Stability Augmentation_, AIAA paper No. 71-785, July 12-14, 1971.

15. Kehrer, W. T., _Design Evolution of the Boeing 2707-300 Supersonic Transport, Part II, Design Impact of Handling Qualities Criteria, Flight Control System Concepts, and Aeroelastic Effects on Stability and Control_, AGARD-CP-147, Volume I, October 1973.

16. Kehrer, William T., _Flight Control and Configuration Design Considerations for Highly Maneuverable Aircraft_ AGARD-CP-262, May 1979.

17. Hoh, Roger H., David G. Mitchell, Irving L. Ashkenas, Richard H. Klien, and Robert K. Heffley, _Proposed MIL Standard - Handling Qualities of Piloted Airplanes_, Systems Technology, Inc., AFWAL-TR-82-   , December 1981. (Preliminary)

18. Hoh, Roger H., David G. Mitchell, Irving L. Ashkenas, Richard H. Klien, and Robert K. Heffley, _Proposed MIL Handbook - Handling Qualities of Piloted Airplanes_, Systems Technology, Inc., AFWAL-TR-82-   , December 1981. (Preliminary)

19. Anon, _Military Standard, Flying Qualities of Flight Vehicles,_ _(Preliminary Draft),_ Interim Technical Report 1163-1, Systems Technology, Inc., September 1980.

20. Carlson, E. Frank, _Impact of Key Flying Qualities Requirements on_ _the YC-14/C-14 Design,_ Proceedings of AFFDL Flying Qualities Symposium Held at Wright State University, 12-15 September 1978, p. 187, AFFDL-TR-78-171, December 1978.

21. Arnold, J. I., et. al., _B-52 CCV Control System Synthesis,_ AFFDL-TR-74-92, Volume II, January 1975.

22. Sudderth, Robert W., Jeff G. Bohn, Martin A. Caniff, and Gregory R. Bennett, _Development of Longitudinal Handling Qualities Criteria for_ _Large Advanced Supersonic Aircraft,_ Boeing Commercial Airplane Company, NASA CR-137635, March 1975.

23. Chalk, C. R., _Recommendations for SCR Flying Qualities Design_ _Criteria_ NASA CR 159236 (Calspan Report No. 6241-F-5), April 1980.

24. Wasserman, Richard and John F. Mitchell, _In-Flight Simulation of_ _Minimum Longitudinal Stability for Large Delta-wing Transports in_ _Landing Approach and Touchdown, Volume I: Technical Results,_ AFFDL-TR-72-143, Volume I, February, 1973.

25. Askenas, Irving L., Roger H. Hoh, and Samuel J. Craig, _Recommended_ _Revisions to Selected Portions of MIL-F-8785B(ASG) and Background_ _Data,_ AFFDL-TR-73-76, August 1973.

26. Chalk, C. R., _Flight Evaluations of Various Phugoid Dynamics and_ $1/T_{h_1}$ _Values for the Landing Approach Task,_ AFFDL-TR-66-2, February, 1966.

27. Mayhew, D. R., _A Digital Computer Program for the Calculation of_ _Parameters Necessary to Satisfy the Closed-loop Criteria of T. P._ _Neal,_ AFFDL/FGC TM 73-110, August 1973.

28. Bull, G., _Minimum Flyable Longitudinal Handling Qualities of Airplanes_, TB-1313-F-1, Cornell Aeronautical Laboratory, Inc., December 1959.

29. Chalk, C.R., _Additional Flight Evaluations of Various Longitudinal Handling Qualities in a Variable-Stability Jet Fighter_, WADC TR-57-719, July 1958.

30. McFadden, Normal M., Richard F. Vomaske and Donovan R. Heinle, _Flight Investigation Using Variable Stability Airplanes of Minimum Stability Requirements for High-Speed, High-Altitude Vehicles_, NASA TN D-779, April 1961.

31. Chalk, C. R., _Flight Evaluation of Various Short-Period Dynamics at Four Drag Configurations for the Landing Approach Task_, FDL-TDR-64-60, October 1964.

32. Tomlinson, L. R., _Problems and Solutions Related to the Design of a Control Augmentation System for a Longitudinally Unstable Supersonic Transport_, AIAA Paper No. 72-871, August 14-16, 1972

33. Crother, C. A., "Flight Management System: Key to the Advanced Technology Fighter", _Astronautics and Aeronautics_, AIAA, June 1981.

34. Hall, G. W. and E. M. Booth, _An In-Flight Investigation of Lateral-Directional Dynamics and Roll-Control Power Requirement for the Landing Approach_, AFFDL-TR-70-145, October 1971.

35. Stalony-Dobrzanski, Janusz and Naren Shah, _Improvement of Fighter Aircraft Maneuverability Through Employment of Control Configured Vehicle Technology_, AGARD-CP-260, ?tability and Control, September 1978.

36. Watson, John H., _Control Requirements for Control Configured Vehicles_, AIAA Paper No. A72-45349, 2nd AIAA Atmospheric Flight Mechanics Conference, September 1972.

37. Grantham, et al., <u>Ground-Based and In-Flight Simulator Studies of Low-Speed Handling Characteristics of Two Supersonic Cruise Transport Concepts</u>, NASA Technical Paper 1240, July 1978.

38. Urie, David M., <u>L-1011 Active Controls, Design Philosophy and Experience</u>, AGARD-CP-260, September 1978.

39. Roskam, Jan, <u>Airplane Dynamics and Automatic Flight Controls</u>, Roskam Aviation and Engineering Corp., Lawrence, Kansas, 1979.

40. Bowser, David K., <u>Limiting Flight Control Systems</u>, AGARD-CP-199, November 1975.

41. Lamers, John P., <u>YF-16 High Angle of Attack Flight Test Experience</u>, AGARD-CP-199, November 1975.

42. Buckner, J. K., J. E., Walker III, and C. K. Clark, <u>The Design of the F-16 High-Alpha Flight Control Characteristics and Control System Concept</u>, AIAA paper No. 79-0403, January 1979.

43. Hall, G. W. and R. P., Harper, <u>In-Flight Simulation of the Light Weight Fighters</u>, AIAA Paper 75-985, August 1975.

44. Berry, Donald T., "Flying Qualities: A Costly Lapse in Flight-Control Design?", AIAA <u>Astronautics and Aeronautics</u>, April 1982.

45. Eggers, James A. and William F. Bryant J., <u>Flying Qualities Evaluation of the YF-16 Prototype Lightweight Fighter</u>, AFFTC-TR-75-15, July 1975.

46. Radford, Robert C. and Rogers E. Smith, "Approach and Landing Flying Qualities Requirements", <u>Flying Qualities Design Criteria, Proceedings of AFFDL Flying Qualities Symposium - October 1979</u>, AFWAL-TF-80-3067, May 1980.

47. Preliminary Design Group, Integrated Application of Active Controls Technology to an Advanced Subsonic Transport - Initial ACT Configuration Design Study, Boeing Commercial Airplane Company, NASA Contractor Report 159, 249, July 1980.

48. Etkin, Bernard, Dynamics of Atmospheric Flight, John Wiley & Sons, Inc., New York, 1973.

49. F-111 Stability and Control Group, Final Preliminary Stability and Control Aerodynamic Data for the F-111A Airplane, General Dynamics Corporation Dept. FZM-12-4198, 1 October 1965.

50. McRuer, Duane, Irving Askenas and Dunstan Graham, Aircraft Dynamics and Automatic Control, Princeton University Press, Princton, New Jersey, 1973.

51. Cooper, G. E. and R. P. Harper, The Use of Pilot Rating in the Evaluation of Aircraft Handling Qualities, NASA TN-D-5153, April 1969.

52. Booth, Edward M., Robert T. N. Chen, and Charles R. Chalk, A Two Phase Investigation of Longitudinal Flying Qualities for Fighters, Calspan Report AK-5280-F-2. (AFFDL-TR-74-9), April 1974.

53. D'Azzo, John J. and Constantine H. Houpis, Linear Control System Analysis and Design, McGraw-Hill, Inc., USA, 1975.

54. Wasserman, Richard, John F. Mitchell, William R. Rikard, Ronald W. Huber, and Arno E. Schelborn, In-Flight Simulation of Minimum Longitudinal Stability for Large Delta-Wing Transports in Landing Approach and Touchdown, Volume 11: Supporting Technical Data and Analysis, AFFDL-TR-72-143, Volume II, Febvruary, 1973.

55. System/Subsystem Summary Report (YF-16), Volume 4, Stability and Flight Control, General Dynamics Report FZM-401-069-4, 14 December 1973.

56. Barr, N.M., Gangsaas, D. ana Schaeffer, D.R., Wind Models for Flight Simulator Certification of Landing and Approach Guidance and Control Systems, Report No. FAA-RD-74-206, December 1974.

57. Schultz, L. A., Visual Flight Simulator (VFS) Applications Software Standard/Library Program User's Manual, Boeing Report D180-20115-1, 1 October 1976.

58. U. S. Standard Atmosphere, U. S. Government Printing Office, 1962, Revised May 1963.

59. Carlson, Frank, C-14 Flight Control System Design Requirements and Objectives, D162-12058-1TN The Boeing Co., January 29, 1976.

60. Anon, YC-14 Advanced Medium STOL Transport Final Flight Test Report - Summary, Boeing Document No D748-10130-1, October 8, 1977.

61. Lee, Alan H., YC-14 Flight Control System Development Experience, Paper presented at Flight Control Systems Symposium, Naval Postgraduate School, Monterey, California, July 11-13, 1978.